CARLOS HENRIQUE GOMES

ANÁLISE ESTATÍSTICA DOS PARÂMETROS MODAIS DE SISTEMAS RANDÔMICOS

FLORIANÓPOLIS

2011

UNIVERSIDADE FEDERAL DE SANTA CATARINA
PROGRAMA DE PÓS-GRADUAÇÃO
EM ENGENHARIA MECÂNICA

ANÁLISE ESTATÍSTICA DOS PARÂMETROS MODAIS DE SISTEMAS RANDÔMICOS

Tese submetida à
Universidade Federal de Santa Catarina
como parte dos requisitos para a
obtenção do grau de Doutor em Engenharia Mecânica

CARLOS HENRIQUE GOMES

Florianópolis, Outubro de 2011

Catalogação na fonte pela Biblioteca Universitária
da
Universidade Federal de Santa Catarina

G633a Gomes, Carlos Henrique
Análise estatística dos parâmetros modais de sistemas randômicos [tese] / Carlos Henrique Gomes ; orientador, Samir Nagi Yousri Gerges. - Florianópolis, SC, 2011.
632 p.: il., grafs., tabs

Tese (doutorado) - Universidade Federal de Santa Catarina, Centro Tecnológico. Programa de Pós-Graduação em Engenharia Mecânica.

Inclui referências

1. Engenharia mecânica. 2. Incerteza - (Teoria da informação). 3. Análise estatística energética. 4. Análise modal - Teses. 5. Matrizes (Matemática). I. Gerges, Samir Nagi Yousri. II. Universidade Federal de Santa Catarina. Programa de Pós-Graduação em Engenharia Mecânica. III. Título.

CDU 621

ANÁLISE ESTATÍSTICA DOS PARÂMETROS MODAIS DE SISTEMAS RANDÔMICOS

CARLOS HENRIQUE GOMES

Esta Tese foi julgada adequada para obtenção do Título de Doutor em Engenharia Mecânica, Área de concentração Vibrações e Acústica, e aprovada em sua forma final pelo Programa de Pós Graduação em Engenharia Mecânica da Universidade Federal de Santa Catarina.

Samir Nagi Yousri Gerges, PhD.
Orientador

Eduardo Alberto Fancello, D. Sc
Coordenador do Programa de Pós-Graduação em Engenharia Mecânica

Banca Examinadora:

Samir Nagi Yousri Gerges, PhD.
Presidente

Moyses Zindeluk, Dr. Eng.
Relator

Erasmo Felipe Vergara Miranda, Dr. Eng.

Marcelo Krajnc Alves, PhD.

Julio Apolinário Cordioli, Dr. Eng.

Dedico este trabalho à familía Burg Gomes, em especial à minha esposa Raquel.

Sempre acreditei nos números. Nas equações e na lógica que leva à razão.
E após uma vida toda de buscas, pergunto: o que realmente é a lógica?
Quem decide a razão?

Minha procura me levou através do físico, do metafísico, do ilusório e de volta. E fiz a descoberta mais importante da minha carreira.

A descoberta mais importante da minha vida. É somente nas misteriosas equações do amor que qualquer lógica ou razão pode ser encontrada.

Discurso de John F. Nash Jr.
Prêmio Nobel de Economia de 1994

Filme: Uma Mente Brilhante
(Titulo original: A Beautiful Mind)

AGRADECIMENTOS

Inicialmente gostaria de agradecer o meu orientador celestial, Deus, que sempre me acompanhou e mostrou a luz nos caminhos mais difíceis.

Agradeço a minha família, em especial a minha esposa Raquel, por sempre me apoiar e lutar conjuntamente pelas conquistas dos nossos objetivos.

Os meus sinceros agradecimentos ao meu orientador Prof. Samir Gerges que me introduziu ao mundo da acústica e sempre me ofereceu as melhores condições de trabalho e de aprendizagem durante a minha permanência no Laboratório de Vibrações e Acústica (LVA). Agradeço também aos outros professores, técnicos e colegas do LVA pela amizade, os bons momentos compartilhados e lições aprendidas.

Gostaria de agradecer o Prof. Brian Mace pela oportunidade de um intercambio técnico na Universidade de Southampton - UK e por discutir pacientemente diversos pontos técnicos do meu trabalho. Agradeço também as contribuições proporcionadas pelo Prof. Neil Ferguson e demais colegas do grupo de Dinâmica.

Agradeço o apoio financeiro proporcionado pelo Conselho Nacional de Desenvolvimento Científico e Tecnológico (CNPq), sem o qual muitos estudos de pós-graduação não seriam possíveis.

Finalmente, os meus sinceros agradecimentos a todos que contribuíram de alguma forma para a realização deste trabalho!

RESUMO

A confecção de um sistema mecânico está sempre sujeita às imperfeições e incertezas oriundas do seu processo de fabricação que podem eventualmente estabelecer diferenças significativas entre o desempenho desejado inicialmente em projeto e aquele efetivamente apresentado pelo sistema real. Como conseqüência deste fato, uma variação aleatória das respostas dinâmicas é certamente esperada ao longo de um *ensemble* composto de sistemas similares, dificultando de forma considerável as análises de engenharia nas regiões de médias e altas frequências. Assim, com o objetivo de garantir que os requisitos de projeto e certificação sejam devidamente cumpridos, um engenheiro projetista deve considerar os principais efeitos decorrentes destas incertezas na elaboração dos seus modelos matemáticos. Neste sentido, intensos esforços têm sido realizados pela comunidade acadêmica para o desenvolvimento de metodologias eficazes e otimizadas para a descrição estatística das respostas oriundas de sistemas randômicos (i.e. sistemas com propriedades não-determinísticas). Atualmente, a Análise Estatística de Energia (SEA) é uma das principais metodologias para análise vibroacústica nas regiões de médias e altas frequências, visto que seus resultados predizem o comportamento médio esperado de um *ensemble* composto de sistemas similares, como por exemplo: carros que saem de uma linha de montagem ou aviões produzidos em série. Recentemente, as formulações analíticas de SEA foram estendidas para predizer a variância da resposta energética. Nestas formulações, as estatísticas dos parâmetros modais (frequências naturais e formas modais) foram descritas pelas estatísticas dos auto-valores e auto-vetores de uma matriz do tipo GOE (*Gaussian Orthogonal Ensemble*) oriunda da Teoria da Matriz Randômica. Diversos trabalhos experimentais e numéricos têm confirmado um estabelecimento satisfatório da estatística GOE para as frequências naturais de sistemas suficientemente randômicos. Entretanto, alguns desvios significativos em relação ao modelo GOE têm sido identificados para as formas modais correspondentes afetando sensivelmente o desempenho das predições da variância de SEA. Neste trabalho de doutorado, as estatísticas dos parâmetros modais de sistemas randômicos foram sistematicamente investigadas com o auxílio dos resultados dos observadores estatísticos oriundos da Teoria da Matriz Randômica. Duas classes de problemas foram analisadas: ondas longitudinais em barras e ondas de flexão em placas. Para as estatísticas de cada um dos parâmetros modais, os níveis de concordância com o modelo GOE (ou de Poisson) foram prontamente avaliados. Além disso, os valores da média e da variância relativa da densidade de

energia cinética foram calculados e comparados com as predições analíticas de SEA baseadas nos modelos GOE e de Poisson. Os possíveis impactos, ou degradações, no desempenho das predições da variância de SEA baseadas no modelo GOE foram investigados para os casos em que as estatísticas dos parâmetros modais não concordam plenamente com a estatística descrita pelo modelo GOE. Dentre as principais contribuições deste trabalho de doutorado destacam-se o estabelecimento de métricas eficientes para a verificação do nível de concordância de cada um dos parâmetros modais com as estatísticas descritas pelos modelos GOE e de Poisson, bem como a obtenção de uma melhor compreensão das relações existentes entre as estatísticas do modelo GOE (ou de Poisson) e as estatísticas esperadas para os parâmetros modais de sistemas vibroacústicos de engenharia.

Palavras Chaves: Incertezas, Análise Estatística Energética (SEA), Parâmetros Modais, Teoria da Matriz Randômica, Estatística GOE.

ABSTRACT

A component of a mechanical system is always affected by the imperfections and uncertainties arising from the manufacturing and assembly processes, which can lead to the establishment of substantial differences between the vibroacoustical performance presented by the real engineering system and that initially targeted in the first design stage. As a direct consequence of this, a random variation in the dynamic responses occurs across the ensemble, making it difficult to carry out vibroacoustical analysis in the mid and high-frequency ranges. In order to guarantee compliance with the design and certification requirements, a design engineer must take into account the effects of uncertainty in the derivation of the mathematical models. In this regard, several efforts have been made by the academic community to develop optimized methods to accurately predict the statistical moments of dynamic responses of random systems (i.e., systems with non-deterministic properties). Statistical Energy Analysis (SEA) is one of main methodologies employed for vibroacoustical analysis in the mid and high-frequency ranges, since its results predict the average response of an ensemble composed of similar systems, such as cars from an assembly line or aircraft manufactured in series. Recently, the SEA predictions were extended to evaluate the relative variance of energy responses. In these new formulations, the statistics of the modal parameters (natural frequencies and mode shapes) were described through the statistics of the eigenvalues and eigenvectors of a special class of matrices known as the Gaussian Orthogonal Ensemble (GOE) of the Random Matrix Theory (RMT). Several experimental and numerical studies have confirmed the satisfactory establishment of GOE statistics for the natural frequencies of sufficiently random systems. However, some deviations in relation to the GOE model have been identified for the corresponding mode shapes, affecting substantially the performance of SEA variance predictions. In this doctoral study, the statistics of the modal parameters of random systems were systematically investigated through the statistical results of particular metric functions from the Random Matrix Theory (RMT) called statistical observables. Two classes of structural systems were investigated: longitudinal rods and flexural plates. The level of agreement with the GOE (or Poisson) model was evaluated for each one of the modal parameter statistics. Additionally, the mean and relative variance of the kinetic energy density results were calculated and compared with the analytical SEA predictions based on the GOE and Poisson models. The possible impacts on the performance of the SEA variance prediction based on the GOE model

were highlighted for the cases in which the modal parameter statistics do not conform perfectly with the statistics described by the GOE model. The main contributions of the study reported herein are the investigation of the efficient metric function for each one of the modal parameters to verify the agreement between the modal parameter statistics and those described by the GOE and Poisson models. Furthermore, an improved understanding was obtained regarding the relationship between the GOE (or Poisson) statistics and those expected for the modal parameters of random vibroacoustical systems.

Keywords: Uncertainties, Statistical Energy Analysis (SEA), Modal Parameters, Random Matrix Theory, GOE statistics.

LIST OF FIGURES

1 Magnitudes of FRFs from 99 nominally identical vehicles, Kompella and Bernhard (9). . . . . p. 61

2 Magnitudes of responses from 41 nominally identical beer cans acoustically excited, Fahy (7). . . . . p. 62

3 Experimental cross-mobility results from an artificial ensemble of beams with randomly attached point masses, Johnson (21). . . . . p. 63

4 The energy responses from the random plates for three distinct ensemble approaches, Langley *et al* (4). . . . . p. 66

5 The energy response variances from three distinct ensemble approaches, Langley *et al* (4). . . . . p. 67

6 Examples of numerical simulations in the automobile field: comparison between deterministic and statistical approaches. Sub-figure (a): FEM and BEM variables. Sub-figure (b): SEA variables, Gomes (28). . . . . p. 71

7 Parameters used in the modal overlap factor definition: half-power band and mean natural frequency spacing, both frequency band average values, Gomes (28). . . . . p. 75

8 Examples of performance of the revised SEA relative variance predictions for the case of a single punctual excitation. Upper Plot: The relative standard deviation of energy density compared to analytical predictions: numerical results (gray solid line); GOE theoretical prediction with $K = 3$ (gray dashed-dotted line); modified GOE prediction with $K = 2.74$ (black solid line). Lower Plot: Relative standard deviation of energy density for 32 member ensemble: experimental results (gray solid line); band average of experimental results (black solid line); GOE theoretical prediction with $K = 3$ (black dotted line); and GOE theoretical prediction with $K = 2.5$ (black dashed line), Langley and Brown (18). . . . . p. 84

9 Measured mode shape patterns from a disordered plate with Bunimovich shape, Schaadt (70). . . . . p. 87

10 Plot(a): The PDF of adjacent eigenvalue spacings. Plot (b): the level repulsion parameter β_r for intermediate eigenvalue statistics $P(s)$ plotted against the scaling parameter, $x_s = b_w^2/N$. For the matrix dimensions: $N = 400(+)$, $N = 800(\Delta)$, and $N = 1600(\diamondsuit)$. Each β_r value was obtained by a fitting process from the numerical data for eigenvalue spacing distribution, Casati *et al* (78). . . . . p. 90

11 Scaled localization length (β_s) versus scaling parameter (x_s) for random matrix dimensions: $N = 200(\bullet)$, $N = 400(\triangle)$, $N = 600(\circ)$, and $N = 800(\blacksquare)$. The dashed line relates to the fitting of numerical data and follows the standard formulation: $\beta_s = \gamma_s x_s/(1+\gamma_s x_s)$, where γ_s is a real constant. Plot (a): the numerical data show a notable trasition (scaling) pattern with the scaling parameter. Plot (b): complete range of scaling parameters in log-log plot, where $y = \beta_s/(1-\beta_s)$, Casati *el al* (79). . . . . p. 92

12 Schematic representation of the typically expected pattern of the modal parameter statistics for an ensemble composed of similar systems with uncertain or non-deterministic parameters. The effects of an increase in the amount of randomness on the statistical characteristics of each one of the modal parameters are illustrated for a fixed frequency range, Gomes (10). . . . . p. 99

13 Examples of energy level spectra of nuclear systems, Mehta (24). . . . . p. 109

14 Examples of staircase function for two aluminum plates. Plot (a): Square geometry. Plot (b): Sinai stadium geometry. The step function is associated with numerical results and the dashed line represents the analytical prediction of Weyl's formula. The zoom plots emphasize the differences between Square and Sinai stadium results, Gomes and Gerges (93). . . . . p. 114

15 The oscillatory components of unfolded staircase functions of plates, Gomes and Gerges (93). Plot (a): Square geometry. Plot (b): Sinai geometry. . . . . p. 116

16 The PDFs of adjacent eigenvalue spacings for Poisson (Exponential) and Wigner (Rayleigh) model statistics . . . . . p. 119

17 The GOE two-level correlation function and Rayleigh PDF for adjacent unfolded eigenvalues, Guhr *et al* (57, 63). . . . p. 122

18 Number variance: GOE and Poisson eigenvalue statistics, Gomes and Gerges (101). . . . . p. 123
19 Example of the evaluation process of Δ_3- statistics, Gomes and Gerges (93). . . . . p. 124
20 Δ_3 - statistics: GOE and Poisson eigenvalue spectra, Gomes and Gerges (101). . . . . p. 126
21 Example of Fourier transform of staircase function fluctuations of a rectangular Sinai ($a = 56\,cm$, $b = 20\,cm$ and $r = 7\,cm$). Inset Figure: identification of main periodic orbits, Stöckmann and Stein (92). . . . . p. 133
22 Periodic orbit effects on the spectral natural frequency statistics. Plot(a): fluctuations or oscillatory component of staircase function. Plot(b): Power spectrum from the FFT of the staircase function fluctuations. Plot(c): resultant fluctuations from Fourier unfolding process, Schaadt (69). p. 135
23 Examples of the effects of periodic orbits on the Δ_3 - statistics results. Upper Plot: Sinai block, Schaadt (69). Lower Plot: Microwave cavity resonator, Gräf *et al* (96). . . . . p. 137
24 Numerical modal analysis of an automotive dash panel using FEM models. Plot (a): structural FEM mesh model. Plots (b) - (d): Mode shapes corresponding to the following natural frequencies: 61.215 Hz, 101.088 Hz, and 114.507 Hz, respectively, Gomes (10). . . . . p. 140
25 Examples of Porter-Thomas distribution: GOE prediction, Sinai Billiard, and Sinai Stadium measured results, Kudrolli *et al.* (71). . . . . p. 144
26 Examples of regular or integrable mode shapes and their PT- distributions from a rectangular plate of quartz, Schaadt (69). In these plots, the smooth and well-behaved function is the analytical formulation of PT-distribution for perfect GOE eigenvectors, Equation (2.24), and the results with step function-like format expresses the experimental measurements. Plot (a): Natural frequency of 419.6 kHz. Plot (b): Natural frequency of 437.7 kHz. . . . . p. 145
27 Typical examples of GOE mode shapes of chaotic billiards. Plot (a): Sinai stadium geometry, McDonald and Kaufman (126). Plot (b): 1/4 Sinai geometry, Pradhan and Sridhar (73). Plot (c): cardioid geometry, Backer (127). . . . . p. 146

28 Definitions of kurtosis averaging approaches. Plot (a): Ensemble mode shapes. Plots (b - d): Graphical representations of the spatial, spectral, and ensemble kurtosis averaging approaches, respectively, Gomes and Gerges (101). . p. 149
29 Representation of the effects of an increase in the amount of uncertainty associated with the unfolded natural frequency of a random system. Plot (a): Example of spaghetti unfolded frequency curves, Schaadt (70). Plot (b): Modal parameter characteristics of the avoided crossing region (mixing of mode shapes), Schaadt (69). . . . . p. 157
30 Example of a typical bouncing ball state of a quarter Sinai rectangular billiard. Plot (a): Main periodic orbits. Plot (b): squared mode shape amplitudes. Plot (c): Porter-Thomas distribution results, Kudrolli and Sridhar (72). . . . . p. 160
31 Examples of mode shapes associated with periodical orbits, Sridhar and Heller (119). . . . . p. 161
32 Examples of the wavefunctions of disordered billiard systems demonstrating the establishment of Anderson Localization. Plot (a): weak localization regime. Plot (b): strong localization regime, Pradhan and Sridhar (73, 74). . . . . p. 163
33 Examples of squared spatial correlation functions of the mode shape components for weak and strong localization regimes, Kudrolli *et al* (71). . . . . p. 165
34 Porter - Thomas results for weakly and strongly localized mode shapes: experimental and analytical patterns based on nonlinear sigma model of supersymmetry, Kudrolli *et al* (71). . . . . p. 168
35 Examples of the nonlinear sigma model forms for chaotic and disordered systems. In the top panel: chaotic Sinai-stadium billiard. In the middle and bottom panels: disordered billiards under weak and strong localization regimes, respectively. The solid lines represent the calculations based on the nonlinear sigma model, Pradhan and Sridhar (73). p. 169
36 Spatial squared mode shape correlation functions of Sinai (chaotic) and disordered (localized) billiards with fixed disordered strength $2kl$ (dotted lines). The analytical nonlinear sigma model results: - - - Equation (2.60) (dashed line) and —— Equation (2.62) (solid line), Pradhan and Sridhar (74). . . . . p. 170

37 Pendulum system: a chain of pendulums coupled by springs, Hodges and Woodhouse (150). . . . . p. 173

38 Pictorial example of a long tail response distribution expected for an ensemble of localized structures: the linear or arithmetic mean (the center of mass) and the typical value (probabilistic mode or peak) of the distribution are very distinct, adaptation of Hodges and Woodhouse (140). . . . p. 176

39 An example of the FEM model of a typical random rod investigated in this study. . . . . p. 193

40 Natural frequency performance: FEM model results and analytical predictions. . . . . p. 195

41 Mode shape performance: FEM model results and analytical predictions. Plots: (a) Mode 05, (b) Mode 25, (c) Mode 36, and (d) Mode 80 (higher order mode - zoom plot). . . p. 197

42 The unfolded natural frequency spacing PDF results and analytical predictions: Gaussian (Normal), Poisson (Exponential), and GOE (Rayleigh) (spectral averaging approach). Plots: (a) Nominal, (b) Uniform (20%), (c) Mass (20%), (d) Gaussian (10%), (e) Gaussian (20%), and (f) Gaussian (30%). . . . . p. 203

43 Correlation coefficient of the natural frequency spacings: the random rod results are compared to the eigenvalue correlation function results of the *dim* (500*500) GOE and Poisson matrices (spectral averaging approach). Plots: (a) Nominal, (b) Uniform (20%), (c) Mass (20%), (d) Gaussian (10%), (e) Gaussian (20%), and (f) Gaussian (30%). . p. 208

44 The number variance results for the nominal and random rods, and GOE and Poisson analytical predictions (spectral averaging approach). Plots: (a) Nominal, (b) Uniform (20%), (c) Mass (20%), (d) Gaussian (10%), (e) Gaussian (20%), and (f) Gaussian (30%). . . . . p. 212

45 The Δ_3-statistics results for the nominal and random rods and analytical predictions of the GOE and Poisson models (spectral averaging approach). Plots: (a) Nominal, (b) Uniform (20%), (c) Mass (20%), (d) Gaussian (10%), (e) Gaussian (20%), and (f) Gaussian (30%). . . . . p. 215

46 Lyon's Mode Shape Statistics Factor or spatial kurtosis results for the nominal and random rods (spatial averaging approach). Plots: (a) Nominal, (b) Uniform (20%), (c) Mass (20%), (d) Gaussian (10%), (e) Gaussian (20%), and (f) Gaussian (30%). . . . . p. 219
47 PDFs of spatial kurtosis from the Gaussian random rods (spatial averaging approach). Plots: (a) Gaussian (10%), (b) Gaussian (20%), and (c) Gaussian (30%). . . . . p. 223
48 The spatial Lilliefors Test results for the nominal and random rods (spatial averaging approach). Plots: (a) Nominal, (b) Uniform (20%), (c) Mass (20%), (d) Gaussian (10%), (e) Gaussian (20%), and (f) Gaussian (30%). . . . . p. 228
49 PT-distribution results for the nominal and random rods and GOE predictions (Gaussian mode shapes) (spatial averaging approach). Plots: (a) Nominal, (b) Uniform (20%), (c) Mass (20%), (d) Gaussian (10%), (e) Gaussian (20%), and (f) Gaussian (30%). . . . . p. 232
50 Examples of the main three classes of mode shape statistics: almost-nominal (sinusoidal), almost-GOE (or Gaussian), and structural localized statistics (spatial averaging approach). The Gaussian (30%) numerical results (for preselected mode shapes) and analytical prediction (sinusoidal and Gaussian statistics). . . . . p. 244
51 Spectral kurtosis results for the nominal and random rods and analytical predictions, GOE and sinusoidal statistics (spectral averaging approach). Plots: (a) Nominal, (b) Uniform (20%), (c) Mass (20%), (d) Gaussian (10%), (e) Gaussian (20%), and (f) Gaussian (30%). . . . . p. 249
52 Hamiltonian matrix patterns of the nominal and Gaussian random rod structures. Plots: (a) Nominal Hamiltonian Matrix - 3D view, (b)-(d) Hamiltonians of nominal structure; Gaussian structures (10%, 20%, and 30%, respectively); and Hamiltonian differences. The Hamiltonian elements are shown in terms of the absolute values. . . . . p. 252
53 Hamiltonian patterns of the nominal and Uniform random rod structures. Plots: (a) - (b) Nominal structure; Uniform structures (10% and 20%, respectively); and Hamiltonian differences. The Hamiltonian elements are shown in terms of the absolute values. . . . . p. 254

54 Hamiltonian patterns for the nominal and mass-loaded random rod structures. Plots: (a) Nominal ; (b) mass-loaded rod structures, Mass (10% and 20%, respectively); and Hamiltonian differences. The Hamiltonian elements are shown in terms of the absolute values. . . . . p. 255

55 Kinetic energy density results for the nominal rod excited by unitary longitudinal single point-loading at left end of rod (spectral averaging approach). Plots: Damping Loss Factors: (a) 0.03, (b) 0.06, (c) 0.12, and (d) 0.24. . . . . p. 260

56 Spectral relative variances of kinetic energy density results for the nominal rod excited by unitary longitudinal single point-loading at the left end of the rod (spectral averaging approach). Plots: Damping Loss Factors: (a) 0.03, (b) 0.06, (c) 0.12, and (d) 0.24. . . . . p. 263

57 Kinetic energy density results for the random and nominal rods in terms of the narrow and 1/3 octave frequency band domains subjected to unit single point excitation. The analytical SEA predictions are also plotted. . . . . p. 266

58 Spectral relative variance of kinetic energy density results for the random and nominal rods subjected to unit single point-loading (spectral averaging approach). The analytical predictions for relative variance based on the Poisson and GOE models. . . . . p. 267

59 Spectral mean and relative variance of kinetic energy density results for the random and nominal rods with DLF = 0.24 (spectral averaging approach). The analytical predictions for relative variance are based on Poisson and GOE statistics models. . . . . p. 269

60 Spectral relative variance of kinetic energy density results from the Mass (20%) and Gaussian (30%) random rods subjected to spatially-averaged (spectral averaging approach) excitation. Several DLF are considered. Plots: (a) 0.03, (b) 0.06, (c) 0.12, and (d) 0.24. . . . . p. 272

61 Distribution of the rod cross-sectional area values from: (a) the spatially independent Gaussian (30%) rod, (b) the spatially-correlated Gaussian rod: Homogeneous isotropic Gaussian random field, and (c) the spatially- correlated Gaussian rod: Markovian stochastic process random field. p. 278

62 The spectral natural frequency statistical observable results for the spatially correlated random rod structures: PDF of adjacent natural frequency spacings and Δ_3-statistics results (spectral averaging approach). . . . . p. 283

63 The spatial mode shape statistical observable results for the spatially- correlated random Gaussian rods: spatial kurtosis values and spatial Lilliefors Test results (spatial averaging approach). . . . . p. 287

64 Spatial kurtosis results for the Gaussian spatially correlated random rods expressed in terms of the normalized parameter (spatial averaging approach). . . . . p. 289

65 Spatial mode shape statistics results from an ensemble composed of 500 spatially-correlated longitudinal rods (spatial averaging approach). Plot (a): Spatial kurtosis values. Plot (b): Spatial Lilliefors Test results. The correlation length range adopted was from $L_c = 0.01$ to $L_c = 1.00$ with constant steps. . . . . p. 291

66 Previous spatial mode shape statistics results from an ensemble composed of 500 spatially correlated longitudinal rods: (a) spatial Lilliefors Test results expressed in terms of the mode order domain, and (b) Histogram of the spatial Lilliefors Test results expressed in terms of the correlation length domain. . . . . p. 293

67 Kinetic energy density statistics of the Gaussian spatially-correlated rods subjected to an unitary single point-loading (spectral averaging approach). Plot(a): energy density results expressed in the narrow frequency domain. Plot(b): spectral mean values expressed in terms of the 1/3 oct. frequency band domain. Plot(c): spectral relative variance results expressed in terms of the 1/3 oct. frequency bands. p. 295

68 Kinetic energy density statistics of the spatially-correlated rods subjected to spatially-averaged excitation (spectral averaging approach). Plot(a): energy density results expressed in narrow frequency domain. Plot(b): spectral mean value results expressed in terms of the 1/3 oct. frequency band domain. Plot(c): spectral relative variance results expressed in terms of the 1/3 oct. frequency bands. p. 298

69 Spectral relative variance of the kinetic energy density results in the frequency band domain with fixed bandwidth (spectral averaging approach). Plot(a): unitary single point-loading. Plot(b): spatially-averaged excitation. . . . p. 301
70 PDF of adjacent unfolded natural frequency spacings: numerical results for the mass-loaded rod ensemble and analytical predictions based on: Gaussian (Normal), GOE (Rayleigh), and Poisson (Exponential) statistics (ensemble averaging approach). Plots: (a) Mode 10, (b) Mode 20, (c) Mode 30, (d) Mode 42, (e) Mode 60, and (f) Mode 80. . . p. 311
71 Number variance results of the mass-loaded rod ensemble. Analytical predictions: GOE and Poisson models (ensemble averaging approach). Plots: (a) Mode 10, (b) Mode 20, (c) Mode 30, (d) Mode 42, (e) Mode 60, and (f) Mode 80. . p. 316
72 Δ_3-statistics results for the mass-loaded rod ensemble (ensemble averaging approach). Analytical predictions: GOE and Poisson models. Plots: (a) Mode 10, (b) Mode 20, (c) Mode 30, (d) Mode 42, (e) Mode 60, and (f) Mode 80. . . p. 319
73 Confidence levels for chi-squared test results for the mass-loaded string: — test for Rayleigh PDF and - - - test for exponential PDF, Brown (1). . . . . p. 321
74 Statistical overlap factor results for a mass-loaded rod ensemble (ensemble averaging approach). Plot (a): global natural frequency spacing, local natural frequency spacings, natural frequency standard deviations. Plot (b): Statistical overlap factor: based on global and local mean values of the natural frequency spacings. . . . . p. 323
75 Spatial analysis of the mode shape statistics of a mass-loaded rod ensemble (spatial averaging approach). Plot (a): spatial kurtosis results. Plot (b): spatial Lilliefors Test results. . . . . p. 326
76 Spectral analysis of the mode shape statistics (spectral averaging approach). Plot (a): spectral kurtosis results. Plot(b): spectral Lilliefors Test results. . . . . p. 328
77 Ensemble kurtosis results: individual members, typically expected, arithmetic and geometric mean values (ensemble averaging approach). . . . . p. 329
78 Ensemble Lilliefors Test results: bi-dimensional graphical representation (ensemble averaging approach). . . . . p. 330

79 Ensemble Porter-Thomas distribution results for localized mode shapes: numerical results for the mode shape component located at 0.658 m, GOE prediction and non-linear sigma model fitted patterns (weak and strong localization regimes) (ensemble averaging approach). Plots: (a) mode 26, (b) mode 39, (c) mode 72, and (d) mode 93. . . . . p. 333

80 Mode shape SEA parameters of the mass-loaded rod ensemble (ensemble averaging approach). Plot (a): Parameter P_a. Plot (b): Parameter Q_a. . . . . p. 335

81 Mode shape SEA parameter of the mass-loaded rod ensemble: parameter Z (ensemble averaging approach). . . . . p. 336

82 Ensemble spatial decay analyses: averaging process performances and localization factor values (ensemble averaging approach). Plot (a): Vicinities of Modes 09 and 10: excitation frequency of 4.5 kHz - almost sinusoidal mode shape statistics. Plot (b): Vicinities of Modes 21 and 22: excitation frequency of 10 kHz - sinusoidal to Gaussian transition mode shape statistics. Plot (c): Vicinities of Modes 41 and 42: excitation frequency of 20 kHz - almost Gaussian mode shape statistics. Plot (d): Vicinities of Modes 62 and 63: excitation frequency of 30 kHz - localized mode shape statistics. . . . . p. 340

83 Localization factor results as a function of excitation frequency: arithmetic and geometric decay evaluation (ensemble averaging approach). . . . . p. 343

84 Kinetic energy density results for spatially-averaged excitation: members, ensemble arithmetic and geometric mean values and SEA prediction (ensemble averaging approach). p. 345

85 Relative variance of kinetic energy density results for spatially-averaged excitation based on: ensemble arithmetic and geometric mean values (ensemble averaging approach). The Poisson and GOE analytical predictions are also plotted. . . . . p. 346

86 Ensemble mean and relative variance values of the mass-loaded longitudinal rods subjected to a single point-loading at excitation points X_0, X_2, and X_3: numerical results and analytical predictions based on GOE and Poisson models (ensemble averaging approach). . . . . p. 350

87 Ensemble kurtosis results for the mass-loaded rod ensemble: excitation points X_0, X_2 and X_3 (ensemble averaging approach). . . . . p. 353

88 Ensemble Lilliefors Test results for the mass-loaded rod ensemble (ensemble averaging approach). Plot (a): Excitation point X_0. Plot (b) Excitation point X_2. Plot (c): Excitation point X_3. . . . . p. 354

89 Results for natural frequency statistical observables for Gaussian spatially-correlated random rods (ensemble averaging approach). Plot (a): Mode 10. Plot (b): Mode 20. Plot (c): Mode 35. Plot (d): Mode 40. Plot (e): Mode 65. Plot (f): Mode 80. Plot (g): Mode 95. . . . . p. 365

90 Statistical overlap factor results for a Gaussian spatially-correlated rod ensemble (ensemble averaging approach). Plot (a): global natural frequency spacing, local natural frequency spacings, natural frequency standard deviations. Plot (b): Statistical overlap factor: based on the definitions of global and local mean values for the natural frequency spacings. . . . . p. 367

91 Spatial kurtosis results for the Gaussian spatially-correlated rods: individual members, probabilistic mode, arithmetic and geometric mean values and analytical predictions (sinusoidal and GOE) (spatial averaging approach). p. 368

92 Spatial Lilliefors Test results for the Gaussian spatially-correlated rod ensemble: individual member values and arithmetic mean values (spatial averaging approach). . . . p. 369

93 Spatial Lilliefors Test results in terms of: (a) member number and (b) correlation length associated with each member of the ensemble (spatial averaging approach). . . . . p. 371

94 Spectral kurtosis results for the Gaussian spatially-correlated rods: individual members, probabilistic mode, arithmetic and geometric mean values and analytical predictions (sinusoidal and GOE) (spectral averaging approach). p. 372

95 Spectral Lilliefors Test results for the spatially-correlated rod ensemble: individual member values and arithmetic mean values (spectral averaging approach). . . . . p. 373

96 Ensemble kurtosis results for the Gaussian spatially correlated rods: individual member, probabilistic mode, arithmetic and geometric mean values (ensemble averaging approach). . . . . p. 374

97 Ensemble Lilliefors Test results for a Gaussian spatially-correlated rod ensemble (ensemble averaging approach). Plot (a): bi-dimensional graphical representation. Plot (b): individual member and the mean values as a function of the mode order value. . . . . p. 375

98 Mode shape normalized SEA parameters of the Gaussian spatially-correlated random rods (ensemble averaging approach). Plot (a): parameter P_a. Plot (b): parameter Q_a. . . . p. 377

99 Mode shape SEA parameter of the spatially-correlated rod ensemble: parameter Z (ensemble averaging approach). . . p. 378

100 Kinetic energy density results for spatially-averaged excitation: some individual members, ensemble arithmetic and geometric mean values and SEA predictions (ensemble averaging approach). Plot (a): frequency-constant DLF. Plot (b): constant modal superposition DLF. . . . . p. 380

101 Ensemble relative variance of spatially-averaged kinetic energy density results based on: arithmetic and geometric mean values. The analytical predictions are based on Poisson and GOE models (ensemble averaging approach). Plot (a): frequency-constant DLF. Plot (b): constant modal superposition DLF. . . . . p. 382

102 Histogram of the spatially-averaged kinetic energy density responses for Gaussian spatially-correlated rods excited by spatially-averaged forces, $\eta = 0.03$, 500 members, at various frequencies f (or the modal overlap factors m). The arithmetic and geometric mean values are also presented. . p. 384

103 Kinetic energy density results for single point-excited Gaussian spatially-correlated rods (ensemble averaging approach). Plot (a): arithmetic mean results - excitation point X_0 and frequency-constant DLF. Plot (b): arithmetic mean results - excitation point X_0 and constant modal superposition DLF. Plot (c): arithmetic mean results - excitation points X_2 and X_3 and frequency-constant DLF. Plot (d): arithmetic mean results - excitation points X_2 and X_3 and constant modal superposition DLF. Plot (e): relative variance results - excitation points X_0, X_2 and X_3 and frequency- constant DLF. Plot (f): relative variance results - excitation points X_0, X_2 and X_3 and constant modal superposition DLF. . . . . p. 389

104 Kinetic energy density results for excitation point X_2 (ensemble averaging approach). Plot (a): frequency-constant DLF. Plot (b): constant modal superposition DLF. . . . . p. 391

105 Relative variance of the kinetic energy density results for excitation point X_2 (ensemble averaging approach). Plot (a): frequency-constant DLF. Plot (b): constant modal superposition DLF. . . . . p. 392

106 Ensemble statistics of the mode shape components at excitation point X_2 (ensemble averaging approach). Plot:(a) Kurtosis values, Plot (b): Skewness values. Plot (c): Lilliefors Test results. . . . . p. 394

107 PDF of mode shape components at excitation point X_2 across the Gaussian spatially-correlated rod ensemble - 30*th* mode: numerical results and best-fit Gaussian PDF curve (ensemble averaging approach). . . . . p. 395

108 Spectral mode shape statistics parameters at excitation point X_2 (spectral averaging approach). Plot (a): individual ensemble member results, arithmetic and geometric mean values and sinusoidal and GOE analytical predictions. Plot (b): Histogram of spectral kurtosis results and their statistical parameters. . . . . p. 397

109 Kinetic energy density results for excitation point X_0 (ensemble averaging approach). Plot (a): frequency-constant DLF. Plot (b): constant superposition DLF. . . . . p. 399

110 Relative variance of kinetic energy density results for excitation point X_0 (ensemble averaging approach). Plot (a): frequency-constant DLF. Plot (b): constant superposition DLF. . . . . p. 400

111 Ensemble statistics of the mode shape components at excitation point X_0 (ensemble averaging approach). Plot (a): kurtosis values. Plot (b): Skewness values. Plot (c): Lilliefors Test results. . . . . p. 402

112 Spectral mode shape statistics parameters at excitation point X_0 (spectral averaging approach). Plot (a): individual member spectral kurtosis results, arithmetic and geometric mean values and sinusoidal and GOE analytical predictions. Plot (b): Histogram of spectral kurtosis results and their statistical parameters. The typically expected, arithmetic and geometric mean values are respectively 2.82, 3.97 and 3.63. . . . . p. 404

113 Kinetic energy density results for excitation point X_3 (ensemble averaging approach). Plot (a): frequency-constant DLF. Plot (b): constant superposition DLF. . . . . p. 406

114 Relative variances of kinetic energy density results for excitation point X_3 (ensemble averaging approach). Plot (a): frequency-constant DLF. Plot (b): constant superposition DLF. . . . . p. 407

115 Ensemble statistics of the mode shape components at excitation point X_3 (ensemble averaging approach). Plot (a): kurtosis values. Plot (b): Skewness values. Plot (c): Lilliefors Test results. . . . . p. 409

116 Spectral mode shape statistics parameters at excitation point X_3 (spectral averaging approach). Plot (a): individual member spectral kurtosis results, arithmetic and geometric mean values and sinusoidal and GOE analytical predictions. Plot (b): Histogram of spectral kurtosis results and their statistical parameters. The probabilistic mode, arithmetic and geometric mean values are, respectively, 2.83, 3.53 and 3.38. . . . . p. 411

117 Illustrations of the flexural plate geometries: square, rectangular, rectangular with one arc at corner, polygonal, circular and 1/4 Sinai stadium, respectively. . . . . p. 422

118 Flexural wavenumbers: traditional formulation based on the corresponding infinite plate system - Equation (4.2), and improved high-frequency formulation - Equation (4.3). p. 427
119 Natural frequency statistical observable results for the square plate (spectral averaging approach). Plot (a): PDF of adjacent natural frequency spacings. Plot (b): Δ_3 - statistics. . . . . p. 430
120 The natural frequency degeneracy factor (n_{av}) for the square plate: analytical prediction, individual and mean values. . . . . p. 431
121 Analysis of the sensitivity of the Δ_3 - statistics results to the distinct magnitudes of the cut-off times used in the Fourier unfolding process (spectral averaging approach). The legends of Δ_3 - statistics results are that the same as those of Figure 119 (b). . . . . p. 433
122 Natural frequency statistical observable results for the circular plate (spectral averaging approach). Plot (a): PDF of adjacent natural frequency spacings. Plot (b): number variance. Plot (c): Δ_3 - statistics. . . . . p. 435
123 Natural frequency statistical observable results for rectangular plate (spectral averaging approach). Plot (a): PDF of adjacent natural frequency spacings. Plot (b): natural frequency correlation coefficient. Plot (c): number variance. Plot (d): Δ_3 - statistics. . . . . p. 438
124 Natural frequency statistical observable results for the rectangular plate with an arc at one corner (spectral averaging approach). Plot (a): PDF of the adjacent natural frequency spacings. Plot (b): natural frequency correlation coefficient. Plot (c): number variance. Plot (d): Δ_3 - statistics. . . p. 440
125 Natural frequency statistical observable results for the 1/4 Sinai stadium plate (spectral averaging approach). Plot (a): PDF of the adjacent natural frequency spacings. Plot (b): natural frequency correlation coefficient. Plot (c): number variance. Plot (d): Δ_3 - statistics. . . . . p. 443
126 Natural frequency statistical observable results for polygonal plate (spectral averaging approach). Plot (a): PDF of the adjacent natural frequency spacings. Plot (b): natural frequency correlation coefficient. Plot (c): number variance. Plot (d): Δ_3 - statistics. . . . . p. 446

127 Natural frequency statistical observable results for the mass-loaded rectangular plate (spectral averaging approach). Plot (a): PDF of the adjacent natural frequency spacings. Plot (b): natural frequency correlation coefficient. Plot (c): number variance. Plot (d): Δ_3 - statistics results. . . . . p. 448
128 Spatial mode shape statistical observable results for square plate (spatial averaging approach). Plot (a): kurtosis results. Plot (b): Lilliefors Test results. . . . . p. 450
129 Mode shape statistical observable results for square plate: Mode 145 (spatial averaging approach). Plot (a): spatial PDF of mode shape components. Plot (b): spatial configuration. Plot (c): squared mode shape amplitudes. Plot (d): Porter-Thomas distribution. . . . . p. 452
130 Mode shape statistical observable results for square plate: Mode 255 (spatial averaging approach). Plot (a): spatial PDF of mode shape components. Plot (c): spatial configuration. Plot (b): squared mode shape amplitudes. Plot (d): Porter-Thomas distribution. . . . . p. 454
131 Representation of two classes of modes and their symmetry characteristics, Bertelsen (90, 66). . . . . p. 455
132 Schematic illustration of the superposition of modes, Schadt (69). . . . . p. 456
133 Spatial normalized mode shape correlation results for the square plate: Mode 255 (spatial averaging approach). Plot (a): linear correlation function (P_1). Plot (b): squared correlation function (P_2). . . . . p. 457
134 Spectral mode shape statistical observable results for the square plate (spectral averaging approach). Plot (a): kurtosis results. Plot (b): Lilliefors Test results. . . . . p. 459
135 Spatial mode shape statistical observable results for the circular plate (spatial averaging approach). Plot (a): kurtosis values. Plot (b): Lilliefors Test results. . . . . p. 461
136 Spatial mode shape characteristics for the circular plate: Mode 142 (spatial averaging approach). Plot (a): spatial PDF of mode shape components. Plot (b): spatial configuration. Plot (c): squared mode shape amplitudes. Plot (d): Porter-Thomas distribution. . . . . p. 463

137 Spatial mode shape characteristics for the circular plate: Mode 229 (spatial averaging approach). Plot (a): spatial PDF of mode shape components. Plot (b): spatial configuration. Plot (c): squared mode shape amplitudes. Plot (d): Porter-Thomas distribution. . . . . p. 466

138 Spectral mode shape characteristics of the circular plate (spectral averaging approach). Plot (a): kurtosis values. Plot (b): Lilliefors Test results. . . . . p. 467

139 Spatial mode shape statistical observable results for the rectangular plate (spatial averaging approach). Plot (a): spatial kurtosis. Plot (b): Lilliefors Test. . . . . p. 468

140 Spatial mode shape statistical observable results for the rectangular plate: Mode 68 (spatial averaging approach). Plot (a): spatial PDF of mode shape components. Plot (b): spatial configuration. Plot (c): squared mode shape component amplitudes. Plot (d): Porter-Thomas distribution. . p. 471

141 Spatial mode shape statistical observable results for the rectangular plate: Mode 186 (spatial averaging approach). Plot (a): spatial PDF of mode shape components. Plot (b): spatial configuration. Plot (c): squared mode shape component amplitudes. Plot (d): Porter-Thomas distribution. . p. 473

142 Spatial normalized mode shape correlation function results for the rectangular plate: Mode 186 (spatial averaging approach). Plot (a): linear correlation function (P_1). Plot (b): squared correlation function (P_2). . . . . p. 475

143 Spectral mode shape statistical observable results for the rectangular plate (spectral averaging approach). Plot (a): kurtosis results. Plot (b): Lilliefors Test results. . . . . p. 477

144 Spatial mode shape statistical observable results for the rectangular plate with an arc at one corner. Plot (a): kurtosis values (spatial averaging approach). Plot (b): Lilliefors Test results. Plot (c): PT-distribution results. . . . . p. 478

145 Spatial representation of the mode shape components and corresponding PT-distribution results for some almost-Gaussian mode shapes of the rectangular plate with an arc at one corner (spatial averaging approach). Plot (a): mode 137. Plot (b): mode 218. . . . . p. 480

146 Spatial representation of the mode shape components and corresponding PT-distribution results for some low-frequency mode shapes of the rectangular plate with an arc at one corner (spatial averaging approach). Plot (a): mode 08. Plot (b): mode 11. Plot (c): mode 44. . . . . p. 483

147 Spatial mode shape statistical observable results for 1/4 Sinai stadium plate (spatial averaging approach). Plot (a): kurtosis values. Plot (b): Lilliefors Test results. . . . . p. 485

148 Spatial representation of the mode shape components and corresponding PT-distribution results for the 1/4 Sinai stadium plate (spatial averaging approach). Plot (a): mode 61. Plot (b): mode 186. Plot (c): mode 249. . . . . p. 488

149 Spectral mode shape statistics results for the 1/4 Sinai stadium plate (spectral averaging approach). Plot (a): kurtosis results. Plot (b): Lilliefors Test results. . . . . p. 489

150 Spatial mode shape statistical observable results for the polygonal plate (spatial averaging approach). Plot (a): kurtosis values. Plot (b): Lilliefors Test results. . . . . p. 490

151 Spatial representation of the mode shape components and corresponding PT-distribution results for some mode shapes of the polygonal plate (spatial averaging approach). Plot (a): mode 198. Plot (b): mode 220. . . . . p. 493

152 Spectral mode shape statistics results for the polygonal plate (spectral averaging approach). Plot (a): kurtosis results. Plot (b): Lilliefors Test results. . . . . p. 494

153 Spatial mode shape statistical observable results for the mass-loaded rectangular plate (spatial averaging approach). Plot (a): kurtosis values. Plot (b): Lilliefors Test results. . . . . p. 495

154 Histograms of the spatial skewness coefficients and kurtosis values for the mass-loaded rectangular plate. . . . . p. 496

155 Spatial mode shape characteristics of the mass-loaded rectangular plate: PDF of the mode shape components and spatial representation of the squared mode shape amplitudes (spatial averaging approach). Plot (a): Mode 207 - almost-Gaussian. Plot (b): Mode 230 - weakly localized. Plot (c): Mode 003 - almost-nominal. . . . . p. 499

156 Porter-Thomas distribution results for the mass-loaded rectangular plate (spatial averaging approach). Plot (a): some typical mode orders. Plots (b) and (c): modes 180 and 207 (almost-Gaussian mode shape statistics), respectively. Plot (d): mode 230 (weak localization statistics) and non-linear sigma model expression (fitted with $d_L = 0.36$ - Equation 2.53). . . . . p. 502

157 Spatial normalized mode shape correlation results for the mass-loaded rectangular plate: modes 153, 167,180, and 207 (spatial averaging approach). Plot (a): linear correlation function (P_1). Plot (b): squared function (P_2). . . . . p. 504

158 Spectral mode shape statistics results for the mass-loaded rectangular plate (spectral averaging approach). Plot (a): kurtosis results. Plot (b): Lilliefors Test results. . . . . p. 505

159 Spatially-averaged kinetic energy density results for the bare rectangular plates with $\eta = 0.010$. Plot (a): individual responses and spatially-averaged value - narrow frequency band domain (spatial averaging approach). Plot (b): individual responses and spatially-averaged value - 1/3 oct. frequency band domain (spatial averaging approach). Plot (c): spectral relative variance of spatially-averaged kinetic energy density response (spectral averaging approach). . . p. 510

160 Relative variance of the spatially-averaged kinetic energy density results for the bare rectangular plate with $\eta = 0.015$ and 0.030, respectively (spectral averaging approach). . . p. 511

161 Spatially-averaged kinetic energy density results for the mass-loaded rectangular plates with $\eta = 0.010$. Plot (a): individual responses and spatially-averaged value - narrow frequency band domain (spatial averaging approach). Plot (b): individual responses and spatially-averaged value - 1/3 oct. frequency band domain (spatial averaging approach). Plot (c): spectral relative variance of the spatially-averaged kinetic energy density response (spectral averaging approach). . . . . p. 514

162 Relative variance of the spatially-averaged kinetic energy density responses for the mass-loaded rectangular plates with $\eta = 0.015$ and 0.030, respectively (spectral averaging approach). . . . . p. 515

163 Spectral mean and relative variance values of the kinetic energy response for the bare and mass-loaded rectangular plates subjected to single-point loading with $\eta = 0.010$ (spectral averaging approach). Plot (a): kinetic energy density response of the bare rectangular plate - narrow and 1/3 oct. frequency domains. Plot (b): relative variance of the bare rectangular plate - 1/3 oct. frequency band domain. Plot (c): kinetic energy density response of the mass-loaded rectangular plate - narrow and 1/3 oct. frequency domains. Plot (d): relative variance of the mass-loaded rectangular plate - 1/3 oct. frequency band domain. . . . . p. 518

164 Relative variance of the single-point loading kinetic energy density responses for the bare and mass-loaded rectangular plates with $\eta = 0.015$ and 0.030 (spectral averaging approach). Plot (a): spectral relative variance of the single-point loading kinetic energy density response for a bare rectangular plate with $\eta = 0.015$. Plot (b): spectral relative variance of the single-point loading kinetic energy density response for a bare rectangular plate with $\eta = 0.030$. Plot (c): spectral relative variance of the single-point loading kinetic energy density result for a mass-loaded rectangular plate with $\eta = 0.015$. Plot (d): spectral relative variance of the single-point loading kinetic energy density response for a mass-loaded rectangular plate with $\eta = 0.030$. . . . p. 521

165 Natural frequency statistical observable results for the random rectangular plates (ensemble averaging approach). Plot (a): Mode 20. Plot (b): Mode 80. Plot (c): Mode 120. Plot (d): Mode 200. . . . . p. 531

166 Natural frequency statistical observable results for nominal and random rectangular plates: spectral and ensemble averaging approaches. . . . . p. 534

167 Statistical overlap factor results for an ensemble of the random rectangular plates (ensemble averaging approach). Plot (a): global natural frequency spacing, local natural frequency spacings, natural frequency standard deviations. Plot (b): Statistical overlap factor: based on global and local mean values of the natural frequency spacings. . . . . p. 536

168 Spatial mode shape statistics results for the random rectangular plates (spatial averaging approach). Plot (a): spatial kurtosis results: individual members, arithmetic and geometric mean values and analytical predictions (sinusoidal and GOE). Plot (b): spatial Lilliefors Test results: individual member values and arithmetic mean values. . . . . p. 538

169 Spectral mode shape statistics results at excitation point X_0 for the random rectangular plates (spectral averaging approach). Plot (a): spectral kurtosis: individual members, arithmetic and geometric mean values and analytical predictions (sinusoidal and GOE models). Plot (b): spectral Lilliefors Test results: individual member and arithmetic mean values. . . . . p. 540

170 Ensemble mode shape statistics results at excitation point X_0 for the random rectangular plates (ensemble averaging approach). Plot (a): ensemble kurtosis, spectral arithmetic mean value and analytical predictions (sinusoidal and GOE models). Plot (b): ensemble Lilliefors Test results. . . . . p. 541

171 PDF values of the mode shape amplitudes associated with the excitation point X_0 for the random rectangular plates: spectral and ensemble averaging approaches. . . . . p. 543

172 Mean and relative variance of the spatially-averaged kinetic energy density results for the random rectangular plates with $\eta = 0.01$ (ensemble averaging approach). Plot (a): mean values. Plot (b): relative variance values. . . . . p. 546

173 Mean and relative variance for the spatially-averaged kinetic energy density results of the random rectangular plates with $\eta = 0.015$ (ensemble averaging approach). Plot (a): mean values. Plot (b): relative variance values. . . . . p. 548

174 Mean and relative variance of the spatially-averaged kinetic energy density results for the random rectangular plates with $\eta = 0.030$ (ensemble averaging approach). Plot (a): mean values. Plot (b): relative variance values. . . . . p. 549

175 Mean and relative variance of the single-point kinetic energy density results for the random rectangular plates with $\eta = 0.01$ (ensemble averaging approach). Plot (a): mean value. Plot (b): relative variance values. . . . . p. 550

176 Mean and relative variance of the single-point kinetic energy density results for the random rectangular plates with $\eta = 0.015$ (ensemble averaging approach). Plot (a): mean values. Plot (b): relative variance values. . . . . p. 552

177 Mean and relative variance of the single-point kinetic energy density results for the random rectangular plates with $\eta = 0.030$ (ensemble averaging approach). Plot (a): mean values. Plot (b): relative variance values. . . . . p. 553

178 Natural frequency statistical observable results for the mass-loaded rectangular plates (ensemble averaging approach). Plot (a): Mode 30. Plot (b): Mode 35. Plot (c): Mode 50. Plot (d): Mode 175. Plot (e): Mode 230. Plot (f): Mode 250. . . . . p. 560

179 Natural frequency statistical observable results for mass-loaded rectangular plates: spectral and ensemble averaging approaches. . . . . p. 564

180 Statistical overlap factor results for an ensemble of the mass-loaded rectangular plates (ensemble averaging approach). Plot (a): global natural frequency spacing, local natural frequency spacings, natural frequency standard deviations. Plot (b): Statistical overlap factor: based on global and local mean values for the natural frequency spacings. . p. 565

181 Spatial mode shape statistics results for the mass-loaded rectangular plates (spatial averaging approach). Plot (a): spatial kurtosis results: individual members, arithmetic and geometric mean values and analytical predictions (sinusoidal and GOE). Plot (b): spatial Lilliefors Test results: individual member values and arithmetic mean values. . . . . p. 567

182 Spectral mode shape statistics results at excitation point X_0 for the mass-loaded rectangular plates (spectral averaging approach). Plot (a): spectral kurtosis: individual members, arithmetic and geometric mean values and analytical predictions (sinusoidal and GOE models). Plot (b): spectral Lilliefors Test results: individual member and arithmetic mean values . . . . . p. 569

183 Ensemble mode shape statistics results at excitation point X_0 for the mass-loaded rectangular plates (ensemble averaging approach). Plot (a): ensemble kurtosis, spectral arithmetic mean value and analytical predictions (sinusoidal and GOE models). Plot (b): ensemble Lilliefors Test results. . . . . p. 570
184 PDF values for the mode shape amplitudes associated with the excitation point X_0 for the mass-loaded rectangular plates: spectral and ensemble averaging approaches. . . . . p. 572
185 Mean and relative variance of the spatially-averaged kinetic energy density results for the mass-loaded rectangular plates with $\eta = 0.01$ (ensemble averaging approach). Plot (a): mean values. Plot (b): relative variance values. . . . . p. 574
186 Mean and relative variance for the spatially-averaged kinetic energy density results for the mass-loaded rectangular plates with $\eta = 0.015$ (ensemble averaging approach). Plot (a): mean values. Plot (b): relative variance values. . . . . p. 575
187 Mean and relative variance of the spatially-averaged kinetic energy density results for the mass-loaded rectangular plates with $\eta = 0.030$ (ensemble averaging approach). Plot (a): mean values. Plot (b): relative variance values. . . . . p. 576
188 Mean and relative variance of the single-point kinetic energy density results for the mass-loaded rectangular plates with $\eta = 0.01$ (ensemble averaging approach). Plot (a): mean value. Plot (b): relative variance values. . . . . p. 578
189 Mean and relative variance of the single-point kinetic energy density results for the rectangular mass-loaded plates with $\eta = 0.015$ (ensemble averaging approach). Plot (a): mean values. Plot (b): relative variance values. . . . . p. 580
190 Mean and relative variance of the single-point kinetic energy density results for the mass-loaded rectangular plates with $\eta = 0.030$ (ensemble averaging approach). Plot (a): mean values. Plot (b): relative variance values. . . . . p. 581
191 The spacing PDF predictions for the superimposed GOE and Poisson distributions, Gomes and Gerges (101). . . . . p. 619
192 Δ_3 - statistics: superimposed GOE and Poisson predictions, Gomes and Gerges (101). . . . . p. 619
193 The spacing PDFs of several 2 GOE spectra with distinct relative densities, Gomes and Gerges (101). . . . . p. 620

194 The Δ_3 - statistics results for several 2 GOE spectra with distinct relative densities, Gomes and Gerges (101). . . . . p. 621
195 Δ_3-statistics results for the 100 GOE matrices with *dim* (300 x 300). Plot (a): individual spectral mean values and ensemble mean value. Plot (b): individual spectral variance values and ensemble mean value of spectral variances. Additionally, the analytical GOE predictions are also plotted, Gomes and Gerges (101). . . . . p. 624
196 Plot (a): Ensemble variance value of Δ_3 - statistics results. Plot (b): statistical convergence analysis of the mean value of spectral variance results across the ensemble, Gomes and Gerges (101). . . . . p. 626
197 Results from the numerical methodology to estimate the ensemble mean values of Δ_3 - statistics results and corresponding spectral variance values. The experimental data from nuclei systems are also plotted, Bohigas *et al* (114). Plot (a): ensemble mean values of Δ_3- statistics results. Plot (b): ensemble mean value of the spectral variances of Δ_3 - statistics results, Gomes and Gerges (101). . . . . p. 627
198 Numerical variance results of Δ_3 - statistics values from the ensembles of GOE random matrices with different dimensions, Gomes and Gerges (101). . . . . p. 629
199 Numerical investigation of the finite dimension effects on the spatial and spectral kurtosis metrics: the expected ensemble kurtosis mean values and respective variance values from the finite GOE matrices with the following dimensions: 30, 50, 100, 300 and 500 elements are compared with available analytical predictions, using Equation (2.63). . . p. 631

LIST OF TABLES

1 The adjusted mode shape statistics factor (K) from SEA variance studies performed with artificial random systems reported in the recent SEA variance literature. The values were obtained through the fitting processes between the numerical (or measured) relative variance results and best fitted revised SEA relative variance predictions based on the GOE model. . . . . p. 85

2 Main characteristics of Gaussian ensembles: nomenclature, abbreviation, random matrix structure and Dyson's index (β), Andersen (68). . . . . p. 111

3 Analogies between the Quantum and Vibroacoustic systems, Bertelsen (90) and Schaadt (70). . . . . p. 129

4 Nominal longitudinal rod: geometric dimensions. . . . . p. 194

5 Nominal longitudinal rod: material properties - standard carbon steel. . . . . p. 194

6 Random rod descriptions - spectral averaging approach: nomenclature, random variable, statistical distribution, and randomness level. . . . . p. 199

7 Descriptions of the random mass-loaded rods - spectral averaging approach: nomenclature, random variable, statistical distribution, and randomness level. . . . . p. 199

8 Mode shapes investigated: subfigure, mode order, spatial kurtosis, and mode shape statistics. . . . . p. 234

9 Localization factor analysis for longitudinal random mass-loaded rods: several excitation frequencies and damping loss factor magnitudes (ensemble averaging approach). . . p. 341

10 Three excitation points considered in the statistical analysis of the kinetic energy density results: point nomenclature, spatial coordinates, and brief statistical description. . . . . p. 347

12 Description of the geometrical dimensions of plate systems: square, rectangular, rectangular with one arc at corner, polygonal, circular and 1/4 Sinai stadium. . . . . p. 423

13 Standard aluminum properties. . . . . p. 423

LIST OF SYMBOLS

Latin Alphabet

a, b, c, d	Flexural plate dimensions
a_0, b_0	Nominal dimensions of rectangular plates
$\mathbf{A}$	Diagonal matrix of eigenvalues λ_i of Hamiltonian H
$b(\theta)$	Fourier transform of Y_2
b_w	Band half-width of matrix
B	Bandwidth parameter defined by Equation (2.85)
c_L	Longitudinal wave speed
c_L^p	Longitudinal wave speed in a plate
c_{ij}	Covariance matrix element
c_t	Second material property constant of Equation (4.4)
$\mathbf{C}$	Damping matrix
C_1, C_2	Normalization constants of Equations (2.57) and (2.58)
$C_2(\Lambda)$	Natural frequency correlation coefficient
$\mathbf{C_m}$	Covariance matrix defined by Equation (3.17)
d_e	Eigenvector dimension
d_L	Disorder localization parameter
d_p	Perpendicular distance between two points
d_r	Diameter of longitudinal rod
dB	Decibel
D	Flexural rigidity of plate system
$\mathbf{D}_k$	Mode shape matrix of k-th mode shape across the ensemble

e_i	i-th energy level of a complex nuclei
E	Total subsystem energy
E_i	Total energy from i-th subsystem
E_{ym}	Young's modulus
f	Frequency (Hz)
f_i	i-th natural or resonance frequency of system
f_{MF}	Mirlin-Fyodorov correction factor for weak localization
F	External force vector
F	Force amplitude
$F(\theta)$	Auxiliar function defined by Equation (2.87)
$F_z(x)$	Empirical cumulative distribution function
g	Dimensionless conductivity
g_i	Relative density of superimposed spectra
h	Plate thickness
H	Hamiltonian matrix
Hz	Hertz
I	Identity matrix
I_2	Inverse Participation Ratio
I_k	k-th statistical moment of normalized squared mode shape amplitude
J	Joule
J_n	Squared generalized force of n-th mode shape
k	Wavenumber
k_f	Flexural wavenumber

K	Spatial factor of mode shape or kurtosis
K	Stiffness matrix
K_1	First material property constant of Equation (4.4)
l	Mean free path
L	Spectral length in eigenvalue or natural frequency space
L_c	Correlation length
L_r	Rod length
m	Meter
$m, m(\omega)$	Modal overlap factor
M	Mass subsystem
$\mathbf{M}$	Mass matrix
$n(f), n(\omega)$	Modal density
$n_{av}(L)$	Natural frequency degeneracy constant
n_i	Modal density of *ith* subsystem.
N	Newton
N	Random matrix size
$N(f)$	Staircase function - frequency domain
$N\left(k_f\right)$	Staircase function - flexural wavenumber domain
$N_{av}(f)$	Average component of staircase function
N_e	Number of members (size of ensemble)
$N_{fluc}(f)$	Oscillatory component of staircase function
N_i	Number of resonant modes in frequency band from i-th subsystem
N_L	Number of source or excitation points

N_R	Number of receiver or response points
$\widetilde{N}(z)$	Unfolded staircase function
$\widetilde{N}_{av}(z)$	Average component of unfolded staircase function
$\widetilde{N}_{fluc}(z)$	Oscillatory component of unfolded staircase function
$\left\langle \overline{p^2} \right\rangle$	Time-space average of squared pressure
$P(k)$	SEA Parameter P of *kth* mode shapes across the ensemble
$P(s)$	Probability Density Function of adjacent eigenvalue spacings
$P_1(kr)$	Linear spatial correlation function of the mode shape components
$P_2(kr)$	Squared spatial correlation function of the mode shape components
$P(\lvert\psi\rvert^2)$	Porter-Thomas distribution
$P_a(k)$	Normalized SEA Parameter P of *kth* mode shapes across the ensemble
$P_{I_2}(I_2)$	Probability Density Function of Inverse Participation Ratio
P_{nD}	Spatial PDF of n-dimensional mode shapes, where $n = 1, 2,$ or 3.
P_P	Perimeter of plate
P_{PT}	Porter-Thomas distribution function
$Q(k)$	SEA Parameter Q of *kth* mode shapes across the ensemble
$Q_a(k)$	Normalized SEA Parameter Q of *kth* mode shapes across the ensemble
r	Internal (or smaller) plate radius
r_T^2	Relative energy density variance
R	External (or circular) plate radius
$\mathbf{R}$	Auxiliar mode shape matrix defined by Equation (2.49)

R_2	Two-level correlation function
R_a	Surface area of flexural plate
R_f	Acoustic field correlation function
R_{HG}	Correlation function of homogeneous Gaussian Field
R_{MS}	Correlation function of Markovian Stochastic process
R_s	Narrow-band spatial correlation function
R_u	System or unit span
R_ω	Frequency band domain
s	Second
s	Spacing between adjacent unfolded natural frequencies
s_i	Statistical overlap factor of i-th natural frequency
S	Cross-section area of longitudinal rod
$\mathbf{S}$	Diagonal Matrix of singular values
S_{LT}	Test statistics parameter of Lilliefors Normality Test
t_c	Cut-off time in the Fourier unfolding process
T	Kinetic energy density
T_{60}	Structural decay or acoustical reverberation times
TL	Threshold limit value of SEA Parameters P and Q
$\mathbf{u}$	Vector of Karhunen-Loeve expansion
$\overline{\mathbf{u}}$	Mean or nominal vector of Karhunen-Loeve expansion
u_i	i-th eigenvector or wave function of Hamiltonian H
$\mathbf{u}_j^i$	k-th mode shape from i-th ensemble member
u_n	n-th wave function
U	Matrix with Hamiltonian eigenvectors

U_g	Gaussian random variable with zero mean and unit standard deviation
$\langle\overline{v^2}\rangle$	Time-space average of squared structural velocity
$\mathbf{V}$	Matrix of orthogonal input basis vectors from the SVD
V_a	Volume of acoustical system
x_f	Excitation force point
x_n	n-th energy level
x_s	Scaling parameter
(x, y)	Cartesian coordinates
X	Response vector
X_0, X_2, X_3	Excitation points
X_i	Empirical data (Lilliefors Test)
$Y(\omega)$	Mobility function
Y_2	Two-level cluster function
W_i	External input power from i-th subsystem
W_{ij}	Transmitted power flow between i-th and j-th subsystems
$\mathbf{W}$	Matrix of orthogonal output basis vectors from the SVD
z	Unfolded natural frequency
Z	SEA Parameter Z of *kth* mode shapes across the ensemble
z_i	i-th unfolded natural frequency
Z_0	Starting eigenvalue point, Equations (2.13) and (2.18)
Z_i	Normalized sample value (Lilliefors Test)

Greek Alphabet

α	Spatial factor
$\overline{\alpha}$	Averaged absorption coefficient
α_d	Fraction of degenerate spacings
α_i	i-th expansion coefficient of Equations (4.5) and (4.6)
β	Dyson's index
β_c	Geometrical constant for clamped boundary condition
β_{ff}	Geometrical constant for free-free boundary condition
β_g	Microwave cavity geometric constant
β_p	Geometrical constant for boundary condition, Equation (4.1)
β_r	Level repulsion parameter
β_s	Scaled localization length
β_{ss}	Geometrical constant for simply supported boundary condition
γ	Euler's constant
γ_S	Real constant, Figure 11
δ	Amount of uncertainty or randomness
δf	Natural frequency spacing
δ_{MS}^{GOE}	Universal limit of mode shapes
δ_{NF}^{GOE}	Universal limit of natural frequencies
Δ_3	Delta3-statistics function
$\Delta\lambda$	Interval in the eigenvalue domain
ε_p	Randomness level of rectangular plate system
η	Frequency average damping loss factor

η_i	Damping loss factor from i-th subsystem
η_{ij}	Coupling loss factor between i-th and j-th subsystems
$\theta_n(L_c)$	Normalized parameter for n-th mode order and a given L_c
λ	Eigenvalue space variable
λ_n^0	Wavelength of n-th mode shape of nominal rod
λ_i	i-th Hamiltonian eigenvalue
λ_k	k*th* eigenvalue from eigenvalue space
λ_n^{rand}	Wavelength of n-th mode shape of random rod
λ_u	Wavelength of resonance frequency
Λ	Number of natural frequency spacings
μ_i	Ensemble mean spacing between i-th and (i+1)-th natural frequencies
μ_T	Mean value of kinetic energy density
μ_X	Mean value of empirical data (Lilliefors Test)
Π_{diss}	Dissipated power of a subsystem
Π_{diss}	Input power of a subsystem
Π_{ij}	Power transmitted from the ith-subsystem to the jth-subsystem
Π_j	Power dissipated by the jth-subsystem
ρ	Mass density
ρ_0	Volumetric density of a fluid
ρ_d	Mass per unit span (length, area, or volume)
$\rho'(x)$	Mass distribution function
σ	Standard deviation
σ_T^2	Variance value of kinetic energy density

σ_X	Standard deviation value of empirical data (Lilliefors Test)
$\sigma_{\omega i}$	Standard deviation of i-th natural frequency
$\Sigma^2(L)$	Number variance function
υ	Poisson's coefficient
ϕ_i, φ_i	i-th mass normalized mode shape
Φx	Gaussian cumulative distribution function of variable x
$\|\psi\|^2$	Normalized squared mode shape amplitude
Ω	Dimensionless frequency
Ω_s	Spatial domain of subsystem
ω	Angular frequency (rad/s)
ω_i	i-th natural angular frequency (rad/s)
ω_0	Central value of frequency band

Abbreviations and Acronyms

BEM	Boundary Element Method
BGS	Bohigas-Giannoni-Schmit
BRM	Band Random Matrices
BT	Berry-Tabor
CLF	Coupling Loss Factor
DLF	Damping Loss Factor
EBK	Einstein, Brillouin and Keller methods
FEM	Finite Element Method
FFT	Fast Fourier Transform
FRF	Frequency Response Function

GOE	Gaussian Orthogonal Ensemble
GSE	Gaussian Symplectic Ensemble
GUE	Gaussian Unitary Ensemble
IFT	Inverse Fourier Transform
IPR	Inversion Participation Ratio
NNSD	Nearest Neighbor Spacing Distribution
PDF	Probability Density Function
PIM	Power Inject Method
POT	Periodical Orbit Theory
PT	Porter Thomas
RMT	Random Matrix Theory
SEA	Statistical Energy Analysis
SFEM	Stochastic Finite Element Method
SPOT	Short Periodic Orbit Theory
SVD	Singular Value Decomposition
WBKJ	Wentzel, Kramers, Brillouin and Jeffreys methods

Notation

$\langle\,\rangle_{Z_0}$	Averaging process over all possible starting point Z_0
$\delta(x)$	Dirac delta function
$\mathbf{A}^T$	Transpose of a matrix $\mathbf{A}$
$E[x]$	Expected value of variable x
$E_1(x)$	Exponential integral function of variable x
$H_n^{(1)}(x)$	Hankel function of first kinf of x

J_0	Zeroth order Bessel function
$K_1(x)$	Macdonald function of variable x
$K_{el}^1(x)$	Complete elliptic integral of first kind of variable x
$Re(x)$	Real part of variable x
$sup(x)$	Maximum value of variable x
$Var(x)$	Statistical variance value of variable x
$x!!$	Double factorial or Factorial2 of variable x
$\dot{x}$	First order time derivative of variable x
$\ddot{x}$	Second order time derivative of variable x

CONTENTS

1 INTRODUCTION . . . . . p. 59
1.1 Overview . . . . . p. 59
1.2 The Physics of High-Frequency Range . . . . . p. 64
1.3 Methods of Response Prediction of Complex Systems . . . p. 68
1.4 Statistical Energy Analysis . . . . . p. 70
1.4.1 SEA Overview . . . . . p. 70
1.4.2 SEA Equations . . . . . p. 71
1.4.3 Basic Assumptions of SEA . . . . . p. 72
1.4.4 SEA Parameters . . . . . p. 73
1.5 SEA Variance . . . . . p. 76
1.6 Universal Statistics . . . . . p. 80
1.6.1 Random Matrix Theory . . . . . p. 80
1.6.2 Establishment of GOE Statistics . . . . . p. 82
1.7 Summary and Discussion . . . . . p. 94
1.8 Scope, Aims and Outline of the Thesis . . . . . p. 102
1.8.1 Open Problems and Motivations . . . . . p. 103
1.8.2 Aims and Scope of this Thesis . . . . . p. 104
1.8.3 Outline of the Thesis . . . . . p. 105

2 LITERATURE REVIEW . . . . . p. 107
2.1 Introduction . . . . . p. 107
2.2 Random Matrix Theory . . . . . p. 107
2.2.1 Historical Context . . . . . p. 108
2.2.2 Gaussian Ensembles of Random Matrices . . . . . p. 110
2.2.3 Unfolding Process . . . . . p. 111
2.2.4 Eigenvalue Statistics . . . . . p. 117
2.2.5 Universality . . . . . p. 127
2.2.6 Analogies: Quantum and Vibroacoustic Systems . p. 128
2.2.7 Finite Wavelength Effects . . . . . p. 131
2.2.8 Effects of Periodic Orbits . . . . . p. 132
2.3 Mode Shape Statistics . . . . . p. 138
2.3.1 Eigenvector Applications . . . . . p. 139
2.3.2 Eigenvector Statistical Observables . . . . . p. 142
2.3.3 Mode Shape SEA Parameters . . . . . p. 154
2.3.4 Nonuniversal Eigenvector Statistics . . . . . p. 159
2.3.5 Structural Localization Phenomenon . . . . . p. 173

2.4 Theory of SEA Variance . . . . . p. 177
2.4.1 Energy Response Statistics . . . . . p. 177
2.4.2 Random Point Process . . . . . p. 179
2.4.3 Band-Averaged Energy Response Statistics . . . . p. 182
2.4.4 Comments on Spatial Factor Characteristics . . . . p. 184
2.4.5 Non-universal Mode Shape Statistics Deviations . p. 185
2.5 Summary and Discussions . . . . . p. 188

3 NUMERICAL ANALYSIS OF RANDOM LONGITUDINAL RODS . . . . . p. 191
3.1 Overview . . . . . p. 191
3.2 Longitudinal Rod Characteristics . . . . . p. 192
3.3 Finite Element Model: Longitudinal Rod . . . . . p. 192
3.3.1 FEM Model Development . . . . . p. 192
3.3.2 FEM Model Validation . . . . . p. 194
3.4 Spectral Averaging Approach . . . . . p. 197
3.4.1 Breaking the Geometrical Regularity . . . . . p. 198
3.4.2 Random Point Masses . . . . . p. 199
3.4.3 Spectral Natural Frequency Statistics . . . . . p. 200
3.4.4 Spatial and Spectral Mode Shape Statistics . . . . p. 217
3.4.5 Analysis of Hamiltonian Matrix Structures . . . . p. 251
3.4.6 Spectral Kinetic Energy Density Statistics . . . . . p. 256
3.4.7 Spatially-Correlated Gaussian Rods . . . . . p. 274
3.4.8 Discussions and Remarks . . . . . p. 302
3.5 Ensemble Averaging Approach . . . . . p. 308
3.5.1 Random Point Masses . . . . . p. 308
3.5.2 Breaking the Geometrical Regularity . . . . . p. 357
3.5.3 Discussion and Remarks . . . . . p. 412
3.6 Summary and Discussion . . . . . p. 417

4 NUMERICAL ANALYSIS OF RANDOM FLEXURAL PLATES . . . . . p. 421
4.1 Overview . . . . . p. 421
4.2 Descriptions of Flexural Plates . . . . . p. 421
4.2.1 Geometrical Characteristics . . . . . p. 422
4.2.2 FEM Model Development . . . . . p. 424
4.3 Spectral Averaging Approach . . . . . p. 424
4.3.1 Spectral Natural Frequency Statistics . . . . . p. 425
4.3.2 Spatial and Spectral Mode Shape Statistics . . . . p. 449

4.3.3 Kinetic Energy Density Statistics . . . . . p. 506
4.3.4 Discussion and Remarks . . . . . p. 522
4.4 Ensemble Averaging Approach . . . . . p. 526
4.4.1 Random Rectangular Plates . . . . . p. 526
4.4.2 Random Mass-Loaded Plates . . . . . p. 553
4.4.3 Discussion and Remarks . . . . . p. 582
4.5 Summary and Final Discussion . . . . . p. 586

5 CONCLUSIONS AND FURTHER WORK . . . . . p. 593
5.1 Conclusions . . . . . p. 593
5.2 Suggestions for Further Work . . . . . p. 597

Appendix A – Statistical Properties of Superimposed Spectra . . . . . p. 617
A.1 Two Independent GOE Eigenvalue Sequences . . . . . p. 617
A.2 Several Independent GOE Eigenvalue Sequences . . . . . p. 617
A.3 Two GOE Eigenvalue Sequences with Distinct Densities . p. 620

Appendix B – Finite Dimension Effects on the Eigenvalue Statistics p. 623

Appendix C – Finite Dimension Effects on the Mode Shape Statistics p. 631

1 INTRODUCTION

1.1 Overview

The vibroacoustical response of a complex built-up system is strongly dependent upon the frequency of excitation. The excitation sources are usually classified according to three major ranges: low-frequency, medium-frequency or high-frequency. At low-frequency range only the first modes of a vibroacoustic system are excited, and the dynamical response can normally be predicted with good accuracy using a well-established deterministic method of analysis (1), for example, the *Finite Element Method* (FEM), Zienkiewicz (2).

In medium to high-frequency ranges, many hundreds of modes can be excited and it becomes extremely difficult to predict the precise dynamical response of the system (3). Indeed, beyond the first modes, a large variability of the energy response is expected, meaning that a detailed and accurate deterministic model of a system with *nominal* parameters would provide inaccurate results (4, 5, 1).

High-frequency excitations lead to the establishment of wavelengths much smaller than the system dimensions (1). As a direct consequence, these higher-order modes become very sensitive to small variations introduced during the manufacturing process[1], leading to a significant random spread in the energy responses across an ensemble of *nominally identical systems*[2] (7, 3, 1).

A typical example of the practical investigation of the dynamical response variability in ensembles composed of nominally identical structures from a production line is the research carried out in the automotive industry field. Kompella and Bernhard (8, 9), through an extensive experimental analysis, showed the relevance of response variability in an ensemble composed of 99 nominally identical vehicles. The *Frequency Response Functions* (FRFs) for both transmission paths, structure-borne and air-borne, were evaluated for a high number of similar vehicles. In their work, only the uncertainties originating from the assembly processes were considered. Although the vehicles were considered nominally identical, their FRF measurements

[1] In most engineering structures, the variation of the mechanical component parameters may occur over the ensemble, in space or over time (1). It is important to emphasize that the physical parameters from an individual mechanical component may also be gradually modified with time due to wear, environmental and working conditions (6).

[2] The *nominal ensemble* is defined, hereafter, as an ensemble composed of similar vibroacoustic systems with uncertain or non-deterministic parameters which are commonly considered nominally identical in a production line.

showed a range of response variability up to 10 dB for a fixed frequency range. In Figures 1 (a) and (b), two examples of FRF measurements are shown in detail.

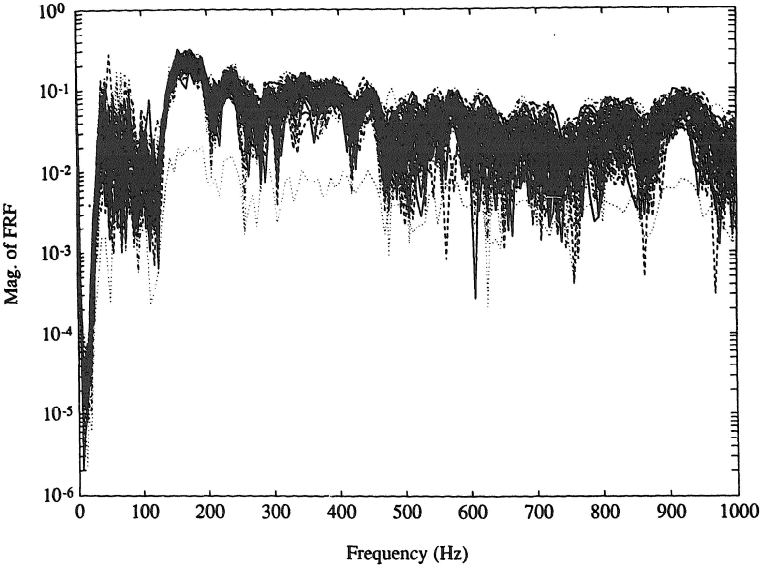

(a)

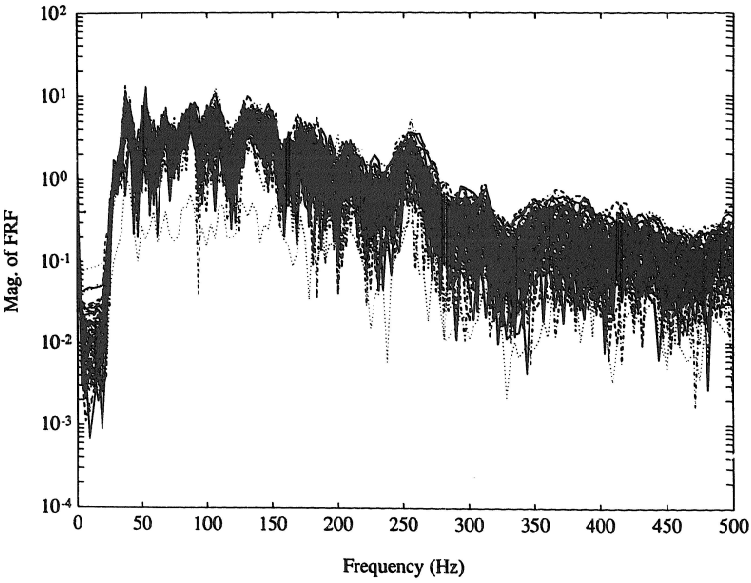

(b)

Figure 1: Magnitudes of FRFs from 99 nominally identical vehicles, Kompella and Bernhard (9).

As shown in Figures 1 (a) and (b), the largest response variability occurs mainly toward the high-frequency range. In this frequency range, the wavelength reduces and it is expected that the dynamical response becomes very sensitive to the presence of *structural uncertainty*[3] (4, 5, 1).

Another practical example of the uncertainty effects on the energy responses from an ensemble composed of nominally identical structures was shown by Frank Fahy (7). In his work, the responses from 41 aluminum cans acoustically excited were measured, Figure 2.

[3] *Structural uncertainty*, or *randomness*, is defined as mass, stiffness, or damping perturbations able to cause a variation in the dynamical response of the system, even when the system is subjected to purely deterministic excitation, Brown (1).

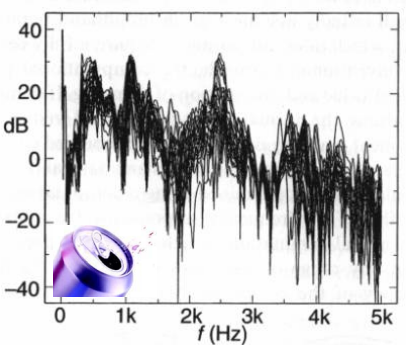

Figure 2: Magnitudes of responses from 41 nominally identical beer cans acoustically excited, Fahy (7).

As shown in Figure 2, the large variability in the can responses is strictly associated with the high intensity of uncertainty effects on the frequency range investigated (7). Additionally, these results emphasize the evident necessity for further detailed investigations on how to include the contributions from the uncertainty effects in the analytical and numerical methods for the prediction of the energy response statistics (4, 5, 6, 10).

In order to investigate systematically the main effects of structural uncertainties on the energy response statistics, several research studies have adopted the use of numerical and experimental approaches in which the ensembles of simple random structures are artificially generated (11, 12, 13, 14, 15). Such artificial ensembles are traditionally composed of perturbed systems with simple geometries such as beams, plates, and cylinders; Langley *et al* (4, 16, 3, 17, 18), Brown (1) and Cordioli *et al.* (19, 20). Additionally it is important to note that this investigative approach is a very convenient mean to reproduce and also to assess the main effects of several sources and different levels of structural uncertainty on the modal parameter statistics as well as on the statistical moments of the energy responses (10).

Johnson (21), using a simple beam structure, investigated experimentally the effects of the structural uncertainties on the dynamical responses. In his work a beam ensemble was artificially generated using twelve small point masses attached randomly onto the surface of a nominal beam along the length direction. The point masses were adopted in order to represent mass distribution uncertainties along beam structures. For each beam member of

the artificial ensemble, the point mass locations were randomly modified to produce an ensemble composed of 20 random beam structures. The transfer mobility functions were measured between two fixed points for each one of the random beam members. The FRF measurements form an *ensemble* of results, Figure 3.

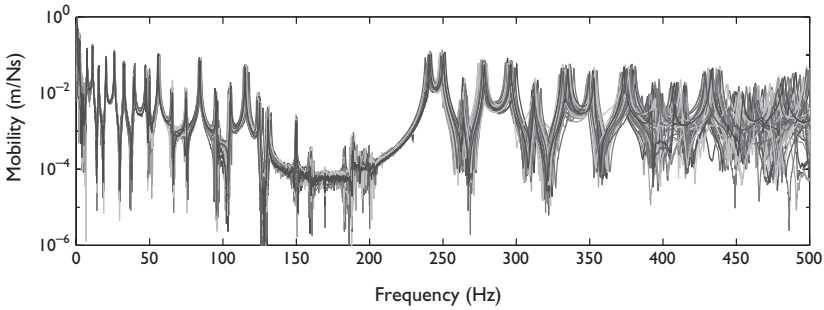

Figure 3: Experimental cross-mobility results from an artificial ensemble of beams with randomly attached point masses, Johnson (21).

As shown in Figure 3, the FRF results from the random beams suggest that the beam responses are almost insensitive to the presence of point masses in the low-frequency range, since the natural frequency locations are almost-deterministic across the ensemble. However, for the high-frequency range, the beam responses become very sensitive to the presence of the point masses and the natural frequency locations are very random in the frequency domain as well as across the ensemble.

Although the experimental results reviewed previously are associated with a particular group of random systems, an evident conclusion arises: *the dynamical response of a real engineering system is very sensitive to the presence of uncertainties in the mechanical properties and its sensitivity to uncertainty effects is amplified as the excitation frequency increases*, Langley *et al.* (4). In this regard, the accurate prediction of the statistical characteristics of the dynamical response expected across the ensemble is essential to meet the design and product certification requirements.

In what follows, the physics of uncertainties associated with random systems are discussed and their main effects on the energy response statis-

tics are highlighted. In the following sections, the performances of various prediction methods of the dynamical response applicable to the analysis of built-up systems are considered and briefly commented on. Special attention is given to *Statistical Energy Analysis* (SEA) which is an appropriate method for the energy diffusion analysis of uncertain or random systems in mid- to high-frequency ranges. The problem of predicting the SEA variance of the energy responses is discussed and the main conclusions and contributions from the current SEA variance literature are reviewed and summarized.

Next, a brief overview of the statistical models from the *Random Matrix Theory* (RMT) and their application to elastodynamic structures is provided. The main aspects associated with the statistics of each of the modal parameters (natural frequencies and corresponding mode shapes) and the application of RMT models are discussed with reference to recent results from the SEA variance and quantum physics fields published in the literature. The review is then summarized and some conclusions are initially drawn regarding the *universal* establishment of *GOE statistics*[4] for the natural frequencies and the corresponding mode shapes of real engineering systems with uncertain or non-deterministic parameters (10). Finally, the examples of the open problems identified from the current review are highlighted, and based on the gaps identified, the scope and aims of the current work are presented (10).

1.2 The Physics of High-Frequency Range

In a typical automotive or aerospace application, the equations of dynamic equilibrium can be easily generated using a commercial Finite Element software program and several degrees of freedom are necessary (4). The dynamic equilibrium equations are given by (22):

$$\mathbf{M}\ddot{X} + \mathbf{C}\dot{X} + KX = \mathbf{F}, \tag{1.1}$$

where **M**, **C** and **K** are the mass, damping and stiffness matrices, respectively, and X and **F** are the response and external force vectors, respectively.

In the engineering context, the main goal of a dynamical analysis is to evaluate the system performance and contribute to the design process as well as the product certification (4). For a complete dynamical analysis, it is necessary to solve a system of linear equations described by Equation (1.1) for several loading cases as well as for several design proposals (4). In this

[4]The statistical characteristics of GOE model will be presented and discussed in next chapter.

methodology, a large number of degrees of freedom is usually applied and the computational processing cost becomes high and prohibitive in several engineering applications (5, 6, 4, 1, 20).

As discussed by Langley *et al.* (4), a complete and efficient computational model must offer the design engineer not only information regarding the dynamical response from the perfect nominal system, but also a good estimate of the expected response variability. However, in the development of such models the following difficulties are encountered (5, 4): (*i*) *input-data regarding uncertainty statistics:* information on the system properties is extremely limited; and (*ii*) *computational cost:* even provided with a complete probabilistic description of the system parameter uncertainties, the analytical and computational task of converting this data into a response description, through motion equations, is immense and prohibitive for almost all ensembles of engineering systems.

In order to solve this engineering problem, a good understanding of the physical phenomena associated with the energy response statistics from uncertain systems is essential to provide effective methodologies to predict the statistical moments of the ensemble responses. According to Langley (4) and Mace (6) as the excitation frequency, or the uncertainty level (or randomness amount) increases, it is expected that *the ensemble response statistics will become independent of the detailed nature of the uncertainties, provided that the systems are random enough across the ensemble*. Indeed, under this particular condition, the analytical problem becomes easier due to the establishment of a physical phenomenon called *Universality* (23, 4). The main statistical aspects of the Universality concept applied to dynamical random systems were demonstrated through a numerical example performed by Langley *et al* (4) and the main conclusions will be described below.

In order to evaluate the sensitivity of response statistics to different sources and levels of uncertainties, three distinct plate ensembles were numerically generated. The uncertainty sources for each plate ensemble were: 9 random edge springs, 10 random located point masses (corresponding to 20% plate mass absent of uncertainties), and 5 randomly located point masses (corresponding to 5% plate mass absent of uncertainties). The ensembles were composed of 200 random plate members. For each plate ensemble, a point force was applied to each plate member and their energy responses were evaluated. The randomization approaches, the individual and ensemble mean energy responses are shown in Figure 4.

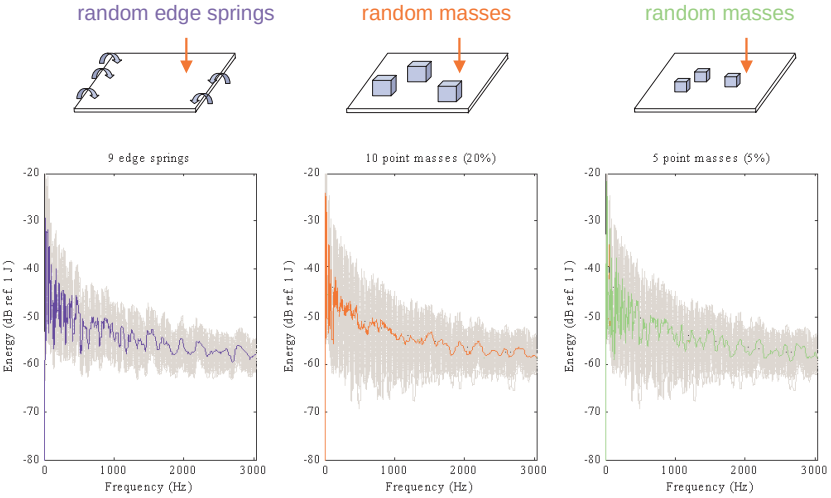

Figure 4: The energy responses from the random plates for three distinct ensemble approaches, Langley *et al* (4).

As shown in Figure 4, the ensemble mean values for the energy responses show distinct curve patterns for each of the randomization approaches in the low-frequency range. For the high-frequency range, the curve patterns of the ensemble mean values are surprisingly similar and seem to be independent of the randomization approaches adopted. In order to understand in detail the application of the Universality concept, the energy response variances were also evaluated for all random plate ensembles, Figure 5.

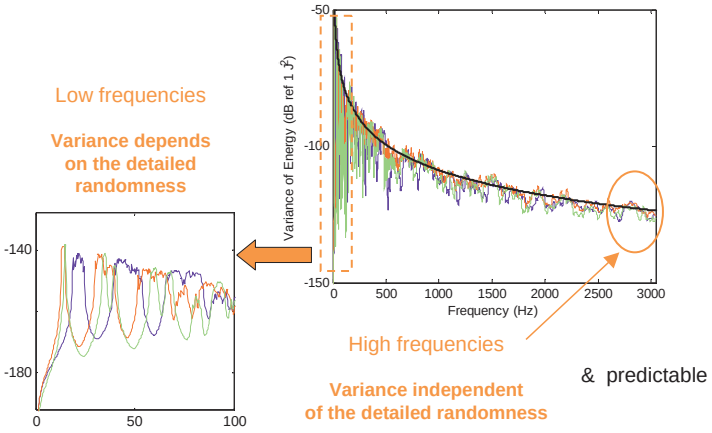

Figure 5: The energy response variances from three distinct ensemble approaches, Langley *et al* (4).

According to Figure 5, the energy response variances from the random plate ensembles are clearly dependent on the uncertainty source characteristics in the low-frequency range. However, when the excitation frequency increases, the energy response variance results for three distinct random plate ensembles become very similar and only small differences were observed between them.

In summary, these numerical results suggest that, for sufficiently random engineering systems, the ensemble mean and variance curve patterns may be independent of the detailed nature of the system randomness at high frequencies (4). Thus, it might be anticipated that *the energy response statistics at high frequencies will be exclusively dependent on the natural frequency and mode shape statistics* (4). Indeed, this physical behavior provides a fundamental hypothesis for the evaluation of the prediction methods based on the application of the Universality concept from the Random Matrix Theory (RMT), Mehta (24) and Langley (23).

1.3 Methods of Response Prediction of Complex Vibroacoustical Systems with Uncertain Parameters

Most built-up engineering systems have components with complex geometries and are composed of a large range of materials and distinct structural connections (5). In principle, the construction of a detailed deterministic model of such systems, such as the well-established FEM models, would be feasible and its application would provide the linear response to applied forces/displacements at any frequency and at any point, Fahy and Langley (5).

In the context of the Finite Element Method (FEM) (2), the vibroacoustical system is split up into a mesh of discrete finite elements, and the elastic and kinetic energies of these elements are described in terms of displacements and their time derivatives (1). Although, the application of FEM models is a well-established approach in the engineering field, due to its high performance in terms of accurately modeling a wide range of complex systems, the FEM model is traditionally limited to the low and mid-frequency range engineering applications. Indeed, there are two major factors that hinder the direct use of the deterministic approaches, such as the FEM, BEM, or Rayleigh-Ritz method, in high-frequency range applications (5).

The first factor is associated with the fact that the size of the finite elements used to represent any component must be considerably smaller than the minimum wavelength in that component at any frequency[5] (1, 5). That is, the mesh size needs to become increasingly smaller at higher frequencies in order to describe accurately the variation in the modal displacement (5). As demonstrated in several structural applications, the number of elements, or the model size, increases exponentially with an increase in the excitation frequency and with the geometric and material complexities of a model (5).

The second factor is more evident and is associated with *irreducible uncertainties* related to the high-order modes (5). Although it is, in principle, possible for current computers to extend deterministic modeling to the high-frequency range, this approach suffers from the unavoidable impossibility of possessing complete and exact knowledge of the mechanical and material properties of any real systems (4, 6, 5).

According to Mace *et al* (6, 25), the response variation due to the uncertainty effects is usually described using two major approaches. The first approach comprises the *possibilistic methods* in which the physical properties of a system are assumed to lie within certain ranges and no attempt is made to

[5] According to F. Fahy (5), the usual recommendation is at least 6 nodes per half wavelength of deformation.

describe any probabilistic distributions within these ranges *et al* (6, 25). Indeed, the main objective is to provide the expected boundaries of the response given a certain set of input values (1, 25). However, setting the limits for the ranges is also very problematical (6). The application of internal or fuzzy analyses to FE models are examples of possibilistic approaches (25). An excellent overview of the publications available on the possibilistic approach has been presented by Elishakoff (26).

On the other hand, the second approach is associated with *probabilistic methods* in which the physical properties of a system are assumed to have statistical distributions and the main aim is to predict the response statistics (6). However, quantifying the statistics of the physical properties is very problematical, especially in an industrial field (6). In practice, the engineer is likely to make estimates of input parameter uncertainties based on prior experience and perhaps based on a very limited number of measurements (6). The stochastic FE method (SFEM), perturbation methods and procedures based on Monte Carlo simulation are examples of probabilistic approaches (25).

Considering the dynamical behavior of a complex vibroacoustic system in the high-frequency range, the effects resulting from the uncertainties are substantial and thus their natural frequencies and corresponding mode shapes should be considered *random variables* (1, 27). The high-frequency dynamical behaviors of random vibroacoustical systems are usually investigated through an *energy flow approach*, which considers statistical concepts in order to take into account the uncertainty effects on the energy responses (28). The most traditional energy flow method is known as *Statistical Energy Analysis* (SEA), in which the results predict the expected mean value of the energy responses from an ensemble composed of similar systems with uncertain or non-deterministic parameters, Lyon and Dejong (29). One of the main limitations to this approach is the impossibility to extend SEA results with accuracy to higher statistical moments of the energy responses (30, 1, 7).

Recently, a nonparametric approach (31, 6) has been presented which considers the uncertainty effect directly in the eigensolutions of the system in order to predict the energy response statistics of non-deterministic systems in the high-frequency range, Langley and Brown (18, 3). As stated previously, the uncertainties of the physical parameters of the system will lead to the establishment of uncertainty in the natural frequencies and corresponding mode shapes (1, 27). In most practical engineering structures is expected that the level of uncertainty is sufficiently large so that the detailed statistics of the physical parameters of the system do not need to be considered to predict high-frequency energy response statistics, Langley *et al* (4, 23). For these

random systems, the natural frequencies can therefore be considered as *random variables* on the frequency axis so that the well-established statistical models can be adopted to model the modal parameter statistics (1, 4, 23, 27). In this regard, the analytical formulations can be conveniently determined to predict the expected ensemble response variance associated with SEA results in the mid and high-frequency ranges, regardless of the detailed nature of the uncertainties of the physical parameters of the system (1, 4, 23, 27). In next section, the main concepts and basic hypothesis of the SEA method are briefly reviewed.

1.4 Statistical Energy Analysis

1.4.1 SEA Overview

Several academic texts can be recommended for an introduction to the basic concepts of Statistical Energy Analysis (SEA), for example: Lyon and Dejong (29), Fahy (32), Woodhouse (33) and Gerges (34). In this methodology, an energy diffusion analysis associated with low computational effort may be performed for several classes of complex built-up systems, applying only previously known global design characteristics (34, 28).

The main differences between deterministic and energy flow methods (or *statistical* methods) in terms of their conceptualizations and application fields are broadly shown in Figure 6, Gomes (28). In deterministic methods, such as Finite and Boundary Element Methods, the system of interest is divided into the finite or semi-infinite elements. The deterministic input parameters are discrete forces and displacements and their output results are sound pressures and local displacements of specific points of the system (the nodes), Figure 6 (a).

In contrast, in the statistical methods, such as SEA, the system is split up into subsystems and the input parameters are described by time-averaged steady-state input powers and their results are the expected energy mean value across the ensemble, Lyon and Dejong (29). The SEA results take into account the spatial characteristics of high-order modes which are very sensitive to parametric variations from the manufacturing process and assembly conditions, Figure 6(b).

It is important to emphasize that the deterministic and statistical prediction methods are complementary analysis tools in which FEM and BEM are the most appropriate methods for dynamical analysis in the low-frequency range and SEA is a methodology most convenient for energy diffusion analy-

sis in the mid and high-frequency ranges, Gomes (28).

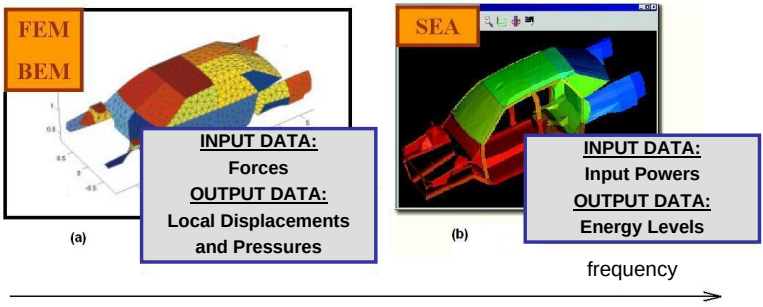

Figure 6: Examples of numerical simulations in the automobile field: comparison between deterministic and statistical approaches. Sub-figure (a): FEM and BEM variables. Sub-figure (b): SEA variables, Gomes (28).

1.4.2 SEA Equations

In the SEA context, the analyzed system is divided into basic units which are called *subsystems*. According to Lyon and Dejong (29), the subsystems may correspond to different regions of the structure, or different mode (or wave) types within a single region, for example: longitudinal vibration beam modes, acoustical cavity modes, bending (or *flexural*) plate modes, among others. In SEA modeling, each subsystem represents a local mechanism of energy storage or the expected mean modal energy from a wave type associated with a particular component of a complex built-up system (34, 28).

The basic SEA equations have been presented by several researches using distinct approaches, (35) (29). Traditionally, the SEA equations are given as following:

$$W_i = \omega\eta_i E_i + \sum_{j\neq i}\omega\eta_{ij}N_i\left[\frac{E_i}{N_i} - \frac{E_j}{N_j}\right] \; i = 1, 2, 3, ..., k; \tag{1.2}$$

where k is the number of subsystems, W_i is the external input power of the i^{th} subsystem, E_i is the total energy of the i^{th} subsystem, η_i is the damping loss factor of the i^{th} subsystem, η_{ij} is the coupling loss factor between the i^{th} and j^{th} subsystems, N_i is the number of resonant modes in the analyzed frequency

band of the i^{th} subsystem. All terms from Equation (1.2) are averaged over time, over the ensemble of the system considered, and spatially, over the relevant subsystems, over the frequency band of interest, wherever these distinct types of averaging processes are appropriate, (1).

The first term on the right side of Equation (1.2) represents the internal power dissipated by mechanical loss in a particular subsystem and the second term represents the power transmitted to other subsystems. The key to the SEA method is the hypothesis of local dynamical behavior. In other words, the power flow between two subsystems is proportional to the difference between their modal energies, regardless of the energy distributions in other subsystems. The expression of the transmitted power flow is given as follows:

$$W_{ij} = \omega \eta_{ij} N_i \left[\frac{E_i}{N_i} - \frac{E_j}{N_j} \right], \tag{1.3}$$

where W_{ij} is transmitted power flow between subsystem i and subsystem j.

1.4.3 Basic Assumptions of SEA

In the derivation of the SEA equations certain simplified assumptions are made, which may limit the application of the SEA model. The basic assumptions of the SEA theory are the following (29, 28):

- The subsystems are weakly coupled and the coupling between the subsystems is linear and conservative (non-dissipative).
- Each mode is considered to store energy and the modal energy equipartition is considered valid for a set of resonant modes contained within a particular frequency range.
- For all subsystems, the absence of coupling or interation between modes inside or outside the frequency range of interest is considered (*i.e.*, modal incoherence). A practical analogy may be established with piano keys. That is, each key is understood to be a resonant mode and its behavior is independent of the others (28).
- For practical convenience, the damping loss factor is assumed to be constant for all modes belonging to the frequency band of interest (resonant modes) for each subsystem. This practical hypothesis is very convenient and simplifies the energy diffusion analysis.

- Each mode corresponding to a natural frequency (f_i) is considered to be a random variable and has uniform probability to lie inside ith frequency band. This hypothesis is directly associated with the fact that subsystems considered nominally identical have randomly distributed parameters, mainly in the high-frequency range.

- The dissipated power flow is mainly provided by resonant modes associated with the frequency band of interest. The external loadings are adequately considered random forces with uncorrelated phases or broad-band pressure fields.

- The reciprocity relationship among subsystems is considered valid.

1.4.4 SEA Parameters

In this section, the main SEA parameters are briefly reviewed. The best-known procedures for the determination of SEA parameters are also presented and discussed (28). Further information on the analytical evaluation and experimental obtaining of SEA parameters are available in: Lyon and Dejong (29); Brown (1) and Cordioli (20).

Subsystem Energy

The subsystem energy is defined in terms of the spatial squared velocity or pressure integrated in the frequency band, Lyon and Dejong (29). For structural subsystems, the total subsystem energy is given by (29):

$$E = M\left\langle \overline{v^2} \right\rangle, \tag{1.4}$$

where M is the mass subsystem and v is the structural velocity.

For acoustical subsystems, the total subsystem energy is given by (29):

$$E = \frac{V_a}{\rho_0 c_0^2}\left\langle \overline{p^2} \right\rangle, \tag{1.5}$$

where V_a is the volume of the acoustical subsystem, $\left\langle \overline{p^2} \right\rangle$ is the time-space average of squared pressure, ρ_0 is the volumetric density of fluid, and c_0 is the sound velocity in a fluid.

Damping Loss Factor

The input power to a subsystem is dissipated through several loss mechanisms: acoustical radiation, structural damping, weld or screw junctions, etc. Generally, analytical expressions are not available to determine the damping loss factor from the structural components and acoustical cavities.

The *Damping Loss Factor* (DLF), η, can be evaluated through experimental techniques: half-power band, structural decay (or acoustical reverberation time) (T_{60}) or *Power Inject Method* (PIM), Fahy *et al* (36) and De Langhe (37). The damping loss factor amplitude can be easily related to other well-known parameters: critical damping ratio (ζ), reverberation time (T_{60}) and averaged absorption coefficient ($\overline{\alpha}$) (29, 30, 5).

Modal Density

The modal density, $n(f)$, is defined as the number of resonant modes that lie within the frequency band limits divided by frequency band width, Lyon and Dejong (29).

For subsystems with simple geometries, for example: beams, plates and rectangular acoustic cavities, the analytical formulations are available, Lyon and Dejong (29), Cremer *et al* (38), and Gomes (28). However, for systems with complex geometries, the modal density can be adequately estimated through experimental or numerical techniques. For structural components, the Point Mobility Method is traditionally applied; Clarkson (39, 40), Brown and Norton (41), and Ranky and Clarkson (42).

Modal Overlap Factor

The modal overlap factor, m, is defined as the ratio between the half-power band width, $f\eta$, and the mean natural frequency spacing, δf , that is (29):

$$m = \frac{\langle f\eta \rangle}{\langle \delta f \rangle}, \tag{1.6}$$

where angular brackets $\langle\ \rangle$ represent the average value for the frequency band. In Figure 7, a graphical representation illustrates the modal overlap definition, Gomes (28).

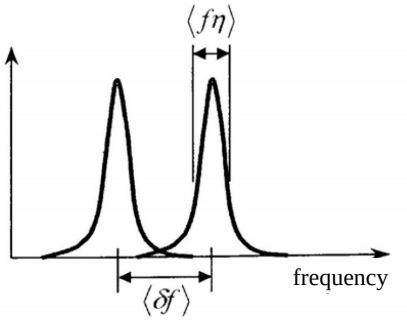

Figure 7: Parameters used in the modal overlap factor definition: half-power band and mean natural frequency spacing, both frequency band average values, Gomes (28).

The mean natural frequency spacing is directly related to the modal density parameter by the following relationship (29):

$$\langle \delta f \rangle = \frac{1}{n(f)}. \tag{1.7}$$

Substituting Equation (1.7) into Equation (1.6), the modal overlap factor is given by:

$$m(f) = f\eta n(f), \tag{1.8}$$

or it can also be expressed in terms of angular frequency, ω, by:

$$m(\omega) = \omega\eta n(\omega). \tag{1.9}$$

According to Rodrigues (43), it is expected that the modal superposition occurs under the following conditions:

$$m > 1 \Rightarrow f\eta > \frac{1}{n(f)} \Rightarrow f\eta > \delta f \Rightarrow f\eta n(f) > 1. \tag{1.10}$$

In the SEA context, the modal overlap factor is a relevant parameter in the description of the expected response variability from an ensemble composed of similar systems as well as in the analysis of the validity of SEA assumptions, Lyon and Dejong (29) and Gomes (28).

Coupling Loss Factor

The *Coupling Loss Factor* (CLF) is an exclusive SEA parameter. Generally, the calculation of the CLF parameter can be associated with other relevant physical parameters (29, 28). In the case of vibroacoustical structures, the CLF associated with flexural panel - acoustic cavity junctions is directly associated with *frequency band-averaged acoustic radiation efficiency*, Gomes (28).

For structural junctions, there are difficulties associated with the evaluation of CLF parameters. Indeed, the coupling between two structural subsystems is dependent on several parameters, such as the spatial extension of the structural components, the geometry and the nature of the junctions (28). Traditionally, the evaluation of CLF associated with structural junctions is based on the *coefficient of transmitted energy*, Cremer and Heckel (38). Several studies have been performed in order to evaluate analytically the CLFs for particular structural junctions, for example: Langley and Heron (44), Craik and Smith (45), and Bosmans and Vermeir (46), Meeds and Vermeir (47) and others.

1.5 SEA Variance

Over several years, a great amount of effort has been dedicated to extending the SEA model capacity to predict the higher statistical moments of energy responses from an ensemble composed of similar systems with non-deterministic parameters (48, 49, 50, 18, 30, 51, 5). Broadly, these research works on SEA variance may be divided into two major approaches, Brown (1) and Cordioli (20). The first approach comprises the *numerical investigation* activities, where probabilistic models are adopted for the physical parameters of the system, whereby the energy response from each member of the ensemble is calculated and then the response statistics are subsequently evaluated across the ensemble (1, 20). On the other hand, the second approach is based on the *random point processes*, where probabilistic models are adopted for the dynamical properties of the ensemble, that is, statistical models are assumed for natural frequency and mode shape statistics (1, 20). In what follows, some literature examples and basic concepts from each one of these SEA variance approaches are briefly presented and discussed. Excellent overviews of the available publications on the existing approaches to the dynamic analysis of uncertain structures have been presented by Brown (1) and Cordioli (20).

In the SEA context, several studies with dynamical systems with non-

deterministic parameters and properties have been adopting the *numerical approach* in order to investigate the relationship between the modal overlap factor value and the energy response statistics across the ensemble (11, 12, 14).

Fahy and Mohammed (13) investigated numerically several structural systems comprised of coupled beams and plates. In order to generate the ensembles of the systems, the Monte Carlo Method was used. The effects of small perturbations in the subsystem geometries on the determination of the coupling loss factors as well as on the frequency-averaged transmitted power flows were investigated. The results suggested that the transmitted power flow and coupling loss factor variance values are strictly dependent on the modal overlap factor values and decreased with an increase in the latter.

Manohar and Keane (15) investigated the performance of SEA predictions for a system of two multimodal, random, one-dimensional subsystems coupled through a spring and subjected to single frequency forcing. The variability of the dissipated power spectrum was investigated numerically through the Monte Carlo Method. The energy flow calculations were based on an exact formulation which uses the Green functions from the uncoupled subsystems, which are expressed as summations over the uncoupled modes. The effects on the energy response resulting from different damping models, loading natures and probabilistic models for the structural parameters statistics were investigated in detail. The results suggested that the damping model of a structure may be related to the statistical convergence of the frequency mean value, and the convergence speed is directly associated with the modal overlap factor value. The analysis of the Probability Density Function (PDF) of the natural frequencies shows that there is a high superposition of PFDs as the excitation frequency or system randomness level increases. Thus, an increase in the PDF superpositions may be associated with an increase in resonant modes that contribute to the response and the establishment of a smooth response along the excitation frequency range. In this regard, a new parameter was proposed in order to quantify the randomness level of the system and the minimum cut-off frequency beyond which the response statistics are no longer dominated by individual modes. This new parameter was denominated the *statistical overlap factor*, for the i*th* natural frequency, and its definition is given by:

$$s_i = \frac{2\sigma_{\omega_i}}{\mu_i} \tag{1.11}$$

where σ_{ω_i} is the standard deviation associated with the i*th* natural frequency

and μ_i is the ensemble mean spacing between the i*th* and (i+1)*th* natural frequencies. Manohar and Keane also showed that the statistical overlap factor may be related to a cut-off frequency beyond which the oscillations on statistical moments of the energy responses becomes smoothed.

In the second approach, *random point process*, probabilistic models are adopted in order to describe the statistics of the system modal parameters, that is, statistical hypothesis are considered for natural frequencies and their corresponding mode shapes (1, 20). Historically, the initial studies on the response statistics from a single subsystem were associated with *acoustic rooms*[6], (52, 53, 54).

One of pioneering work was carried out by Lyon (48), where the natural frequencies of a single system were described by the *Poisson Point Process* (55) and analytical predictions were proposed for the energy response variance from single geometry systems, such as a rectangular plate and box-shaped acoustical cavity. Additionally, the mode shapes were considered as a product of the sinusoidal functions. For the case of a subsystem subjected to point-loading, the results demonstrated that the statistical characteristics of mode shapes exert a substantial influence on the energy response variance prediction through a parameter called *Spatial Factor of Mode Shapes*[7] (K). Additionally, the effect of application of the non-Poisson distribution for natural frequency spacings was evaluated using an empirical distribution formula. Lyon shows that when the empirical distribution formula is considered, the energy response variance is reduced in comparison to that which is based on the Poisson distribution. However, an analytical prediction using the empirical distribution formula was not proposed at that time.

Davy (53, 54) extended Lyon's formulations (48), the analytical predictions based on Poisson and non-Poisson models were derived for several source and receiver points. Considering the ensemble-frequency ergodicity considered valid for the averaging process, the spectral statistics of the experimental measurements were compared with the analytical predictions. The analytical predictions based on the non-Poisson empirical distribution provided a better performance than the previous formulation based on the Poisson model. An experimental investigation of the spatial factor of mode shapes was carried out in detail. The results showed that the hypothesis of sinusoidal mode shapes provided an overestimated prediction in comparison with the experimental measurements. In this regard, it was suggested that the ac-

[6]For acoustic room systems, there are several acoustic modes in the audible frequency range and thus the use of determinist models becomes prohibitive in several applications (1).

[7]This SEA parameter will be introduced and discussed in the following chapters (48, 18, 35).

curate determination of this factor is essential to obtaining good analytical predictions for cases of single point excitation.

In general, the natural frequency statistics adopted by Lyon (48) and Davy (53) are considered invalid for most of engineering systems (35, 4, 23). Several studies, mainly in the physics field, have established that natural frequency statistics from the random dynamical systems may be correctly described by eigenvalue statistics from the *Gaussian Orthogonal Ensemble* (GOE) of *Random Matrix Theory* (RMT)[8], (24). However, the GOE statistics are not expected for systems with several symmetries, such as a simply supported perfect rectangular plate or a box-shaped acoustic space (35, 23). For this class of systems, the Poisson statistical hypothesis initially proposed by Lyon (48) and also supported by Davy (53) is correct, but the presence of small perturbations in the system parameters may lead to changes in the system symmetries and the establishment of GOE statistics is expected for the high-frequency range.

Langley and Brown (18) considered the GOE model for modal parameter statistics and proposed analytical formulations for the energy response variance from an ensemble composed of similar subsystems. In their work, the original and complete formulation of the two-level cluster function[9] was used for modeling the *local* correlations of the natural frequencies. Numerical simulations and experimental measurements with flexural plates perturbed with small point masses were performed for single point and rain-on-the-roof excitations. For rain-on-the-roof excitation, the analytical prediction conformed very well with the energy results. On the other hand, for the point-loading case, the GOE prediction over-predicted the energy variance results. The analytical formulation was fitted with numerical results, considering the mode shape statistics factor as an independent variable. The best-fitted value of K was lower than the GOE value proposed by RMT, that is, $K < 3$.

According to Lobkis *et al* (50), this finding may be associated with the presence of complex mode shapes. However, the proportional damping approach was adopted in Langley's formulation which provides fully real mode shape components, thus discarding Lobkis' hypothesis (18). Langley and Brown (18) conclude that further investigations are necessary to evaluate the most adequate value for the mode shape spatial factor.

Although the studies described above are limited to the evaluation of energy response variance from a single subsystem, several attempts have been

[8]The RMT literature related to GOE eigenvalue and eigenvector statistics is very well-established in the physics and mathematics fields (24, 56, 57, 58).

[9]The definition of *two-level cluster function* will be introduced in next chapter.

made to extend the SEA variance prediction to complex engineering systems composed of several connected or coupled subsystems, (16, 35, 4), as well as to FEM-SEA hybrid systems, (59, 60). Further details concerning SEA variance theory are presented in Chapter 4.

1.6 Universal Statistics

1.6.1 Random Matrix Theory

As mentioned in the previous section, the spacing distribution of eigenvalues (or natural frequencies) and their spectral correlations are essential key points during the development of analytical methods aimed at predicting the variance in the energy response of vibroacoustical systems (1, 51). In this section, the main concepts of the *Random Matrix Theory* (RMT) are briefly reviewed with the focus being on its application to random vibroacoustical systems. The RMT analytical results for the eigenvalue statistics are usually adopted in derivations of analytical formulations to predict the variance of the energy responses, (18, 48).

Random Matrix Theory (RMT) arose in the early 1960's and its main goal was to give mathematical support to the statistical analysis of spectra of the *energy levels*[10] of complex nuclei, Wigner (61) (62). In nuclear systems, the energy levels are evaluated through a finite Hermitian matrix operator call a *Hamiltonian* (H), Guhr *et al.* (57, 63). In general, the eigenproblem associated with a Hamiltonian matrix H is described as in (23):

$$Hu_i = \lambda_i u_i, H = U\Lambda U^T, UU^T = I, \tag{1.12}$$

where λ_i and u_i are the i^{th}eigenvalue and eigenvector of the Hamiltonian H, respectively. The matrix U has eigenvectors in its columns and the matrix Λ is diagonal and contains the eigenvalues in diagonal elements.

In a series of studies, Wigner (61, 62) showed that the statistical properties of energy levels from nuclear systems with complex nuclei can be adequately represented by the statistics of eigenvalues from random matrices with large dimensions.

Recently, several studies have obtained promising results for the application of RMT concepts in the analysis of natural frequency statistics from systems with several physical natures (64, 65, 66, 20) . Indeed, a surprising conclusion arises from the numerical and experimental analysis of random

[10] In nuclear systems, a graph of the resonance levels shows several peaks which corresponding to *energy levels*, Mehta (24).

systems: in most of them the natural frequency statistics are described by statistics from the *Gaussian Orthogonal Ensemble* (GOE) of Random Matrix Theory (RMT) (23, 6, 20).

One of the pioneering studies on the application of RMT concepts in vibroacoustical systems was carried out by Weaver (64). In his work, the natural frequencies of aluminum blocks were measured and their statistics shown excellent agreement with analytical RMT predictions. Additionally, Langley and collaborators (4, 17, 51, 16, 18, 3, 35, 23) and Cordioli (20) have shown that the RMT models can also be applied to describe the natural frequency statistics of random dynamical systems.

It is also important to emphasize that there is, as yet, no explicit proof as to why the RMT concepts are so widely applicable to random systems from many different areas (67, 23). The matrices arising from the mathematical modeling of any physical system differ considerably from the RMT random matrices (23). Some authors postulate that this good agreement is supported by the establishment of the *Universality* concept (4, 6, 23). Therefore, the conditions necessary for the *universal* establishment of GOE statistics for each modal parameter have been investigated by several researchers; Bohigas *et al* (67), Langley (23), Cordioli (20) and others.

In the RMT context, analytical expressions are proposed to describe eigenvalue statistics from the universal classes of large random matrices which are called as *Gaussian Ensembles*, Andersen (68). According to Bohigas *et al* (67), the eigenvalue statistics from a Hamiltonian matrix associated with a random *chaotic* system[11] are expected to correspond to those of the eigenvalues from the GOE[12] matrices.

In GOE statistics, the universal statistics of the eigenvalues from the large symmetric random matrices present *spectral rigidity* and *level repulsion* characteristics and thus their spectral statistics obey the *Wigner surmise* which states that the PDF of adjacent eigenvalue spacings is described by a Rayleigh PDF, Weaver (64, 1). The *level repulsion* characteristic is associated with the establishment of a low probability of small spacings between the adjacent levels (or natural frequencies) and the *spectral rigidity* is associated with the establishment of a perfect uniform spacing distribution between the adjacent natural frequencies along the spectrum, that is, there are no small or large

[11] In the classic context, *chaotic systems* are systems whose ray trajectories are unstable with respect to the initial conditions, that is, the distance between two particles inside a billiard scatters in an exponential way over time, covering the entire surface of the system due to scattering at the boundaries, Bohigas *et al* (67).

[12] The statistical characteristics of a GOE model associated with natural frequency and the corresponding mode shape statistics are presented in detail in Chapter 2.

level spacings (64, 1).

Considering the complete establishment of *universal* statistics, the GOE eigenvectors are expected to be *statistically independent*, and thus their distribution of eigenvector (or eigenfunction) components is assumed to be *Gaussian*, (69, 70, 71). Additionally, the components of GOE eigenvectors (or mode shapes) present normal distribution and therefore the mode shape statistics factor value (K) is expected to be equal to 3 for perfect GOE mode shapes, $K^{GOE} = 3$ (1, 18).

Traditionally, the hypothesis of the universal establishment of GOE statistics has been extended to the corresponding mode shapes in the derivation of analytical methods to predict the response variance of random vibroacoustical systems, Langley *et al* (16, 3, 18, 4). However, relevant numerical and experimental results have suggested non-trivial deviations of mode shape statistics from the GOE eigenvector statistics (35, 49, 3, 17, 18, 4).

Recently, considerable effort has been directed toward the Quantum Physics field in order to quantify and classify the deviations of the mode shape statistics from the GOE eigenvector statistics, Kudrolli and Pradhan (71, 72, 73, 74). On the other hand, a reduced number of similar studies has been performed for random vibroacoustical systems (10). In this regard, further investigations are necessary to characterize the non-universal statistics of mode shapes of random engineering systems, Gomes (10).

1.6.2 Establishment of GOE Statistics

Considering the ensemble response variability in the SEA variance context, an excellent performance of the revised SEA relative variance predictions[13] is confirmed provided that the system modal parameters are considered to be sufficiently random across the ensemble, Langley *et al.* (18, 3, 17, 4). Under this particular condition, it is expected that the modal parameter statistics across the ensemble have *universal* characteristics and are adequately described by the statistics from a Gaussian Orthogonal Ensemble (GOE) of Random Matrix Theory (RMT), (23, 4, 6, 1).

Although the hypothesis that modal parameter statistics of random engineering structures have GOE statistics across the ensemble is commonly adopted in the SEA variance context (18, 49, 75, 50), several numerical and experimental results from the artificially generated random systems investiga-

[13]The *revised SEA relative variance predictions* are based on the hypothesis that complete establishment of GOE statistics occurs for both system modal parameters, natural frequencies and corresponding mode shapes, Langley and Brown (18, 3).

ted recently in the SEA literature show strong evidence that while the natural frequency statistics are accurately described by the GOE model, the corresponding mode shape statistics do not completely conform to the GOE model and present *almost-Gaussian* characteristics (35, 49, 3, 17, 16, 18, 4, 10). Thus, a partial establishment of the GOE model occurs for the mode shape statistics and the revised SEA relative variance predictions based on complete GOE statistics over predict the ensemble relative variance results for such artificial random systems (18, 1, 35, 76, 10).

In Figure 8, examples of the performance of the revised SEA relative variance prediction are shown for random systems subjected to a single point-loading[14]. These examples clearly indicate that the revised SEA relative variance prediction based on the complete GOE statistics model over predicts the ensemble relative variance results (18, 3). However, an excellent performance of the revised SEA normalized variance prediction is obtained when the mode shape statistics factor values are adequately adjusted. Indeed, the adjusted value of the mode shape statistics factor provides an excellent agreement between the numerical (or experimental) results and revised SEA variance predictions, (18, 3).

In Table 1, examples of adjusted mode shape statistics factor values are shown for the random artificial systems investigated previously in the current SEA variance literature (35, 49, 3, 18, 17, 16, 18, 20, 4). The adjusted mode shape statistics factor values were obtained through the fitting processes between the numerical (or measured) relative variance results and best fitted revised SEA variance predictions based on the GOE model.

[14]In cases of a single point-loading, the contributions of the mode shape statistics to the energy response statistics are more substantial than in the case of other types of excitation, (18, 48).

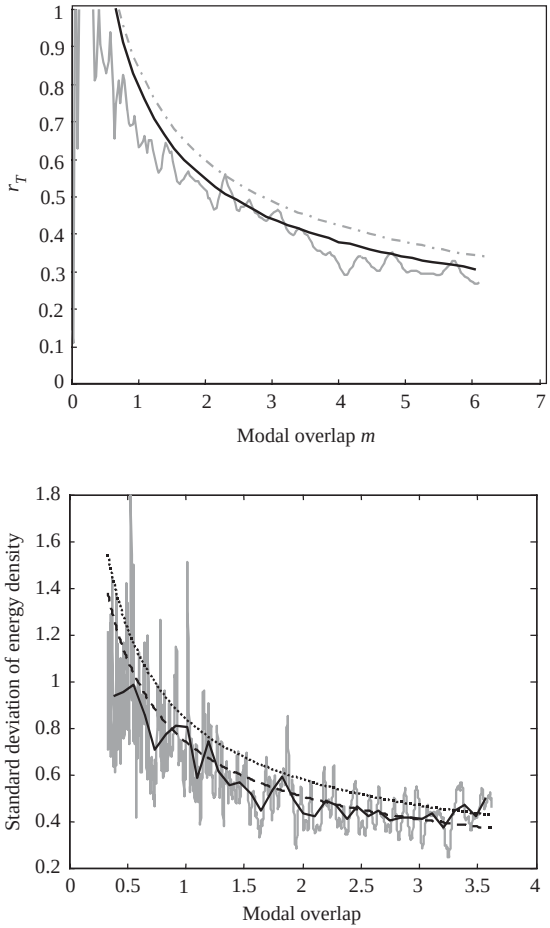

Figure 8: Examples of performance of the revised SEA relative variance predictions for the case of a single punctual excitation. Upper Plot: The relative standard deviation of energy density compared to analytical predictions: numerical results (gray solid line); GOE theoretical prediction with $K = 3$ (gray dashed-dotted line); modified GOE prediction with $K = 2.74$ (black solid line). Lower Plot: Relative standard deviation of energy density for 32 member ensemble: experimental results (gray solid line); band average of experimental results (black solid line); GOE theoretical prediction with $K = 3$ (black dotted line); and GOE theoretical prediction with $K = 2.5$ (black dashed line), Langley and Brown (18).

Table 1: The adjusted mode shape statistics factor (K) from SEA variance studies performed with artificial random systems reported in the recent SEA variance literature. The values were obtained through the fitting processes between the numerical (or measured) relative variance results and best fitted revised SEA relative variance predictions based on the GOE model.

System/Approach	System Description	Literature Reference	Modified K
Single/Numerical	Mass-loaded plates	Langley and Cotoni (35)	2.87
Single/Numerical	Reverberation room	Weaver (49)	2.60
Single/Numerical	Mass-loaded plates	Langley and Brown (3)	2.75
Single/Numerical	Mass-loaded plates	Langley and Brown (18)	2.74
Single/Numerical	Mass-loaded plates	Cordioli (20)	2.50
Built-up/Numerical	Line-connected plates	Cotoni and Langley (17)	2.70
Built-up/Numerical	Point-connected plates	Langley and Cotoni (16)	2.75
Single/Experimental	Mass-loaded plates	Langley and Brown (18)	2.50
Built-up/Experimental	Cylinder-plate structures	Cotoni and Langley (17)	2.70
Built-up/Experimental	Cylinder-plate structures	Langley and Shorter (4)	2.75

As shown in Table 1, the adjusted (or modified) mode shape statistics factor values obtained through a fitting process are obviously smaller than the expected GOE value, that is, $K < 3$ for all random systems investigated. Additionally, the adjusted mode shape statistics factor values are very distinct for each random system investigated and also strongly suggest the *incomplete* establishment of GOE statistics for the mode shapes (76, 10).

It is also important to emphasize that for the artificial random systems

investigated in Table 1, although their mode shape statistics do not perfectly conform to GOE model, the revised SEA relative variance predictions using the best fitted mode shape statistics factor conform very well with the numerical (or experimental) relative variance results. Indeed, the uncertainty levels associated with these artificial random systems seem to be only able to provide the *universal* establishment of the GOE characteristics for the natural frequency statistics, while for the corresponding mode shapes some residual non-universal characteristics are clearly observed due to the contributions associated with system-dependent effects (76, 10).

In the elastodynamics field, Schaadt (70) carried out an experimental investigation of flexural wave physics from a disordered system in order to assess the *universal* establishment of GOE statistics for modal parameters as the frequency increases. In his work, the spectral fluctuation statistics (*i.e.*, natural frequency statistics) were assessed for a thin disordered fused quartz plate in Bunimovich shape. In order to introduce a certain degree of disorder (uncertainties) in the analyzed system, small holes were drilled on the surface of the plate. The spectral statistics of natural frequencies were determined in five different frequency ranges in order to assess the distinct strengths of the effects of disorder on the natural frequency statistics. The natural frequency statistics results suggested a gradual transition pattern from almost Poisson statistics to GOE statistics as the frequency increases[15].

As known in RMT context, GOE model can be established for eigenvalue statistics through the introduction of the off-diagonal coupling elements in the Hamiltonian matrix structure (63, 77). The presence of the off-diagonal elements couples the unperturbed eigenvalues and provides the establishment of *universal* level repulsion and spectral rigidity characteristics on the eigenvalue spectrum (77, 78).

Schaadt (70) also investigated experimentally the effect of the introduction of a certain amount of disorder (uncertainties) on the mode shape statistics. However, due to experimental difficulties, it was not possible to measure the corresponding mode shapes for the same Bunimovich plate in which the natural frequency statistics was previously evaluated (70). In this second stage of his analysis, a reduced model of the aluminum Bunimovich plate was used to understand the physical phenomena resulting from the pre-

[15] Similar results were also presented in Cordioli's work (20). Using metric functions of RMT, the natural frequency statistics of flexural plates with structural uncertainties were investigated in detail. The good agreement with GOE predictions for short and long-range fluctuation statistics was obtained as the frequency increases and suggested the occurrence of Univervality phenomenon toward the high-frequency range.

sence of disorder in the mode shape statistics. Its important to note that no attention was given to compare the convergence speed characteristics for the universal establishment of GOE statistics for each of the modal parameters, (10). In Figure 9, the spatial characteristics of the disordered mode shapes investigated are presented for distinct natural frequencies.

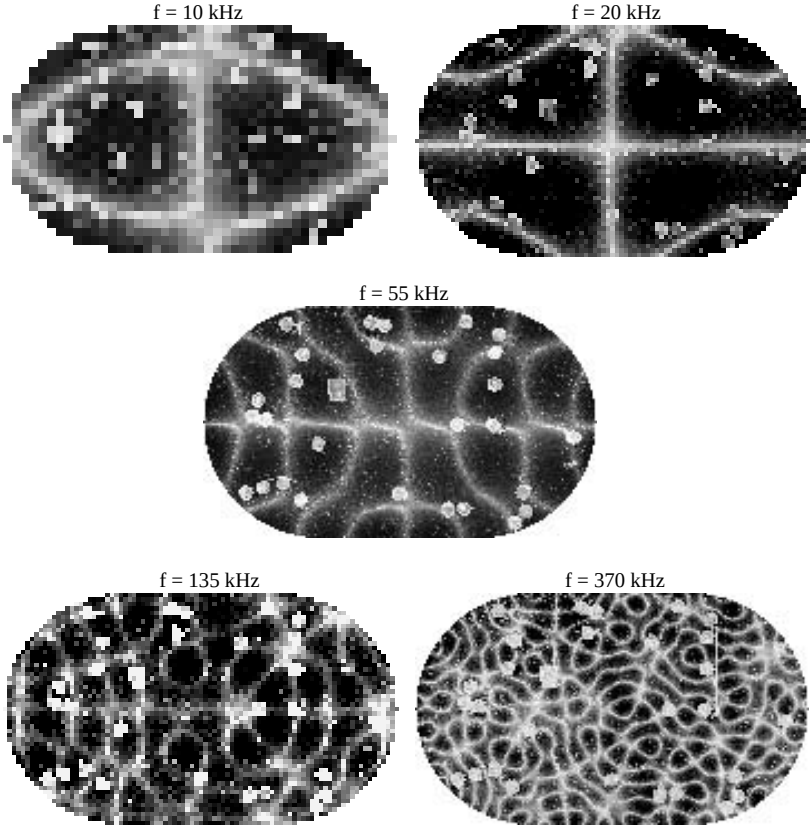

Figure 9: Measured mode shape patterns from a disordered plate with Bunimovich shape, Schaadt (70).

As discussed by Schaadt, the experimental results shown in Figure 9

suggest that the mode shapes are not obviously localized for all frequencies investigated (70). Indeed, the low-frequency wavelengths are not affected by the holes and the mode shape symmetry is not broken. As the frequency increases, the disorder effects of the holes become more and more relevant. The nodal line and symmetry characteristics evidence clearly a gradual frequency statistical transition toward almost-GOE statistics (70). Considering the mode shape associated with the natural frequency of 135 kHz, the spatial mode shape characteristics shows that the symmetry around the vertical axis is certainty broken, but the symmetry around the horizontal axis seems almost unbroken. For the highest frequency analyzed (375 kHz) the spatial mode shape characteristics showed that both symmetry axes were completely broken and the GOE characteristics were adequately established.

Unfortunately, no conclusions regarding the convergence speed characteristics of the modal parameter statistics to the *universal* establishment of GOE statistics can be drawn from the experimental results obtained by Schaadt (70), because the natural frequency and mode shape statistics were obtained from distinct disordered systems (10). Nevertheless, it can be verified that the presence of uncertainties (or disorder) provides a gradual and continuous frequency transition of the mode shapes from almost-deterministic statistics to GOE statistics as the excitation frequency increases and wavelength reduces[16], Gomes (10). According to Schaadt (70), his analysis was incomplete and further investigations are needed in order to obtain clear information on the convergence speed characteristics of the modal parameter statistics to the universal establishment of the GOE statistics in disordered systems.

Additionally, a series of numerical experiments with *Band Random Matrices* (BRM) have been carried out to investigate the convergence speed characteristics for the establishment of GOE statistics for each of the modal parameters, Casati *et al* (77, 78, 79). The BRM are traditionally applied to model the Hamiltonian of perturbed integrable or regular systems of solid state physics (78). This type of random matrix is able to model the transition from Poisson statistics to GOE statistics (77). Casati *et al* (78, 79) showed, through a set of numerical studies using the band random matrices, that the scaling (transition) characteristics are dependent only on the *scaling parameter*[17] which is defined as $x_s = b_w^2/N$, where b_w is the band half-width and N

[16] Although the modal parameter statistics were only evaluated as a function of excitation frequency, similar results are also expected when the modal parameter statistics are evaluated in function of uncertain level under a fixed excitation frequency range, Gomes (10).

[17] The *scaling parameter* describes the statistics of modal parameters in the regime of full classical chaos. The term b_w^2 is proportional to the localization length associated with the rate of

is the random matrix size.

In the RMT context, the scaling parameter can be seen as a parameter used to quantify the level of coupling between the unperturbed eigenvalues, since this parameter is directly related to the number of non-zero off-diagonal elements of the Hamiltonian (79). Indeed, an eigenvalue convergence to GOE statistics is expected to occur with an increase in non-zero elements, that is, when the off-diagonal coupling elements are introduced in a symmetric Hamiltonian matrix (78).

Casati *et al* (78, 79) in their numerical analysis adopted a BRM ensemble which is defined as the set of real symmetric diagonal matrices with half bandwidth b_w. The matrix elements were chosen as independent random variables with Gaussian distributions. Diagonal elements have the double variance of off-diagonal ones, similarly to traditional GOE matrices. Thus, the band matrix structure allowed the intermediate and extreme modal parameter statistics to be reproduced (*i.e.*, Poisson and GOE matrices). For the case of the diagonal matrices ($b_w = 1$), the eigenvalues are expected to be uncorrelated and the PDF of the adjacent eigenvalue spacings, $P(s)$, conformed very well with Poisson statistics. In the opposite case, for fully random matrices ($b_w = N$), the $P(s)$ results conform well with GOE statistics which are described by the well-known *Wigner surmise* (*i.e.*, Rayleigh distribution).

The relationship between spectral eigenvalue statistics and the scaling parameter (x_s) was investigated using a *phenomenological formula* for PDF of adjacent eigenvalue spacings which is associated with the *level repulsion parameter* (β_r), Casati *et al* (78). This formula also allows the correct characterization of the intermediate eigenvalue statistics during a Poisson-GOE crossover transition as well as the best known eigenvalue statistics. For $\beta_r = 0$, they reduce to Poisson statistics and for $\beta_r = 1, 2, 4$ to Gaussian Orthogonal, Unitary and Symplectic Ensembles (GOE, GUE and GSE), respectively. The numerical experiments were performed using several ensembles of the band random matrices composed of different matrix dimensions and bandwidths. The level repulsion parameter (β_r) was fitted for each corresponding scaling parameter (x_s) in order to describe in detail the eigenvalue statistics during a Poisson-GOE crossover transition. The main eigenvalue statistics results related to the scaling parameter dependence are shown in Figure 10.

exponential decay of the eigenvectors at the limit of infinite size ($N \to \infty$). Further information on the physical meaning of scaling parameter and its application to statistical analysis of quantum systems are available in Casati and Molinari (78, 79).

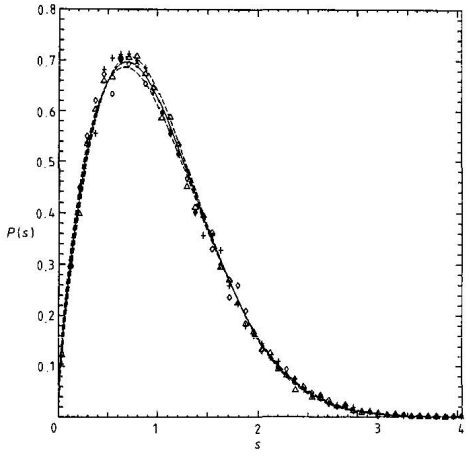

(a)

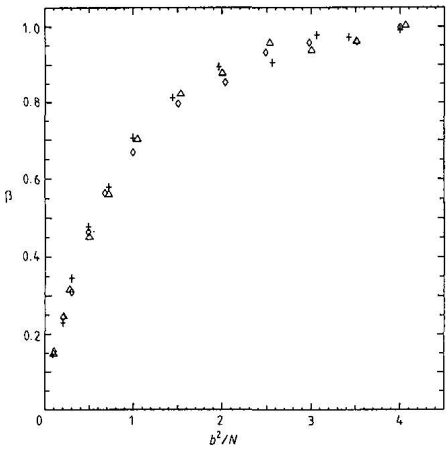

(b)

Figure 10: Plot(a): The PDF of adjacent eigenvalue spacings. Plot (b): the level repulsion parameter β_r for intermediate eigenvalue statistics $P(s)$ plotted against the scaling parameter, $x_s = b_w^2/N$. For the matrix dimensions: $N = 400(+)$, $N = 800(\Delta)$, and $N = 1600(\diamondsuit)$. Each β_r value was obtained by a fitting process from the numerical data for eigenvalue spacing distribution, Casati *et al* (78).

According to Figure 10, the results suggested that as the matrix bandwidth (or scaling parameter) increases, the eigenvalue statistics tend to conform to the GOE model (78). Surprisingly, one can note that the GOE model is established for eigenvalue statistics even for non complete fully random matrices (78). That is, it is not necessary to have a complete insertion of the off-diagonal coupling elements in the Hamiltonian for the eigenvalue statistics to satisfactorily obey the GOE model.

In a complementary study, Casati *et al* (79) also investigated the statistics of corresponding eigenvectors in the Poisson-GOE statistics transition and their relationship with the scaling parameter (x_s). Based on the definition of the *entropy localization length*[18] of normalized squared eigenvectors of the BRM matrices (78), a measure parameter called the *scaled localization length*[19](β_s) was proposed, in order to quantified the deviations from GOE eigenvector statistics[20]. In cases of extreme statistics, the scaled localization length is unitary for GOE statistics and null for perfectly diagonal matrices with a large N-limit (79).

Similarly to Casati *et al* (78), the scaled localization length was evaluated for normalized squared eigenvectors of the band random matrices with several sizes and bandwidths in order to characterize the eigenvector statistics during Poisson-GOE crossover transition and investigate their relationship with the scaling parameter (x_s). The main eigenvector statistics results for the Poisson-GOE statistics transition are shown in Figure 11 for several band random matrix dimensions.

[18]The *entropy localization length* is a measure parameter based on the difference between the effective number of nonzero components of a given eigenvector and its corresponding GOE eigenvector, Casati and Molinari (78). Further information on the calculation and practical application of entropy localization length for wavefunctions of quantum systems are available in: Casati and Molinari (78), and Mirlin and Fyodorov (77).

[19]The *scaled localization length* is defined as the average of the entropy localization lengths of the eigenvectors divided by the random matrix size, Casati and Molinari (78).

[20] In current investigation, the *level repulsion* and *scaled localization length* parameters proposed by Casati and Molinari (78, 79) are not used to verify the agreement with the GOE model statistics. In principle, there is no apparent limitations for the application of these parameters to statistical analysis of natural frequencies and corresponding mode shapes of real engineering systems. Therefore, systematical investigations on the performance of application of these parameters to verify the establishment of GOE statistics are needed for random systems with several natures.

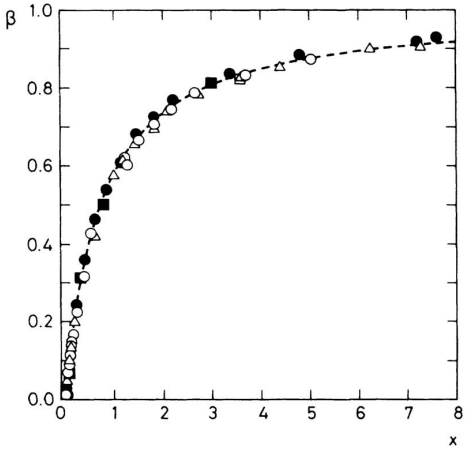

(a)

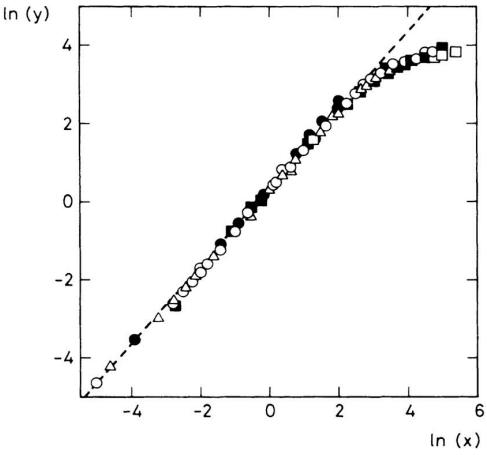

(b)

Figure 11: Scaled localization length (β_s) versus scaling parameter (x_s) for random matrix dimensions: $N = 200(\bullet)$, $N = 400(\triangle)$, $N = 600(\circ)$, and $N = 800(\blacksquare)$. The dashed line relates to the fitting of numerical data and follows the standard formulation: $\beta_s = \gamma_s x_s/(1+\gamma_s x_s)$, where γ_s is a real constant. Plot (a): the numerical data show a notable trasition (scaling) pattern with the scaling parameter. Plot (b): complete range of scaling parameters in log-log plot, where $y = \beta_s/(1-\beta_s)$, Casati *el al* (79).

As shown in the eigenvector statistics results, as the matrix bandwidth increases there is an asymptotic tendency toward GOE statistics, (79). Similarly to the eigenvalue scaling behavior, the scaling parameter values can easily be associated with the level of establishment of the *chaotic* (or universal) statistics of the eigenvectors of the band random matrices.

Additionally, important conclusions can be directly drawn when the scaling parameter results for the modal parameters are compared. For eigenvalue statistics, it is considered that GOE statistics are satisfactorily established when the level repulsion parameter (β_r) is approximately unitary, that is, it corresponds to the scaling parameter value of $x_s = 4$, Figure 10. On the other hand, for the corresponding eigenvector statistics results, it is also expected that GOE statistics will occur when the scaled localization length (β_s) is approximately unitary. According to the eigenvector statistics results in Figure 11, the pattern of the asymptotical results suggests that this universal cut-off limit will be reached for large values of the scaling parameter, $x_s > 8$.

Thus, these BRM numerical results provide convincing evidence that the dependencies of the scaling parameter (uncertainty level) are distinct for eigenvalue and the corresponding eigenvector statistics. In other words, the convergence speed characteristics for the universal establishment of GOE statistics show different patterns for each modal parameter (10). Indeed the requirements to establish GOE statistics for eigenvectors seem to be more stringent and a higher level of coupling between Hamiltonian matrix elements is necessary for eigenvectors, in comparison to the corresponding eigenvalues, that is, the universal cut-off limit for the establishment of GOE statistics can be reached more easily for eigenvalues than the corresponding eigenvectors (10).

Considering the extension of the previous BRM numerical results to the modal parameter statistics of random engineering systems with uncertain or non-deterministic parameters, the scaling parameter value can be directly associated with the uncertainty level of a given real engineering system. It seems reasonable to assume that the conclusions obtained previously regarding the convergence speed characteristics of BRM modal parameter statistics could be extended to modal parameter statistics from real engineering systems. That is, the amount of randomness necessary to establish GOE statistics for mode shapes is greater than that necessary for the corresponding natural frequencies and, thus, for real random engineering systems it is expected that the universal establishment of GOE statistics is easier for natural frequencies than for the corresponding mode shapes (10).

However, it is important to emphasize that there is no explicit evidence

that the Hamiltonians of random engineering systems with non-deterministic parameters are adequately described by the BRM when randomness effects are introduced into the Hamiltonian matrices from the nominal engineering systems. For the quantum systems, an excellent performance of the BRM statistics is expected to describe the modal parameter statistics in the Poisson-GOE transition range, (79, 77). Therefore, further investigations are required to verify the BRM performance in order to describe the modal parameter statistics of real random engineering systems with uncertain or non-deterministic parameters, Gomes (10).

Cordioli in (20) investigated the conformity level between the modal parameter statistics of engineering systems and the universal statistics described by GOE model. Considering several ensembles of random flexural plates with distinct levels and natures of structural uncertainty, the agreement between the natural frequency statistics and GOE model statistics were systematically evaluated through the results of RMT metric functions. The statistical overlap factor and mode shape statistics factors were also evaluated for natural frequencies and mode shapes, respectively. Additionally two new parameters based on mode shapes, Parameters P and Q, were proposed to analyze the agreement with GOE eigenvector statistics. The results provided an improved understanding of main aspects associated with the establishment of universal GOE statistics for real engineering systems. More information on these new SEA parameters is available in (20).

1.7 Summary and Discussion

This chapter presented a brief review of the energy response statistics across a nominal ensemble which is composed of similar engineering systems with uncertain or non-deterministic parameters and properties. As is already known, the effects of the presence of uncertainties become more relevant as the excitation frequency increases (5). In the low-frequency range, the long wavelengths are not substantially affected by uncertainty effects (1). Thus a well-established deterministic model of an engineering structure which considers the nominal physical parameters is able to provide a satisfactory prediction of the dynamical response (6).

In the mid to high-frequency ranges, the statistics of the modal parameters are highly complex and the evaluation of the dynamical response statistics using analytical formulations or numerical deterministic methods becomes a vigorous task due to two major factors (5). The first is associated with the fact that the application of the Monte Carlo method for an ensemble

of complex structures, through the FEM models, may become an extremely hard task and requires a high computational cost, since short wavelengths and data on several input parameters are involved in this process (5). The second factor is associated with the total or partial absence of statistical data from the system parameters or properties of real engineering systems (4). Even though these statistics of the system parameters are in principle available, the prediction of the response variance across the ensemble, based on a probabilistic method, is considered a prohibitive task for most engineering companies (5).

Considering that the real engineering systems have several uncertain physical properties, the *Statistical Energy Analysis* (SEA) is an appropriate analytical method to predict the ensemble average response for complex systems, mainly in the mid to high-frequency ranges (29). The SEA formulations take into account the high-frequency uncertainty effects on the energy response and thus their results provide the expected mean value of the energy responses from an ensemble composed of similar systems (29, 32, 33, 34).

Although the SEA performance is satisfactory in several real engineering applications to predict the ensemble average results, two key parameters have a significant influence on the response variability across the ensemble (1). The first parameter is the *modal overlap factor*. Several studies have shown that with an increase in this factor, multi-modal characteristics are established and the dynamic response becomes smooth making it difficult to identify the contributions of the individual modes (11, 12, 13, 14). The second parameter is the *statistical overlap factor* which defines how much the position of any natural frequency tends to change across the ensemble of systems (15, 1, 4, 80).

In the past, the earliest analytical investigations to predict the mean and variance of the energy responses were developed in the room acoustics context, (52, 48). In these pioneering works, the Poisson Point Process approach (55) were considered. The Poisson model was initially adopted for the natural frequency statistics due to analytical convenience (48). Additionally, the mode shapes were assumed to be a product of sinusoidal functions. Later, the analytical predictions were conveniently extended in order to allow multiple source and microphone points as well as the adoption of alternative and empirical non-Poisson statistical models for the natural frequencies, (52, 48). Satisfactory agreement was obtained for the analytical formulation based on the Poisson model, but surprisingly improved agreement with experimental results was established when an empirical non-Poisson model from quantum physics was applied (53, 54, 49). Indeed, these improved analytical results demonstrated the establishment of two main spectral characteristics associ-

ated with real engineering systems: the *level repulsion* and *spectral rigidity* (49, 75, 50, 18).

Some years ago, relevant experimental and numerical results from the elastodynamics field suggested that the natural frequency statistics can be adequately described by the eigenvalue statistics from the Gaussian Orthogonal Ensemble (GOE) of Random Matrix Theory (RMT) (64, 67).

The establishment of GOE statistics has also been extended to random systems of many different areas of physics, including acoustical and structural dynamics (23, 4, 50). For the modal parameters from these systems, a statistical transition from deterministic statistics to GOE statistics is expected with an increase in the frequency or a increase in the degree of asymmetry or disorder of system (6). A typical example of this gradual statistical transition to GOE was clearly demonstrated in (70) by Schaadt's mode shape results in the elastodynamic field, Figure 9. It is also important to note that the GOE matrices are clearly differ from the large matrices of the mathematical models associated with the these random systems (23, 4). Indeed, the main reason why the GOE statistics are so widely applicable to a large number of systems with distinct natures is not totally explicit (23).

Although, much effort has been made to provide the required conditions for the establishment of GOE statistics in random systems (23), the explicit reasons for the establishment of distinct universal limits for each of the modal parameters are not totally clear for random engineering systems (4, 23, 20). In particular, a large number of investigations have been performed on the statistics of natural frequencies from random systems, (67, 23). However, a reduced number of studies has been performed to investigate the conditions necessary for the establishment of the GOE statistics for corresponding mode shapes, (81, 20). Further investigations in this direction are certainly necessary, Gomes (10).

Several results in the SEA variance field reported in the literature have suggested the existence of a well-established cut-off frequency (or cut-off randomness amount) at which an increase of the excitation frequency (or randomness amount in the system physical properties) does not affect substantially the modal parameter statistics (27, 4, 15). Thus, the precise sources of uncertainty in the physical properties of a system seem to be less important and it becomes more adequate to describe the uncertainty effects directly in terms of uncertainties in the dynamical properties of the system, that is, in terms of statistical models for system modal parameters (6, 27, 4). Above this cut-off limit, the modal parameter statistics seem to have a high degree of *universal* statistics and are adequately described by the GOE model (27).

Thus the precise description of uncertainty sources as well as the statistics of uncertainties in the physical properties of a system become unnecessary to model accurately the modal parameter statistics (1, 18, 4).

In the SEA variance context, this cut-off limit, also called the *universal limit*[21], represents a saturation point at which an increase in the uncertainty level of the system physical properties (or an increase in the excitation frequency) does not cause significant changes in the dynamical properties of the system. Therefore, the accurate identification of the universal limit for the establishment of GOE statistics for the modal parameters makes the problem more appropriate from the analytical point of view (10). Indeed, under this condition, simple statistical expressions based on the GOE model can be adopted for the mode shape and natural frequency statistics. Thus, it is possible to develop analytical formulations to predict the mean and corresponding relative variance of the energy responses across a nominal ensemble (1, 82).

Langley and Brown (18, 3) considered that the real engineering systems are sufficiently random to ensure that both modal parameter statistics in the high-frequency range are described by the GOE model in an accurate way. Indeed, the adoption of the GOE model for modal parameters reproduces adequately some relevant dynamical characteristics expected for most real engineering systems with uncertain or non-deterministic properties, for example the *level repulsion* and *spectral rigidity* phenomena associated with the natural frequencies (64, 51, 23).

Currently, the best performance of SEA variance predictions based on the GOE model is observed for the response variance of sufficiently random engineering systems subjected to spatially distributed loadings, for example *rain-on-the-roof* loading (18, 16, 17). There are two main reasons for the good performance of SEA variance predictions associated with spatially-distributed loadings. The first is related to the fact that the contribution of the mode shape statistics to the energy response statistics is not substantial for most systems excited by spatially-distributed loading[22]. The second reason is associated with the fact that most real practical engineering systems are considered sufficiently random to ensure that their high-frequency natural frequencies are adequately described by the GOE model (6, 4, 23). Therefore, the major contributions to the energy response statistics from a random system subjected to spatially-distributed excitation are expected to be from the natural frequency statistics (1, 48), which, in turn, are expected to present

[21] According to AutoSEA Variance Manual (27), this limit is also known as the *acoustic limit*.

[22] The same conclusion can be extended to the spatially-averaged response statistics, Brown (1).

GOE characteristics for sufficiently random systems, thus providing a good agreement between the experimental (or numerical) results and GOE variance predictions.

In cases where random engineering systems are subjected to a single point-loading, the energy response statistics are highly sensitive to mode shape statistics (1, 48), that is, small changes in the statistical characteristics of the mode shapes may have a substantial effects on the response variability (10). As discussed, an incomplete establishment of GOE statistics seems to be expected for real random engineering systems in the high-frequency range, at least for artificially generated systems usually considered sufficiently random in SEA variance analysis (10). Indeed, it is expected that the natural frequency spacings obey adequately the Rayleigh PDF and the corresponding mode shapes are *near*-Gaussian, not complying perfectly with the universal eigenvector statistics proposed by the GOE model which predicts perfect Gaussian mode shapes (18, 10). In Table 1.1, these mode shape discrepancies expressed by the mode shape statistics factor values seem to explain the reduced performance of the revised SEA variance theory for cases of single point-loaded systems as well as why the improved performance is obtained when the mode shape statistics factor value is adequately modified (18, 16, 17).

Extending the main conclusions from the previous BRM results to random engineering systems, it seems that the level of uncertainty necessary to establishment of universal statistics, which is described by GOE model, may be very distinct for the natural frequencies and the corresponding mode shapes (20). As demonstrated previously by the BRM numerical results in Figures 10 and 11, the necessary conditions associated with eigenvectors for the establishment of GOE statistics seem to be more stringent and require a higher level of uncertainty than the corresponding conditions associated with eigenvalues.

Considering the most practical random engineering systems, the level of uncertainty in their physical parameters seems to be sufficient to ensure that the universal limit associated with natural frequencies (δ_{NF}^{GOE}) is reached, and thus their natural frequency statistics are correctly described by the GOE model in the high-frequency range (10). However, it is important to emphasize that the same conclusion cannot necessarily be extended to the corresponding mode shapes. It has been shown that the effects of such uncertainties on the mode shapes are not sufficient to ensure that the universal limit associated with mode shapes (δ_{MS}^{GOE}) is reached, at least for high-frequency modes (10).

Based on the results from the SEA variance and BRM literature previ-

ously shown in the Section 1.6.2, an initial sketch is proposed in Figure 12 for the statistical patterns expected for each one of the modal parameter statistics when structural uncertainties are introduced in a typical engineering system with perfect nominal characteristics; Gomes (10), Langley and Cordioli (76). In the current proposal, the expected effects of the increase in the amount of randomness, or uncertainty level, on each one of the modal parameter statistics across the ensemble are illustrated for a fixed frequency range[23].

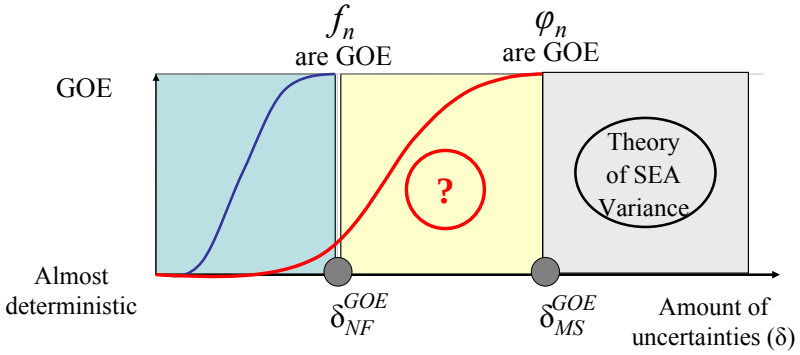

Figure 12: Schematic representation of the typically expected pattern of the modal parameter statistics for an ensemble composed of similar systems with uncertain or non-deterministic parameters. The effects of an increase in the amount of randomness on the statistical characteristics of each one of the modal parameters are illustrated for a fixed frequency range, Gomes (10).

As shown in Figure 12, it is expected that the increase in the level of uncertainty in the physical parameters of engineering systems provides a gradual statistics transition for both modal parameters from an *almost-deterministic* statistics (i.e., almost complete absence of uncertainties) to a *universal* statistics which is described by the GOE model (4, 23, 6, 10). As previously discussed, the speeds of convergence to GOE statistics may be substantially different for each modal parameter and thus distinct universal limits occur for natural frequencies and their corresponding mode shapes (10).

[23] Similar statistical behavior is expected under partner conditions as the uncertainty level of system ensemble is considered fixed and the excitation frequency increases, Langley *et al* (4) and Gomes (10).

For the natural frequencies, it is expected that the presence of a small amount of disorder in the system may provide a fast convergence toward the universal establishment of GOE statistics, and therefore universal limited δ_{NF}^{GOE} is expected to be more easily reached for most real engineering systems (20). On the other hand, an asymptotic slow speed convergence for GOE statistics is expected for the corresponding mode shape (eigenvector) statistics, since in order to reach the limit of universal statistics δ_{MS}^{GOE} , the mode shape statistics seems to require a larger disorder in the system parameters than the corresponding natural frequency statistics (10). Thus, in principle the δ_{MS}^{GOE} is expected to be larger than δ_{NF}^{GOE} and may be not readily reached in the case of practical engineering systems, Gomes and Langley (10, 76). Indeed, it is expected that the conditions necessary to comply with GOE statistics for natural frequencies are less stringent than for their corresponding mode shapes (10).

In summary, Figure 12 suggests that the statistical characteristics of modal parameters from a random engineering system are divided into three major groups (10). In the first region, below the δ_{NF}^{GOE} and δ_{MS}^{GOE} universal limits, the amount of randomness in the physical parameters of the system is relatively low and thus only incipient uncertainty effects are observed on the statistics of the natural frequencies and corresponding mode shapes (6). Indeed, the level of disorder provided by such structural uncertainties is not able to ensure the establishment of GOE statistics for both modal parameters (10). As shown in Figure 12, the universal limits associated with the natural frequencies (δ_{NF}^{GOE}) and mode shapes (δ_{MS}^{GOE}) are not reached and the statistical characteristics of the modal parameters are *completely non-universal*, having system-dependent characteristics (10). That is, their modal parameter statistics are strongly dependent on the statistical characteristics of the uncertainties of the physical parameters of the system (27). Indeed, transitory statistics with intermediate characteristics between the almost-deterministic and GOE models is established for both modal parameters in this first region (10).

At the other extremity, in the last region, the amount of randomness is sufficiently large to ensure that both universal limits are adequately reached and the universal statistics are established for modal parameters and thus the GOE model is perfectly applicable to describe the ensemble statistics of the natural frequencies and corresponding mode shapes (1, 23). For this region, *universal* statistics are completely established across the ensemble so that both modal parameters are practically independent of precise sources of uncertainties in the physical properties of a subsystem (27, 4, 23). The natural

frequencies are expected to obey the *Wigner surmise* which states that the adjacent natural frequency spacings are Rayleigh distributed and there is the establishment of level repulsion and spectral rigidity phenomena in the natural frequency correlations (64, 1). Additionally, the corresponding mode shapes are expected to be statistically independent and their component amplitudes uncorrelated and *Gaussian* distributed, so that the value of the mode shape statistics factor is $K = 3$ (27, 4, 1).

In the second region, intermediate range, an incomplete establishment of universal statistics occurs where only the universal limit associated with one of modal parameters is reached (10). According to Figure 12, the literature results discussed above suggest that, in principle, the universal limit of natural frequencies δ_{NF}^{GOE} is effectively reached while the universal limit of corresponding mode shapes δ_{MS}^{GOE} is not (10). In this regard, the statistics of natural frequencies are adequately described by the GOE model and present universal characteristics, that is, the natural frequency statistics are expected to be independent of the precise sources of the structural uncertainties of the system physical parameters (6, 4, 23). On the other hand, the mode shape universal limit (δ_{MS}^{GOE}) is not effectively reached and it is expected that the corresponding mode shapes will still present some residual *non-universal* characteristics, where the *system-dependent effects* may be relevant to the statistics of the mode shapes (10). Indeed, a mode shape component distribution with *near-Gaussian* characteristics is expected for this intermediate region and the mode shape statistics factor values are lower than the expected Gaussian value, that is, $K < K_{GOE} = 3$ (18, 16, 17).

Considering the SEA variance context, the revised analytical formulation of the relative variance derived by Langley and Brown (18, 1) assumes that both modal parameter statistics comply with the GOE model. This condition is associated with a complete establishment of *universal* statistics simultaneously for both modal parameters. According to Figure 12, the condition of the complete establishment of *universal* statistics is expected, in principle, to be ensured only beyond the mode shape universal limit (δ_{MS}^{GOE}) where the natural frequency as well as the mode shape statistics are perfectly described by the GOE model (10). Indeed, the best performance of the revised SEA variance formulations based on the complete GOE model is expected for random engineering systems in which the modal parameter statistics are similar to those associated with the third region of Figure 12 (10).

Based on the above discussion of the results available in the literature for energy response variance, the discrepancies observed between the experimental measurements (or numerical) results and analytical variance predicti-

ons based on the GOE model seem to be explained by the existence of deviations of the mode shape statistics in relation to *universal* statistics (10). Indeed, the characteristics of the modal parameter statistics from the random systems investigated in the SEA variance literature seem to correspond to the modal parameter statistics associated with the second region of Figure 12 (10). As shown in Table 1.1, an incomplete establishment of universal statistics for modal parameters is certainly expected for most random engineering systems in which the level of uncertainty of the system parameters is not large enough to guarantee the establishment of GOE statistics for mode shapes although these are adequately established for natural frequencies across the ensemble (10). Therefore, systematic investigations are also required to provide a better understanding of the effects of non-universal mode shape statistics on the energy response statistics of real engineering systems subjected to different natures of excitation, so that it will be possible to estimate with good accuracy the errors associated with the application of the revised SEA variance prediction based on the complete GOE model to real engineering vibroacoustic systems in which an incomplete establishment of GOE statistics is expected for the mode shapes, Gomes (10, 83, 84).

1.8 Scope, Aims and Outline of the Thesis

The main goal of current work is to provide a better understanding on the performance of SEA method to predict the energy response statistics of random engineering structures in the mid and high-frequency ranges. Several investigations on the application of SEA models have been carried out at Laboratory of Vibration and Acoustics (LVA) from Federal University of Santa Catarina (UFSC) with aeronautical structures: Rodrigues (43), Gomes (28), Gomes *et al.* (85), Cordioli and Gerges (86); and with automotive structures: Calçada (87) e Gomes *et al.* (88). Recently, research activities have been carried out on the use of SEA models to predict the higher statistical moments of energy responses. In overall, the basic assumptions and performance of Theory of SEA Variance have been discussed: Corlioli and Gerges (19), Cordioli (20) and Gomes (10).

In this regard, the problem of interest investigated in this thesis is associated with the characterization of deviations of the modal parameter statistics in relation to *universal* statistics described by a Gaussian Orthogonal Ensemble (GOE) from Random Matrix Theory (RMT) (10). This study also aims to investigate the main effects of the *non-universal* characteristics of the modal parameters on the energy response statistics and their possible impacts on the

performance of SEA variance theory which considers a complete establishment of GOE statistics for both modal parameters (10).

1.8.1 Open Problems and Motivations

From the previous discussions based on the existing literature results, it is clear that in spite of extensive research efforts, many issues regarding the extension of the validity of the Universality concept for random vibroacoustic systems with uncertain or non-deterministic parameters as well as the complete establishment of GOE model for their modal parameters are not still sufficiently clear to academic community (10). The following questions are examples of the main open problems which are of interest in this study and they can be broadly divided as follows (10):

1. Investigation of statistical characteristics of modal parameters in the high-frequency range

- In real engineering structures, what type of statistics are most probable for each of the modal parameters in the high-frequency range? Is the universal establishment of GOE statistics expected for the mode shapes? How much randomness is needed to ensure it?

- If the mode shapes are not perfectly GOE in the high-frequency range, which are the most effective metric functions to verify the agreement level (or possible deviations) between the real engineering system mode shape statistics and GOE eigenvector statistics?

2. Statistical transition process of the universal establishment of GOE statistics for each modal parameter

- Is the initial proposal for the expected transition pattern of modal parameter statistics, shown in Figure 12, valid for all random engineering systems, or is its validity limited to only a particular group of random engineering systems?

- Are the characteristics of the convergence of mode shape statistics toward GOE model dependent on the system characteristics or dimensionality? If the answer is positive, what would be the expected statistical transition pattern for each modal parameter?

- Is there a well-defined sequence between the modal parameters for the *universal* establishment of GOE statistics? In other words, is it always expected that the mode shapes will require a higher level of disorder than the corresponding natural frequency to comply with the *universal* statistics described by the GOE model?

3. Impacts on performance of SEA variance prediction due to the incomplete establishment of GOE statistics

- For the cases of an incomplete establishment of GOE statistics, what are main impacts on the performance of the revised SEA variance predictions if the mode shapes are not considered perfectly GOE? How can we modify the SEA variance theory to allow for this?

- Is the SEA variance prediction based on complete GOE statistics conservative for all real engineering structures? What are the possible statistical parameters based on mode shape statistics which can readily provide this information?

1.8.2 Aims and Scope of this Thesis

In view of the above open problems, the main aims of this thesis are presented below. The three main objectives are the following:

- To gain a better understanding of the relationship between the modal parameter statistics of the GOE ensemble and those expected for real structure ensemble, as well as of how the deviations might be readily verified. Special attention is given to the accurate description of the statistical characteristics of each of modal parameters during the transitory process for the *universal* establishment of GOE statistics, for example, speed convergence and its dependence on the amount of randomness or the excitation frequency to comply with GOE statistics.

- To carry out a global analysis of the main physical phenomena associated with the *non-universal* characteristics of the mode shapes expected in random engineering systems with uncertain or non-deterministic parameters in the high-frequency range. That is, the derivation of an efficient methodology to indentify and quantify the discrepancies between the mode shapes of real engineering systems and GOE eigenvectors.

- A systematic investigation of the effects of the incomplete establishment of GOE modal parameter statistics on the energy response statistics as well as their consequences in terms of the expected performance of the revised SEA variance prediction.

1.8.3 Outline of the Thesis

Motivated by the existing open problems highighted in previous sections, a systematic study on the statistical characteristics of the modal parameters and energy responses of vibroacoustic systems with uncertain or non-deterministic parameters and properties will be carried out. In order to deal with this task, this document is subdivided into the following chapters:

In Chapter 2 a brief literature review is presented on the main aspects associated with the statistical analysis of modal parameters of engineering systems. Initially, the main concepts of Random Matrix Theory (RMT) applied to the statistical analysis of the natural frequencies from vibroacoustical systems are briefly reviewed. In complementary manner, the statistical properties of the corresponding mode shapes are also introduced for GOE and sinusoidal eigenvectors. The main limitations to the direct use of RMT tools in the statistical analysis of vibroacoustic systems are identified and their non-universal physical phenomena (such as *finite wavelength effects*, *periodical orbits*, and *structural Localization*) are also discussed in detail. Considering SEA model applications, the analytical predictions based on the Poisson and GOE models are presented for the energy density variance of a single random dynamical system.

In Chapter 3, a complete statistical analysis is performed with the random one-dimensional structures and the effect of distinct uncertainty sources on the modal parameter statistics are investigated in detail through the metric functions from the RMT. Random longitudinal rods were generated using the Finite Element Method (FEM) and the distinct structural irregularities, or uncertainties, were introduced to a nominal rod structure and different approaches to the uncertainty distribution (randomization approaches) were also considered.

During the numerical analysis, the spectral and ensemble averaging processes were performed for random rod structure responses. In addition, the main effects of the spatial correlation on the rod geometry and of the structural localization phenomenon on the modal parameter statistics were also assessed through RMT tools. The relevant findings were then obtained regarding the *universal* establishment of GOE statistics for each of the modal

parameters as well as for the statistical moments of the kinetic energy density results from the random longitudinal rod structures.

In Chapter 4, a statistical analysis is systematically performed with the random two-dimensional structures. Flexural plates with several geometries (square, rectangular, rectangular with arc at one corner, circle, polygon, 1/4 Sinai stadium) are numerically generated by FEM models. Considering the spectral and spatial averaging approaches, the effects of distinct levels of the system symmetry are assessed and the resulting modal parameter statistics are compared with analytical predictions based on the Poisson and GOE models. Special attention is focused on the main physical phenomena expected for the mode shapes of real engineering systems (i.e., the establishment of stable periodic orbits, the structural localization and others).

In a similar manner to random rod analysis, two distinct ensembles of random flexural plates are also investigated considering the spectral and ensemble averaging processes. The statistics of the point-loading and spatially-averaged kinetic energy density results in terms of the narrow and broad frequency band domains are compared with SEA analytical formulations based on the Poisson and GOE models. Therefore, the performance of the analytical prediction is discussed in terms of the corresponding modal parameter statistics and then conclusions are drawn regarding the application of the universality concept to real engineering systems in the mid and high-frequency ranges.

Finally, Chapter 5 presents the main original conclusions emerging from the present work and gives some directions and suggestions for future research studies.

2 LITERATURE REVIEW

2.1 Introduction

In this chapter the basic theoretical concepts on the modal parameter statistics are briefly reviewed. The main aspects on the statistical analysis of natural frequencies and corresponding mode shapes are introduced and discussed in detail[1].

Initially, the main tools of Random Matrix Theory (RMT) applied to the statistical analysis of the natural frequency statistics from vibroacoustical systems are presented. The limitations to the direct use of RMT tools in the statistical analysis of vibroacoustic systems are also highlighted and discussed using illustrative literature examples and results from numerical studies using finite GOE matrices.

The statistical properties of the corresponding mode shapes are introduced in Section 2.3. The main metric functions adopted to characterize the statistics of the mode shapes of random systems are defined and the analytical predictions are presented for GOE and sinusoidal eigenvectors. The two classes of mode shape statistics deviations from the *universal* GOE eigenvector statistics are identified and illustrated through results for microwave cavity systems reported in the literature.

Finally, the analytical predictions, based on the Poisson and GOE models, are presented for the energy density variance. Based on the results reported in the SEA variance literature, a detailed discussion is presented regarding the effects of the mode shape statistics factor on the performance of relative SEA variance predictions.

2.2 Random Matrix Theory

In this section the main RMT concepts are briefly reviewed. Initially, the historical context and the first applications in the Quantum Physics field are presented. The best known Gaussian ensembles from RMT are classified and their statistical characteristics are described. The RMT *statistical observables* applied to evaluate the spectral statistics of eigenvalues of large random matrices are introduced. Typical examples of the application of sta-

[1] Further information is available in Cordioli (20) and Brown (1).

tistical observables in the description of spectral characteristics of chaotic and integrable (or regular) systems are shown.

The principal analogies between quantum and vibroacoustic systems are emphasized and the limitations to the use of RMT tools in the analysis of spectral natural frequency statistics are also presented and illustrated. The link between the theory of variance of *Statistical Energy Analysis* (SEA) and RMT statistics models is highlighted. Finally, the application of RMT concepts to describe the response statistics of dynamical systems is discussed in detail.

2.2.1 Historical Context

The *Random Matrix Theory* (RMT) appeared in the early 1960s and its main goal was to give mathematical support to the statistical analysis of the spectra of the energy levels of complex nuclei, (62). For atoms with light nuclei, there are few energy levels on the spectrum and it is possible to carry out a complete description of the energy level behavior using both experimental and analytical approaches. On the other hand, for atoms with heavy nuclei, the energy level density is extremely high and the identification of individual energy levels may become prohibitive. In the latter cases, a statistical description of the spectral proprieties is strongly recommended, Mehta (24).

In Figure 13, examples of energy level spectra are shown for two typical nuclear systems. The peak curves correspond to energy levels. A large number of peaks is expected mainly for the high energy range since the spectra relate to nuclear systems with heavy nuclei, Mehta (24).

In quantum nuclear systems, the energy levels are evaluated through a Hermitian matrix operator known as *Hamiltonian*. For continuous systems, the Hamiltonian is described by an infinite number of eigenvalues[2], Almeida (58). For practical applications, a truncation process is necessary and a large limited number of eigenvalues is considered in the statistical analysis. In this context, based on the statistical properties of the Hamiltonian matrix and considering some hypothesis concerning its structure (*i.e.*, presence of symmetries), the main aim of RMT is to describe the global statistical characteristics of the eigenvalues and eigenvectors of Hamiltonian matrices.

The main conclusions of Wigner's studies showed that the statistical spectral properties of nuclear systems with complex nuclei can be adequately

[2] In the vibroacoustic context, the Hamiltonian matrix H of a dynamic system can be evaluated through the combination of the mass and stiffness matrices, $H = M^{-1}K$. For continuous vibroacoustic systems, their Hamiltonians are described by an infinite number of degrees of freedom, Meirovitch (89).

described by the eigenvalue statistics of random matrices with large dimensions, (61, 62). However, the eigenvalue statistics of large random matrices can not be used to predict in detail an energy level sequence of a nuclear system, but the RMT statistical models are only able to describe correctly the global statistics and the level of irregularity expected from the nuclear system spectra.

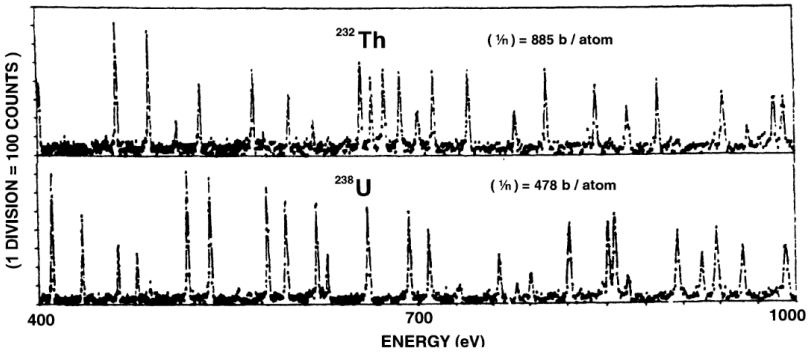

Figure 13: Examples of energy level spectra of nuclear systems, Mehta (24).

Recently, several studies have showed a series of promising results for the use of RMT tools in the analysis of the eigenvalue statistics of physical systems with several natures. These results suggest that the application of RMT concepts are not limited to nuclear systems. One of the pioneering works in this regard was carried out by Weaver (64). In his work, the natural frequencies of aluminum blocks were measured and their spectral statistics showed an excellent agreement with analytical RMT predictions. Some years later, Langley and other researchers (4, 17, 51, 18, 3, 35, 23) showed that the RMT models could be applied to describe the natural frequency statistics of random dynamical systems. In particular, a good and promising agreement was found for large symmetric random matrices in vibroacoustic applications, (16, 18, 4, 35, 23).

It is also important to emphasize that there is, as yet, no explicit explanation as to why the RMT concepts are so widely applicable to several systems with different natures. The matrices arising from the mathematical model of any physical system are considerably different than the random ma-

trices of RMT. Some studies propose that this good agreement is based on the validity of the *Universality* concept. Therefore, the conditions required for the occurrence of *universal* statistics have been strongly investigated by several researchers, Bohigas *et al* (67), Langley (23) and others. The mathematical details concerning RMT concepts and the derivation of their results are beyond the scope of the current work and will not be discussed in detail below. Further information is available in: Mehta (24), Brody (56), Almeida (58), and Guhr *et al* (57, 63).

2.2.2 Gaussian Ensembles of Random Matrices

In this section, the three best known Gaussian ensembles from Random Matrix Theory (RMT) are introduced, they are: the *Gaussian Orthogonal Ensemble* (GOE), the *Gaussian Unitary Ensemble* (GUE) and the *Gaussian Symplectic Ensemble* (GSE), Mehta (24).

According to Langley *et al.* (4, 23), the *Gaussian Orthogonal Ensemble* (GOE) is the Gaussian ensemble most commonly adopted in general applications, since its most attractive characteristic is the invariance of the matrix probability distribution function under *orthogonal transformations* (*i.e.*, change of basis). The corresponding results can be extended to Hermitian matrices in which the *Gaussian Unitary Ensemble* (GUE) pdf is statistically invariant under *unitary transformation*s. Similarly, the *Gaussian Symplectic Ensemble* (GSE) is composed of quaternion-real self-dual matrices, and its pdf function is invariant under *symplectic transformation*.

In order to classify the Gaussian ensembles, the Hamiltonian matrix structure is considered as the main factor in the classification process, Andersen (68). Traditionally, *Dyson's Index* (β) is adopted for the identification of each Gaussian ensemble, Guhr (57, 63). In Table 2, the main characteristics of Gaussian ensembles are described, Andersen (68).

The *Gaussian Orthogonal Ensemble* (GOE) is composed of real symmetric random matrices and its main characteristics are the following (23):

- the entries have zero mean and are uncorrelated Gaussian random variables,
- the diagonal elements have twice the variance of the off-diagonal elements, and
- the Hamiltonian is invariant under orthogonal transformation $H \rightarrow W^T H W$, where W is an orthogonal matrix, (90).

Table 2: Main characteristics of Gaussian ensembles: nomenclature, abbreviation, random matrix structure and Dyson's index (β), Andersen (68).

Nomenclature	Abbreviation	Random Matrix Structure	Dyson's Index (β)
Gaussian Orthogonal Ensemble	GOE	Real Symmetric	$\beta = 1$
Gaussian Unitary Ensemble	GUE	Hermitian	$\beta = 2$
Gaussian Symplectic Ensemble	GSE	Quaternion-real self-dual	$\beta = 4$

Although the structure of a GOE matrix is completely distinct from those of the matrices of the mathematical models of engineering systems, the statistics of the eigenvalues are surprisingly similar to the natural frequency statistics of the matrices associated with the mathematical model of random dynamical systems, Langley (23).

The *Gaussian Unitary Ensemble* (GUE) has an eigenvalue spectrum described by the Hermitian matrix (68). According to Weaver (64), the GUE statistics are not expected to apply to vibroacoustic systems, except for the cases in which there is a gyroscopic force in one of system components, for example: a Coriolis force which is dependent on the component velocity, Santos (91).

In this context, a general statement of the *Universality* principle would be to claim for large matrices that, apart from well defined exceptions, all symmetric random matrices should have local GOE eigenvalue statistics, all Hermitian random matrices should have local GUE eigenvalue statistics, and all quaternion-real self-dual matrices should have local GSE eigenvalue statistics, (4, 23). Further detailed descriptions of GUE and GSE statistics are available in the physics literature, (24, 56, 58, 68).

2.2.3 Unfolding Process

In the RMT context, before starting a statistical analysis of any spectrum of a certain physical system, it is necessary to carry out a normalization process in order to extract from the spectrum the particular characteristics which are dependent on the nature of the system under analysis, *i.e.*, the secularities, (64, 90). This normalization process is traditionally known as the *unfolding process* and its resultant spectrum as the *unfolded spectrum*. The

main advantage provided by the unfolding process is that the unfolded spectral statistics of systems with different natures can be directly compared to each other and also to RMT analytical predictions.

By definition, the eigenvalues of RMT matrices show a *unitary mean spacing* between two successive eigenvalues, (23, 24, 56). Thus, an efficient unfolding process has to provide appropriate conditions, so that a direct and systematic comparison can be made between the spectral statistics of the system analyzed and the analytical RMT predictions, Brody *et al* (56).

In the Quantum Physics context, the *staircase function* is defined as a step function which counts the number of energy levels present below a particular energy level, e_i, Bertelsen (90). Similarly for vibroacoustic systems, the staircase function describes the number of natural or resonant frequencies below a particular frequency, f_i , Weaver (64). The staircase function can be decomposed into two major components and is given by (69, 90):

$$N(f) = N_{av}(f) + N_{fluc}(f), \tag{2.1}$$

where $N_{av}(f)$ and $N_{fluc}(f)$ are the average and oscillatory components of the staircase function, respectively.

The average (or monotonic) component of the staircase function, also called the smooth component, expresses the expected average number of natural frequencies of a particular system and is associated with the global behavior of the staircase function, Stöckmann and Stein (92). On the other hand, the oscillatory component of the staircase function is associated with the staircase function fluctuations and describes the level of interaction among the natural frequencies. According to Bertelsen (90), the average component of a staircase function has *system-dependent* characteristics and its behavior differs for physical systems of different natures. In contrast, the oscillatory component of the staircase function shows a *universal* behavior regardless of the particular physical properties of the system. In this regard, the unfolding process tends to emphasize the *universal statistics* of the oscillatory component of the staircase function and provides ideal conditions for direct and normalized analysis of the spectral fluctuations and their respective natural frequency interactions.

The evaluation of the average staircase function component can be carried out using analytical functions, for example: Weyl's formula, Stöckmann (92) and Brown (1). Hereafter in this document, the unfolding process which employs analytical asymptotic functions will be referred to as the *standard unfolding process*.

For thin plates, the analytical asymptotic functions for average stair-

case function are dependent only on the geometrical dimensions and material properties, Lyon and Dejong (29) and Bertelsen (90). In Figure 14, examples of the smooth component evaluations of the staircase functions are shown for two aluminum plates: Square and 1/4 Sinai stadium geometries, Gomes and Gerges (93).

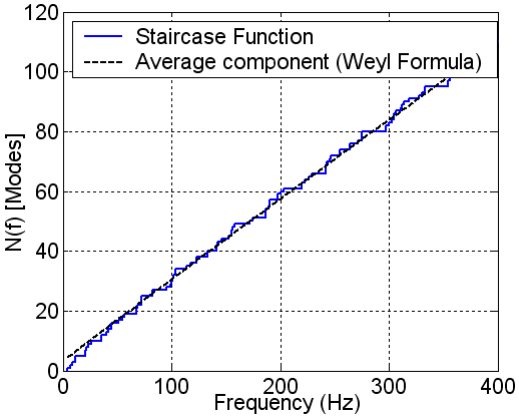

(a_1) square plate

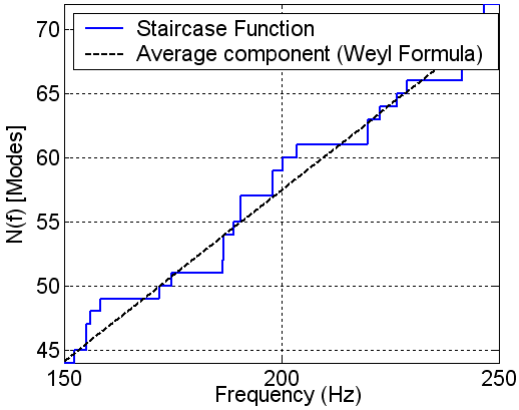

(a_2) zoom plot

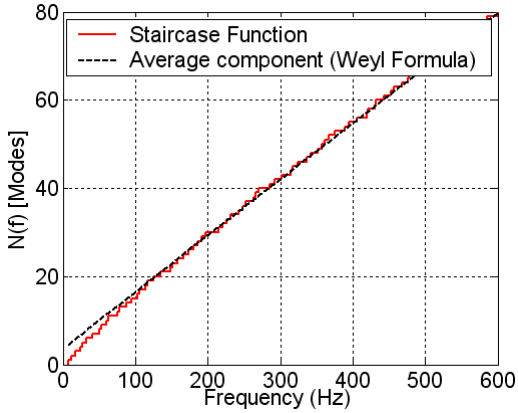

(b_1) sinai plate

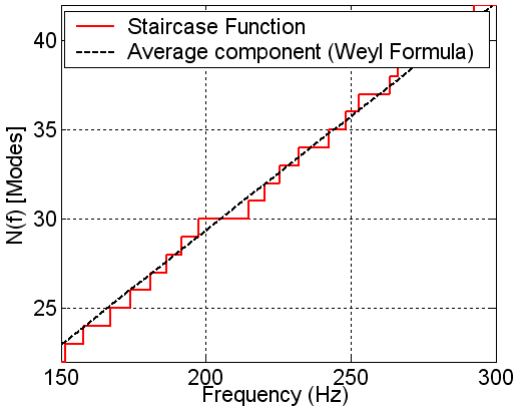

(b_2) zoom plot

Figure 14: Examples of staircase function for two aluminum plates. Plot (a): Square geometry. Plot (b): Sinai stadium geometry. The step function is associated with numerical results and the dashed line represents the analytical prediction of Weyl's formula. The zoom plots emphasize the differences between Square and Sinai stadium results, Gomes and Gerges (93).

In the zoom plots, relevant differences can be noted between the fluctuation characteristics of the plates. In general, the fluctuation magnitudes of

the Square plate are expected to be larger than those of the Sinai stadium plate due to the establishment of the periodic orbits, Gomes and Gerges (93).

In order to evaluate the universal fluctuations of a particular spectrum, the unfolding process must be carried out. According to Weaver (64), once there is a satisfactory estimate for the average component of staircase function, $N_{av}(f)$, the data of the original spectrum can be normalized by the following transformation:

$$z_i = N_{av}(f_i), \tag{2.2}$$

where z_i, is the ith unfolded (or normalized) natural frequency which corresponds to the ith natural frequency, f_i. The unfolded frequencies have an unitary mean spacing and their statistics can be directly compared to analytical RMT predictions, Weaver (64). According to Bertelsen (66), the unfolded staircase function has the same fluctuations as the original staircase function, $\widetilde{N}_{flu}(z) = N_{fluc}(f)$, but its smooth component is given by $\widetilde{N}_{av}(z) = z$. Then, the unfolded staircase function is given by (69, 90):

$$\widetilde{N}(z) = N_{av}\left(N_{av}^{-1}(z)\right) + N_{fluc}\left(N_{av}^{-1}(z)\right) = z + N_{fluc}(f(z)). \tag{2.3}$$

It is very important to emphasize that the unfolded spectra from different systems can be directly compared to each other since the normalization process (or unfolding process) provides an unitary mean spacing (64, 90). As discussed by Bertelsen (90), it is no trivial task to evaluate correctly the smooth (or average) component of a staircase function, mainly for complex geometries where the asymptotic analytical formulations are not available. The main difficulty is to correctly ascertain how close the smooth component should be near to the original staircase function. If the smooth component is too close to the original staircase function, the universal properties of the fluctuations can be erroneously removed. On the other hand, if the smooth component is too far from the original staircase function, the *system-dependent effects* are not removed and the resultant oscillatory component of the staircase function will be present in the *non-universal* spectral fluctuations. According to Bertelsen (90), good performance of unfolding process can be observed by the following condition:

$$\widetilde{N}(z) - z \lesssim 1. \tag{2.4}$$

Additionally, it is also expected that the fluctuations follow a Gaussian

distribution, Fujisaka and Tohyama (94). In Figure 15, the condition proposed by the Equation (2.4) can be verified for both plates, Square and Sinai geometry. The high amplitudes of unfolded staircase fluctuations are mainly observed for Square plates, and for Sinai plates these are reduced.

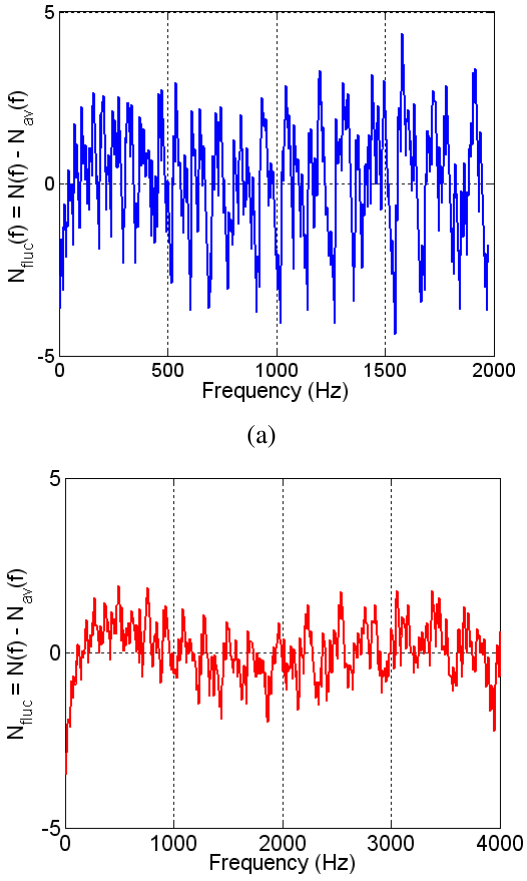

Figure 15: The oscillatory components of unfolded staircase functions of plates, Gomes and Gerges (93). Plot (a): Square geometry. Plot (b): Sinai geometry.

Some researchers uphold that the reasons for the discrepancies are the presence of the periodic orbits: Bertelsen (90), Schaadt (69), Deland *et al* (95), Gräf *et al* (96) and Wright & Ham (97). They have been shown that the effects resulting from the presence of periodic orbits modify strongly the spectral statistics. Therefore, further investigations are also necessary in order to evaluate the effects of the periodic orbits on the eigenvalue statistical observable results for random dynamical systems, (98, 99, 100).

2.2.4 Eigenvalue Statistics

In this section, the best known *statistical observables* associated with eigenvalues from Gaussian ensembles are introduced. In the RMT context, the *statistical observables* are defined as particular functions (metrics) which are able to describe the statistical characteristics of a spectrum, Guhr *et al* (57, 63) and Brody *et al* (56). Asymptotic analytical formulations are available for the spectral eigenvalue statistics of random matrices with well-established statistical characteristics, such as Poisson and Gaussian Ensemble statistics.

The analytical formulations for eigenvalue statistical observables will be introduced for short and long-range spectral fluctuations. These are based on eigenvalues normalized by the unfolding process, that is, the mean spacing of adjacent eigenvalues must be unitary and frequency-constant, Mehta (24). It is important to emphasize that under these conditions, it is possible to compare spectral natural frequency statistics from systems with different natures as well as with different modal densities, Gomes *et al* (101, 93) and Bertelsen *et al* (90, 66).

PDF of Adjacent Eigenvalue Spacings

One of the best known statistical observables is the *Probability Density Function of adjacent eigenvalue spacings*, $P(s)$. This function is traditionally used to evaluate the local characteristics of a spectrum (*i.e.*, the short-range fluctuation statistics). In the Quantum Physics field, this statistical observable is also known as the *Nearest Neighbor Spacing Distribution (NNSD)*, Mehta (24), Brody *et al* (56), and Bertelsen (90). Further details on the statistical properties of PDF are described in Soong (102) and Montgomery & Runger (103).

In the Quantum Physics context, there are two best known classes of statistical behaviors: *integrable* (or *regular*) and *chaotic*. The first class is associated with the group of systems in which the eigenproblems can be solved

analytically. These systems are usually denominated *regular* or *integrable systems*, Schaadt (69).

In the vibroacoustic field, the regular systems are generally associated with systems with simple geometry characteristics. A simply supported rectangular plate or a box-shaped acoustic space represent typical examples of regular systems, Lyon (48) and Langley and Cotoni (35). The spectral natural frequency statistics of the integrable systems conforms very well with the *Poisson distribution model* (also called the *random number statistics*, Soong (102)). The PDF of adjacent eigenvalue spacings for the Poisson distribution model, $P^{(Poisson)}(s)$, is given by:

$$P^{(Poisson)}(s) = e^{-s}, \tag{2.5}$$

where $s_i = z_{i+1} - z_i$ is the distance between adjacent unfolded natural frequencies. According to Equation (2.5), the spacing distribution of the Poisson model statistics is described by an *Exponential PDF*.

On the other hand, there is a second best known class of systems which is denominated *chaotic systems*. In the classical context, the chaotic systems are systems whose trajectories are unstable with respect to the initial conditions, that is, the distance between two particles inside of a *billiard*[3] scatter in an exponential way over time, Bohigas *et al* (67). In the vibroacoustic context, the chaotic systems are commonly associated with systems in which the acoustic waveguides propagate in a very disordered way within the system. For a spectrum of a chaotic system, the unfolded natural frequency statistics can be adequately described by eigenvalue statistics from a *GOE matrix*. According to Brody *et al* (56), the spacing PDF for chaotic systems is given by:

$$P^{(GOE)}(s) = \frac{\pi}{2} s \exp\left(-\frac{\pi}{4} s^2\right). \tag{2.6}$$

According to Equation (2.6), the spacing distribution of the GOE statistics is described by a *Rayleigh* PDF, Montgomery and Runger (103). This distribution is also known as the *Wigner surmise* in the Quantum Physics field, since Wigner proposed it in 1957, Bohigas *et al* (67). In Figure 16, the PDFs of adjacent eigenvalue spacings for Poisson (Exponential) and Wigner (Rayleigh) model statistics are shown.

[3] A *classical billiard* consists of a point particle which moves freely in a compact domain of d - dimensional space and reflects elastically in the boundary of this domain, Guhr *et al* (57, 63).

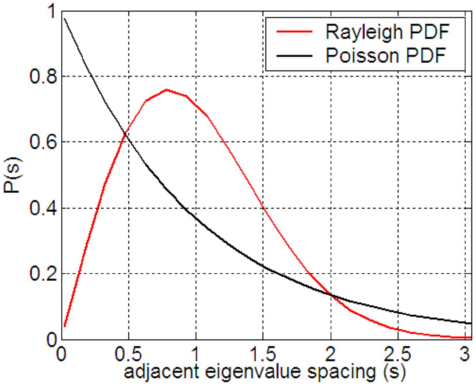

Figure 16: The PDFs of adjacent eigenvalue spacings for Poisson (Exponential) and Wigner (Rayleigh) model statistics

As shown in Figure 16, the most relevant difference between the Poisson and Rayleigh PDFs is noted for a small eigenvalue spacing range. For the Poisson PDF, there is a large probability for the occurrence of small eigenvalue spacings, that is, a strong tendency toward eigenvalue clustering is observed. On the other hand, for the Rayleigh PDF there is a small probability for the occurrence of small eigenvalue spacings. This veering phenomenon is traditionally known as *level repulsion* in the Quantum Physics field; Mehta (24), Brody *et al* (56), Guhr *et al* (57, 63), and Stöckmann (104). The *level repulsion phenomenon* is characterized by a strong tendency for the eigenvalues to repel each other, avoiding clustering. Therefore, a low probability is expected for the occurrence of small eigenvalue spacings. It is very important to emphasize that the Rayleigh distribution is also characterized by a low probability for the occurrence of large eigenvalue spacings. These properties of the Rayleigh PDF are associated with high *spectral rigidity* characteristics of the eigenvalues of the GOE matrices, Bohigas *et al* (67).

Correlation Functions

The PDF of adjacent natural frequency spacings is one of the most important statistical observables in RMT, but great practical interest is traditionally directed toward *correlation functions* associated with two eigenvalue interactions which is also known as the *two-level correlation function*, $R_2(\lambda_1,\lambda_2)$, Mehta (24), Brody *et al* (56), Guhr *et al* (57, 63) Langley (23), and Cordioli (20). According to Cordioli (20), this function may be interpreted as the probability of at least two eigenvalues have been found in small distinct regions $d\lambda$ around λ_1 and λ_2 respectively, independent of the presence of other eigenvalues outside these regions. The two-level correlation function is given by (20):

$$R_2(\lambda_1,\lambda_2) = R_2(\lambda_1-\lambda_2) = R_2(\Delta\lambda) = 1 - Y_2(\Delta\lambda), \tag{2.7}$$

where $Y_2(\Delta\lambda)$ is the *two-level cluster function*, Stöckmann (104). It can be noted that the two - level correlation function is dependent only on the eigenvalue difference, that is, it is a *translation invariant* through the spectrum, Cordioli (20) and Guhr *et al* (57, 63).

For the Poisson case, correlations between eigenvalues are absent. This reflects the fact that the $k-$level correlation function involves only one-level correlation functions and is given by (57, 63):

$$R_k(\lambda_1,\lambda_2,\ldots,\lambda_k) = \frac{N!}{(N-k)!}\prod_1^k R_1(\lambda_k) = 1. \tag{2.8}$$

In Equation (2.8), the correlation functions are unitary for all eigenvalues in the Poisson case. Thus, the two-level cluster function, $Y_2(\Delta\lambda)$, acceptably measures the deviation from the uncorrelated Poisson case, Guhr *et al* (57, 63). An analytical evaluation of the two-level cluster for the GOE case was proposed by Stöckmann (104) and it is given by:

$$Y_2(\Delta\lambda) = \left[\frac{\sin(\pi\Delta\lambda)}{\pi\Delta\lambda}\right]^2 + \left[\frac{\pi}{2}\mathrm{sgn}(\Delta\lambda) - \mathrm{Si}(\Delta\lambda)\right]\left[\frac{\cos(\pi\Delta\lambda)}{\pi\Delta\lambda} - \frac{\sin(\pi\Delta\lambda)}{(\pi\Delta\lambda)^2}\right], \tag{2.9}$$

where the $\mathrm{sgn}(\triangle\lambda)$ function is given by:

$$\mathrm{sgn}(\Delta\lambda) = \begin{cases} 1 & \text{if} \quad \Delta\lambda > 0 \\ 0 & \text{if} \quad \Delta\lambda = 0 \\ -1 & \text{if} \quad \Delta\lambda < 0 \end{cases}, \tag{2.10}$$

and the $\mathrm{Si}(x)$ function is given by:

$$\mathrm{Si}(x) = \int_0^x \frac{\sin(t)}{t}\, dt. \tag{2.11}$$

It is important to emphasize that the two-level cluster function is used in the analytical prediction of the revised SEA variance, Brown and Langley (18, 1, 3).

According to Guhr *et al* (57, 63), the eigenvalue spacing PDF for GOE model can be approximated by the two - level correlation function for small spectral distances:

$$R_2^{(GOE)}(\Delta\lambda) \approx P^{GOE}(\Delta\lambda). \tag{2.12}$$

On other hand, for a large range of the eigenvalue spacings, the two-level correlation function, $R_2^{(GOE)}(\Delta\lambda)$, saturates to unitary amplitude and Rayleigh PDF, $P^{GOE}(\Delta\lambda)$, tends asymptotically to zero. According to Guhr *et al* (57, 63), the two-level correlation function may be interpreted as a joint probability density function with the additional requirement that the two levels considered are adjacent, *i.e.,* there are no levels between them. Thus, although the adjacent eigenvalue spacing distribution mathematically involves all level correlations, it gives, in practice, meaningful information only regarding the two-level correlation.

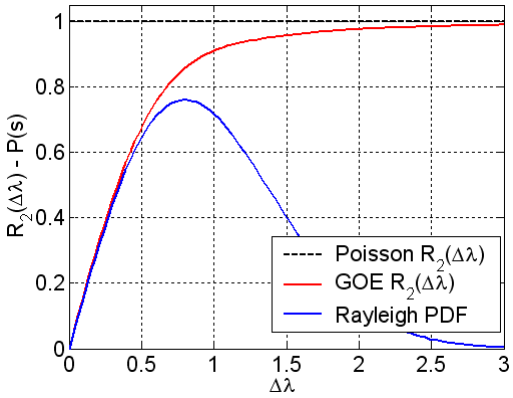

Figure 17: The GOE two-level correlation function and Rayleigh PDF for adjacent unfolded eigenvalues, Guhr *et al* (57, 63).

In order to evaluate the global statistics of a spectrum, the statistical observables for long-range fluctuations are recommended, Brody *et al* (56). In what follows, the best known statistical observables employed for the evaluation of long-range fluctuation characteristics will be defined.

Number Variance

By definition, the expected average number of eigenvalues in an interval of length L in an unfolded spectrum is L, Weaver (64) and Guhr *et al* (57, 63). According to Weaver (64), the *number variance*, $\Sigma^2(L)$, refers to the expected mean-square fluctuation of the eigenvalues lying in a range of L mean spacings. In the RMT context, the *number variance* is defined by (68):

$$\Sigma^2(L) \equiv \left\langle \widetilde{N}^2(L,Z_0) \right\rangle_{Z_0} - \left\langle \widetilde{N}(L,Z_0) \right\rangle_{Z_0}^2, \tag{2.13}$$

where $\widetilde{N}(L,Z_0)$ is the number of eigenvalues that lie within the interval $[Z_0, Z_0+L]$ and the angular brackets describe the averaging process over all possible starting points Z_0.

According to Andersen (68), the number variance is a measure of the long-range fluctuation statistics and it can be related to the two-level cluster

function, $Y_2(r)$, by the relation:

$$\Sigma^2(L) = L - 2\int_0^L (L-r)\,Y_2(r)\,dr. \tag{2.14}$$

For large spectral lengths, $L \gtrsim 2$, Andersen (68) shows that the number variance associated with GOE statistics is analytically given by:

$$\Sigma^2(L) = \frac{2}{\pi^2}\left[\ln(L) + \ln(2\pi) + \gamma + 1 - \frac{\pi}{8}\right], \tag{2.15}$$

where $\gamma = 0.5772$ is the Euler constant.

For Poisson statistics, the two-level cluster function is null due to the absence of eigenvalue correlations, Guhr *et al* (57, 63). Then, the number variance for Poisson statistics is given by (68):

$$\Sigma^2(L) = L. \tag{2.16}$$

In Figure 18, examples of number variance functions are shown for GOE and Poisson eigenvalue statistics.

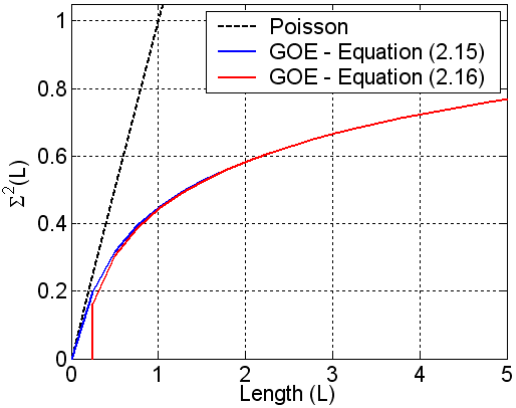

Figure 18: Number variance: GOE and Poisson eigenvalue statistics, Gomes and Gerges (101).

A periodicly spaced array of eigenvalues would have the number va-

riance $\Sigma^2(L) = 0$ for all integer L, Weaver (64). Thus, the establishment of small number variance values means that there is a small deviation from periodicity, that is, the spectrum has *high spectral rigidity* characteristics.

Δ_3 - *statistics*

The *spectral rigidity* or Δ_3- *statistics* is one of most popular measures of spectral rigidity characteristics and long-range fluctuation in the RMT context, Mehta (24) and Guhr *et al.* (57, 63). Here, Δ_3 - *statistics* is defined as the least-square deviation of the unfolded staircase function from its best fitted straight line and is given by (90, 64):

$$\Delta_3(Z_0, L) = \frac{1}{L} min_{A,B} \int_0^L \left[\widetilde{N}(z) - Az - B\right]^2 dz, \tag{2.17}$$

where A and B are the particular line coefficients associated with the best straight line fit for each interval $[Z_0, Z_0 + L]$.

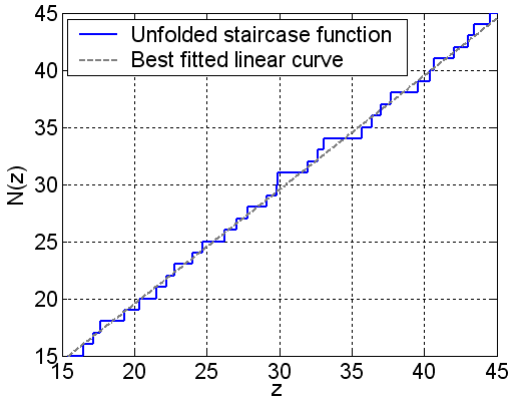

Figure 19: Example of the evaluation process of Δ_3- statistics, Gomes and Gerges (93).

According to Bertelsen (90), the mean value can be evaluated over possible points Z_0 by considering many non overlapping intervals of length L, and computing the $\Delta_3(Z_0, L)$ for each interval. Therefore, the $\Delta_3(L)$ is now

defined as this averaged value over all possible starting points and is given by (90):

$$\Delta_3(L) = \frac{1}{L} min_{A,B} \left\langle \int_0^L \left[\widetilde{N}(z) - Az - B \right]^2 dz \right\rangle_{Z_0}, \tag{2.18}$$

where the angular brackets indicate an averaging process over starting points Z_0.

The ensemble-averaged Δ_3- statistics can be related to the two-level cluster function using the following expression (68):

$$\Delta_3(L) = \frac{L}{15} - \frac{1}{15L^4} \int_0^L (L-x)^3 \left(2L^2 - 9Lx - 3x^2\right) Y_2(x)\, dx. \tag{2.19}$$

For $L \gtrsim 10$, it is expected that the GOE eigenvalues show a logarithmic behavior, Weaver (64). According to Andersen (68), an asymptotic prediction for large spectral distances (or long-range fluctuations) is given by:

$$\Delta_3(L) = \frac{1}{\pi^2} \left[\ln(L) + \ln(2\pi) + \gamma - \frac{5}{4} - \frac{\pi^2}{8} \right], \tag{2.20}$$

where $\gamma \approx 0.5772$ is the constant of Euler.

For a sequence of uncorrelated eigenvalues as in Poisson statistics, the two-level cluster function is null for all eigenvalue spacings and the resultant Δ_3 - statistics can be express by (68):

$$\Delta_3(L) = \frac{L}{15}. \tag{2.21}$$

In Figure 20, examples of Δ_3-statistics results are shown for GOE and Poisson eigenvalues. The logarithmic and linear behaviors can be easily noted throughout the spectra, respectively.

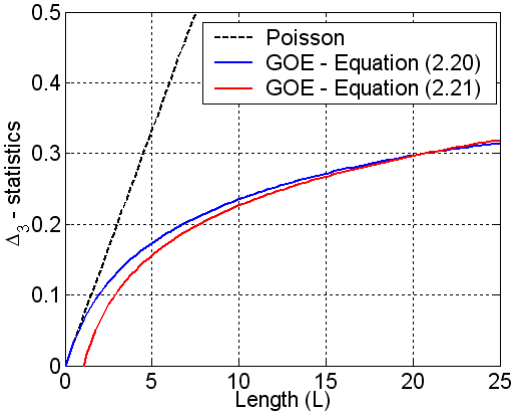

Figure 20: Δ_3 - statistics: GOE and Poisson eigenvalue spectra, Gomes and Gerges (101).

Although not discussed here in detail, the presence of system symmetries is a relevant factor in the resultant dynamical behavior of a system, Cordioli (20). The breaking of the system symmetries leads to very strong effects on the spectrum and an analysis of these effects aids the physical understanding of existent interactions among the natural frequencies.

As discussed in Physiscs literature (64, 90, 69), the spectrum of a system can be understood as superposition of independent spectra. Indeed, it is believed that the number of independent spectra needed to describe the spectral natural frequency statistics of a given system is associated with the number of symmetries in this system (90, 69) or is associated with the number of uncoupled substructures of systems which do not interact with the others (64).

According to Weaver (64), the superposition of independent spectra leads to a decrease in the spectral rigidity characteristics, that is, an increase in the Δ_3- statistics values. In Appendix A the analytical predictions are shown for the eigenvalue statistical observables of a spectrum composed of several independent GOE eigenvalue sequences.

2.2.5 Universality

The Universality concept was initially associated with Bohigas' work which investigated experimentally a microwave cavity with Sinai geometry, Bohigas *et al* (67). In his work, the results suggested that the statistics of spectral fluctuations from the chaotic systems can be correctly described by the statistics of the eigenvalues of the Gaussian Orthogonal Ensemble (GOE). Since that time, Random Matrix Theory (RMT) has been become a powerful tool for the statistical analysis of the spectral properties of chaotic systems. A relevant characteristic of chaotic systems is that their eigenvalue statistics show *universal statistics* provided that the spectrum of the original system is correctly unfolded. In other words, the resultant spectrum from the unfolding process must have a unitary mean spacing, Mehta (24).

In the RMT context, the *Bohigas-Giannoni-Schmit* (BGS) conjecture states that: *Spectra of systems whose classical analogues are fully chaotic show correlation properties as modeled by the Gaussian ensembles*, Bohigas *et al* (67). On the other hand, the *Berry-Tabor* (BT) conjecture is complementary and states: *Spectra of systems whose classical analogues are fully regular show correlation properties which are often those of the Poisson type*, Guhr *et al* (57, 63). Several research works A general statement of the principle of *Universality* would be to claim that, for large matrices, apart from well defined exceptions, all symmetric random matrices should have local GOE eigenvalue statistics, all Hermitian random matrices should have local GUE eigenvalue statistics, and all quaternion-real self-dual matrices should have local GSE eigenvalue statistics, Langley (23).

Although the RMT was initially developed to describe the nuclear spectra statistics, it is expected that the RMT concepts are global and applicable to systems of several natures: quantum billiard systems (92), microwave cavities (105), metal blocks (64), membranes (106), elastic plates (66), financial correlations (107), and others. For all of these above-mentioned fields, excellent agreements are observed between the RMT analytical predictions and eigenvalue statistics. However, it is also very important to emphasize that there is a relevant limitation to extending the use of RMT concepts to systems of several natures. Pandey (108) showed analytically that the Universality concept is restricted only in a *local* sense, that is, it is valid only for a set of adjacent eigenvalues with almost constant mean spacing. For a set of eigenvalues where the spacings are larger than the mean spacing, the fluctuations are not universal and are dependent on the particular system analyzed (*system-dependent effects*). In these cases, the spectral statistics may not be

correctly described by RMT analytical predictions, Langley (23).

Several results from studies on uncertain or non-deterministic vibroacoustic systems have suggested that the statistics of the natural frequencies may be adequately described by the GOE model provided that there is a sufficiently large amount of randomness in the system parameters, Langley *et al* (23, 4, 18). Recently, analytical and numerical investigations have been carrying out in order to highlight the conditions required for the occurrence of Universality for the modal parameter statistics of vibroacoustic systems: Langley (23), Cordioli (20), etc.

2.2.6 Analogies: Quantum and Vibroacoustic Systems

In principle, it is believed that all RMT concepts from the Quantum Chaos field can be adequately applied to classical wave vibroacoustic systems, since the RMT assumptions are very general and do not include any quantum mechanical arguments, Schaadt (69).

In recent decades, several researchers have carried out experimental activities with systems of distinct natures and their spectral natural frequency statistics have been successfully comparing to RMT predictions(105, 64, 66). However, it is important to emphasize that there is no analytical proof to ensure that the random dynamical systems are completely described by RMT, (64) (66) (109). In general, it is recommended that all *system-dependent effects* be removed from the original spectrum in order to compare the spectral statistics of the random engineering systems with the universal RMT statistics. Inspired by the success of experimental studies, complementary theoretical work was performed to describe the main analogies between the quantum mechanical and vibroacoustic systems. Several evidences confirm this attractive possibility, (92, 105, 106). On the other hand, there are some particular characteristics which can become very complex the direct use of this quantum-vibroacoustic analogy, (64) (69) (110)(70)(95). In the present study, these details will be presented and discussed for random dynamical systems in the context of SEA variance theory. In order to highlight the analogies between the quantum and vibroacoustic phenomena, the well-established similarities are shown in Table 3.

Table 3: Analogies between the Quantum and Vibroacoustic systems, Bertelsen (90) and Schaadt (70).

Quantum system	Vibroacoustic system
Quantum mechanics	Theory of elasticity
Schrödinger equation	Acoustic wave equation
Energy levels	Natural frequencies
Eigenfunctions	Mode shapes or Standing waves
Semi-classical limit	Acoustic ray theory
Ray splitting	Modal conversion

One of pioneering application of RMT models to systems with natures distinct to those of nuclear and quantum systems was carried out by Weaver (64). In his work, the aluminum rectangular blocks were perturbed by drills (slits) on their faces in different ways in order to break the system symmetries. The natural frequencies from each one of the blocks with different degrees of symmetry were measured and their corresponding unfolded spectra were also evaluated. The eigenvalue statistical observable results were determined and compared with analytical predictions from GOE and 2 GOE spectra. The results showed that the natural frequency statistics of the most perturbed block, which has all symmetries broken, presents a *universal* behavior adequately described by the GOE model. For less perturbed block, one reflection symmetry was retained and their spectral natural frequency statistics were in good agreement with the 2 GOE model predictions.

Bertelsen *et al* (90, 66) investigated experimentally the spectral natural frequency statistics of free plates with a shape of the quarter Sinai Stadium billiard (chaotic billiard shape). For the plates investigated, two type waves were considered: transverse (symmetric and antisymmetric) and in-plane waves. The statistical observable results displayed 2 GOE statistics (*i.e.*, one GOE spectrum for each type of wave), since for the experimental range of natural frequencies investigated, both waves types contribute to the same extent. In order to confirm this conclusion, two cuts were made in one plate face to break the symmetry in the up-down or thickness direction, where flexural and in-plane modes are strongly coupled. The resultant statistical observable results displayed GOE statistics due to the occurrence of coupling between the two wave types.

Fujisaka and Tohyama (94) investigated numerically acoustic fields

surrounded by 2D-semi-stadium-type boundaries, as examples of boundaries where chaotic properties are hidden, in order to understand the spectral characteristics of complex sound fields and to gain new insight into sound field design. Several geometries were parametrically investigated, from regular to completely chaotic. Through the statistical observable results, the natural frequency statistics, including the mode shapes, were described. The statistical characteristics from the modal parameters in the Poisson-GOE crossover region were demonstrated, and an excellent agreement was observed for the extreme limit statistical cases.

Weaver, Stöckmann and Kuhl published an excellent review paper (111), describing the technical and analytical details regarding the transport properties of classical waves through chaotic systems with special emphasis on microwaves and sound waves.

Based on the successful results obtained from the initial parametric study performed by Bertelsen (90) with a 1/4 Sinai stadium plate, Schaadt (110, 70) investigated the parametric variation of the natural frequencies when a chaotic plate is subjected to a perturbation via an external parameter. In his study, the size of the plate was adopted as the external parameter. The normalized correlation metrics associated with the first and second derivatives as a function of the external parameter were evaluated and the dynamics of the natural frequencies from a chaotic plate was accurately characterized. The experimental results were compared to RMT numerical results for large random matrices presented in the physics literature, Li and Robnik (112). An excellent agreement was observed for both derivative metrics, suggesting that the RMT correlation results can be extended to wave systems other than quantum systems.

As observed here, excellent results can be obtained with the application of the quantum-vibroacoustic analogy to practical engineering situations where the natural frequency statistics of sufficiently random engineering systems may be adequately described by the GOE model of RMT. However, most random vibroacoustic systems do not have the conditions necessary for a direct comparison between the quantum mechanics and vibroacoustics results, Bertelsen (90). A good example of a direct application of the quantum-vibroacoustic analogy may be expected in the *Geometric Acoustic Ray* field where the acoustic wavelengths tend to reach the semi-classical limit, Deland *et al* (95) and Schaadt (70).

In what follows, the main effects provided by some system-dependent phenomena, such as *finite wavelengths* (113) and *periodic orbits* (95) and others (69, 70), are discussed with regard to the establishment of the semi-

classical limit in vibroacoustic systems.

2.2.7 Finite Wavelength Effects

Within the analogy with RMT applied to dynamics, GOE statistics are expected when the classical limit (here geometrical acoustics limit) exhibits chaotic[4]behavior, (113). The *geometrical acoustics limit* corresponds to the deterministic motion of a point-like particle propagating in straight lines inside the system and being specular reflecting at the system boundaries, Bohigas *et al* (113). In other words, the geometrical acoustics limit corresponds to the lower cut-off frequency in which the geometrical ray approach is valid.

Considering again Weaver's results (64), slits on the faces of rectangular aluminum blocks were made to break the system symmetry. A good agreement was observed between the spectral statistics of the natural frequencies and GOE model predictions, although the classical geometrical ray acoustics trajectories are not chaotic. According to Bohigas *et al* (113), the perturbed block systems used by Weaver belong to the class of pseudointegrable systems that are both regular (integrable) but non-separable in orthogonal variables.

As discussed by Bohigas *et al* (113), a possible explanation for the good agreement of Weaver's results arises from the comparative analysis of the scale magnitude of the acoustic wavelength and the characteristic size of the system. For the frequency range considered, the corresponding wavelengths are typically of the order of centimeters and are much larger than typical dimensions of slits cut in the block faces for which the scale is of the order of millimeters. As a consequence, the typical acoustic wave inside the block can not distinguish a thin straight split from a wider split with a spherical tip. Although the spherical tip has a diameter of the order of the wavelength, it acts as a strong focusing element and ensures the existence of *deterministic chaos*. That is, this geometrical perturbation at the boundaries of the order of the wavelength results in focusing or defocusing effects which also lead to a very rapid divergence of trajectories initially separated by a distance of the order of the wavelength.

In summary, based on the above discussion, the following behavior is expected for a random engineering system along the frequency domain. For the natural frequencies where the wavelengths approximately match the

[4]In the classic context, chaotic systems are systems whose ray trajectories are unstable with respect to the initial conditions, that is, the distance between two particles inside a billiard scatters in an exponential way over time, covering the entire surface of the system due to scattering at the boundaries, Bohigas *et al* (67).

dimensions of the focusing or defocusing boundaries present in the system, the classical motion may be expected to have a chaotic behavior described by the GOE statistics model.

According to Bohigas *et al* (113), for the much higher frequencies, other physical parameters beyond boundary perturbation, such as surface roughness and material heterogeneity, can no longer be neglected and the corresponding wavelength becomes similar in size to the scale of the material imperfections, a regular motion in the geometrical acoustic limit must be recovered and the spectral natural frequency statistics become Poissonian.

In the low-frequency range, where the wavelengths are longer than the focusing or defocusing boundary spans, the acoustic waves can not resolve the geometrical perturbations and thus it may be that the low natural frequencies are not strongly coupled each other, leading to *non-universal* effects on the modal parameter statistics, Schaadt (69). In the Quantum Physics literature (69, 113), these classes of nonuniversal behaviors are traditionally denominated *finite wavelength effects*. Therefore, an efficient quantification of these effects on the modal parameter statistics is essential in order to extend the analogy of random matrix theory to engineering applications in the vibroacoustics field, Gomes (10).

In Appendix B, the finite wavelength effects are numerically investigated using GOE random matrices with several dimensions. The main effects are investigated on the Δ_3 - statistics results. Additionally, the expected fluctuations along the spectral domain and across the ensemble are determined and compared to analytical predictions available in RMT literature, Bohigas *et al.* (114). The numerical analysis shown that large fluctuations in the Δ_3 - statistics results across the ensemble are expected for random matrices with small dimensions.

2.2.8 Effects of Periodic Orbits

Considering the context of Ray Acoustics, *periodic orbits* are defined as ray paths in an acoustic system that return to their starting position with the same direction of motion. The establishment of periodic orbit effects can lead to significant changes in the spectral statistics of natural frequencies as well as in the statistical characteristics of the corresponding mode shapes.

According to C. Ham (115), the periodic orbits are classified into three major classes: stable, unstable or marginally stable. A periodic orbit is *stable* if each ray on it belongs to some interval such that every orbit starting from an arbitrary point in the interval converges to the periodic orbit. A periodic

orbit is *unstable* if each ray on it belongs to some interval such that every orbit starting from an arbitrary point in the interval diverges from the periodic orbit. A periodic orbit is *marginally stable* if each ray on it belongs to some interval such that every orbit starting from an arbitrary point in the interval neither converges to or diverges from the periodic orbit.

In the *quantum chaology*[5] field, periodic orbits have been used as a semiclassical tool in the statistical analysis of billiard systems, (92, 96, 95, 97, 115). Stable periodic orbits can be identified through the application of Fourier transform on the unfolded staircase function fluctuations considering the wavenumber as an independent variable, Delande *et al* (95). In Figure 21, an example of the results from the Fourier transform of the staircase function fluctuations of a rectangular Sinai microwave cavity is presented. The peaks of the Fast Fourier Transform correspond to the lengths of the most relevant periodic orbits, Stöckmann and Stein (92).

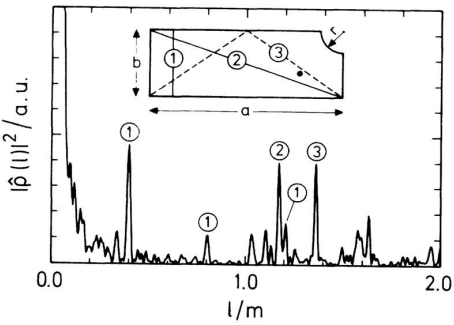

Figure 21: Example of Fourier transform of staircase function fluctuations of a rectangular Sinai ($a = 56\,cm$, $b = 20\,cm$ and $r = 7\,cm$). Inset Figure: identification of main periodic orbits, Stöckmann and Stein (92).

In the inset of the Figure 21, a typical example of the identification of periodic orbits through the Fourier transform of staircase function fluctuations is presented. The numbered peaks in the Fourier transform results are associated with periodic orbits. In particular, large contributions to spectral statistics are expected for *bouncing ball* orbits (orbit number 1 in inset).

[5] *Quantum chaology* is the study of how chaos in classical mechanics arises at the limit of quantum mechanics, Stöckmann (104).

The bouncing ball orbits are a special class of periodic orbits which propagate perpendicularly to two parallel system boundaries. As observed, the establishment of stable periodical orbits seems to be directly associated with the presence of system symmetries as well as the regularity of system geometry. Indeed, further systematical investigations are certainly necessary to highlight the exact relationship between the geometrical characteristics of a vibroacoustical system and the periodical orbit effects on the modal parameter statistics.

The main effects of the periodic orbits are directly observed in the oscillatory component of the natural frequency staircase function. In general, the fluctuations are large, corresponding to the deviation of several natural frequency spacing units from the average or smooth component of the staircase function, which is usually evaluated by polynomial functions or the Weyl formula. An illustrative example of fluctuations from the aluminum block, which are affected by the bouncing ball periodic orbit effects, is presented in Figure 22 (a), Schaadt (69).

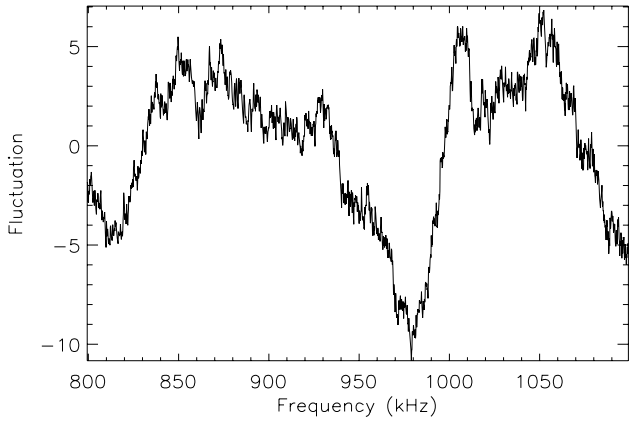

(a)

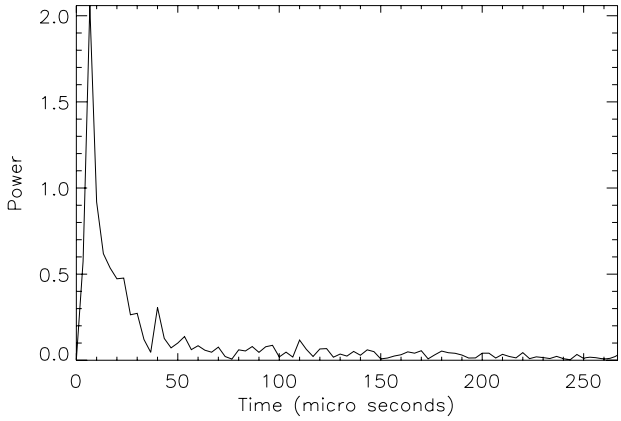

(b)

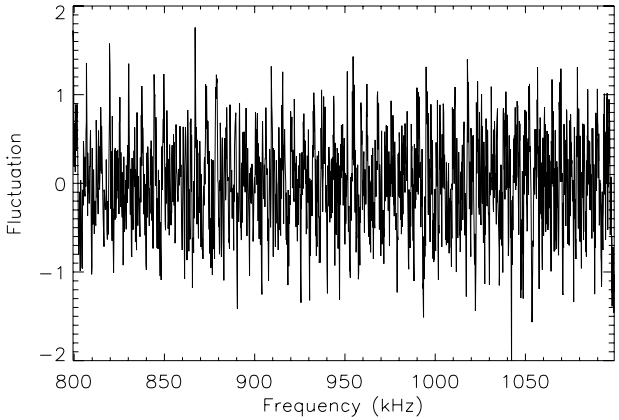

(c)

Figure 22: Periodic orbit effects on the spectral natural frequency statistics. Plot(a): fluctuations or oscillatory component of staircase function. Plot(b): Power spectrum from the FFT of the staircase function fluctuations. Plot(c): resultant fluctuations from Fourier unfolding process, Schaadt (69).

The identification of the periodic orbits and respective lengths is not a trivial task in the case of vibroacoustic systems. However, on performing the *Fast Fourier Transform* (FFT) of the fluctuations, their peaks on the power spectrum (with time or length on the x-axis) identify the dominant frequencies of the fluctuations, Schaadt (69) and Delande *et al* (95). Indeed, the peak locations on the power spectrum may be directly associated with stable periodic orbits which contribute significantly to the large scale oscillatory pattern of the staircase fluctuations, Figure 22 (b).

In order to quantify the periodic orbit contributions to the average or smooth staircase function component of stable periodic orbits and remove them from the staircase function, the *Inverse Fourier Transform* (IFT) is performed, including only those Fourier components that lie below some cut-off time, t_c. That is, all Fourier components above the cut-off time t_c are discard (set to zero), and one keeps only the Fourier components which are lower than t_c. In this new unfolding process, here referred to as the *Fourier unfolding process*, the effective average staircase function component is evaluated as the sum of the polynomial component and the inverse Fourier transform contributions. Note that the total procedure is similar to a *low-pass filter* applied to the staircase function fluctuations. In Figure 22 (c), the resultant fluctuations obtained from the Fourier unfolding process are presented for a certain cut-off frequency.

The choice of cut-off time is essential to obtaining a good performance of the Fourier unfolding process. According to Schaadt (69, 70), a short cut-off time will not take into account all of the significant contributions from the periodic orbits, and the resultant fluctuations will present nonuniversal characteristics. On the other hand, for an excessively long cut-off time, the universal characteristics are erroneously removed and a saturation point is expected beyond some spectral eigenvalue distance. Thus, the adopted value for the cut-off time must be selected so as to avoid the effects described above and simultaneously provide a resultant unfolded spectrum in which all of the *universal* characteristics are not affected by the unfolding process, (90, 69, 70).

Considering the results for the natural frequency statistical observables, the contributions of the periodic orbit effects on these results are expected to be gradually more pronounced only for large spectral distances. In Figure 23, illustrative examples of Δ_3-statistics results affected by the effects of the bouncing ball periodic orbits are presented. The Δ_3- statistics results based on the standard unfolded spectra are compared to results based on the Fourier unfolded spectrum in which the effects of periodic orbits are removed.

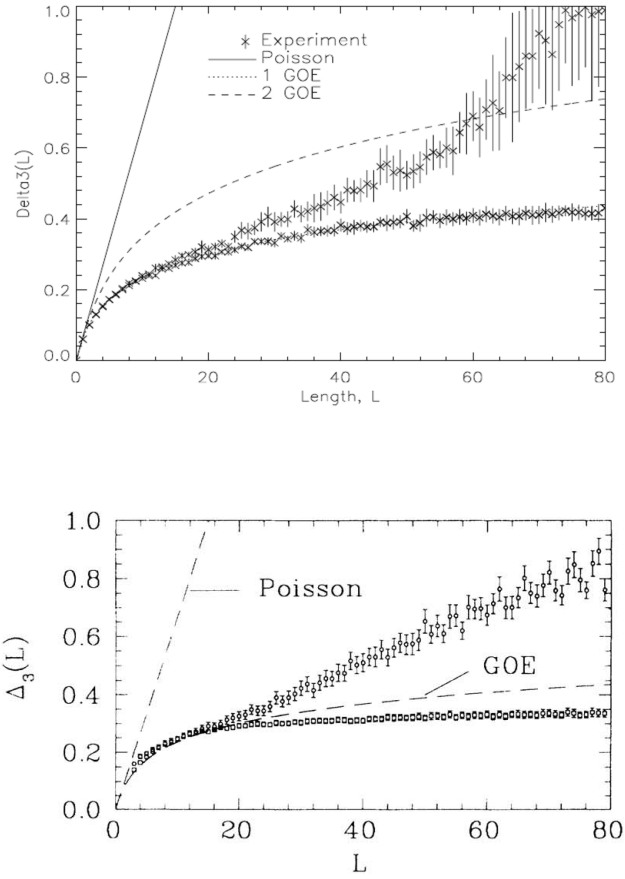

Figure 23: Examples of the effects of periodic orbits on the Δ_3 - statistics results. Upper Plot: Sinai block, Schaadt (69). Lower Plot: Microwave cavity resonator, Gräf *et al* (96).

As shown in Figure 23, the effects of the periodic orbits lead to a slightly higher increase in the Δ_3 - statistics than expected. Using the Fourier unfolding process appropriately, all such effects were totally removed and a good agreement with GOE statistics was observed, Figure 23 (a). However, when the time cut-off is too long the universal characteristics are removed in the resultant Fourier unfolded spectrum and the corresponding Δ_3 - statistics

curve saturates beyond a certain spectral distance, Figure 23 (b). Thus, it can be noted that the periodic orbit effects can not be removed without saturating the Δ_3 - statistics curve, Bertelsen (90).

An alternative approach to understanding natural frequency statistics was introduced by the Gutzwiller *trace formula*, (104, 116). In this semiclassical approximation, the oscillatory staircase function component can be described as a sum of all classical periodic orbits, (92, 96). Although the semiclassical approach is very attractive in the periodic orbit application field, its application to vibroacoustic systems is very limited for the following reasons: (*i*) a large number of periodic orbits is required to provide a good approximation of the staircase function, (*ii*) the accuracy of the results increases exponentially with the number of periodic orbits, and (*iii*) the characterization of the classical periodic orbits is very complex or at least prohibitive. Recently, the main limitations and performances of the extension of the semiclassical tools to vibroacoustic systems applications have been investigated in detail and their results support the interdisciplinary research field known as *Semiclassical Acoustics*, Wright and Howls (117).

2.3 Mode Shape Statistics

In this section the statistical properties of eigenvectors of large random matrices are presented and discussed in detail. The main eigenvector statistical observables are introduced along with the analytical predictions for GOE and sinusoidal eigenvectors. A complete statistical characterization is performed for mode shapes from chaotic and regular systems. Additionally, the main classes of mode shape statistics deviations from the GOE eigenvector statistics are identified and their effects on the mode shape statistical observables results are discussed and illustrated through results reported in the literature for microwave cavity systems.

Lastly, the effects of Localization phenomenon are discussed for quantum billiard and vibroacoustic systems. The performance of the applications of non-linear sigma models from the Supersymmetry theory to describe the characteristics of the mode shape statistics deviations from the GOE eigenvector statistics is discussed for weak and strong localization regimes.

2.3.1 Eigenvector Applications

In a vibroacoustic system, a vibration or acoustic mode is characterized by a natural (or modal) frequency and a mode shape (spatial interference pattern - standing wave), Ewins (118). The natural frequencies and mode shapes are characteristic of a particular structure and its boundary conditions, but are independent of the form of excitation, Fahy (5). If the system is placed exactly in one of its mode shape configurations and left to vibrate freely, it will present a harmonic motion and its vibrating frequency will be associated with a particular natural frequency corresponding to that mode shape. However, in practical situations, when a system vibrates freely or in a forced manner, assuming linear behavior, its total displacement will be a superposition of the mode shapes of the individual modes.

In engineering structures, an eigenproblem equation can be conveniently written and the undamped modal parameters, natural frequencies and corresponding mode shapes, can be easily determined. The natural angular frequencies ω_j and mode shapes ϕ_j of the system satisfy the following equation:

$$-\omega_j^2 \mathbf{M}\phi_i = \phi_j \mathbf{K}, \tag{2.22}$$

where $\mathbf{M}$ and $\mathbf{K}$ are the mass and stiffness matrices of system, respectively.

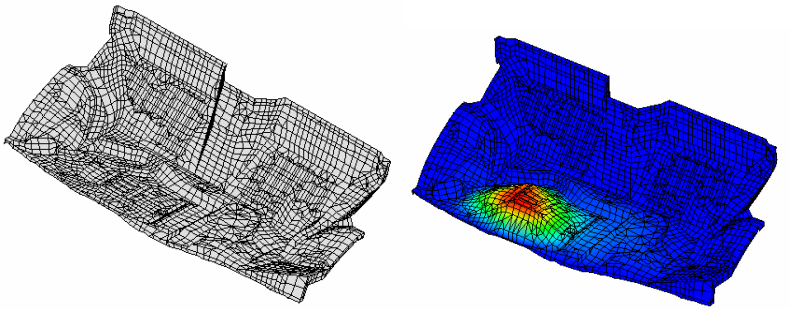

(a) (b)

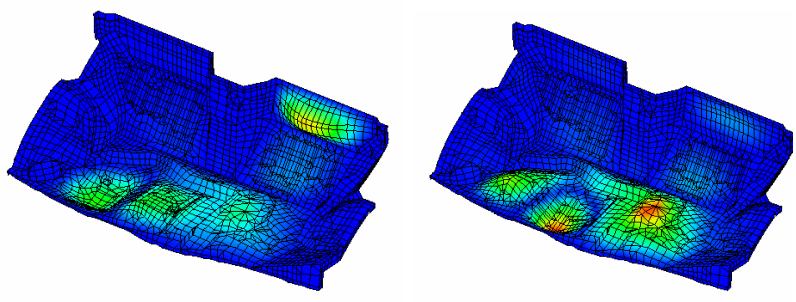

(c) (d)

Figure 24: Numerical modal analysis of an automotive dash panel using FEM models. Plot (a): structural FEM mesh model. Plots (b) - (d): Mode shapes corresponding to the following natural frequencies: 61.215 Hz, 101.088 Hz, and 114.507 Hz, respectively, Gomes (10).

Nowadays, the high processing capacity and storage characteristics of computers allow numerical methods to be employed in the dynamical analysis of engineering structures. One of these methods, the *Finite Element Method* (FEM) presents excellent versatility and performance for almost all practical applications, Zienkiewicz (2). In the case of relatively complex engineering structures, the mass and stiffness matrices can be satisfactorily evaluated through numerical methods, and the characteristic equation can be adequately established. In Figure 24, some mode shapes of a typical vehicle dash panel obtained in numerical modal analysis using FEM models are presented, Gomes (10).

In a complementary way to numerical models, there are well established experimental methods which allow the evaluation of mode shapes from a given vibroacoustic system. *Modal analysis*, or more accurately *experimental modal analysis*, is the field of measuring and analyzing the dynamic response of structures and or fluids when excited by an external input, Ewins (118). The modal testing and analysis methods seek to determine the modal parameters, such as natural frequencies, damping ratios and mode shapes, from the measured transfer functions, and then fit a damping matrix to these data. However, the experimental methods for the evaluation of modal parameters are traditionally restricted to low order modes.

In the Quantum Physics field, the *Hamiltonian* operator from the nuclear systems is modeled through large random matrices, Mehta (24). Addi-

tionally to the spectral statistics of energy levels (x_n) which are traditionally evaluated through the eigenvalue statistics from a large random matrix H, the statistics of the wave functions (u_n) can also be investigated considering the corresponding eigenvectors, Guhr *et al* (57, 63). The typical eigenproblem associated with a nuclear system is given by:

$$Hu_n = x_n u_n \,, n = 1, 2, \ldots, N. \tag{2.23}$$

where N is the size of Hamiltonian matrix H.

While the characteristics of the spectral statistics of the energy levels are well known for nuclear systems, only a small number of experimental investigations have been carried out regarding the statistical characteristics and properties of the corresponding wave functions. The main reason for this apparently low interest is associated with the lack of accessibility to wave functions in nuclear systems. In atoms and complex nuclei systems, the wave function characteristics are expressed through the indirect parameters as transition amplitudes and widths which also provide information on the matrix elements of a transition operator, Guhr *et al* (57, 63) and Brody *et al* (56). In order to overcome these experimental difficulties, the *quantum billiard systems*[6] with classically chaotic geometries have been used as convenient experimental models to represent chaotic nuclear systems, since their natural frequencies and corresponding mode shapes can be easily measured and their modal parameter statistics adequately compare to analytical predictions from the RMT.

The main experimental method used to evaluate the wave functions from the quantum billiard systems is the technique of *Microwave Cavity Perturbation*, developed by Kudrolli and Sridhar (105). In this experimental technique, a small metal bead (perturber) is introduced into the microwave cavity at coordinate (x,y). If the bead is sufficiently small compared to the wavelength, the resultant shift in the natural frequencies, Δf_n, due to the perturbation, is proportional to the square of the Electric field (hence, the wave function), at the location of the bead (x,y). By moving the bead with a magnet, the wave function can be mapped out. In overall, one of the main advantages of this method is the direct visualization of the eigenfunctions without inserting a probe into the cavity. The literature results form the quantum physics field has been shown excellent performance of this experimental method for a variety of microwave cavity geometries, including integrable, pseudo-

[6] A *billiard* is defined as a dynamical system in which a particle alternates between motion in a straight line and specular reflections from a boundary.

integrable, isospectral and chaotic, (72, 71, 105, 119, 120, 121).

Recently, the mode shape statistics have currently become a significant area of interest in the quantum physics field. The main topics of research associated with the wave function statistics of billiard systems in the quantum physics field are: physical interpretation of wave functions in terms of classical trajectories, including the *scar phenomena* predicted by Heller (122); transition of wave function statistics over a localization-delocalization regime in disordered systems (100, 74, 123, 73, 71), and other subjects (97, 115, 117).

It is also important to emphasize the increasing and substantial advances in the *semi-classical acoustics* research area in relation to modal parameter statistics, Wright and Howls (117). Semi-classical acoustics is a multidisciplinary research field which uses tools from the semi-classical theory of Quantum Physics such as *periodic orbit theory* (SPOT, WBKJ and EBK approximations) (97, 115) and the *Weyl series* (124) to address engineering problems in the vibroacoustics field. The mathematical details regarding the analogy between the Schrodinger and Helmohtz equations are beyond the scope of this current work and further information is available in (71, 105, 119, 120).

2.3.2 Eigenvector Statistical Observables

In this section, the statistical observables associated with the eigenvectors of large random matrices are defined and their performance in characterizing the eigenvector statistics are briefly discussed. The characteristics of the mode shape statistics of classically chaotic and integrable (or regular) systems are introduced and demonstrated through typical examples of eigenvector statistical observables results.

Porter-Thomas Distribution

The Porter-Thomas distribution, $P_{PT}(|\psi|^2)$, is the most traditional eigenvector statistical observable used to characterize the GOE eigenvector statistics in the RMT field. This metric function is defined as the probability density function of squared mode shape amplitudes[7] (normalized to have unit mean). For a system respecting time reversal invariance, Haake (116) demonstrated that for classically chaotic systems the Porter-Thomas distribu-

[7] In the Quantum Billiard context, the probability density function of squared mode shape amplitudes is also known as the *density distribution*, Sridhar (120).

tion[8] is a universal GOE eigenvector feature and is given by:

$$P_{PT}^{GOE}\left(|\psi|^2\right) = \frac{1}{\sqrt{2\pi|\psi|^2}} \exp\left(-\frac{|\psi|^2}{2}\right), \tag{2.24}$$

where $|\psi|^2$ is the normalized squared mode shape amplitude[9], which is defined as:

$$|\psi|^2 = \frac{\phi^2}{\langle\phi^2\rangle}, \tag{2.25}$$

where ϕ is the mass-normalized mode shape amplitude and angular bracket $\langle\,\rangle$ denotes the mean value from an averaging process over the eigenvector component domain (*i.e.* over the spatial domain of the system).

The Porter-Thomas analytical prediction proposed for GOE eigenvectors has been confirmed in several experimental studies on two dimensional chaotic microwave cavities (71, 74) and elastodynamical system plates (69, 93) as well as in numerical studies with large random matrices (79, 101).

A typical example of an experimental investigation on the distribution of normalized squared mode shape amplitudes of chaotic systems can be observed in Kudrolli *et al* (71). In their work, the normalized squared mode shape amplitudes, $|\psi|^2$, from two microwave cavities with Sinai Stadium and Billiard geometries were measured using the cavity perturbation technique, which considers that the Schrodinger and Helmholtz equations coincide. The distributions of normalized squared mode shape amplitudes of such microwave cavities were compared with the Porter-Thomas distribution predictions for GOE eigenvector statistics, Figure 25.

[8] Traditionally, this function is evaluated considering the spatial domain of system (*i.e.*, spatial averaging approach). Illustrative examples of its application for billiard systems are available in quantum physics literature, (71, 74, 69).

[9] For this normalization process, the scalar parameter $|\psi|^2$ can be understood as simplified notation of the *i-th* squared mode shape component of a mode shape normalized to have a unit mean, (71, 69).

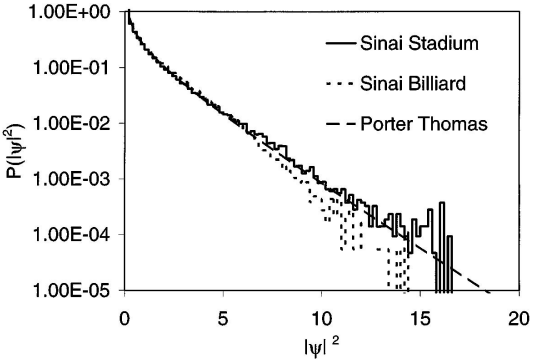

Figure 25: Examples of Porter-Thomas distribution: GOE prediction, Sinai Billiard, and Sinai Stadium measured results, Kudrolli *et al.* (71).

As shown in Figure 25, the GOE prediction for Porter-Thomas distribution shows that universal mode shapes present a finite, although exponentially vanishing, probability of finding large mode shape amplitudes. A good agreement is observed for the Sinai Stadium, while the Sinai Billiard results display slight deviations in the large mode shape amplitude range[10] due to the establishment of *non-universal* statistics associated with *bouncing-ball orbits*[11] (125, 72).

For integrable systems, the distribution of normalized squared mode shape amplitudes is often truncated at some finite value of $|\psi|^2$ and is not universal, Haake (116). In the case of a rectangular geometry, it is expected that a truncation point occurs approximately at $|\psi|^2 = 4$, Schaadt (69). In Figure 26, the flexural mode shapes of the rectangular quartz plate and their respective Porter-Thomas distribution results are presented, Schaadt (69).

For pseudo-integrable systems, their mode shapes have, simultaneously, the statistical characteristics of regular and chaotic systems. Overall, the non-universal mode shape characteristics are mainly established in the range of large mode shape amplitudes, where the Porter-Thomas distribution amplitudes of the large mode shape amplitude range are usually less than

[10]The main difference between these Sinai geometries is the existence of parallel sides for the Sinai billiard one which provide the establishment of stable periodical orbits of type *bouncing ball*, more details will be presented and discussed along the text.

[11]Further details regarding the effects of bouncing ball orbits on the mode shape statistics are presented in the section 2.2.8.

or greater than the universal expected amplitudes described by the GOE PT-distribution, (123, 74, 125, 72).

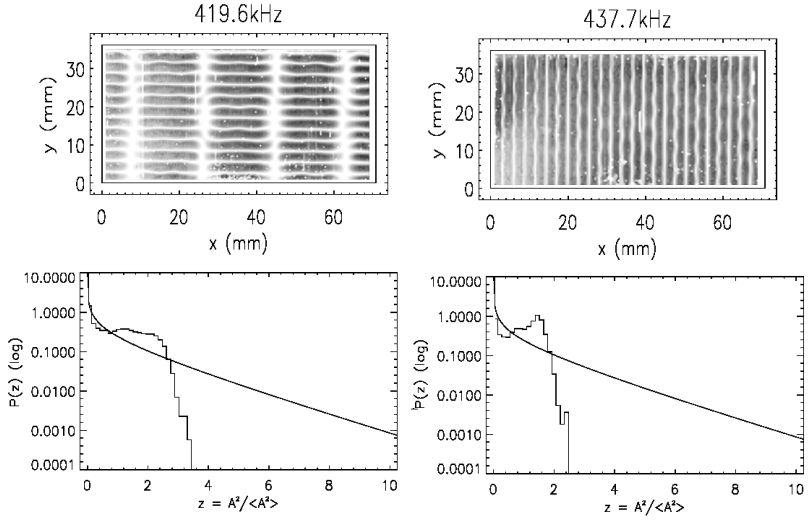

Figure 26: Examples of regular or integrable mode shapes and their PT- distributions from a rectangular plate of quartz, Schaadt (69). In these plots, the smooth and well-behaved function is the analytical formulation of PT-distribution for perfect GOE eigenvectors, Equation (2.24), and the results with step function-like format expresses the experimental measurements. Plot (a): Natural frequency of 419.6 kHz. Plot (b): Natural frequency of 437.7 kHz.

Spatial Distribution of the Mode Shape Components

Considering the spatial mode shape characteristics, the chaotic or GOE mode shapes are traditionally identified by the presence of disordered nodal line curves which have the orientations quite random inside the body, (126, 73, 127). In Figure 27, some examples of chaotic or GOE mode shapes are presented.

For classically chaotic systems as well as large symmetric random matrices, such as perfect GOE matrices, the mode shapes (or eigenvectors) are expected to be *Gaussian distributed*, that is, a normal distribution for their eigenvector (mode shape) components is established over the mode shape (or eigenvector) component domain, (71, 90, 69, 128). Indeed, a Gaussian mode shape component can be understood as being a random superposition of real plane waves reflected from the boundaries (or discontinuities) of the system, Lobiks *et al* (50). If the system boundaries or irregularities are sufficiently to scatter the waveguides in several directions, the central limit theorem will be applicable. This theorem states that the sum of a large number of random variables tends asymptotically to present Gaussian distribution characteristics, provided that the random variables are independent or identically distributed, Conover (129).

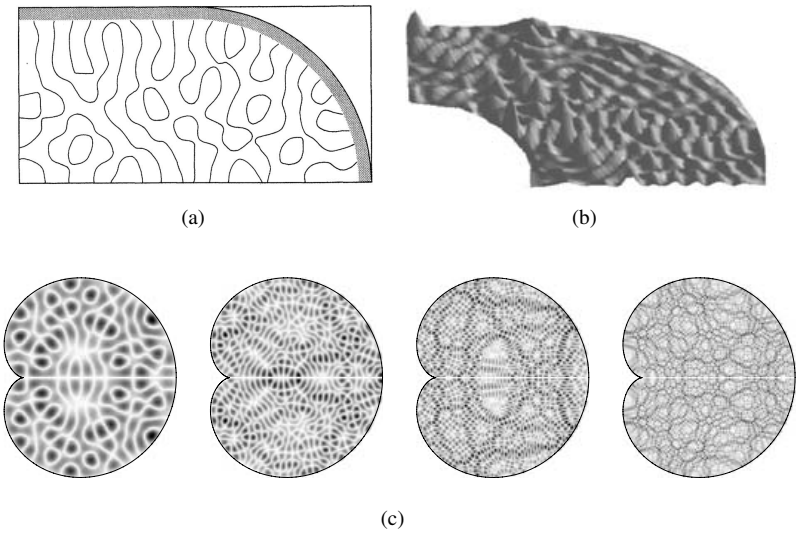

Figure 27: Typical examples of GOE mode shapes of chaotic billiards. Plot (a): Sinai stadium geometry, McDonald and Kaufman (126). Plot (b): 1/4 Sinai geometry, Pradhan and Sridhar (73). Plot (c): cardioid geometry, Backer (127).

Waterhouse (130) proposed analytical expressions for the spatial PDF

(with the sample space taken to be the area of the system) of sinusoidal mode shapes for one, two, and three-dimensional systems, and these expressions are given by, respectively:

$$P_{1D}(\phi) = \frac{2}{\pi}\left(1-\phi^2\right)^{-\frac{1}{2}}, \text{if } -1 \leq \phi \leq 1, \tag{2.26}$$

$$P_{2D}(\phi) = \frac{4}{\pi^2} K_{el}^1\left(1-\phi^2\right), \text{if } -1 \leq \phi \leq 1, \tag{2.27}$$

$$P_{3D}(\phi) = \frac{8}{\pi^3}\int_{\phi}^{1} \frac{K_{el}^1\left(1-\phi^2\right)}{\left(u^2-\phi^2\right)} du, \text{if } -1 \leq \phi \leq 1, \tag{2.28}$$

where $K_{el}^1(x)$ is the complete elliptic integral of the first kind of x and:

$$P_{1D}(\phi) = P_{2D}(\phi) = P_{3D}(\phi) = 0, if\, |\phi| > 1. \tag{2.29}$$

Lilliefors Test

In order to evaluate the agreement between the Gaussian PDF[12] and the PDF of mode shape components from a random system, the Lilliefors normality test can be considered adequate[13], Conover (129). The Lilliefors test is an adaptation of the Kolmogorof-Smirnoff Test, which is applied to verify the establishment of normal statistics for a set of data.[14] In the Lilliefors normality test, the test statistics (S_{LT}) are defined as:

$$S_{LT} = \underset{x}{sup}|\Phi(x) - F_Z(x)|, \tag{2.30}$$

where $\Phi(x)$ is the standard Gaussian cumulative distribution function and the $sup(x)$ function refers to the maximum value of the difference over the range

[12] According to RMT, Gaussian or normal distribution is expected for eigenvector components of classically chaotic systems, Mehta (24).

[13] In probability theory and the statistics field, the *skewness coefficient* is a measure of the asymmetry of the probability distribution of a random variable. For normal distribution (or any perfectly symmetric distribution), the skewness coefficient is zero, (131, 132, 103). In the present study, some analysis carried out with mode shape components used this metric function as an auxiliary or complementary result to investigate indirectly the degree of the establishment of GOE (or Gaussian) statistics for the mode shapes of random engineering systems.

[14] A detailed description of the most well known normality tests is available in Conover (129) and Montgomery & Runger (103).

of x considered, and $F_Z(x)$ is the empirical cumulative distribution function of the normalized sample values which is defined as:

$$Z_i = \frac{X_i - \mu_X}{\sigma_X}, \tag{2.31}$$

where μ_X and σ_X are the mean and standard deviation values from the empirical data.

The Lilliefors test is implemented in the standard libraries of several mathematical software programs, for instance: *Statistics* and *Matlab* (133, 131, 132). The Lilliefors test results are based on the corresponding level of significance for a particular value of a certain statistic. In the Matlab software, the Lilliefors test results are presented in terms of two distinct values. If the Lilliefors test result is unity, the hypothesis that variable X_i has a normal distribution can be rejected. On the other hand, if the Lilliefors test result is null (zero), the hypothesis of the normal distribution cannot be rejected.

Kurtosis Metrics

The *kurtosis* is a statistical observable which measures how outlier-prone a distribution is, that is, it quantifies the degree to which a uni-modal distribution is peaked, Montgomery and Runger (103). In the mode shape context, the definition of kurtosis is given by:

$$K = \frac{E\left[\phi^4\right]}{E\left[\phi^2\right]^2}, \tag{2.32}$$

where $E[\,]$ usually denotes the expected value from the averaging process over the mode shape component domain.

Regardless of the averaging process approach adopted, the kurtosis can be adequately defined as the ratio of the fourth central moment divided by the square of the second central moment. If the distribution is normal, then the kurtosis value is exactly equal to 3. A kurtosis value greater than 3 indicates the presence of several values in the neighborhood of the mean value, that is the distribution is more peaked than the normal distribution. If the kurtosis value is less than 3, the distribution curve is flatter than the normal distribution.

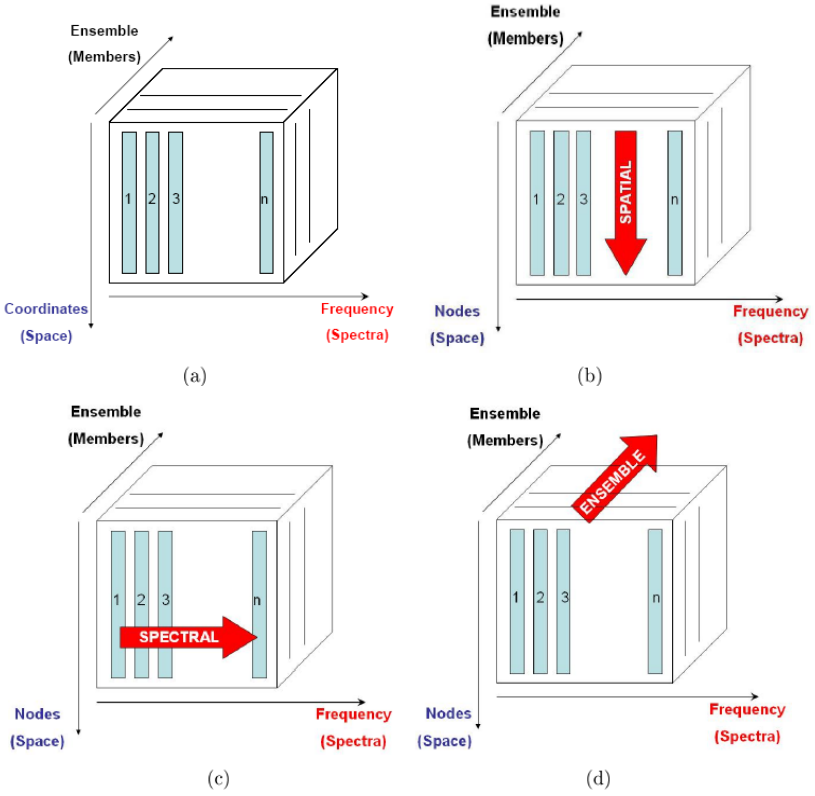

Figure 28: Definitions of kurtosis averaging approaches. Plot (a): Ensemble mode shapes. Plots (b - d): Graphical representations of the spatial, spectral, and ensemble kurtosis averaging approaches, respectively, Gomes and Gerges (101).

Although the kurtosis evaluation for mode shapes traditionally considers the expected values from an averaging process over the spatial domain (*i.e.*, over the mode shape component domain), other alternative kurtosis averaging approaches can be considered and their statistical results provide relevant information about the mode shape statistics, Gomes and Gerges (101).

In the present study, three distinct mode shape averaging approaches

were considered for the kurtosis evaluation from the mode shapes: spatial, spectral, and ensemble averaging approaches. In Figure 28, the kurtosis averaging approaches are illustrated.

Mode Shape Statistics Factor

The parameter known as the *Mode Shape Statistics Factor* (K) was initially proposed by Lyon (48) in order to represent the spectral statistics of mode shapes in the Theory of SEA variance, (48, 53, 54, 49, 50). The definition of the Mode Shape Statistics Factor (K) is given by:

$$K = \frac{E\left[\phi^4\left(x_f\right)\right]}{E\left[\phi^2\left(x_f\right)\right]^2}, \tag{2.33}$$

where x_f is the excitation force point.

In order to simplify the evaluation of the mode shape statistics factor, Lyon (48) considered, for convenience, the mode shapes as *sinusoidal functions* and the term $E[\,]$ denoted the expected values from the *spatial averaging process*. It is important to emphasize that, for mass normalized mode shapes with zero mean amplitudes, Lyon's mode shape statistics factor definition becomes identical to the spatial kurtosis, Equation (2.32). For mode shapes described by sinusoidal functions, the spatial kurtosis values are $K_{sin} = 1.5, 2.25$ and 3.375, for one, two, and three-dimensional systems, respectively.

Considering the context of the energy response variance across the ensemble, Langley and Brown (18) adopted the *ensemble averaging approach* in the evaluation of the mode shape statistics factor. Thus, for mass normalized mode shapes with zero mean amplitudes, Langley's mode shape statistics factor definition becomes identical to the ensemble kurtosis definition for any given mode shape component (*i.e.*, at a fixed excitation point) across the ensemble. In SEA variance predictions, Langley and Brown (18) considered the GOE model for both modal parameter statistics, and thus the ensemble mode shape statistics at the excitation point was assumed to be Gaussian and an ensemble kurtosis value of 3 was adopted, regardless of the system dimensionality.

Inverse Participation Ratio

In the disordered Quantum Billiard context, the *Inverse Participation Ratio - IPR* (I_2) is an eigenvector statistical observable which measures the

disorder strength from the mode shapes, Pradhan and Sridhar (123). According to Pradhan and Sridhar (73), the kth statistical moment of nth normalized squared mode shape amplitudes (I_k) is given by:

$$I_k(n) = \int_{\Omega} |\psi_n(\overrightarrow{r})|^{2k} d\Omega, \tag{2.34}$$

where Ω is the spatial domain of system and $|\psi_n(\overrightarrow{r})|^2$ is the nth normalized squared mode shape amplitude at spatial position $\overrightarrow{r}$, which is normalized to have unit mean:

$$I_1(n) = \int_{\Omega} |\psi_n(\overrightarrow{r})|^2 d\Omega = 1. \tag{2.35}$$

The definition of the *Inversion Participation Ratio* arises from the second statistical moment of normalized squared mode shape amplitudes (normalized to have unit mean) as follows:

$$I_2(n) = \int_{\Omega} |\psi_n(\overrightarrow{r})|^4 d\Omega = E\left[|\psi_n^2(\overrightarrow{r})|^2\right], \tag{2.36}$$

where $E[\,]$ denotes the value expected from the averaging process over the spatial system domain.

According to Equation (2.36), the Inversion Participation Ratio definition can be considered identical to Lyon's Mode Shape Statistics Factor or the spatial kurtosis when they are evaluated considering normalized squared mode shapes instead of mass normalized mode shapes. Burhhardt and Weaver (75) called this factor the *Modal Participation Ratio*.

The second statistical moments (I_2) and their probabilistic distribution $P_{I_2}(I_2)$ are very important measures of the statistical properties of the chaotic and disordered eigenfunctions, (73, 74). For finite chaotic systems, it is expected that the spectral mean value of I_2, $\langle I_2 \rangle$, is close to that of the universal GOE limiting value of $\langle I_2 \rangle = 3.0$, with small mode-to-mode fluctuations $\delta I_2 \ll \langle I_2 \rangle$, resulting in a nearly symmetric distribution around $\langle I_2 \rangle$. On the other hand, the statistical moments I_k of squared normalized mode shape amplitudes from an infinite classically chaotic system are expected to have fixed values with no mode-to-mode fluctuations, with $I_2 = 3.0$, *i. e.*, $P_{I_2}(I_2) = \delta(I_2 - 3.0)$.

Similarly to the spatial kurtosis values, the inverse participation values of $I_2 = 1.5$, 2.25, and 3.375 are expected for all mode shapes from the one, two and three-dimensional regular or integrable systems, respectively, in which their mode shapes are described as product of sinusoidal functions.

Spatial Correlation of Mode Shape Components

Another eigenvector statistical observable is the *spatial correlation function of the mode shape components* which describes the spatial correlation of mode shape amplitudes, (71, 73). In the present study, two types of spatial correlations are investigated: the linear and squared mode shape spatial correlation functions, $P_1(kr)$ and $P_2(kr)$, respectively.

In the Quantum Billiard field, the linear and squared spatial mode shape correlation functions of the n-th mode shape, $P_1(k_n r)$ and $P_2(k_n r)$ respectively, are defined as:

$$P_1(k_n r) = \left\langle |\psi_n(\overrightarrow{k_n r_0})|\, |\psi_n(\overrightarrow{k_n r_0} + \overrightarrow{k_n r})| \right\rangle, \tag{2.37}$$

and:

$$P_2(k_n r) = \left\langle |\psi_n(\overrightarrow{k_n r_0})|^2\, |\psi_n(\overrightarrow{k_n r_0} + \overrightarrow{k_n r})|^2 \right\rangle, \tag{2.38}$$

where ψ_n is the nth normalized mode shape amplitude (normalized to have unit mean), k_n is the wave number of n-th mode, r is the magnitude of the distance between $\overrightarrow{r}$ and $\overrightarrow{r_0}$ points, and the angular brackets $\langle\ \rangle$ denote the averaging process over $\overrightarrow{k_n r_0}$, and angles between $\overrightarrow{k_n r_0}$, and $\overrightarrow{k_n r}$. Traditionally, an averaging process over many mode shapes (wave functions) is adopted in order to obtain more robust and representative results, and thus the angular brackets also include the averaging process over different mode shapes.

Since the mode shapes are traditionally scaled to unit-generalized mass in the vibroacoustics field, the definition of the frequency-averaged linear mode shape correlation function can be conveniently re-written as:

$$P_1(kr) = M\,E\left[\phi_n(\mathbf{x}_0)\phi_n(\mathbf{x})\right], \tag{2.39}$$

where ϕ_n is the n-th mass-normalized mode shape, M is system mass and $E[\,]$ denotes the expected frequency-averaged value of the product of the mode shape amplitudes at the $\mathbf{x}_0$ and $\mathbf{x}$ positions.

Considering that the mode shapes form a homogeneous random field, the linear mode shape correlation function is identical to the acoustic field correlation function (R_f):

$$P_1(kr) = M\,E\left[\phi_n(\mathbf{x}_0)\phi_n(\mathbf{x})\right] = R_f(\mathbf{x}-\mathbf{x}_0). \tag{2.40}$$

For the ideal diffuse acoustic field, Cremer and Heckel (38) defined analytical expressions of diffuse field correlation functions for two and three-dimensional systems as:

$$R_f(\mathbf{x}-\mathbf{x}_0) = \begin{cases} J_0(kr), & \text{2D-systems,} \\ \sin(kr)/(kr), & \text{3D-systems,} \end{cases} \tag{2.41}$$

where J_0 denotes the zeroth order Bessel function.

Langley and Cotoni (35) showed that the diffuse field correlation functions can be directly extended to classically chaotic dynamical systems in which the mode shape statistics conform to the GOE model. Prigodin (134) also showed that the same correlation function expressions can also be obtained through the Friedel functions in the ballistic regime for wave functions from the 2D- and 3D-quantum chaotic disordered systems.

Similarly to the linear correlation function of the mode shape components, the definition of the squared correlation function of the mode shape components can be re-written in terms of the mass-normalized mode shapes:

$$P_2(kr) = M^2 E\left[\phi_n^2(\mathbf{x}_0)\phi_n^2(\mathbf{x})\right]. \tag{2.42}$$

Considering the statistical characteristics of covariance function, the P_2 definition is conveniently expressed as an expansion of ϕ_n terms, (35):

$$P_2(kr) = M^2 E\left[\phi_n^2(\mathbf{x}_0)\right] E\left[\phi_n^2(\mathbf{x})\right] + 2M^2 E\left[\phi_n(\mathbf{x}_0)\phi_n(\mathbf{x})\right]^2. \tag{2.43}$$

Considering that the linear correlation function of the mode shape components is adequately described by a diffused field correlation function and the fact that the mode shapes are scaled to unit generalized mass so that $E\left[\phi_n^2(\mathbf{x}_0)\right] = 1/M$, the frequency-averaged squared correlation function of the mode shape components for GOE mode shapes is given by:

$$P_2^{GOE}(kr) = 1 + c_{GOE} J_0^2(kr), \tag{2.44}$$

where $c_{GOE} = 2$ for chaotic systems.

A similar expression to Equation (2.44) was also obtained by Prigodin *et al* (135, 134) through the use of disordered system models at the ballistic or extreme diffusive limit. An excellent agreement with this analytical prediction has recently been confirmed with mode shape correlation results from the chaotic systems such as the Sinai stadium and other classically chaotic geometries, (71, 135, 134, 136).

According to Equation (2.44), $P_2(kr) \to 1$ for large distances since $J_0^2(kr) \to 0$ for $r \to \infty$. Therefore, it is expected that the squared mode shape amplitudes are uncorrelated for sufficiently large distances. The coefficient c_{GOE}, in front of the Bessel function term, corresponds to $P_2(0) - 1$ and is in agreement with the Porter-Thomas distribution for GOE mode shapes, Equation (2.24), and thus:

$$P_2(0) = \left\langle |\psi_n(\overrightarrow{k_n r_0})|^2 \, |\psi_n(\overrightarrow{k_n r_0})|^2 \right\rangle = \left\langle |\psi_n(\overrightarrow{k_n r_0})|^4 \right\rangle = \int_0^\infty z^2 P_{PT}^{GOE}(z) dz = 3, \tag{2.45}$$

where $z = |\psi_n(\overrightarrow{k_n r_0})|^2$.

2.3.3 Mode Shape SEA Parameters

In the SEA variance context, the mode shape statistics provides a significant contribution to the energy response from an ensemble composed of similar random engineering structures with uncertain or non-deterministic parameters. Therefore, major effects of the mode shape statistics on the statistical moments of energy responses are expected for cases of structures subjected to single point-loadings rather than the spatially-distributed excitations, Brown (1).

The definitions of mode shape SEA parameters are described in detail below. These mode shape parameters are metric functions which quantify the level of randomness of random systems through the measurement of mode shape dispersion characteristics across the ensemble.

Additionally, it is generally considered that, in principle, the results from these mode shape SEA parameters also allow the correct identification of the level of uncertainty necessary to guarantee that the universal statistics threshold limit is reached and a GOE model can be completely established for both modal parameter statistics.

In the Quantum Physics field, good results have been obtained in the quantifying of *universal* statistics based on the eigenvector statistics. Karol Zyczkowski (81) showed through a single parameter, called $M(r)$, which is based on the minimal number of relevant eigenstates, that the level of *universal* statistics associated with a certain system can be correctly identified through the number of eigenbases present on their eigenvectors. For a classically chaotic system, a large number of eigenbases is expected since the *disorder effects* are strongly established across the eigenvector domain. However, only a small number of eigenbases is required to describe the eigenvectors

of integrable or regular systems. Additionally, the proposed parameter based on the minimal number of relevant eigenstates also allows three known universality symmetry classes to be distinguished, GOE, GUE and GSE.

Based on a similar concept to Zyczkowski's, Cordioli (20) employed the *Singular Value Decomposition* (SVD) techniques and proposed SEA parameters based on the mode shape statistics in order to verify the applicability of GOE statistics to the modal parameters from an ensemble composed of similar random structures. The definitions of these parameters are reviewed below. Further information concerning the performance of these mode shape SEA parameters will not be discussed here in detail, but is available in Cordioli (20).

Let us consider that N mode shapes are presented in terms of increasing natural frequencies for each ensemble member and the size of the ensemble is N_e members. For the kth mode shapes across the ensemble, the mode shape matrix $\mathbf{D}_k$ is defined as:

$$\mathbf{D}_k = \left[\begin{array}{cccc} \mathbf{u}_k^1 & \mathbf{u}_k^2 & \dots & \mathbf{u}_k^{N_e} \end{array} \right], \tag{2.46}$$

where $\mathbf{u}_k^i$ is the kth mode shape from the ith ensemble member.

According to Singular Value Decomposition (SVD)(137), the mode shape matrix $\mathbf{D}_k$ can be decomposed as:

$$\mathbf{D}_k = \mathbf{W}_k \mathbf{S}_k \mathbf{V}_k, \tag{2.47}$$

where the $\mathbf{W}_k$ and $\mathbf{V}_k$ are matrices which contain a set of the orthonormal *output* and *input* (or *analysing*) basis vectors displayed in their columns, respectively, and $\mathbf{S}_k$ is the diagonal matrix which presents the corresponding singular values.

In order to determine the minimum number of relevant singular values (or eigenstates) of the mode shape matrix, a particular threshold limit (TL) is adopted for convenience, considering that all important basis vectors are included. Therefore, the first mode shape SEA parameter, Parameter $P(k)$, which quantifies the number of important basis vector, is defined as:

$$\sum_{i=1}^{P(k)} \left(S_i^k \right)^2 = TL \sum_{i=1}^{N} \left(S_i^k \right)^2, \tag{2.48}$$

where S_i is the i-th singular value for kth mode shapes, which is assumed to be labeled in order of decreasing magnitude. Traditionally, the threshold limit value (TL) adopted is $TL = 0.90$ or 0.99, (81, 20).

Before introducing the second mode shape SEA parameter, Parameter $Q(k)$, the concept of the *eigenvector mixing* phenomenon is illustrated through the results from a parametric study with an externally perturbed quantum chaotic billiard system performed by Schaadt *et al* (69, 110, 70). In parametric studies of billiard systems in the Quantum Physics field, the representation of effects of an increase in the level of disorder (external parameter) on the modal parameters is performed through the curves of unfolded energy levels (eigenvalues) as a function of the disorder level (external parameter magnitude). Thus, a set of curves of unfolded natural frequencies are simultaneously represented for each mode order, which present a pattern similar to *spaghetti* in appearance, Figure 29 (a).

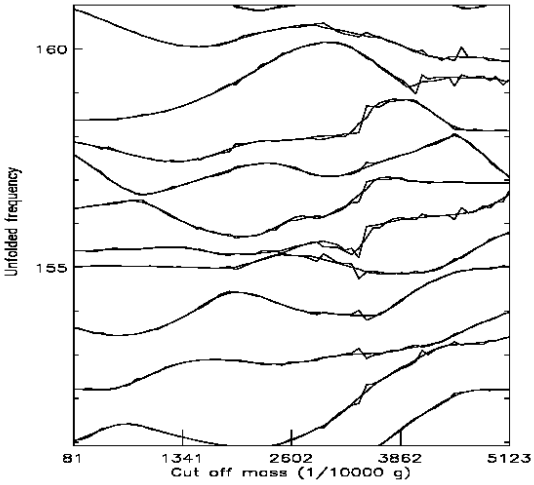

(a)

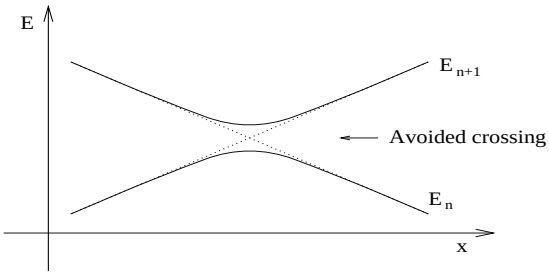

(b)

Figure 29: Representation of the effects of an increase in the amount of uncertainty associated with the unfolded natural frequency of a random system. Plot (a): Example of spaghetti unfolded frequency curves, Schaadt (70). Plot (b): Modal parameter characteristics of the avoided crossing region (mixing of mode shapes), Schaadt (69).

Due to the *level repulsion effects* expected for classically chaotic systems, no natural frequency curves can cross each other. As shown in Figure 29 (b), the natural frequencies close to the crossing region have avoided crossing characteristics, that is, the natural frequencies repel each other due to the level repulsion effects and move apart again. Although the natural frequencies do not cross the corresponding mode shapes do cross. Now consider that the mode shape of the n-th natural frequency before the avoided crossing region is the same as the mode shape of the $(n+1)$-th natural frequency after the avoided crossing region. This phenomenon of a change in the mode shape position in the natural frequency domain is known as the *mixing of eigenvectors*.

It is also important to emphasize that for structures in which several classes of modes exist, only mode shapes of the same mode class will show avoided crossing characteristics, while two mode shapes from distinct mode classes will cross each other without any iteration.

Considering the avoided crossing phenomena, Cordioli (20) proposed a second mode shape SEA parameter, Parameter $Q(k)$, which is related to the mixing of eigenvectors. For the kth mode shapes across the ensemble, the level of eigenvector mixing is evaluated through the auxiliary matrix ($\mathbf{R}_k$) which is defined as the projection of each $\mathbf{u}_k$ on the SVD basis vectors of the

$\mathbf{D}_k$, that is:

$$\mathbf{R}_k = (\mathbf{W}_k)^T \mathbf{D}_k = \left[\begin{array}{cccc} \mathbf{r}_1^k & \mathbf{r}_2^k & \cdots & \mathbf{r}_{N_e}^k \end{array} \right], \tag{2.49}$$

where the matrix dimensions are: $dim(\mathbf{R}_k) = (N, N_e)$, $dim(\mathbf{W}_k) = (N, N)$ and $dim(\mathbf{D}_k) = (N, N_e)$, respectively.

Therefore, each vector $\mathbf{r}_i^k$ has a unitary module and contains the internal product of the kth mode shape of the ith ensemble member with the basis vector from $\mathbf{W}_k$. For cases where a particular $\mathbf{r}_i^k$ component is large, a high alignment is expected with a specific basis vector. On the other hand, if several $\mathbf{r}_i^k$ amplitudes are significant, the $\mathbf{r}_i^k$ vector is composed of several basis vectors. Similarly to the determination of the Parameter $P(k)$, the number of relevant basis vectors, $Q^k(i)$ of each $\mathbf{r}_i^k$ vector is given by:

$$\sum_{z=1}^{Q^k(i)} \left(r_{i,z}^k \right)^2 = TL, \tag{2.50}$$

where the components of the $\mathbf{r}_i^k$ vector are labeled in order of decreasing magnitude.

The Parameter $Q(k)$ associated with the k-th mode shapes across the ensemble is defined as the ensemble mean of the $Q^k(i)$ parameters and is given by:

$$Q(k) = \frac{1}{N_e} \sum_{i=1}^{N_e} Q^k(i). \tag{2.51}$$

In order to verify the number of symmetries of system, a third mode shape SEA parameter, Parameter Z, was also proposed by Cordioli (20). Based on the Parameters $P(k)$ and $Q(k)$ results, the Parameter $Z(k)$ associated with the k-th mode shapes across the ensemble is given by:

$$Z(k) = \frac{P(k)}{Q(k)}. \tag{2.52}$$

For systems with several symmetries as those have Poisson statistics, large values are expected for Parameter Z results. Further information concerning the application and performance of the Parameter Z is available in Cordioli (20).

2.3.4 Nonuniversal Eigenvector Statistics

As discussed in the previous section, some relevant mode shape statistics deviations in relation to the expected GOE eigenvector statistics are observed for most random engineering systems, Gomes (10). The main physical phenomena associated with the establishment of *nonuniversal* mode shape statistics can be classified into two major deviation classes. In first mode shape deviation class, the phenomena are related to the effects of the presence of *stable periodic orbits* which are strongly associated with the geometrical characteristics of the system, (92, 96, 95, 97, 115). The second mode shape deviation class is associated with the *structural localization* effects of the presence of impurities and structural irregularities along the spatial domain of system, (136, 138, 71, 139, 140)

In the following subsections, the effects of periodic orbits and structural localization phenomena on the mode shape statistics are discussed in detail and illustrated in terms of the eigenvector statistical observables results.

Effects of Periodic Orbits on the Mode Shapes

In the *quantum chaology*[15] field, periodic orbits have been used as a semiclassical tool in the spectral analysis of the energy levels from billiard systems, (92, 96, 95, 97, 115). From the mode shape statistics point of view, periodic orbits provide an efficient means to clarify the connections between the mode shape characteristics and the system geometry characteristics since every mode shape is considered to be composed of resonance functions which are constructed on periodic orbits at the semiclassical limit, (97, 115).

Considering the effects of periodic orbits on the mode shape statistics, the presence of stable periodic orbits leads to the establishment of the *scars* phenomenon of the mode shapes, (141, 119). According to Kudrolli and Sridhar (105), the scars are defined as mode shape regions of enhanced intensity along the periodic orbits. Some scarred mode shapes of billiard systems investigated in the recent literature are presented below and examples are discussed in order to illustrate how the effects of periodic orbits may become significant in terms of the mode shape statistics characteristics. In Figure 30, an example of the *bouncing ball*[16] state and its respective Porter Thomas distribution results are presented, Kudrolli and Sridhar (72). The main stable

[15] *Quantum chaology* comprises the study of how chaos in classical mechanics arises it the limit of quantum mechanics, Stockmann (104).

[16] The *bouncing ball orbits* are a special class of periodic orbits which propagate perpendicularly to two parallel system boundaries.

periodic orbits of a quarter Sinai rectangular billiard are shown in Figure 30 (a).

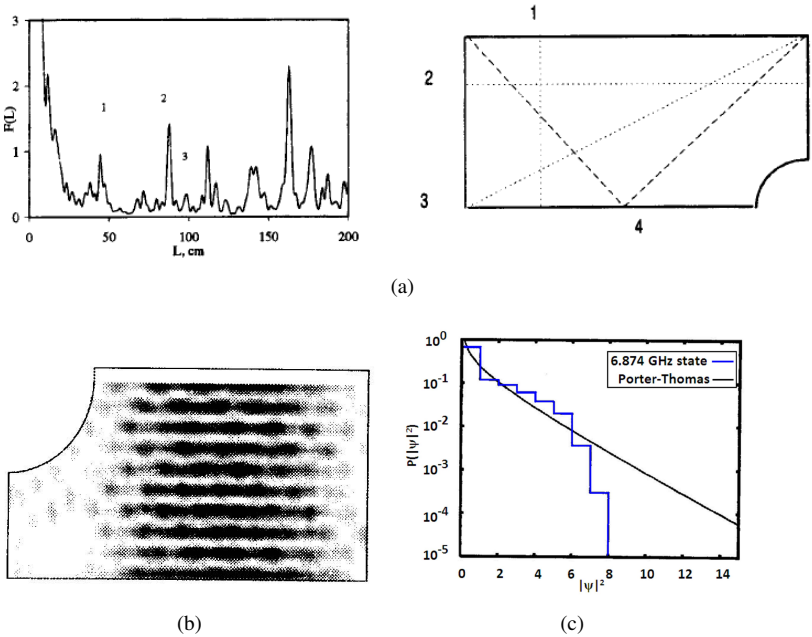

Figure 30: Example of a typical bouncing ball state of a quarter Sinai rectangular billiard. Plot (a): Main periodic orbits. Plot (b): squared mode shape amplitudes. Plot (c): Porter-Thomas distribution results, Kudrolli and Sridhar (72).

As shown in Figures 30 (b) and (c), the establishment of bouncing ball periodic orbits provides significant changes mainly in the range of mode shape components with large amplitudes. Indeed, the quarter Sinai rectangular billiard presents some geometrical characteristics similar to classical regular systems, where the periodic orbits with bouncing ball characteristics are established and their effects reduce the probability of the occurrence mode shape components with large amplitudes.

In Figure 31, other examples are presented from an experimental investigation with disordered Sinai billiard micro-cavities, Sridhar *et al* (119, 122).

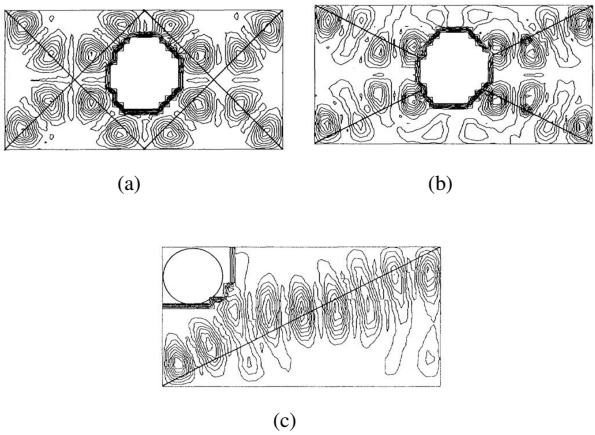

(a) (b)

(c)

Figure 31: Examples of mode shapes associated with periodical orbits, Sridhar and Heller (119).

As shown in Figures 31 (a) and (b), the periodical orbits are the half diagonal lines and main diagonal lines, respectively. While the qualitative association with the periodical orbits is easily determined, the evaluation of the corresponding natural frequency through simple geometric rules is sometimes a very complex task, Sridhar (119). In Figure 31 (c), the enhanced mode shape amplitudes are established predominantly along the diagonal direction, while the corresponding periodic orbits are not perfectly isolated.

For a regular or integrable system like a rectangular billiard, the stable periodic orbits provide an asymptotic tendency to establishment of good quantum numbers, that is, the establishment of well-defined modal indexes associated with each mode shape, (119). For vibroacoustical systems, the good quantum numbers correspond to the wavenumbers which allow adequately to describe the spatial configuration of a mode shape and evaluate its corresponding natural frequency.

On the other hand, for systems with classically chaotic or sufficiently disordered geometries, an exact identification of quantum numbers becomes very complex, (119). In these cases, the complexity arises because in chaotic geometries, natural frequency is the only well-defined parameter, while other quantum numbers, like k_x and k_y wavenumbers for regular geometry, are absent.

Disorder and Anderson Localization Effects

The second class of the nonuniversal deviations of the mode shape statistics is related to the establishment of *localization* phenomena[17]. The localization phenomenon was initially predicted by the American physicist P. W. Anderson, also known as *Anderson localization*, Anderson (142). In general, the localization concept is associated with the absence of the diffusion of waves in a random medium and can be extended to a general wave phenomenon that applies to the transport of electromagnetic waves, acoustic waves, quantum waves and spin waves, etc.

The several experimental observations of the localization phenomena have been made in disordered billiard systems in the quantum physics field. For disordered systems such as microcavities perturbed with small metallic scatters (tiles), there are three characteristic lengths which may affect the statistical behavior of the mode shapes, or wavefunctions. They are the system size or span length (R_u), the mean free path[18] (l), and the wavelength of the resonance frequency (λ_u).

The most relevant physical phenomenon associated with disordered quantum billiard systems is *Anderson Localization* or simply *Localization* which is established under conditions where the wavelength is similar to mean free path, $\lambda_u \sim l$, Sridhar (120). Examples of the experimental localized wavefunctions are shown in Figure 32.

[17] The occurrence of this physical phenomena can be attributed to the existence of a the large degree of randomness of the impurities or defects inside the system domain, (71, 120).

[18] The *mean free path* of a particle is the average distance covered by a particle between subsequent impacts.

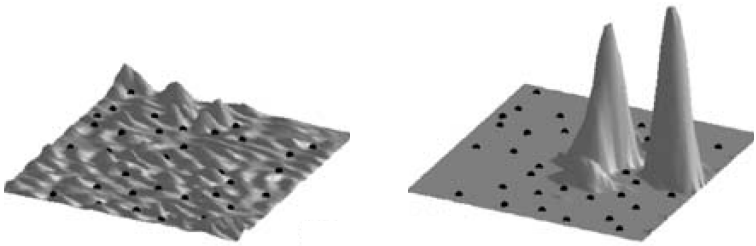

(a) (b)

Figure 32: Examples of the wavefunctions of disordered billiard systems demonstrating the establishment of Anderson Localization. Plot (a): weak localization regime. Plot (b): strong localization regime, Pradhan and Sridhar (73, 74).

As shown in Figure 32, the localization effects on mode shape amplitudes are significant and provide the confinement of large mode shape amplitudes in certain spatial mode shape regions. Furthermore, the degree of localization varies, either changing the frequency range or changing the mean free path through an increase or decrease in the uncertainty level of system (tiles, irregularities, or discontinuities). In general, two major regimes of localization are established: weak and strong localizations, Figures 32 (a) and (b), respectively.

For localized wavefunctions (or mode shapes), the probability density function of squared normalized mode shape amplitudes, $P_{PT}(|\psi|^2)$, deviates significantly from the universal GOE PT-distribution, $P_{PT}^{GOE}(|\psi|^2)$, Equation (2.24). The localization effects lead to the probability density function of squared normalized mode shape amplitudes, $P_{PT}(|\psi|^2)$, being much larger than the prediction of the *universal* GOE PT-distribution, $P_{PT}^{GOE}(|\psi|^2)$ for range of large $|\psi|^2$ magnitudes, Pradhan and Sridhar (123). Additionally, a slight reduction in the universal GOE PT-distribution, $P_{PT}^{GOE}(|\psi|^2)$, is also expected for the region of small normalized squared mode shape amplitudes for strong localization regime[19].

According to Sridhar (120), the degree of localization of wavefunc-

[19]Examples of PT-distribution results for weak and strong localization regimes are presented in Figure 34.

tions (or mode shapes) can be correctly expressed by the higher statistical moments of the normalized squared mode shape amplitudes as the *Inverse Participation Ratio*, I_2, that is $P_2(0)$. For disordered wavefunctions (or mode shapes) subjected to the establishment of localization phenomenon, values of $I_2 > 3$ are expected. For a weak or incipient localization regime, the mode shapes are almost delocalized and most values of I_2 are expected to be slightly greater that the universal value $I_2^{GOE} = 3$ as $I_2 \sim 4$, as well as present a small level-to-level variation. However, for a strong localization regime, the values of I_2 are expected to be very large in comparison to the universal value as $I_2 \sim 20$ for extremely localized mode shape.

Besides the individual values of I_2 for each mode shape, important conclusions concerning the spectral characteristics of mode shape statistics can be obtained when the Probability Density Function of I_2 is also evaluated for disordered systems.

For chaotic geometries, such as the 1/4 Sinai stadium, the mode shapes are *delocalized* and the $P_{I_2}(I_2)$ is expected to be nearly symmetric around to spectral mean value of I_2 which is identical to the expected universal value of $I_2^{GOE} = 3$. Due to finite dimensions, the boundary scattering phenomenon on the system length scale, leads to the incipient establishment of nonuniversal correlations, which is not consistent with the RMT hypothesis of Gaussian fluctuations of eigenfunction amplitude, and provides fluctuations in the distribution of $P_{I_2}(I_2)$, although of narrow distribution width, Pradhan

For disordered structures, the mode shapes tend to be spatially localized for some frequencies. As discussed above, the degree of localization of a certain mode shape can be associated with the I_2 value, and thus a strong localization leads to large values of I_2, which may be as high as $I_2 \sim 20$. In general, the $P_{I_2}(I_2)$ is asymmetric and the spectral mean value, $\langle I_2 \rangle$, is higher than the expected universal GOE value $I_2^{GOE} = 3$ [20].

Since the establishment of the localization phenomenon provides the absence of wave diffusion, the significant localization effects on the energy spatial distribution as well as on the spatial correlation of mode shapes are expected for localized mode shapes. In Figure 33, examples of the evaluation of squared spatial correlation functions of the mode shape components are presented for weak and strong localization regimes, Kudrolli *et al* (71).

[20] Practical examples of the PDF of I_2 are depicted for disordered systems under ballistic (*i.e.*, chaotic) and strong localization regimes Figure 35, respectively.

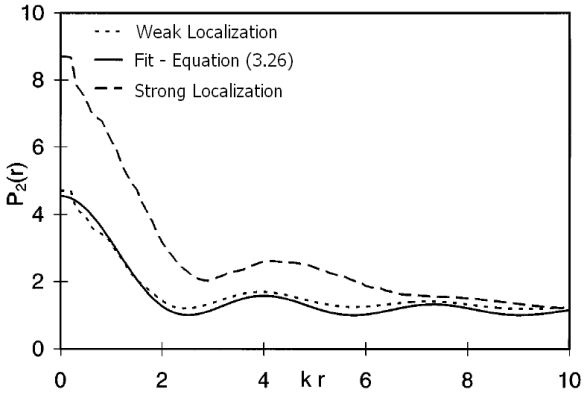

Figure 33: Examples of squared spatial correlation functions of the mode shape components for weak and strong localization regimes, Kudrolli *et al* (71).

As observed in Figure 33 the squared spatial mode shape correlation function results do not obey the universal GOE expression proposed by Equation (2.44). The amplitudes of spatial mode shape correlation function results are larger than those of the universal GOE prediction, mainly for a small kr region. This pattern shows clearly that the localization effects cause an increase in the spatial correlation between the mode shape components mainly for small distances. Additionally, the amplitudes of the spatial correlation functions of localized mode shapes die out faster with an increase in the magnitude of kr and tend to be uncorrelated for large distances.

Theory of Supersymmetry: Nonlinear Sigma Model

The Theory of Supersymmetry is an alternative approach which enables us to describe of spectral correlations of disordered systems, such as the natural frequency spacing statistics, the linear and squared mode shape amplitude distributions and the spatial correlation of squared mode shape amplitudes, Efetov (136, 138).

From the perspective of transport in disordered systems, the chaotic systems correspond to disordered systems with a *ballistic* or *diffusive* limit where the mean free path and conductance[21] are infinite, (138, 123, 73). Due

[21] Details regarding the conductance parameter are provided later in this section.

to the establishment of incipient localization effects, the universal properties are no longer ensured and the modal parameter statistics deviates substantially from the RMT predictions. Thus, a perturbative treatment has been achieved using *nonlinear sigma models* from the supersymmetry theory, (138). Originally, the development of these models was motivated by the problem of electrons in a disordered metal.

In general, the nonlinear sigma model has proven to be a very powerful tool for the characterization of the statistical properties of energy levels (natural frequencies) and eigenfunctions (mode shapes) in disordered and chaotic systems, (71, 73, 123). The main advantage of nonlinear sigma models is associated with the ballistic regime, $kl > 1$, where the expressions proposed by nonlinear sigma models reduce to RMT predictions for both modal parameters.

As the disorder level increases the finite mean free path and conductance are established and the modal parameter statistics are no longer universal and can be not described by the RMT predictions. Through 1D sigma models, a perturbative correction is taken into account due to the finite conductance g and a finite disorder strength parameter $2kl$. Further details regarding the theory of supersymmetry are beyond the scope of this work and are available in the related literature, (138, 143, 104).

The main expressions of eigenvector statistical observables based on the nonlinear sigma model of supersymmetry theory are presented below and examples of their applications are demonstrated through illustrative results from the quantum physics literature.

Mirlin and Fyodorov (77) investigated analytically and numerically the higher moments of the normalized squared mode shape amplitudes of large random matrices with a band structure. They were able to describe the localization correlation of weak localized mode shapes of a quasi-one dimensional wire, using the 1D nonlinear sigma model of supersymmetry. For incipient localization, Mirlin and Fyodorov show that the distribution of normalized squared mode shape amplitudes can be expressed as a correction function for the universal GOE PT-distribution and is given by:

$$P_{PT}^{WL}(|\psi|^2) = f_{MF}\left(|\psi|^2\right) P_{PT}^{GOE}(|\psi|^2), \tag{2.53}$$

where f_{MF} is the Mirlin - Fyodorov correction function for weak localization

is given by:

$$f_{MF}(|\psi|^2) \cong 1 + d_L \left[\frac{1}{4} - \frac{|\psi|^2}{2} + \frac{\left(|\psi|^2\right)^2}{12} \right], \tag{2.54}$$

where d_L is the fitted disorder localization parameter.

For a strong localization regime, large deviations are expected for the $P_{PT}(|\psi|^2)$ results, which can not be described by the localization corrections proposed for $P_{PT}^{WL}(|\psi|^2)$, as in Equation (2.54). Mirlin and Fyodorov proposed the following PT-distribution expression for the strong localization regime:

$$P_{PT}^{SL}\left(|\psi|^2\right) = \frac{8}{d_L^2} \sqrt{\frac{d_L}{2\left(|\psi|^2\right)}} K_1 \left[2\sqrt{\frac{2\left(|\psi|^2\right)}{d_L}} \right], \tag{2.55}$$

where $K_1(x)$ is the MacDonald Function, or modified Bessel function of the second kind of first order, (144). In the Mathematics field, the modified Bessel functions of the second kind are sometimes also called the Basset functions, modified Bessel functions of the third kind, or MacDonald functions. The definition of the modified Bessel function of the second kind of nth order is given by:

$$K_n(x) = \frac{1}{2}\pi i^{n+1} H_n^{(1)}(ix), \tag{2.56}$$

where $H_n^{(1)}(x)$ is the Hankel function of the first kind of x, (131, 132). In Figure 34, examples of the good performance of PT- distribution expressions for localization in weak and strong regimes are presented, Kudrolli *et al* (71).

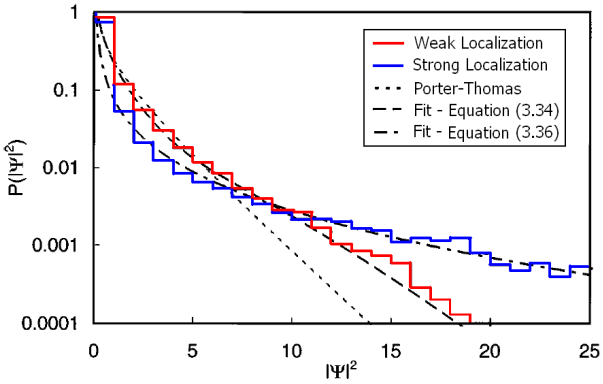

Figure 34: Porter - Thomas results for weakly and strongly localized mode shapes: experimental and analytical patterns based on nonlinear sigma model of supersymmetry, Kudrolli *et al* (71).

Analytical developments regarding the distribution of Inverse Participation Ratio values have been performed by Prigodin and Altschuler (145). Based on nonlinear sigma models from the mesocopic systems, they showed that the PDF of I_2 values, $P_{I_2}(I_2)$, follows an exponential decay law and, for $I_2 < \langle I_2 \rangle$, is given by:

$$P_{I_2}(I_2) = C_1 \frac{g}{2} \exp\left[-\frac{g}{6}(I_2 - \langle I_2 \rangle) - \frac{\pi}{2} e^{-\frac{g}{3}(I_2 - \langle I_2 \rangle)}\right], \tag{2.57}$$

while, for $I_2 \gg \langle I_2 \rangle$, the $P_{I_2}(I_2)$ is given by:

$$P_{I_2}(I_2) = C_2 \sqrt{\frac{g}{I_2}} \exp\left[-\frac{\pi}{6} g I_2\right], \tag{2.58}$$

where C_1 and C_2 are the normalization constants. For a mesoscopic system, the spectral distribution of I_2, $P_{I_2}(I_2)$, is dependent on the *dimensionless conductivity* g of a system which is defined as:

$$g = \frac{ln\left(\frac{R_u}{l}\right)}{\langle w \rangle}, w = \frac{(I_2 - 3)}{6}, \tag{2.59}$$

where R_u is the system size, l is the mean free path and $\langle \cdots \rangle$ denotes the expected averaged value for a fixed *disorder strength*, $2kl$.

In Figure 35, examples of the good performance of fitted forms of PDF of values I_2, $P_{I_2}(I_2)$, proposed by nonlinear sigma model of supersymmetry theory are presented for chaotic and disordered systems, Pradhan and Sridhar (73).

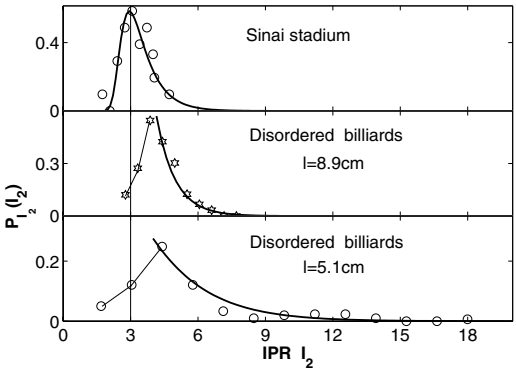

Figure 35: Examples of the nonlinear sigma model forms for chaotic and disordered systems. In the top panel: chaotic Sinai-stadium billiard. In the middle and bottom panels: disordered billiards under weak and strong localization regimes, respectively. The solid lines represent the calculations based on the nonlinear sigma model, Pradhan and Sridhar (73).

Pradhan and Sridhar (74) have extended the calculation of the spatial squared mode shape correlation functions of chaotic to localized mode shapes. The spatial squared mode shape correlation function for a moderate disorder regime is given by:

$$P_2(k_n r) = \left\langle |\psi_n(\overrightarrow{k_n r_0})|^2 \, |\psi_n(\overrightarrow{k_n r_0} + \overrightarrow{k_n r})|^2 \right\rangle = 1 + (I_2 - 1)\, K_L\left(k\,|r|\right), \quad (2.60)$$

where the function $K_L(x)$ is defined as:

$$K_L(x) = \left| \frac{1}{\pi} \int_{-\infty}^{+\infty} \frac{1}{1+y^2} J_0\left[kx(1+\frac{1}{2kl}y)\right] dy \right|^2 . \quad (2.61)$$

Since the evaluation of the function $K(x)$ is a very complex task, the Equation (2.60) can be approximately expressed in a region $r \lesssim l$ by a decay-

length scale of scattering mean path length l as follows:

$$P_2(k_n r) = \left\langle |\psi_n(\overrightarrow{k_n r_0})|^2 \, |\psi_n(\overrightarrow{k_n r_0} + \overrightarrow{k_n r})|^2 \right\rangle = 1 + (I_2 - 1) J_0^2 (k|r|) e^{-kr/kl}. \tag{2.62}$$

As observed in the Equation (2.62), the decay length of the spatial squared mode shape correlation function is a classical mean free path l. In Figure 36, examples of both analytical evaluations of the spatial squared mode shape correlation function, Equations (2.60) and (2.62), are presented for chaotic and moderate localized regimes for fixed disorder strength $2kl$, Pradhan and Sridhar (74).

Additionally, for large disordered strength $2kl$, corresponding to a ballistic or chaotic regime, the above expressions, Equations (2.60) and (2.62), will converge to the expression of a classically chaotic system, Equation (2.44).

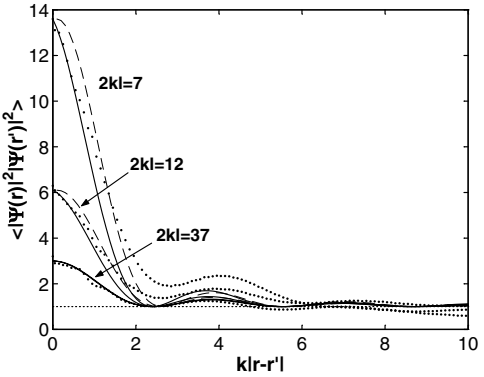

Figure 36: Spatial squared mode shape correlation functions of Sinai (chaotic) and disordered (localized) billiards with fixed disordered strength $2kl$ (dotted lines). The analytical nonlinear sigma model results: - - - Equation (2.60) (dashed line) and —— Equation (2.62) (solid line), Pradhan and Sridhar (74).

Mode Shape Component Correlations and Finite Size Effects

Although the use of random matrices with finite dimensions is relevant in certain applications of RMT models, only a few studies have been performed to evaluate and quantify the effects of the truncation process on the results for the statistical observables of the modal parameters.

Izrailev (128) investigated the statistical properties of the eigenfunctions in a quantum model with a finite number of states. In his work, the effects of the truncation process on the eigenfunction statistical characteristics were numerically investigated considering the kicked rotor Hamiltonians with a distinct number of states (that is, a distinct number of the mode shape components). The eigenfunction component distribution results suggested that the best agreement with the GOE analytical prediction is observed when a large number of states (*i.e.*, large number of the eigenvector components) was considered.

One of the pioneering analytical studies regarding the correlations between the Hamiltonian elements was carried out by Ullah and Porter (146). They showed analytically that there are no correlations between the diagonal and off-diagonal matrix elements and between the off-diagonal matrix elements, while the diagonal elements are correlated for some (invariant) eigenvalue distribution. In this study, no reference was made to the possible relationship between the performance of the truncation process and the effects of the correlation of the Hamiltonian elements on the modal parameter statistics.

Brody *et al* (56) investigated the level of correlation between the eigenvector components. In their study, they showed analytically for a GOE matrix that the distinct components of the same eigenvector, as well as the same component from distinct eigenvectors are not completely uncorrelated for finite eigenvector dimensions. However, they could only affirm that the eigenvector component distribution becomes asymptotically Gaussian with an increase in the eigenvector size. Additionally, Brody *et al* (56) also suggested that the correlation of the eigenvector components of sufficiently large eigenvectors would be likely considered weak and they could be neglected for convenience. However, it was noted that for other cases where the contributions of the component correlations on the eigenvector statistics are substantial they should certainly be considered.

Considering the orthogonally invariant statistics, Brody *et al* (56) proposed analytical expressions for the statistical moments of a d_e-dimensional eigenvector, Langley and Cotoni (35). The odd statistical moments are iden-

tically null and the even statistical moments of an entry of the eigenvector components are given by:

$$E\left[\phi_n^{2v}(z)\right] = \frac{(2v-1)!!\,(d_e-2)!!}{(d_e+2v-2)!!}, \tag{2.63}$$

where $x!!$ means the *Double Factorial*[22] of variable x. According to Weisstein (147), the definition of the Double Factorial ($x!!$) is given by:

$$x!! \equiv \begin{cases} n.(n-2)\ldots 5.3.1 & n>0\, odd \\ n.(n-2)\ldots 6.4.2 & n>0\, even \\ 1 & n=-1,0 \end{cases}. \tag{2.64}$$

Cordioli in (20) investigated the effects of spectral correlations between the mode shape components on the performance of SEA variance predictions based on GOE model. In his analysis, the point-loading variance results were numerically evaluated considering the excitation point location as a random variable across the ensemble. An improved agreement was obtained between numerical results and GOE prediction with $K = 3$. The direct comparison with variance results evaluated under fixed excitation point location suggested that the spectral correlations between the mode shape components are substantially reduced when the averaging process was carried for different components of different mode shapes. It was also argued that the spectral correlations between mode shape components play role in the kinetic energy statistics and may be the main reason for the deviations between the numerical (or measured) results and GOE prediction with $K = 3$ extensively reported in SEA literature.

A numerical investigation of the effects of finite dimensions on the evaluation of kurtosis metrics is presented in Appendix C. The kurtosis values were evaluated for several sets of perfect GOE matrices with distinct finite dimensions. The spatial and spectral averaging approaches were considered. The mean and variance values of kurtosis results were calculated and compared with available analytical predictions. In overall, the kurtosis results demonstrate indirectly that the mode shape statistical observables evaluated under spectral averaging approach may be more susceptible to finite dimension effects. In order to minimize possible finite dimension effects, it was recommended that the maximum number of available modes should be used during the evaluation of the results for the spectral mode shape statistical

[22]The *Double Factorial* is also known as *Factorial 2*. More information regarding the definition and properties of double factorial are available in Weisstein (147).

observable results.

2.3.5 Structural Localization Phenomenon in Vibroacoustic Systems

Although the localization phenomenon is well established in solid physics, mainly in disordered quantum systems, the corresponding localization effects in structural dynamics are less understood and explored. Indeed, one of the reasons for this is that in engineering system must always deal with *finite* structures, and considering the limit as the structure becomes infinite - as is typically applied in localization proofs in solid state physics - is of limited practical relevance.

The pioneering studies in the structural dynamics field considered simple systems such as coupled pendulums and string, and they were only a concept proof, not addressing the possibility of localization effects in practical structures, (140, 139, 148). In typical periodic engineering structures, such as turbine and compressor rotors of airplanes where the mounted blades are nominally equidistant to each other, any imperfection or disorder may break the blade-to-blade periodicity and induce the establishment of structural localization. Thus, in-depth knowledge of the localization effects is essential to estimating the dynamical stresses and fatigue life as well as the expected range of dynamical response, Bendiksen (149).

In order to introduce the physical concept of the *structural localization* phenomenon, a simple system composed of a row of N identical pendulums is considered, Figure 37. In this system, each pendulum is weakly coupled to its two neighbors with all couplings being identical, so that the pendulum system can be considered to have one-dimensional periodic characteristics, Hodges and Woodhouse (150).

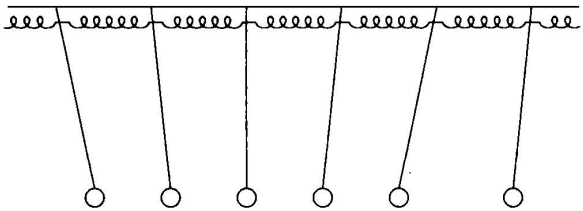

Figure 37: Pendulum system: a chain of pendulums coupled by springs, Hodges and Woodhouse (150).

When the pendulum system is excited at one of the ends and its vibrations can propagated unattenuated along the chain structure, this excitation frequency is within the *pass bands*. For excitation frequencies outside this range, that is, within the *stop bands*, the vibrations can not propagate along the chain at all and an exponential decaying near-field around the driving point is observed.

In order to understand the effects of pass and stop-bands on the mode shapes of the pendulum chain, let's consider the ideal case where the coupling strength between the pendulums is null. In this case, the mode shapes of the N independent pendulums would consist simply of each pendulum separately, vibrating at its natural frequency. Since the pendulums are identical, their frequencies are all the same and the N-fold natural frequency degeneracy is established. However, if there is a small degree of coupling between the pendulums, the natural frequency degeneracy will be no longer valid and a frequency cluster will be established close to the natural frequency of an uncoupled pendulum. The frequency region corresponding to this frequency cluster is defined as the *passband* region.

It is also important to emphasize that the mode shapes associated with the passband frequencies are *extended* throughout the whole structure and have amplitudes which vary sinusoidally with distance along the chain, (150). On the other hand, if there is some disorder (or randomness) in the pendulum system, and thus the pendulums have slightly distinct natural frequencies, the pendulum system mode shapes can be very distinct to those expected for a pendulum system absent of disorder.

Therefore, it is clearly intuitive that when at least one of pendulum natural frequencies is sufficiently different, the pendulum system mode shapes will be *localized* around individual pendulums. Considering that the individual pendulum frequencies are not degenerate, the coupling between pendulums is no longer strong enough to produce extended mode shapes in which all pendulums contribute more or less equivalent amplitudes. In this regard, it is important to point out that the establishment of structural localization is substantially dependent on the trade-off relationship between the disorder level and coupling strength, that is, the magnitude of the *disorder to coupling ratio*.

In the *strong localization* regime, where a large disorder to coupling ratio is established, large structural localization effects are expected for highly disordered periodical systems with weak couplings between their periodical substructures. On the other hand, for the *weak localization* regime, the disorder to coupling ratio is not so large and only incipient localizations effects are

observed. Indeed, the weak localization effects are very similar to the dynamical behavior of the wave interference between multiple-scattering paths.

Although the pendulum system described above is really a very simple system, their qualitative conclusions regarding the structural localization phenomenon characteristics can be adequately extended to almost periodic or random engineering structures.

In real engineering structures, the structural localization phenomenon can be understood as the vibration confinement due to the presence of irregularity over the spatial domain of a structure. For localized systems, the energy is confined spatially to a particular structural region close a driving point and at particular frequencies, Pierre (148). For practical purposes, the localization effects can be considered to be similar to damping effects, since they lead to spatial decay of the vibration amplitude along the structure, even though for localized vibrations the energy is confined to near the source of excitation, while for damping it is dissipated as it propagates, Pierre (148). Additionally, in general, it is known that the dynamic response of a typical disordered structure would decay exponentially moving away from the driving point, where the decay constant is referred to as the the *localization factor*, Pierre (148).

With respect to the statistical moments of energy responses across an ensemble of engineering structures, the establishment of localization phenomena in some of the ensemble members may strongly affect the statistical moments of the energy response as well as the significance of the expected energy response in terms of a typical individual member of the ensemble. The structural localization effects may lead to energy response distributions with *long tail characteristics* where the mean and probabilistic mode values of the response distribution across the ensemble are substantially distinct, as shown in Figure 38.

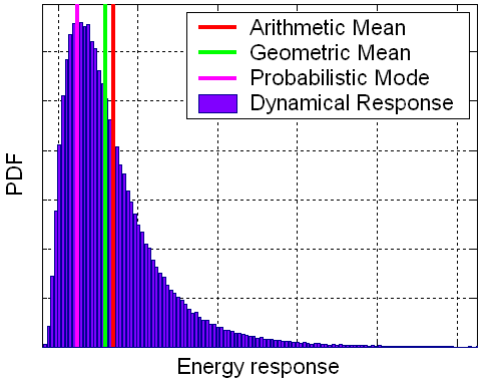

Figure 38: Pictorial example of a long tail response distribution expected for an ensemble of localized structures: the linear or arithmetic mean (the center of mass) and the typical value (probabilistic mode or peak) of the distribution are very distinct, adaptation of Hodges and Woodhouse (140).

Considering the variability of the dynamical responses of an ensemble composed of engineering structures with non-deterministic parameters, the *arithmetic mean* or *linear average* is usually applied over the configurations in the ensemble and satisfactory results are obtained. However, under certain circumstances, such as that presented in Figure 38, the *geometric mean* or *logarithmic average* value over the ensemble can be adequately applied to estimate the *typically expected value* for the responses across the ensemble (that is, the *probabilistic mode* or *peak* value of distribution). Indeed, the geometric averaging process is less sensitive to anomalous or sporadic contributions that occur in the energy response distributions with long tail characteristics, Hodges and Woodhouse (140).

In the SEA context, perfect energy diffusion is considered in the derivation of the analytical predictions through the establishment of a reverberant field in subsystems, Lyon and Dejong (29). For systems composed of reverberant and weak-coupled subsystems, a satisfactory agreement is expected between the SEA predictions and the ensemble mean value, regardless of the averaging process adopted, Fahy (30).

On the other hand, the establishment of structural localization phenomenon across the ensemble inhibits a good agreement between the SEA predictions and the typically expected value across the ensemble. Indeed, in

this situation, perfect energy diffusion and modal equipartition conditions do not occur over the system spatial domain and the *linear average* is no longer representative for the evaluation of the typically expected response across the ensemble members.

Detailed reviews of the implications of the structural localization effects on the performances of SEA and other diffusive transport theories are presented in Hodges and Woodhouse (151) and Fahy (30).

2.4 Theory of SEA Variance

In the high-frequency range, a large variability in the energy responses across the ensemble is expected due to small variations introduced during the manufacturing and assembly processes, and thus successive nominal systems from a production line may present a significant random spread in their dynamical performances. In order to determine if the statistics of the dynamical responses over an ensemble composed of random similar products meet the design and certification requirements, extensive effort has been directed by the vibroacoustic community toward developing robust and widely applicable analytical methods.

In this section, the analytical predictions of the energy density variance are presented for a single random dynamic system subjected to a generic nature of excitation. The Poisson and GOE models are considered for the statistics of the natural frequencies[23]. The narrow and broad frequency band analytical formulations for the relative variance are obtained for each statistical model. Based on the current results reported in the SEA variance literature, a detailed discussion is presented regarding the effect of the mode shape statistics factor (K) on the performance of relative variance predictions.

2.4.1 Energy Response Statistics

The response of a linear dynamical system can be correctly described using the method of modal superposition, Meirovitch (22). The complex mobility function between a sinusoidal force at frequency ω and drive point x_0 and the velocity of the response point at x is given by:

[23] Although it is not discussed here in details, the SEA variance literature has been shown that distinct statistics can be established for the modal parameter statistics, these being directly associated with degree of uncertainty and the characteristics of the geometrical irregularities present in the random system, (48, 54, 1, 18, 3).

$$Y(x, x_0, \omega) = \sum_n \frac{i\omega\phi_n(x)\,\phi_n(x_0)}{\omega_n^2 - \omega^2 + i\eta\,\omega_n^2}, \tag{2.65}$$

where ϕ_n is the nth mode shape, ω_n is nth natural frequency and η is the damping loss factor. For cases of engineering systems in which the performances of the damping effects are spatially distributed, for convenience, the damping loss factor can be adopted as the frequency-constant parameter, Gomes (28).

The time-space averaged kinetic energy density T of a system subjected to sinusoidal single excitation at frequency ω, location x_0 and magnitude F, is given by:

$$T(\omega, x_0) = \frac{F^2}{4R_u} \int_{R_u} \rho_d \left|Y(\omega, x_0, x)\right|^2 dx, \tag{2.66}$$

where R_u is the system or unit span. The energy density given by Equation (2.66) is the average over the main spatial dimensionality associated with the system of interesting for a single excitation point at x_0.

Therefore, using the orthogonal relationship, the simplified expression for kinetic energy density is given by,(22):

$$T(\omega) = \frac{\omega^2}{4R_u} \sum_n \frac{c_n}{\left(\omega_n^2 - \omega^2\right)^2 + \left(\eta\,\omega_n^2\right)^2}. \tag{2.67}$$

This equation might represent, for example, the spatially-averaged kinetic energy density of a system when excited by a point-loading. In this excitation case c_n is equal to the square of the nth mode shape at the drive point x_0 multiplied by the square of the force amplitude:

$$c_n = F^2 \phi_n^2(x_0). \tag{2.68}$$

In the derivation of SEA analytical formulations, the *rain-on-the-roof* excitation is defined as a spatially distributed loading where the point forces are considered statistically independent and delta-correlated in the space domain.

On the other hand, several numerical investigations on SEA variance have considered an averaging process over the force positions, that is, spatially-averaged excitation. Therefore, it is important to emphasize that both excitations remove the effects of the mode shape statistics on the res-

ponse variance results, since the set of c_n values is averaged out, Brown (1).

The spatially-averaged response to a single point force for a homogeneous system is given by:

$$\overline{T(\omega)} = \frac{F^2\omega^2}{4\rho_d R_u^2}\sum_n \frac{1}{4\omega^2(\omega_n-\omega)^2+(\eta\omega\omega_n)^2}, \tag{2.69}$$

where the over bar notation denotes the averaging process over all possible excitation points. It is also important to note that the following approximation was assumed given that each mode bandwidth is small in comparison to the natural frequency[24]:

$$\left(\omega_n^2-\omega^2\right)^2+(\eta\omega\omega_n)^2 = 4\omega^2(\omega_n-\omega)^2+\left(\eta\omega^2\right)^2. \tag{2.70}$$

2.4.2 Random Point Process

As stated previously, the statistics of the kinetic energy density results can be adequately evaluated through the random point process approach, (82, 55). Assuming a unitary punctual force, Equation (2.67) is conveniently rewritten and is given by:

$$T(\omega) = \sum a_n g(\omega_n-\omega), \tag{2.71}$$

where a_n is given by:

$$a_n = \frac{\phi_n^2(x_0)}{4R_u}, \tag{2.72}$$

and the function $g(\theta)$ is given by:

$$g(\omega_n-\omega) = \frac{\omega^2}{4\omega^2(\omega_n-\omega)^2+(\eta\omega^2)^2}. \tag{2.73}$$

In the next sections, the analytical predictions based on Poisson and GOE modes are presented for the relative variance of the kinetic energy den-

[24] Although it will not be demonstrated here, Equation (2.70) also provides a good performance for almost homogeneous systems, such as mass-loaded structures, Langley and Brown (16, 3, 18, 4).

sity results. Further details are available in Langley and Brown (18, 3, 1) and Cordioli (20).

Poisson Statistics

The pioneering studies on the energy response variability were performed in the room acoustics field. These adopted the Poisson model to describe the resonant or natural frequency statistics due to its analytical convenience, Lyon (48). That is, the natural frequencies were considered to form a *Poisson Point Process* (55, 51) on the frequency axis, where the natural frequencies are *uncorrelated* and their adjacent spacings have an *exponential* distribution. For the natural frequency statistics which obeys the Poisson model, the *relative variance* of the kinetic energy density results (r_T^2) is given by:

$$r_T^2 = \frac{\sigma_T^2}{(\mu_T)^2} = \frac{\alpha}{\pi m}, \tag{2.74}$$

where m is the modal overlap factor and the parameter α is the *spatial factor* which is given by:

$$\alpha = \frac{E\left[a_n^2\right]}{E\left[a_n\right]^2}. \tag{2.75}$$

The term α describes the influence that spatial matching between the excitation field and the mode shapes of the subsystem has on the relative variance, (18, 27).

For the case of systems subjected to a single point loading, the spatial factor (α) is identical to *mode shape statistics factor* (K) proposed initially by Lyon (48), which is a function dependent exclusively on the mode shape characteristics:

$$\alpha = K = \frac{E\left[\phi_n^4\right]}{E\left[\phi_n^2\right]^2}. \tag{2.76}$$

For a rain-on-the-roof excitation in which the response is averaged over the loading statistics prior to considering the statistics over the system ensemble, the value of $\alpha = 1$ is expected. According to Langley and Brown (3), the value of $\alpha = 1$ also occurs for the cases where the response to a single point force is averaged over all possible locations of the point-loading, prior to considering the ensemble statistics.

GOE Statistics

Langley and Brown (18) considered that the natural frequencies are substantially correlated and their *local* iteration across the ensemble is described accurately by the eigenvalue statistics from the large random symmetric matrices of GOE type from RMT. In order to model the correlation of two adjacent natural frequencies the *two-level cluster function* (Y_2) was considered in the derivation of analytical formulation. Therefore, the modal parameter statistics which obeys the GOE model, the *relative variance* of the kinetic energy density results (r_T^2) is given by:

$$r_T^2 = \frac{\sigma_T^2}{(\mu_T)^2} = \frac{1}{\pi n}\int_0^\infty \left[\alpha - b\left(\frac{\theta}{2\pi n}\right)\right]\exp(-\eta\omega\theta)d\theta, \tag{2.77}$$

where $b(\theta)$ is the Fourier transform of the two-level cluster function. This function was described by Mehta (24), being given by:

$$b(\theta) = \int_{-\infty}^{\infty} Y_2(r)\exp(-2\pi i r\theta)dr = \begin{cases} 1-2|\theta|+|\theta|\ln(1+2|\theta|), & |\theta|\leq 1 \\ -1+|\theta|\ln\left(\frac{2|\theta|+1}{2|\theta|-1}\right) & |\theta|\geq 1 \end{cases}, \tag{2.78}$$

Brown (1) evaluated the integral of Equation (2.77), so that:

$$r_T^2 = \frac{1}{\pi m}\left\{\alpha - 1 + \frac{1}{2\pi m}\left[1-\exp(-2\pi m)\right] + E_1(\pi m)\left[\cosh(\pi m) - \frac{1}{\pi m}\sinh(\pi m)\right]\right\}. \tag{2.79}$$

Here, $E_1(x)$ is the exponential integral and is given by:

$$E_1(x) = \int_x^\infty \frac{\exp(-t)}{t}dt. \tag{2.80}$$

Using an expansion of the exponential integral valid for large arguments, it is possible to demonstrated that Equation (2.79) can be correctly simplified to provide:

$$r_T^2 \approx \frac{(\alpha-1)}{\pi m} + \frac{1}{(\pi m)^2}. \tag{2.81}$$

According to Brown (1), the accuracy of Equation (2.81) is guaranteed only for $m > 0.6$. In the case of single point excitation when ($\alpha = K$), it can be observed that the first term of equation (2.81) agrees with Weaver's result (49), and thus the relative variance is predominantly proportional to $1/(\pi m)$. However, in the case of spatially-averaged excitation, with $\alpha = 1$, the energy variance is proportional to $1/(\pi m)^2$. The term proportional to $1/(\pi m)^2$ does not appear in the previous expression given by Weaver (49), demonstrating the high accuracy of the expression given by Equation (2.81).

2.4.3 Band-Averaged Energy Response Statistics

In several engineering applications, the external excitation does not perform at a single frequency ω but rather over a broad frequency band. If the kinetic energy is averaged over the frequency band $R_\omega = [\omega_0 - \Delta\omega/2,\ \omega_0 + \Delta\omega/2]$, it is given by:

$$T_\Delta(\omega, \Delta\omega) = \frac{1}{\Delta\omega}\int_{R_\omega} T(\omega)\, d\omega, \tag{2.82}$$

where $\Delta\omega$ is the averaging bandwidth.

Neglecting the small contributions from the modes outside the frequency band of interest (non-resonant modes), Equation (2.82) can be adequately simplified as, (48):

$$T_\Delta(\omega, \Delta\omega) \approx \frac{1}{\rho_d}\sum_{n=N_1}^{n=N_2} \frac{a_n}{\Delta\omega}\frac{\pi}{2\eta\,\omega_0}, \tag{2.83}$$

where N_1 is the sequence number of the lowest natural frequency in the frequency band and N_2 the sequence number of the highest natural frequency in the band.

The analytical expressions of the relative variance of frequency band-averaged kinetic energy density responses are presented below considering modal parameter statistics based on the Poisson and GOE models, respectively. Further details concerning the analytical derivation of the frequency-band averaged relative variance formulations are available in the SEA variance literature: (1, 53, 54, 3, 48).

Poisson Statistics

Davy (53) extended the Lyon's work and proposed analytical expressions for the case of multiple source and receiver positions in the room acoustics field. The Poisson model was adopted to describe the natural frequency statistics and the mode shapes were assumed to be the product of sinusoidal functions. The proposed analytical expression for the relative variance of the frequency-band averaged kinetic energy density results is given by:

$$r_T^2 = \left\{ \frac{1}{N_L N_R} \frac{m}{\Delta\omega} + \frac{1}{n(\omega)\Delta\omega} \left[\frac{K}{N_L} + 1 - \frac{1}{N_L} \right] \left[\frac{K}{N_R} + 1 - \frac{1}{N_R} \right] \right\} F(B), \tag{2.84}$$

where N_L is the number of source points (or excitation points), N_R is the number of receiver points (or response points) and the bandwidth parameter B is defined as:

$$B = \frac{\Delta\omega}{\omega\eta}. \tag{2.85}$$

In the case of a system subjected to a single point excitation, that is, $N_L = 1$ and $N_R = \infty$, the relative variance is given by:

$$r_T^2 = \frac{K}{n(\omega)\Delta\omega} F(B), \tag{2.86}$$

where the function $F(B)$ is defined as:

$$F(B) = \left(\frac{2}{\pi} \right) \arctan(B) - \frac{1}{\pi\eta} \ln\left(1 + B^2\right). \tag{2.87}$$

In the case of a system subjected to a spatially-averaged excitation, that is, $N_L = \infty$ and $N_R = \infty$, the relative variance is given by:

$$r_T^2 = \frac{1}{n(\omega)\Delta\omega} F(B). \tag{2.88}$$

GOE Statistics

Langley and Brown (3) extended the relative variance analytical formulation based on the GOE model for a narrow frequency domain, Equation

(2.81), to the case of a frequency-band averaged response. The relative variance of the frequency-band averaged kinetic energy density results is given by:

$$r_T^2(\omega,\Delta\omega) = \frac{(\alpha-1)}{\pi m}\left(\frac{1}{B^2}\right)\left\{2B\left[\frac{\pi}{2}-\arctan\left(\frac{1}{B}\right)\right]-\ln\left(1+B^2\right)\right\}+$$

$$+\frac{1}{(\pi m)^2}\left(\frac{1}{B^2}\right)\ln\left(1+B^2\right). \tag{2.89}$$

According to Brown (1), the accuracy of Equation (2.89) with the adjusted spatial parameter[25] (for instance $\alpha \approx 2.7$) is guaranteed within the range of $m > 0.4$ for a single point excitation. For a spatially distributed excitation where $\alpha \approx 1$, such as a rain-on-the-roof loading, Equation (2.89) is expected to have good accuracy for $m > 1$, Langley *et al* (18, 3, 16, 4).

2.4.4 Comments on Spatial Factor Characteristics

Regardless of the nature of the excitation, the kinetic energy density response of a particular subsystem can be written as (18, 3):

$$T(\omega) = \frac{\omega^2}{2}\sum_n \int_{\omega+-\Delta/2}^{\omega+\Delta/2} \frac{J_n}{\left(\omega_n^2-\omega^2\right)^2+\left(\eta\omega\omega_n\right)^2} d\omega \tag{2.90}$$

where the summation is taken over the local modes of the subsystem, and J_n is the modulus squared generalized force associated with the nth mass-normalized mode shape. Thus, the spatial factor α, defined previously in Equation (2.75), can be rewritten as:

$$\alpha = \frac{E\left[J_n^2\right]}{E\left[J_n\right]^2}. \tag{2.91}$$

In cases where the power arises from a spatially-distributed force applied over the spatial domain Ω of the subsystem, the squared generalized force J_n is written as (27):

$$J_n = \int_\Omega \int_\Omega \phi_n(\mathbf{x}) R_s\left(\mathbf{x},\mathbf{x}'\right) \phi_n\left(\mathbf{x}'\right) d\mathbf{x} d\mathbf{x}', \tag{2.92}$$

[25] Note that Gaussian mode shapes or perfect GOE eigenvector would yield $\alpha = 3$, Mehta (24).

where ϕ_n is the nth mode shape of the subsystem and R_s represents the *narrow-band spatial correlation function* of the excitation. As observed in Equation (2.92), the value of the spatial factor α is dependent on the spatial characteristics of the excitation field and the statistics of the subsystem mode shapes. Physically, this term indicates the sensitivity of the joint acceptance function[26] between the excitation and modes of the subsystem to changes in the mode shapes of the subsystem.

As discussed by Langley and Brown (1, 18, 3), the value of parameter α varies typically between 1 and 3 depending on the spatial characteristics of the excitation field and the main dimensionality of the subsystem of interest. The minimum value of the statistical factor is equal to unity and this is expected when the joint acceptance function is independent of changes in the mode shapes of the subsystem. For the particular case of spatially incoherent rain-on-the-roof excitation the term is unity and thus the input power to a subsystem is not sensitive to the mode shape statistics of the subsystem. For example, an upper value of approximately 3 will occur for a three dimensional cavity with Gaussian mode shapes excited by a single point excitation.

2.4.5 Non-universal Mode Shape Statistics Deviations

For the case of single point excitation, the spatial factor (α) is identical to the mode shape statistics factor (K) and the input power to a subsystem is highly sensitive to the mode shape statistics of the subsystem. In 1969, Lyon (48) defined the mode shape statistics factor using a spatial averaging approach. Considering, for convenience, the mode shapes as a product of the sinusoidal functions, mode shape statistics factor values of $K = 1.5$, $K = 2.25$, and $K = 3.375$ were obtained for uni, bi, and tri-dimensional systems, respectively.

The hypothesis of sinusoidal mode shapes has commonly been adopted for SEA variance predictions based on the Poisson natural frequency statistics, Lyon (48) and Davy (53, 54). However, it is important to emphasize that the mode shapes associated with Poisson natural frequency statistics are not necessarily sinusoidal and the sinusoidal mode shape hypothesis is very limited, being only valid for certain cases, such as simple geometry systems,

[26]The *joint acceptance* function is a measure of the strength of coupling between two wave fields where they are joined along a line or over an area, taking into account the relative amounts of phase reinforcement and cancellation over the space of the junction, Mead and Richards (152). In other words, the joint acceptance is a type of correlation-coupling function which describes how well the vibration modes harmonize with the spatial characteristics of the external excitation field, Gomes (28).

for example: a simply supported rectangular plate or a box-shaped acoustic space[27], Langley and Cotoni (35).

Recently Langley and Brown (18) defined the mode shape statistics factor using the ensemble averaging approach and assumed that the mode shape components of random engineering system are statistically independent and have a Gaussian distribution across the ensemble as described by the GOE model. For perfect Gaussian mode shapes, a value of $K = 3$ is obtained, regardless of the system dimensionality, (35).

In the SEA variance literature, an excellent agreement was reached between the predicted single-loading relative variance values and the numerical (or experimental) results when a value of K lower than 3 was adopted. Indeed, it is usually argued that the good agreement with the SEA variance theory for $K < 3$ is due to the distribution of the mode shape components not being perfectly Gaussian as predicted by the GOE model of the RMT.

The main factors and influences associated with these mode shape statistics factor discrepancies between the mode shape statistics of random engineering systems and the GOE eigenvector statistics have been the subject of several academic research studies. In the RMT field, Brody *et al* (56) suggested that the GOE mode shapes become asymptotic Gaussian with an increase in the eigenvector dimension and thus a value of $K = 3$ is only expected in the case of very large random matrices. In the elastodynamics field, the numerical and experimental results obtained in Lobkis' studies showed that the natural frequency statistics conform very well with the GOE model, although some deviations have been identified for the corresponding mode shapes, (50). Lobkis *et al* suggested that these mode shape statistics discrepancies and low values of K may be associated with the presence of complex modes. Subsequently, Langley and Brown (18, 3, 1) investigated the mode shape statistics of mass-loaded plate systems. The typical values of K found were significantly lower than the Gaussian value of $K = 3$. Since the mode shape components were considered to be fully real numbers, the postulation, proposed previously by Lobkis *et al* (50), that the mode shape statistics factor will be lowered if the mode shapes are complex, was definitively discarded.

Additionally, Brown in (1) suggested that the establishment of correlations between the same component of different mode shapes may be responsible for the discrepancies observed between the numerical (or experimental)

[27] In the present study, the SEA variance predictions based on Poisson model for natural frequency statistics consider that the corresponding mode shapes have sinusoidal statistics, while those based on GOE model for natural frequency statistics consider that the corresponding mode shape have Gaussian statistics.

results and the theoretical variance prediction based on the GOE model, since the theory assumes statistical independence of the mode shape components and does not allow for correlations between different mode shapes. In particularly, in the case of mass-loaded plates, the point masses attached to the plate surface could make the plate effectively *clamped* at those point mass locations and lead to the introduction of significant correlations between different mode shapes at the force position. Indeed, if large amounts of point masses were placed randomly on the plate, the variance of the energy response for a point excitation could under predict the analytical expression due to this clamping effect.

Recently, Langley and Cotoni (35) investigated numerically the statistical moments of the mode shape amplitudes across an ensemble composed of very perturbed mass-load plates. The statistical moments of the mode shape amplitudes across an ensemble were also compared with analytical predictions based on Gaussian and sinusoidal mode shapes. A value of $K = 2.87$ was observed for the mode shape statistics factor associated with the excitation point across the ensemble. The results suggested that the distribution of the mode shape components is expected to be *almost Gaussian* when an ensemble mode shape averaging approach is considered. Considering that the mode shapes are almost Gaussian, the current value of the mode shape statistics factor from the numerical analysis of the statistical moments of the mode shape components was employed in point-loading relative variance formulations. The adjusted theoretical variance prediction was compared with numerical results from an ensemble composed of 200 mass-loaded plate members. Again, the adjusted theoretical variance prediction, surprisingly, over predicted the numerical results. Additional numerical simulations were performed using 10,000 realizations for four discrete frequencies and the numerical variances were in closer agreement with variance prediction based on GOE model. These results indicate that the performance of theoretical variance prediction is dependent on the size of the ensemble adopted, that is, the ensemble must include a sufficient number of members to yield realistic results for the energy response statistics.

Based on the above discussion, several possible reasons for the establishment of non-Gaussian statistics for the mode shapes of sufficiently random systems were identified and further investigations are certainly required to determine the precise contributions from each mode shape deviation class to the energy variance results, Gomes (10).

2.5 Summary and Discussions

In this chapter a brief literature review were carried on the main aspects associated with the statistical analysis of natural frequencies and corresponding mode shapes of vibroacoustic systems.

Initially, the main concepts of Random Matrix Theory (RMT) applied to statistical analysis for the natural frequencies of random systems were reviewed. Particular attention was given to descriptions of the statistical characteristics of a particular ensemble composed of large random symmetric matrices known as the *Gaussian Orthogonal Ensemble* (GOE). As shown in the literature, the eigenvalue statistics of GOE matrices are expected to be surprisingly very similar to the natural frequency statistics of sufficiently random vibroacoustic systems. The definitions of particular metric functions called *statistical observables* were introduced for short and long fluctuation ranges. These functions shown to be able to describe correctly the typically physical phenomena expected for the natural frequency spectrum of real engineering systems, such as *level repulsion* and *spectral rigidity*.

Although the excellent results have been founded for the use of RMT concepts in the statistical analysis of random vibroacoustic systems, some limitations to the direct use of RMT concepts have been identified in studies carried out with elastodynamical systems. Two classes of non-universal natural frequency statistics deviations were identified: the effects of the *finite wavelengths* and the establishment of *stable periodic orbits*. The main effects on natural frequency statistics due to the establishment of non-universal effects were also discussed in terms of the statistical observable results for short and long fluctuation ranges.

Considering the corresponding mode shapes, a complete characterization of the universal GOE statistics of mode shapes was performed using the results for the eigenvector statistical observables. Besides the proposed analytical predictions presented extensively in RMT literature, the definitions of the kurtosis metrics and Lilliefors normality test were introduced and their applications were discussed for statistical mode shape analysis of the vibroacoustic systems. The possible kurtosis averaging approaches to evaluation of the Mode Shape Statistics Factor were reviewed in the SEA context.

Although the universal characteristics of mode shapes are extremely convenient from an analytical point of view, some non-universal characteristics are observed in the mode shape statistics of random engineering systems. Therefore, the main possible deviations from *universal* mode shape statistics were identified and discussed in the context of vibroacoustic systems. Two

classes of non-universal mode shape deviations were considered: the establishment of periodical orbits and the effects of structural localization.

In last section the main aspects associated with SEA variance theory were discussed. The analytical predictions based on Poisson and GOE models for the relative variance of the energy responses across the ensemble were presented for single subsystem subjected to point-loading and spatially-averaged excitations. The main details associated with the evaluation of the spatial factor parameter and its relationship with the joint acceptance function, which quantifies the degree of harmonization between the mode shapes and the spatial characteristics of the excitation field, were highlighted. For the case of single point-loading, the possible reasons for the establishment of the *non-universal* characteristics of the mode shapes of random engineering systems were highlighted and discussed in detail.

In the next chapters, the systematic numerical analysis of random systems will be carried in order to understand the main practical aspects associated with the establishment of *universal* statistics as well as the resultant performance of the relative variance predictions based on the complete GOE model. The main statistical observables reviewed in this chapter will be employed to verify the agreement of each modal parameter statistics with the *universal* statistics described by the GOE model. Additionally, the typical *non-universal* characteristics of modal parameters expected from the real random engineering systems will be identified and classified. The main impacts of the non-universal contributions on the performance of the SEA variance prediction based on a complete GOE model will be investigated in detail.

3 NUMERICAL ANALYSIS OF RANDOM LONGITUDINAL RODS

3.1 Overview

Although the application of Random Matrix Theory concepts to the statistical analysis of engineering systems has been the subject of many publications in recent years, some important questions still remain unclear. The issue regarding the complete establishment of *universal* GOE statistics for modal parameters[1] of real engineering systems as well as the validity of *ergodicity* concept[2] are aspects of recent interest and further investigations are required, Gomes (10).

In this chapter, a complete statistical analysis is performed with random one-dimensional structures[3]. The effects of distinct uncertainty sources on the modal parameter statistics are investigated through the *statistical observables* of Random Matrix Theory (RMT). In this study, the random longitudinal rods were generated using Finite Element Method (FEM). The distinct structural irregularities, or uncertainties, were introduced on a nominal rod structure and different approaches to the uncertainty distribution (randomization approaches) were also considered. In the numerical analysis, the spectral and ensemble averaging processes were performed for random rod energy responses. In addition, the main effects of the spatial correlation from the rod geometry and of the structural localization phenomenon on the modal parameter statistics were also investigated using the RMT statistical observables.

Finally, important contributions were obtained regarding the establishment of *universal* statistics for each one of the modal parameters as well as for the statistical moments of the kinetic energy density results of random longitudinal rod structures.

---

[1] In the Dynamics field, the system modal parameters comprise the natural frequencies and the mode shapes (or eigenvalues and eigenvectors, respectively), Meirovitch (22, 89).

[2] The validity of ergodicity concept ensures that there is an equivalence between the theoretically calculated ensemble average and the physically more relevant spectral average, Pandey (108).

[3] The work presented in this chapter was carried out under the supervision of and with the collaboration of professors Brian R. Mace and Neil S. Ferguson from the Dynamics Group, Institute of Sound and Vibration Research (ISVR) at the University of Southampton; Gomes and Gerges (153); Gomes and Mace (83); Gomes, Mace and Ferguson (154).

3.2 Longitudinal Rod Characteristics

In order to investigate the *universal* establishment of GOE statistics for the modal parameters of random one-dimensional structures, the numerical analysis was performed using longitudinal rods with uncertain or nondeterninistic parameters and properties. The main reasons for adopting this class of nominal structure are:

- *frequency-constant modal density:* the natural frequency spectrum of a nominal longitudinal rod shows frequency-constant natural frequency spacings, as well as stationary statistical properties along the frequency domain, Timoshenko and Young (155). These characteristics are very convenient for performing direct comparisons between numerical results and RMT analytical predictions, since the latter are based on the unitary and frequency-constant eigenvalue spacing mean, Mehta (24).

- *sinusoidal mode shapes:* the longitudinal mode shapes of the nominal rod structure are perfectly sinusoidal. Considering sinusoidal eigenvector statistics, the available analytical predictions provide a complete description of the mode shape statistics, Waterhouse (130). In this regard, the sinusoidal analytical predictions are efficient tools to characterize the main effects of the introduction of the uncertainties on the nominal mode shape statistics.

- *low computational cost:* since the system analyzed is one-dimensional, low computational processing skills are required and thus several classes of uncertainty sources can be easily investigated with low computational cost.

3.3 Finite Element Model: Longitudinal Rod

In this study, the random rod structures investigated were generated using the Finite Element Method (FEM), Zienkiewicz (2). The FEM model characteristics and validation process are described in detail below.

3.3.1 FEM Model Development

For the development of numerical models of random longitudinal rod structures, the FEM commercial software ANSYS was used, (156, 157). In the current work, the investigated system comprises a longitudinal cylindrical

rod with uncertain or non-deterministic parameters. The random rod parameters may vary across the ensemble or spatially along its length. In addition, some random rods investigated also considered small point masses attached to the rod surface in the randomization process, in order to simulate the possible irregularities of mass distribution along the rod length, (18) (35).

In order to obtain a good description of the dynamical behavior from a rod structure subjected to a longitudinal loading, the finite element BEAM3 was adopted, (156). This finite element is a uniaxial element with tension, compression, and bending capabilities. The element has three degrees of freedom at each node: translations in the nodal x and y directions and rotation about the nodal z - axis.

For the FEM representation of structural point masses, the finite element MASS21 was adopted. This element is a point element having up to six degrees of freedom: translations in the nodal x, y, and z directions and rotations about the nodal x, y, and z - axes. In Figure 39, a typical example of a random rod structure investigated in this study is shown. In this FEM model, 20 small point masses (corresponding to 20% rod mass absent of uncertainties) are randomly attached onto the rod surface along its length.

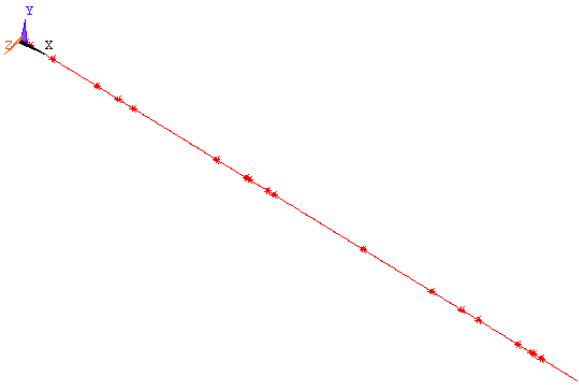

Figure 39: An example of the FEM model of a typical random rod investigated in this study.

3.3.2 FEM Model Validation

In order to validate the numerical FEM model performance, a direct comparison was made between the modal parameters obtained from the FEM model and those evaluated from the analytical predictions for a longitudinal rod with a circular cross-sectional area; Thomson (158), and Timoshenko & Young (155). The FEM model was built considering a nominal rod, the parameters of which are absent of uncertainties. In Tables 4 and 5, the geometric dimensions and material properties of the nominal rod are described, respectively.

Table 4: Nominal longitudinal rod: geometric dimensions.

Geometric parameter	Value
Longitudinal length (L_r)	5 m
Cross-section diameter (d_r)	1 cm

Table 5: Nominal longitudinal rod: material properties - standard carbon steel.

Material property parameters	Value
Young's modulus (E_{ym})	210 G Pa
Poisson ratio (ν)	0.3
Density (ρ)	7860 kg/m^3

During the FEM model development, the common rule of 12 finite elements for the smallest longitudinal wavelength was considered, Zienkiewicz (2). Additionally, it is important to emphasize that the validity conditions of the analytical models were also respected for the highest frequency of interest. That is, the smallest longitudinal wavelength is larger than the rod cross-sectional dimension, Timoshenko and Young (155).

The free-free boundary condition was considered. The frequency range considered was from 0 to 50 kHz and the first 100 longitudinal modes were evaluated for both model approaches. In Figure 40, the FEM model performance is shown in terms of natural frequencies.

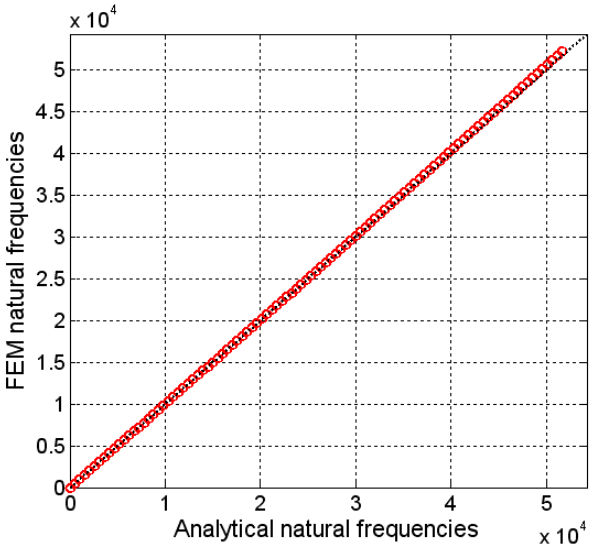

Figure 40: Natural frequency performance: FEM model results and analytical predictions.

According to Figure 40, the natural frequency results suggest only small discrepancies for the high order mode range. In general, the natural frequency results obtained from the FEM model conform very well with the analytical predictions. In Figure 41, some longitudinal mode shapes obtained from the FEM model are compared to those corresponding to the analytical formulation. The mode shapes are normalized to have unit maximum amplitude.

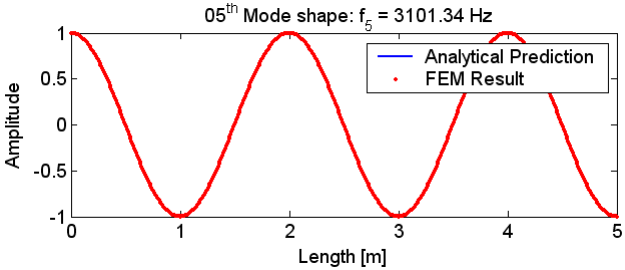
05th Mode shape: f5 = 3101.34 Hz
Analytical Prediction
FEM Result
Amplitude
Length [m]

(a)

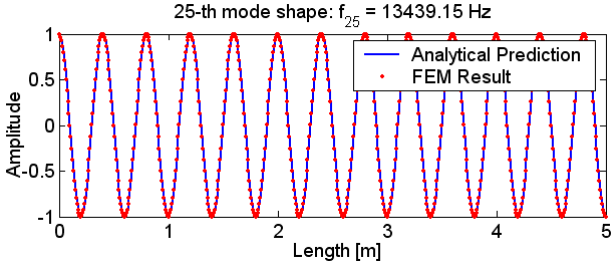
25-th mode shape: f25 = 13439.15 Hz
Analytical Prediction
FEM Result
Amplitude
Length [m]

(b)

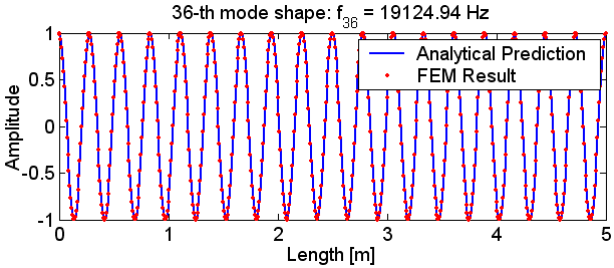
36-th mode shape: f36 = 19124.94 Hz
Analytical Prediction
FEM Result
Amplitude
Length [m]

(c)

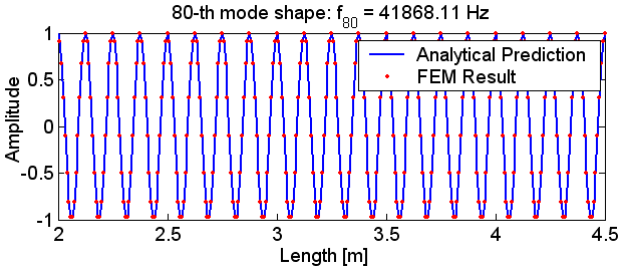

(d)

Figure 41: Mode shape performance: FEM model results and analytical predictions. Plots: (a) Mode 05, (b) Mode 25, (c) Mode 36, and (d) Mode 80 (higher order mode - zoom plot).

Similarly to the natural frequency results, the excellent performance of the FEM model was also confirmed for the corresponding mode shapes. Indeed, the FEM mode shapes conformed very well with the sinusoidal predictions.

In summary, based on Figures 40 and 41, in relation to the modal parameter performance results, it appears that the numerical FEM models are able to represent adequately the modal parameter statistics for the class of rod structure investigated herein.

As described, several FEM models were developed in order to investigate the main effects of the uncertainties on the modal parameter statistics as well as on the statistical moments of the kinetic energy density results obtained from the distinct natures of external loadings.

3.4 Spectral Averaging Approach

In this section, the main effects of different uncertainty sources are evaluated through the use of the statistical observables of the Random Matrix Theory (RMT). The spectral statistics of the modal parameters, natural frequencies and corresponding mode shapes, are evaluated and compared with analytical predictions obtained using the best known statistical models: *Poisson* statistics[4] and the statistics of the *Gaussian Orthogonal Ensemble* (GOE)

[4] *Poisson statistics* is also known as *random number statistics*, Montgomery and Runger (103).

of RMT, Mehta (24).

In the following sections, the *spectral averaging approach* is initially adopted in the first stage of this study, and statistical analysis of the kinetic energy density results was performed in the 1/3-octave frequency band domain for each random rod structure investigated. Additionally, the relationship between the statistical moments of the kinetic energy density results and the modal parameter statistics are highlighted and discussed.

In the next subsections, the two main classes of random rod structures investigated hereafter are described in terms of their uncertainty levels and sources. The numerical results of the spectral analysis are presented and discussed in terms of the modal parameter statistics as well as in terms of the statistical moments of the kinetic energy density results as the random rods are excited by a single point-loading or spatially-averaged excitation.

3.4.1 Breaking the Geometrical Regularity

The first rod class investigated considers the cross-sectional area of the circular rod as a random variable along the rod length. The other rod parameters: length and material properties, are adopted to be identical to nominal rod parameters, that is, absent of uncertainties. In this context, it appears that a breaking of the geometry regularity is obtained as the cross-sectional area varies sufficiently along the rod length.

In order to evaluate the sensitivity of the statistical moments of the energy responses to different randomization approaches, distinct probabilistic distributions are considered for the rod cross-sectional area values (uniform and normal distributions). Additionally, different randomness (or uncertainty) levels[5] are also considered for each randomization approach. Therefore, several FEM models were built with several randomness levels and distinct source probabilistic distributions. In Table 6, the main characteristics adopted in the development of the random longitudinal rods investigated hereafter are described in detail.

[5]The randomness levels of the rod cross-sectional area were defined in relation to the nominal cross-sectional area.

Table 6: Random rod descriptions - spectral averaging approach: nomenclature, random variable, statistical distribution, and randomness level.

Nomenclature	Random variable	Statistical distribution	Randomness level (%)
Nominal	Cross-sectional area	Dirac delta	Null
Gaussian (10 %)	Cross-sectional area	Gaussian	10
Gaussian (20 %)	Cross-sectional area	Gaussian	20
Gaussian (30 %)	Cross-sectional area	Gaussian	30
Uniform (10 %)	Cross-sectional area	Uniform	10
Uniform (20 %)	Cross-sectional area	Uniform	20

3.4.2 Random Point Masses

In order to evaluate the effects of mass distribution irregularities on the modal parameters and the kinetic energy response statistics, a second class of random rod structures was also investigated. These random rods were generated through the attachment of 20 small point masses on the nominal rod surface.

A uniform spatial distribution is adopted for point mass locations and mass perturbation levels of 10% and 20% are considered in relation to the bare nominal rod mass. In this second class of the rod structures, the rod parameters and properties are considered identical to those of the nominal rod, that is, with the absence of uncertainties. In Table 7, the descriptions of the random mass-loaded rods are shown in detail.

Table 7: Descriptions of the random mass-loaded rods - spectral averaging approach: nomenclature, random variable, statistical distribution, and randomness level.

Nomenclature	Random variable	Statistical distribution	Randomness level (%)
Mass (10%)	Point mass location	Spatially uniform	10 % of bare rod mass
Mass (20%)	Point mass location	Spatially uniform	20 % of bare rod mass

It is import to emphasize that bi-dimensional random mass-loaded structures similar to ones presented in Table 7 have been commonly adopted in numerical and experimental validations of revised SEA variance predictions which consider in their derivation the GOE model for both modal parameter statistics, Langley *et al* (16, 3, 18, 4, 35, 17) and Cordioli *et al.* (19) and Cordioli (20).

In the present work, particular interest is focused on one-dimensional random mass-loaded structures since, for this particular group of structures, the establishment of the *structural localization* phenomenon is expected. As shown by Hodges *et al* (140, 139, 151, 159), the structural localization effects may modify significantly the probabilistic distribution characteristics of kinetic energy responses of engineering structures, because their effects are directly associated with the occurrence of energy confinement to certain spatial regions of the structure. In this regard, numerical investigations were performed in this study in order to establish a consistent relationship between structural localization effects and the SEA prediction performance.

3.4.3 Spectral Natural Frequency Statistics

In the following sections, the statistical characterizations of the natural frequencies of random longitudinal rod structures, described in previous subsections, are performed using the RMT eigenvalue statistical observable results.

Probability Density Function of Adjacent Natural Frequency Spacings

The first eigenvalue statistical observable evaluated is the Probability Density Function (PDF) of adjacent natural frequency spacings, which describes the *short-range fluctuation* statistics. In Figure 42, the numerical PDF results for random rods described previously are shown[6]. The analytical predictions: Gaussian (Normal), Poisson (Exponential), and GOE (Rayleigh) are also plotted. It is important to emphasize that all numerical spacing PDF results were evaluated from the *unfolded spectra* where the mean value of the natural frequency spacings is frequency-constant and unitary.

[6]The modal parameter statistics of the Uniform (10%) and Mass (10%) rod structures are evaluated indirectly through the Hamiltonian matrix structural analysis performed in the section 3.4.5.

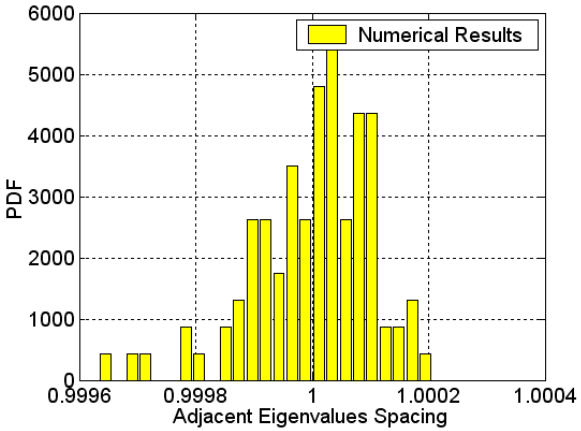
Numerical Results
PDF
6000
5000
4000
3000
2000
1000
0
0.9996
0.9998
1
1.0002
1.0004
Adjacent Eigenvalues Spacing

(a)

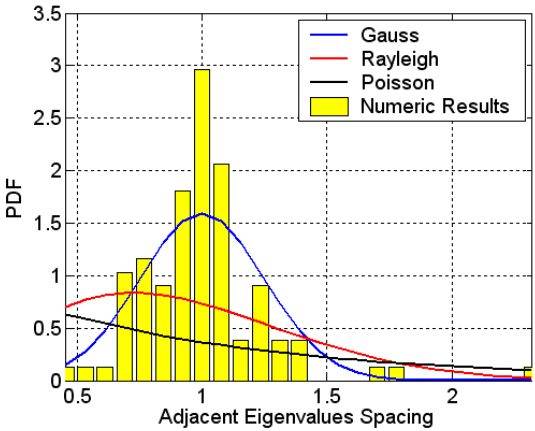
Gauss
Rayleigh
Poisson
Numeric Results
PDF
3.5
3
2.5
2
1.5
1
0.5
0
0.5
1
1.5
2
Adjacent Eigenvalues Spacing

(b)

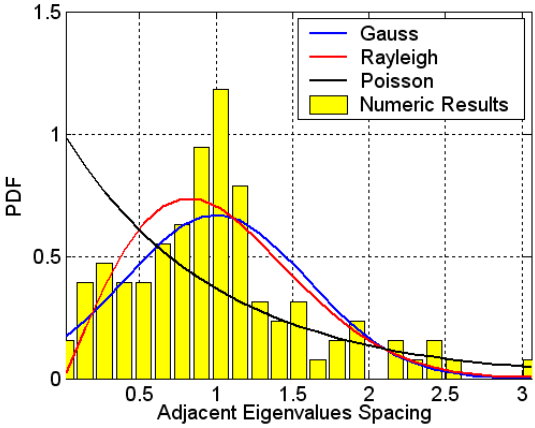
Gauss
Rayleigh
Poisson
Numeric Results
PDF
Adjacent Eigenvalues Spacing
0
0.5
1
1.5
2
2.5
3

(c)

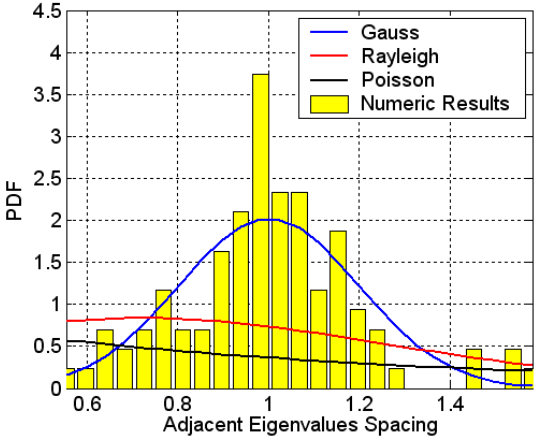
Gauss
Rayleigh
Poisson
Numeric Results
PDF
Adjacent Eigenvalues Spacing
0
0.5
1
1.5
2
2.5
3
3.5
4
4.5
0.6
0.8
1
1.2
1.4

(d)

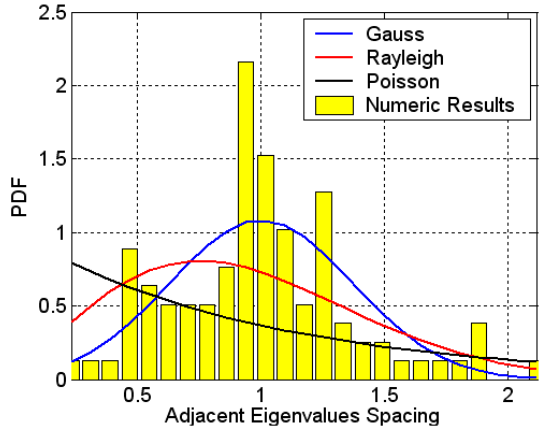

(e)

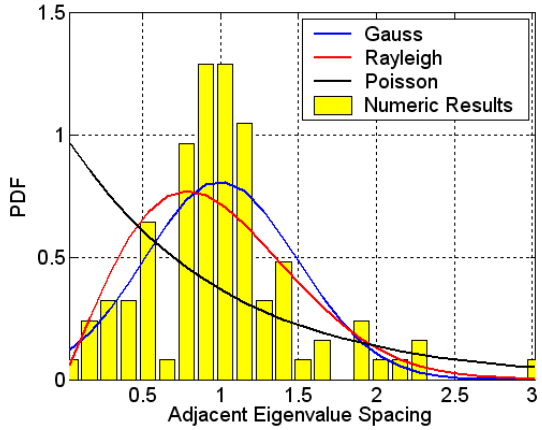

(f)

Figure 42: The unfolded natural frequency spacing PDF results and analytical predictions: Gaussian (Normal), Poisson (Exponential), and GOE (Rayleigh) (spectral averaging approach). Plots: (a) Nominal, (b) Uniform (20%), (c) Mass (20%), (d) Gaussian (10%), (e) Gaussian (20%), and (f) Gaussian (30%).

As shown in Figure 42 (a), the spacing PDF result for the nominal rod has a curve pattern similar to Delta Dirac (pulse) function. Indeed, as expected for the nominal rod structure, the natural frequency spacings are practically frequency-constant, Timoshenko and Young (155).

As shown in Figures 42 (b) - (f), the numerical PDF results suggest the establishment of the *high spectral rigidity characteristics* in the natural frequency spectra for all random rods investigated. That is, a large probability associated with the occurrence of unitary natural frequency spacings is clearly observed, regardless of the uncertainty sources and levels.

As the randomness level increases, the spectral spacing statistics of the nominal unfolded natural frequencies, which is similar to Dirac Delta distribution, are significantly perturbed and disordered statistics are clearly established for the random rods with a high level of randomness. As observed in Figure 42, the intermediate distribution similar to those of the *Normal* and *Rayleigh* cases (Gaussian and GOE statistics, respectively) are expected during the statistical transition process from nominal to disordered statistics. A good example of this statistical transition process is observed in the random Gaussian rods as the randomness level increases in a gradual manner.

Natural Frequency Correlation Coefficient

In order to assess the spectral correlations between the natural frequencies, the *eigenvalue correlation coefficient*[7] was evaluated for each one of the random rods investigated, Brody *et al* (56).

The definition of the natural frequency correlation coefficient is given by:

$$C_2(\Lambda) = \frac{E\left[\left(z_i - \overline{z}\right)\left(z_{i+\Lambda} - \overline{z}\right)\right]}{E\left[\left(z_i - \overline{z}\right)^2\right]}, \tag{3.1}$$

where z_i is the ith unfolded spacing, $\overline{z}$ is the spectral spacing mean value, and Λ is the number of spacings between values. For GOE eigenvalues, this correlation coefficient has been evaluated to be $C_2(\Lambda) = -0.271$ for $\Lambda = 1$, Brody *et al* (56).

According to Langley and Brown (1, 18), the natural frequency correlation has significant influence on the energy response variance in the SEA context. The natural frequency correlation reduces the response variance,

[7] The *eigenvalue correlation coefficient* is also known as the *correlation function of the natural frequency spacings*, Brody *et al* (56).

since larger fluctuations in the kinetic energy density results arise when there is a succession of small or large natural frequency spacings. Additionally, it is also expected that natural frequency correlation effects become more relevant as the modal overlap increases.

The natural frequency correlation coefficient results are shown in Figure 43. The correlation coefficient results computed for the eigenvalues of large random matrices with GOE and Poisson statistics are also plotted, Gomes and Gerges (101).

In Figure 43 (a), the nominal rod results suggest a high correlation level between the natural frequencies even for large spectral natural frequency distances. On the other hand, the eigenvalues from the large GOE and Poisson random matrices shown *almost*-null correlation coefficient values for most of spacing numbers (Λ), suggesting the establishment of spectral rigidity characteristics lower than those displayed by the natural frequencies of nominal rod[8].

As shown in Figures 43 (b) - (f), the presence of uncertainties leads to a significant reduction in the spectral natural frequency correlation for all random rods investigated. Indeed, it is also relevant to observe that all random rod results showed negative values for unitary spacing ($\Lambda = 1$), suggesting the establishment of the *level repulsion phenomenon* for natural frequencies. On the other hand, the presence of small discrete peaks is observed for large spectral distances, showing some residual high *spectral rigidity characteristics* which are associated with the expected spectral characteristics of the nominal rod.

[8]More details on the physical interpretation of the correlation coefficient results for random dynamical systems are available on Langley and Brown (18) and Brown (1).

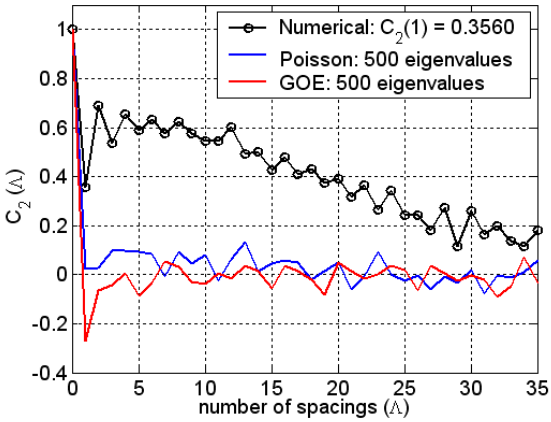
Numerical: C2(1) = 0.3560
Poisson: 500 eigenvalues
GOE: 500 eigenvalues
C2 (Λ)
number of spacings (Λ)

(a)

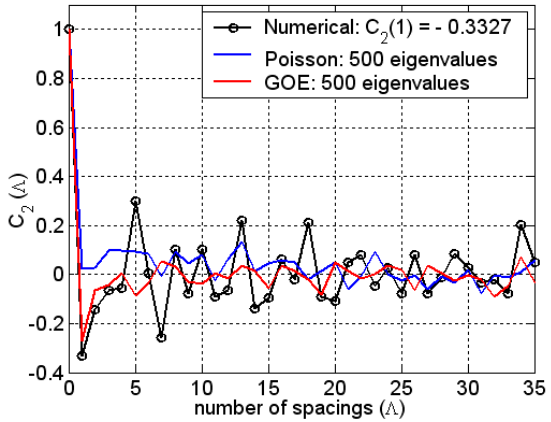
Numerical: C2(1) = - 0.3327
Poisson: 500 eigenvalues
GOE: 500 eigenvalues
C2 (Λ)
number of spacings (Λ)

(b)

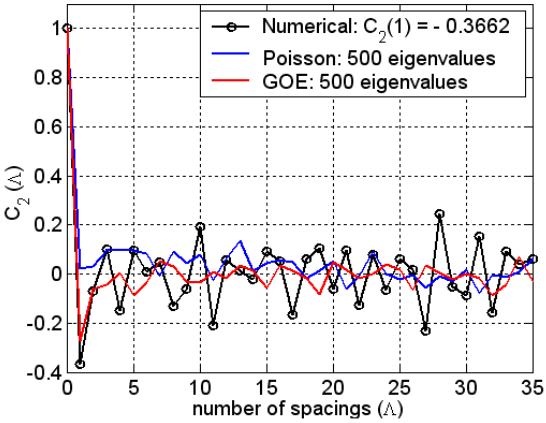
Numerical: C2(1) = - 0.3662
Poisson: 500 eigenvalues
GOE: 500 eigenvalues
C2 (Λ)
number of spacings (Λ)

(c)

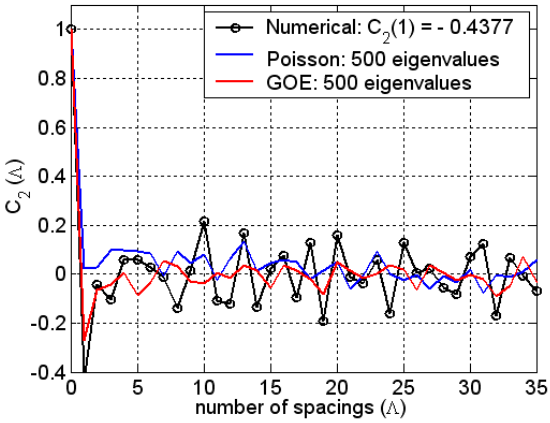
Numerical: C2(1) = - 0.4377
Poisson: 500 eigenvalues
GOE: 500 eigenvalues
C2 (Λ)
number of spacings (Λ)

(d)

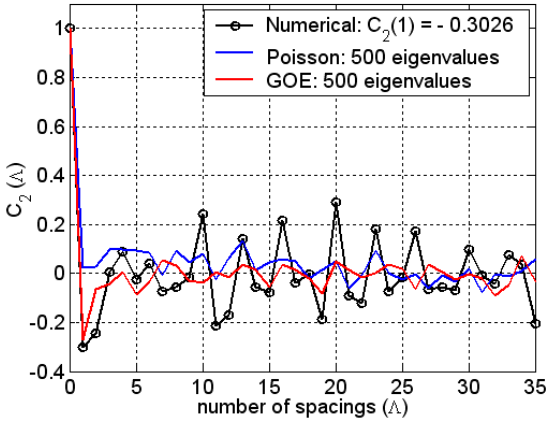

(e)

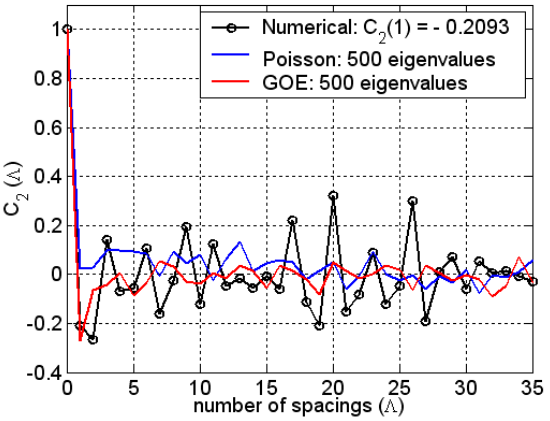

(f)

Figure 43: Correlation coefficient of the natural frequency spacings: the random rod results are compared to the eigenvalue correlation function results of the *dim* (500*500) GOE and Poisson matrices (spectral averaging approach). Plots: (a) Nominal, (b) Uniform (20%), (c) Mass (20%), (d) Gaussian (10%), (e) Gaussian (20%), and (f) Gaussian (30%).

Number Variance and Δ_3-statistics

The measure functions of the *long-range fluctuation* statistics used traditionally in the random matrix literature are the number variance and the Δ_3-statistics, Mehta (24). In Figure 44, the number variance results for the nominal and random longitudinal rods are compared to the GOE and Poisson model predictions.

For the nominal rod, it is expected that number variance values are null for integer spectral natural frequency spacings, Weaver (64). As shown in Figure 44 (a), the number variance results comply with this hypothesis mainly in the small spacing range, but some small discrepancies are clearly observed in the large spacing range. In fact, it appears that these small disagreements are due to slightly reduced FEM model performance associated with the high-frequency range.

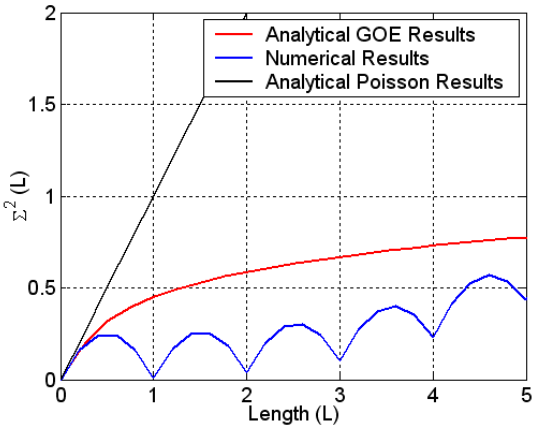

(a)

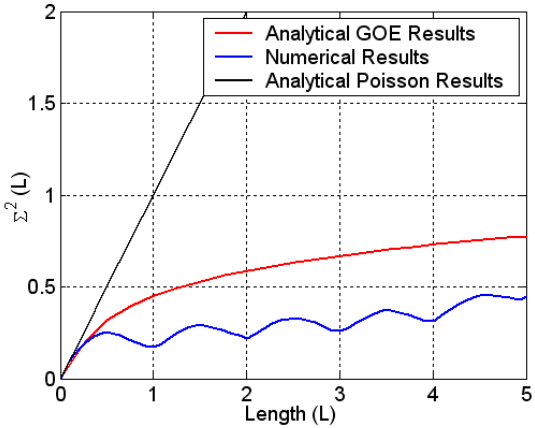
Analytical GOE Results
Numerical Results
Analytical Poisson Results
Σ^2 (L)
Length (L)
0
0.5
1
1.5
2
0
1
2
3
4
5

(b)

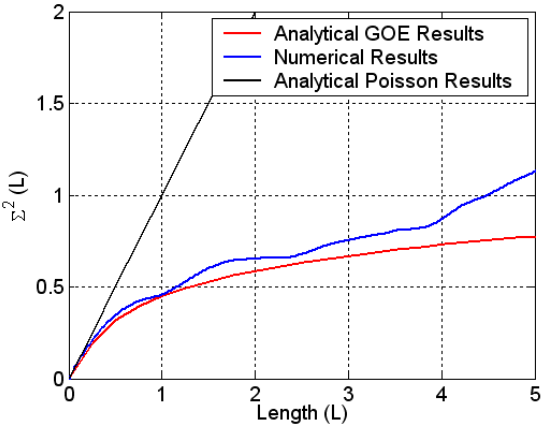
Analytical GOE Results
Numerical Results
Analytical Poisson Results
Σ^2 (L)
Length (L)
0
0.5
1
1.5
2
0
1
2
3
4
5

(c)

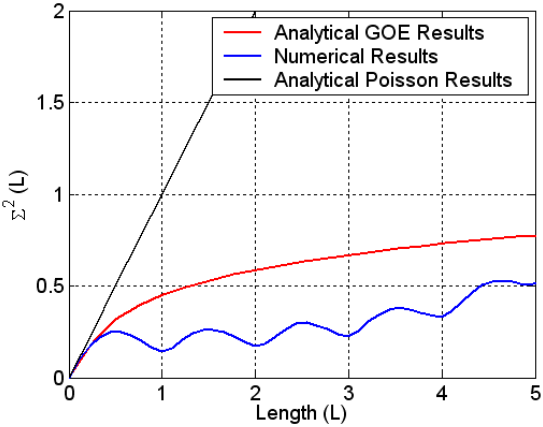
Analytical GOE Results
Numerical Results
Analytical Poisson Results
Σ^2 (L)
Length (L)
0
0.5
1
1.5
2
0
1
2
3
4
5

(d)

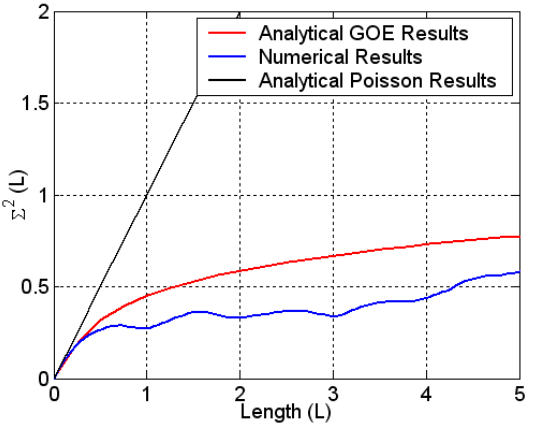
Analytical GOE Results
Numerical Results
Analytical Poisson Results
Σ^2 (L)
Length (L)
0
0.5
1
1.5
2
0
1
2
3
4
5

(e)

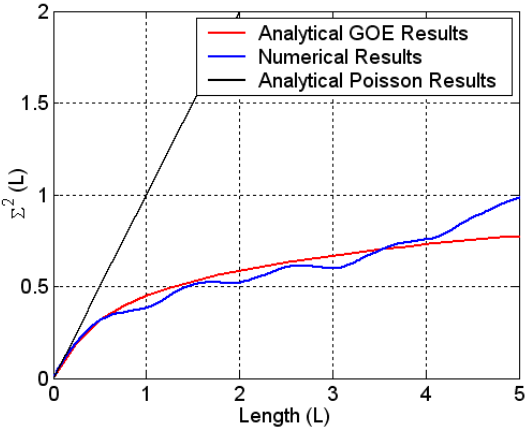

(f)

Figure 44: The number variance results for the nominal and random rods, and GOE and Poisson analytical predictions (spectral averaging approach). Plots: (a) Nominal, (b) Uniform (20%), (c) Mass (20%), (d) Gaussian (10%), (e) Gaussian (20%), and (f) Gaussian (30%).

On the other hand, for random rod structures, Figures 44 (b) - (f), the uncertainty effects reduce the spectral rigidity characteristics and lead to an increase in the number variance values. The number variance results suggest different levels of spectral rigidity characteristics for each one of the randomization approaches investigated. In general, as the uncertainty level increases, there is a strong tendency for the establishment of statistics described by the GOE model. This tendency is observed in the number variance results for the Mass (20%) and Gaussian (30%) random rod structures, Figures 44 (c) and (f), respectively. Although the uncertainty sources of these rod structures are completely distinct, their spectral natural frequency statistics are very similar and show approximately GOE natural frequency statistics. In Figure 45, the Δ_3-statistics results for the nominal and random rods are displayed.

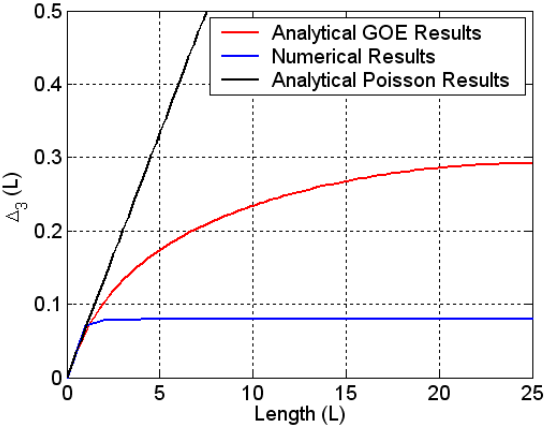
Analytical GOE Results
Numerical Results
Analytical Poisson Results
Δ_3 (L)
Length (L)
0
0.1
0.2
0.3
0.4
0.5
0
5
10
15
20
25

(a)

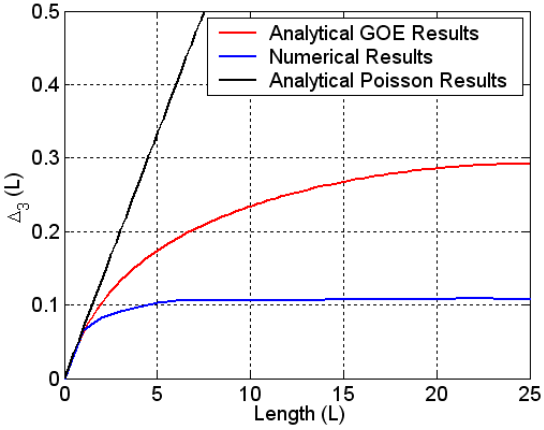
Analytical GOE Results
Numerical Results
Analytical Poisson Results
Δ_3 (L)
Length (L)
0
0.1
0.2
0.3
0.4
0.5
0
5
10
15
20
25

(b)

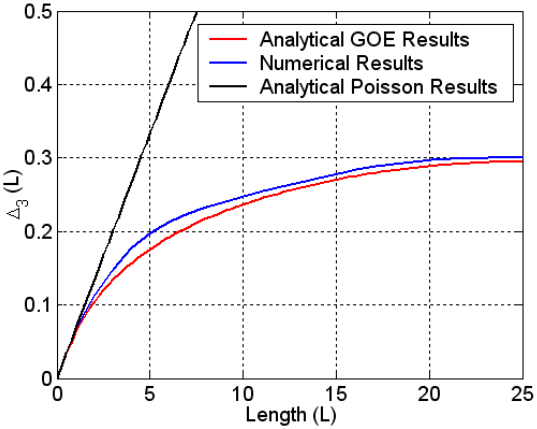
Analytical GOE Results
Numerical Results
Analytical Poisson Results
Δ3 (L)
Length (L)
0
0.1
0.2
0.3
0.4
0.5
0
5
10
15
20
25

(c)

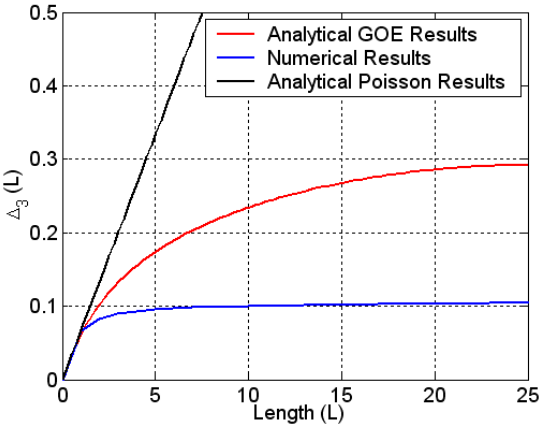
Analytical GOE Results
Numerical Results
Analytical Poisson Results
Δ3 (L)
Length (L)
0
0.1
0.2
0.3
0.4
0.5
0
5
10
15
20
25

(d)

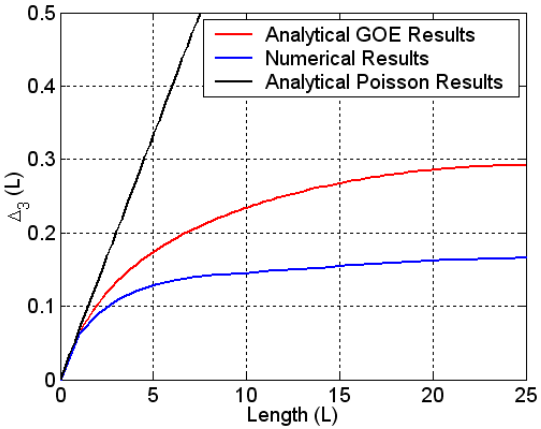

(e)

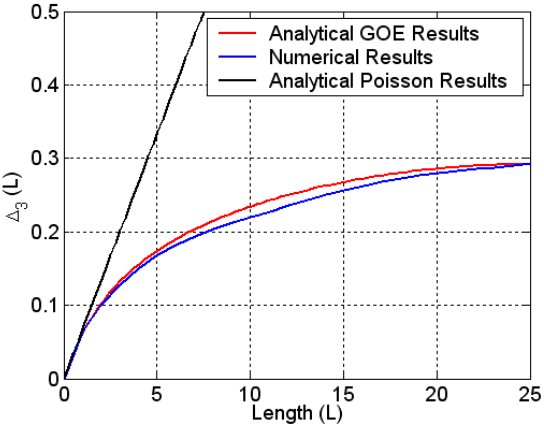

(f)

Figure 45: The Δ_3-statistics results for the nominal and random rods and analytical predictions of the GOE and Poisson models (spectral averaging approach). Plots: (a) Nominal, (b) Uniform (20%), (c) Mass (20%), (d) Gaussian (10%), (e) Gaussian (20%), and (f) Gaussian (30%).

According to Figures 45 (a) - (b) and (d), the Δ_3-statistics results for the nominal and random rod structures with a low level of randomness showed an almost constant value throughout the natural frequency spacing domain. Indeed, this global pattern for the Δ_3 - statistics results occurs due to significant spectral rigidity characteristics associated with this particular group of structures. For Uniform (20%) and Gaussian (10%) random rods, the Δ_3 - statistics results suggest a small and uniform reduction in the spectral rigidity characteristics throughout the natural frequency spacing domain, that is, uniform and slightly increasing of Δ_3 - statistics values. Therefore, it appears that the increase in the randomness level leads to a transition from *high spectral rigidity* statistics to GOE statistics in Figures 45 (d) - (f). The results for the Gaussian rod structures suggest that the reduction in the spectral rigidity characteristics begins at large spectral natural frequency distances (long-range fluctuation) and continues until small spectral natural frequency distances (short-range fluctuation). Similarly to the number variance results, the Δ_3- statistics results for the Mass (20%) and Gaussian (30%) random rods also show a certain level of *universal* characteristics and conform well with the GOE analytical predictions, Figures 45 (c) and (f), respectively.

Although the Δ_3 - statistics function is successfully applied to the spectral analysis of random systems with distinct natures, some relevant issues must be highlighted regarding the performance of its use to characterize the spectral natural frequency statistics.

Considering the natural frequency statistics results for the Gaussian (30%) and Mass (20%) random rods, an excellent agreement with the analytical prediction based on the GOE model is observed for Δ_3 - statistics as well as the number variance results. However, the corresponding natural frequency statistics results for the statistical observables for short-range fluctuation, the spacing PDF and natural frequency correlation coefficient, shown high spectral rigidity characteristics for the small natural frequency spacing range, Figures 42 and 43, respectively. In other words, the short-range fluctuation statistics results for both random rods showed a high probability for the natural frequency spacings to be close to unitary magnitude (expected mean value of the nominal unfolded natural frequency spacings). Thus, it appears that the spectral natural frequency statistics for these random rods do not conform completely with the *universal* statistics described by the GOE model and that they have *system-dependent* characteristics.

It is important to emphasize that the long-range fluctuation statistical observables, the Δ_3 - statistics and number variance Σ^2, provide the averaged results in the natural frequency domain and they can opportunely mask natu-

ral frequency statistics characteristics associated with a particular range of the natural frequency domain. In conclusion, from the previous discussion arises a relevant observation: the natural frequency statistics from any random system is only correctly characterized when all results from several eigenvalue statistical observables are analyzed together and compared to each other, regardless of their individual performance in the characterization of the spectral natural frequency statistics.

3.4.4 Spatial and Spectral Mode Shape Statistics

In addition to the natural frequency analysis, a statistical investigation of the corresponding mode shapes of the nominal and random rod structures was also carried out. The best known eigenvector statistical observables of RMT were evaluated and their results were compared with analytical predictions, GOE (Gaussian) and sinusoidal mode shape statistics.

Spatial Kurtosis

In the current analysis, the *kurtosis*[9] is defined as the ratio of the fourth statistical moment of the eigenvector components to the square of second one, Montgomery and Runger (103). According to Gomes and Gerges (101, 93), Lyon's mode shape statistic factor can be also understood as *spatial kurtosis*, since a spatial averaging approach is adopted in the evaluation of eigenvector component statistical moments. In other words, the evaluation of the eigenvector component statistical moments for each eigenvector mode order is performed along the eigenvector components (*i.e.*, spatial domain of system). Therefore, in order to emphasize the averaging approach adopted in the kurtosis parameter evaluation, the nomenclature of *spatial kurtosis* will be intentionally adopted herein for Lyon's Mode Shape Statistics Factor. In Figure 46, the spatial kurtosis results are shown for each rod structure investigated.

[9]The *kurtosis* is a metric parameter reflecting whether the data are peaked or flat relative to a normal distribution. That is, data sets with high kurtosis tend to have a distinct peak near the mean, decline rather rapidly, and have heavy tails. Data sets with low kurtosis tend to have a flat top near the mean rather than a sharp peak. A uniform distribution would be considered as the extreme case, Montgomery and Runger (103).

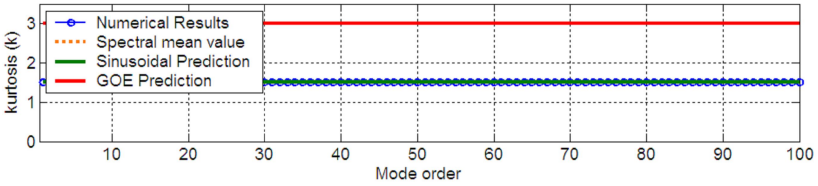
Numerical Results
Spectral mean value
Sinusoidal Prediction
GOE Prediction
kurtosis (k)
Mode order

(a)


Numerical Results
Spectral mean value
Sinusoidal Prediction
GOE Prediction
kurtosis (k)
Mode order

(b)

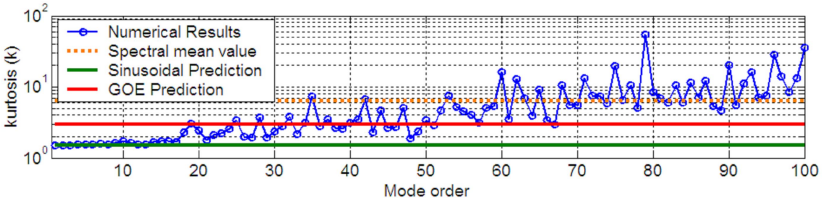
Numerical Results
Spectral mean value
Sinusoidal Prediction
GOE Prediction
kurtosis (k)
Mode order

(c)

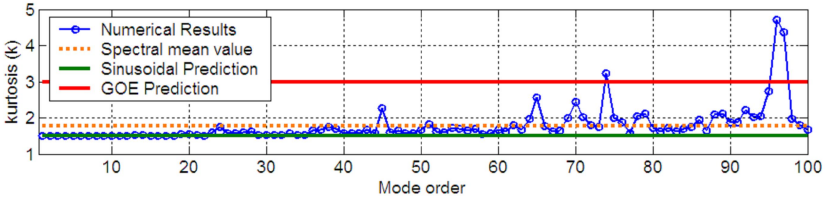
Numerical Results
Spectral mean value
Sinusoidal Prediction
GOE Prediction
kurtosis (k)
Mode order

(d)

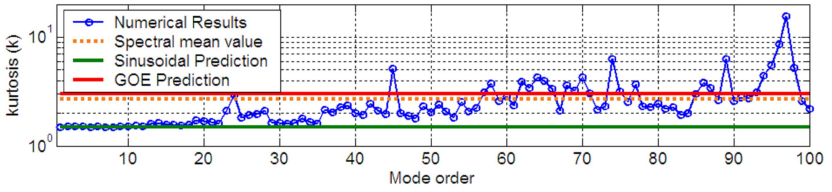

(e)

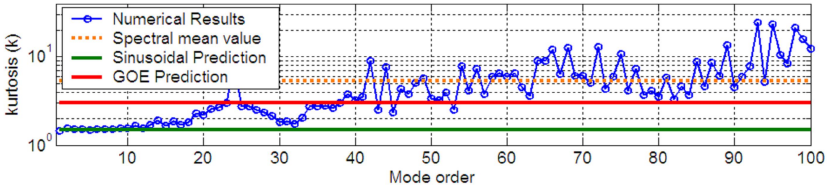

(f)

Figure 46: Lyon's Mode Shape Statistics Factor or spatial kurtosis results for the nominal and random rods (spatial averaging approach). Plots: (a) Nominal, (b) Uniform (20%), (c) Mass (20%), (d) Gaussian (10%), (e) Gaussian (20%), and (f) Gaussian (30%).

According to Figure 46 (a), the nominal rod spatial kurtosis results suggest that the mode shapes are perfectly sinusoidal. For spatial kurtosis results for the random rods, Figures 46 (b) - (f), distinct intensities of the randomness effects in the mode order domain are clearly observed for each of random rods investigated.

For almost all of the random rods, small deviations in comparison to the nominal mode shape statistics occurs for the low-frequency range (or low mode order range). As expected, the large randomness effects are observed in the mid and high-frequency ranges for all random rods investigated.

Overall, the random rod spatial kurtosis results suggest that as the mode order (or excitation frequency) increases, a mode shape statistics transition occurs from almost *sinusoidal statistics* to *disordered statistics*. For *disordered* mode shape statistics, the spectral mean values of the spatial kurtosis results for the random rods are larger than the sinusoidal and GOE predicted values.

As observed in Figure 46, the spatial kurtosis results for the random

rods show a high level of dispersion around the global spectral tendency, and the degree of spatial kurtosis variability becomes more intense as the excitation frequency (mode order) or the randomness level increases.

In the current analysis, the spatial kurtosis results for the Gaussian random rods show a typical example of the effects of the different randomness levels on the mode shape statistics. Considering a fixed frequency range, for example, around the 70*th* mode order vicinities, the spatial kurtosis results for the Gaussian (10%) random rod show a smooth curve with values close to $K \simeq 2.00$. For the Gaussian (20%) random rod, the spatial kurtosis results vary moderately between $3 \lesssim K \lesssim 5$. On the other hand, for the Gaussian (30%) random rod, the spatial kurtosis results vary considerately between $5 \lesssim K \lesssim 10$. Indeed, for the Gaussian rod structures, as the level of randomness increases for a fixed frequency range, a simultaneous increase in the spatial kurtosis values and in their spectral variability is expected due to the gradual establishment of the *structural localization* effects on the mode shapes.

Besides investigating the kurtosis magnitudes, it is also relevant to analyze the spatial kurtosis distribution in the mode order domain, Gomes and Gerges (101). According to Pradhan and Sridhar (73, 123, 74), a perfect Dirac delta function for the spatial kurtosis distribution centered at $K^{GOE} = 3$ is no longer expected for a *classically chaotic* engineering system due to the finite system dimension effects. In Figure 47, the spatial kurtosis PDF results are presented for each of the Gaussian random rods. Additionally, the nonlinear sigma model expressions from the supersymmetry theory for the exponential decay law of spatial kurtosis (or Inverse Participation Ratio) values, Equation (2.59), are also plotted (linear and logarithmic plots, respectively). The dimensionless conductivity (g) and the normalization constant (C_2) values from the fitting processes are: $g = 10$ and $C_2 = 8.10^4$ for Gaussian (10%) rod, $g = 0.8$ and $C_2 = 60$ for Gaussian (20%) rod and, $g = 0.28$ and $C_2 = 75$ for Gaussian (30%) rod.

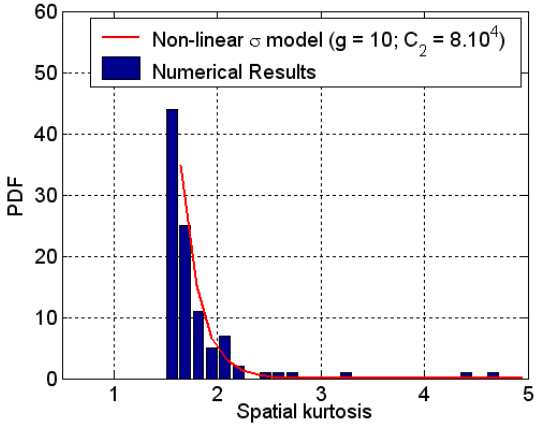
Non-linear σ model (g = 10; C2 = 8.10^4)
Numerical Results
PDF
Spatial kurtosis
0
10
20
30
40
50
60
1
2
3
4
5

(a_1)

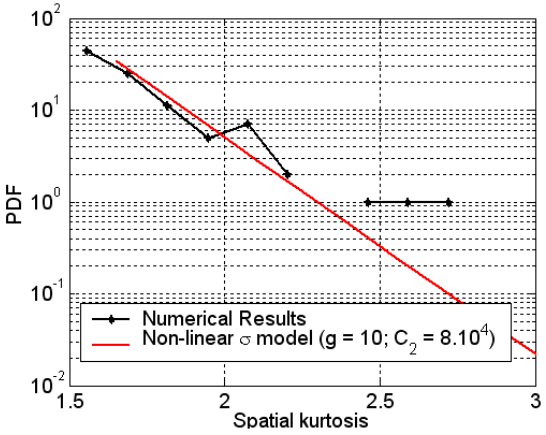
Numerical Results
Non-linear σ model (g = 10; C2 = 8.10^4)
PDF
Spatial kurtosis
10^2
10^1
10^0
10^-1
10^-2
1.5
2
2.5
3

(a_2)

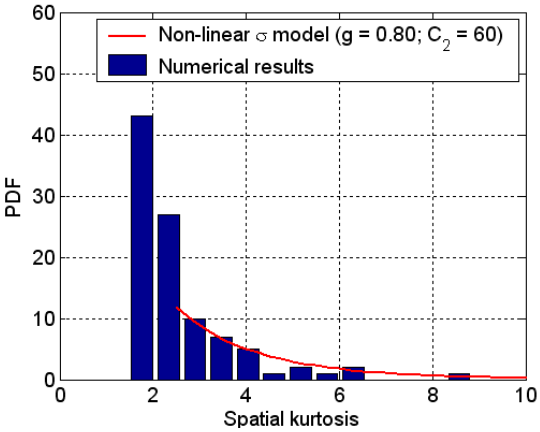
Non-linear σ model (g = 0.80; C2 = 60)
Numerical results
PDF
Spatial kurtosis
0
10
20
30
40
50
60
0
2
4
6
8
10

(b_1)

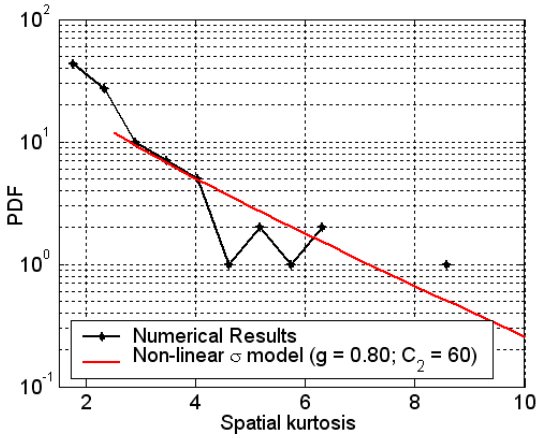
Numerical Results
Non-linear σ model (g = 0.80; C2 = 60)
PDF
Spatial kurtosis
10^2
10^1
10^0
10^-1
2
4
6
8
10

(b_2)

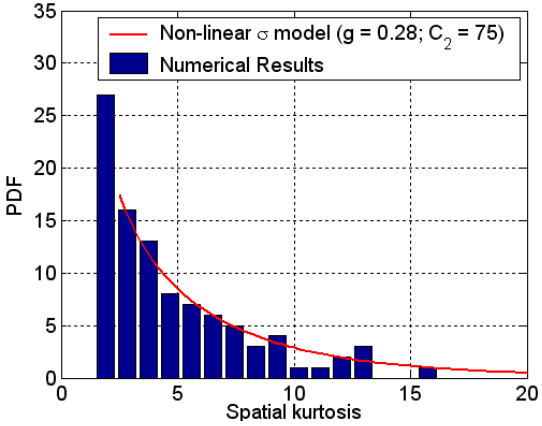

(c_1)

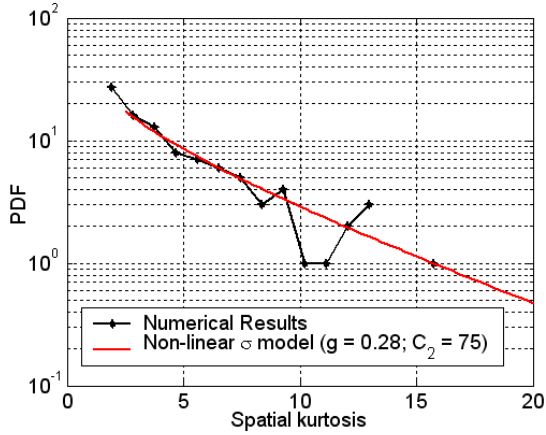

(c_2)

Figure 47: PDFs of spatial kurtosis from the Gaussian random rods (spatial averaging approach). Plots: (a) Gaussian (10%), (b) Gaussian (20%), and (c) Gaussian (30%).

As shown in Figure 47, for all Gaussian random rods, the spatial kurtosis PDF results suggest a large PDF kurtosis amplitude for kurtosis values close to the nominal value. In fact, the patterns of these PDF results may be

directly associated with the poor performance of the randomization processes in the low-frequency range (or low mode order range). Considering the results for the Gaussian random rods, it can be noted that the increase in the randomness level leads to an increase in the PDF kurtosis amplitudes associated with large spatial kurtosis values. In fact, none of the spatial kurtosis PDF results show a tendency toward a Gaussian distribution and their spectral mean or probabilistic mode values are very distinct from the kurtosis value expected for the GOE model. Similarly to the main conclusions drawn from the previous analysis of the spatial kurtosis values, the patterns of the spatial kurtosis PDF results also confirm that the performance of the randomization process is not homogeneous over the frequency domain for all Gaussian random rods.

In the Statistics field, a distribution with large kurtosis values is called *leptokurtic*, or *leptokurtotic*. In terms of distribution shape, a leptokurtic distribution has a more acute *peak* around the mean value[10]. For the mode shapes with large spatial kurtosis values it is expected that most of their mode shape components have amplitudes close to the probabilistic mode value and only a small number of mode shape components have large amplitudes beyond the probabilistic mode value. Therefore, these distribution characteristics suggest the existence of large localized mode shape component amplitudes confined to a *particular* (or spatially limited) region of Gaussian random rods. It is also important to note that these effects are very similar to those of the *structural localization* phenomenon, Hodges *et al* (139).

Considering again the spatial kurtosis results for the Mass (20%) random rod, Figure 46 (c), a similar conclusion regarding the effects of an increase in uncertainty level on the mode shape statistics can be also extended to the effects of an increase in excitation frequency on the mode shape statistics of a structure with a fixed randomness level. Indeed, the Mass (20%) spatial kurtosis results suggest that the effects of randomness on the low-frequency range are almost negligible and the spatial kurtosis values are very similar to the kurtosis value predicted for sinusoidal mode shapes (*i.e.*, nominal kurtosis value). As the excitation frequency (or the mode order) increases, the pattern of spatial kurtosis curve becomes gradually discontinuous (looks like a *zigzag*) and dispersed.

As shown in the previous spatial kurtosis analysis for all random rods, there is an evident tendency toward the establishment of large kurtosis values in the mid and high mode order ranges. For almost-periodic structures, large values for the spatial kurtosis can be easily associated with the *struc-*

[10] For most practical distributions, the mean value is equal to the probabilistic mode value.

tural localization phenomenon, Hodges *et al* (139, 151). A similar tendency has been established for disordered billiard systems in the Quantum Physics field, (71, 100, 120). In such studies, the localized wave function amplitudes occur in a certain region of the microwave cavity due to energy confinement provided by small tiles (disorder or irregularity).

Considering the Mass and Gaussian random rods, they may be considered possible candidates for the establishment of structural localization effects, (140, 139, 159). In Figures 46 (c) and (f), the results for the Mass (20%) and Gaussian (30%) random rods showed the large spatial kurtosis values as well as a high dispersion around the spectral mean value mainly in the high mode order range. Although, this global pattern of results is very similar to those observed for the disordered billiard systems, it is important to emphasize that there is no evident reasons to affirm that the predictions from the supersymmetry models valid for quantum nuclear or billiard systems can be directly extended to the random dynamical structures.

Considering the spatial kurtosis PDF results for the Gaussian (20% and 30%) rods, the Figures 47 (b) and (c), a satisfactory performance of the non-linear sigma model expression is observed mainly in the kurtosis range associated with weak and moderate localization characteristics, that is $3.5 \lesssim K \lesssim 9$. At the tail of the kurtosis distribution, a dispersion of kurtosis PDF around the fitted non-linear sigma model expression is clearly noted. Indeed, it is also important to emphasize that the spatial kurtosis values associated with the tail kurtosis distribution have strong and extremely strong localization characteristics, being strictly sensitive to *system-dependent effects*. For the Gaussian (10%) rod, as discussed previously, the localization characteristics are only established for a small number of mode shapes and thus it is expected that the non-linear sigma model expression is no longer valid. However, the non-linear sigma model expression was fitted to the numerical kurtosis results, Figure 47 (a). The fitted non-linear sigma model expression showed good versatility and performance in describing the exponential decay law as the spatial kurtosis value increases.

Although the *Universality* concept states that the modal parameter statistics (inclusive mode shape statistics) tends asymptotically to be independent of uncertainty sources and converge to the GOE model, the current spatial kurtosis results did not confirm this *universal* tendency for the frequency range investigated. For all random rods investigated, their spatial kurtosis results showed distinct high-frequency asymptotic tendencies and their asymptotic values did not conform well to the GOE predicted value. Indeed, the relevant *non-universal* mode shape characteristics were identified

for all of the random rods investigated, since their mode shape statistics seem to have *structural localization* characteristics, showing *system-dependent effects*, Bertelsen *et al* (90, 66).

Spatial Lilliefors Test

In order to evaluate the agreement between the mode shape statistics of the random rods and GOE statistics, the Lilliefors Test was also adopted, since the Gaussian distribution is expected for the GOE eigenvector components, Mehta (24). The Lilliefors Test is able to identify the particular frequency range (or mode order range) in which the mode shape statistics are almost-Gaussian (GOE), Montgomery and Runger (103). In Figure 48, the spatial Lilliefors Test results are shown for all rods investigated.

According to Figure 48, the spatial Lilliefors Test results from all random rods show that the Gaussian distribution hypothesis is rejected for the mode shape components in the low mode order range. For this range, the mode shapes are weakly affected by randomness effects and their component distributions are similar to those expected for the sinusoidal mode shapes.

However, as the excitation frequency or randomness level increases, a statistical *transition* occurs initially from almost-nominal to GOE statistics. Thus, the establishment of almost-Gaussian mode shapes (or GOE mode shape statistics) occurs in a particular limited frequency region (or mode order) for each of the random rod structures investigated.

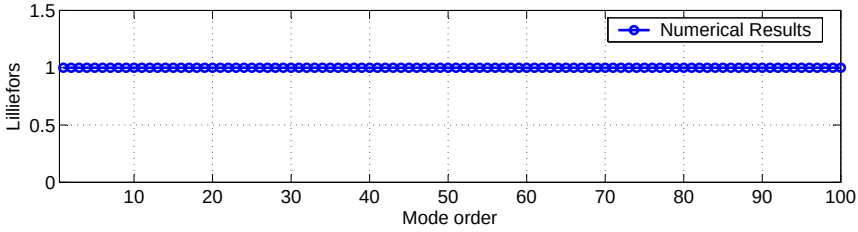

(a)

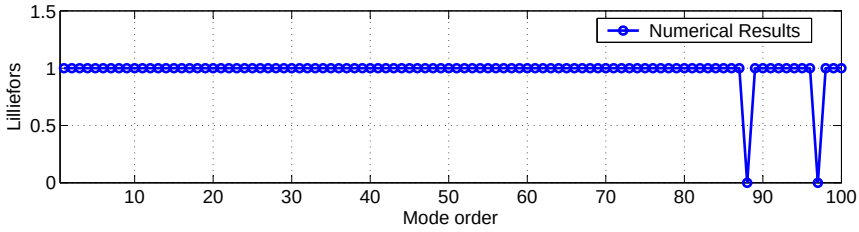
Numerical Results
Lilliefors
Mode order
1.5
1
0.5
0
10
20
30
40
50
60
70
80
90
100

(b)

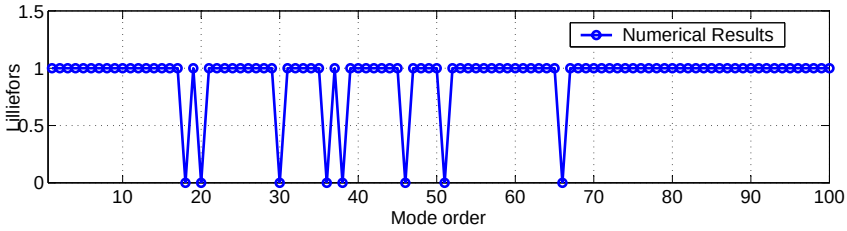
Numerical Results
Lilliefors
Mode order
1.5
1
0.5
0
10
20
30
40
50
60
70
80
90
100

(c)

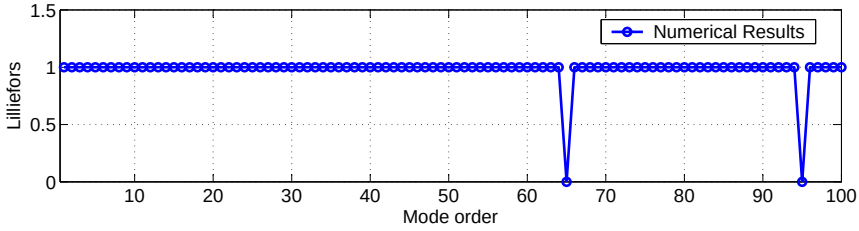
Numerical Results
Lilliefors
Mode order
1.5
1
0.5
0
10
20
30
40
50
60
70
80
90
100

(d)

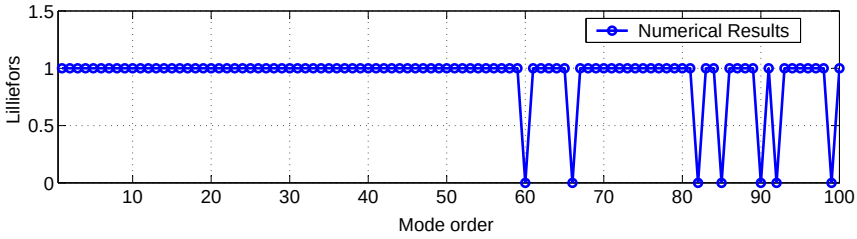
Numerical Results
Lilliefors
Mode order
1.5
1
0.5
0
10
20
30
40
50
60
70
80
90
100

(e)

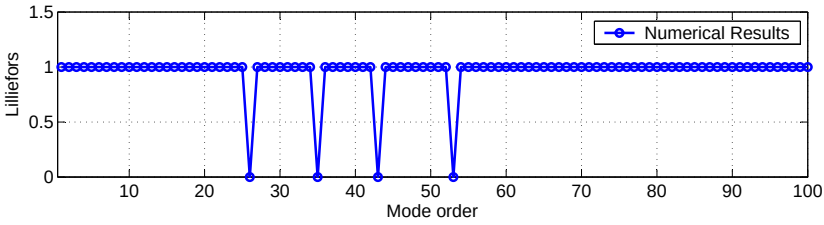

(f)

Figure 48: The spatial Lilliefors Test results for the nominal and random rods (spatial averaging approach). Plots: (a) Nominal, (b) Uniform (20%), (c) Mass (20%), (d) Gaussian (10%), (e) Gaussian (20%), and (f) Gaussian (30%).

For the high mode order range, beyond the Gaussian mode shape region, the spatial Lilliefors Test results showed that the spatial distribution of the mode shape components is no longer Gaussian and the Gaussian distribution hypothesis is again rejected for the mode shape components. Based on the previous and current eigenvector statistical observable results, it appears that these mode shapes might establish the *structural localization phenomenon* in the high mode order range. Indeed, this fact once again upholds the evidence that the mode shape statistics have *non-universal* characteristics in the high-frequency range for random rod structures.

Overall, the spatial Lilliefors Test results in the mode order domain suggest three well defined patterns for the spatial mode shape statistics: *almost-nominal statistics*, *almost-GOE statistics*, and *structural localized statistics*, respectively.

Porter-Thomas Distribution

In the RMT context, the one of the best known eigenvector statistical observables is the *Porter-Thomas distribution*, also known as the *PT-distribution*, kudrolli *et al.* (71). This metrics is based on the distribution of normalized squared mode shape amplitudes (to have unit mean value), and its application is commonly used to verify the agreement between the random system eigenvector statistics and the GOE eigenvector statistics, Brody *et al* (56). In addition, the PT-distribution results also allow the identification of the deviation classes of a particular mode shape statistics in comparison

to the expected *universal* GOE mode shape statistics. In other words, it is possible to identify correctly the sources (or their class) of eigenvector deviation which lead to *non-universal* behavior in the mode shape statistics, (119, 72, 160, 74). In the RMT context, the main physical phenomena associated with *non-universal* mode shape statistics can be classified into two major classes: *periodical orbits* (presence of geometrical symmetries) and *structural localization* (spatial confinement of energy). In Figure 49, the PT-distribution results are shown for the nominal and random longitudinal rods investigated.

For the nominal rod, the mode shapes are perfect sinusoidal functions and the PT-distribution results are very similar for all mode shapes in the frequency range investigated, Figure 49 (a). In addition, it can be noted that, for all nominal mode shapes, the normalized squared amplitudes are less than 2 and the PT-distributions have a well defined pattern. Indeed, for the nominal longitudinal rod, the mode shapes are written as $\phi(x) = A_x sin(x)$ and thus $\langle \phi^2 \rangle = \frac{A_x}{2}$ and $max(\phi^2) = A_x^2$. For the normalized squared mode shape amplitude $z_A = \frac{A_x^2}{\langle A_x^2 \rangle}$, and $max(z_A) = 2$ as observed in Figure 49(a).

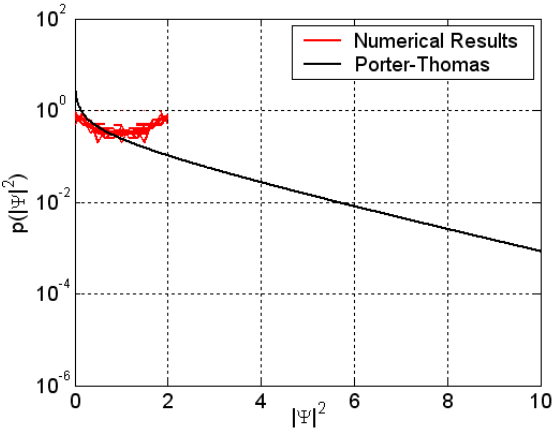

(a)

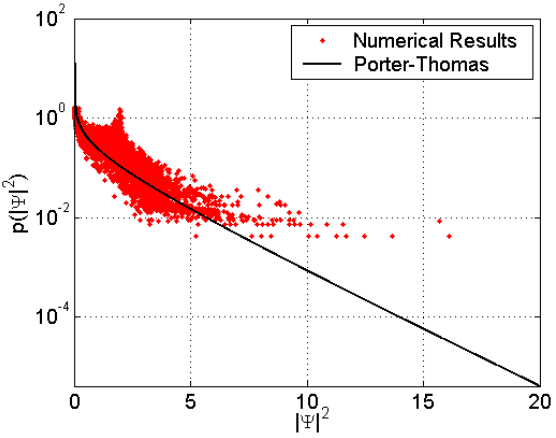
Numerical Results
Porter-Thomas
10^2
10^0
10^{-2}
10^{-4}
$p(|\Psi|^2)$
0
5
10
15
20
$|\Psi|^2$

(b)

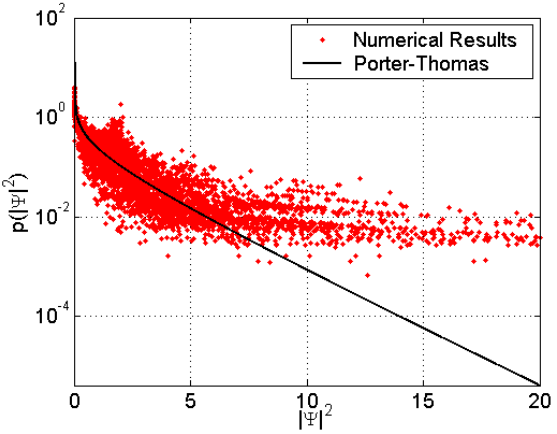
Numerical Results
Porter-Thomas
10^2
10^0
10^{-2}
10^{-4}
$p(|\Psi|^2)$
0
5
10
15
20
$|\Psi|^2$

(c)

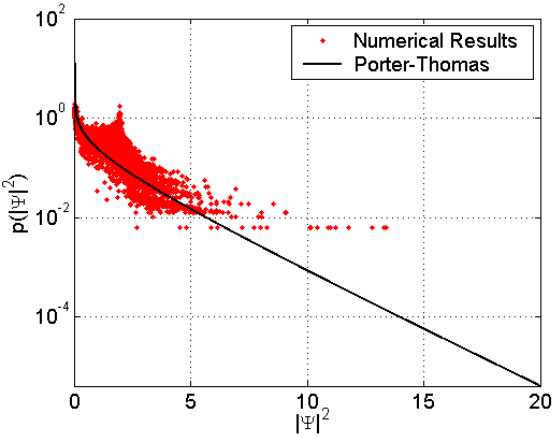
Numerical Results
Porter-Thomas
10^2
10^0
10^{-2}
10^{-4}
$p(|\Psi|^2)$
0
5
10
15
20
$|\Psi|^2$

(d)

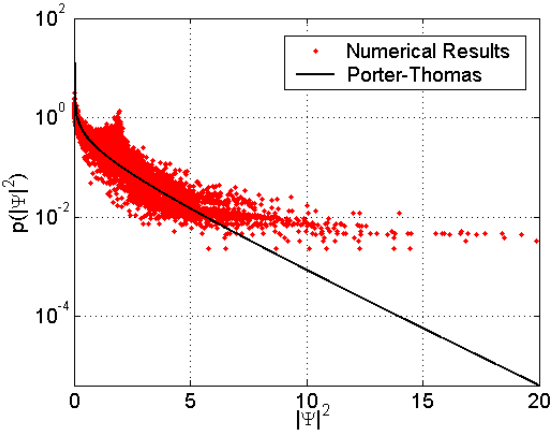
Numerical Results
Porter-Thomas
10^2
10^0
10^{-2}
10^{-4}
$p(|\Psi|^2)$
0
5
10
15
20
$|\Psi|^2$

(e)

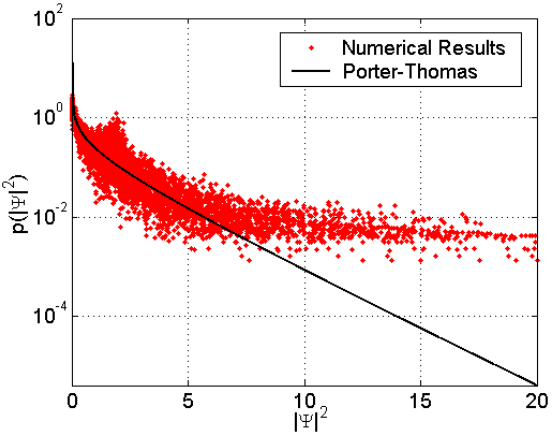

(f)

Figure 49: PT-distribution results for the nominal and random rods and GOE predictions (Gaussian mode shapes) (spatial averaging approach). Plots: (a) Nominal, (b) Uniform (20%), (c) Mass (20%), (d) Gaussian (10%), (e) Gaussian (20%), and (f) Gaussian (30%).

For all random rods investigated, the PT-distribution results suggest a partial elevation of tail distribution for some higher mode orders. This characteristic traditionally occurs due to the establishment of a certain degree of *structural localization* of the mode shapes, (71, 73).

For the low order mode shapes, the randomness effects are almost negligible and it is expected that their PT-distribution results are very similar to the nominal results. In contrast, as the frequency increases the structural irregularities lead to the establishment of structural localization associated with the high probability of large normalized mode shape amplitudes. As shown in Figures 49 (b) - (c), the PT-distribution results allow the identification of the different levels of *non-universal* characteristics as well as the effects of the different randomization processes (or distinct randomness sources) on the mode shape statistics.

Nevertheless, it is also important to emphasize that the large normalized squared mode shape amplitudes are very sensitive to *system-dependent effects* and thus they become a key point in the checking process of the universal establishment of GOE mode shape statistics. In Figures 49 (d) - (f),

the PT-distribution results suggest that the increase in randomness level reinforces the structural localization effects since the tail distribution becomes thicker and the occurrence of large normalized mode shape amplitudes is expected.

Spatial PDF of Mode Shape Components

In this study, a detailed analysis was performed with some particular mode shapes from each random rod structure in order to investigate the establishment of the *universal* GOE statistics and structural localization characteristics (*non-universal* effects). Due to the large amount of data obtained in this analysis and the high similarity of some results obtained, only the most relevant results will be shown below. Based on complete set of results, it appears that the mode shape statistical results for the Gaussian (30%) random rod are very representative and demonstrate the most relevant physical phenomena of all of the random rods investigated, Gomes (84).

The statistical characteristics of the three major classes of mode shape statistics will be presented in detail below. These main mode shape statistical classes are: *almost-nominal* (sinusoidal), *almost-GOE* (or Gaussian), and *structural localized* statistics.

In Table 8, the statistical characteristics of the Gaussian (30%) mode shapes investigated in this section are presented in detail. These pre-selected mode shapes are representative samples of each mode shape statistics class. Additionally, some mode shapes are also considered in order to investigate the statistical transition characteristics between the well-defined mode shape statistics classes.

In Figure 50, the spatial representation of mode shape amplitudes, the PDF of mode shape components, and the PT-distribution results are presented for some pre-selected mode shapes of the Gaussian (30%) random rod. The analytical predictions for sinusoidal and Gaussian mode shape statistics are also compared to numerical results. Additionally, the performance of the PT-distribution based on the non-linear sigma model expressions of the supersymmetry, Equations (2.53) and (2.55), are verified for the mode shapes with weak and strong localization characteristics.

Table 8: Mode shapes investigated: subfigure, mode order, spatial kurtosis, and mode shape statistics.

Sub-figure	Mode order	Spatial kurtosis (K)	Mode shape statistics
Figure 50 (a)	05	1.498	almost-nominal
Figure 50 (b)	20	2.182	nominal - Gaussian transition
Figure 50 (c)	26	2.773	almost-Gaussian
Figure 50 (d)	35	2.786	almost-Gaussian
Figure 50 (e)	39	3.759	Gaussian - localized transition
Figure 50 (f)	72	13.024	structural localized
Figure 50 (g)	93	24.492	structural localized

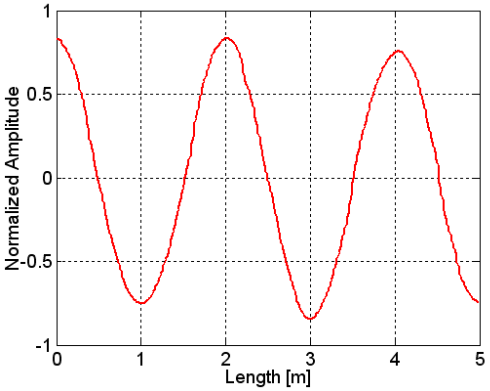

(a_1) Mode 05: almost-nominal

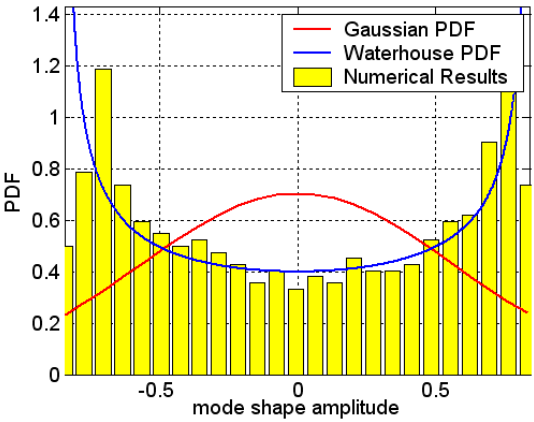

(a_2) Mode 05: almost-nominal

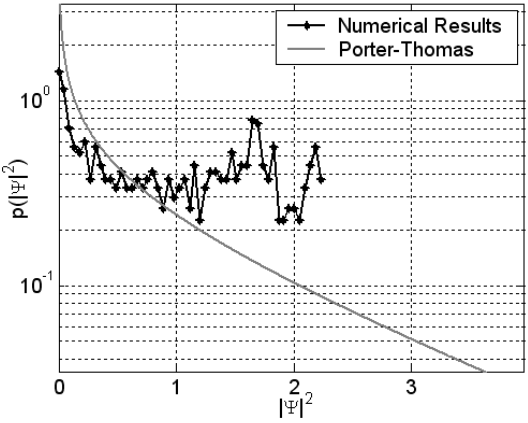

(a_3) Mode 05: almost-nominal

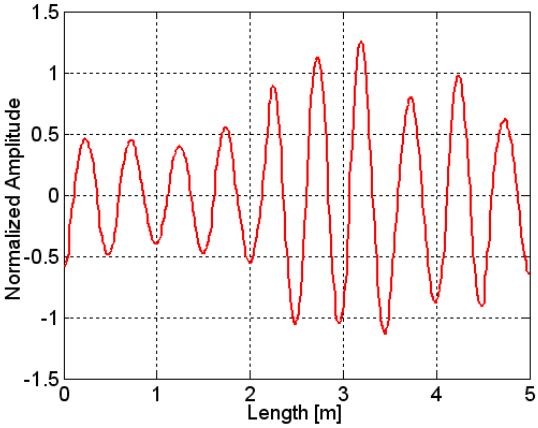

(b_1) Mode 20: nominal to Gaussian transition

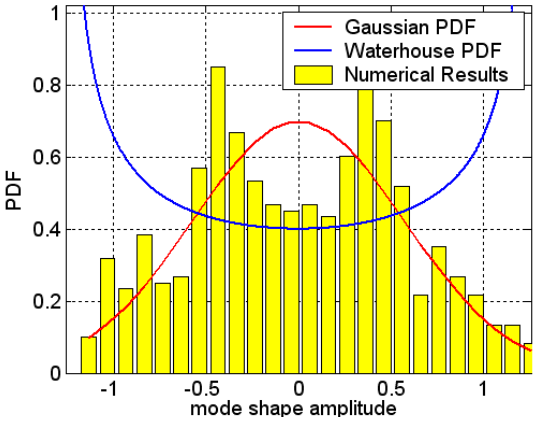

(b_2) Mode 20: nominal to Gaussian transition

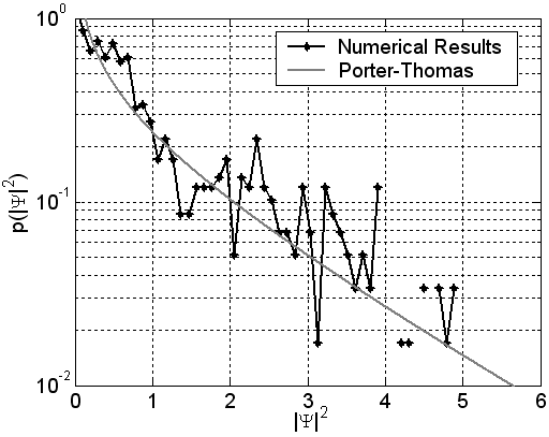

(b_3) Mode 20: nominal to Gaussian transition

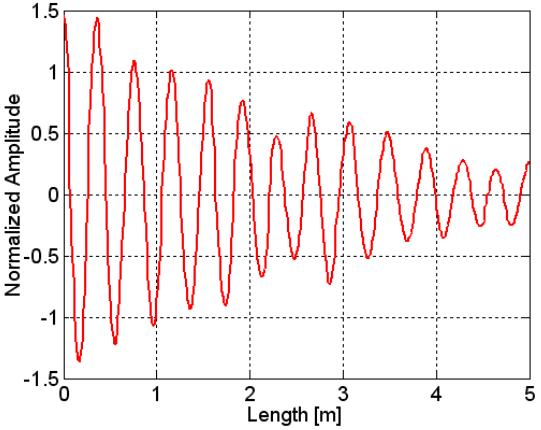

(c_1) Mode 26: almost-Gaussian

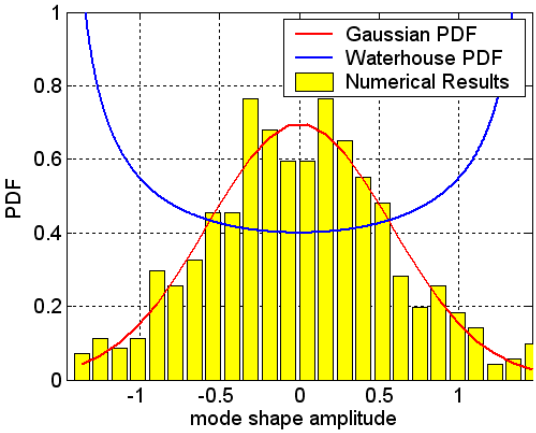

(c_2) Mode 26: almost-Gaussian

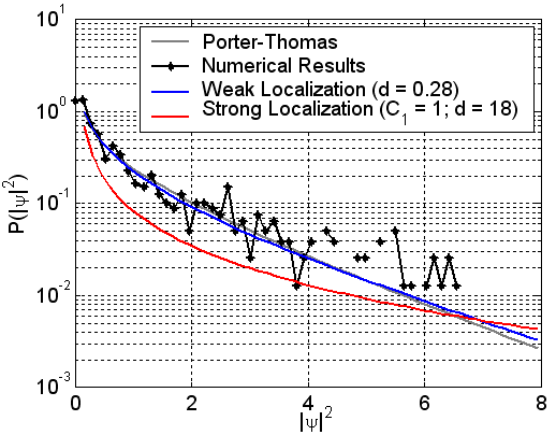

(c_3) Mode 26: almost-Gaussian

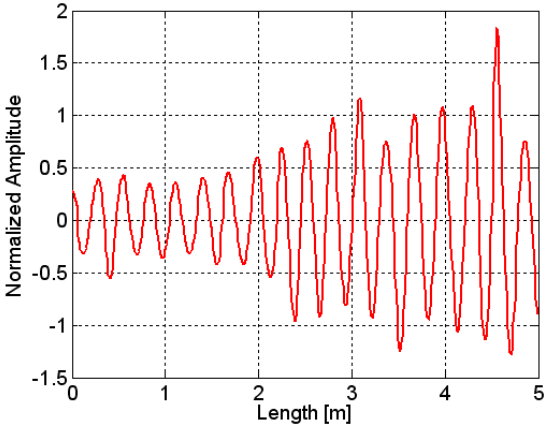

(d_1) Mode 35: almost-Gaussian

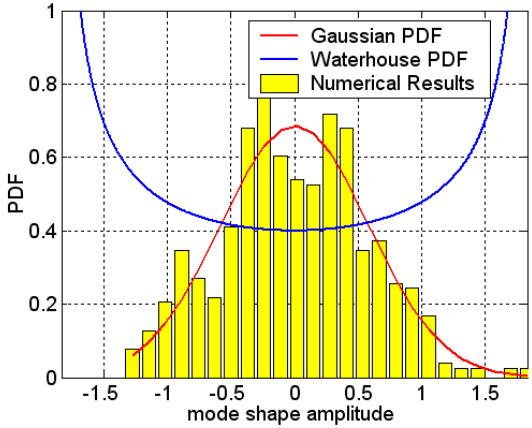

(d_2) Mode 35: almost-Gaussian

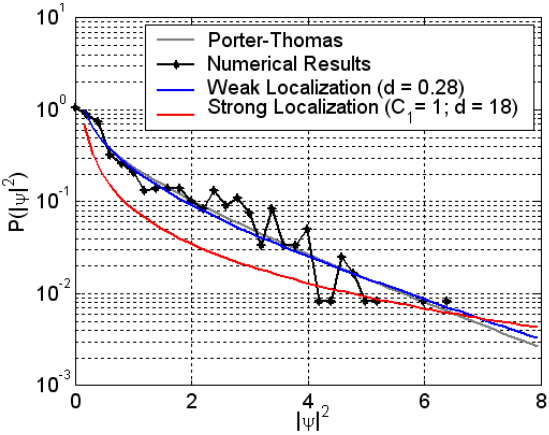

(d_3) Mode 35: almost-Gaussian

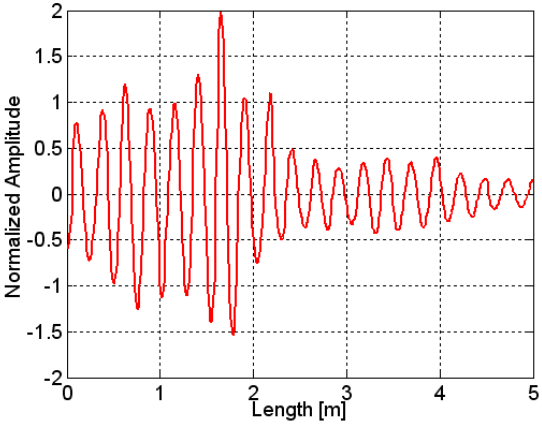

(e_1) Mode 39: Gaussian to localized transition

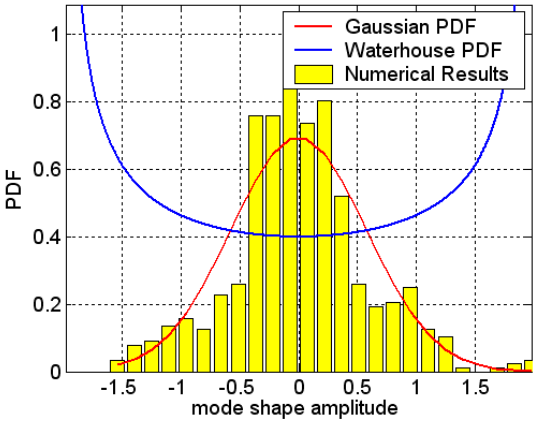

(e_2) Mode 39: Gaussian to localized transition

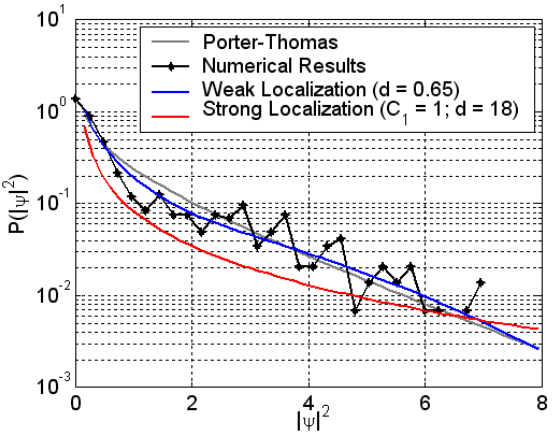

(e_3) Mode 39: Gaussian to localized transition

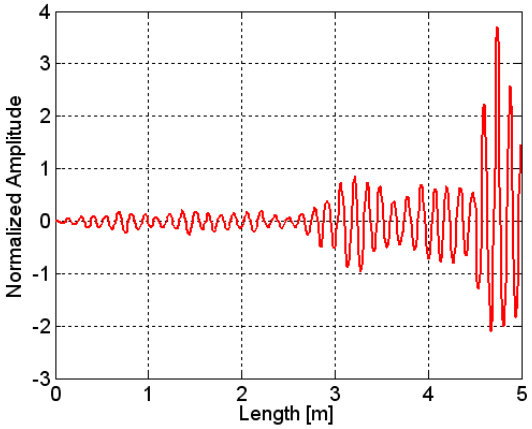

(f_1) Mode 72: Localized

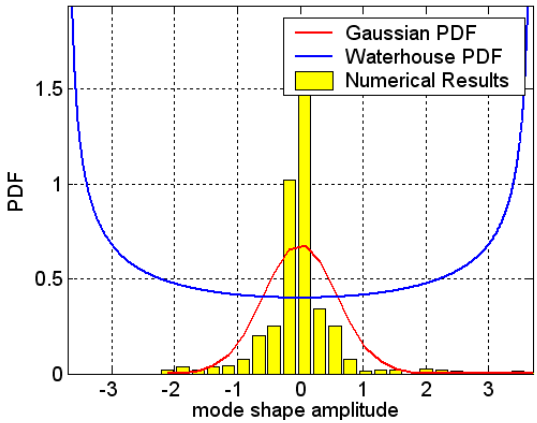

(f_2) Mode 72: Localized

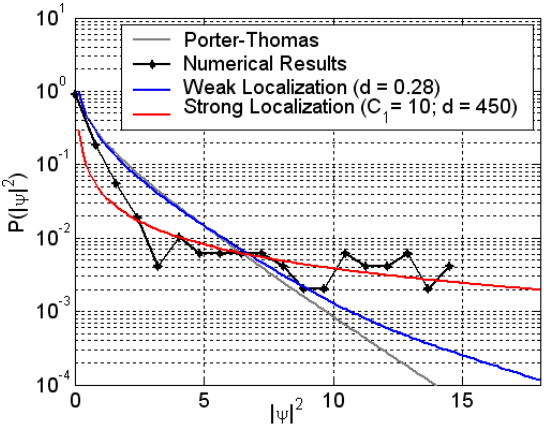

(f_3) Mode 72: Localized

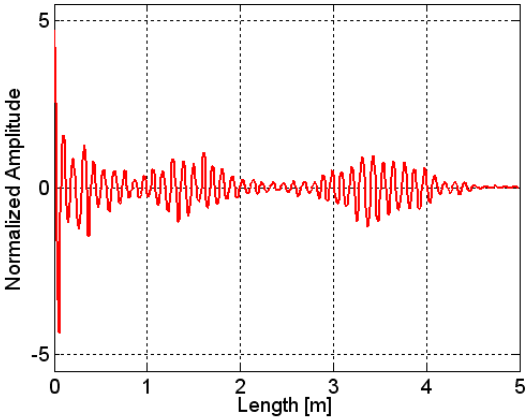

(g_1) Mode 93: Extreme localized

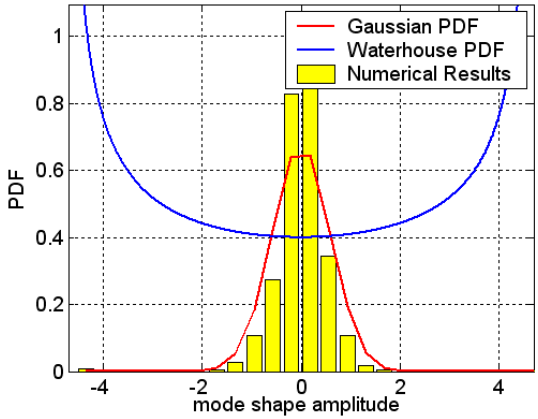

(g_2) Mode 93: Extreme localized

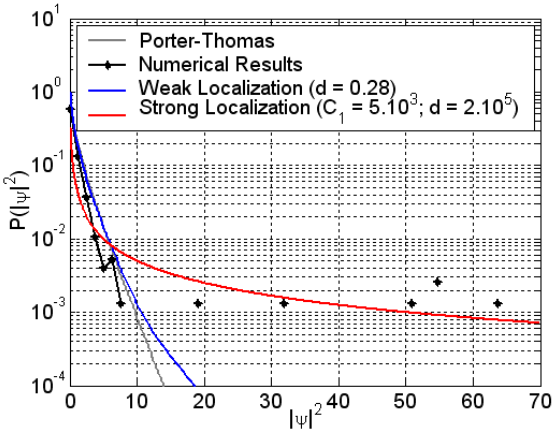

(g_3) Mode 93: Extreme localized

Figure 50: Examples of the main three classes of mode shape statistics: almost-nominal (sinusoidal), almost-GOE (or Gaussian), and structural localized statistics (spatial averaging approach). The Gaussian (30%) numerical results (for pre-selected mode shapes) and analytical prediction (sinusoidal and Gaussian statistics).

As shown in Figure 50, the three distinct statistics classes and their transitions are easily identified in the mode shape analysis of the Gaussian (30%) random rod. These numerical results illustrate the effects of the presence of randomness on the mode shape statistics and the statistical mode shape characteristics as the excitation frequency increases.

For the low mode order range (or low-frequency range), small deviations are observed in comparison to nominal mode shape statistics and thus the Waterhouse PDF analytical prediction for one-dimensional sinusoidal mode shapes, Equation (2.26), conforms well with numerical results, Figure 50 (a).

For modes 26 and 35; Figures 50 (c) and (d), respectively; a good agreement was obtained between the numerical results and the GOE analytical prediction which states that the GOE mode shapes are statistically independent and their eigenvector components have an asymptotic Gaussian distribution.

For the high mode order range (or high-frequency range), the confinement of large mode shape amplitudes to a particular rod region characterizes the establishment of the *structural localization* phenomenon. That is, the PDF of localized mode shape components shows a high probability for mode shape component amplitudes closer to the mean value and a low probability for eigenvector amplitudes larger or smaller than the mean value. Additionally, the PT-distribution results for such localized mode shapes show large magnitudes for the tail region of the distribution, that is, large mode shape component amplitudes are expected in comparison with the PT-distribution of the *universal* GOE mode shapes. In Figures 50 (f) and (g), examples of moderate and strong structural localization degrees are presented in terms of the PT-distribution for the mode shapes 72 and 93, respectively.

Although it is not discussed above in detail, an intermediate or transitory statistical behavior occurs between the well-defined mode shape statistics classes. Indeed, two main transitory statistics are: nominal to almost-GOE transition, Figure 50 (b) - Mode 20, and almost-Gaussian to localized transition, Figure 50 (e) - Mode 39.

Considering the performance of the PT-distribution expressions based on the non-linear sigma model for weakly and strongly localized mode shapes, a good performance of the weak localization expression is observed to describe the small perturbations due to incipient localization effects, Mode 39 - Figure 50 (e). For strongly localized mode shapes, a normalization constant (C_{PT}) was introduced into the non-linear sigma model expression in order to improve the fit. Indeed, satisfactory performance of the modified PT-distribution expression based on the non-linear sigma model is verified

for strong localization regime, Figure 50 (f). However, some small discrepancies are also observed in the large mode shape amplitude range where the PT-distribution results are sensitive to small changes in the system-dependent contributions.

For extremely localized regime, as the case of mode 93, extremely large values occur in the PT-distribution curve for the large mode shape amplitude range. Although the PT-distribution expression based on the non-linear sigma model is not expected to be valid for the extremely localized regime, a satisfactory performance is surprisingly observed in Figure 50 (g), showing its capacity to describe the effects of the non-universal perturbations on the Gaussian PT-distribution curve.

Spectral Kurtosis

Although the Lyon's Mode Shape Statistics Factor (or spatial kurtosis) considers the spatial averaging approach for each mode shape (*i.e.,* an averaging process over the mode shape component domain), the relevant statistical mode shape characteristics are also obtained when the mode shape statistical moments are evaluated for a fixed mode shape component across the frequency domain (or mode order domain), that is, the *spectral averaging approach* is adopted, Gomes and Gerges (101). The relevance of the spectral kurtosis analysis arises from the fact that the kinetic energy density evaluation for a system subjected to a single point-loading is partially dependent on the mode shape component amplitudes at excitation point. Thus, a statistical investigation of the amplitudes of a fixed mode shape component associated with forcing point is essential, in order to provide a detailed understanding of the system energy statistical characteristics.

In the revised theory of SEA variance, the GOE statistics model is adopted for both system modal parameters, Langley *et al* (18, 3). Therefore, it is expected that mode shapes are *statistically independent* and the mode shape component distribution is *asymptotically Gaussian*, that is, the mode shape components are considered *uncorrelated Gaussian variables*.

In the current analysis, the kurtosis value associated with each mode shape component, here referred to as *spectral kurtosis*, was evaluated for all rod structures investigated in order to verify compliance with the assumption of sinusoidal and GOE (or Gaussian) mode shape statistics. In Figure 51, the spectral kurtosis results are shown for all rods investigated.

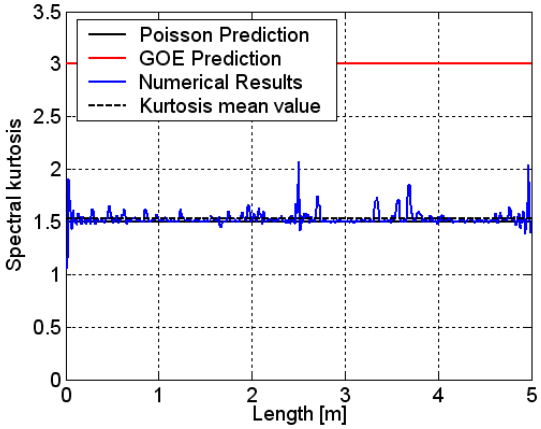
Poisson Prediction
GOE Prediction
Numerical Results
Kurtosis mean value
Spectral kurtosis
Length [m]
0
0.5
1
1.5
2
2.5
3
3.5
0
1
2
3
4
5

(a)

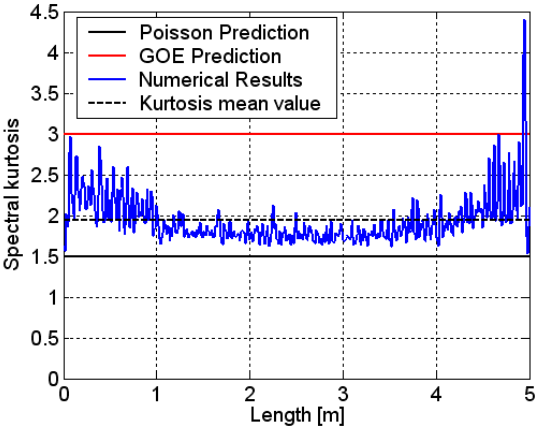
Poisson Prediction
GOE Prediction
Numerical Results
Kurtosis mean value
Spectral kurtosis
Length [m]
0
0.5
1
1.5
2
2.5
3
3.5
4
4.5
0
1
2
3
4
5

(b)

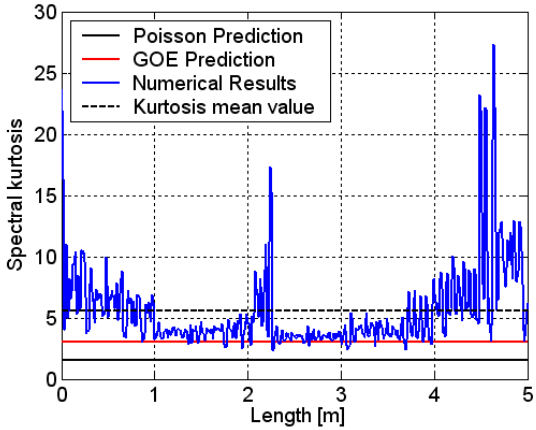
Poisson Prediction
GOE Prediction
Numerical Results
Kurtosis mean value
Spectral kurtosis
Length [m]
0
5
10
15
20
25
30
0
1
2
3
4
5

(c)

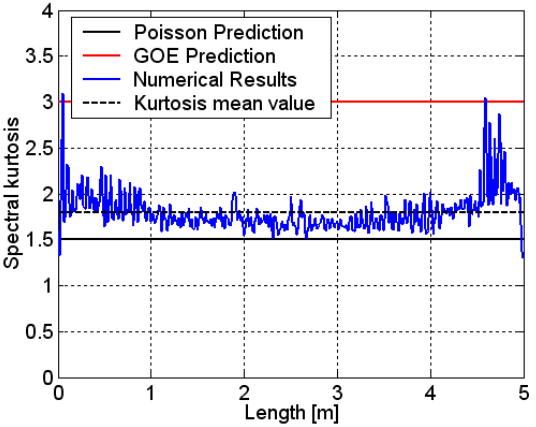
Poisson Prediction
GOE Prediction
Numerical Results
Kurtosis mean value
Spectral kurtosis
Length [m]
0
0.5
1
1.5
2
2.5
3
3.5
4
0
1
2
3
4
5

(d)

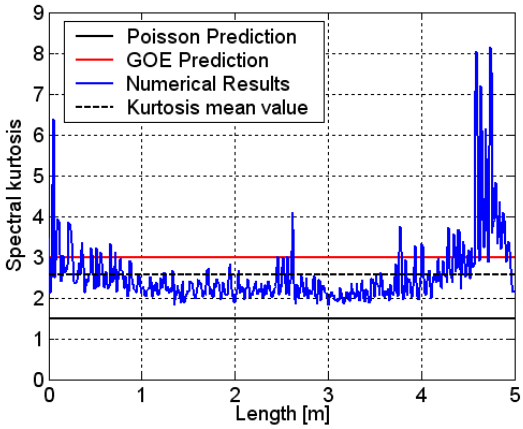

(e)

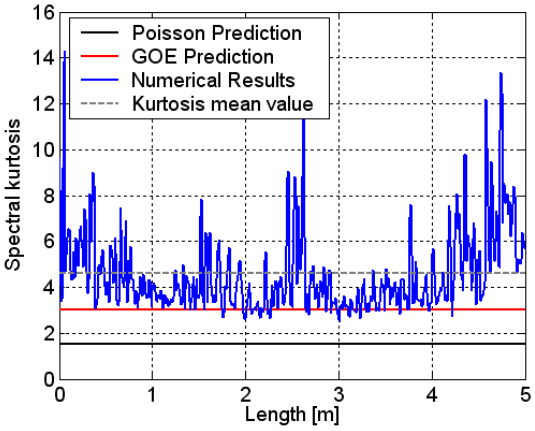

(f)

Figure 51: Spectral kurtosis results for the nominal and random rods and analytical predictions, GOE and sinusoidal statistics (spectral averaging approach). Plots: (a) Nominal, (b) Uniform (20%), (c) Mass (20%), (d) Gaussian (10%), (e) Gaussian (20%), and (f) Gaussian (30%).

According to Figure 51, the nominal spectral kurtosis results conform very well to the sinusoidal analytical predictions and to the spatial kurtosis results obtained in previous spatial kurtosis analysis. In this regard, the nominal rod results suggest that the sinusoidal mode shape statistics are practically *ergodic* in terms of the spatial and spectral average statistics being equivalent, Lyon (48).

For the random rods, the randomness effects are relevant and large spectral kurtosis values are observed for the rod regions closer to the rod end vicinities. In a similar way to the spatial kurtosis results, the spectral kurtosis results also evidence the *non-universal* characteristics of the mode shapes of the random rods investigated. In most of the mode shape components, the spectral kurtosis values are distinct from the kurtosis value associated with a perfect Gaussian distribution, suggesting the existence of correlations between the same component of different mode shapes for all of the random rod structures investigated. According to Langley *et al* (18, 35), the correlation between the different mode shapes at the force point may be the main reason for the reduced performance associated with revised SEA variance theory based on the GOE model, which does not allow the existence of spectral correlations between the force point component of different mode shapes.

Based on the spectral kurtosis results, it can be suggested that most of mode shape components present spectral or inter-modal correlations and can not be considered to have asymptotic uncorrelated characteristics. However, it is important to emphasize that the spectral kurtosis results only provide an indirect analysis regarding mode shape component correlations and it is not possible to establish a direct or linear relationship between the spectral kurtosis values and the spectral correlation level of different mode shapes at a fixed mode shape component, Gomes and Gerges (101).

Although it was not investigated here, for the case of the highest frequency range, it appears that the mode shapes may show asymptotically well established statistics. Considering the extreme condition where the longitudinal wavelength is smaller than the structural irregularity span, the rod becomes effectively *clamped* at the structural irregularity locations. Therefore, independent sets of modes with similar statistics can exist in the various sections between the structural irregularities. According to Brown (1) and Bertelsen (90, 66), an asymptotic exponential PDF is expected for the natural frequency spacings, since the sum of a large number of statistically independent sets of random variables has an exponential PDF. However, a similar conclusion can not be directly extended to the corresponding mode shapes due to their system-dependent characteristics. In this regard, further

investigations are necessary in order to clarify the establishment of possible asymptotic mode shape statistics toward the high-frequency region.

3.4.5 Analysis of Hamiltonian Matrix Structures

In order to understand the effects of uncertainties on the structure of mass and stiffness matrices, an analysis was performed in relation to the matrix characteristics of the nominal rod structure. The current matrix analysis is performed in terms of the Hamiltonian matrix which is defined as a combination of the mass and stiffness matrices. According to Brown (1), the Hamiltonian (H) is the matrix operator which is given by:

$$H = M^{-1}K. \tag{3.2}$$

In Figure 52, the Hamiltonian matrices are shown for the nominal and Gaussian random rods investigated. The magnitudes of the Hamiltonian elements are presented in terms of the absolute values. In order to visualize the randomness effects in the Hamiltonian matrix structure, the absolute differences between the Hamiltonian elements of the nominal and each of the random rod structures are also presented.

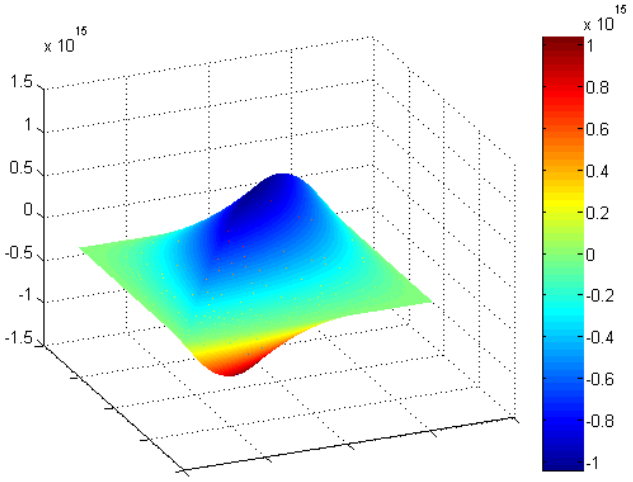

(a)

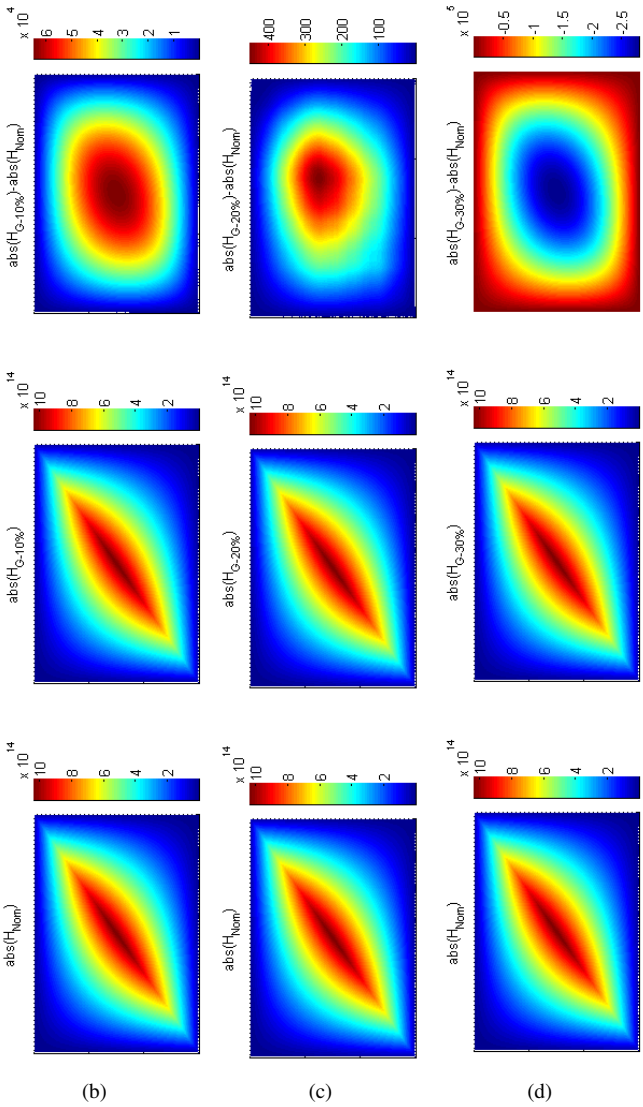

(b) (c) (d)

Figure 52: Hamiltonian matrix patterns of the nominal and Gaussian random rod structures. Plots: (a) Nominal Hamiltonian Matrix - 3D view, (b)-(d) Hamiltonians of nominal structure; Gaussian structures (10%, 20%, and 30%, respectively); and Hamiltonian differences. The Hamiltonian elements are shown in terms of the absolute values.

As shown in Figure 52 (a), the Hamiltonian matrix structure of the nominal rod structure does not clearly have the band-matrix characteristics. Additionally, the large absolute magnitudes are observed for diagonal matrix elements.

In relation to Figures 52 (b) - (d), the changes in the magnitude of the Hamiltonian elements occur gradually from the corner to the center of matrix operator and the patterns are similar for all Gaussian random rods investigated. Regarding the changes in the magnitude of the Hamiltonian element, it can be noted that the relationship between the randomness level of the random rod structures and the changes in the magnitude of Hamiltonian elements is not linear.

In Figure 53, the Hamiltonian results are shown for random rod structures which consider a Uniform distribution for the cross-sectional area values during the randomization process.

The results for the Uniform random rod structures do not suggest a clear tendency for changes in the magnitude of the nominal Hamiltonian matrix structure. Both results for the Uniform rods showed distinct ranges for the changes in the amplitude of Hamiltonian elements as well as different patterns for the changes in the Hamiltonian matrix structure due to the presence of randomness.

In Figure 54, the Hamiltonian results are shown for each one of the mass-loaded random rod structures. The results for the mass-loaded random rod structures show explicitly that the perturbed Hamiltonian structure is very similar to the nominal Hamiltonian structure. It is important to emphasize that this randomization approach is traditionally applied to induce the universal establishment of GOE statistics, Langley *et al* (16, 3, 18, 4, 35).

As shown previously in the natural frequency analysis, the spectral natural frequency statistics of this class of random rod structure presents a high level of GOE statistics in comparison to other random rod structures. However, the Hamiltonian structures of mass-loaded rod structures seems to be, surprisingly, almost absent of magnitude changes in the Hamiltonian matrix elements. This suggests that the modifications in the Hamiltonian structure do not have a direct relationship with the universal establishment of GOE statistics for the modal parameters.

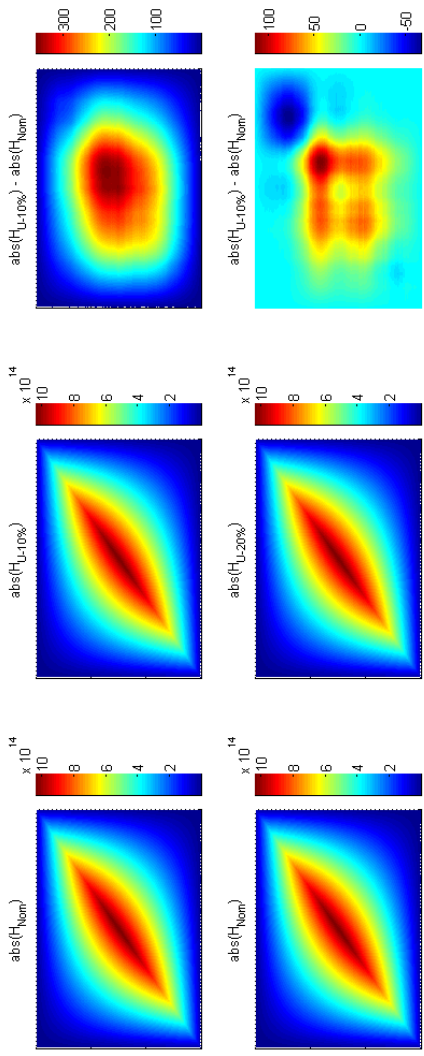

(a) (b)

Figure 53: Hamiltonian patterns of the nominal and Uniform random rod structures. Plots: (a) - (b) Nominal structure; Uniform structures (10% and 20%, respectively); and Hamiltonian differences. The Hamiltonian elements are shown in terms of the absolute values.

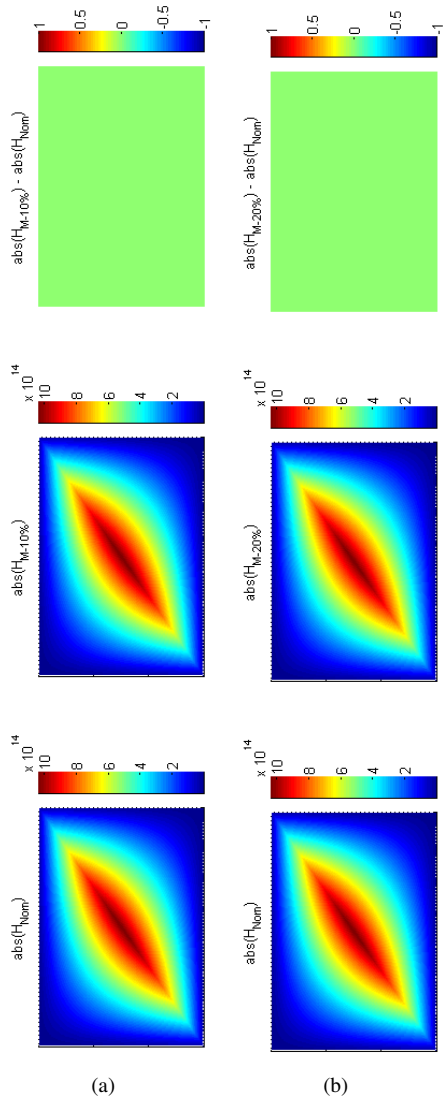

Figure 54: Hamiltonian patterns for the nominal and mass-loaded random rod structures. Plots: (a) Nominal ; (b) mass-loaded rod structures, Mass (10% and 20%, respectively); and Hamiltonian differences. The Hamiltonian elements are shown in terms of the absolute values.

Although not shown in detail, it is also important to emphasize that the number of non-zero matrix elements did not change for the stiffness and mass matrices of all random rod structures investigated when randomness was inserted in the nominal rod structure, Gomes (84). However, it is not clear how the small changes in matrix element magnitudes due to point mass uncertainties led to modifications in the level of coupling between Hamiltonian elements and in the modal parameters, natural frequencies and mode shapes, for the mass-loaded random rod structures investigated.

In conclusion, important evidence arises from the results of this analysis: the universal establishment of GOE statistics can not be evaluated directly through analysis of the mass and stiffness matrix structures, or the changes in the magnitude of Hamiltonian matrix structure. Based on this evidence, the investigation approach based on the matrix structure will not be applied in the following statistical analysis of the other random structures investigated in this study.

3.4.6 Spectral Kinetic Energy Density Statistics

In this subsection, the statistical characteristics of the first two statistical moments of the kinetic energy density results are investigated for the nominal and random longitudinal rod structures. Initially, the general considerations regarding the kinetic energy density evaluation in the SEA prediction context are shown in detail for the case of a longitudinal rod.

SEA Predictions

For a single subsystem, like the longitudinal rod structure considered, the SEA power balance states that the power input (Π_{in}) to the structure is equal to the dissipated power (Π_{diss}):

$$\Pi_{in} = \Pi_{diss} = E\omega\eta\,. \tag{3.3}$$

In SEA analysis, the variables are usually taken as band-averaged variables and the frequency ω is assumed to be the frequency-band central frequency. According to Cremer *et al* (38), the power input for a single point force is given by:

$$\Pi_{in} = \frac{1}{2}F^2\left\langle Re\left(Y(\omega)\right)\right\rangle, \tag{3.4}$$

where $\langle\,\rangle$ denotes the spatial average and $Y(\omega)$ is the input mobility. Lyon in (48) showed that the spatial mean of the real part of the mobility can be adequately estimated from the real part of the input mobility results of a corresponding infinite (or semi-infinite) system, $Y_\infty(\omega)$. This assumption is usually adopted in the analytical SEA field. Thus, Equation (3.4) can be rewritten as:

$$\Pi_{in} = \frac{1}{2}F^2 Re\left(Y_\infty(\omega)\right). \tag{3.5}$$

Considering a unit point force and substituting Equation (3.5) into Equation (3.3), the total energy is given by:

$$E_{SEA} = \frac{Re\left(Y_\infty(\omega)\right)}{2\omega\eta}. \tag{3.6}$$

Therefore, the kinetic energy density for a longitudinal rod is given by:

$$T_{SEA} = \frac{E_{SEA}}{2L_r} = \frac{Re\left(Y_\infty(\omega)\right)}{4L_r\omega\eta}, \tag{3.7}$$

where L_r is the rod length.

The analytical mobility expressions for infinite and semi-infinite rods subjected to a single point-excitation are available in the literature. According to Fahy and Walker (5), the analytical mobility expression for semi-infinite rods is given by:

$$Y_{\frac{1}{2}\infty}(\omega) = \frac{1}{S\sqrt{E_{ym}\rho}} = \frac{1}{\rho S c_l}. \tag{3.8}$$

and for infinite rod systems is given by:

$$Y_\infty(\omega) = \frac{1}{2S\sqrt{E_{ym}\rho}} = \frac{1}{2\rho S c_l}, \tag{3.9}$$

where c_l, S, and ρ are the longitudinal wave speed, rod cross-sectional area, and mass density, respectively. The longitudinal wave speed (c_l) of a rod is given by:

$$c_l = \sqrt{\frac{E_{ym}}{\rho}}. \tag{3.10}$$

Substituting the previous analytical mobility expressions into Equa-

tion (3.7), the kinetic energy density for a longitudinal rod subjected to a unitary single point force is given by:

$$T_{SEA} = \frac{1}{4\rho S L_r \omega c_l \eta}, \tag{3.11}$$

and the spatially-averaged kinetic energy density is given by:

$$T_{SEA} = \frac{1}{8\rho S L_r \omega c_l \eta}. \tag{3.12}$$

Spectral Kinetic Energy Density Statistics: Single Point-Excitation

In this current analysis, the spectral approach will be adopted for the averaging processes of kinetic energy density results. Therefore, the evaluation of the energy response variability was performed within the 1/3 octave frequency band limits. Similar averaging processes have been applied in experimental investigations of the energy response variability in the room acoustics field, Davy *et al* (53, 54).

In this regard, the kinetic energy density results are evaluated, using the Equation (2.67), for each of the rod structures subjected to a unitary longitudinal single point-loading at the left rod end. Additionally, the damping loss factor (DLF) was considered to be *frequency-constant*, since the mechanical loss mechanisms for the structure class investigated were considered to be spatially distributed, (28, 161). Based on the recent literature, four the DLF values were adopted in order to provide distinct levels of the modal superposition, Langley and Brown (1, 18). The DLF values adopted are η = 0.03, 0.06, 0.12 and 0.24.

The kinetic energy density results for the nominal rod are initially evaluated for each DLF in terms of the narrow frequency domain with 10 Hz frequency intervals. A sufficiently large number of modes was adopted in the superposition process to provide the correct response convergence in frequency range investigated.

In Figure 55, the kinetic energy density results for the nominal rod are presented in terms of the narrow frequency domain as well as in terms of the 1/3 octave frequency bands domain. Additionally, the SEA analytical predictions were also evaluated and compared with the numerical results.

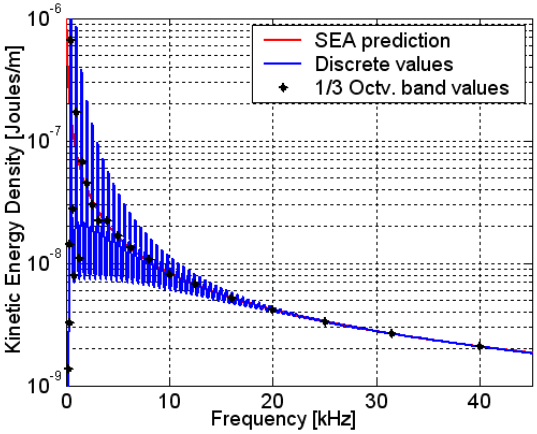
SEA prediction
Discrete values
1/3 Octv. band values
Kinetic Energy Density [Joules/m]
Frequency [kHz]
10^-6
10^-7
10^-8
10^-9
0
10
20
30
40

(a)

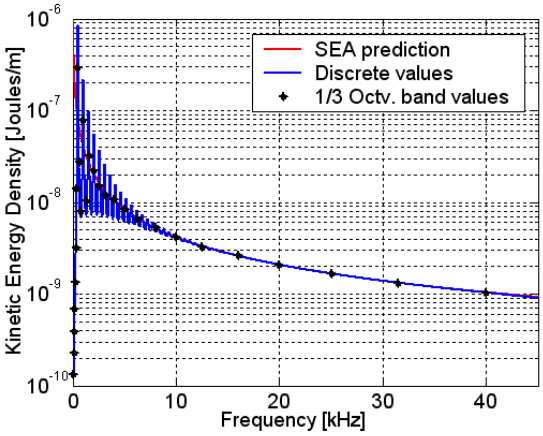
SEA prediction
Discrete values
1/3 Octv. band values
Kinetic Energy Density [Joules/m]
Frequency [kHz]
10^-6
10^-7
10^-8
10^-9
10^-10
0
10
20
30
40

(b)

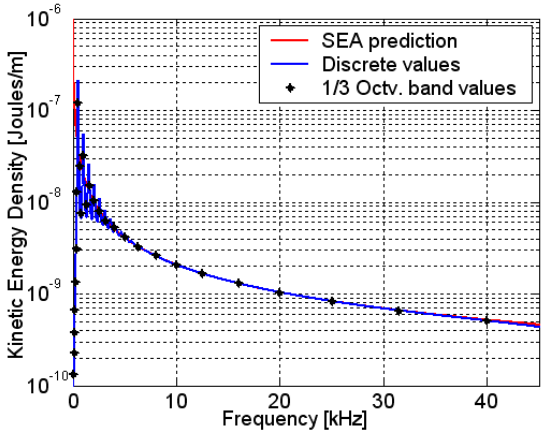

(c)

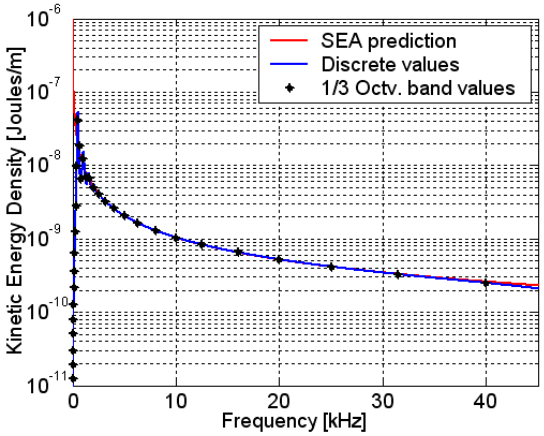

(d)

Figure 55: Kinetic energy density results for the nominal rod excited by unitary longitudinal single point-loading at left end of rod (spectral averaging approach). Plots: Damping Loss Factors: (a) 0.03, (b) 0.06, (c) 0.12, and (d) 0.24.

According to Figure 55, the numerical energy results for the nominal rod conform very well with the SEA predictions mainly in the high-frequency range, regardless of the damping loss factor value considered. In general, as the DLF magnitude increases, the numerical energy results become smooth and a reduction in the oscillation behavior of the energy response curve occurs around the analytical SEA predicted values.

Considering a spectral averaging process, the relative variances of the kinetic energy density results, associated with each 1/3 octave frequency band, were also evaluated for the nominal rod response. In order to identify clearly the effects on the spectral relative variance of different levels of modal superposition, the relative variance results for the four DFLs considered are plotted in terms of the corresponding modal overlap factors, Figure 56.

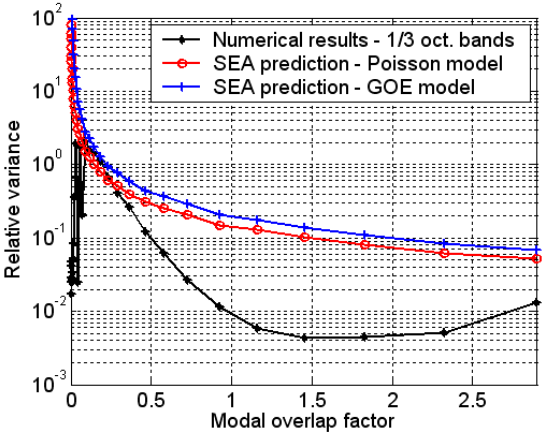

(a)

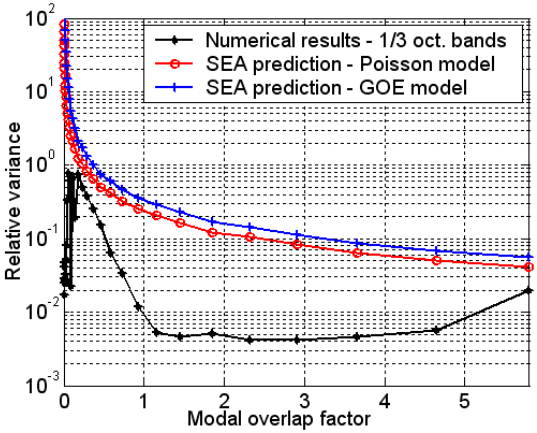
Numerical results - 1/3 oct. bands
SEA prediction - Poisson model
SEA prediction - GOE model
Relative variance
Modal overlap factor

(b)

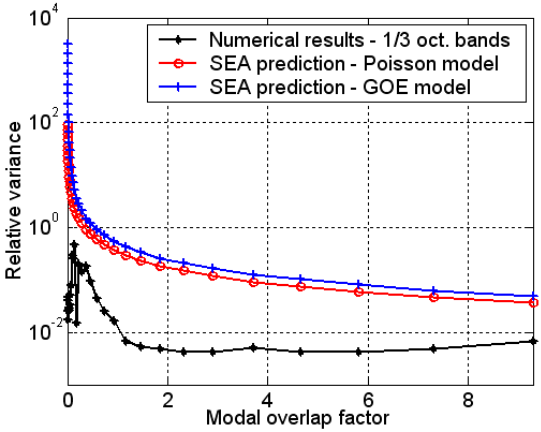
Numerical results - 1/3 oct. bands
SEA prediction - Poisson model
SEA prediction - GOE model
Relative variance
Modal overlap factor

(c)

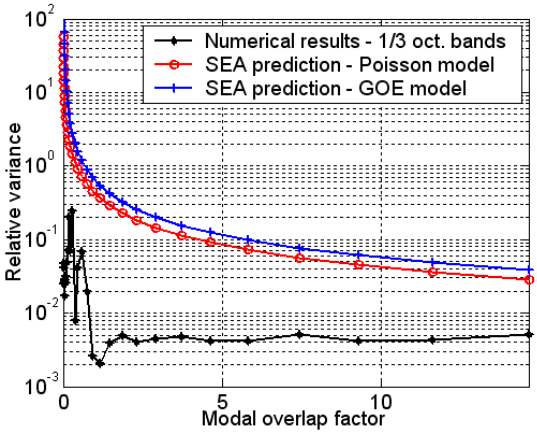

(d)

Figure 56: Spectral relative variances of kinetic energy density results for the nominal rod excited by unitary longitudinal single point-loading at the left end of the rod (spectral averaging approach). Plots: Damping Loss Factors: (a) 0.03, (b) 0.06, (c) 0.12, and (d) 0.24.

As shown in Figure 56, the numerical results of the spectral relative variance present lower values in comparison to the expected analytical predictions for all of the DFLs considered. It can be noted that as the DLF value increases, the energy response becomes multimodal and an asymptotic reduction in the energy response variability is expected. Indeed, good agreement occurs between the averaged numerical results and the SEA predictions for high modal overlap factor magnitudes, Figure 55. In terms of the spectral relative variance results, similar behavior occurs, since an almost constant plateau curve with small amplitude is established for high overlap modal factor values.

Although the SEA variance analytical prediction based on the Poisson model considers sinusoidal mode shapes like those observed for the nominal rod structure, the spectral relative variance numerical results for the nominal rod are much lower than the Poisson predictions, Figure 56. It appears that this discrepancy is mainly due to differences between the natural frequency statistics of the nominal rod and Poisson model.

Considering the nominal longitudinal rod structure, the natural fre-

quency statistics presents *high spectral rigidity* characteristics as well as the establishment of a relevant spectral correlation. On the other hand, the SEA variance prediction based on the Poisson model considers that the natural frequencies are completely uncorrelated. In this regard, the numerical spectral relative variance results for the nominal rod are expected to be lower than the analytical predictions based on the Poisson model as well as on the GOE[11] model.

As shown in the SEA literature, the relative variance predictions based on the Poisson statistics are traditionally expected to be larger than those based on the GOE model for all two and three-dimensional real engineering systems (16, 35). In the current analysis, the SEA variance predictions based on the Poisson model for a longitudinal rod subjected to a single point-loading are surprisingly lower than corresponding results based on the GOE model, as presented in Figure 56.

As discussed previously, the point-loading relative variance predictions are highly dependent on the mode shape statistics through the Mode Shape Statistics Factor (K), Brown *et al* (1, 18, 3). Considering the SEA relative variance predictions based on the Poisson model, the mode shapes are assumed to be sinusoidal and thus the Mode Shape Statistics Factor is equal to $K = 1.5$ for one-dimensional systems[12], Lyon (48). On the other hand, the relative variance predictions based on the GOE model consider Gaussian mode shape statistics in which the Mode Shape Statistics Factor is equal to $K = 3.0$, regardless of the system dimensionality, Mehta (24).

The natural frequency effects associated with Poisson statistics on the energy results lead to a large variability in the energy response compared with those associated with GOE statistics. The current rod relative variance predictions strongly suggest that the contribution from the mode shape statistics on the energy density results can be significantly greater than the contribution the natural frequency statistics for the case of a longitudinal rod subjected to a single point-loading. Indeed, the statistical moments of the kinetic energy density response from the engineering structure subjected to a single point-loading are strongly influenced by the mode shape statistics and thus small modifications in the mode shape statistics can lead to relevant changes in the response variance magnitudes.

In summary, lower amplitudes of the point-loading relative variance

[11] The GOE model considers Rayleigh correlated natural frequencies, Mehta (24).

[12] For sinusoidal mode shapes, the spatial kurtosis values are dependent on the system dimensionality and thus the spatial kurtosis values are 1.5, 2.25, and 3.875 for one, two, and tri-dimensional systems, respectively, Lyon (48).

prediction based on the Poisson model can be easily explained considering the following factors:

- the sinusoidal spatial kurtosis value is much lower than the GOE value for one-dimensional structures, that is $K_{sin}^{1D} = 1.5 < K_{GOE} = 3$, and
- the effects of the mode shape statistics on the energy results become predominantly greater than the corresponding natural frequency statistics effects for cases where a structure is subjected to a single point-loading.

Considering random rod structures, the kinetic energy density results were evaluated in terms of the narrow frequency domain as well as the 1/3 octave frequency-band domain. In Figure 57, the numerical energy results for the random rods are presented and compared with the SEA analytical predictions as well as the nominal rod result[13].

In these plots, only the spectral variances of the kinetic energy density results, with $\eta = 0.03$, are present for random rods. This technical choice is based on the premise that small DFL magnitudes provide low modal superposition characteristics and allow a direct visualization of the effects of the modal parameter statistics on the statistical moments of kinetic energy density results.

[13] It is relevant to point out that the comparison with the nominal results provides an efficient investigation of the performance of the randomization process and the corresponding uncertainty effects. In other words, this direct comparison enables the identification of the minimum cut-off frequency at which the energy responses of the random rods are effectively perturbed by the presence of randomness.

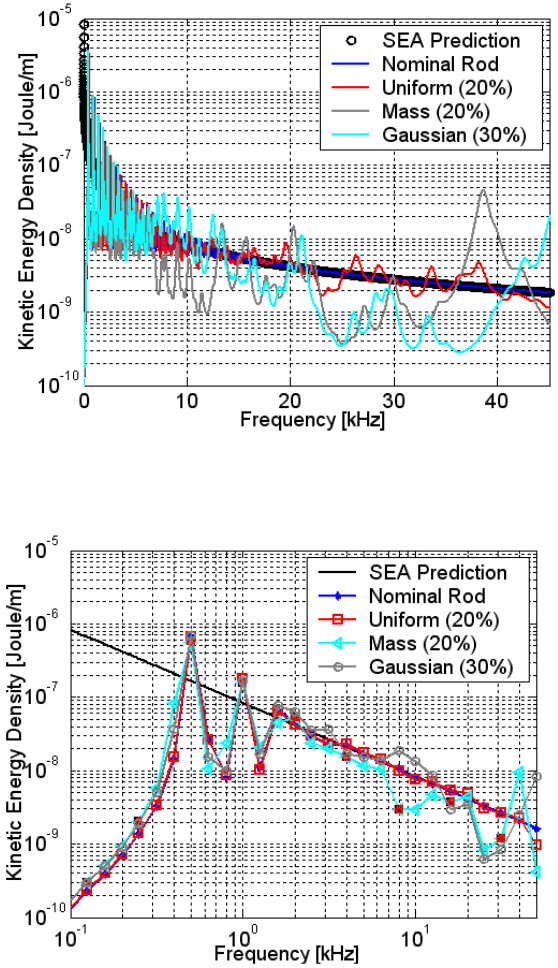

Figure 57: Kinetic energy density results for the random and nominal rods in terms of the narrow and 1/3 octave frequency band domains subjected to unit single point excitation. The analytical SEA predictions are also plotted.

In addition to the kinetic energy density analysis, the spectral relative variances of the kinetic energy density results were evaluated for the random and nominal rod structures. The analytical predictions of the relative vari-

ance based on the Poisson and GOE models were also evaluated in terms of the 1/3 octave frequency band domain, Figure 58. The DLF magnitude was considered to be frequency-constant and equal to 0.03 (3%).

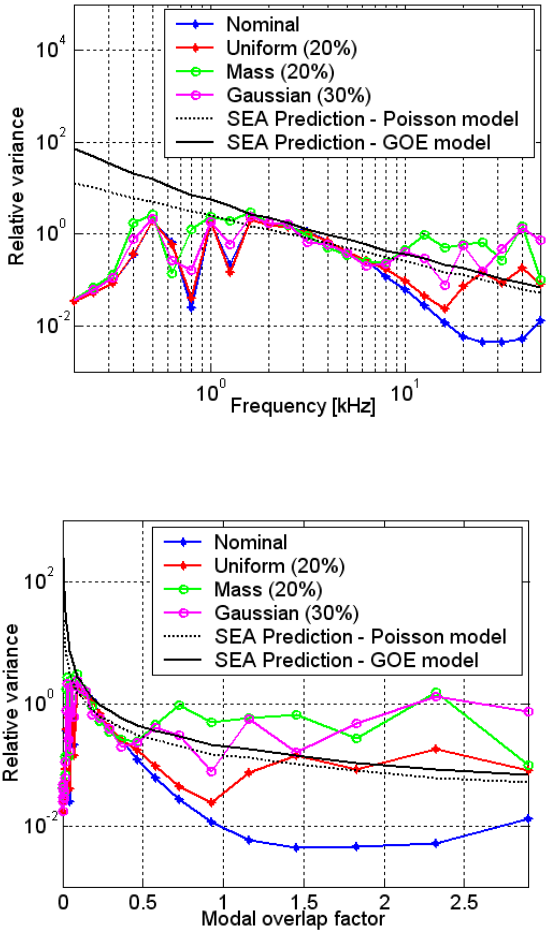

Figure 58: Spectral relative variance of kinetic energy density results for the random and nominal rods subjected to unit single point-loading (spectral averaging approach). The analytical predictions for relative variance based on the Poisson and GOE models.

According to Figure 58, the results for the random rods suggest that the spectral relative variances are dependent on the randomization approach adopted in the mid and high-frequency ranges. Even though a certain level of *universal* statistics is expected for modal parameters toward the high-frequency range[14], the spectral relative variance results showed distinct behaviors as well as *system-dependent effects* in the high-frequency range. Nevertheless, it appears that these distinct behaviors are due to large differences in the mode shape statistics of the random rod structures considered. Indeed, the statistical moments of the energy responses for a single point excited structure are strictly dependent on mode shape statistics and thus small changes in the mode shape statistics may provide relevant changes in the spectral relative variance results.

In order to evaluate the effects of the high modal superposition condition, the statistical moments of the kinetic energy density results were evaluated considering a large DLF value for the nominal and random rod structures. A large frequency-constant DLF, $\eta = 0.24$, was adopted, providing a range of modal overlap factor values from 0 to 12 modes. In Figure 59, the spectral mean and relative variance results are shown for the nominal and random rods with $\eta = 0.24$.

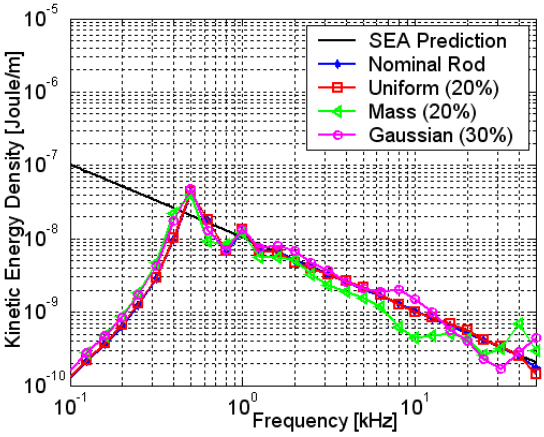

[14] In other words, it is expected that the energy response statistics becomes independent of the uncertainty sources for a sufficiently random system, Langley *et al* (4, 23).

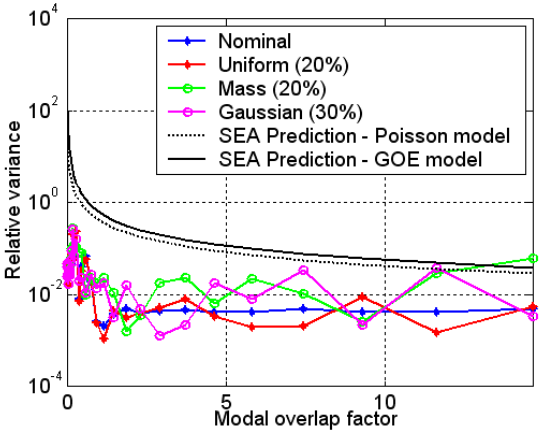

Figure 59: Spectral mean and relative variance of kinetic energy density results for the random and nominal rods with DLF = 0.24 (spectral averaging approach). The analytical predictions for relative variance are based on Poisson and GOE statistics models.

As shown in Figure 59, the high DLF values provide a smoother mean response curve than those for the rods with low DLFs. In general, it can be noted that there is a reduction in the oscillatory behavior around the SEA predictions and a better agreement is obtained mainly for the 1/3 octave frequency band results.

For spectral relative variance results, lower magnitudes were observed for all random rod structures. As expected, the high modal superposition condition tends to reduce substantially the spectral relative variance magnitudes and thus the spectral relative variance magnitudes for the random rods are similar to that for the nominal rod.

Indeed, the global patterns of the spectral variance results for the random rods are very similar to each other, and it seems that small differences in the relative variance magnitudes of the random rods occurs due to the effects of the distinct randomization processes adopted during the generation of these random structures. However, it is important to emphasize that the differences in the spectral relative variances are very significant for the case of lightly damped random rod structures, Figures 57 and 58.

Spectral Kinetic Energy Density Statistics: Spatially-Averaged Excitation

From the natural frequency statistical observable results, it can be noted that the spectral natural frequency statistics of the Mass (20%) and Gaussian (30%) random rod structures shows a degree of *universal* characteristics as well as good agreement between the GOE eigenvalue predictions and the natural frequency statistics of these rod structures.

Based on the concept of *Universality*, the establishment of GOE natural frequency statistics is expected for sufficiently random engineering systems, Langley *et al* (23, 18, 4). Under this particular condition, the statistics of the kinetic energy results for the engineering structures subjected to *spatially-averaged excitation*[15] are practically independent of the precise sources of uncertainty in the physical properties of system. Thus similar structures with sufficiently random parameters could give approximately the same mean and relative variance results in mid and high-frequency ranges. Additionally, it is also expected that the spatially-averaged mean and relative variance results can be adequately predicted by the SEA model based on the GOE model for natural frequency statistics.

In order to verify the validity of the Universality concept for natural frequency statistics of sufficiently random rod systems, the spatially-averaged relative variance results for the Mass (20%) and Gaussian (30%) random rod structures were evaluated for several DFL magnitudes. Considering that the natural frequency statistics results for the Mass (20%) and Gaussian (30%) random rods are very similar and conform well with GOE statistics, it is expected that spatially-averaged energy results for such rod structures will comply with the Universality concept and thus the spectral spatially-averaged relative variances are independent of uncertainty sources and conform very well to the revised SEA relative variance prediction based on the GOE eigenvalue statistics.

In Figure 60, the spatially-averaged relative variance results are presented for both random rod structures. The analytical predictions based on Poisson and GOE models are also plotted for all cases investigated.

[15] As shown in the SEA literature, the spatially-averaged process of a single point-loading leads to energy results equivalent to those of *rain-on-the-roof* excitation. It is very important to emphasize that in both excitation cases the effects of the mode shape statistics are completely removed from the energy response and thus the kinetic energy density results are dependent only on the natural frequency statistics.

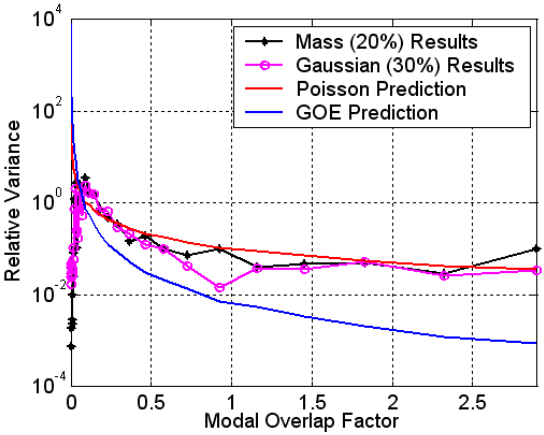
Mass (20%) Results
Gaussian (30%) Results
Poisson Prediction
GOE Prediction
Relative Variance
Modal Overlap Factor
10^4
10^2
10^0
10^-2
10^-4
0
0.5
1
1.5
2
2.5

(a)

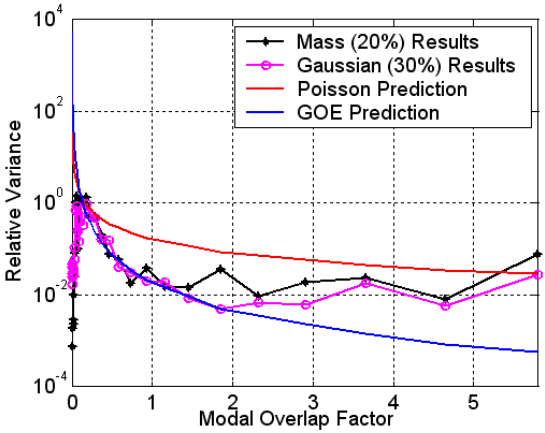
Mass (20%) Results
Gaussian (30%) Results
Poisson Prediction
GOE Prediction
Relative Variance
Modal Overlap Factor
10^4
10^2
10^0
10^-2
10^-4
0
1
2
3
4
5

(b)

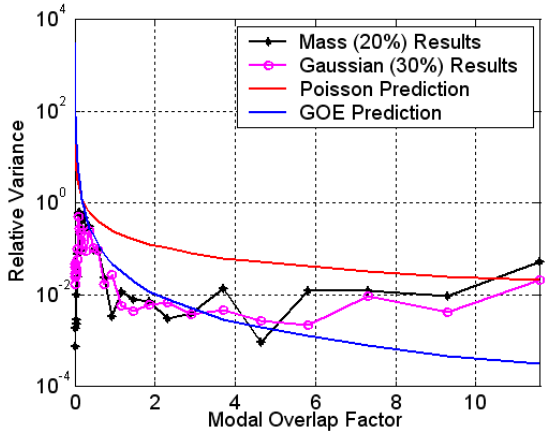

(c)

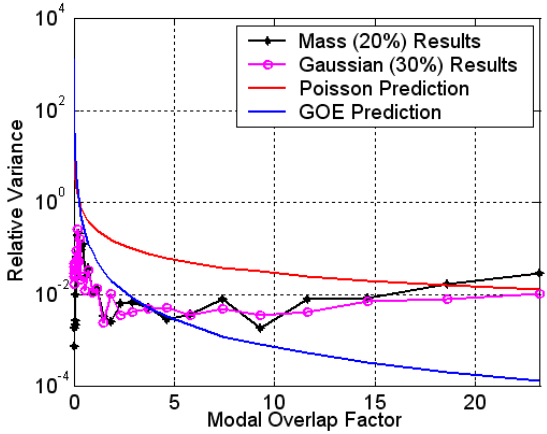

(d)

Figure 60: Spectral relative variance of kinetic energy density results from the Mass (20%) and Gaussian (30%) random rods subjected to spatially-averaged (spectral averaging approach) excitation. Several DLF are considered. Plots: (a) 0.03, (b) 0.06, (c) 0.12, and (d) 0.24.

As shown in Figure 60, the spectral relative variance results for the

Mass (20%) and Gaussian (30%) rods are very similar, except for the presence of some small discrepancies, regardless of the DFL value considered.

In Figure 60 (a), the numerical results surprising do not conform well with the variance prediction based on the GOE model, but a good agreement with the prediction based on the Poisson model is observed mainly in the high-frequency range. Indeed, although a spectral averaged behavior similar to GOE statistics is expected for the natural frequencies, the statistical characteristics vary substantially in the frequency domain, from *almost-nominal* statistics in the lower frequency range with high spectral rigidity characteristics to *structural localized* statistics in the higher frequency range in which the natural frequencies have statistical characteristics similar to the *Poisson* model.

In Figures 60 (b) - (d), the effects of an increase in the damping level are investigated. For the random rod structures investigated, the increase in DLF values is linearly related to the increase in the degree of modal superposition. Indeed, a large number of modes is expected to contribute to the energy response and thus the presence of spectral correlations between the natural frequencies may become more and more relevant and reduces substantially the spectral variability of the energy responses.

Considering the effects of the increase in damping levels on the performance of the variance prediction based on the Poisson model, the discrepancies between the numerical results and analytical prediction become more and more pronounced as the damping level increases. Additionally, it can be observed that the numerical results deviate from the Poisson prediction differently over the frequency range. Indeed, large deviations of the numerical results are expected for low and mid-frequency ranges, where the spectral natural frequency correlations are expected to be more intensive.

Based on the above discussions, it appears that the natural frequencies of both random rods have well established asymptotic statistics for the extremely high-frequency range. In fact, considering the extreme condition where the longitudinal wavelength is smaller than the structural irregularity span, the random rods become effectively *clamped* on the structural irregularity locations. Therefore, the structural localization phenomenon is completely established and independent sets of modes with similar statistics exist in the various sections between the structural irregularities, providing an asymptotic exponential PDF for the natural frequency spacings described approximately by Poisson model, since the sum of a large number of statistically independent sets of random variables has an exponential PDF.

3.4.7 Spatially-Correlated Gaussian Rods

In order to investigate the effects of the spatial correlation of the geometrical irregularities on the spectral response variability for the one-dimension real engineering structures, the statistical characteristics of spatially-correlated longitudinal random rods were investigated considering several levels of spatial correlation.

In the engineering context, the spatial variation of the physical and material properties can be appropriately represented by the *random fields*, Vanmaercke (162). If the spatial variations in the geometric dimensions are considered, the application of a continuous random field becomes very appropriate. However, for cases of an existing FEM discretization, a practical approach is traditionally considered where the random field values in each finite element domain are considered to be constant throughout on the finite element extension. It is also important to emphasize that the discretized random field model includes the spatial inter-dependencies between the finite element random field values based on a probabilistic approach, such as the Monte Carlo simulation.

The essential concepts from the random field theory are briefly presented below. The random field characteristics adopted in the FEM model development of Gaussian spatially correlated random rods are discussed in detail. The effects of the spatial correlation on the modal parameter statistics are investigated for several correlation length magnitudes. In the last stage, the relationship between the establishment of GOE characteristics for the modal parameter statistics and the correlation length magnitudes is also investigated in the spectral response variability context.

Random Field Theory Background

A simple random field model considered in the engineering context is a *homogeneous isotropic Gaussian field*. In this field, the random field variables have a Gaussian distribution with parameters independent of direction and location. That is, the interdependency between two random variables is dependent only on the perpendicular distance between the two points considered. According to Hinke and Mace (25), the correlation function between two Gaussian random variables is given by:

$$R_{HG}(d_p, L_c, \sigma) = \sigma^2 \exp\left(-\left|\frac{d_p}{L_c}\right|^2\right), \tag{3.13}$$

where σ is the standard deviation, L_c is the correlation length and d_p is the perpendicular distance between the two points considered.

According to Sakar and Ghanem (163), an alternative correlation function of the *Markovian stochastic process* is given by:

$$R_{MS}(d_p, L_c) = \exp\left(-\left|\frac{d_p}{L_c}\right|\right). \tag{3.14}$$

On comparing the previous random field correlation function definitions, distinct dependencies on the absolute ratio of the perpendicular distance to the correlation length magnitude are clearly observed. The Markovian process correlation function has a linear dependence while the homogeneous Gaussian one has a square dependence on the absolute ratio of the distance to the correlation length. Although both correlation functions show a decreasing exponential pattern, a more abrupt profile variation in the spatial domain is expected for the homogeneous Gaussian function due to its square dependence characteristics.

For n random variables, the covariance matrix $\mathbf{C_m}$ is a symmetric and completely positive matrix. The elements of the n x n covariance matrix c_{ij} are given by:

$$c_{ij} = R(d_{ij}, L_c, \sigma) \;\; i, j = 1, 2, ..., n. \tag{3.15}$$

A one-dimensional random field, given by a vector $\mathbf{u}$ of length n, can be adequately represented by the Karhunen-Loeve expansion in the form:

$$\mathbf{u}(\mathbf{x}, \zeta) = \bar{\mathbf{u}}(x) + \sum_{i}^{r \leq n} \sqrt{\lambda_i}\phi_i(\mathbf{x})\,\psi_i(\zeta), \tag{3.16}$$

where $\bar{\mathbf{u}}$ denotes the mean, ψ_i are uncorrelated standard normal random variables (zero mean and unit variance) and λ_i and ϕ_i are the eigenvalues and eigenfunctions of the covariance matrix respectively, which are obtained from the eigenvalue problem:

$$\mathbf{C_m}\phi_i = \lambda_i\phi_i. \tag{3.17}$$

The mean $\bar{\mathbf{u}}$ and the eigenfunctions ϕ_i are deterministic and only contain the spatial coordinate $\mathbf{x}$. The randomness of the field is included through the $\psi_i(\zeta)$ parameter. There are n eigensolutions, but in general it is sufficient to consider only the most important eigenfunctions, which provide a good approximation to the random field.

Development of the Spatially-Correlated Longitudinal Random Rods

In order to assess the effects of different levels of the geometry spatial correlation on the modal parameter statistics, as well as on the statistical moments of kinetic energy density results, the spatially-correlated longitudinal random rods were built considering the rod cross-sectional areas as *Gaussian correlated random variables* along the rod length domain. The random rod cross-sectional area values were calculated through the Karhunen-Loeve expansion based on the modal parameters of the covariance matrix, similarly to Equation (3.16).

In the current analysis, the random field correlation function definition based on the Markovian stochastic process was adopted in the FEM models development for Gaussian spatially-correlated random rods, Equation (3.14). The main reason for adopting this random field correlation function definition is based on the performance of the results, which provide a distribution very close to that of the spatially independent Gaussian values, although the rod cross-sectional area values are spatially correlated along the rod length direction.

In contrast, the homogeneous isotropic Gaussian field results present a distribution which is slightly non-symmetric around the mean value and also shows small deviations from the Gaussian distribution pattern. The Lilliefors Test results for both random fields confirm that the Markovian stochastic random field values have a more Gaussian distribution than that of the random field results for the homogeneous isotropic Gaussian case.

In order to perform a direct comparison between the statistical characteristics of the spatially correlated random rod structures and the spatially independent Gaussian (30%) rod structure, in which the rod cross-section areas are not spatially correlated along the rod length direction, the random field cross sectional area values were adjusted to provide a spatially Gaussian correlated distribution with the same width distribution and mean value as the cross-sectional area distribution of the spatially independent Gaussian (30%) rod structure investigated in the spectral analysis performed in previous section 3.4.1.

In Figure 61, the distribution of the random field results are shown for the Markovian stochastic process and homogeneous isotropic Gaussian correlation functions. In order to compare the distributions of all of the numerical results, the cross-section area distribution of the spatially independent Gaussian (30%) rod structure is also presented.

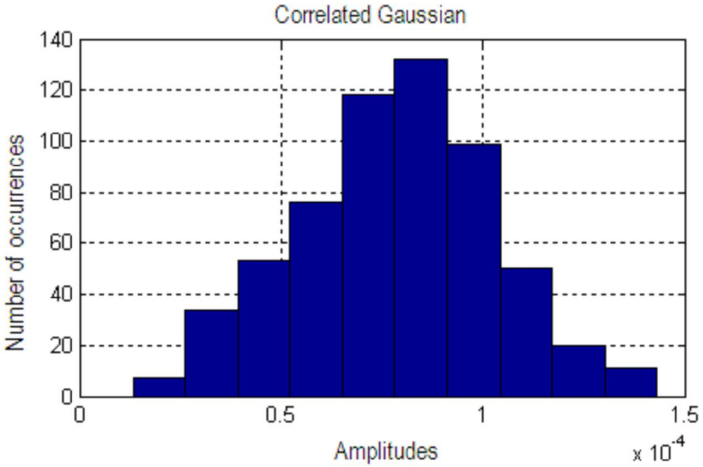
Correlated Gaussian
Number of occurrences
Amplitudes
x 10^-4
0
20
40
60
80
100
120
140
0
0.5
1
1.5

(a)

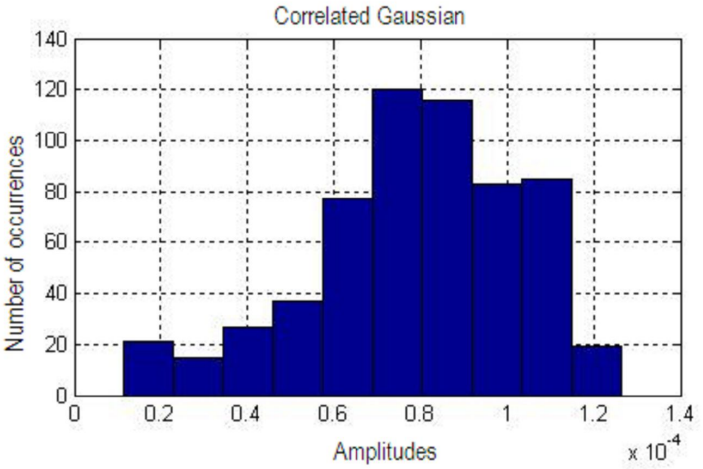
Correlated Gaussian
Number of occurrences
Amplitudes
x 10^-4
0
20
40
60
80
100
120
140
0
0.2
0.4
0.6
0.8
1
1.2
1.4

(b)

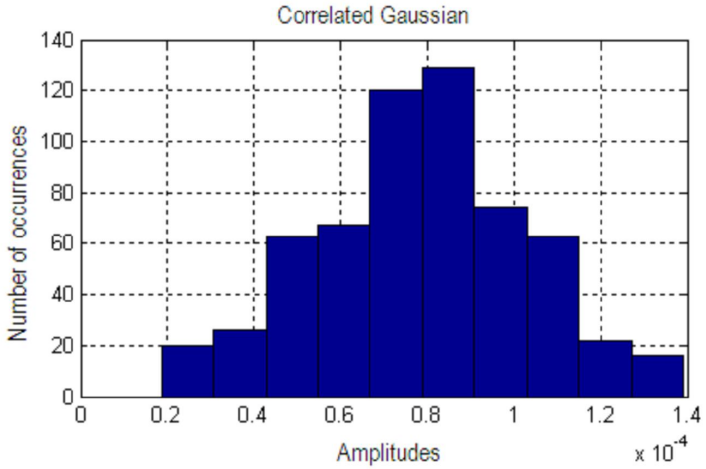

(c)

Figure 61: Distribution of the rod cross-sectional area values from: (a) the spatially independent Gaussian (30%) rod, (b) the spatially-correlated Gaussian rod: Homogeneous isotropic Gaussian random field, and (c) the spatially- correlated Gaussian rod: Markovian stochastic process random field.

In addition, it is also important to note that good performance was obtained in the application of the random fields based on decreasing linear exponential correlation functions, such as that proposed in Equation (3.14), in the numerical studies regarding the response variability in which the correlation effects on the geometry of the one-dimensional real engineering structures were considered, Sakar and Ghanem (163).

In the current analysis, a large range of the correlation length magnitudes was considered in order to ensure a complete statistical analysis of the most representative effects due to spatial correlation, including two extreme conditions of spatial correlation, that is, rods with spatially independent Gaussian cross-sectional areas provided by the asymptotic null correlation length magnitudes and, under another extreme condition, rods with cross-sectional areas strongly spatially correlated which are provided by the asymptotic large correlation length magnitudes, similar to the nominal rod cross-sectional area

distribution. The following magnitudes of the correlation length (L_c) were considered in the spectral analysis: 0.01, 0.06, 0.1, 0.2, 1, 5, and 10; as well as very large L_c magnitude (approximately infinite correlation length almost corresponding to the nominal rod).

In the following sections, the spectral statistics of the modal parameters are investigated for each of the spatially-correlated random rods.

Spectral Natural Frequency Statistics

The current spectral analysis of the unfolded natural frequencies considers only the following eigenvalue statistical observables: the PDF of adjacent natural frequency spacings and Δ_3-statistics. As discussed previously, these statistical observables are very efficient in terms of describing the statistical characteristics associated with short and long-range fluctuations, respectively.

The spectral natural frequency statistics obtained for each of the spatially-correlated random rods are shown in Figure 62.

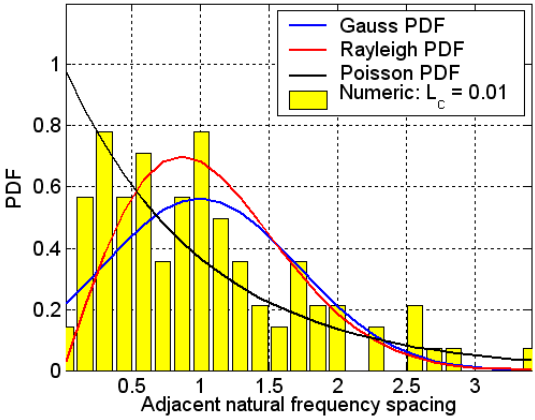

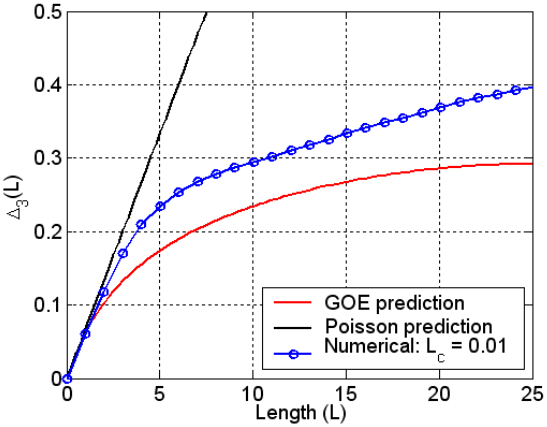
0.5
0.4
0.3
0.2
0.1
0
$\Delta_3(L)$
0
5
10
15
20
25
Length (L)
GOE prediction
Poisson prediction
Numerical: L_c = 0.01

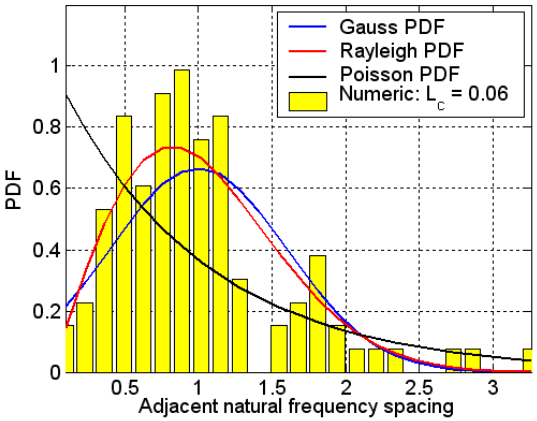
1
0.8
0.6
0.4
0.2
0
PDF
0.5
1
1.5
2
2.5
3
Adjacent natural frequency spacing
Gauss PDF
Rayleigh PDF
Poisson PDF
Numeric: L_c = 0.06

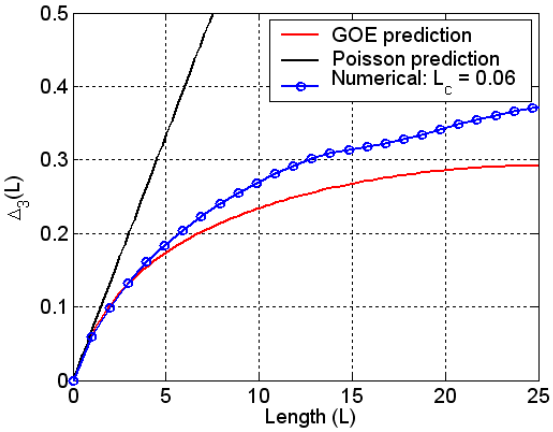
GOE prediction
Poisson prediction
Numerical: L_c = 0.06
Δ3(L)
Length (L)
0
0.1
0.2
0.3
0.4
0.5
5
10
15
20
25

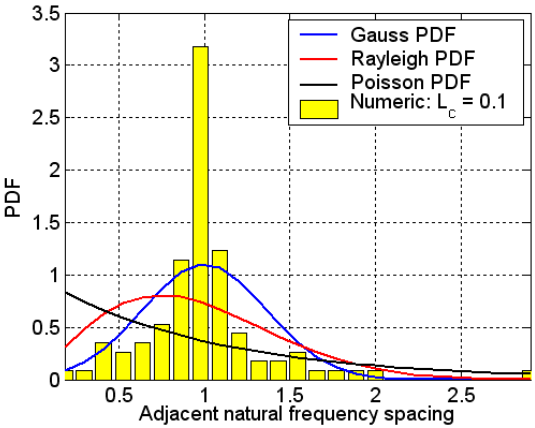
Gauss PDF
Rayleigh PDF
Poisson PDF
Numeric: L_c = 0.1
PDF
Adjacent natural frequency spacing
0
0.5
1
1.5
2
2.5
3
3.5

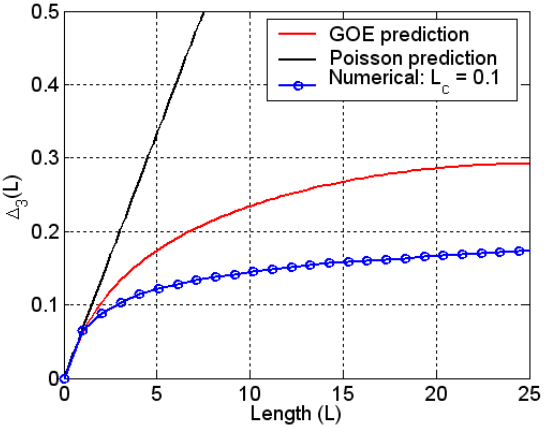
GOE prediction
Poisson prediction
Numerical: L_c = 0.1
Δ3(L)
Length (L)
0
0.1
0.2
0.3
0.4
0.5
0
5
10
15
20
25

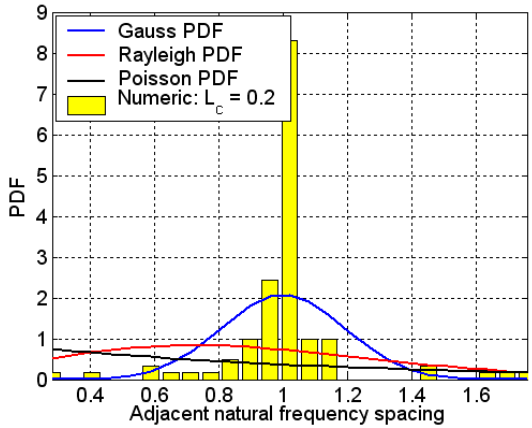
Gauss PDF
Rayleigh PDF
Poisson PDF
Numeric: L_c = 0.2
PDF
Adjacent natural frequency spacing
0
1
2
3
4
5
6
7
8
9
0.4
0.6
0.8
1
1.2
1.4
1.6

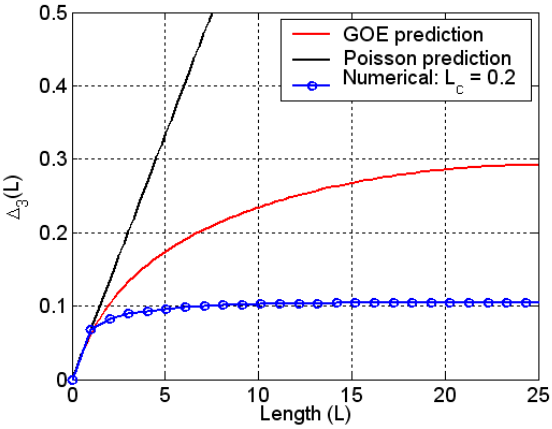

Figure 62: The spectral natural frequency statistical observable results for the spatially correlated random rod structures: PDF of adjacent natural frequency spacings and Δ_3-statistics results (spectral averaging approach).

As shown in Figure 62, the greatest effect of the spatial correlation occurred for the smallest correlation lengths investigated. For $L_c = 0.01$, the spacing PDF results suggest a partial establishment of spectral characteristics similar to those of the uncorrelated natural frequency statistics, that is, Poisson statistics. On the other hand, the presence of the *level repulsion* characteristics is clearly observed for the smallest natural frequency spacing range. Additionally, the Δ_3-statistics results also showed moderate spectral rigidity characteristics for large natural frequency spacing range, evidencing the establishment of some discrepancies in relation to Poisson model.

The occurrence of the Poisson model characteristics for small correlation lengths can be easily explained by the discontinuities introduced by geometrical irregularities which become the nominal rod structure into a built-up system composed by several substructures connected each other by the irregularities in their extremes. Therefore, for each substructure, there is a set of natural frequencies which is independent on the natural frequencies associated with others substructures. As discussed by Weaver (64), the spectra of real system can be adequately described by the superposition of independent spectra associated with the number of non-interacting substructures or the number of geometrical symmetries presented by complex vibroacoustic

system. Thus, a superposition of large number of statistically independent natural frequency sets has a Exponential PDF and agrees satisfactorily with the Poisson model PDF spacing, Brown (1).

For $L_c = 0.06$, the natural frequency statistics results have statistical characteristics similar to GOE eigenvalue statistics in the short-range fluctuation. For the other greater correlation lengths investigated, the spectral natural frequency statistics obtained are very similar to nominal statistics, that is, there was a very notable presence of the spectral rigidity characteristics in the natural frequency domain and an asymptotic delta function distribution was established for the expected nominal unfolded natural frequency spacing value.

In addition, the Δ_3-statistics results associated with the small spacing range also suggest that for $L_c = 0.06$ the spectral short-range fluctuation statistics are similar to GOE statistics. As shown in Figure 62, for the spatially-correlated rods with $L_c < 0.06$, the spectral natural frequency statistics are asymptotically uncorrelated with the reduction in the correlation length magnitude. In contrast, the Δ_3-statistics results for $L_c > 0.06$ also suggested that the spectral natural frequency statistics in the short-range fluctuation range tends to be similar to that of the nominal rod as the correlation length magnitude increases.

For the long-range fluctuations, the Δ_3-statistics results suggest relevant spectral rigidity characteristics for all correlation lengths investigated. In general, the increase in the correlation length magnitude leads to a reduction in the Δ_3-statistics for long spectral distances, that is, an increase in the spectral rigidity effects on the long-range fluctuations.

Although it is not shown here, most of the unfolded natural frequency spacings of the spatially-correlated rods with small correlation lengths were perturbed throughout the mode order domain, while the large correlation lengths perturbed only in a limited range of the mode order domain. Indeed, it appears that there is a direct relationship between the correlation length magnitude and the wavelength associated with the frequency affected by the correlation effects.

Considering the spatially correlated rods with large correlation lengths, the results suggest that the geometrical perturbations due to correlation effects are practically negligible for the longitudinal wavelengths of the frequency range investigated and thus the unfolded natural frequency spacings magnitudes are approximately equal to the expected nominal unfolded spacing magnitude.

Spatial Mode Shape Statistics

In this subsection, the effects of distinct magnitudes of the correlation length on the mode shape statistics are investigated considering only the *spatial averaging approach*. The following eigenvector statistical observables were considered: spatial kurtosis and Lilliefors Test metric functions. In Figure 63, the spatial mode shape statistics results are shown as a function of the mode order domain.

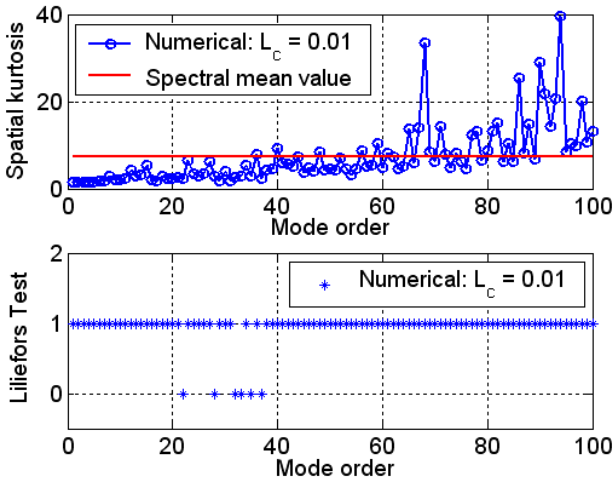

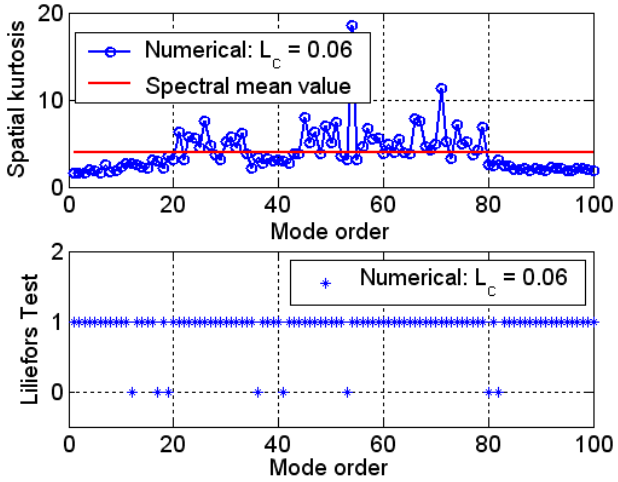
Spatial kurtosis
Numerical: L_C = 0.06
Spectral mean value
Mode order
Liliefors Test
Numerical: L_C = 0.06
Mode order

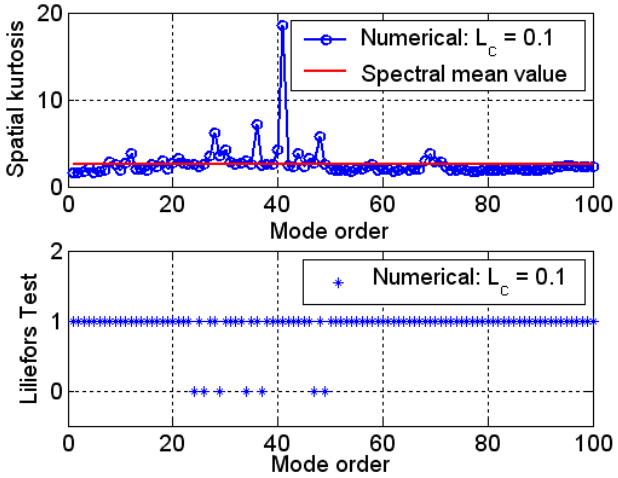
Spatial kurtosis
Numerical: L_C = 0.1
Spectral mean value
Mode order
Liliefors Test
Numerical: L_C = 0.1
Mode order

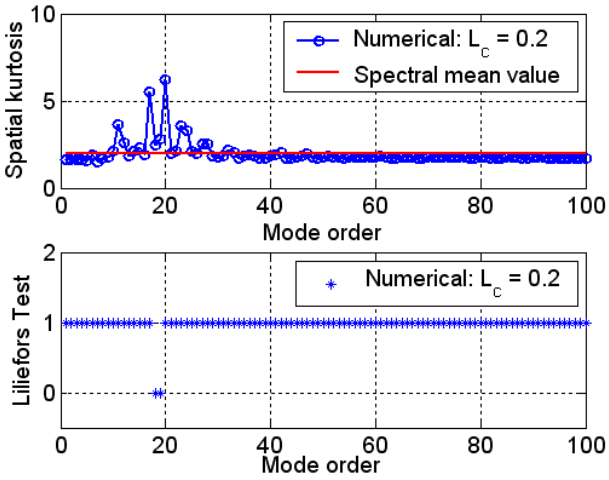

Figure 63: The spatial mode shape statistical observable results for the spatially- correlated random Gaussian rods: spatial kurtosis values and spatial Lilliefors Test results (spatial averaging approach).

As shown in Figure 63, the spatial mode shape statistics results reveal a direct relationship between the correlation length magnitude and the frequency region affected by geometrical perturbation due to spatial correlation effects. For the frequency range considered, the spatial mode shape statistics results suggest that the effects of the smaller correlation length are relevant and affect almost the whole mode shape order range considered.

For $L_c = 0.01$, the large magnitudes of the spatial kurtosis are associated with the structural localization phenomenon, mainly in the high mode order range. As the mode order increases, a gradual increase is observed for the spatial kurtosis magnitudes and for the corresponding dispersion characteristics. Indeed, the spatial kurtosis results suggest a statistical transition from *almost-deterministic statistics* (sinusoidal mode shapes) to *disordered statistics* (structurally localized mode shapes) as frequency increases. Additionally, the spatial Lilliefors Test results also suggest the establishment of intermediate statistics in which the characteristics are *almost-Gaussian* in the restricted (limited) mode order region (or frequency region) around the $30th$ mode order.

For $L_c = 0.06$, the several spatial kurtosis values are weakly localized

and slightly larger than the GOE or Gaussian value, and thus the spectral mean value of the spatial kurtosis is approximately $K = 3.90$. Additionally, the spatial kurtosis results show that the correlation effects are manifested mainly in the central region of the frequency range investigated. In this central frequency region, the spatial kurtosis results suggest the establishment of a weak structural localized statistics, since most of the spatial kurtosis values affected by the correlation effects are around $K = 3.5$ (spectral probabilistic mode value). In addition, the spatial Lilliefors Test results show that the frequency range associated with GOE or Gaussian mode shapes is wider than those of other correlation lengths.

For $L_c > 0.06$, the spatial mode shape statistics results show that the effects of a given correlation length magnitude are restricted to a particular frequency range and that the spatial mode shape statistics associated with mode shapes lying outside this particular frequency range converge asymptotically to nominal statistics as the correlation length magnitude increases. Furthermore, it appears that with an increase in the correlation length magnitude, the establishment of almost-Gaussian (or almost-GOE) mode shape statistics becomes more and more restricted to a small frequency range (or mode order range) and the spatial mode shape statistics present asymptotically similar characteristics to those of sinusoidal statistics corresponding to nominal mode shape statistics in which a flat pattern for the spatial kurtosis results is established in the mode order domain.

Non-dimensional Analysis of Mode Shape Statistics

In order to establish a good understanding of the relationship between the correlation length and its effects on the mode shape statistics, a non-dimensional analysis was performed. A normalized parameter (or non-dimensional parameter) is proposed, which relates the correlation length and wavelength magnitudes.

Considering the assumption that the wavelength of *nth* mode shape from the random rod is almost equal to that correspond to the nominal rod[16], that is, $\lambda_n^{rand} \approx \lambda_n^0$, the normalized parameter (θ_n) associated with each *nth* mode and a certain correlation length (L_c) is given by:

$$\theta_n(L_c) = \frac{L_c}{\lambda_n^0}, \tag{3.18}$$

[16]Detailed analysis performed with extremely localized mode shapes showed that a maximum error of 2% is associated with the application of this assumption. It appears that the errors are probably associated with the dispersive nature of rod system investigated, Graff (164).

where λ_n^0 is the nominal wavelength of nth mode shape.

In Figure 64, the spatial kurtosis results are presented in terms of the normalized parameter domain. This graphical presentation pattern allows the identification of the frequency range affected by a certain correlation length as well as the results to be extended to several other random one-dimensional longitudinal structures.

As shown in Figure 64, for the normalized parameter range in which the values are greater than unity, an almost flat behavior of spatial kurtosis results is observed and an asymptotic convergence toward the nominal spatial kurtosis value occurs as the correlation length increases. On the other hand, for normalized parameter with magnitudes of less than unity, the corresponding mode shape statistics are clearly affected by the spatial correlation effects and large spatial kurtosis magnitudes are observed.

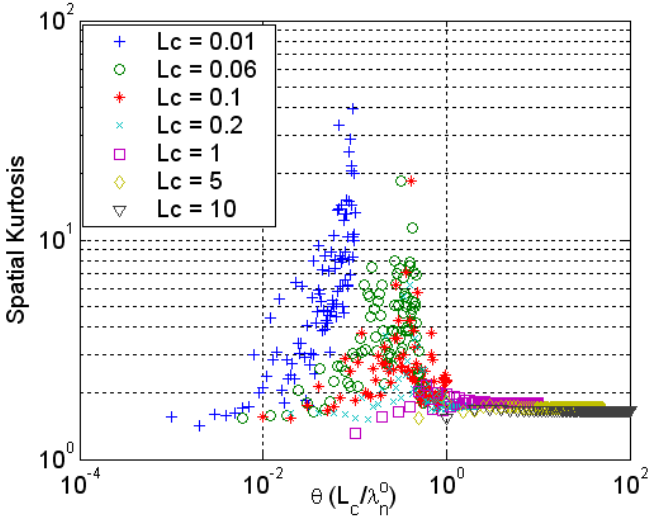

Figure 64: Spatial kurtosis results for the Gaussian spatially correlated random rods expressed in terms of the normalized parameter (spatial averaging approach).

In order to identify the particular correlation length magnitude at which the corresponding mode shapes have the highest probability of the

establishment of GOE eigenvector statistics, the spatial mode shape statistics was investigated throughout an ensemble composed of 500 spatially correlated longitudinal rods. The correlation length magnitude was considered constant for each member and variable across the ensemble. The correlation length range was considered from $L_c = 0.01$ to $L_c = 1.00$ with constant steps. In a similar manner to the previous analysis, only the rod cross-sectional area was considered as a variable parameter in the rod length direction. The other rod parameters were considered fixed across the frequency and ensemble domains.

In Figure 65, the spatial kurtosis and corresponding spatial Lilliefors Test results are presented for each of the ensemble members. Again, the mode shape statistics results are presented in terms of the normalized parameter domain.

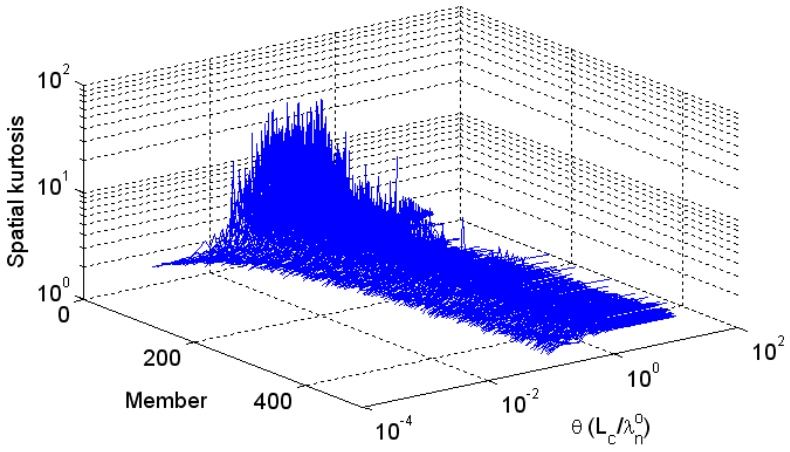

(a)

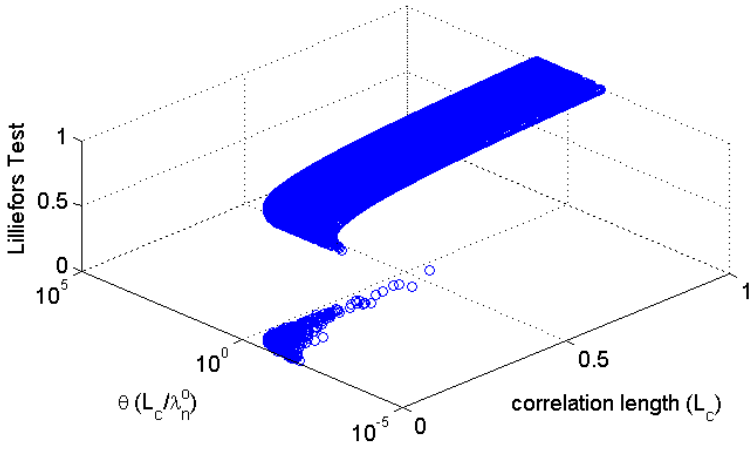

(b)

Figure 65: Spatial mode shape statistics results from an ensemble composed of 500 spatially-correlated longitudinal rods (spatial averaging approach). Plot (a): Spatial kurtosis values. Plot (b): Spatial Lilliefors Test results. The correlation length range adopted was from $L_c = 0.01$ to $L_c = 1.00$ with constant steps.

The spatial mode shape statistics results confirm the main conclusions obtained from the previous results of the initial non-dimensional analysis for some discrete correlation length magnitudes, Figure 64, that is, the establishment of GOE mode shape statistics is restricted to a particular frequency region and its extension is dependent on the ratio of the correlation length to the wavelength magnitude.

As shown in Figure 65 (a), the spatial kurtosis results suggest the establishment of spatial localized mode shape statistics for the small normalized parameter and small correlation length ranges. In general, structural localized mode shapes are expected for the normalized parameter range of 0 to unity, that is, $0 \lesssim \theta_n \lesssim 1$. However, weakly structural localized mode shapes with spatial statistical characteristics similar to those of GOE statistics occur for the following normalized parameter range: $0.02 \lesssim \theta_n \lesssim 0.6$ as observed in Figure 65 (b). In other words, for this normalized parameter range, the discrete occurrence of Gaussian mode shapes in the frequency domain is expected.

Additionally, the spatial Lilliefors Test results were expressed in terms of the mode order domain for each of ensemble members[17], Figure 66 (a).

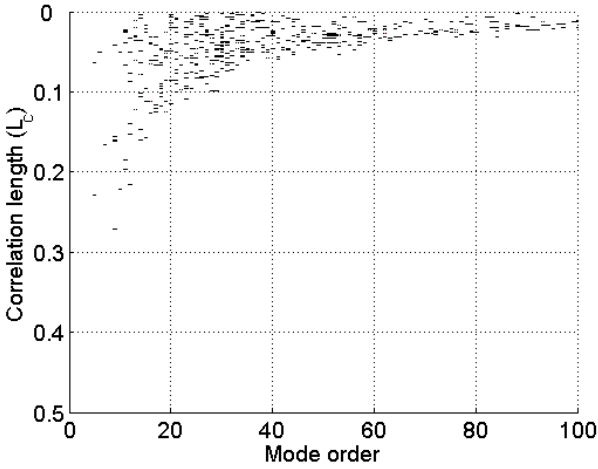

(a)

[17] The variation of the correlation length magnitude across the ensemble members occurs in constant steps, that is, an exclusive correlation length magnitude is defined for each rod member and the difference between the correlation lengths of two successive members remains unaltered across the ensemble.

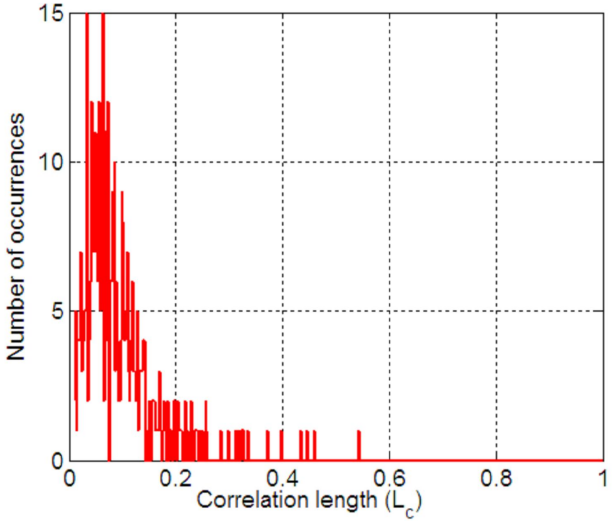

(b)

Figure 66: Previous spatial mode shape statistics results from an ensemble composed of 500 spatially correlated longitudinal rods: (a) spatial Lilliefors Test results expressed in terms of the mode order domain, and (b) Histogram of the spatial Lilliefors Test results expressed in terms of the correlation length domain.

The spatial Lilliefors Test results suggest that the increase in the correlation length magnitude reduces the number of Gaussian (or almost Gaussian) mode shapes along the mode order domain. In Figure 66 (b), the histogram associated with spatial Lilliefors Test results in Figure 66 (a) is shown. The histogram of spatial Lilliefors Test results shows that the largest number of Gaussian mode shapes is associated with a correlation length range around $L_c \approx 0.05$ for the spatially correlated random longitudinal rods investigated in this study.

As shown in Figure 64, for the spatially- correlated rods with $L_c \gtrsim 0.05$, the spatial mode shape statistics presents an asymptotic statistical transition from GOE statistics (or Gaussian statistics) to the nominal statistics (or almost deterministic - sinusoidal statistics) as the correlation length magnitude increases. Considering the non-dimensional spatial mode shape statistics

analysis, very similar results were established for the following normalized parameter range: $\theta_n \gtrsim 1.00$.

Spectral Statistics of the Kinetic Energy Density Results

Similarly to the spectral analysis performed previously in Section 3.4.6, the spectral statistics of the kinetic energy density results was also investigated for Gaussian spatially-correlated random longitudinal rods considering two natures (types) of loadings: unitary single point-loading at the rod end and spatially-averaged excitation. The damping loss factor magnitude wass considered frequency-constant and equal to $\eta = 0.06$, providing a range of modal overlap factor magnitudes of 0 to 6 modes. In addition, the SEA mean and relative variance for 1/3 octave frequency band predictions were also evaluated considering the Poisson and GOE models. In Figure 67, the spectral mean and relative variance values are presented for the Gaussian spatially correlated random longitudinal rod structures subjected to a unitary single point-loading.

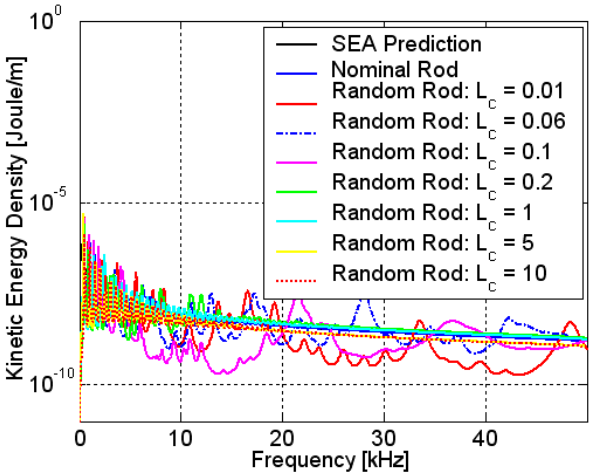

(a)

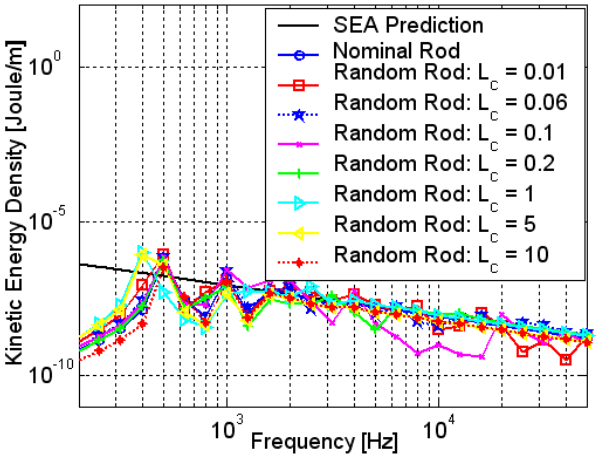

(b)

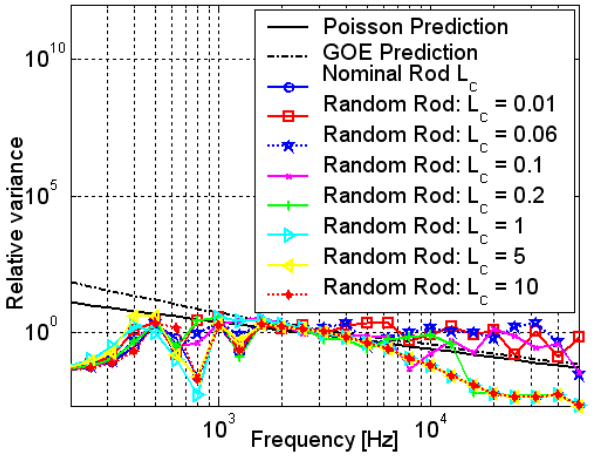

(c)

Figure 67: Kinetic energy density statistics of the Gaussian spatially-correlated rods subjected to an unitary single point-loading (spectral averaging approach). Plot(a): energy density results expressed in the narrow frequency domain. Plot(b): spectral mean values expressed in terms of the 1/3 oct. frequency band domain. Plot(c): spectral relative variance results expressed in terms of the 1/3 oct. frequency bands.

Considering the case of rod structures subjected to a unitary single point-loading, the energy density results in the narrow frequency domain showed clearly that the effects of each of the correlation length magnitudes can be associated with a particular frequency range, Figure 67 (a). Outside the particular frequency range affected by the spatial correlation effects, the modal parameter statistics are very similar to those presented by the nominal rod and a good agreement is expected between the narrow frequency energy density results and the SEA analytical prediction. Although they are slightly shifted, similar narrow response patterns to those presented by the nominal rod are presented for the energy results of the rod structures with large correlation lengths, that is, $L_c \gtrsim 1$.

For the Gaussian spatially-correlated rods with small correlation lengths, large discrepancies in relation to the SEA predictions are noted in the particular frequency range affected by the correlation effects. For the spatially Gaussian correlated rod with $L_c = 0.06$, the correlation effects are smoother and a moderate oscillatory pattern is established around the SEA predicted values throughout the frequency domain investigated.

In Figure 67 (b), the spectral mean values in terms of the 1/3 oct. frequency band domain lead to the same conclusions obtained previously from the narrow frequency kinetic energy results. Additionally, the frequency regions affected by correlation effects can be easily identified due to energy discrepancies in relation to the 1/3 oct. frequency band SEA predictions.

Considering the spectral relative variance results, a large spectral variability of the energy density response is expected for the spatially -correlated rods with small correlation magnitudes in the frequency region affected by the correlation effects. Since the *spectral averaging approach* is considered in this current analysis, the spectral relative variance magnitudes are very sensitive to large changes in the spectral response pattern present within the frequency band limits. It is important to stress that small relative variance magnitudes do not express the existence of a good agreement between the rod energy responses and SEA mean value predictions. The small magnitudes of the spectral relative variance represent effectively the occurrence of small response variability in relation to the response mean value associated with the frequency band. Indeed, small relative variance magnitudes express the nonexistence of abrupt oscillations of the energy response pattern within the frequency band limits.

As shown in Figure 67 (c), the performance of the relative variance predictions were neither satisfactory nor conservative for the spatially Gaussian correlated rods investigated. Indeed, it appears that the large relative

variance values for the Gaussian spatially correlated rods are mainly due to the correlation effects which induce the establishment of the *structural localization phenomenon* in the mode shape statistics. It is important to emphasize that the statistical characteristics of the energy response of a system subjected to a single point-loading are very sensitive to mode shape statistics. Thus, the distinct relative variance patterns associated with each of the correlation length magnitudes can probability be attributed to the different mode shape statistics obtained for each of the correlation lengths considered.

For the case of a rod structure subjected to *spatially-averaged excitation*, the kinetic energy density results are independent of the mode shape statistics. In Figure 68 (a), the narrow frequency results of the kinetic energy density show a good agreement between the SEA prediction and the numerical rod results for all correlation lengths investigated. As shown Figure 68 (b), although distinct spectral natural frequency statistics were obtained for each correlation length magnitude, the spectral mean value of the kinetic energy density results were found to be practically independent of the natural frequency statistics and an excellent agreement with the band-averaged SEA prediction was noted for all Gaussian spatially correlated rods investigated.

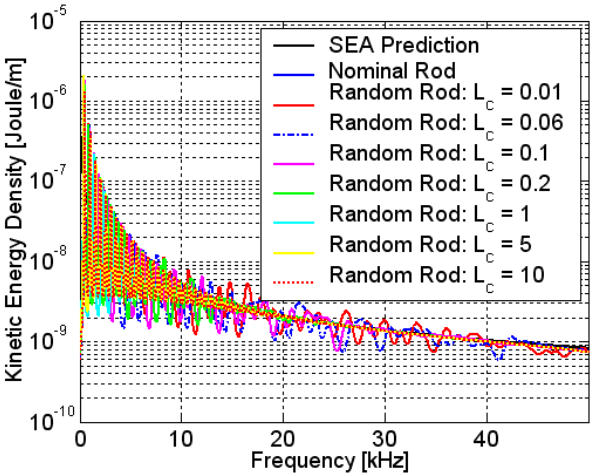

(a)

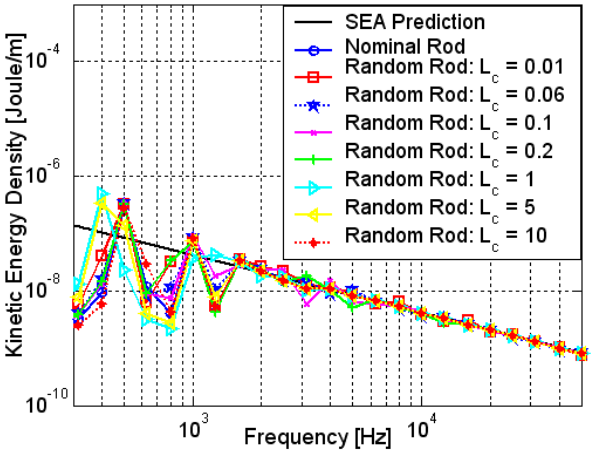

(b)

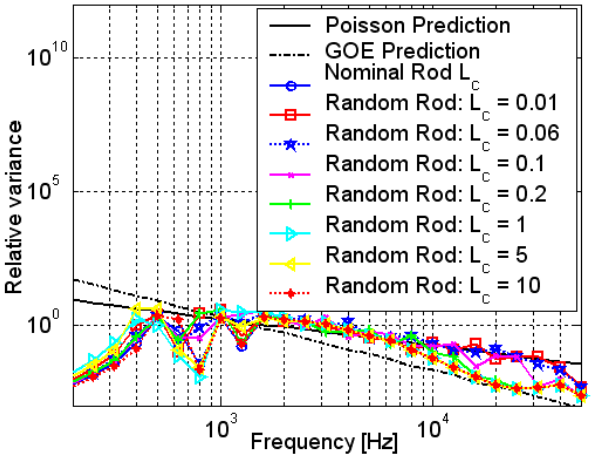

(c)

Figure 68: Kinetic energy density statistics of the spatially-correlated rods subjected to spatially-averaged excitation (spectral averaging approach). Plot(a): energy density results expressed in narrow frequency domain. Plot(b): spectral mean value results expressed in terms of the 1/3 oct. frequency band domain. Plot(c): spectral relative variance results expressed in terms of the 1/3 oct. frequency bands.

In Figure 68 (c), the spatially-averaged relative variance results suggested the establishment of small magnitudes for the spatially-correlated rods with large correlation length magnitudes. In such rod structures, the modal parameter statistics are very similar to those of the nominal longitudinal rod and thus small spectral response variability is expected for the high-frequency range.

Furthermore, the spectral relative variance values for the spatially - correlated rods with small correlation lengths are clearly higher than those of the rods with large correlation length, mainly in the high-frequency range, Figure 68 (c). Regarding the performance of the SEA relative variance predictions, that based on the GOE model under predicted the numerical results with $L_c \gtrsim 0.1$. On the other hand, the SEA relative variance prediction based on the Poisson model is very conservative and over predicted all of the rod numerical results throughout the frequency range investigated. Indeed, as discussed in the preceding section, asymptotic uncorrelated natural frequency statistics (or almost Poisson statistics) are expected for natural frequencies of structurally localized rod structures.

As observed in Figure 68 (c), the spectral relative variance results for rods with small correlation length magnitudes are not explicit regarding the effects of distinct correlation length magnitudes on the spectral variability of kinetic energy responses. Indeed, the current spectral relative variance results are directly influenced by two main factors: the variable degree of modal superposition in the frequency domain and the distinct number of resonant modes associated with each frequency band.

In order to evaluate the exact contribution of the correlation length effects to the spectral variability of the kinetic energy responses, the spectral relative variance results were calculated considering the following assumptions:

- *fixed modal superposition*: the frequency-constant modal overlap factor is obtained if the damping loss factor magnitude is defined as being inversely proportional to the angular frequency (ω) and directly proportional to the longitudinal sound speed (c_L):

$$\eta(\omega) = \frac{c_L}{\omega}. \tag{3.19}$$

- *constant number of resonant modes*: since the 1/3 octave frequency bands have varying bandwidths, the number of resonant modes is variable. Therefore, the use of the frequency band domain with fixed

bandwidth is very convenient and also avoids the contribution from a variable number of resonant modes in the spectral relative variance magnitudes.

In Figure 69, the spectral relative variance of the kinetic energy density results are shown for the single point and spatially-averaged excitations, respectively. In such spectral relative variance results, the DLF definition proposed in Equation (3.19) was considered and provided the frequency-constant modal overlap factor magnitudes of approximately 1.6 modes along the frequency domain investigated[18]. Additionally, a fixed frequency bandwidth of 5 kHz was also considered along the frequency domain in order to obtain a constant resonant modes contribution to the spectral relative variance magnitudes.

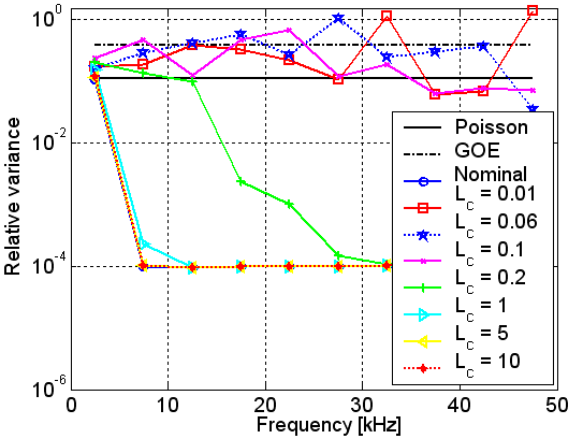

(a)

[18]The DLF magnitudes obtained for the spatially Gaussian correlated longitudinal rods were considered adequate since their values are very similar to those of numerical investigations with similar rod structures in the open literature, (161) (163).

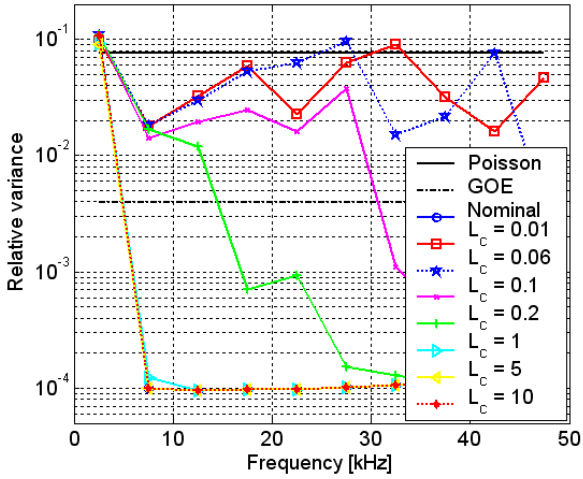

(b)

Figure 69: Spectral relative variance of the kinetic energy density results in the frequency band domain with fixed bandwidth (spectral averaging approach). Plot(a): unitary single point-loading. Plot(b): spatially-averaged excitation.

As shown in Figure 69 (a), the point loading relative variance results show that the spatially correlated rods with large correlation length magnitudes present low spectral response variability and thus the correlation length effects are not distinguishable in the spectral relative variance results for spatially correlated rods with $Lc \gtrsim 1$ for the frequency range investigated herein.

For the spectral relative variance results for spatially correlated rods with small correlation lengths, a good agreement with the GOE model prediction is obtained for the spatially correlated rod with $L_c = 0.06$, although a slight oscillatory behavior around the GOE prediction is observed in the frequency range investigated. It is important to note that the modal parameter statistics results for the spatially correlated rod with $L_c = 0.06$ present almost GOE statistics for the frequency range investigated. As shown previously in the modal parameter statistics results, the spectral natural frequency statistics of the spatially correlated rod with $L_c = 0.06$ is expected to be similar to GOE statistics in the short-range fluctuations (local behavior) and also a higher number of almost GOE mode shapes is expected in the frequency

range investigated. Indeed, the modal parameter statistics of the Gaussian spatially-correlated rod with $L_c \simeq 0.06$ leads to the most favorable statistical condition for the establishment of GOE statistics for the frequency range investigated and explains the good performance of the relative variance prediction based on the GOE model.

In Figure 69 (b), the Gaussian spatially-averaged relative variance results of the spatially-correlated rods with $L_c \gtrsim 0.1$ suggest that an increase in the correlation length magnitude leads to a reduction in the spectral response variability. Indeed, the spectral natural frequency statistics results showed that, for the frequency range considered, as the correlation length magnitude increases the spectral natural frequency statistics tends asymptotically to be similar to that presented for the nominal rod. As shown in Figure 69 (b), a poor agreement occurs between the numerical relative variance results for random rods with $L_c = 0.06$ and the GOE prediction, even though the spectral natural frequency statistics characteristics of the Gaussian spatially- correlated rod with $L_c = 0.06$ are very similar to the GOE statistics characteristics in the short-range fluctuations. However, it is important to emphasize that spectral eigenvalue statistical observables are spectrally-averaged metrics which may eventually mask a certain unexpected statistical characteristics associated with a particular frequency region. As shown previously, the correlation length effects are observed in different frequency regions for distinct correlation length magnitudes. Therefore, this characteristic hinders a direct comparison with the correlation effects for rods with distinct correlation lengths in a fixed frequency range.

Overall, it is important to note that the spatially-averaged relative variance prediction based on the Poisson natural frequency statistics presents an excellent performance, since the spectral statistical characteristics of the spatially-averaged energy responses are independent of the mode shape statistics and an asymptotic Poisson statistics is expected for the structurally localized one-dimensional structures as in the case of the Gaussian spatially-correlated rods with small correlation length magnitudes.

3.4.8 Discussions and Remarks

In this initial stage of the statistical investigations of the random longitudinal rods, a complete analysis of the modal parameter statistics was carried out considering the spectral averaging approach for the natural frequencies and the spatial and spectral averaging approaches for the corresponding mode shapes. The random longitudinal rods with several natures and levels

of randomness were systematically investigated using the RMT statistical observable results.

Considering the RMT eigenvalue statistical observables, the good performance of their results allowed accurate evaluation of the spectrally-averaged effects of distinct natures and levels of randomness on the natural frequency statistics in the short and long-range fluctuations. Although the number variance and Δ_3-statistics results have faster convergence characteristics and provide the averaged results in the natural frequency domain, these metric functions can unintentionally mask the *local* characteristics of the natural frequency statistics associated with a particular range in the frequency domain.

As discussed in section 3.4.3, it appears that the natural frequency statistics from any random system is only correctly characterized when all results for the several natural frequency statistical observables are compared to each other, independent of their individual performance in the description of spectral natural frequency statistics. Indeed, the spectral natural frequency statistics results for the Mass (20%) and Gaussian (30%) random rods demonstrated this particular situation, where the long-range fluctuation statistical observable results suggest the establishment of spectrally-averaged statistics very similar to those of the GOE model, although at the extremes of frequency range investigated the local spectral natural frequency statistics are completely distinct to the statistical characteristics expected for the GOE model.

Concerning the spatial mode shape statistics, the eigenvector statistical observable results allowed an accurate characterization of the effects of the randomness on the mode shape statistics. Additionally the main non-universal physical phenomena, such as the structural localization, were correctly identified and quantified for each individual mode order, allowing a complete description of the local mode shape statistics in terms of the spatial averaging approach. Indeed, the main characteristics of the well-defined mode shape statistics classes (sinusoidal, Gaussian and structurally localized) as well as their statistical transitions were adequately described and compared with the analytical predictions.

In the current spatial mode shape statistics analysis, the PDFs of spatial kurtosis values for the Gaussian random rods were fitted to expressions of the non-linear sigma model of the Supersymmetry theory which are traditionally applied in experimental studies of disordered billiards with Anderson localization characteristics. The agreement between the numerical results and the fitted non-linear sigma model expressions was satisfactory for the mode-

rate and strong localization regimes, except for the presence of small discrepancies in the distribution tail region, which is extremely sensitive to the details of the system nature, Figure 47. In a similar manner, the PT-distribution results were also fitted to the weak and strong localization non-linear sigma model expressions, Figure 50. The excellent agreement confirmed the high performance and versatility of the non-linear sigma expressions to describe accurately the spatial mode shape statistics characteristics in the weak and strong localization regimes. To the best of the knowledge of the author, this is the first application of non-linear sigma model expressions to describe the non-universal localization characteristics of the mode shape statistics of vibroacoustic systems.

The spectral mode shape statistics was investigated through the kurtosis metrics, proving indirect information on the spectral correlation level for a fixed mode shape component in the mode order domain. The spectral kurtosis results for the nominal rod showed that the sinusoidal mode shapes are practically ergotic in terms of the spectral and spatial average approaches, validating the hypothesis proposed initially by Lyon (48) during the evaluation of the mode shape statistics factors of regular systems, such as a simply supported rectangular plate or box acoustic room. On the other hand, the spectral kurtosis results for the random rods also suggested that most of the mode shape components present some significant spectral or inter-modal correlations across the mode order domain. However, some mode shape components of the Mass (20%) and Gaussian (30%) random rods, located in the vicinity of the central rod domain, were shown to be approximately asymptotic Gaussian variables. Nevertheless, it is important to emphasize that the spectral kurtosis as well as the corresponding spectral Lilliefors Test results provide only an indirect analysis regarding the spectral mode shape component correlations, and thus it is not possible to establish a linear relationship between the spectral kurtosis values and spectral correlation level of different mode shapes for a fixed mode shape component.

In general, the modal parameter statistical observable results suggest that the local statistical characteristics of the modal parameters of the random longitudinal rods vary substantially in the frequency domain, from an almost-deterministic or nominal statistics in the lower frequency range toward structural localized statistics in the higher frequency range, where intermediate statistics with characteristics similar to those of the GOE model is certainly established for a limited frequency range. For almost-deterministic or nominal statistics, the natural frequencies have high spectral rigidity characteristics and the corresponding mode shapes are practically sinusoidal, presenting

practically constant statistical characteristics for the spatial and spectral mode shape averaging approaches over the mode order domain.

At the other extreme, the establishment of the structural localization phenomenon in the high-frequency range leads to local spectral natural frequency statistics with statistical characteristics similar to the Poisson model, where the spacings seem to be almost uncorrelated. Additionally, the corresponding mode shapes present energy confinement in the restricted spatial region of the rod length domain which establishes strong spectral and spatial correlations between the mode shape components. It is also important to note that the localized mode shapes did not show asymptotic well-defined statistics in the high-frequency range due to their relevant *non-universal* characteristics associated with the details of the system nature. As demonstrated by the previous mode shape statistics results, a large mode-to-mode dispersion is clearly observed in the high mode order range, hindering the accurate description of the mode shape statistics by analytical models as well as the derivation of an efficient analytical methodology to predict the kinetic energy density statistics.

The kinetic energy density results associated with random rods subjected by a single point-loading were clearly shown to be dependent on the randomness characteristics. Indeed, the point-loading kinetic energy density results for light damped rod structures seem to have a significant dependence on the mode shape statistics and thus small changes in mode shape statistics become extremely relevant in terms of the energy response statistics. The spectral point-loading relative variance results for the random rods investigated here showed very distinct curve patterns as well as a poor agreement with the analytical predictions based on the Poisson and GOE models. Based on the spatial and spectral mode shape statistics results, the large values of the point-loading relative variance are certainly explained by the establishment of the structural localization phenomenon and its corresponding effects on the modal parameter statistics.

In order to investigate the establishment of the universal characteristics for natural frequency statistics, Mass (20%) and Gaussian (30%) random rods were considered since their spectrally-averaged natural frequency statistics are very similar to those of GOE statistics. Additionally, the spatially-averaged excitation was adopted whereas the kinetic energy results are exclusively dependent on the contributions of the natural frequency statistics. Thus, the spectral relative variance of the spatially-averaged kinetic energy density results for the Mass (20%) and Gaussian (30%) random rods were also calculated and compared to the analytical prediction based on the Poisson and

GOE models for several levels of the modal superposition. The relative variance curve pattern of the numerical results showed clearly that the local spectral natural frequency statistics varies substantially in the frequency domain, from almost-nominal statistics in the lower frequency range with high spectral rigidity characteristics to structural localized statistics in the higher frequency range in which the natural frequencies have statistical characteristics similar to the Poisson model.

In second part of the current statistical analysis, systematic investigations were performed with Gaussian spatially correlated random longitudinal rods with several correlation length magnitudes. The spectral natural frequency statistical observable results showed that the characteristics of natural frequency statistics change in a sensitive way for each range of correlation length magnitudes. As shown in Figure 62, a natural frequency statistical transition from almost-Poisson to high spectral rigidity statistics is observed as the correlation length magnitude increases for the frequency range investigated.

Considering the spatial mode shape statistics, the statistical observable results showed that the level of the localization effects on modal parameter statistics is clearly dependent on the ratio between the correlation length and the typical wavelength, and thus for a given correlation length only a limited frequency range is effectively affected. The results for the non-dimensional mode shape statistics analysis indicated explicitly this wavelength dependency, showing that for correlation lengths larger than the typical expected wavelength, the modal parameters statistics converges asymptotically to nominal statistics as the excitation frequency increases. Additionally, the spatial modal parameter statistics results showed that for correlation lengths close to $L_c \approx 0.05$ the corresponding modal parameters have spectrally-averaged statistics with characteristics similar to those of the GOE model and thus the best agreement is expected to be between the spectral relative variance results and the analytical prediction based on the GOE model.

In a manner similar to the previous investigations performed with independent Gaussian random rods, the point-loading kinetic energy results for the Gaussian spatially-correlated random rods expressed in terms of the narrow frequency band domain also allowed prompt identification of the structural localization effects associated with each correlation length investigated. The corresponding results expressed in terms of the 1/3 octave frequency bands seem to minimize the localization effects and thus an improved agreement with the SEA predictions was only observed for random rods with large correlation lengths. For Gaussian spatially- correlated random rods with

small correlation lengths, some discrepancies were clearly observed. Indeed, it is expected that these random rods do not have a perfect energy reverberant field due to the establishment of the strong localization phenomenon on their modal parameters and thus large deviations occur in relation to SEA basic assumptions, reducing the performance of the frequency-band mean value predicted by the standard SEA model.

Considering the point-loading relative variance evaluated for the spectral averaging approach, the results associated with rods with small correlation lengths showed large amplitudes as a direct consequence of the localization phenomenon contribution of the mode shape statistics. Indeed, the analytical predictions based on the GOE and Poisson models under predicted the numerical results for these random rods. For the other random rods, their relative variance results are very similar to those for the nominal rod.

The spatially-averaged kinetic energy density results expressed in terms of the narrow frequency band domain showed a good agreement with the SEA prediction, although small oscillations were observed. It is important to note that the spatially-averaged excitation removes completely the contributions of the localized mode shape statistics to the energy results. The corresponding relative variance results showed clearly the characteristics of the spectral natural frequency statistics for each of the correlation lengths investigated and suggested clearly that the spatially-averaged relative variance prediction based on the Poisson model seems to be a conservative formulation at least for cases of random rods with strong localization characteristics.

Besides the statistical investigations with the frequency-constant DLF, the spectral statistics kinetic energy density results for point-loading and spatially-averaged excitations were also investigated using fixed frequency bandwidths and an alternative DLF definition which provides a constant number of resonant modes in each frequency band and a fixed modal superposition condition in the frequency domain, respectively. These spectral relative variance results under constant modal superposition condition allowed immediate visualization of the contributions of the modal parameter statistics to the variance results as well as the performance of the SEA variance predictions. Overall, the relative variance results also suggested that the increase in the correlation length reduces the spectral variance for the frequency range investigated.

3.5 Ensemble Averaging Approach

In this section the modal parameter statistics across the ensemble are investigated in order to assess the conditions necessary to establish GOE statistics for each of the modal parameters as well as to establish a good performance of the relative variance prediction based on the GOE model. Two random longitudinal rod ensembles are considered: point mass-loaded and Gaussian spatially-correlated.

In the following sections, the main SEA parameters as well as the RMT statistical observables, which are applied traditionally in spectral analysis, were adapted in order to allow the evaluation of the statistics of the a fixed mode order (or spacing) of interest across the ensemble, that is, the adapted statistical observables are able to characterize the modal parameter statistics in terms of the ensemble averaging approach.

3.5.1 Random Point Masses

In this subsection the statistical characteristics of an ensemble composed of point mass-loaded rods are investigated across the ensemble. The manufacturing uncertainties are represented by small point masses attached to the surface of each rod member of the ensemble in order to reproduce the possible structural irregularities of the mass distribution in the rod length direction, (4, 3, 17, 35, 18).

For each rod member, 20 point masses (each point mass with 1% of the total mass of the bare nominal rod) are randomly distributed along the length on the nominal rod surface. In the current work, an ensemble size of 500 members was considered in order to guarantee the convergence of the statistical results for the kinetic energy density statistics as well as for the modal parameter statistics across the ensemble.

Natural Frequency Statistics

Since a large range of the mode orders was considered in the FEM modal analysis, six particular mode orders, or spacings, were selected in order to present the main physical phenomena of the modal parameter statistics across the rod ensemble. The mode orders considered in the current analysis are: mode 10, mode 20, mode 30, mode 42, mode 60, and mode 80. In Figure 70, the PDFs of adjacent unfolded natural frequency spacings are shown for the mode orders considered.

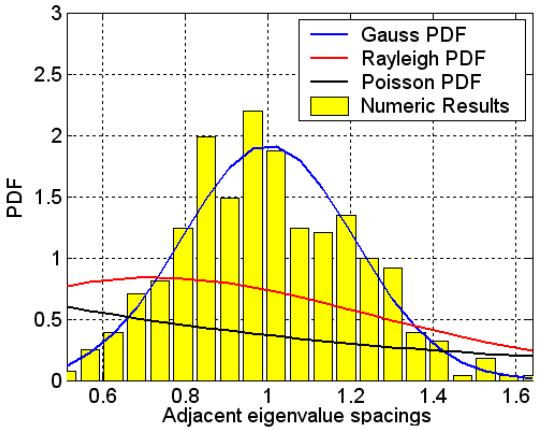
Gauss PDF
Rayleigh PDF
Poisson PDF
Numeric Results
PDF
Adjacent eigenvalue spacings
0
0.5
1
1.5
2
2.5
3
0.6
0.8
1
1.2
1.4
1.6

(a)

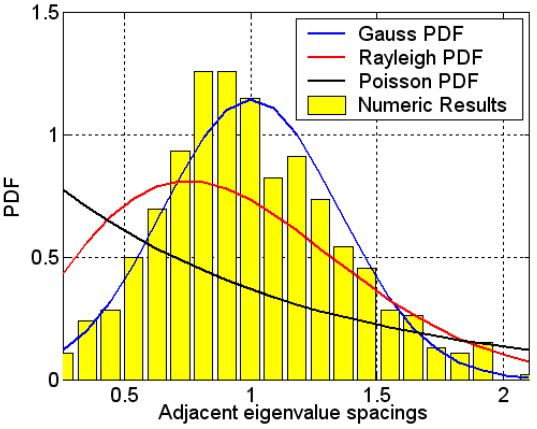
Gauss PDF
Rayleigh PDF
Poisson PDF
Numeric Results
PDF
Adjacent eigenvalue spacings
0
0.5
1
1.5
0.5
1
1.5
2

(b)

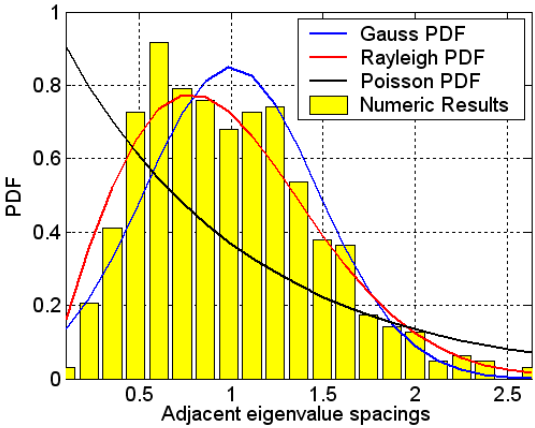
Gauss PDF
Rayleigh PDF
Poisson PDF
Numeric Results
PDF
Adjacent eigenvalue spacings
0
0.2
0.4
0.6
0.8
1
0.5
1
1.5
2
2.5

(c)

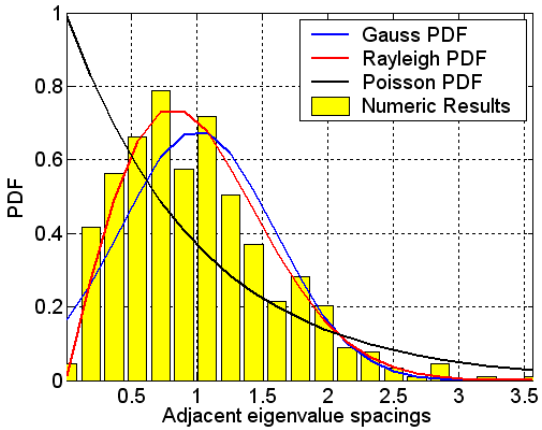
Gauss PDF
Rayleigh PDF
Poisson PDF
Numeric Results
PDF
Adjacent eigenvalue spacings
0
0.2
0.4
0.6
0.8
1
0.5
1
1.5
2
2.5
3
3.5

(d)

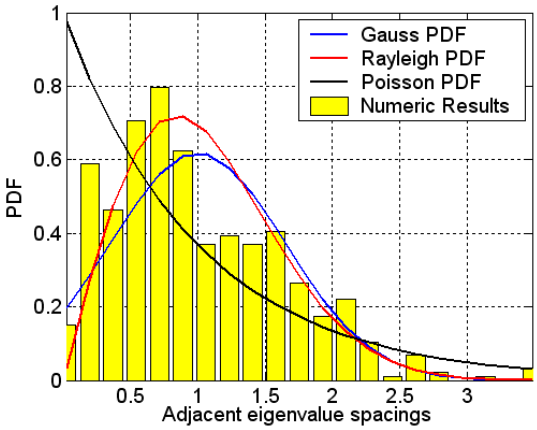

(e)

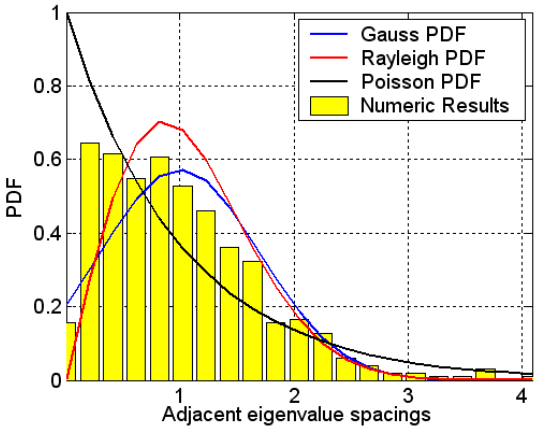

(f)

Figure 70: PDF of adjacent unfolded natural frequency spacings: numerical results for the mass-loaded rod ensemble and analytical predictions based on: Gaussian (Normal), GOE (Rayleigh), and Poisson (Exponential) statistics (ensemble averaging approach). Plots: (a) Mode 10, (b) Mode 20, (c) Mode 30, (d) Mode 42, (e) Mode 60, and (f) Mode 80.

As shown in Figure 70, the short-range fluctuation statistics vary significantly in the frequency domain (or mode order domain). For the low-frequency range, for example in the vicinity of mode 10, an approximate *sharp Gaussian* distribution is symmetrically established on the unitary spacing value, suggesting a statistical transition from the Delta Dirac function to Gaussian statistics. Considering mode 20, the spacing PDF results suggest the establishment of almost-Gaussian statistics. Indeed, a reduction in the spectral rigidity characteristics associated with nominal rod natural frequencies leads to a more spread out spacing distribution in which several spacing values are distinct from unitary spacing[19].

Thus, as the frequency increases, the longitudinal wavelength reduces and the ensemble natural frequency statistics becomes very sensitive to structural irregularities and thus the uncertainty effects induce a statistical transition from *almost Delta Dirac statistics* to *almost Poisson statistics*. Additionally, intermediate natural frequency statistics are also established in the frequency domain as *Gaussian* and *Rayleigh*[20] statistics. For a mass-loaded rod ensemble, the closest natural frequency spacing statistics to GOE statistics (Rayleigh PDF) occurs for the mode order range close to the vicinity of mode 42 which corresponds to the frequency range around 20 kHz. Besides this particular frequency, due to the nature of the randomization process considered, there is also an increase in the occurrence of small natural frequency spacings across the ensemble. The higher mode order results, modes 60 and 80, suggest the establishment of an asymptotic Poisson statistics toward the high-frequency range.

The establishment of the almost-Poisson model characteristics for high frequency range occurs because the rod becomes effectively clamped at the point mass locations, actuating as mechanical discontinuities. Indeed, under this particular condition, a high number of mode sets can exist in the various rod sections between the point masses which do not interact each other, Weaver (64). In this regard, a statistics similar to those of Poisson model is expected for the natural frequencies since the superposition of large number of statistically independent spectra has an exponential PDF, Brown (1).

In Figure 71, the number variance results are shown. For the low-

[19]The mean value of the unfolded natural frequency spacings is expected to be frequency-constant and unitary for the nominal rod.

[20]The establishment of a Rayleigh distribution for natural frequency spacings is classically associated with the eigenvalue statistics of the Gaussian Orthogonal Ensemble (GOE), Mehta (24).

frequency range, an ensemble natural frequency statistics with high spectral rigidity characteristics is clearly established. Similarly to the spectral number variance results for the nominal rod, for which null values of the number variance are expected for integer spectral natural frequency spacings, the ensemble number variance results also show an oscillatory pattern and present null values for some integer natural frequency spacings, Weaver (64). Indeed, this oscillatory pattern of ensemble number variance results is associated with high spectral rigidity characteristics established across the ensemble and the low performance of the point mass randomization process in the low-frequency range, Figure 71 (a).

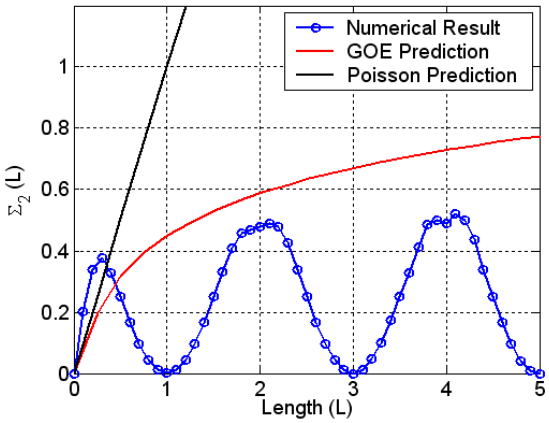

(a)

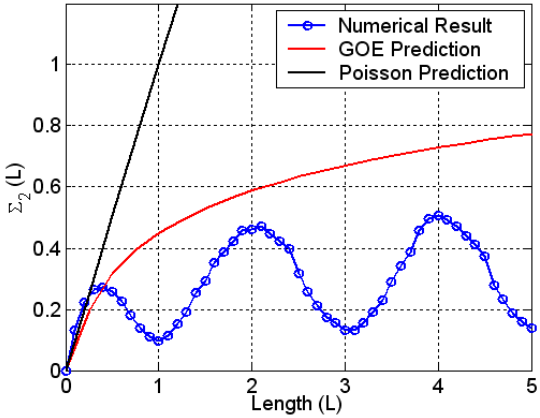
Numerical Result
GOE Prediction
Poisson Prediction
Σ_2 (L)
Length (L)
0
0.2
0.4
0.6
0.8
1
0
1
2
3
4
5

(b)

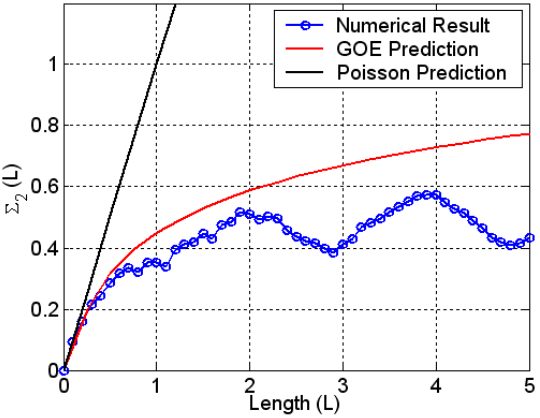
Numerical Result
GOE Prediction
Poisson Prediction
Σ_2 (L)
Length (L)
0
0.2
0.4
0.6
0.8
1
0
1
2
3
4
5

(c)

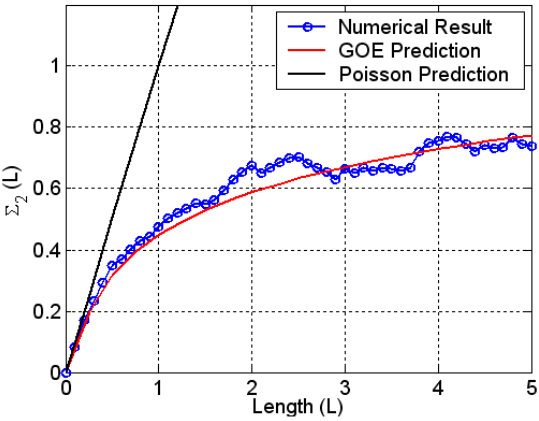
Numerical Result
GOE Prediction
Poisson Prediction
Σ_2 (L)
Length (L)
0
0.2
0.4
0.6
0.8
1
0
1
2
3
4
5

(d)

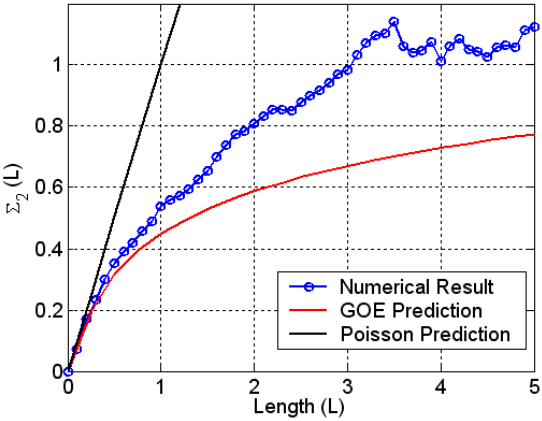
Numerical Result
GOE Prediction
Poisson Prediction
Σ_2 (L)
Length (L)
0
0.2
0.4
0.6
0.8
1
0
1
2
3
4
5

(e)

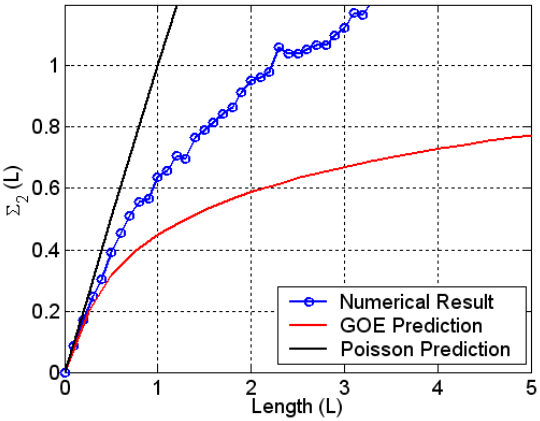

(f)

Figure 71: Number variance results of the mass-loaded rod ensemble. Analytical predictions: GOE and Poisson models (ensemble averaging approach). Plots: (a) Mode 10, (b) Mode 20, (c) Mode 30, (d) Mode 42, (e) Mode 60, and (f) Mode 80.

As shown in Figure 71 (b), the ensemble number variance results for mode 20 present moderate oscillatory characteristics with small non-zero values. The increase in the number variance values is associated with a reduction of the *spectral rigidity* characteristics which occurs gradually from the long to short fluctuation range. Thus, the largest ensemble number variance values are expected to occur for large natural frequency distance ranges. Similarly to the spacing PDF results, the mode 42 results conform very well to the GOE prediction and the establishment of a certain level of *universal* statistics is again suggested for this narrow frequency range, Figure 71 (d). The number variance results for modes 60 and 80 also present an asymptotic Poisson statistics toward the high-frequency range, Figures 71 (e) and (f), respectively. In Figure 72, the Δ_3 - statistics results are presented for the mode orders investigated.

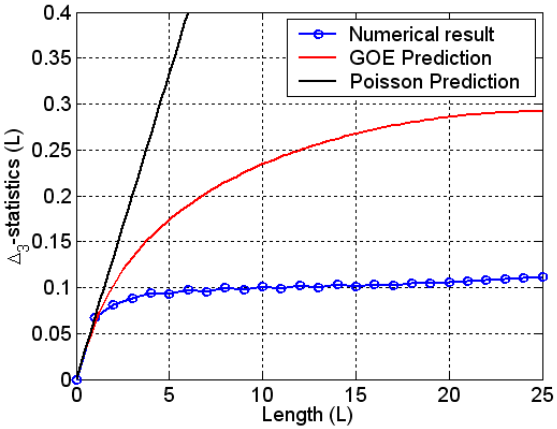
Numerical result
GOE Prediction
Poisson Prediction
Δ_3-statistics (L)
Length (L)
0
0.05
0.1
0.15
0.2
0.25
0.3
0.35
0.4
0
5
10
15
20
25

(a)

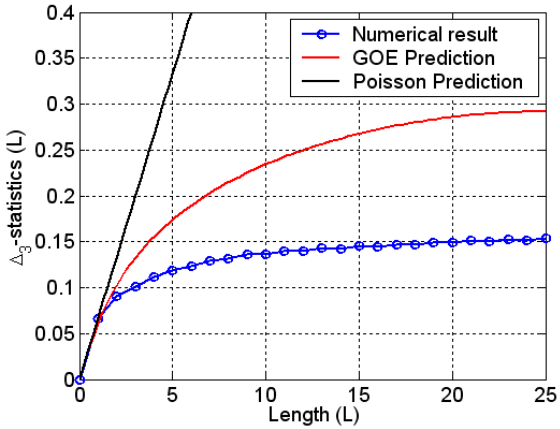
Numerical result
GOE Prediction
Poisson Prediction
Δ_3-statistics (L)
Length (L)
0
0.05
0.1
0.15
0.2
0.25
0.3
0.35
0.4
0
5
10
15
20
25

(b)

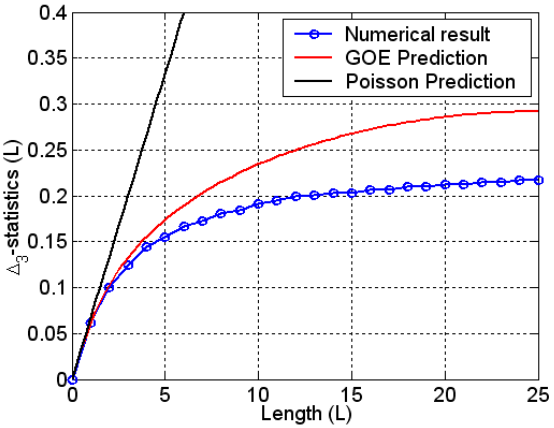
Numerical result
GOE Prediction
Poisson Prediction
Δ_3-statistics (L)
Length (L)
0.4
0.35
0.3
0.25
0.2
0.15
0.1
0.05
0
0
5
10
15
20
25

(c)

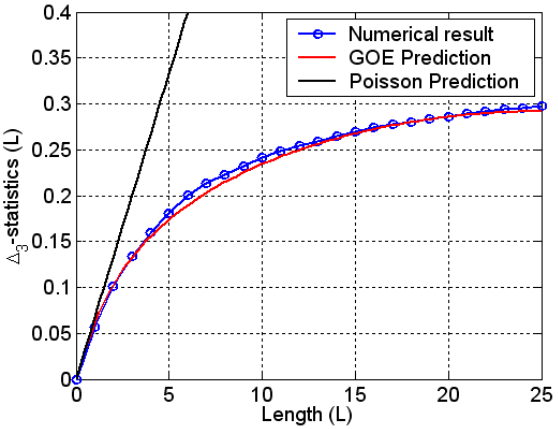
Numerical result
GOE Prediction
Poisson Prediction
Δ_3-statistics (L)
Length (L)
0.4
0.35
0.3
0.25
0.2
0.15
0.1
0.05
0
0
5
10
15
20
25

(d)

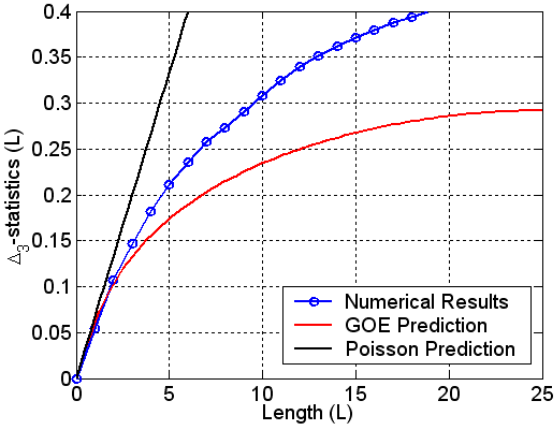

(e)

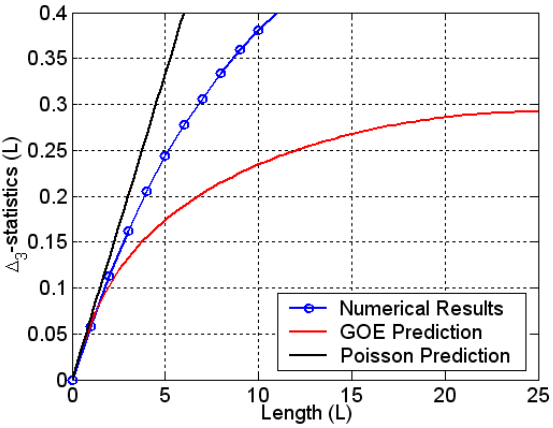

(f)

Figure 72: Δ_3-statistics results for the mass-loaded rod ensemble (ensemble averaging approach). Analytical predictions: GOE and Poisson models. Plots: (a) Mode 10, (b) Mode 20, (c) Mode 30, (d) Mode 42, (e) Mode 60, and (f) Mode 80.

As observed in Figure 72, similar conclusions to those of the previ-

ous statistical observable results are obtained for the characterization of the natural frequency statistics across the ensemble. Therefore, the simultaneous analysis of the natural frequency statistical observable results leads to the following global understanding: the ensemble statistics of the natural frequencies in the low-frequency range, below mode 10 (corresponding approximately to the frequency of 5 kHz), present an intermediate distribution between Dirac Delta (nominal) and Gaussian statistics. As the frequency increases, a statistical transition to GOE statistics occurs where an intermediate statistics with characteristics similar to those of the Gaussian model is also established. The establishment of an almost-GOE statistics occurs in the vicinity of mode 42 which corresponds approximately to a frequency of 20 kHz. In this frequency range, the natural frequency spacing PDF is adequately described by a Rayleigh distribution and the occurrence of the moderate spectral rigidity characteristics and *level repulsion* phenomenon can be clearly observed, Mehta (24).

On the other hand, for the mid and high-frequency ranges, that is above 20 kHz (*i.e.*, higher than mode 42), the establishment of an asymptotic Poisson statistics occurs as the excitation frequency increases. In this frequency range, the spectral rigidity characteristics is significantly reduced and the natural frequencies seem to be almost uncorrelated. In summary, three distinct major statistics can be adequately established for ensemble natural frequency statistics in the frequency domain, which are: *almost-deterministic statistics*, *almost-GOE statistics*, and *asymptotic-Poisson statistics*.

Similar conclusions regarding the natural frequency statistics of one-dimensional mass-loaded string structures were surprisingly obtained in Brown's work (1). In his study, Brown (1) investigated the spectral natural frequency statistics from a simply supported string with randomly placed small point masses. Considering a fixed frequency range, the modal parameters were numerically obtained for distinct sizes of point masses. Instead of the complete set of spectral eigenvalue statistical observables, the chi-square tests for Rayleigh and Exponential (Poisson) PDFs were adopted in order to evaluate the confidence levels as a function of the point masses added to the string surface.

A qualitative comparison[21] is performed between the current natu-

[21] It is important also to note that similar dynamical behaviors are expected for two distinct conditions: (*i*) as the frequency range of interest is considered fixed and the randomness level increases, and (*ii*) as the randomness level is considered unaltered and the excitation frequency increases. For both approaches, it is expected that the increase in the random level (or excitation frequency) leads to the establishment of *universal* natural frequency statistics which are described by the Gaussian Orthogonal Ensemble (GOE), (23).

ral frequency statistics obtained across the mass-loaded rod ensemble and Brown's main spectral results. In Figure 73 a plot of the chi-squared confidence intervals is shown for the test results for the Exponential and Rayleigh PDFs as a function of the size of 5 randomly placed masses.

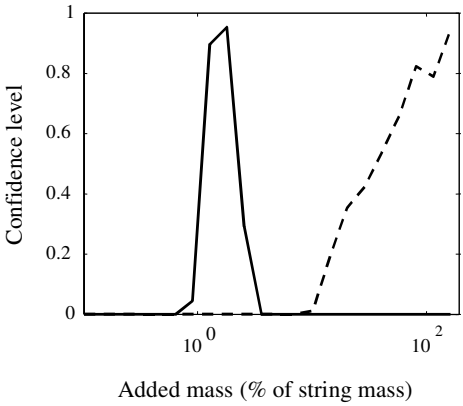

Figure 73: Confidence levels for chi-squared test results for the mass-loaded string: — test for Rayleigh PDF and - - - test for exponential PDF, Brown (1).

As shown in Figure 73, the results for the mass-loaded string are very similar to those for the current mass-loaded rod. In both cases, the natural frequency statistics is dependent on the excitation frequency (or randomness level). A global pattern of statistical transition from an *almost-nominal statistics* to *asymptotic-Poisson statistics* is clearly observed[22]. The asymptotic statistical trend towards an exponential PDF occurs because the string becomes effectively *clamped* at the point mass locations. Indeed, under this particular condition, a high number of independent mode sets can exist in the various string sections between the point masses. Thus, the sum of a large number of statistically independent sets of variables has an exponential PDF.

The current results for the statistical observables also showed that the

[22] Although it is not shown here, similar results were also obtained by Cordioli (20) using an artificial approach. In his study, distinct levels of matrix structure symmetry and randomness were systematically considered for the random stiffness matrix. The two statistical crossover regions were individually shown for the natural frequencies under ensemble averaging approach: GOE model to high spectral rigidity statistics and GOE model to Poisson model statistics.

establishment of the GOE model for natural frequency statistics occurs only for a limited and narrow frequency range or randomness level limits, respectively. It is also important to emphasize that there is no formal evidence regarding the relationship between the system dimensionality and the frequency range extension of GOE natural frequency statistics. This aspect has recently been attracting interest and further investigations are required, Gomes (10).

Natural Frequency SEA Parameter: Statistical Overlap Factor

Traditionally, the statistical overlap factor has been used to quantify the level of randomness of an ensemble composed of random engineering structures, (18, 3, 4, 14). According to Langley *et al* (18, 4), statistical overlap factor values greater than unity provide a condition appropriate for the use of the GOE model to describe accurately the modal parameter statistics. Under such condition, it supposes that the statistics of the energy responses, which is dependent on the natural frequency and mode shape statistics, will be independent of the detailed nature of the system randomness, Langley *et al* (23, 4) and Cordioli (20).

As discussed by Cordioli (20), two distinct definitions for the statistical overlap factor are traditionally considered in the SEA context. The first considers the *local mean spacing* between natural frequencies, that is, the ensemble mean value of the spacings between two adjacent natural frequencies, (15). On the other hand, the second considers the *global mean spacing* which represents the mean value of the spacings over the ensemble and spectral domains, (18, 35, 4). In Figure 74, the statistical overlap factor results are shown for the mass-loaded rod ensemble.

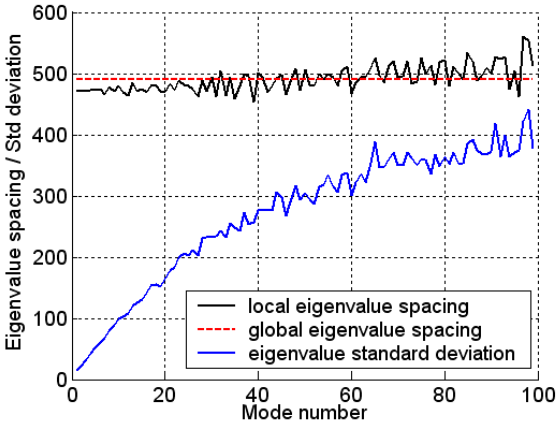

(a)

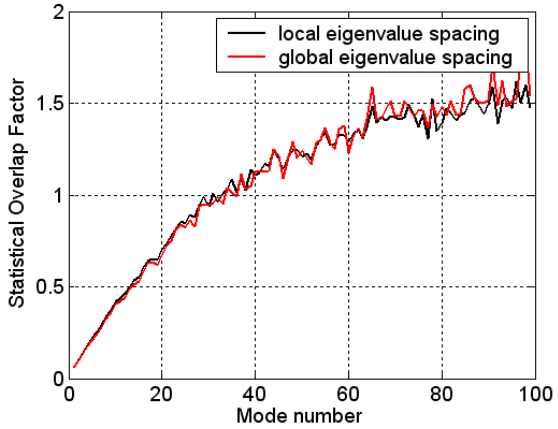

(b)

Figure 74: Statistical overlap factor results for a mass-loaded rod ensemble (ensemble averaging approach). Plot (a): global natural frequency spacing, local natural frequency spacings, natural frequency standard deviations. Plot (b): Statistical overlap factor: based on global and local mean values of the natural frequency spacings.

According to Figure 74 (b), the statistical overlap factor results suggest that, for mode orders greater than mode 35 (corresponding to approximately 17 kHz), the statistical overlap factor values are higher than unity and the system should be considered to have appropriate conditions for the modal parameters to have GOE statistics. Additionally, Figure 74 (a) shows that almost constant mean values for the natural frequency spacings are obtained, regardless of the local or global spacing definitions. On the other hand, large standard deviation magnitudes are observed for the natural frequencies in the high mode order range, providing large statistical overlap factor values.

It is important to emphasize that the statistical overlap factor results are only based on the ensemble natural frequency statistics and any preliminary conclusion based on exclusively its values regarding the establishment of the GOE model for the modal parameter statistics should be avoided, since the statistical overlap factor definition does not take into account directly the ensemble statistics of the corresponding mode shapes, Cordioli (20).

In the following, a complete statistical analysis is performed with corresponding mode shapes. Thus, the mode shape statistics results will contribute to providing a detailed understanding of the modal parameter statistics as well as additional information to investigate the conditions required for the establishment of *universal* statistics described by the GOE model.

Mode Shape Statistics

In a manner similar to the natural frequency statistical analysis, the mode shape statistics were characterized through the use of the eigenvector statistical observables of the Random Matrix Theory (RMT). Although the eigenvector statistical observables were initially defined considering the *spatial* or *spectral* averaging approaches, the results for the eigenvector statistical observables presented below considered also an *ensemble* averaging approach, that is, the statistics of a fixed eigenvector component across the ensemble is evaluated for a given mode shape (or mode order)[23]. In this regard, the routines for the previous eigenvector statistical observables which consider spectral and spatial averaging approaches were modified so as to also allow an evaluation of the ensemble statistics.

In Figure 75, the spatial kurtosis and Lilliefors Test results are shown in detail. Arithmetic and geometric averaging processes were performed on the spatial kurtosis results. The typically expected or probabilistic mode va-

[23]The definitions of the mode shape statistics averaging approaches are presented in detail in Section 2.3.2.

lue for the spatial kurtosis was also determined for each mode order. The analytical kurtosis predictions are also plotted for Gaussian and sinusoidal mode shape statistics (GOE and Poisson models), respectively.

According to Figure 75 (a), the spatial kurtosis results across the ensemble suggest the establishment of three well-defined regions of ensemble mode shape statistics. The first region is associated with low order mode shapes which have almost nominal statistics, that is, very close to sinusoidal statistics. As the mode order, or frequency, increases the typically expected spatial kurtosis values suggest that there is a statistical transition toward GOE or Gaussian statistics and thus, around the vicinity of mode 40, the typically expected spatial kurtosis values are close to the expected Gaussian value, that is, $K \sim 3$. In the last statistical region, beyond the almost-GOE range, large values of the spatial kurtosis are clearly observed, suggesting the establishment of the *structural localization* phenomenon, (139, 140, 159). Indeed, as excitation frequency increases, the effects of the structural localization phenomenon become more and more relevant and there is a highly dispersive behavior, or large variability, of individual spatial kurtosis values around the kurtosis mean value curves.

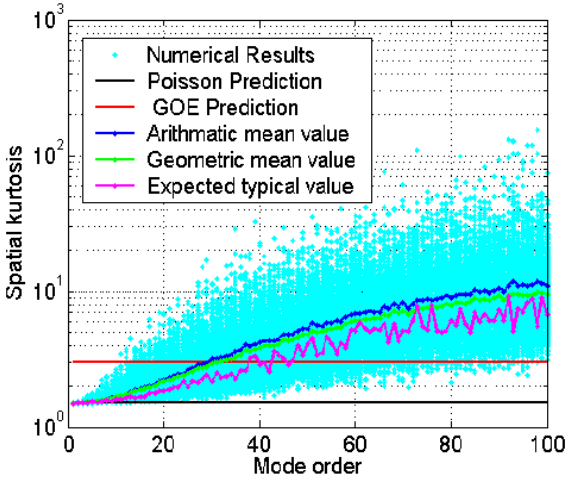

(a)

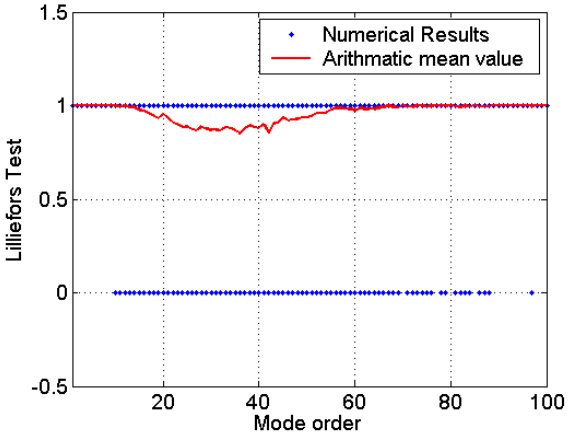

(b)

Figure 75: Spatial analysis of the mode shape statistics of a mass-loaded rod ensemble (spatial averaging approach). Plot (a): spatial kurtosis results. Plot (b): spatial Lilliefors Test results.

Considering that the performance of the mean values to representing the typically expected spatial kurtosis value across the ensemble, the arithmetic as well as geometric mean values are very distinct from the typically expected spatial kurtosis value across the ensemble, mainly in the high-frequency range. Indeed, the low performance of both averaging processes confirms the establishment of a probabilistic distribution with long tail characteristics for the spatial kurtosis values.

Additionally, the spatial Lilliefors Test results, Figure 75 (b), suggest that the largest number of Gaussian mode shapes occurs for a limited mode order range, approximately from mode 26 to mode 42, and only some members of the ensemble, circa 15%, present Gaussian distribution characteristics for this mode order range.

Although the spatial and ensemble kurtosis averaging approaches were adopted by Lyon (48) and Langley (18, 3), respectively, in the definition of the mode shape statistics factor in the SEA variance context, the use of the *spectral averaging approach* for the statistical investigation of the kurtosis parameter can provide important evidence regarding the statistical correlation between the mode shape components, Gomes (101). In this regard, the

spectral kurtosis and Lilliefors Test results were evaluated for each mode shape component and each ensemble member. The statistical parameters of the spectral kurtosis results were investigated using arithmetic and geometric averaging processes across the ensemble. In Figure 76, the spectral kurtosis values and Lilliefors Test results are shown. The Gaussian (GOE) and sinusoidal (Poisson) analytical predictions are also plotted.

As shown in Figure 76 (a), large spectral kurtosis values are observed in the rod regions close to both rod ends. An asymptotic establishment of an almost flat spectral kurtosis mean curve toward the central rod region is also observed, regardless of the averaging process adopted. Additionally, it can be noted that the averaging processes provide distinct kurtosis mean values. Indeed, the spectral kurtosis values also present a probabilistic distribution with long tail characteristics and thus the arithmetic as well as geometric mean values do not represent adequately the typically expected value across the ensemble (ensemble probabilistic mode value).

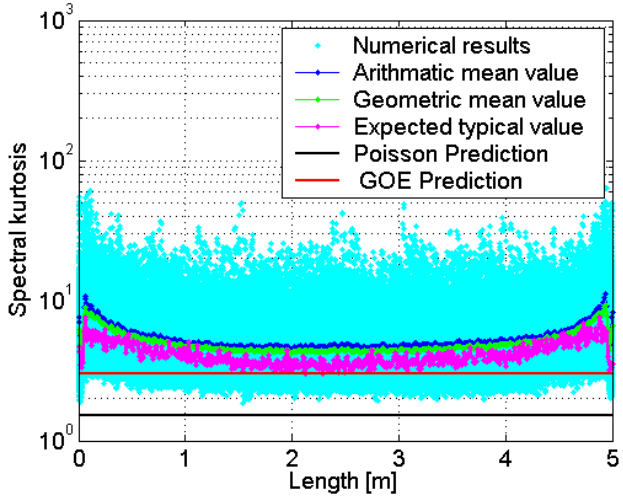

(a)

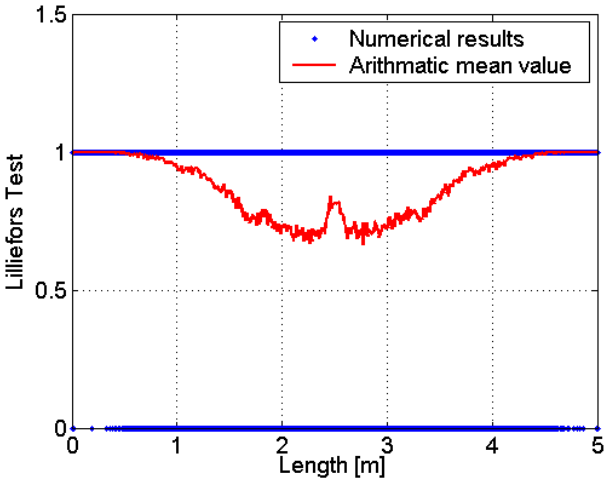

(b)

Figure 76: Spectral analysis of the mode shape statistics (spectral averaging approach). Plot (a): spectral kurtosis results. Plot(b): spectral Lilliefors Test results.

In Figure 76 (b), the spectral Lilliefors Test results for each rod member of the ensemble as well as the arithmetic mean value across the ensemble are shown in detail. Similarly to the spectral kurtosis results, the averaged value of the spectral Lilliefors Test results confirms that the largest number of mode shape components with Gaussian characteristics occurs in the central region of the rod compared to other regions. Indeed, the mean value of the spectral Lilliefors Test results suggests that the establishment of a Gaussian distribution for a fixed mode shape component, located in the vicinity of the central region of the rod, across the mode order domain, is expected for approximately 30% of the rod members of the ensemble. That is, only for 30% of the members of the mass-loaded rod ensemble it is expected that the mode shapes are *statistically independent* at a given excitation point located in the central region of the rod. Therefore, based on the spectral mode shape statistics results, the most favorable condition for the achievement of a good performance of the SEA variance predictions based on GOE model statistics seems to occur when the excitation point is located in the central region of the mass-loaded rod structure.

Considering the *ensemble mode shape averaging approach*, the ensemble kurtosis value for each mode shape component was evaluated as a mode order function. The ensemble kurtosis results for each mode shape component as well as their statistical parameters are shown in Figure 77. The Gaussian (GOE model) and sinusoidal analytical predictions are also plotted.

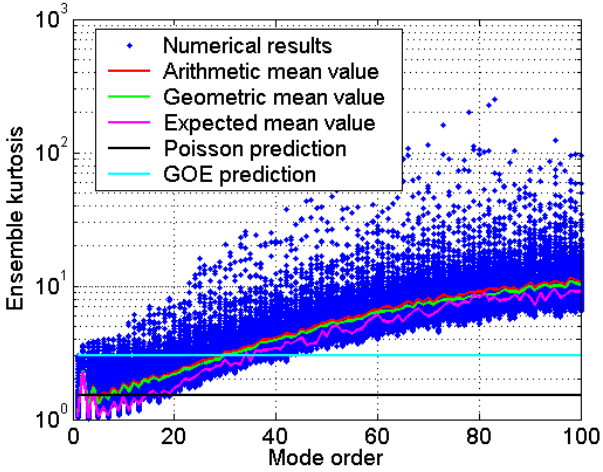

Figure 77: Ensemble kurtosis results: individual members, typically expected, arithmetic and geometric mean values (ensemble averaging approach).

As shown in Figure 77, the ensemble kurtosis results also confirm the global tendency of the mode shape statistics described previously in the spatial kurtosis analysis. However, it is relevant to note that in contrast to the spatial kurtosis variability, which increases gradually as the mode order (or frequency) increases, the ensemble kurtosis variability presents moderate magnitudes in the low and mid-frequency range.

In order to identify the most probable mode shape component (excitation point) and mode order range (or frequency range) for the establishment of *Gaussian* mode shape statistics across the ensemble, the ensemble Lilliefors Test results were evaluated, Figure 78.

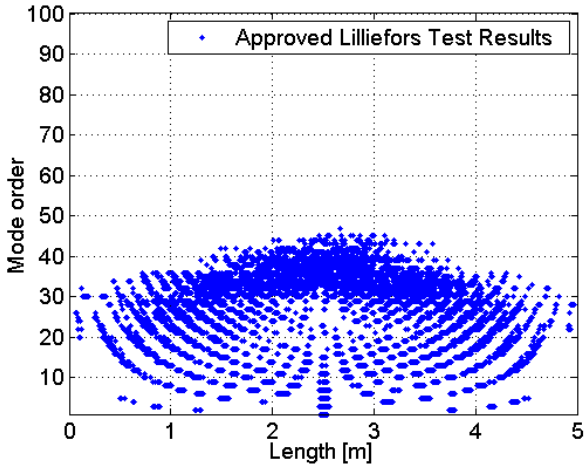

Figure 78: Ensemble Lilliefors Test results: bi-dimensional graphical representation (ensemble averaging approach).

In Figure 78, the points on the ensemble Lilliefors Test results represent the data sets approved by the Lilliefors Normality Test in which a good agreement with GOE or Gaussian mode shape statistics is expected.

It is important to emphasize that the conclusions drawn from the ensemble Lilliefors Test results agree satisfactorily with those of the previous mode shape statistics obtained using spatial and spectral averaging approaches. That is, the establishment of Gaussian mode shape statistics across the ensemble is expected in the vicinity of mode 40 when a single excitation point is located in the central region of the mass-loaded longitudinal rods.

In addition, Figure 78 shows clearly that the high order modes, beyond mode 45, are certainly *non-Gaussian*, regardless of the excitation point location. As discussed previously, this frequency region is characterized by the establishment of *ensemble localization statistics*.

Based on the above discussion, the bi-dimensional representation of the ensemble Lilliefors Test results can be considered an excellent tool to identify the most probable region (mode order range and excitation point location) for the establishment of GOE mode shape statistics.

In the Quantum Billiard field, analytical expressions proposed by the Theory of Supersymmetry are available to describe the statistical characte-

ristics of localized wavefunctions, Sridhar and others (71, 73, 74). Mirlin and Fyodorov (77), based on 1D non-linear sigma model, proposed PT-distribution patterns for weak and strong localization regimes. These expressions and their parameters are reviewed in section 2.3.4 of Chapter 2.

In the following, the performance of these analytical expressions based on the non-linear sigma model are evaluated considering PT-distributions of a fixed mode shape component across the ensemble, instead of the use of a spatial averaging approach over the mode shape components. Two regimes (or disorder levels) are investigated: weak and strong localization.

In Figure 79, the numerical ensemble PT-distribution results, the analytical GOE prediction and the PT-distribution fitted results for the non-linear sigma models are plotted. In a manner similar to the previous spatial mode shape analysis performed in section 3.4.4 of the current chapter, a global normalization constant (C_1) was introduced for the strong localization expression, Equation (2.55).

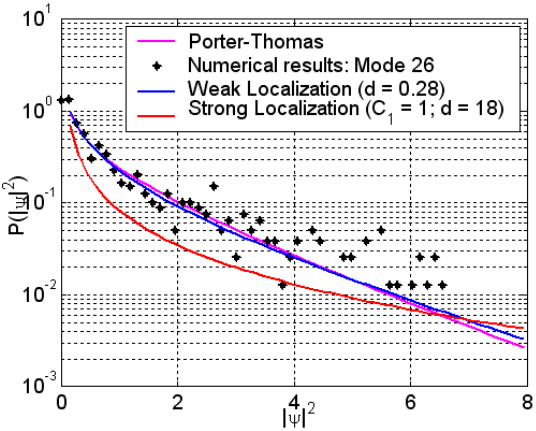

(a)

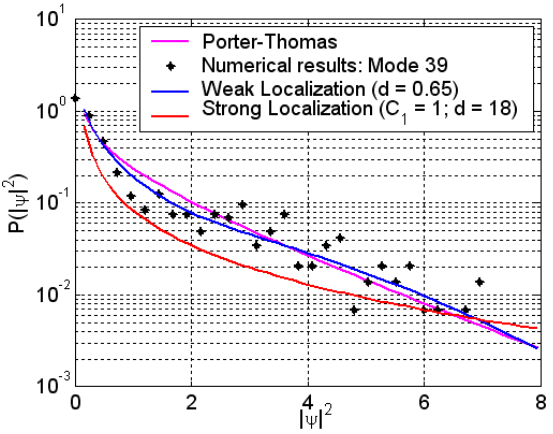
Porter-Thomas
Numerical results: Mode 39
Weak Localization (d = 0.65)
Strong Localization (C1 = 1; d = 18)
P(|ψ|2)
|ψ|2

(b)

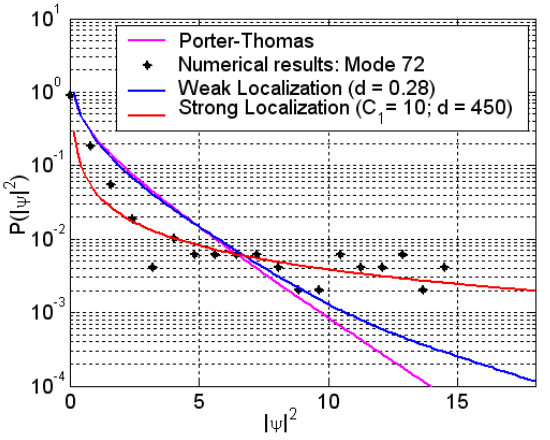
Porter-Thomas
Numerical results: Mode 72
Weak Localization (d = 0.28)
Strong Localization (C1 = 10; d = 450)
P(|ψ|2)
|ψ|2

(c)

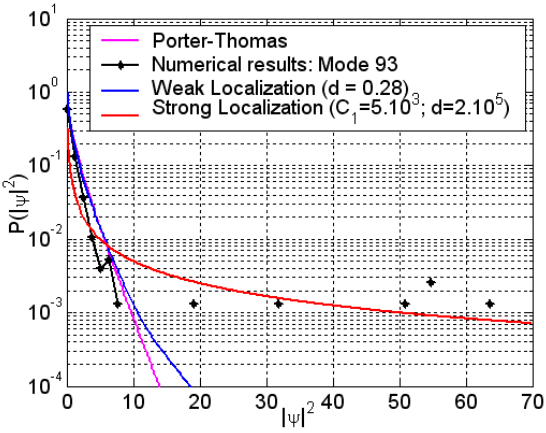

(d)

Figure 79: Ensemble Porter-Thomas distribution results for localized mode shapes: numerical results for the mode shape component located at 0.658 m, GOE prediction and non-linear sigma model fitted patterns (weak and strong localization regimes) (ensemble averaging approach). Plots: (a) mode 26, (b) mode 39, (c) mode 72, and (d) mode 93.

As shown at Figures 79 (a) and (b), the fitted non-linear sigma model curves are not able to describe the non-universal statistical characteristics presented in the PT-distribution results associated with the weakly localized mode shapes across the ensemble. Indeed, a non logical dispersive behavior is clearly observed for the numerical PT-distribution results associated with these mode shape components.

For strongly localized mode shapes, Figures 79 (c) and (d), the fitted non-linear sigma model curves conform very well to the numerical results. Indeed, the PT-distribution expression based on the non-linear sigma model was initially developed for one dimensional disordered systems in which the dynamical characteristics are very similar to those of the structure class investigated in this current work.

Mode Shape SEA Parameters: Normalized Parameters*P* and *Q*

Analogously to the statistical overlap factor results which measure the randomness levels from each natural frequency across the ensemble, the randomness (or disorder) level of the mode shapes can also provide important information required to define the necessary conditions for the *universal* establishment of GOE model for the modal parameter statistics in a given random vibroacoustic system. In general, it is assumed that the disorder level of the mode shapes is directly associated with the number of relevant *eigenbases* across the ensemble, Zyczkowski (81) and Cordioli (20).

In the current study, the parameters P and Q, originally proposed by Cordioli (20), were normalized in terms of the mode shape vector size, that is, the total number of mode shape components, in order to provide appropriate conditions for a direct comparison between vibroacoustical systems with different numbers of the mode shape components, usually associated with distinct meshing characteristics. This normalization process minimizes the effects associated with the meshing characteristics of the vibroacoustical system investigated. In Figure 80, the results for the normalized Parameter P (P_a) and normalized parameter Q (Q_a) are presented for the mass-loaded rod ensemble.

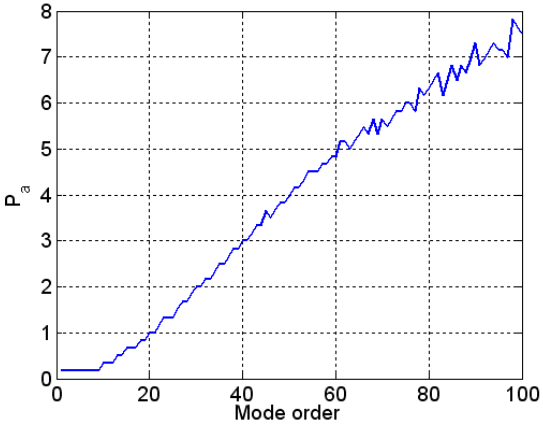

(a)

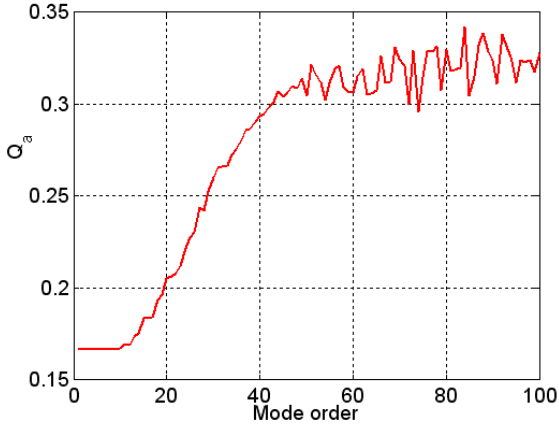

(b)

Figure 80: Mode shape SEA parameters of the mass-loaded rod ensemble (ensemble averaging approach). Plot (a): Parameter P_a. Plot (b): Parameter Q_a.

As shown in Figure 80 (a), the parameter P_a results suggest that the number of relevant bases increases as the frequency or mode order increases. Thus, the statistics for high order mode shapes are expected to be closer to GOE statistics than those for low order mode shapes, that is, an asymptotic establishment of the GOE statistics is expected as the mode order value (or excitation frequency) increases.

Considering the parameter Q_a results, Figure 80 (b), they have a tendency very similar to that of the parameter P_a results in the low mode order range, although the results are very distinct for mid and high mode order ranges. Beyond the vicinity of mode 40, the parameter Q_a results have almost flat characteristics (or a plateau region), except for the presence of small oscillations. Hence, the number of relevant bases beyond mode 40 would be expected to remain approximately constant.

As shown previously in the results for the spatial and ensemble statistical observables, an almost GOE statistics is expected to be established in a limited (or restricted) mode order range in the vicinity of mode 42, and beyond this region the establishment of the structural or ensemble localization phenomena is strongly expected.

Comparing the curve patterns of the spatial and ensemble kurtosis re-

sults with the performances of the parameters P_a and Q_a, only the parameter Q_a results are able to identify that significant changes occur in the mode shape statistics for the mid and high mode order ranges. The parameter P_a performance is only reliable in the low mode order region where the mode shape mixing phenomenon is not established. According to Cordioli (20), it is important to note that the parameter P presents an inadequate performance in identifying the establishment of GOE statistics in certain situations. Similarly to the statistical overlap factor definition, the parameter P definition does not take into account the mode shape *mixing* phenomenon associated with each mode shape investigated across the ensemble; Cordioli (20), Schaadt (110, 69, 70), Bertelsen (90) and Kessissoglou & Langley (80).

On the other hand, the parameter Q_a showed convenient characteristics to evaluate the randomness level from a certain mode shape set across the ensemble, since the mode shape mixing effects are minimized during its evaluation. However, there is no analytical proof to affirm that an explicit connection exists between the parameter Q_a values and the establishment of GOE statistics or the establishment of the *structural* or *ensemble* localization phenomena. Thus, it appears that the parameter Q_a may be employed together with other eigenvector statistical observables as an auxiliary parameter to evaluate the randomness (or disorder) level of mode shapes.

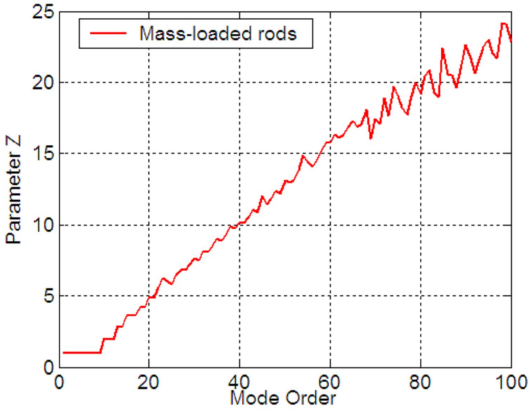

Figure 81: Mode shape SEA parameter of the mass-loaded rod ensemble: parameter Z (ensemble averaging approach).

In Figure 81, the parameter Z results are plotted as function of mode order for the mass-loaded rods. Considering the normalization process adopted for the mode shape SEA parameters P and Q, the evaluation of parameter Z is given by $Z = P_a/Q_a$.

As shown Figure 81, the parameter Z results have a crescent behavior as the mode order increases, suggesting that the number of superimposed spectra increases asymptotically toward the high natural frequency range. For high frequency range, the longitudinal wavelength reduces substantially in comparison to rod dimensions and thus the point masses actuates as mechanical discontinuities, proving the establishment of non-interacting rod substructures which are defined by a rod section limited by two successive point masses, Brown (1). Therefore, a high number of independent mode sets can exist in the various rod sections between the point masses, explaining the establishment of the almost-Poisson model characteristics observed previously for natural frequency statistical observable results[24].

Ensemble Analysis of Structural Localization Phenomenon

As observed in the previous analysis of the modal parameter statistics, the mass-loaded rod ensemble, due to its structural irregularity characteristics, presents a high probability of the establishment of *structural localization phenomenon* in the mid and high-frequency ranges. The main goal of the analysis which follows is to understand the principal aspects associated with the establishment of the localization phenomenon, for instance: the physics of spatial decay and its relationship with the excitation frequency, damping magnitudes, establishment of the GOE statistics for modal parameters and others. These structural localization issues are investigated through the use of the *localization factor* which allows the identification of the *pass-band* and *stop-band* regions, Pierre (148).

Initially, the ensemble-averaged spatial decay along the length was evaluated as each rod member is subjected to unitary longitudinal excitation at the rod end. The frequency-constant and low damping loss factor was adopted in order to minimize the effects of the damping mechanisms on the spatial energy response. The arithmetic and geometric averaging processes were considered and their corresponding localization factors were evaluated

[24] Although it was not discussed here in details, similar effects on the natural frequency statistics are expected for two distinct situations: (*i*) the system has several non-interacting substructures (*i.e.*, mass-loaded rod) or (*ii*) the system has geometric symmetries (*i.e.*, perfectly rectangular block or plate), Weaver (64), and Cordioli (20).

for several excitation frequencies. In Figure 82, the performances of the arithmetic and geometric averaging processes and respective localization factors are shown in detail for distinct mode shape statistics.

As shown in Figure 82, the establishment of the localization phenomenon leads to significant effects on the averaging processes and thus very distinct localization factor values are expected for the arithmetic and geometric averaging processes, mainly for the high excitation frequency range in which the mode shape statistics are localized.

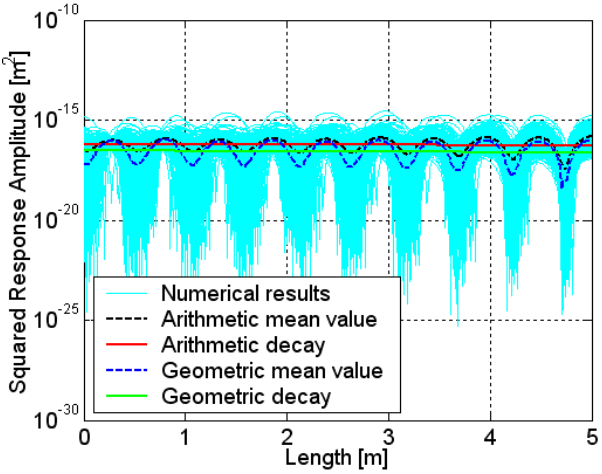

(a)

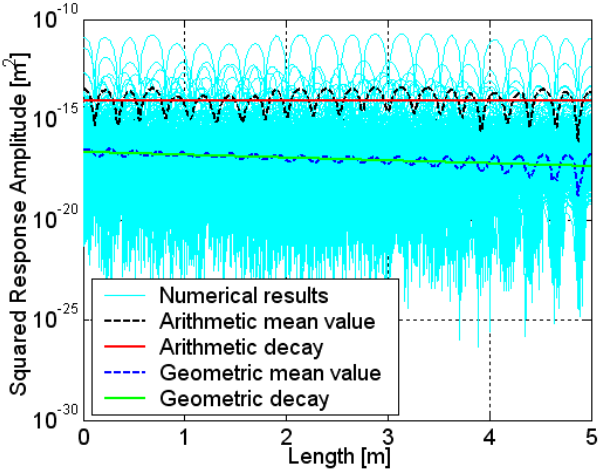
Squared Response Amplitude [m²]
Length [m]
Numerical results
Arithmetic mean value
Arithmetic decay
Geometric mean value
Geometric decay

(b)

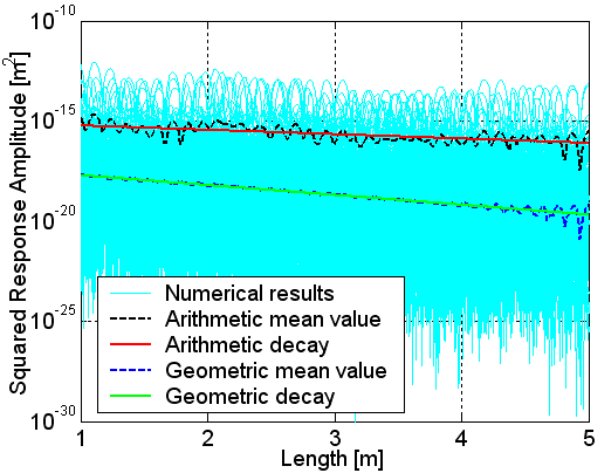
Squared Response Amplitude [m²]
Length [m]
Numerical results
Arithmetic mean value
Arithmetic decay
Geometric mean value
Geometric decay

(c)

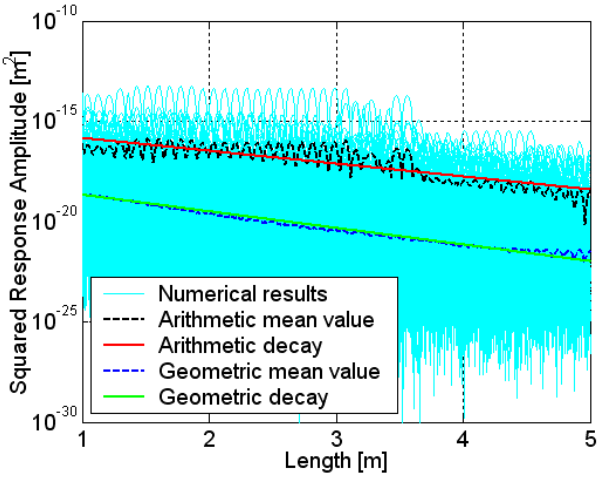

(d)

Figure 82: Ensemble spatial decay analyses: averaging process performances and localization factor values (ensemble averaging approach). Plot (a): Vicinities of Modes 09 and 10: excitation frequency of 4.5 kHz - almost sinusoidal mode shape statistics. Plot (b): Vicinities of Modes 21 and 22: excitation frequency of 10 kHz - sinusoidal to Gaussian transition mode shape statistics. Plot (c): Vicinities of Modes 41 and 42: excitation frequency of 20 kHz - almost Gaussian mode shape statistics. Plot (d): Vicinities of Modes 62 and 63: excitation frequency of 30 kHz - localized mode shape statistics.

In general, the results suggest that the use of the geometric averaging process is more appropriate than the traditional arithmetic averaging process to represent the typically expected response of an ensemble composed of engineering structures with structural irregularities. Similar results with almost-periodical structures were obtained by Hodges (159, 150). Additionally, the expected mean value for the geometric averaging process has a decreasing linear pattern along the rod length. Hence, the linear best-fit decay provides a good evaluation of the localization factor mainly in the frequency range corresponding to localized mode shapes. Indeed, the low performance of the arithmetic averaging process seems to be based on the significant contribution of the sporadic localized results associated with the long-tail characteristics

of the response distribution.

In order to investigate the effects of damping mechanisms on the localized mode shapes, several magnitudes of damping loss factor were considered and the corresponding localization factors were evaluated for four mode shape statistics regions considered in the previous analysis. In Table 9, the localization factors of the arithmetic and geometric decay fitting are presented for distinct mode shape statistics.

Table 9: Localization factor analysis for longitudinal random mass-loaded rods: several excitation frequencies and damping loss factor magnitudes (ensemble averaging approach).

f= 4.5 kHz	Almost sinusoidal statistics	Modes: 09 - 10
Damping Loss Factor	Arithmetic decay	Geometric decay
10^{-2}	0.0004	0.0009
10^{-3}	0.0002	0.0005
10^{-4}	0.0002	0.0004
10^{-6}	0.0002	0.0004
10^{-8}	0.0002	0.0004
10^{-12}	0.0002	0.0004

(a) Vicinities of Modes 09 and 10: excitation frequency of 4.5 kHz - almost sinusoidal mode shape statistics

f= 10 kHz	sinusoidal - Gaussian transition	Modes: 21 - 22
Damping Loss Factor	Arithmetic decay	Geometric decay
10^{-2}	0.0031	0.0038
10^{-3}	0.0032	0.0028
10^{-4}	0.0010	0.0027
10^{-6}	0.0000	0.0027
10^{-8}	0.0000	0.0027
10^{-12}	0.0000	0.0027

(b) Vicinities of Modes 21 and 22: excitation frequency of 10 kHz - sinusoidal to Gaussian transition mode shape statistics

f= 20 kHz	Almost Gaussian statistics	Modes: 41 - 42
Damping Loss Factor	Arithmetic decay	Geometric decay
10^{-2}	0.0080	0.0115
10^{-3}	0.0051	0.0096
10^{-4}	0.0040	0.0094
10^{-6}	0.0042	0.0094
10^{-8}	0.0042	0.0094
10^{-12}	0.0042	0.0094

(c) Vicinities of Modes 41 and 42: excitation frequency of 20 kHz - almost Gaussian mode shape statistics

f= 30 kHz	structural localized statistics	Modes: 62 - 63
Damping Loss Factor	Arithmetic decay	Geometric decay
10^{-2}	0.0165	0.0177
10^{-3}	0.0113	0.0160
10^{-4}	0.0121	0.0159
10^{-6}	0.0123	0.0159
10^{-8}	0.0123	0.0159
10^{-12}	0.0123	0.0159

(d) Vicinities of Modes 62 and 63: excitation frequency of 30 kHz - Localized mode shape statistics

The localization factor results show the significant influence of moderate and large damping loss factor magnitudes on the evaluation of the spatial averaged decay across the ensemble. According to the results, a low damping loss factor provides the most favorable condition for the accurate evaluation of the localization factor. In addition, it can be noted that the localization factor magnitudes of the arithmetic and geometric averaging processes have very distinct characteristics. The localization factors based on the geometric mean value are expected to be larger than those based on the arithmetic mean value for most excitation frequency ranges.

In Figure 83, the localization factor results are shown as a function of the excitation frequency for both decay evaluation averaging processes, that is, arithmetic and geometric. During the localization factor evaluation, very low damping loss factor magnitudes were adopted in order to minimize the

damping effects on the ensemble-averaged spatial decay. The localization factor results are presented in terms of absolute values.

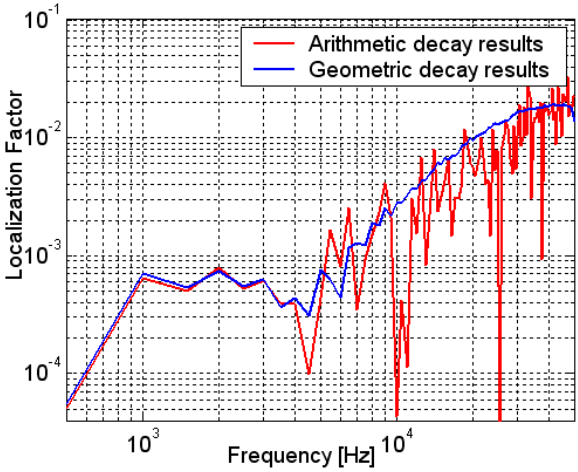

Figure 83: Localization factor results as a function of excitation frequency: arithmetic and geometric decay evaluation (ensemble averaging approach).

The localization factor curve of the arithmetic fitted decay has a very oscillatory behavior and presents some unexpected null as well as negative[25] values for the frequency regions of typical localized mode shape statistics. On the other hand, the localization factor curve of the geometric fitted decay has an almost continuous pattern and well-defined frequency characteristics.

As shown in Figure 83, as the excitation frequency increases, the structural localization phenomenon becomes more relevant and large localization factor values are expected for the high-frequency range. Based on the previous results for the mode shape statistics analysis, for the frequency range closest to the vicinity of 20 kHz, the establishment of GOE statistics is expected for both modal parameters. The localization factor results associated with this frequency region suggest the presence of a moderate localization and magnitudes close to 1% for the localization factor.

[25]The negative values of the localization factors are not emphasized herein because the localization factor results are presented in terms of absolute values.

Additionally, the *pass-band* and *stop-band* frequency limits were adequately identified. In the current localization analysis, the stop-band threshold was adopted as the localization factor magnitude is equal to 1.10^{-3}. In the Pierre's work (148), a similar stop-band threshold magnitude was adopted for several finite oscillator chains and an excellent performance was obtained in the characterization of the pass-band and stop-band frequency regions. For the low-frequency range, a spatial propagation of the longitudinal wave is expected throughout the rod structure domain since the uncertainty or disorder effects are not significant. Therefore, the low localization factor magnitudes confirm the establishment of an almost negligible spatial decay, indicating that the pass-band characteristics are associated with the low-frequency range.

On the other hand, the strong localization and spatial energy confinement phenomena are expected to become more intense as the excitation frequency increases. The localization factor curve shows also that the localization factor magnitude increases gradually as the excitation frequency increases.

Considering the excitation frequency region around 20 kHz, that is, in the vicinities of modes 41 and 42, the establishment of GOE statistics is expected for both modal parameters, as shown in previous results from mode shape statistics analysis. From the localization analysis, the localization factor results suggest the establishment of a moderate localization regime for this excitation frequency region since the presence of disorder or uncertainties reduces the coupling strength between two successive rod sections separated by a point mass.

Kinetic Energy Density Statistics: Spatially-Averaged Excitation

In order to investigate the effects of distinct modal parameter statistics on the kinetic energy density statistics, two distinct excitation classes are considered. The first is a unitary longitudinal *single point-loading* which provides the energy response dependent on both modal parameter statistics. The second considers a *spatially-averaged excitation* which provides the energy results identical to those for *rain-on-the-roof* excitation. It is important to emphasize that the contributions of the mode shape statistics are removed for this second excitation class and thus the kinetic energy density statistics are dependent only on the natural frequency statistics, Brown (1).

In the following, the energy response of each ensemble member is evaluated considering a narrow frequency domain with a fixed frequency interval

of 10 Hz. The modal superposition method was used to evaluate the kinetic energy density results. Considering the FEM model performance, a detailed convergence analysis was performed in order to guarantee the response convergence in the frequency range of interest. The ensemble size adopted was 500 members.

In Figure 84, the spatially-averaged kinetic energy density results for some members are presented for a damping loss factor of magnitude equal to 3%, that is, $\eta = 0.03$. This choice is based on the fact that the modal overlap factor range corresponding to this particular DLF magnitude is adequate to evaluate directly the effects of the modal parameter statistics on the kinetic energy density results, since the establishment of a high modal superposition does not occur. Additionally, the analytical SEA prediction is also plotted.

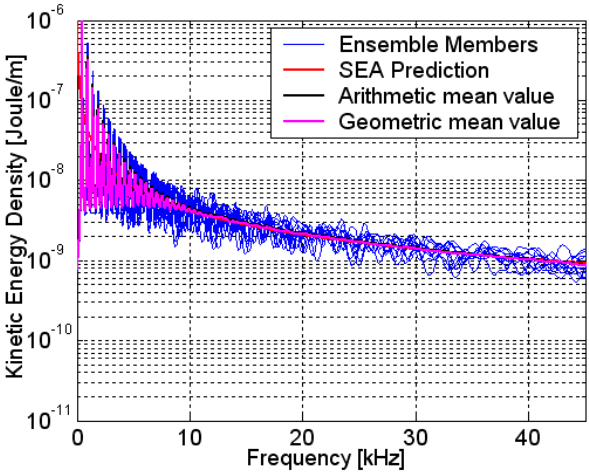

Figure 84: Kinetic energy density results for spatially-averaged excitation: members, ensemble arithmetic and geometric mean values and SEA prediction (ensemble averaging approach).

As shown in Figure 84, an excellent agreement was obtained between the SEA prediction and ensemble mean values mainly in the mid and high-frequency ranges.

In a similar manner, the relative variance of the spatially-averaged kinetic energy density results were also evaluated across the ensemble. The

numerical results and analytical predictions are plotted in Figure 85.

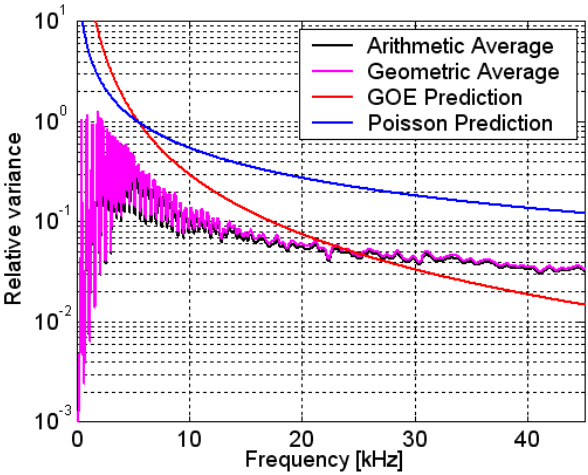

Figure 85: Relative variance of kinetic energy density results for spatially-averaged excitation based on: ensemble arithmetic and geometric mean values (ensemble averaging approach). The Poisson and GOE analytical predictions are also plotted.

As shown in Figure 85, the level of agreement between the numerical values and analytical predictions is low for almost the whole frequency domain. The numerical relative variance results associated with each frequency range can be easily understood when compared to the corresponding ensemble natural frequency statistics. For the low-frequency range, the spectral rigidity characteristics are relevant. Thus, small differences between the random rod response and the nominal rod one are expected since almost negligible deviations occur for the natural frequency locations in comparison to those of the nominal rod.

As the excitation frequency increases the energy response variability across the ensemble becomes more and more relevant due to uncertainty or structural irregularity effects. In the vicinity of 20 kHz (mode 42) the natural frequency statistics presents an almost-GOE statistics and a good agreement is expected between the ensemble relative variance results and the analytical prediction based on the GOE model. Indeed, the relative variance of the

numerical results conforms well with the GOE prediction in this frequency region.

Beyond this frequency range, the structural localization effects on the natural frequency statistics become gradually substantial as the excitation frequency increases. As shown previously, an asymptotic establishment of the Poisson natural frequency statistics occurs toward the high-frequency range and thus the relative variance results from the numerical rod ensemble show intermediate values between the GOE and Poisson analytical predictions.

Based on the performances of the relative variance predictions obtained in these current analyses, it is possible to affirm that for cases of spatially-excited one-dimensional random structures, which are evident candidates for the establishment of the structural localization phenomenon, the relative variance analytical formulations based on the Poisson model can be applied in a conservative way to predict the expected relative variance in the highest frequency range.

Kinetic Energy Density Statistics: Single Point-Excitations

In this section, the characteristics of the energy response statistics of the mass-loaded rods subjected to a unitary longitudinal single point-loading are investigated for three distinct excitation point locations. The ensemble mean and relative variance values of the kinetic energy density results were evaluated considering the arithmetic and geometric averaging processes. Three distinct excitation points (X_0, X_2, and X_3) are described in Table 10.

Table 10: Three excitation points considered in the statistical analysis of the kinetic energy density results: point nomenclature, spatial coordinates, and brief statistical description.

Excitation points	Length coordinate [m]	Brief description
X_0	0	Left rod end
X_2	2.125	Almost-GOE
X_3	0.658	Arbitrary location

In Figure 86, the ensemble mean and relative variance values are shown for each excitation point. The analytical predictions based on GOE and Poisson model statistics are also plotted.

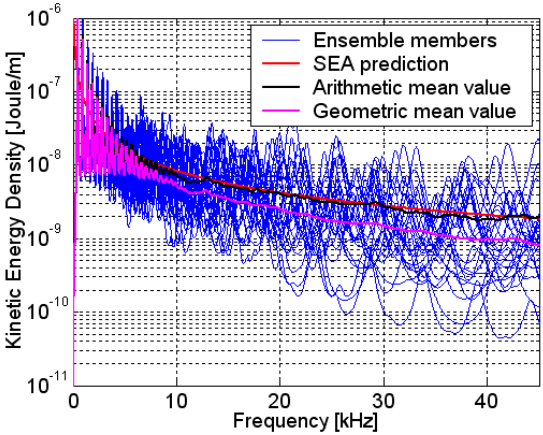

(a_1) Excitation point X_0

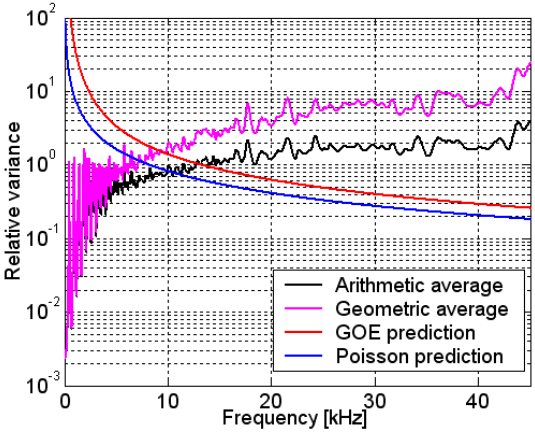

(a_2) Excitation point X_0

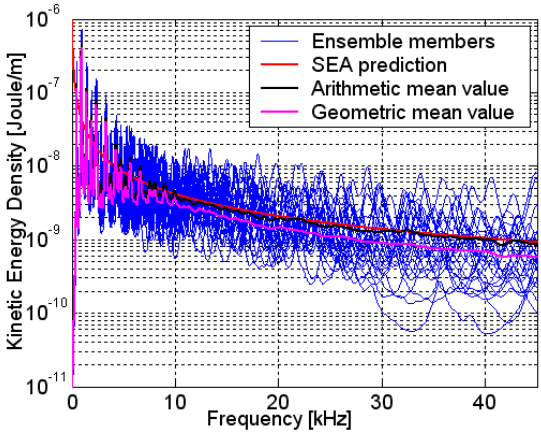

(b_1) Excitation point X_2

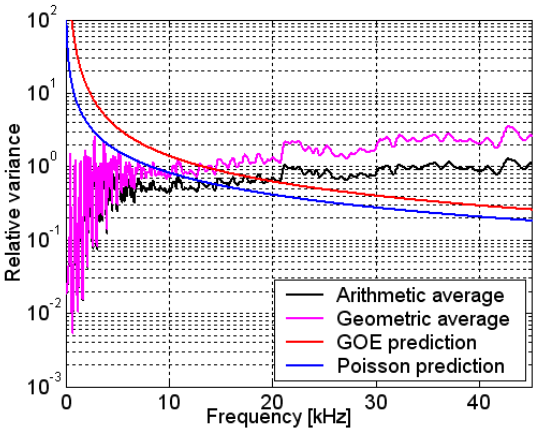

(b_2) Excitation point X_2

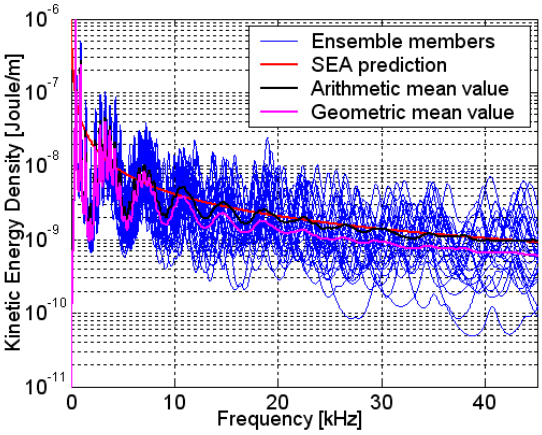

(c_1) Excitation point X_3

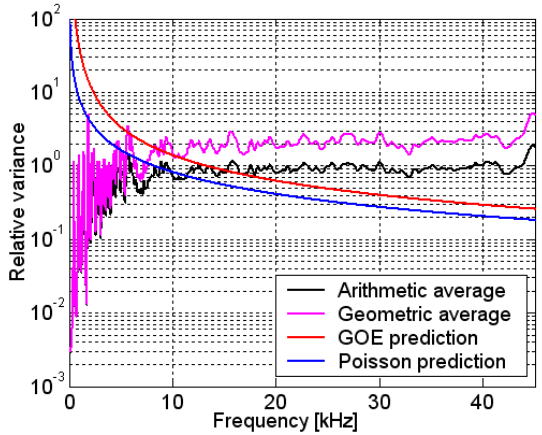

(c_2) Excitation point X_3

Figure 86: Ensemble mean and relative variance values of the mass-loaded longitudinal rods subjected to a single point-loading at excitation points X_0, X_2, and X_3: numerical results and analytical predictions based on GOE and Poisson models (ensemble averaging approach).

According to Figure 86, the ensemble mean and relative variance values present very distinct values for each averaging process considered. Since

the structures investigated have a relevant trend toward the establishment of the structural localization phenomenon, it is expected that the ensemble mean values obtained from the geometric averaging process will represent the typically expected response across the ensemble more adequately than the mean values obtained from the traditional arithmetic averaging process, Hodges *et al* (139, 140, 159).

In general, the ensemble mean values obtained from the geometric averaging process are lower than those of the SEA predictions and arithmetic values throughout the excitation frequency domain for all excitation points investigated. The energy responses of some ensemble members are also plotted and clearly indicate the good performance of the ensemble geometric mean values in representing the expected response of a typical member of the ensemble.

On the other hand, the ensemble mean values obtained from the arithmetic averaging process conform very well to the SEA predictions. Indeed, it is important to emphasize that SEA predictions provide an excellent estimate of the expected arithmetic mean value across the ensemble. As discussed previously, the evaluation of the arithmetic mean value of the energy responses has a weak dependence on the modal parameter statistics and thus an excellent agreement between the SEA predictions and ensemble arithmetic mean values is expected, at least for structure ensembles for which the response distributions have long-tail distribution characteristics.

Considering the ensemble relative variances of the three distinct excitation points investigated, the results based on the geometric mean values present larger amplitudes than those based on the arithmetic mean values, mainly in the mid and high-frequency ranges, for all excitation points investigated. Indeed, the discrepancies between the relative variance results based on the arithmetic and geometric mean values are clearly associated with the establishment, to a high degree, of the ensemble localization phenomenon which is gradually reinforced as the frequency increases.

The numerical variance results based on the geometric mean value are high and clearly overestimate the SEA variance predictions based on the GOE model throughout the frequency range investigated, suggesting that the typically expected variation in the kinetic energy density results across the ensemble obtained from the probabilistic mode values (typically expected values across the ensemble) may be substantially higher than the energy variance predicted by SEA model based on GOE statistics.

Additionally, it is important to emphasize that the ensemble relative variance results are more sensitive to changes in the modal parameter statis-

tics than the ensemble mean values, regardless of the averaging process adopted. Unlike the ensemble spatially-averaged relative variance results, which are dependent only on the natural frequency statistics, the point-loaging relative variance results are dependent on both the modal parameter statistics, that is, natural frequency statistics and a fixed mode shape component statistics corresponding to excitation point. As discussed previously in the spectral relative variance analysis, it is expected that the contribution of the mode shape statistics is usually more predominant for point-loading energy variance values than those of the natural frequency statistics, since small changes in the mode shapes may become significant in terms of the relative variance results.

As observed in Figure 86, the performance of point-loading relative variance analytical predictions is very limited, regardless of the statistical model adopted for the modal parameter statistics. Indeed, the good performance of the point-loading variance prediction based on the GOE model is strictly associated with the establishment of Gaussian characteristics in the ensemble and spectral mode shape statistics at the excitation point.

For all excitation points investigated, the relative variance results conform satisfactorily with the SEA variance prediction only within a limited frequency range. The limits of these frequency ranges, in which the GOE agreement is satisfactory, vary for each excitation point. In Figures 87 and 88, the ensemble kurtosis and Lilliefors Test results are presented for the excitation points X_0, X_2 and X_3, respectively. The analytical predictions for sinusoidal and Gaussian (GOE model) mode shape statistics are also plotted.

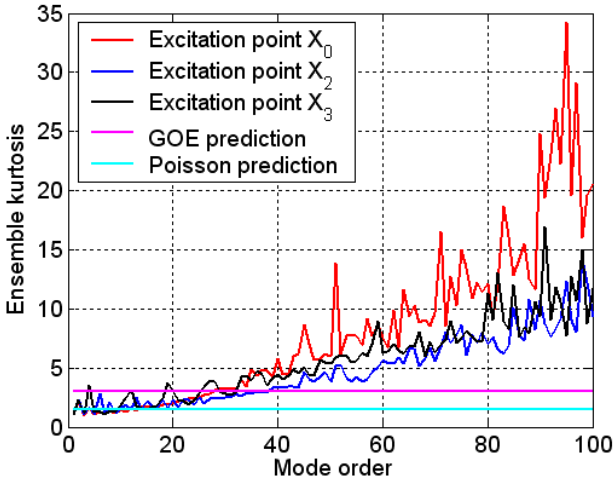

Figure 87: Ensemble kurtosis results for the mass-loaded rod ensemble: excitation points X_0, X_2 and X_3 (ensemble averaging approach).

In general, the ensemble mode shape statistics results for the excitation points agree with the global tendency previously presented in section 3.5.1. For the lower mode order range, the mode shapes are weakly affected by the randomness effects and their statistics are almost-sinusoidal (nominal). As the mode order increases the randomness effects become substantial and a statistical transition occurs from the sinusoidal to almost-Gaussian mode shape statistics. For three excitation points, the establishment of Gaussian statistics is clearly observed in a limited mode order range, although the limits and their extensions vary for each excitation point. Indeed, the achievement of a good performance of the SEA variance prediction based on GOE statistics are strictly associated with the location and extension of the mode order range with Gaussian characteristics. Beyond the Gaussian mode order range, a gradual establishment of the localization characteristics occurs as the frequency (mode order) increases. In the following, the performance of the SEA variance prediction based on the GOE model is discussed in detail for each excitation point in terms of the statistical characteristics of the *ensemble* and *spectral* mode shape statistics results.

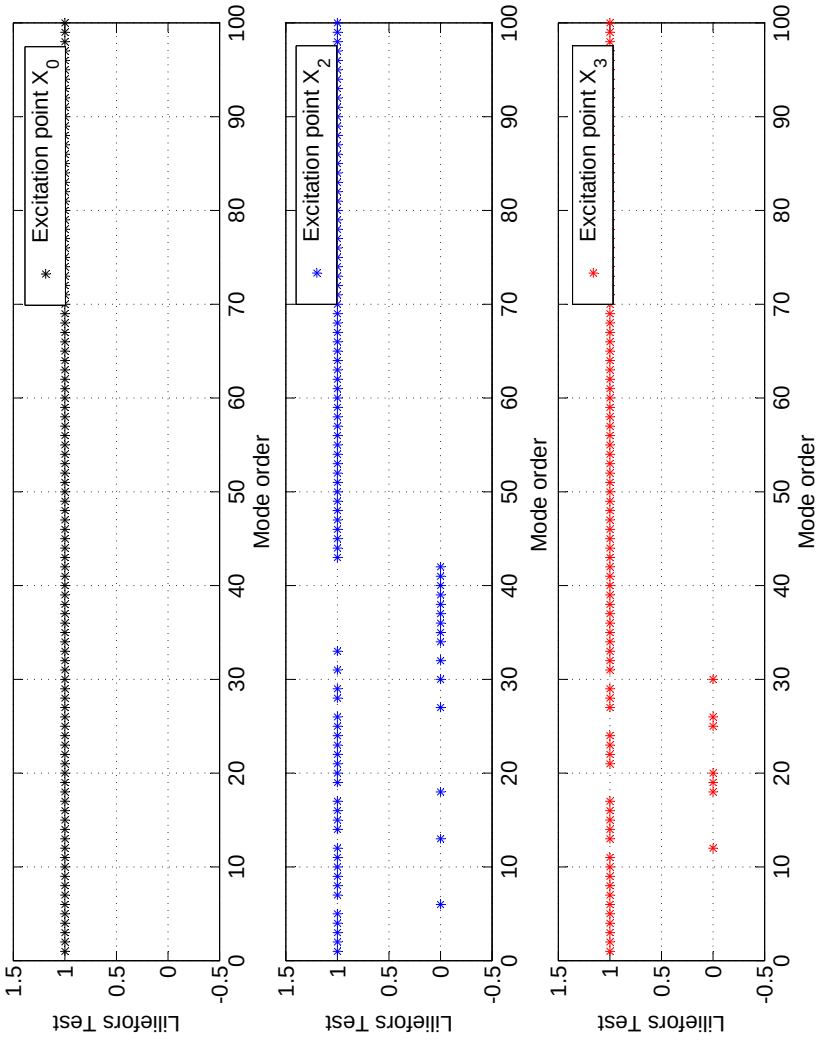

Figure 88: Ensemble Lilliefors Test results for the mass-loaded rod ensemble (ensemble averaging approach). Plot (a): Excitation point X_0. Plot (b) Excitation point X_2. Plot (c): Excitation point X_3.

For *excitation point* X_0, in the frequency range of approximately 12.5 kHz to 15 kHz (corresponding approximately to modes 16-31) there was a satisfactory agreement between the numerical variance results based on the arithmetic mean value and the SEA variance prediction based on the GOE model. Considering the corresponding ensemble mode shape statistics results, Figure 87 and Figure 88 (a), the ensemble kurtosis results associated with this mode order range present values close to $K \sim 3$ (expected Gaussian kurtosis value), although the Lilliefors Test results reject the hypothesis of Gaussian distribution for the mode shape components associated with the excitation point X_0 across the ensemble.

Considering again the relative variance results at the excitation point X_0, Figure 86 (a), some discrete peaks can be easily associated with large values of the ensemble kurtosis results. For example, the narrow peak at approximately 21.5 kHz is correlated to the localization characteristics of mode 45 where the ensemble kurtosis value is strongly localized, that is, $K_{45} \sim 9$, Figure 87. Similarly, the peak centered at approximately frequency 24.3 kHz is strictly associated with the localization characteristics of mode 51 ($K_{51} \sim 15$, strongly localized).

For *excitation point* X_3, three distinct narrow frequency regions show an approximate agreement between the analytical prediction based on the GOE model and the numerical variance results based on the arithmetic mean value. These three narrow frequency ranges are approximately centered in the vicinity of 12.5 kHz (corresponding to modes 25-26) for the first range, in the vicinity of 13.5 kHz (corresponding to modes 29-31) for the second range, and in the vicinity of 16.8 kHz (corresponding to mode 35) for the last frequency range.

Considering the corresponding ensemble mode shape statistics results, Figure 87 (c) and Figure 88, the ensemble kurtosis results show that the mode shapes associated with these mode order ranges present values close to $K \sim 3$ (expected Gaussian kurtosis value), although the Lilliefors Test results reject the hypothesis of Gaussian distribution only for last frequency region.

Between the second and third frequency ranges, a large peak in the relative variance results is clearly established in the vicinity of frequency 15.8 kHz. This peak is correlated to the localization characteristics of successive modes 33 and 34 where the ensemble kurtosis values are moderately localized, that is, $K_{33-34} \sim 4.5$, Figure 87.

For *excitation point* X_2, the arithmetic relative variance results associated with the frequency range from approximately 16.2 kHz to 20.6 kHz (corresponding approximately to modes 34-44) showed a excellent agreement

with the SEA variance prediction based on the GOE model. Considering the corresponding ensemble mode shape statistics results, Figures 87 and 88 (b), the ensemble kurtosis results associated with this mode order range present values close to $K \sim 3$ (expected Gaussian kurtosis value) and the corresponding Lilliefors Test results approve the hypothesis of Gaussian distribution for the mode shape components associated with excitation point X_2 across the ensemble.

As observed in Figure 86 (b), a well-defined shift in the curve of the relative variance results occurs at a frequency of approximately 21 kHz (vicinity of mode order 44) and an approximately flat behavior is established beyond this shift up to a frequency of 29 kHz. Considering the corresponding ensemble kurtosis results, Figure 87, a similar shift from the almost Gaussian ($K_{\sim 42} \sim 3$) to weak localized statistics ($K_{45-58} \sim 4$,) occurs at mode order 45 and a mode order range with weak localization characteristics is established from mode 45 to mode 58.

Considering the *spectral kurtosis* and *Lilliefors Test results*, Figure 76, the degree of the spectral correlation between the mode shape components is very substantial for the excitation points X_0 and X_3. Indeed, the spectral Lilliefors Test results, Figure 76 (b), suggest that for most of the ensemble members, circa 99%, the mode shapes can not be considered to be *Gaussian variables* at these excitation points. Conversely, the spectral results associated with excitation point X_2, Figure 76 (b), suggest that for less than half of ensemble members, circa 30%, the mode shape components can be considered to be almost Gaussian distributed at excitation point X_2.

It is also interesting to note that, although the excitation points X_2 and X_3 have distinct spectral correlation characteristics in terms of the mode shape statistics, their agreements with the analytical prediction based on the GOE model are very similar in the frequency ranges in which the establishment of Gaussian mode statistics is expected. Indeed, their numerical results conform very well with those based on GOE predictions over frequency ranges with similar extensions, suggesting that the presence of an inter-modal correlation between the mode shapes at the excitation point may not be the main factor associated with the reduced performance of the relative variance predictions based on the GOE model observed previously in the SEA variance literature results.

With respect to the establishment of GOE statistics for each of the modal parameters, it is important to note that for excitation points X_0 and X_3 the frequency ranges associated with ensemble mode shape statistics with almost-GOE characteristics are clearly distinct to the frequency range in which the

ensemble natural frequency statistics is approximately described by the GOE model. Although, it is considered that the best performance of the revised SEA variance predictions is exclusively obtained when a complete establishment of GOE statistics occurs for both modal parameter statistics, an excellent agreement between the analytical prediction based on the GOE model and numerical results was observed for the frequency range associated with Gaussian mode shape statistics, independent of the excitation point location. This finding appears to indicate that the mode shape contributions to kinetic energy density response are more predominant than the natural frequency contributions in the case of the single point excited rod ensemble investigated.

Considering the point-loading variance results associated with the excitation point X_2, an excellent agreement is verified between the variance prediction based on the GOE model and arithmetic numerical results for the excitation frequency range close to the vicinity of 20 kHz. As shown in the previous analysis of the modal parameter statistics for the *ensemble averaging approach*, the results for the statistical observables suggest an almost GOE statistics for point X_2 and in the vicinity of 20 kHz frequency (or in the vicinity of mode 42). Considering the ensemble averaging approach, a satisfactory establishment of GOE statistics for the modal parameters is also suggested by the corresponding results for the statistical observables.

On the other hand, it is also important to observe that the *spectral mode shape statistics* results associated with the excitation point X_2 clearly indicate an incomplete establishment of the GOE statistics, since for no more than 30% of the ensemble members the mode shape components are expected to be Gaussian distributed.

Additionally, the *spatial mode shape statistics* results, Figure 75, suggest that the occurrence of Gaussian characteristics in the mode shape component domain is very limited to a mode order range and also the largest number of Gaussian mode shapes occurs for a limited mode order range, approximately modes 26-42, where circa 15% of the ensemble members present Gaussian distribution characteristics.

3.5.2 Breaking the Geometrical Regularity

In this study, a second ensemble composed of 500 Gaussian spatially-correlated random rods was also investigated. In order to break the regularity of the rod geometry along the length, the randomization process considered the rod cross-sectional area as a random variable along the rod axis direction, where the values are spatially correlated. For each rod member, a particu-

lar correlation length is adopted and, using a correlation function, a spatial variation of cross-sectional area along the rod axis direction is obtained and the rod cross sectional area values are Gaussian distributed[26]. The correlation length values vary uniformly across the rod members from $L_c = 0.04$ to $L_c = 0.08$. According to previous results discussed in section 3.4.7, the correlation length range adopted here is associated with the highest probability for the occurrence of Gaussian mode shapes, Figure 66 (b).

Natural Frequency Statistics

In Figure 89, the results for the natural frequency statistical observables are shown for several mode orders (or spacings): PDF of adjacent natural frequency spacings and Δ_3 - statistics results.

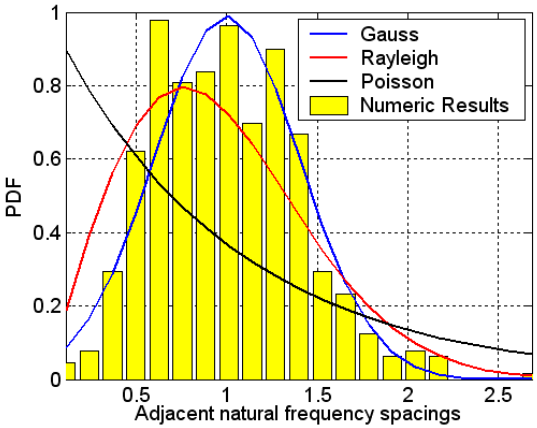

(a_1) Mode 10

[26] A similar randomization process was adopted previously in the spectral analysis of Gaussian spatially-correlated random rods. For more details see section 3.4.7.

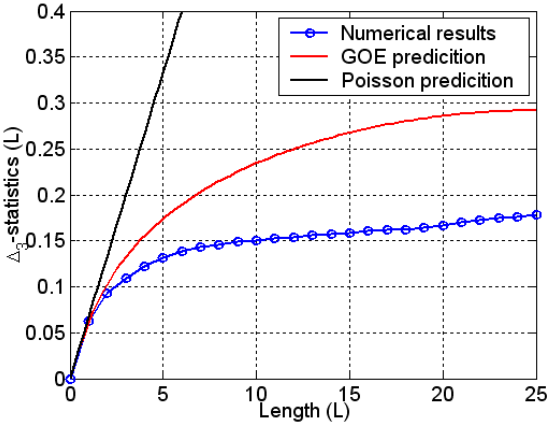

(a_2) Mode 10

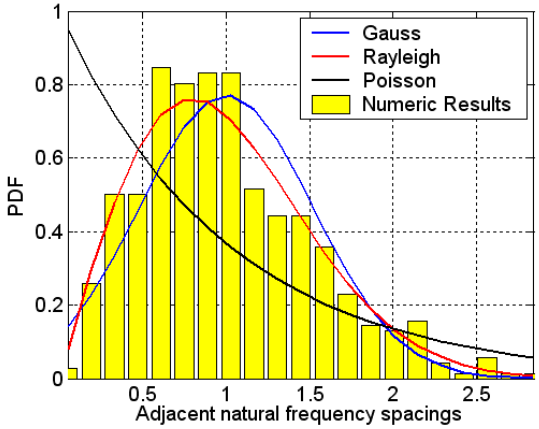

(b_1) Mode 20

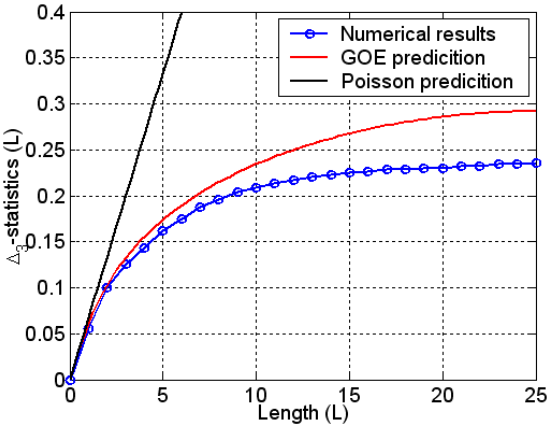

(b_2) Mode 20

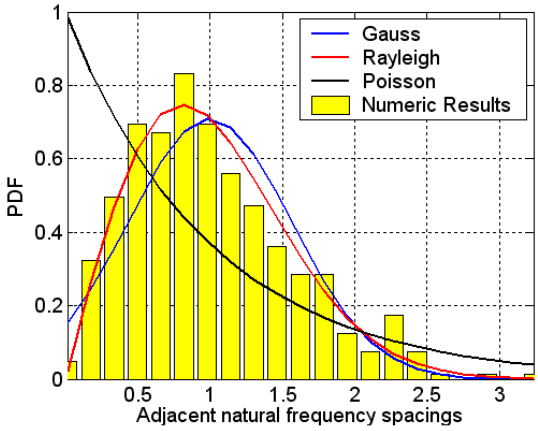

(c_1) Mode 35

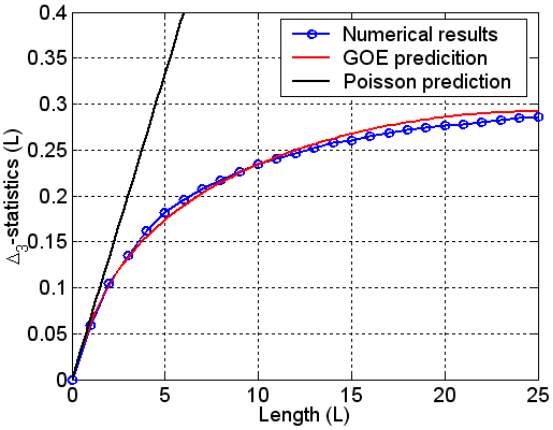

(c_2) Mode 35

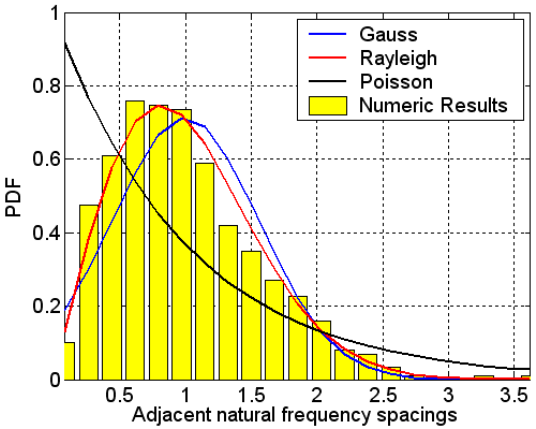

(d_1) Mode 40

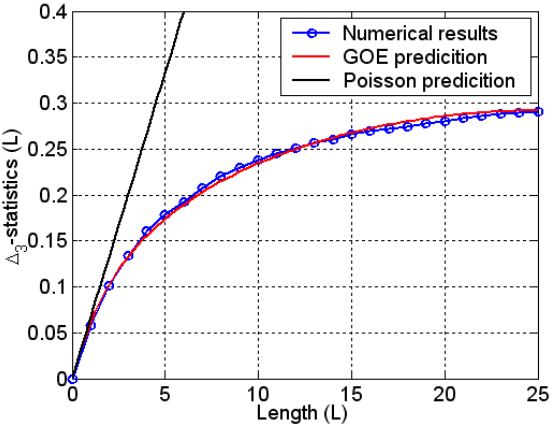

(d_2) Mode 40

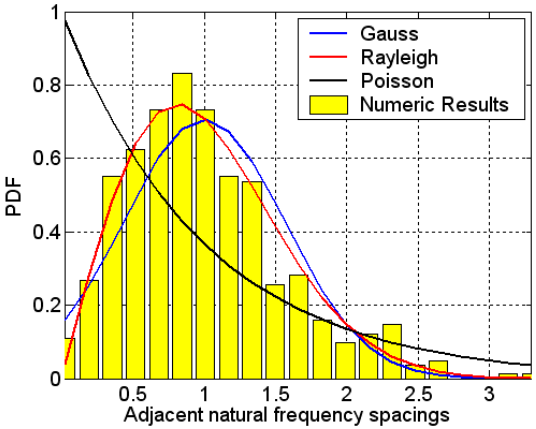

(e_1) Mode 65

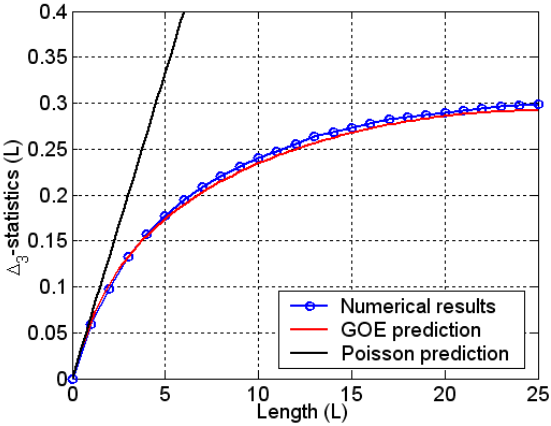

(e_2) Mode 65

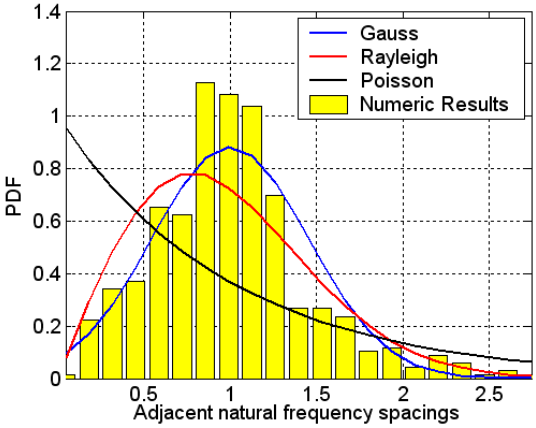

(f_1) Mode 80

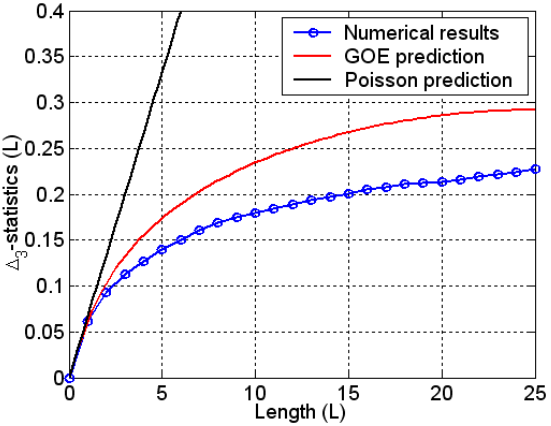

(f_2) Mode 80

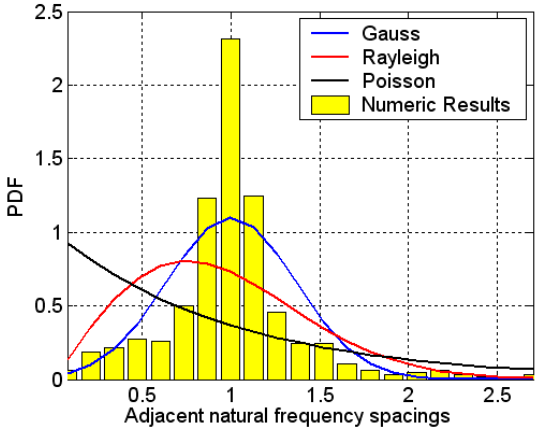

(g_1) Mode 95

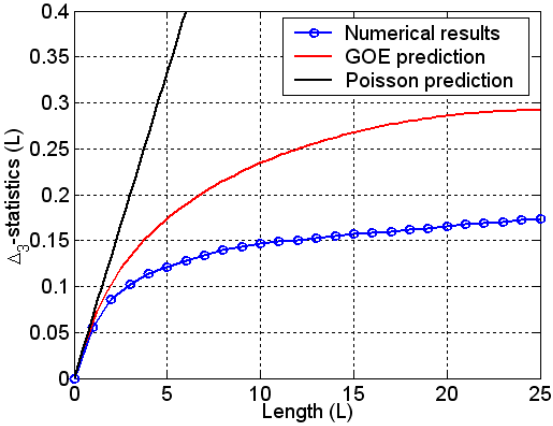

(g_2) Mode 95

Figure 89: Results for natural frequency statistical observables for Gaussian spatially-correlated random rods (ensemble averaging approach). Plot (a): Mode 10. Plot (b): Mode 20. Plot (c): Mode 35. Plot (d): Mode 40. Plot (e): Mode 65. Plot (f): Mode 80. Plot (g): Mode 95.

As shown in Figure 89, the effects of the spatial correlation vary significantly in the frequency range investigated. For mode 10, corresponding approximately to a frequency of 5 kHz, the natural frequency statistics presents deterministic-GOE transition statistics characteristics. The high spectral rigidity characteristics are clearly established due to the low performance of the randomization process. Indeed, the typical wavelength of mode 10 is higher than the values adopted for the correlation lengths, $\bar{\lambda}_{10} \gg L_c$. For mode 20, corresponding approximately to a frequency of 10 kHz, the spatial correlation effects are substantial and a tend toward the establishment of GOE statistics is observed in the small spacing range, breaking the high spectral rigidity characteristics. On the other hand, the correlation effects are not effective for large spectral distances and some residual spectral rigidity characteristics are still observed in the results for the long-range fluctuation statistical observables.

Although it not shown here in detail, for modes that lie in the mode order range of modes 40-65, corresponding approximately to the frequency range of 20,7 kHz to 34,0 kHz, the GOE statistics is satisfactorily established

for short and long spectral distances and an excellent agreement with the RMT predictions is also observed. Beyond this GOE region, the performance of the randomization process becomes inefficient since the typical wavelength is expected to be less than the correlation length values, $\bar{\lambda}_{modes>70} \ll L_c$. In fact, the spatial correlation effects are clearly minimized as the mode order increases and the spectral rigidity characteristics are again gradually reestablished. The natural frequency statistical observable results for modes 80 and 95 showed the establishment of an almost-nominal (deterministic) statistics where high spectral rigidity characteristics are clearly observed.

Natural Frequency SEA Parameter: Statistical Overlap Factor

In the SEA context, the statistical overlap factor has been traditionally used to verify the applicability of the GOE model to random engineering systems. In Figure 90, the global and local natural frequency spacings, and natural frequency standard deviations, as well as the respective statistical overlap factor results, are presented in terms of mode order domain.

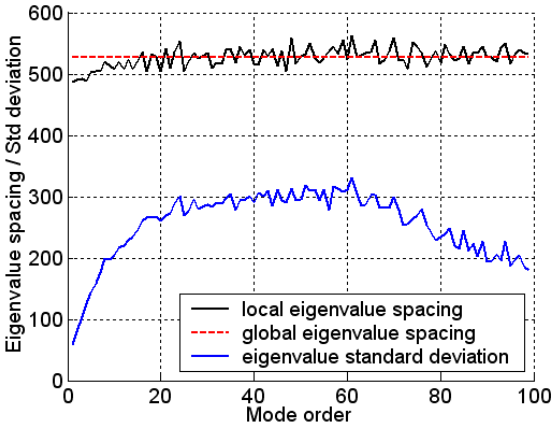

(a)

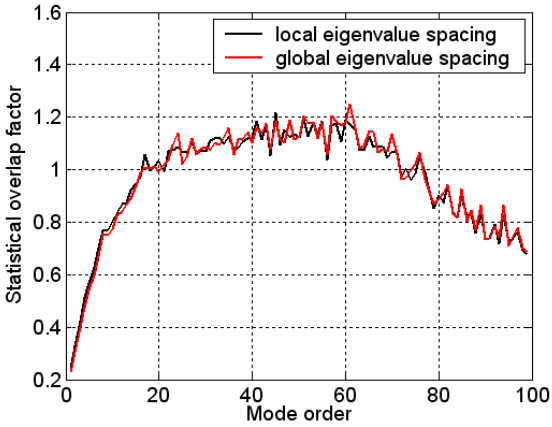

(b)

Figure 90: Statistical overlap factor results for a Gaussian spatially-correlated rod ensemble (ensemble averaging approach). Plot (a): global natural frequency spacing, local natural frequency spacings, natural frequency standard deviations. Plot (b): Statistical overlap factor: based on the definitions of global and local mean values for the natural frequency spacings.

As shown in Figure 90 (a), the standard deviation values are less than natural frequency spacing values throughout the mode order domain investigated. Additionally, it is also observed that the performance of the randomization process is satisfactory uniform in the central region of the frequency domain investigated, since the local and global natural frequency spacing values are very similar.

According to the statistical overlap factor results, Figure 90 (b), the establishment of GOE statistics would be expected for modes where the statistical overlap factor values are large than unity, that is, the frequency range is approximately from 8 kHz to 40 kHz (or the corresponding mode order region which comprises approximately modes 16-77). Conversely, based on the previous results for the natural frequency statistical observables, it can be concluded that the statistical overlap factor analysis clearly failed to identify the frequency region in which the GOE model is applicable to natural frequency statistics. Indeed, the good and satisfactory agreement between the GOE predictions and natural frequency statistics is only observed approxi-

mately in the frequency range of 18 kHz to 35 kHz.

Mode Shape Statistics

In Figure 91, the spatial kurtosis results for each member are presented in terms of the mode order domain. The probabilistic mode values as well as the arithmetic and geometric mean values are also presented. The analytical predictions for sinusoidal and GOE mode shapes are also plotted.

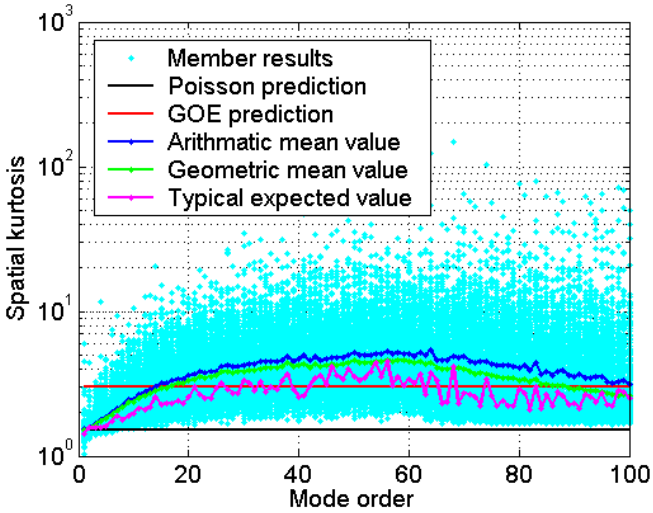

Figure 91: Spatial kurtosis results for the Gaussian spatially-correlated rods: individual members, probabilistic mode, arithmetic and geometric mean values and analytical predictions (sinusoidal and GOE) (spatial averaging approach).

As presented in Figure 91, a high dispersion of spatial kurtosis values is observed throughout the mode order domain. The distinct mean values obtained from the arithmetic and geometric averaging processes clearly evidence a possible establishment of the long-tail distribution characteristics for the mode shapes. Additionally, the high values for the spatial kurtosis are associated with the occurrence of the structural localization phenomenon in the mode shapes, mainly beyond mode 20, Hodges and Woodhouse (139, 140).

Considering again the spatial kurtosis results in Figure 91, the probabilistic mode values suggest that the largest number of Gaussian modes, in terms of the spatial mode shape domain, occurs mainly in the mode order region from mode 35 to mode 65 (approximately from 18 kHz to 34 kHz). In Figure 92, the spatial Lilliefors Test results are presented for individual member values and arithmetic mean values also are plotted.

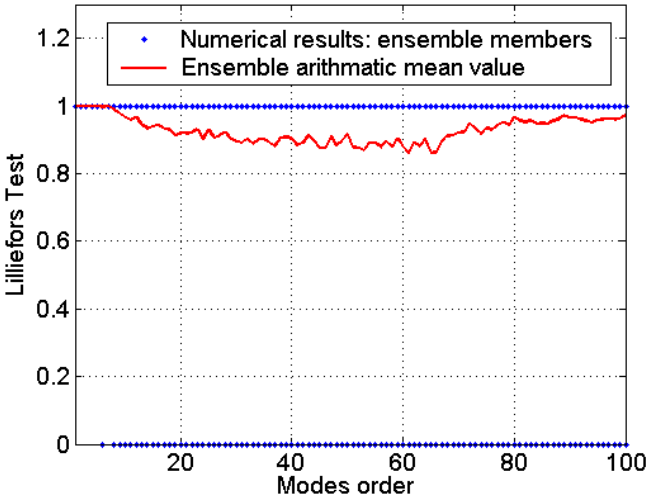

Figure 92: Spatial Lilliefors Test results for the Gaussian spatially-correlated rod ensemble: individual member values and arithmetic mean values (spatial averaging approach).

As shown in Figure 92, the establishment of Gaussian modes in the spatial mode shape domain is expected at least for one member of the ensemble for the mode order range beyond mode 10. Additionally, the results suggest that the largest number of Gaussian mode across the ensemble occurs in the mode order range from mode 35 to mode 70 (approximately from 18 kHz to 36 kHz), where it is expected that approximately 10% of the members have Gaussian mode shape characteristics. Outside this mode order region, a reduced establishment of spatial Gaussian mode shapes is observed and thus less than 10% of the members are expected to have mode shapes with Gaussian characteristics.

In order to assess the establishment of spatial Gaussian mode shapes across the ensemble, the spatial Lilliefors Test results from each member are presented in terms of the mode order domain, Figure 93 (a). The points represent the mode shapes for which the Gaussian hypothesis is held in the spatial mode shape averaging approach. In general, the spatial Lilliefors Test results suggest that the establishment of Gaussian modes is approximately uniform across the ensemble for most mode orders, showing the good performance of the randomization process adopted. In Figure 93 (b), the total number of Gaussian mode shapes is presented for each ensemble member. Rather than presenting the results with the member number on the x-axis, the results are presented in terms of the particular correlation length (L_c) associated with each member of the ensemble.

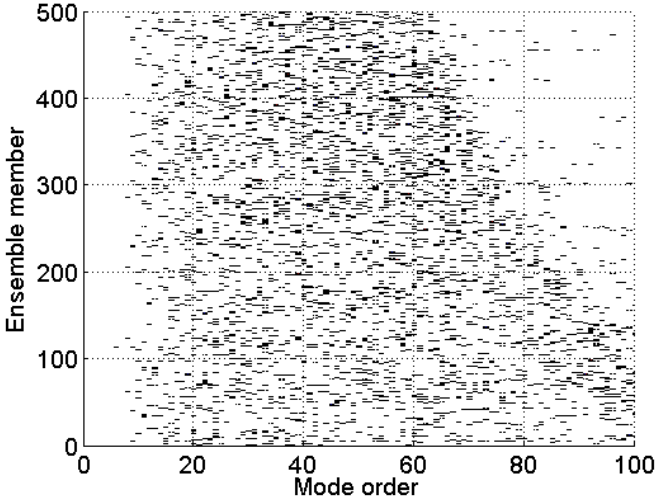

(a)

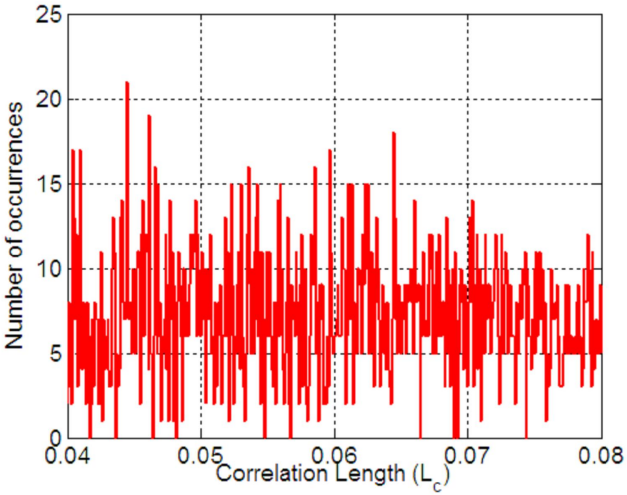

(b)

Figure 93: Spatial Lilliefors Test results in terms of: (a) member number and (b) correlation length associated with each member of the ensemble (spatial averaging approach).

Another relevant characteristic of the mode shapes is the degree of statistical independence of a fixed mode shape component associated with the excitation point. For the case of complete statistical independence, it is expected that the distribution of the mode shape amplitudes associated with a given excitation point is Gaussian. In Figure 94, the spectral kurtosis results for each member are presented in terms of the spatial coordinate domain. The probabilistic mode values are also presented along with the arithmetic and geometric mean values. The analytical predictions for sinusoidal and GOE mode shapes are plotted.

As presented in Figure 94, a high dispersion of the spectral kurtosis values is observed mainly in the rod regions close the ends. Additionally, the expected mean and typical values are highest in these rod regions. For the central rod region, the spectral kurtosis mean values tend asymptotically toward a kurtosis value slightly lower than the GOE prediction value.

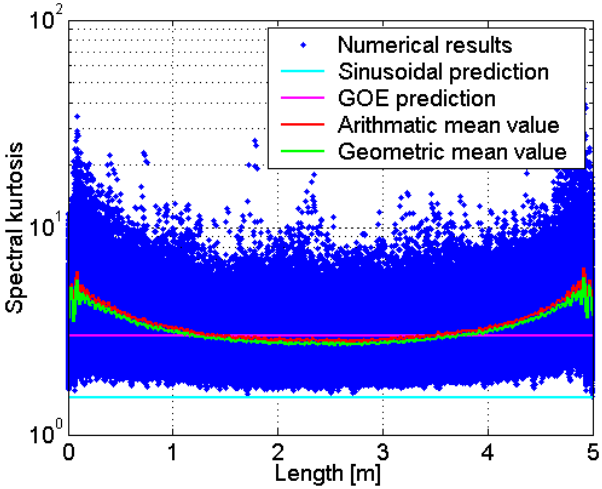

Figure 94: Spectral kurtosis results for the Gaussian spatially-correlated rods: individual members, probabilistic mode, arithmetic and geometric mean values and analytical predictions (sinusoidal and GOE) (spectral averaging approach).

The ensemble mean values of the spectral kurtosis obtained from the arithmetic and geometric averaging processes differ slightly, suggesting a weak effect of the long-tail distribution characteristics on the mode shapes. In Figure 95, the spectral Lilliefors Test results are presented for individual members and arithmetic mean values also are plotted.

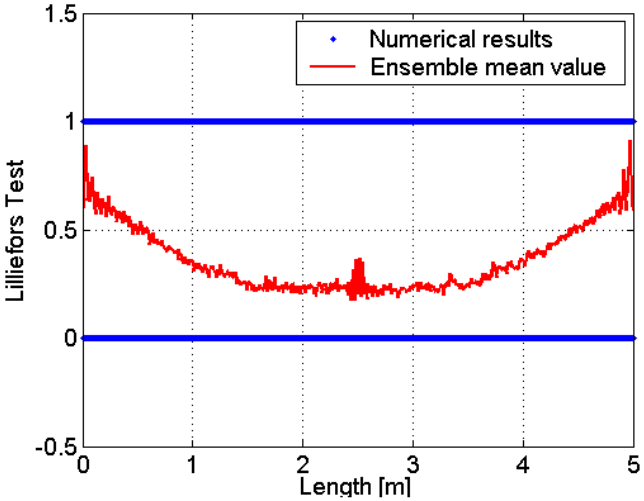

Figure 95: Spectral Lilliefors Test results for the spatially-correlated rod ensemble: individual member values and arithmetic mean values (spectral averaging approach).

As shown in Figure 95, the establishment of Gaussian modes in the spectral averaging approach is expected at least for a member of the ensemble, regardless of the excitation point location. Additionally, the averaged results suggest that the largest number of Gaussian modes across the ensemble occurs in the central rod region, circa 80 % of the members. For other rod regions, a gradual decrease in the number of Gaussian modes across the ensemble is observed from the central to end regions. According to the averaged spectral Lilliefors Test results across the ensemble, the percentages of members which have Gaussian mode shapes on the excitation points X_0, X_2 and X_3 are approximately 27%, 80% and 57%, respectively.

Considering the *ensemble mode shape averaging approach*, the ensemble kurtosis results, as well as their mean and typical values, are shown as a function of mode order in Figure 96. The GOE and sinusoidal analytical predictions are also plotted.

As shown in Figure 96, a high dispersion is expected for all mode orders. Extremely large ensemble kurtosis values are also observed for some mode orders mainly in the mid and high mode order ranges.

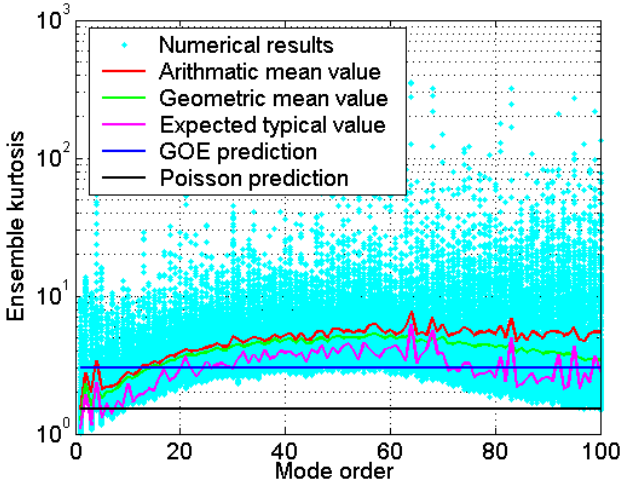

Figure 96: Ensemble kurtosis results for the Gaussian spatially correlated rods: individual member, probabilistic mode, arithmetic and geometric mean values (ensemble averaging approach).

The ensemble averaged results indicate that as the frequency (or mode order) increases, a statistical transition occurs for the mode shapes of the approximately sinusoidal to localized statistics. On the other hand, the typically expected values of the ensemble kurtosis are lower than both the mean values throughout the mode order range and indicate that mode shape statistics similar to GOE are expected to be established for the mode order ranges of approximately modes 17-33 and modes 70-80 (corresponding to the frequency ranges of 7.5 kHz to 18 kHz and 37 kHz to 42 kHz, respectively). For the mode order range of modes 33-70 (corresponding to the frequency range of 18 kHz to 37 kHz), the typical kurtosis results are slightly greater than the GOE values and suggest the establishment of a weak localization phenomenon across the ensemble.

In order to identify the most probable mode shape component (*i.e.*, excitation point) and mode order range (or frequency range) for the establishment of GOE statistics across the ensemble, the ensemble Lilliefors Test results are plotted in a bi-dimensional graphical representation, Figure 97 (a).

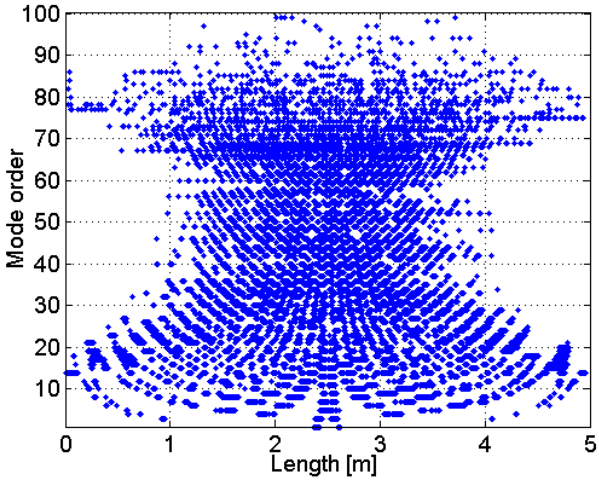

(a)

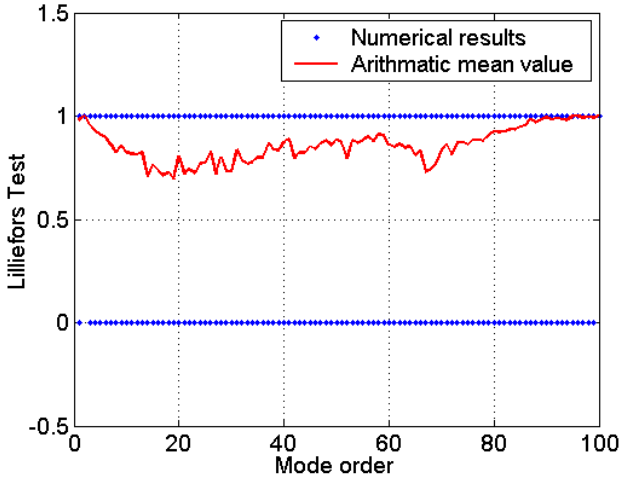

(b)

Figure 97: Ensemble Lilliefors Test results for a Gaussian spatially-correlated rod ensemble (ensemble averaging approach). Plot (a): bi-dimensional graphical representation. Plot (b): individual member and the mean values as a function of the mode order value.

As shown in Figure 97 (a), the large amount of points associated with the central rod region shows the high probability of the establishment of GOE statistics across the ensemble for these mode shape components. In Figure 97 (b), the mean value of the Lilliefors Test results across the ensemble for each mode order value suggests that the mode order region with the largest probability for the establishment of a Gaussian distribution for the mode shape components is approximately from mode 15 to mode 35 (corresponding to the frequency range of 7.5 kHz to 18 kHz). Beyond this region, a reduced number of Gaussian distributed mode shape components is clearly observed due to the establishment of localization phenomenon in the ensemble averaging approach, including the mode order from mode 70 to 80.

Mode Shape SEA Parameters: Normalized Parameters *P* and *Q*

In Figure 98, the results for the normalized parameters P and Q, (P_a and Q_a respectively), are presented as a function of the mode order value. Considering that for parameter P_a values larger than $P_a = 0.4$ the establishment of GOE statistics is expected (20), the current parameter P_a results suggest that the complete establishment of GOE statistics occurs beyond mode 08, Figure 98 (a). These results clearly show that the performance of parameter P_a is totally unsatisfactory under particular situations, since this parameter does not take into account the crossing phenomenon of natural frequencies due to the presence of system randomness, Kessissoglou and Langley (80) and Cordioli (20). As discussed by Cordioli (20), the parameter P is expected to have a performance similar to the statistical overlap factor, which fails when the system is randomized in particular ways or has the presence of geometrical symmetries.

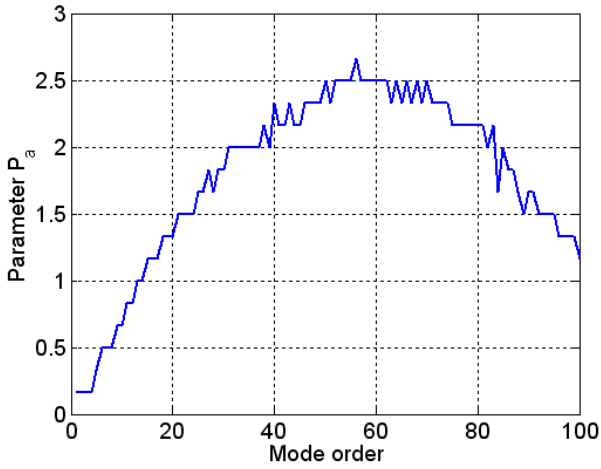

(a)

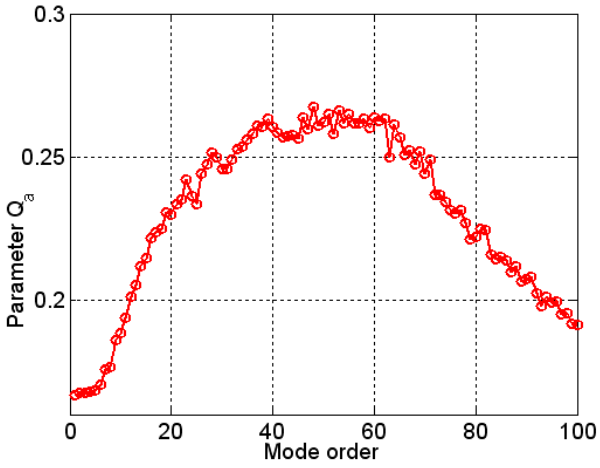

(b)

Figure 98: Mode shape normalized SEA parameters of the Gaussian spatially-correlated random rods (ensemble averaging approach). Plot (a): parameter P_a. Plot (b): parameter Q_a.

Considering the parameter Q_a analysis, Figure 98 (b), the establishment of GOE statistics is expected for values higher than $Q_a = 0.25$, Cordioli (20). Thus, the current parameter Q_a results suggest that the establishment of GOE statistics for the mode shapes is expected to occur for the mode order range of approximately mode 35 to mode 70 (corresponding to the frequency range of 18 kHz to 37 kHz). Surprisingly, it can be observed that conclusions similar to those for parameter Q_a were also obtained from the typically expected spatial kurtosis values in Figure 91.

In Figure 99, the parameter Z results are plotted for the spatially-correlated rods.

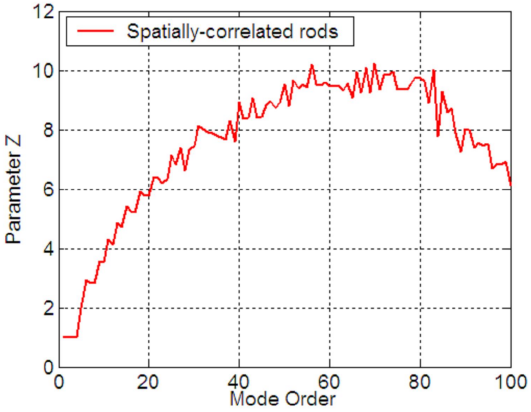

Figure 99: Mode shape SEA parameter of the spatially-correlated rod ensemble: parameter Z (ensemble averaging approach).

As shown Figure 99, the parameter Z results show the highest number of superimposed spectra occurs for mid frequency range. For this frequency range, a large level of spatial interference occurs between the typical longitudinal wavelength and the geometrical irregularities.

On the other hand, for high frequency range, the performance of the randomization process becomes inefficient since the typical wavelength is expected to be smaller than the correlation length values, $\bar{\lambda}_{modes>80} \ll L_c$. In fact, the spatial correlation effects are clearly minimized as the mode order increases and the establishment of an almost-nominal (deterministic) characteristics for both modal parameters statistics is strongly expected. In this

regard, the reduction of parameter Z amplitudes for higher mode orders reflects this situation and the number of non-interacting spectra is gradually decreased as mode order increases.

Kinetic Energy Density Statistics: Spatially-Averaged Random Rod Responses

In a manner similar to previous analysis performed with the mass-loaded rod ensemble, the mean and relative variance values of the kinetic energy density results were also evaluated across the Gaussian spatially-correlated rod ensemble. Two excitation natures are considered: unity single point-loading on the X_0, X_2 and X_3 excitation points and spatially-averaged excitation. Analytical predictions based on the Poisson and GOE modal parameter statistics are compared to all numerical results.

In the current analysis, two approaches to the damping loss factor parameter are considered. The first approach considers a frequency-constant value which is equal to $\eta = 0.03$. This DLF approach with a low and frequency-constant value allows an accurate visualization of the contributions of modal parameter statistics to the kinetic energy density statistics. In the second approach, the DLF is defined as being inversely proportional to the frequency and proportional to the longitudinal sound speed, Equation (3.19). This second DLF approach removes the effects of the distinct degrees of modal superposition.

In Figure 100, the spatially-averaged kinetic energy density results are presented for both damping loss factor approaches. The results for some members along with the arithmetic and geometric mean values are plotted. Additionally, the analytical SEA prediction is also plotted.

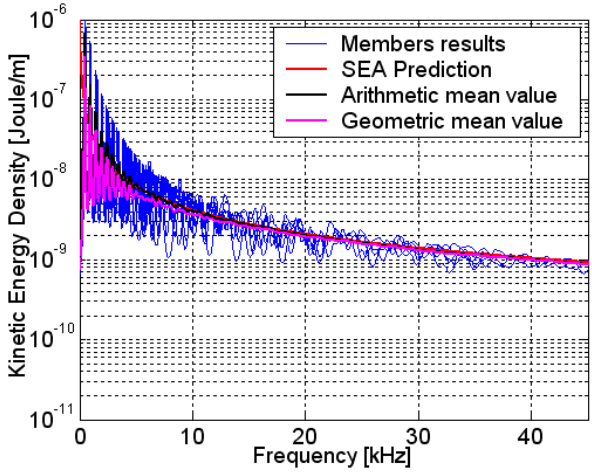

(a)

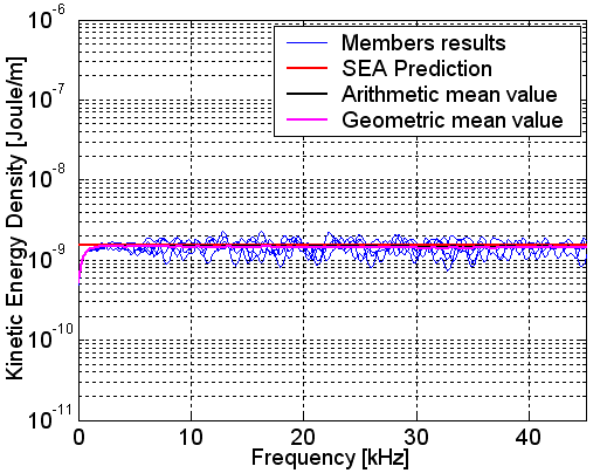

(b)

Figure 100: Kinetic energy density results for spatially-averaged excitation: some individual members, ensemble arithmetic and geometric mean values and SEA predictions (ensemble averaging approach). Plot (a): frequency-constant DLF. Plot (b): constant modal superposition DLF.

As shown in Figure 100 (a), an excellent agreement was obtained between the SEA predictions and ensemble mean values, mainly in the mid and high-frequency ranges, regardless of the averaging process adopted. The same conclusion can be extended to the constant modal superposition energy results throughout the frequency domain, since the modal overlap factor amplitude is greater than unity and the SEA basic assumptions are guaranteed, Figure 100 (b).

In Figure 101, the relative variance of the spatially-averaged kinetic energy density results and analytical predictions are plotted. The evaluation of the spatially-averaged relative variance results was based on the arithmetic and geometric mean values.

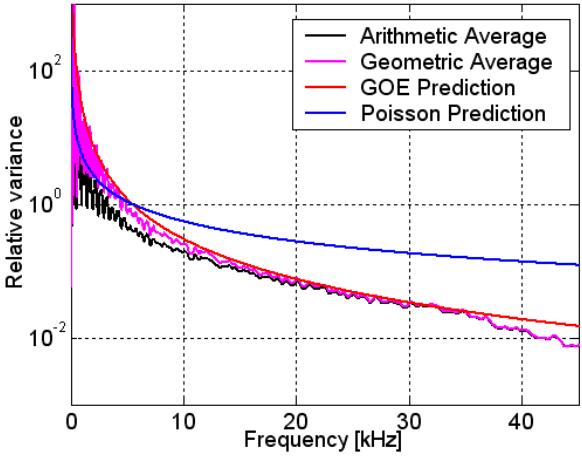

(a)

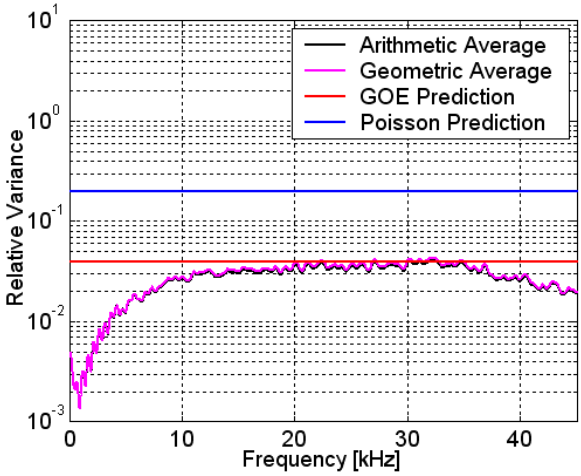

(b)

Figure 101: Ensemble relative variance of spatially-averaged kinetic energy density results based on: arithmetic and geometric mean values. The analytical predictions are based on Poisson and GOE models (ensemble averaging approach). Plot (a): frequency-constant DLF. Plot (b): constant modal superposition DLF.

As shown in Figure 101, the numerical relative variance results conform very well with the GOE analytical predictions for the frequency range of 18 kHz to 35 kHz, which corresponds approximately to the mode order range of modes 35-70. Indeed, this excellent agreement can be attributed to two main factors: (*i*) the natural frequency statistics has GOE characteristics in this frequency range and (*ii*) the mode shape effects are completely removed from the ensemble statistics of the kinetic energy density responses due to the spatially-averaged characteristics of the excitation. Outside this frequency range, the low values for the relative variance are associated with the establishment of the high spectral rigidity characteristics in natural frequency statistics and low perturbation of the natural frequency locations across the ensemble.

Considering the mean and relative variance results obtained from the arithmetic and geometric averaging processes, the substantial effects of the use of the distinct averaging processes are only observed in the low-frequency

range, exclusively for the case of a frequency-constant DLF, Figure 101 (a). In order to investigate these effects, the histogram of the kinetic energy density results across the ensemble for distinct conditions of modal superposition are presented in Figure 102.

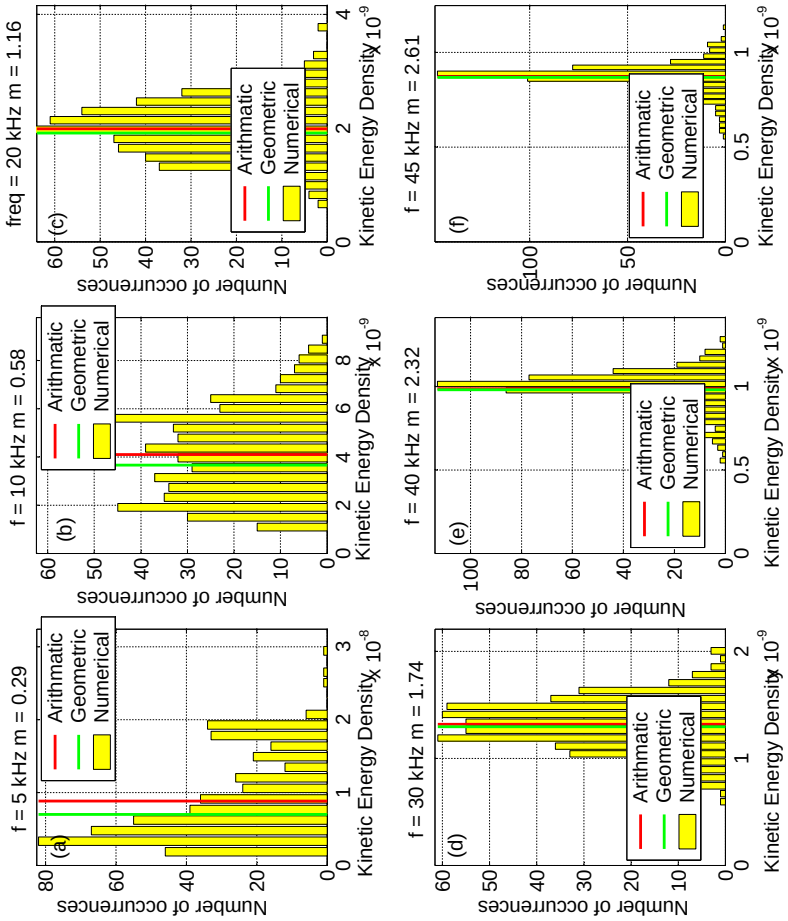

Figure 102: Histogram of the spatially-averaged kinetic energy density responses for Gaussian spatially-correlated rods excited by spatially-averaged forces, $\eta = 0.03$, 500 members, at various frequencies f (or the modal overlap factors m). The arithmetic and geometric mean values are also presented.

As shown in Figure 102 (a), the kinetic energy response distribution for the low-frequency region (or low modal superposition condition) presents a probabilistic distribution with long tail characteristics where the probabilistic mode value is clearly distinct from the arithmetic and geometric mean values. For the kinetic energy response distribution of the excitation frequency $f = 10kHz$ (or modal overlap factor $m = 0.58$), Figure 102 (b), the probabilistic mode value remains distinct for both mean values and an initial statistical transition from the long tail to Gaussian statistics can be observed. Indeed, the typically expected value across the ensemble clearly differs from the mean values obtained from the arithmetic and geometric averaging processes.

In Figures 101 (a) and 102 (a), the effects of non-Gaussian and long tail distribution characteristics of the kinetic energy density responses are clearly observed, since the arithmetic and geometric values are substantially distinct. Additionally, it is expected that the effects of long tail distribution characteristics become increasingly substantial for higher statistical moments of the kinetic energy density responses.

On the other hand, for the frequency region where the natural frequency statistics conforms well to the GOE model, Figures 102 (c) and (d), the probabilistic distribution of the kinetic energy density responses are typically Gaussian and thus the arithmetic and geometric mean values, as well as the probabilistic mode value, are approximately coincident.

For the high frequency range, Figures 102 (e) and (f), the performance of the randomization is reduced and a small dispersion of the energy density results is observed. The probabilistic distribution of the energy density results is clearly peaked and the two mean values and the probabilistic mode value are almost identical.

Although it is not presented here in detail, for the case of constant modal superposition DLF, the degree of modal superposition is high enough to guarantee that the long tail distribution effects are minimized and thus identical amplitudes are obtained in the arithmetic and geometric averaging processes. Indeed, as shown in Figures 100 (b) and 101 (b), the mean and relative variance values are identical for the two averaging processes in the frequency range investigated.

Kinetic Energy Density Statistics: Point-Loaded Random Rod Responses

Considering the kinetic energy density responses of the Gaussian spatially-correlated random rods subjected to a unitary single point-loading

at excitation points X_0, X_2 and X_3, the arithmetic mean values and corresponding relative variances were evaluated for both damping loss factor approaches. In Figure 103, the statistical parameters of the kinetic energy density results are presented for each excitation point. In these results, frequency-constant and constant modal superposition DLF approaches are considered. The analytical SEA predictions based on the Poisson and GOE models are also plotted.

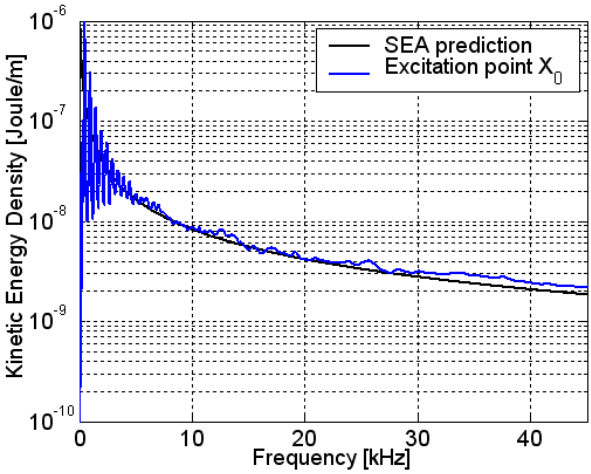

(a)

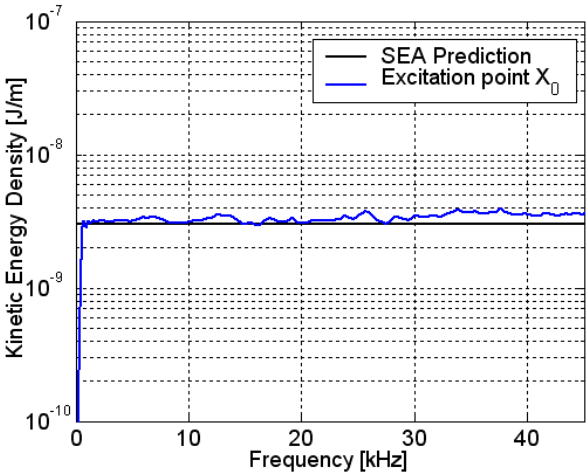
SEA Prediction
Excitation point X0
Kinetic Energy Density [J/m]
Frequency [kHz]
10^-7
10^-8
10^-9
10^-10
0
10
20
30
40

(b)

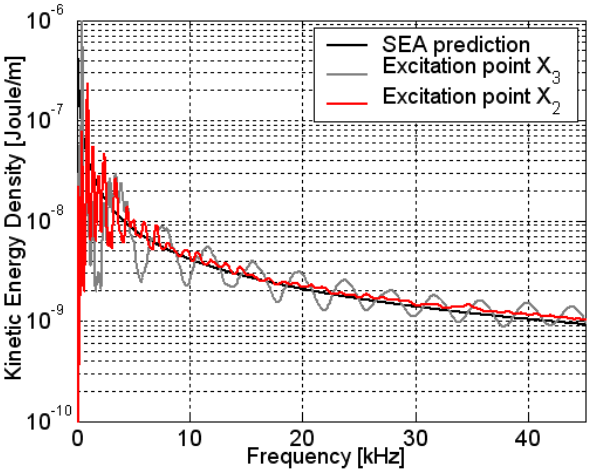
SEA prediction
Excitation point X3
Excitation point X2
Kinetic Energy Density [Joule/m]
Frequency [kHz]
10^-6
10^-7
10^-8
10^-9
10^-10
0
10
20
30
40

(c)

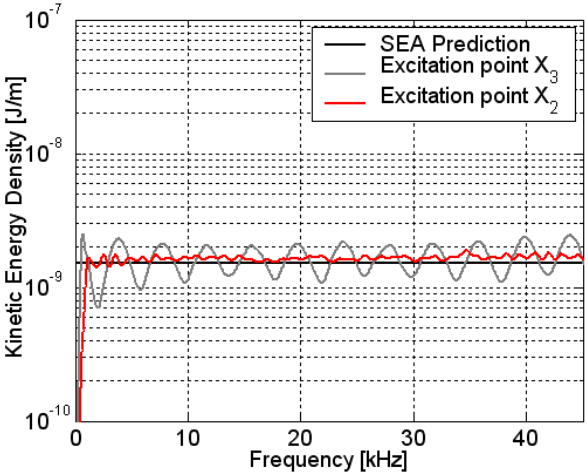
SEA Prediction
Excitation point X3
Excitation point X2
Kinetic Energy Density [J/m]
Frequency [kHz]

(d)

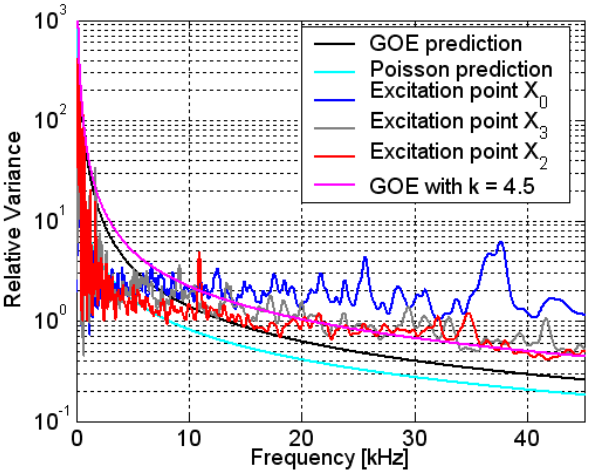
GOE prediction
Poisson prediction
Excitation point X0
Excitation point X3
Excitation point X2
GOE with k = 4.5
Relative Variance
Frequency [kHz]

(e)

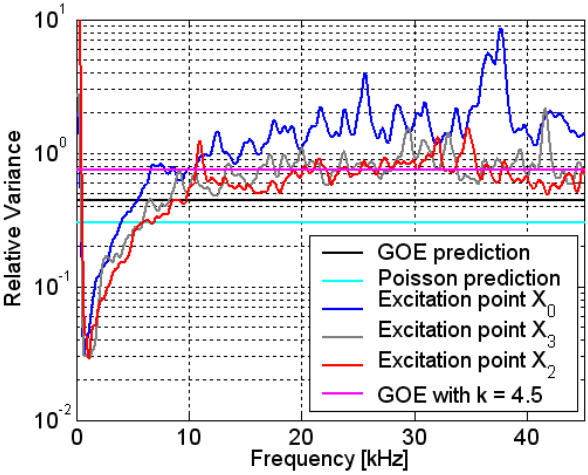

(f)

Figure 103: Kinetic energy density results for single point-excited Gaussian spatially-correlated rods (ensemble averaging approach). Plot (a): arithmetic mean results - excitation point X_0 and frequency-constant DLF. Plot (b): arithmetic mean results - excitation point X_0 and constant modal superposition DLF. Plot (c): arithmetic mean results - excitation points X_2 and X_3 and frequency-constant DLF. Plot (d): arithmetic mean results - excitation points X_2 and X_3 and constant modal superposition DLF. Plot (e): relative variance results - excitation points X_0, X_2 and X_3 and frequency- constant DLF. Plot (f): relative variance results - excitation points X_0, X_2 and X_3 and constant modal superposition DLF.

As shown in Figures 103 (a) - (d), an excellent agreement is observed between all numerical mean results and the analytical SEA predictions, regardless of the DLF approach adopted. Indeed, these results showed that the mean values for the kinetic energy responses are not very sensitive to the statistical characteristics of modal parameters.

Considering the relative variance results, Figures 103 (e) and (f), a poor agreement between the numerical results and the analytical GOE and Poisson predictions is observed. Indeed, the numerical results of the relative variance for point-loading conform approximately to the GOE predictions only in limited frequency ranges and the limits of these ranges vary for each

of the excitation points. Additionally, the relative variance results also suggest that the spatial location of the excitation point seems to affect the degree of the establishment of GOE statistics in the energy results.

At most frequencies, the numerical results are higher than the GOE predictions, mainly in the mid and high-frequency ranges. For the excitation point X_0, some peaks of the relative variance are higher than unity. On the other hand, the variance results for the excitation points X_2 and X_3 are slightly higher than the GOE prediction and present similar behaviors in the mid and high-frequency ranges. Additionally, a modified GOE prediction with $K > 3$ was also evaluated for several values of K and the best fitted results for excitation points X_2 and X_3 were obtained with approximately $K = 4.5$, which corresponds to a mode shape statistics with weak localization characteristics.

In the following, the mean and relative variance of the kinetic energy density results associated with excitation points X_0, X_2 and X_3 are discussed and assessed in terms of modal parameter statistics. The contributions of mode shape statistics are identified and discussed. In order to undertake this task, the ensemble and spectral mode shape statistics results from each excitation point are presented in detail. Additionally, the performance of averaging processes in the evaluation of the typically expected values across the ensemble is investigated in terms of the mean and relative variance values of the kinetic energy density responses.

Statistical Analysis of Excitation Point X_2

Considering initially the energy results for the excitation point X_2, some individual member values, the analytical SEA prediction along with the arithmetic and geometric mean values of the kinetic energy density results are plotted in Figure 104.

As shown in Figure 104, distinct mean values are obtained from the arithmetic and geometric averaging processes. This fact clearly suggests that long tail, or asymmetric, distribution characteristics are presented in the kinetic energy density distribution across the ensemble. Hence, the typically expected values across the ensemble may not be accurately evaluated in the averaging processes. In Figure 105, the relative variance of the kinetic energy density results is presented for mean values evaluated from the arithmetic and geometric averaging processes. The analytical SEA variance predictions based on the Poisson and GOE models are also plotted.

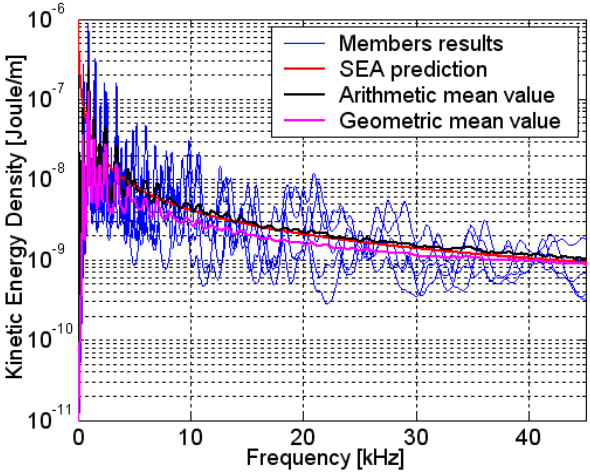

(a)

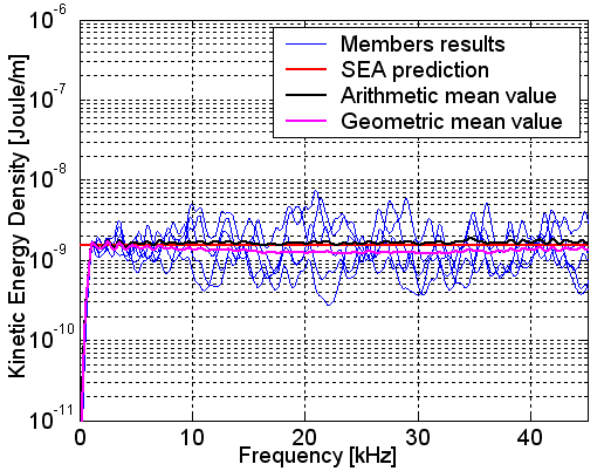

(b)

Figure 104: Kinetic energy density results for excitation point X_2 (ensemble averaging approach). Plot (a): frequency-constant DLF. Plot (b): constant modal superposition DLF.

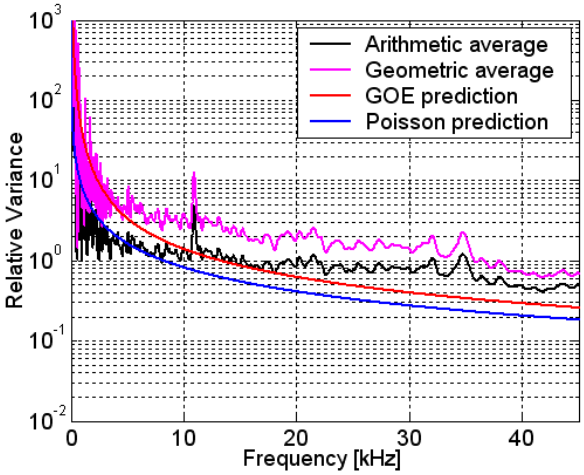

(a)

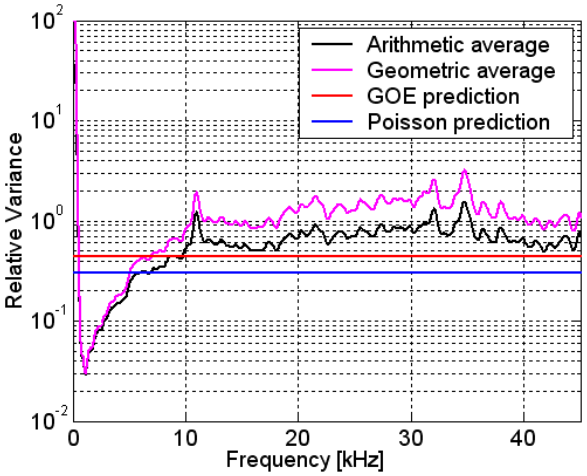

(b)

Figure 105: Relative variance of the kinetic energy density results for excitation point X_2 (ensemble averaging approach). Plot (a): frequency-constant DLF. Plot (b): constant modal superposition DLF.

As observed in Figure 105, two distinct frequency regions show a good agreement with the analytical predictions based on the GOE model. The first frequency range is approximately 6.5 kHz to 9.6 kHz (corresponding to modes 13-19) and the second range is 11.7 kHz to 18 kHz (corresponding to modes 23-35). It is important to note that these frequency ranges are clearly distinct to certain frequency range in which the natural frequency statistics is approximately described by the GOE model. As discussed previously, the establishment of GOE statistics for natural frequencies is expected to occur in the frequency range of 18 kHz to 35 kHz which corresponds, approximately, to the mode order range of mode 35 to mode 70. Indeed, these relative variance results seem to show that the mode shape contributions are more predominant in the kinetic energy density response than the natural frequency contributions for the single point-loaded rod ensemble investigated.

Considering the *ensemble mode shape statistics* results, Figure 106, the mode shapes associated with the first frequency range with GOE agreement have ensemble kurtosis values close to $K \sim 3$ and the corresponding skewness values are slightly positive, showing that the mode shape component distribution at excitation point X_2 is practically symmetric across the ensemble.

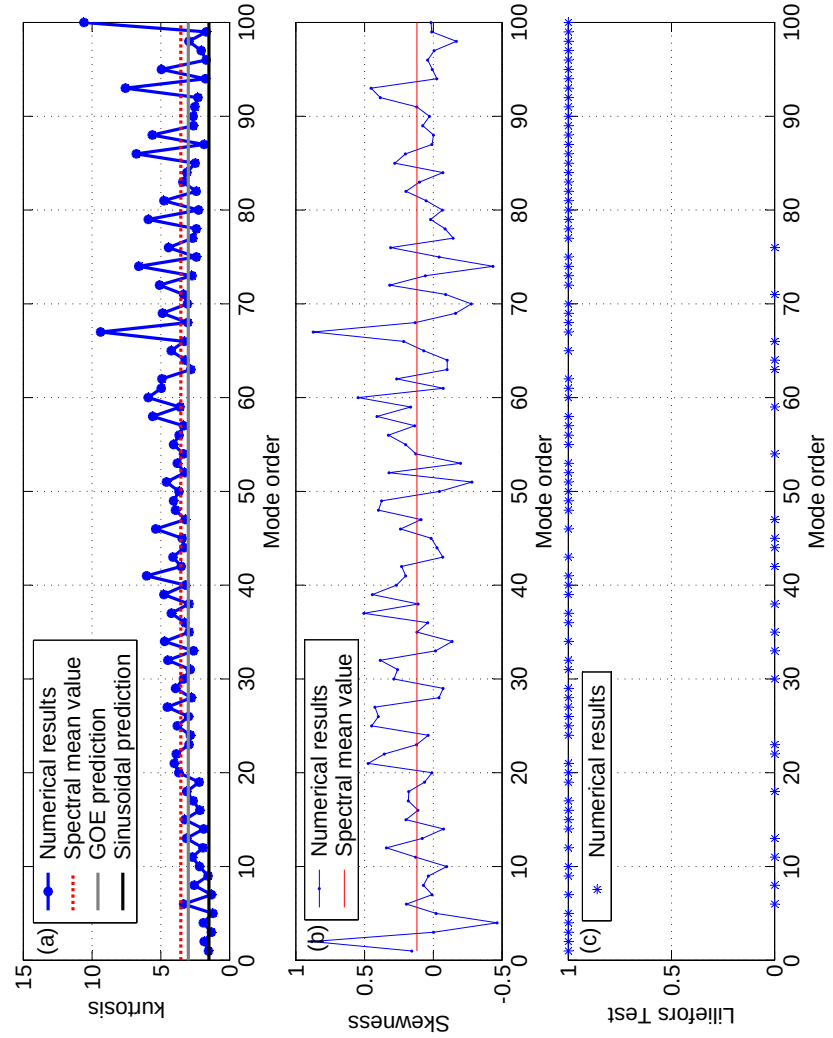

Figure 106: Ensemble statistics of the mode shape components at excitation point X_2 (ensemble averaging approach). Plot:(a) Kurtosis values, Plot (b): Skewness values. Plot (c): Lilliefors Test results.

In the second frequency range of the GOE agreement, from mode 23 to mode 35, the corresponding mode shapes are slightly localized, that is, $K \sim 3.5$, although, the mode shape component distribution at excitation point X_2 are practically Gaussian in the ensemble averaging approach. In Figure 107, an example of a PDF of the mode shape components across the ensemble at excitation point X_2 for $30th$ mode shape is shown in detail. It can be noted that the mode shape component distribution is approximately Gaussian since the Lilliefors test approves the normal distribution hypothesis, although the corresponding ensemble kurtosis value is slight higher than the Gaussian value.

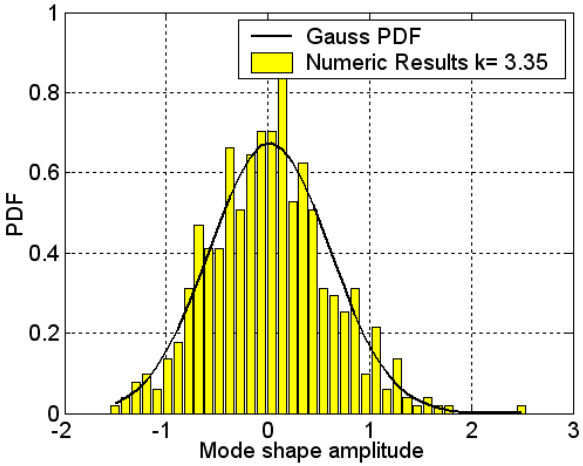

Figure 107: PDF of mode shape components at excitation point X_2 across the Gaussian spatially-correlated rod ensemble - $30th$ mode: numerical results and best-fit Gaussian PDF curve (ensemble averaging approach).

Considering again the relative variance results at excitation point X_2, Figure 105, the large peaks can be easily associated with higher ensemble kurtosis results. For example, the narrow peak at approximately 10.6 kHz is associated with the successive localization characteristics of modes 20 to 22 where the ensemble kurtosis values are weakly localized, that is, $K_{20-22} \sim 4$, Figure 106 (a). The other peaks centered at approximately frequencies 31 and 35 kHz are strictly associated with the localization characteristics of modes

60 to 62 ($K_{60-62} \sim 5$, moderately localized) and of mode 67 ($K_{67} \sim 10$, strongly localized), respectively. Considering the corresponding skewness results, the high positive or right skewness values are associated with these localized mode shapes and apparently suggest that the symmetry of the mode shape component distribution at the excitation point is also an important characteristic associated with the degree of agreement between the relative variance results and GOE predictions.

As shown in Figure 106, the ensemble kurtosis results suggest the establishment of some discrete localized mode shapes in high mode order range which are inserted among almost sinusoidal or GOE mode shapes. Additionally, the ensemble Lilliefors Test results showed clearly that the normal distribution hypothesis is rejected for these high-frequency modes. Indeed, the alternate sequence of localized and almost-nominal (deterministic), or GOE, mode shapes provides a smooth curve of relative variance with values higher than those of the GOE predictions in this frequency range.

Considering the *spectral mode shape statistics* in order to investigate the inter-modal correlation between the mode shapes of an ensemble rod member at excitation point X_2, the spectral kurtosis results at excitation point X_2 across the ensemble are shown in Figure 108. Additionally, a histogram of the spectral kurtosis results with their statistical parameters is shown.

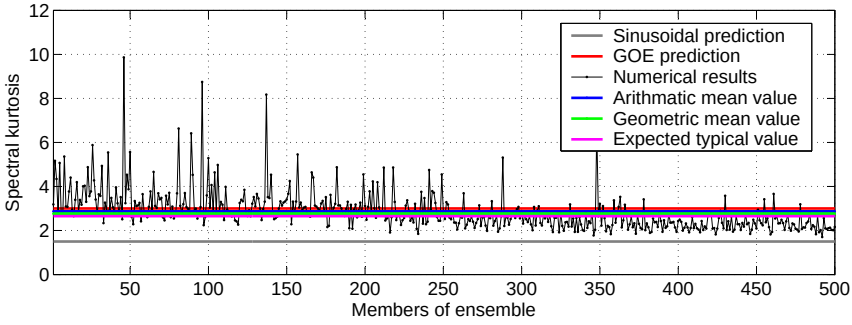

(a)

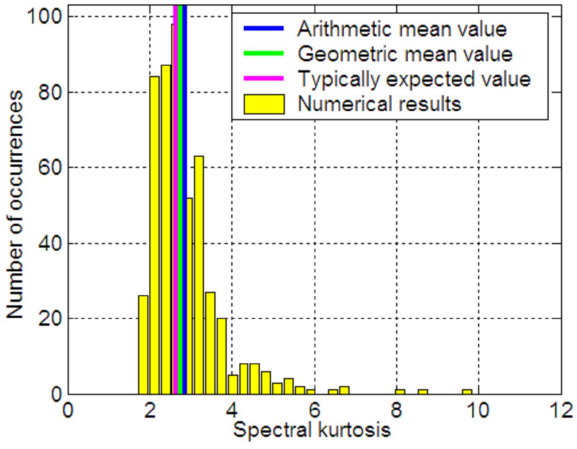

(b)

Figure 108: Spectral mode shape statistics parameters at excitation point X_2 (spectral averaging approach). Plot (a): individual ensemble member results, arithmetic and geometric mean values and sinusoidal and GOE analytical predictions. Plot (b): Histogram of spectral kurtosis results and their statistical parameters.

As shown in Figure 108 (a), most of the members have approximately Gaussian spectral kurtosis values, that is, $K \sim 3$. Additionally, the histogram of the spectral kurtosis results has a well defined peak in the region close to $K = 3$, although a small number of discrete high kurtosis values are observed, Figure 108 (b). These high kurtosis values present moderate localization characteristics and are associated with the first members of the ensemble, as observed in Figure 108 (a). The arithmetic and geometric mean and typically expected (probabilistic mode) values across the ensemble are respectively 2.87, 2.76 and 2.65. Indeed, the spectral kurtosis and Lilliefors Test results, Figure 108 (a) and Figure 95, suggest that for most of the ensemble members, circa 80%, the mode shapes can be considered to be practically Gaussian distributed at excitation point X_2. That is, it is expected that most of the ensemble members have approximately a Gaussian distribution for the mode shape components at excitation point X_2.

Statistical Analysis of Excitation Point X_0

Considering the kinetic energy results for the excitation point X_0, localized at the left rod end, some individual member values, the analytical SEA prediction along with the arithmetic and geometric mean values of energy density results are plotted in Figure 109.

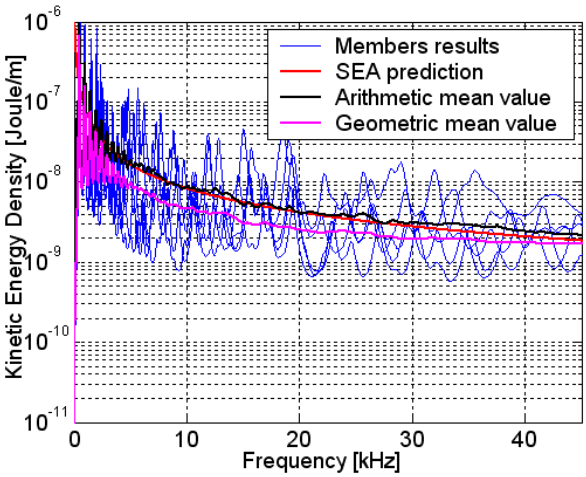

(a)

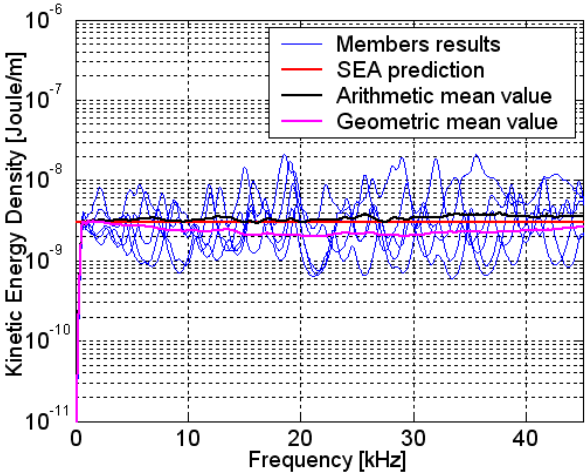

(b)

Figure 109: Kinetic energy density results for excitation point X_0 (ensemble averaging approach). Plot (a): frequency-constant DLF. Plot (b): constant superposition DLF.

As shown in Figure 109, the arithmetic-averaged energy numerical results conform well to the SEA predictions, although some small deviations are observed in the mid and high-frequency ranges. Additionally, distinct arithmetic and geometric mean values suggest the establishment of localization characteristics in the mode shapes, mainly in the mid-frequency range. Indeed, the establishment of a long tail distribution for the kinetic energy density results across the ensemble in mid-frequency range suggests strongly that typically expected values across the ensemble may be not be accurately evaluated in the arithmetic nor geometric averaging processes. In the high-frequency range, the correlation length effects of the randomization process on the mode shapes are gradually minimized as the excitation frequency increases and thus the two mean values tend to conform asymptotically well with the SEA predicted values.

In Figure 110, the relative variances of the kinetic energy density results are presented for the mean values obtained in the arithmetic and geometric averaging processes.

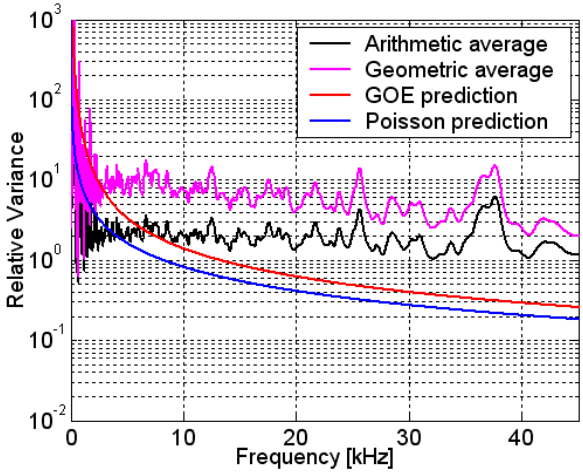

(a)

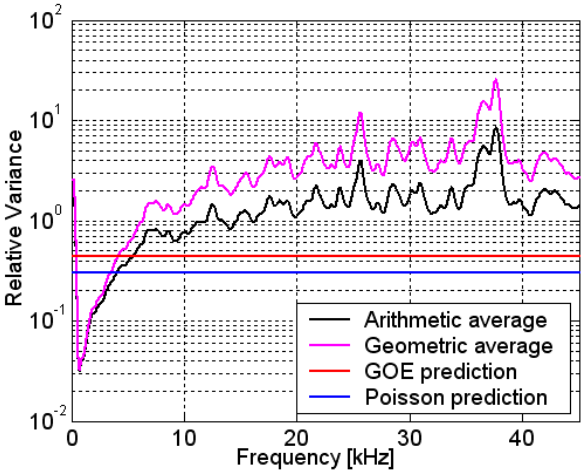

(b)

Figure 110: Relative variance of kinetic energy density results for excitation point X_0 (ensemble averaging approach). Plot (a): frequency-constant DLF. Plot (b): constant superposition DLF.

As observed in Figure 110, a very restricted and limited frequency region shows an approximate agreement between the numerical variance results based on the arithmetic mean value and the analytical predictions based on the GOE model. This frequency range is approximately from 5.5 kHz to 7.0 kHz (corresponding to modes 11-14). Additionally, it is also observed that the numerical variance results based on the geometric mean value are high and clearly overestimate the SEA variance prediction based on the GOE model for the frequency region investigated. These kinetic energy density results suggest that the ensemble variation in relation to typically expected (or mode probabilistic value) is expected to be substantially larger than the energy variance proposed by the SEA prediction based on the GOE model.

Considering the *ensemble mode shape statistics* results at excitation point X_0, Figure 111, the mode shapes associated with the frequency range with GOE agreement have ensemble kurtosis values close to $K \sim 3$ and the corresponding skewness values are slightly positive and present a smooth behavior.

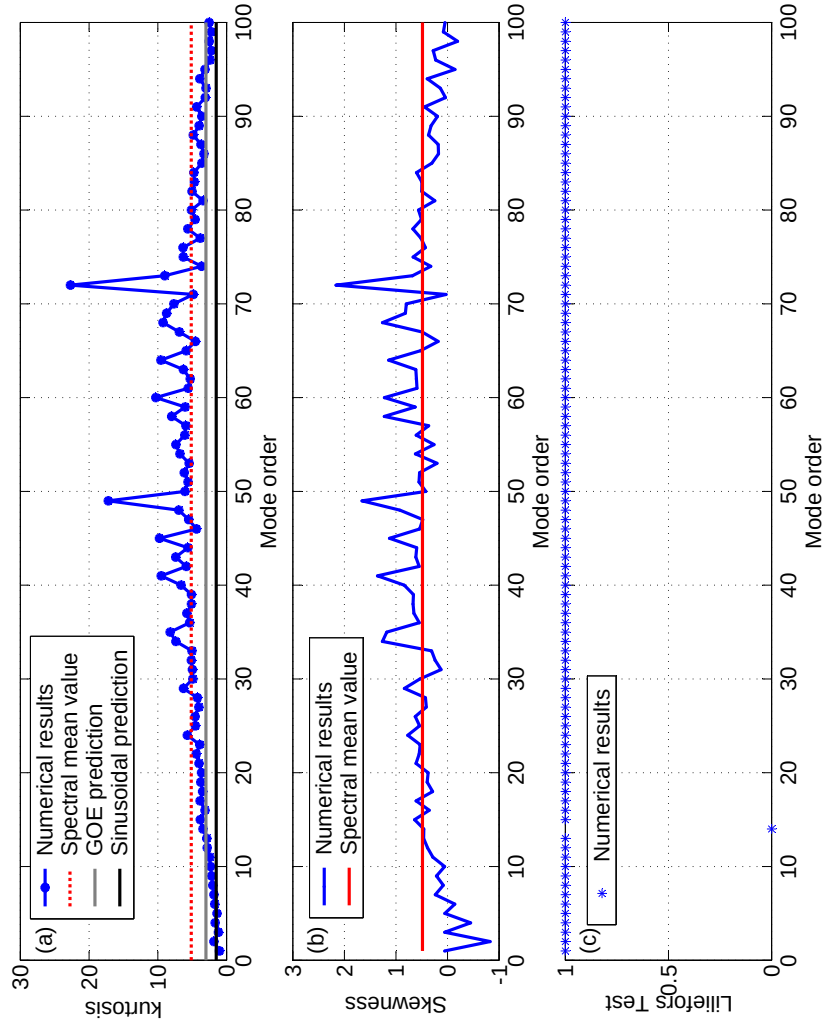

Figure 111: Ensemble statistics of the mode shape components at excitation point X_0 (ensemble averaging approach). Plot (a): kurtosis values. Plot (b): Skewness values. Plot (c): Lilliefors Test results.

As shown in Figure 111, most of the ensemble kurtosis values are around $K \sim 5$ and the corresponding skewness values are positive, suggesting that the mode shapes have moderate localization characteristics and are substantially asymmetric across the ensemble at excitation point X_0. The mode shape statistics results also show some discrete strongly localized mode shapes. In addition, it can be observed that most of ensemble kurtosis values lie in the following interval $1.5 \lesssim K \lesssim 8.5$ and the typically expected value for the ensemble kurtosis is well defined and is approximately located at $K \sim 5$. Additionally, some discrete high kurtosis values associated with strongly localized mode shapes with $K \sim 20$ are also observed. Indeed, the results for the statistical mode shape parameters across the ensemble suggest that the ensemble mode shape statistics at excitation point X_0 presents moderate localization characteristics for most of the mode order values, although the presence of some discrete strongly localized mode shapes is also expected.

Considering the results in Figure 110 for the relative variance at excitation point X_0, the large peaks in the relative variance may be associated with the high ensemble kurtosis results. For example, the narrow peak centered approximately at a frequency of 25 kHz is strictly associated with the localization characteristics of mode 49 ($K_{49} \sim 20$, strongly localized). The peak at approximately 36 kHz is correlated to successive localization characteristics of modes 68 to 70 where the ensemble kurtosis values are moderately localized, that is, $K_{68-70} \sim 8$, Figure 111. The adjacent peak centered at approximately frequency 37 kHz is strictly associated with the localization characteristics of mode 72 ($K_{72} \sim 20$, strongly localized).

For the high-frequency region, beyond mode 72 (approximately 38 kHz), the mode shapes present a statistical transition from moderate localization to almost-sinusoidal statistics as the frequency increases. Although, the ensemble kurtosis results suggest the establishment of some discrete GOE mode shapes, the Lilliefors Test results showed clearly that the normal distribution hypothesis is rejected for these modes in the high-frequency range. Indeed, this asymptotic behavior of the mode shapes toward sinusoidal statistics provides a smooth reduction in the relative variance values as the excitation frequency increases.

In Figure 112, the *spectral kurtosis* results for the excitation point X_0 across the ensemble are shown. Additionally, a histogram of the spectral kurtosis results and their statistical parameters can be observed.

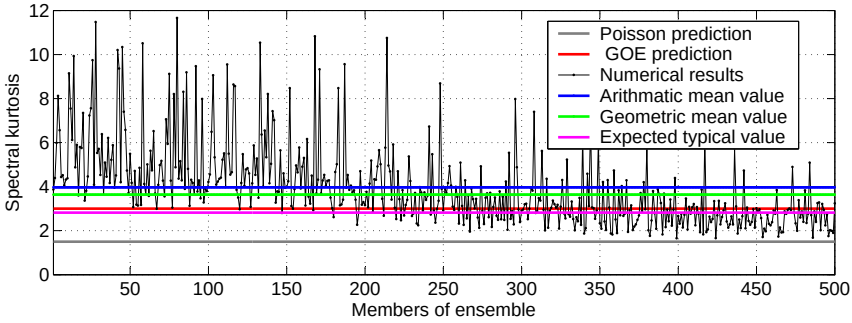

(a)

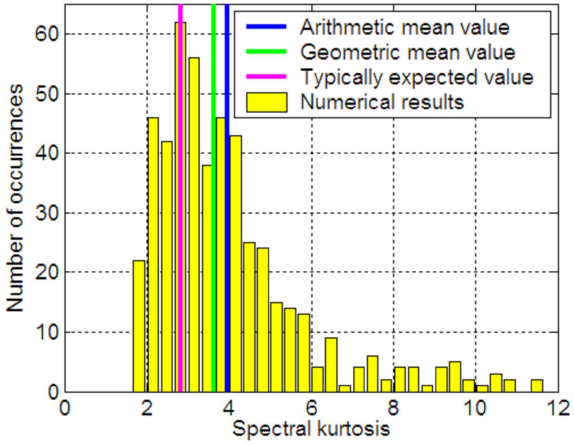

(b)

Figure 112: Spectral mode shape statistics parameters at excitation point X_0 (spectral averaging approach). Plot (a): individual member spectral kurtosis results, arithmetic and geometric mean values and sinusoidal and GOE analytical predictions. Plot (b): Histogram of spectral kurtosis results and their statistical parameters. The typically expected, arithmetic and geometric mean values are respectively 2.82, 3.97 and 3.63.

As shown in Figure 112 (a), most of the first members of the ensemble have high spectral kurtosis values, which suggests the establishment of weak

and moderate localization characteristics of the mode shapes. Conversely, for the last members, the spectral kurtosis values show asymptotic reestablishment of the nominal characteristics due to the low performance of the randomization process.

In Figure 112 (b), the histogram of the spectral kurtosis values also suggests a substantial number of discrete high kurtosis values, which leads to the establishment of a long tail distribution, although the typically expected (probabilistic mode) value of the spectral kurtosis is close to $K \sim 3$. Indeed, the spectral kurtosis and Lilliefors Test results, Figure 112 and Figure 95, suggest that for most of the ensemble members, the mode shapes do not have a Gaussian distribution for their components associated with excitation point X_0, and thus the hypothesis of statistical independence can not likely be ensured at excitation point X_0.

Statistical Analysis of Excitation Point X_3

In Figure 113, the kinetic energy density results for the excitation point X_3 (arbitrary choice) are plotted: some individual member values, analytical SEA prediction along with arithmetic and geometric mean values.

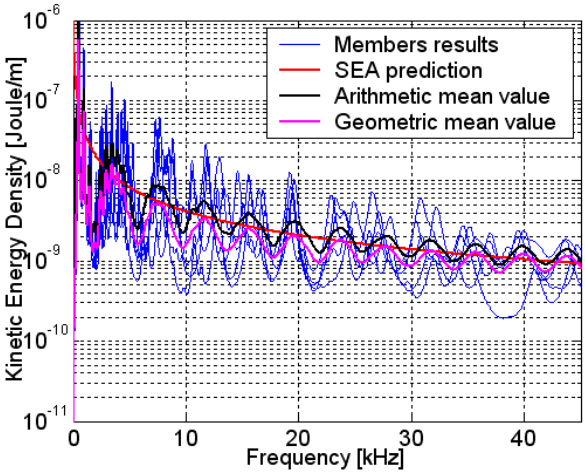

(a)

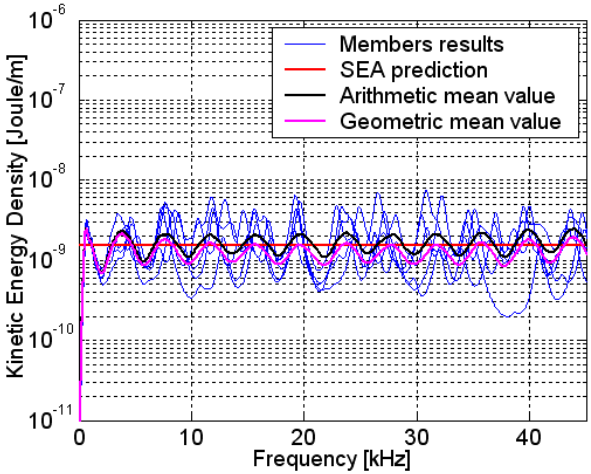

(b)

Figure 113: Kinetic energy density results for excitation point X_3 (ensemble averaging approach). Plot (a): frequency-constant DLF. Plot (b): constant superposition DLF.

As shown in Figure 113, the ensemble mean value for the energy numerical results obtained from the geometric averaging process is slightly lower than that obtained from the arithmetic process and both mean values present an oscillatory behavior throughout the excitation frequency range considered. Indeed, distinct arithmetic and geometric mean values suggest a possible establishment of the long tail distribution for the kinetic energy density results across the ensemble in the mid and high-frequency range. As observed only the numerical mean values obtained from the arithmetic process conform satisfactorily with the SEA predictions, regardless of the DLF approach adopted. In Figure 114, the relative variances of the kinetic energy density results are presented for mean values evaluated from the arithmetic and geometric averaging processes.

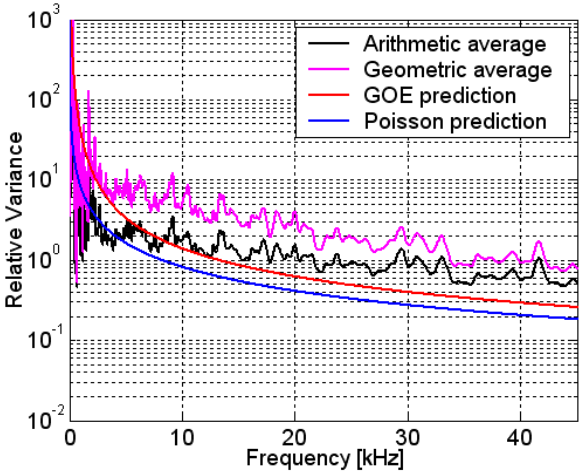

(a)

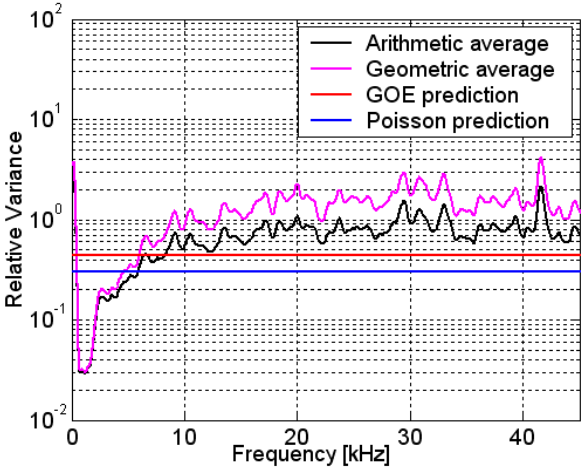

(b)

Figure 114: Relative variances of kinetic energy density results for excitation point X_3 (ensemble averaging approach). Plot (a): frequency-constant DLF. Plot (b): constant superposition DLF.

As observed in Figure 114, three narrow frequency regions show an approximate agreement between the analytical predictions based on the GOE model and the numerical variance results based on the arithmetic mean value. The limits of these three frequency ranges are approximately from 6 kHz to 7 kHz (corresponding to modes 12-14) for the first range, from 11 kHz to 12 kHz (corresponding to modes 22-24) for the second range, and from 15 kHz to 16 kHz (corresponding to modes 29-31) for the last frequency range. Additionally, the numerical variance results based on the geometric mean value are high and clearly overestimate the SEA variance prediction based on the GOE model throughout the frequency region investigated.

Considering the *ensemble mode shape statistics* results obtained for excitation point X_3, Figure 115, the regions of the mode shapes with Gaussian characteristics are clearly inserted between discrete moderately or strongly localized mode shapes, explaining the oscillatory characteristics of the kinetic energy density results.

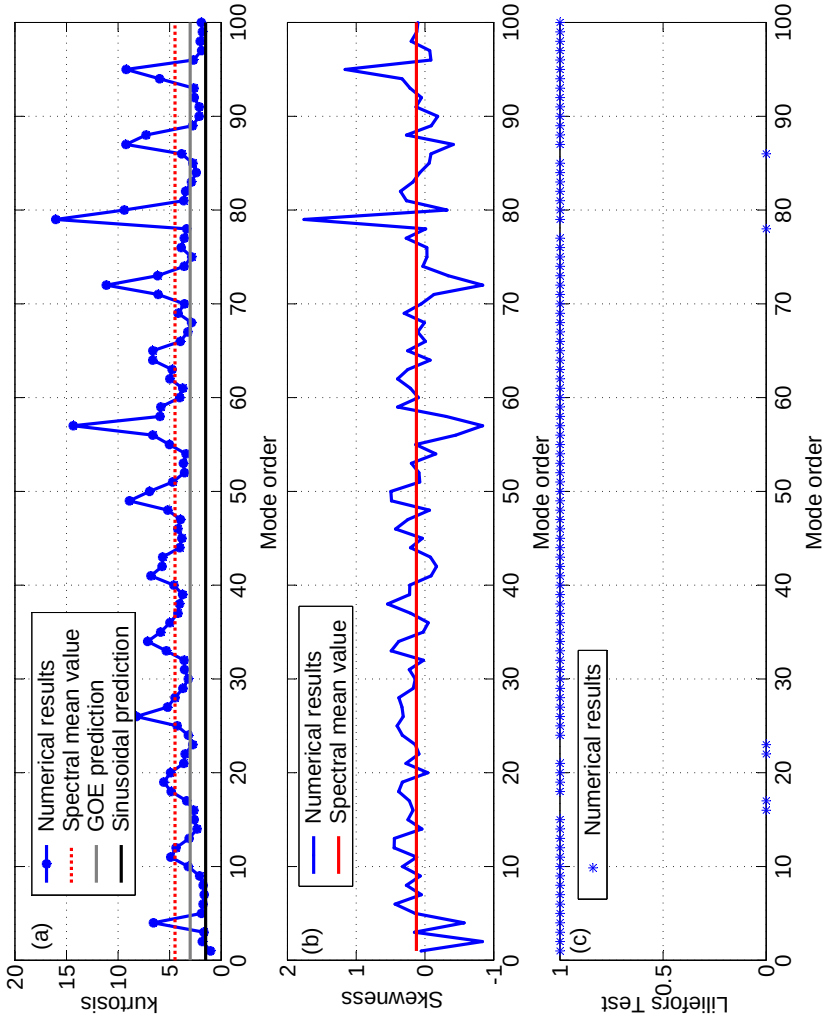

Figure 115: Ensemble statistics of the mode shape components at excitation point X_3 (ensemble averaging approach). Plot (a): kurtosis values. Plot (b): Skewness values. Plot (c): Lilliefors Test results.

As shown in Figure 115, most of the ensemble kurtosis values are around $K \sim 3.75$ and the corresponding skewness values are slightly positive, suggesting that the mode shapes have weak localization characteristics, and are almost symmetric across the ensemble at excitation point X_3. However, several isolated moderate and strong localization mode shapes are uniformly distributed along the mode order domain, inhibiting the establishment of Gaussian statistics. Indeed, the results for the statistical mode shape parameters across the ensemble suggest that the ensemble mode shape statistics at excitation point X_3 presents, in most cases, slight weak localization characteristics for most of the mode order values, interrupted by the presence of the isolated moderately or strongly localized mode shapes.

Considering again the relative variance results at excitation point X_3, Figure 114, several peaks are clearly observed in the frequency range investigated and they are directly associated with the presence of the localized mode shapes which have high ensemble kurtosis values. For example, the establishment of the peaks at around 10 kHz is probably associated with the localization characteristics of modes 18 to 21, where a local maximum point of $K_{19} \sim 5$ occurs on the ensemble kurtosis curve. In addition, the peak centered at approximately frequency 13.5 kHz is directly associated with successive localization characteristics of modes 25 to 27 where the ensemble kurtosis values are moderately localized, that is, $K_{25-27} \sim 8$. Similarly, the narrow peaks centered at approximately frequencies 29.5 and 41.6 kHz are directly associated with the localization characteristics of mode 57 ($K_{57} \sim 15$, strongly localized) and mode 79 ($K_{79} \sim 18$, strongly localized), respectively.

In Figure 116, the spectral kurtosis results at excitation point X_3 across the ensemble are shown. Additionally, a histogram of the spectral kurtosis results and their statistical parameters can be observed.

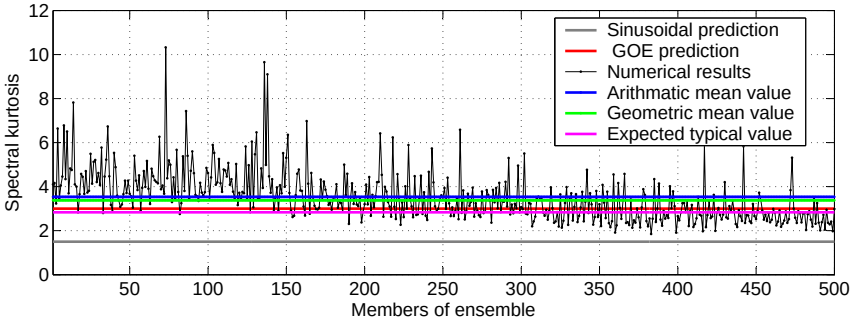

(a)

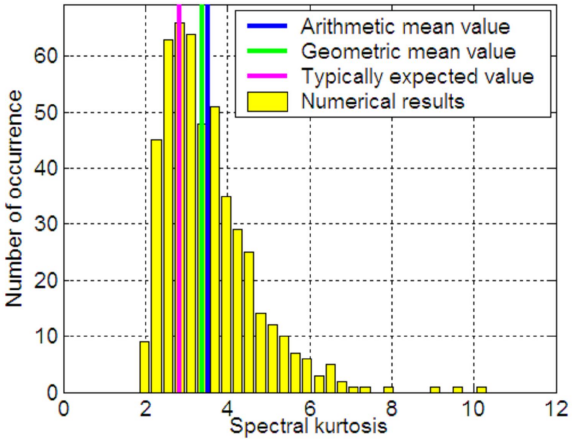

(b)

Figure 116: Spectral mode shape statistics parameters at excitation point X_3 (spectral averaging approach). Plot (a): individual member spectral kurtosis results, arithmetic and geometric mean values and sinusoidal and GOE analytical predictions. Plot (b): Histogram of spectral kurtosis results and their statistical parameters. The probabilistic mode, arithmetic and geometric mean values are, respectively, 2.83, 3.53 and 3.38.

As shown in Figure 116 (a), most of the first members of ensemble have high spectral kurtosis values which suggests the establishment of weak

localization characteristics of the mode shapes. Conversely, for the last members the spectral kurtosis values show an asymptotic reestablishment of the nominal characteristics due to the low performance of randomization process. In Figure 116 (b), the histogram of spectral kurtosis values also suggests a substantial number of discrete large kurtosis values which leads to the incipient establishment of a long tail distribution, although the typically expected (or probabilistic mode) value of spectral kurtosis is close to $K \sim 3$. Indeed, the spectral kurtosis and Lilliefors Test results, Figure 116 and Figure 95, suggest that for more than half of the ensemble members, the mode shapes have a distribution close to Gaussian for the components associated with the excitation point X_3, and thus the hypothesis of statistical independence can not likely be completely ensured at excitation point X_3.

3.5.3 Discussion and Remarks

In this second stage of the statistical investigation of random longitudinal rods, a complete analysis of the modal parameter statistics of the two ensembles of random rods with distinct randomness was carried out considering the ensemble averaging approach for the natural frequencies and the spatial, spectral and ensemble averaging approaches for the corresponding mode shapes.

The first ensemble investigated was composed of mass-loaded rods. The results for the natural frequency statistical observables showed that the ensemble natural frequency statistics vary substantially along the frequency domain from almost-nominal statistics in the low-frequency range to asymptotic-Poisson statistics in the high-frequency range. An intermediate statistics with characteristics similar to those of GOE model is observed in the vicinity of mode 42, which corresponds approximately to a frequency of 20 kHz. On the other hand, the statistical overlap factor results clearly failed to verify the establishment of the GOE statistics, since this factor indicated incorrectly the application of the GOE model beyond mode 35.

In general, the results for the mode shape statistical observables showed in an easily perceptible manner the establishment of the structural localization phenomenon, regardless of the mode shape averaging approach adopted. The spatial mode shape statistics results suggested the occurrence of a small number of the mode shapes with Gaussian distribution characteristics in a narrow frequency range centered at approximately a frequency of 20 kHz (vicinity of mode 42) for no more than 15% of the members of the ensemble.

The spectral mode shape statistics results showed that most of the

mode shape components are not Gaussian distributed in the mode order domain and thus relevant inter-modal correlations may be certainly expected for a fixed mode shape component associated with a given excitation point. Indeed, the spectral Lilliefors Test results suggested that for the mode shape components located in the vicinity of the central rod, no more than 30% of the members have a Gaussian distribution.

Additionally, the ensemble mode shape statistics results confirmed the previous conclusions obtained from the spectral and spatial mode shape statistics analysis, where the most favorable condition for the establishment of Gaussian mode shape statistics across the ensemble occurs in the vicinity of mode 40 when a single excitation point is located in the central region of the mass-loaded longitudinal rods.

Similarly to the spatial mode shape analysis, the PT-distribution results were calculated using the ensemble averaging approach. The typical localized PT-distribution results were fitted to non-linear sigma model expressions for weak and strong localization regimes. Although a poor agreement was observed for weakly localized mode shapes, the fitted expressions conform very well with the strongly localized mode shape results. To the best of the author's knowledge, this is the first application of the PT-distribution metric to a fixed mode shape component of a given mode order across the ensemble, as well as the use of the non-linear sigma model to describe the non-universal characteristics of the mode shape statistics in terms of the ensemble averaging approach.

The results for the normalized mode shape SEA parameters P_a and Q_a did not allow a clear identification of the establishment of Gaussian characteristics for mode shapes along the mode order domain and showed an inadequate performance in the verification of the GOE model applicability to the mass-loaded random rods investigated here. However, these parameter results may be used as an auxiliary metric with other eigenvector statistical observables to evaluate the randomness (or disorder) level of the mode shapes across the ensemble. On the other hand, an excellent performance of parameter Z results was obtained for the indication of the level of superposition of the independent mode sets which exist in various rod sections between the point mass locations. Additionally, this mode shape SEA parameter was able to capture indirectly the some effects on the mode shape statistics due to establishment of structural localization phenomena in the random rods as the frequency increases.

In this study, the establishment of the localization phenomenon was systematically investigated through the localization factor values. The geo-

metric averaging process was found to be more accurate than the traditional arithmetic averaging process in representing the typically expected or probabilistic mode value across the ensemble, mainly when the energy response distribution has long tail characteristics. As shown in Figures 82 and 83, the localization factor values based on the geometric mean values seem to be more appropriate to represent the frequency dependence characteristics of the spatial energy confinement due to the establishment of the structural localization phenomenon. Indeed, the shape of the curve for the geometric localization factor showed clearly a gradual transition as the excitation frequency increases from the weak to strong localization regimes, which was previously indicated by the results for the spatial mode shape statistical observables.

The ensemble mean values of the spatially-averaged kinetic energy density results conform very well with the SEA analytical prediction, regardless of the averaging process adopted. The corresponding relative variance results showed indirectly the gradual transition of the ensemble natural frequency statistics from the nominal to asymptotic Poisson statistics. As expected, a good agreement between the numerical results based on the arithmetic mean value and variance prediction based on the GOE model was observed only within the limited and narrow frequency range in the vicinity of mode 42. On the other hand, the prediction based on Poisson statistics overestimated the numerical results throughout the excitation frequency range investigated, giving a conservative analytical prediction at least for the excitation frequency range under the strong localization regime.

The point-loading kinetic energy density responses were evaluated for three distinct excitation points (X_0, X_2 and X_3) which allowed the systematic investigation of the contributions of the distinct characteristics of the spatial, spectral and ensemble mode shape statistics on the kinetic energy density statistics. The mean values obtained from the arithmetic averaging process showed an excellent agreement with the standard SEA prediction in the mid and high-frequency ranges, regardless of the excitation point location. On the other hand, the mean values based on the geometric averaging process were clearly lower than the arithmetic values, suggesting the establishment of the structural localization phenomenon across the ensemble. Indeed, distinct mean values may indicate, in principle, that the typically expected or probabilistic mode value may not be well represented by the traditional arithmetic mean value across the ensemble due to the long tail characteristics of the kinetic energy distribution in the mid and high-frequency ranges.

Considering the corresponding point-loading relative variances across the ensemble, the results based on arithmetic mean value conform with the

GOE prediction in the distinct frequency regions for each excitation point. Indeed, the frequency range for which there was a good agreement with the GOE prediction is distinct for each excitation point and is easily associated with the ensemble mode shape statistics with almost-Gaussian characteristics. Additionally the notable peaks on the relative variance curve can be directly associated with the ensemble mode shape statistics with moderate and strong localization characteristics.

Unexpected evidence emerged regarding the contributions of the spectral mode shape effects (i.e., inter-modal correlation) on the energy response statistics when the results for the excitation points X_2 and X_3 are compared each other. Their point-loading variance results conform well to the analytical prediction based on the GOE model in the excitation frequency ranges with Gaussian mode shape statistics. However, the excitation points X_2 and X_3 have very distinct spectral correlation characteristics for the mode shape statistics, suggesting likely that the presence of the inter-modal correlations between the mode shapes at the excitation point may not be the main phenomenon which reduces the performance of the relative variance predictions based on the GOE model, as observed in the SEA variance literature results.

Another notable finding is associated with the excitation point X_3 results, where the establishment of GOE statistics occurs in separate frequency regions for each modal parameter. Additionally, a good agreement between the GOE prediction and numerical relative variance results for excitation point X_3 was observed in the frequency range for which the excitation point X_3 ensemble mode shape statistics are almost-Gaussian, suggesting that the mode shape contributions to the kinetic energy density response are larger than those of the corresponding natural frequencies for the case of the mass-loaded rods excited by a single point force.

The second ensemble investigated here is composed of Gaussian spatially-correlated random rods. The ensemble natural frequency statistics results showed that for modes that lie in the mode order range from mode 40 to 65, corresponding to approximately 20.7 kHz to 34.0 kHz, the GOE statistics is satisfactorily established for short and long spectral distances and an excellent agreement with the RMT predictions is also observed. Outside this limited range, the effects of the spatial geometric correlations are minimized and a transition statistics with intermediate characteristics between high spectral rigidity and GOE statistics is established.

Analogously to the mass-loaded rod ensemble, the mode shape statistics were strongly affected by the effects of the structural localization phenomenon and thus the establishment of Gaussian modes occurs in a limited

frequency range (mode order range). Considering the spectral mode shape results, the Lilliefors Test results clearly indicated that for approximately 80% of the members the mode shape components located in the vicinity of the central rod region are almost Gaussian distributed, suggesting that they may be almost uncorrelated in the spectral domain, Figure 95. The ensemble mode shape statistics suggested that the mode order region with the highest probability of the establishment of Gaussian distribution for these mode shape components is approximately from mode 15 to 35 (corresponding approximately to the frequency range of 7.5 kHz to 18 kHz). To the best of the author's knowledge, this is the first explicit demonstration that the establishment of GOE statistics can occur in separate frequency regions for each of the modal parameters.

In order to assess accurately the effects of distinct levels of the establishment of the GOE model on the modal parameter statistics and their relation with the performance of the relative variance predictions based on the complete GOE model, the ensemble statistics of the kinetic energy responses was also evaluated considering constant modal superposition DFLs.

The mean values for the spatially-averaged kinetic energy results conformed very well to the SEA prediction throughout the excitation frequency range investigated, being weakly dependent on the contributions of the ensemble natural frequency statistics. The corresponding relative variance results clearly showed an excellent agreement with the prediction based on the GOE model in a limited frequency range in which the establishment of GOE statistics is obtained for ensemble natural frequency statistics. It is important to note that in this particular frequency range the corresponding mode shapes are weakly localized and their contribution to kinetic energy statistics seems to be negligible, suggesting the strong predominance of the ensemble natural frequency statistics contribution to spatially-averaged kinetic energy results.

The point-loading kinetic energy results were strongly affected by the structural localization effects. The differences between the mean values obtained from the arithmetic and geometric averaging processes illustrated clearly these effects, suggesting that the traditional arithmetic mean value may not estimate efficiently the typically expected value for the energy response across the ensemble. The corresponding point-loading relative variance results only conform well with the analytical GOE prediction in a limited frequency range in which the ensemble mode shape statistics are almost-Gaussian. Indeed, the current point-loading relative variance results showed that a satisfactory performance of the GOE prediction can be obtained at least for an incomplete establishment of the GOE model for the modal parameters, where the natural

frequency statistics does not conform completely with the statistical characteristics of the GOE model.

Additionally, it is interesting to note that the variance results associated with excitation points X_2 and X_3 are very similar, although their spectral correlation levels at the corresponding excitation points seems to be completely distinct, suggesting that the inter-modal correlations between the mode shapes at the excitation point may not be the main reason for the reduction in the performance of the relative variance predictions based on the GOE model.

For mid and high-frequency ranges, the point-loading relative variance results have peaks resulting from the establishment of the structural localization phenomenon in the mode shapes across the ensemble. Indeed, these results showed that the analytical prediction based on complete GOE statistics underestimates the numerical results, showing effectively that the $K = 3$ is not always a totally conservative option as originally expected.

For the current variance results from the excitation points X_2 and X_3, a good agreement with numerical results was obtained in mid and high-frequency ranges when the mode shape statistics factor of the GOE prediction was changed to $K = 4.5$. This surprising agreement seems to show that the good performance of the GOE prediction with the modified mode shape statistics factor is expected at least for modal parameter statistics with incipient or weak localization characteristics.

3.6 Summary and Discussion

In this chapter the modal parameter statistics of random longitudinal rods was systematically investigated through the results for the statistical observables. The main physical phenomena expected in real engineering structures, such as level repulsion and spectral rigidity, were accurately identified and measured. In this regard, the statistical characteristics of the modal parameters were assessed using several statistical averaging approaches (spectral, spatial and ensemble) and the results were compared to those of well-established statistical models (Poisson and GOE models for natural frequencies and sinusoidal and Gaussian for mode shapes).

The complete description of the natural frequency and mode shape statistics provided a detailed analysis of the agreement with the GOE model as well as a possible projection of the expected performance of the SEA variance prediction based on the complete GOE model along the excitation frequency range for the random rod ensembles investigated. Additionally, the results for the statistical observables provided a systematic verification of the perfor-

mance of the SEA parameters presented in the literature used to verify the application of the GOE model. The inefficacy of these SEA parameters under certain situations was highlighted. It was observed that the statistical overlap factor results, which are exclusively based on natural frequency statistics, failed when the mode shape mixing phenomenon is established. In a similar manner, the results for the normalized parameters P_a and Q_a were also unable to identify the frequency range in which the mode shapes are approximately Gaussian, and these parameters are also not sufficiently representative to express the establishment of the structural localization phenomenon in the mode shapes. However, the parameter Z results were able to capture the existence of a superimposed spectra which is composed by superposition of independent mode sets from the non-interacting rod substructures. As discussed, these non-interacting are defined by the various rod sections delimited by structural irregularities which can be interpreted as mechanical discontinuities for longitudinal wave propagation in the high frequency range.

Regarding the convergence characteristics of the modal parameter statistics for the universal establishment of GOE model statistics, it is important to note that the current results for the natural frequency and mode shape statistical observables do not suggest the existence of a well-established priority order, or convergence sequence, between the modal parameters for the establishment of the universal statistics described by the GOE model. The Gaussian spatially-correlated rod results showed that the establishment of GOE statistics may occur in separate frequency regions for each of the modal parameters. In fact, it appears that the level of disorder associated with a fixed level of randomness may be distinct for each of the modal parameters. Therefore, the convergence speed and form characteristics of the statistical transition of each modal parameter to conform to *universal* statistics are probably non-universal characteristics which are strongly dependent on the nature of the randomness and system dimensionality. Further investigations on real engineering systems with distinct dimensionalities are required.

Another important issue investigated in this study was the effect of the establishment of the structural localization phenomenon on the modal parameter statistics. The results for the statistical observables of the localized mode shapes clearly indicated the existence of a strong spatial correlation between the mode shape components due to the energy confinement. In order to describe the disorder effects on the mode shapes, the non-linear sigma model expressions from the supersymmetry theory were used and satisfactory results were obtained for weak and strong localization regimes.

The statistical results obtained for the two ensembles of random rods

investigated here showed that two nominally identical ensembles may have very distinct modal parameter and energy response statistics across the ensemble. Indeed, the current kinetic energy results suggest that the characteristics of the modal parameter statistics have little influence on the mean value of the spatially-averaged kinetic energy density results. Thus, a good agreement with the standard SEA prediction is expected on applying the spectral and ensemble averaging process approaches. In cases of single point-loaded structures, the contributions of the mode shape statistics seem to be substantial and some small discrepancies may be observed, not invalidating the good performance of the SEA prediction.

The corresponding relative variance results were found to be very sensitive to the statistical characteristics of the modal parameters, since small changes in the modal parameter statistics may lead to large changes in the variance responses, mainly in the mid and high-frequency ranges. Additionally, the current relative variance results also suggested that for random systems for which the establishment of *universal* statistics is incomplete or clearly separated over the frequency domain for each of the modal parameters, the performance of the SEA variance prediction based on the complete GOE model is strongly dependent on the nature and spatial characteristics of the excitation. For the random rods investigated herein, two completely distinct situations were clearly identified: the single point-loaded structure for which the energy statistics seems to be dominated by the mode shape statistics contribution; and, on the other extreme, the structure subjected to spatially-averaged excitation where the energy statistics is exclusively dependent on the natural frequency statistics.

An important aspect investigated in this study is the possible effects of the inter-modal correlations at the excitation point on the performance of the SEA variance based on the GOE model. The results of several studies have indicated that the main reason for the reduced performance of the point-loading SEA variance prediction based on the complete GOE model is the existence of inter-modal correlations between the mode shapes. The current point-loading variance results from the random rod ensembles showed that a good agreement with GOE prediction is equally obtained for two excitation points with completely distinct spectral mode shape statistics over the excitation frequency range in which the ensemble mode shape component statistics are almost Gaussian. Indeed, these results seem to reject the initial hypothesis that the inter-modal correlations at the force position leads to an incomplete establishment of Gaussian characteristics for a fixed mode shape component of a given modal order across the ensemble. However, further systematic in-

vestigations are required to ascertain whether this unexpected conclusion can also be extended to real engineering systems with different dimensionalities.

The nature of the random systems investigated here provides important information regarding the main effects on the modal parameter and energy response statistics due to the establishment of the structural localization phenomenon under weak and strong regimes. It was observed that the mean value obtained from the geometric averaging process has a better performance than the value obtained from the traditional arithmetic averaging process in terms of representing the typically expected or probabilistic mode value across an ensemble with long-tail distribution characteristics. In terms of the energy results, the establishment of spatial energy confinement in some limited regions of the system domain leads to a class of dynamic behaviors which is not supported by the basic assumptions of the SEA method. Therefore, large discrepancies are expected in relation to the SEA analytical predictions. The point-loading variance results showed that the prediction based on the GOE model is not conservative for one-dimensional systems with moderate and strong structural localization characteristics. For systems with incipient structural localization characteristics, a unexpectedly good performance of the analytical point-loading variance prediction based on the complete GOE model was obtained when the mode shape statistics factor was changed to a value slightly higher than the Gaussian value. On the other hand, the spatially-averaged variance results for random rods suggested that only the prediction based on the Poisson model is conservative, since the natural frequency statistics becomes asymptotically Poissonian as the excitation frequency increases.

4 NUMERICAL ANALYSIS OF RANDOM FLEXURAL PLATES

4.1 Overview

In this chapter a statistical analysis of the modal parameters of random flexural plates is systematically performed. In the first part of this chapter the effects of distinct levels of the system symmetry on the modal parameter statistics are numerically investigated considering flexural plates with several geometries (square, rectangular, rectangular with arc at one corner, circle, polygon, 1/4 Sinai stadium). These plates were generated using the Finite Element Method (FEM) and their modal parameter statistics are assessed using the statistical observables, considering the *spectral* and *spatial* averaging approaches. Special attention is focused on the main physical phenomena associated with the establishment of the stable periodic orbits, the Shnirelman peaks and structural localization and their possible effects on the modal parameters as well as their corresponding contributions to results for the statistical observables.

The numerical results for the statistical observables are also compared to analytical predictions based on Poisson and GOE model statistics and thus the conditions required to obtain good agreement with these statistics are discussed in detail. Additionally, the spectral mean and relative variance values of the kinetic energy density results of the bare (nominal) and mass-loaded rectangular plates were calculated and compared with SEA analytical formulations based on the Poisson and GOE models.

In the second part of this chapter, the statistical characteristics of two distinct ensembles of flexural random plates are investigated through the modal parameter statistical observables. Distinct approaches to randomize a nominal rectangular plate are considered for each plate ensemble. The statistics of the point-loading and spatially-averaged kinetic energy density results across the ensemble were assessed in terms of the narrow and broad frequency band domains.

4.2 Descriptions of Flexural Plates

In this section the geometrical characteristics of the flexural plates investigated in this study are described in detail. Additionally, the assumptions and limitations of FEM models corresponding to these plates are highlighted and discussed.

4.2.1 Geometrical Characteristics

In order to investigate the main effects of the distinct levels of system symmetry on modal parameter statistics, flexural plates with several geometries were considered: square, rectangular, rectangular with arc at one corner, polygonal, circular, and 1/4 Sinai stadium. These plate geometries are schematically illustrated in Figure 117.

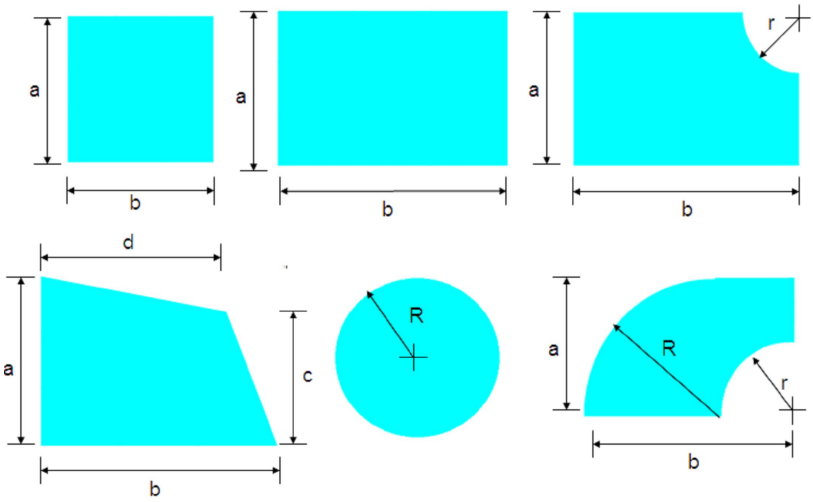

Figure 117: Illustrations of the flexural plate geometries: square, rectangular, rectangular with one arc at corner, polygonal, circular and 1/4 Sinai stadium, respectively.

All flexural plates are composed of standard aluminum and have 2 mm thickness. The main dimensions of the plates and the material proprieties of standard aluminum are described in Tables 12 and 13, respectively.

Table 12: Description of the geometrical dimensions of plate systems: square, rectangular, rectangular with one arc at corner, polygonal, circular and 1/4 Sinai stadium.

Plate Geometry	Plate Dimensions [m]
Square	$a = b = 1.200$
Rectangular	$a = 0.745$ and $b = 1.200$
Rectangular with one arc at corner	$a = 0.745$, $b = 1.200$, and $R = 0.300$
Polygonal	$a = 0.860$, $b = 1.200$, $c = 0.680$, and $d = 0.940$
Circular	$R = 0.500$
1/4 Sinai stadium	$a = R = 0.787$, $b = 1.200$, and $r = 0.414$

Table 13: Standard aluminum properties.

Material Property Parameters	Value
Young's Modulus (E_{ym})	71 G Pa
Poisson Ratio (υ)	0.33
Mass Density (ρ)	2800 kg/m^3

It is important to note that this group of plate geometries leads to very distinct modal parameter statistics. Indeed, the extreme conditions such as those described by the Poisson (regular) and GOE (chaotic) models, as well as the intermediate statistics between them, are expected to be adequately reproduced. Additionally, the modal density of flexural plates is asymptotically frequency-constant in the high-frequency range, providing very attractive characteristics for the spectral natural frequency statistics in order to investigate the universal establishment of the GOE model, since the normalized natural frequency statistics results can be directly compared with the analytical GOE model predictions.

4.2.2 FEM Model Development

For the development of numerical models of random flexural plate structures, the FEM commercial software ANSYS was used, (156, 157). In order to obtain a good description of dynamical behavior from a flexural plate subjected to either single-point or spatially-distributed normal loadings, the finite element SHELL63 was adopted. This finite element has both bending and membrane capabilities. The element has six degrees of freedom at each node: translations in the nodal x, y, and z directions and rotations about the nodal x, y, and z-axes.

The free-free boundary condition and only transversal displacements were considered for all plates investigated herein. The finite element length was defined as being $1/12$ of the bending wavelength. The estimate of the bending wavelength was based on the analytical formulation for the corresponding infinite isotropic plate, Fahy *et al.* (7, 5). For the plate geometries with curved elements (*i.e.* circular arcs) the mesh discretization was defined in order to avoid the corruption of finite elements with inappropriate shape as well as to capture in a satisfactory manner the spatial characteristics of high-frequency mode shapes.

Besides the bare flexural plates described above, some additional random plates with small point masses attached to their surfaces were also investigated. The small point masses were considered in order to reproduce possible irregularities of the mass distribution along the spatial domain of the plate system. The locations of the point masses were randomly distributed on the spatial domain of the plate systems. For dynamical representation of the point masses, the finite element MASS21 was adopted. This element is a point element which has up to six degrees of freedom: translations in the nodal x, y, and z directions and rotations about the nodal x, y, and z - axes.

Considering the recommendations for the FEM development described above, it is believed that the performance of FEM models is sufficiently reliable to provide accurate modal parameters for the flexural plates investigated in this study.

4.3 Spectral Averaging Approach

In this section the modal parameter statistics of the flexural plates with the geometries described previously in Section 4.2 are systematically investigated. The effects of the main physical phenomena which exert substantial influence on each modal parameter are identified and described in terms of

the results for the most representative statistical observables. For natural frequencies, the *spectral* averaging approach is considered and the results for the eigenvalue statistical observables are compared with the analytical predictions based on the Poisson and GOE models[1]. For the corresponding mode shapes, the *spatial* and *spectral* averaging approaches are investigated and the results for the mode shape statistical observables are compared with analytical predictions based on Gaussian and sinusoidal eigenvectors.

4.3.1 Spectral Natural Frequency Statistics

In order to provide a didactic presentation of the main results of the statistical analysis of flexural systems investigated herein, the plate systems are roughly classified in relation to the expected characteristics for the natural frequency statistics: integrable (or regular), mixed, chaotic and disordered systems.

Initially, the main aspects considered during the unfolding process are shown in detail. In subsequent subsections the main physical phenomena which exert a substantial influence on the modal parameter statistics are identified and their possible effects on the energy response statistics are also discussed.

Unfolding Process

For the evaluation of the smooth or average part of the staircase function, the 2-term Weyl formula was adopted, Bogomolny and Hugues (124):

$$N(k_f) = \frac{R_a k_f^2}{4\pi} + \beta_p \frac{P_p k_f}{4\pi}, \tag{4.1}$$

where k_f is the flexural wavenumber, R_a is the surface area of the plate, P_p is the perimeter of the plate, and β_p is a geometrical constant which is dependent

[1] A similar investigation of natural frequency statistics considering the spectral averaging approach was previously carried out by Cordioli (20). In his work, the shape of a flexural plate was gradually perturbed from the perfectly rectangular to polygonal geometries so that a statistical transition was observed from the Poisson to GOE model for spectral natural frequency statistics. In this section of the current work, the effects of the irregularities of system geometry are also investigated in systematical manner for the modal parameter statistics. In particular, special attention is focused on the statistics of corresponding mode shapes when they were evaluated on the spatial and spectral averaging approaches. Additionally, a better understanding of the following physical phenomena is expected under the mode shape statistics context: establishment of stable periodic orbits, structural localization, occurrence of degenerated modes (Peak of Shnirelman), etc.

on the boundary condition and material properties (through the Poisson coefficient υ): clamped boundary condition ($\beta_c = -1.762$) for all υ values, simply supported boundary condition ($\beta_{ss} = -1$) for all υ values, and free-free boundary condition which is directly dependent on the Poisson coefficient, ($\beta_{ff} = 1.7$ for aluminum), Schaadt (70).

The flexural wavenumber (k_f) is traditionally evaluated using the analytical formulation associated with the corresponding infinite plate system, Cremer *et al.* (38):

$$k_f = \left(\frac{\rho h \omega^2}{D} \right)^{\frac{1}{4}}, \tag{4.2}$$

where D is flexural rigidity.

Bertelsen *et al.* (66) proposed an expansion of the dispersion relation for flexural plates in terms of the dimensionless frequency (Ω) which is theoretically expected to be more accurate for the high-frequency range. This improved analytical formulation is given by:

$$k_f = \left\{ \frac{2\sqrt{3}\Omega}{K_1} \left[1 + a_1\Omega + a_2\Omega^2 + a_3\Omega^3 \right] \right\}, \tag{4.3}$$

where h is the plate thickness, and the two material property constants and dimensionless frequency are given, respectively, by:

$$K_1 = \sqrt{\frac{2}{(1-\upsilon)}}, c_t = \sqrt{\frac{E_{ym}}{2\rho(1+\upsilon)}} \text{ and } \Omega = \frac{2\pi f h}{c_t}. \tag{4.4}$$

The first two expansion coefficients of the dispersion relation proposed by Equation (4.3) are analytical functions which are dependent only on the Poisson coefficient, and are given, respectively, by (70):

$$a_1 = \frac{\sqrt{6}(17 - 7\upsilon)}{240\sqrt{1-\upsilon}}, \tag{4.5}$$

and:

$$a_2 = \frac{60\upsilon^2 + 1726\upsilon - 1353}{134400(1-\upsilon)}. \tag{4.6}$$

The third expansion coefficient was evaluated experimentally by Schaadt (70), being $a_3 = 8.68\,10^{-4}$ for aluminum plates. In Figure 118, the tradi-

tional and improved formulations for the flexural wavenumber are compared with each other, considering a plate of 2 mm thickness.

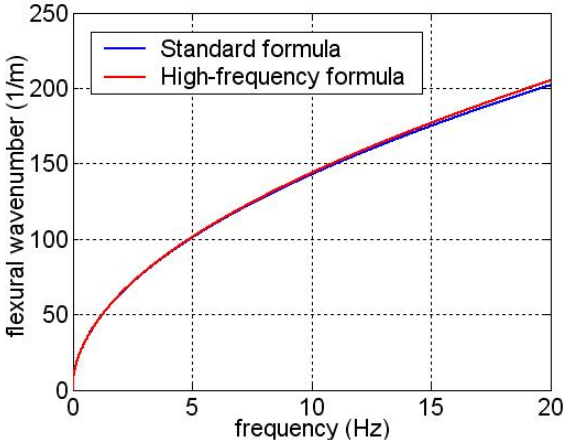

Figure 118: Flexural wavenumbers: traditional formulation based on the corresponding infinite plate system - Equation (4.2), and improved high-frequency formulation - Equation (4.3).

As shown in Figure 118, similar results are obtained up to the frequency of 10 kHz and substantial differences are observed only at around the 20 kHz. Based on these results, the traditional wavenumber formulation, Equation (4.2), will be adopted hereafter for evaluation of the 2-term Weyl formula.

In this study, the natural frequency spectra of all flexural plates, independent of their geometry characteristics, were unfolded using two distinct approaches: the 2-term Weyl formula and the best-fitted third-degree polynomial function. Although not shown in detail here, the best results were obtained for the smooth part of the staircase function based on the 2-term Weyl formula, where the resultant fluctuations of the staircase function are approximately Gaussian distributed and approved by the Lilliefors Normality Test, Fujisaka and Tohyama (94).

Integrable Systems: Square and Circular Plates

For flexural plates with several symmetries, such as a square plate, the fluctuations of the staircase function present clearly an oscillatory pattern, suggesting the presence of some residual contributions from *bouncing ball* orbits, Delande *et al.* (95). Additionally, the relevant contributions from the degenerate natural frequencies are also expected. In order to investigate these effects on the natural frequency statistics, the results for the natural frequency statistical observables were evaluated for the square plate considering two distinct approaches.

In the first approach, the smooth part of the staircase function is evaluated using the *Fourier unfolding process* and the results for the natural frequency statistical observables are compared with analytical predictions based on the Poisson model. In the second approach, the smooth part of the staircase function is calculated through a 2-term Weyl formulation and the results for the natural frequency statistical observables are compared with the *rescaled* Poisson model predictions which are corrected by a degeneracy constant proposed by *Theory Shnirelman Peak*, Chirikov and Shepelyansky (99).

For quasidegenerate systems, the PDF results for the adjacent natural frequency spacings show a well-defined peak in the first bin indicating the occurrence of natural frequency clustering due to the high number of degeneracies present in the spectrum, (99) (160). This phenomenon was physically explained by A. I. Shnirelman in 1993 and named the *Shnirelman peak*. Frahm and Shepelyansky (100) showed that the other spacing bins are described by a *scaled Poisson* distribution, given by:

$$P(s) = (1-\alpha_d)^2 \exp^{-(1-\alpha_d)s}, \tag{4.7}$$

where the α_d is the fraction of degenerate spacings compared to the total number of spacings.

Based on the *Periodical Orbit Theory* (POT), Biswas *et al.* (98) investigated the main effects of the establishment of periodical orbits on the statistical observable results associated with the long-range fluctuations. Additionally, they proposed analytical predictions of the number variance and Δ_3 - statistics for degenerate integrable systems:

$$\Sigma^2(L) = n_{av}(L)\Sigma^2_{Poisson}(L) = n_{av}(L)\,L, \tag{4.8}$$

and:

$$\Delta_3(L) = n_{av}(L)\frac{L}{15}, \tag{4.9}$$

where $n_{av}(L)$ is a natural frequency degeneracy constant which expresses the mean degeneracy of the natural frequencies. This parameter can be written in terms of α_d as $n_{av} = 1 + \alpha_d$. For the square plate investigated in this study, the fraction of degenerate spacings is 24.85%. Thus, the mean degeneracy constant is given by:

$$n_{av} = 1 + \alpha_d = 1 + 0.2485 \Rightarrow n_{av} = 1.2485. \tag{4.10}$$

In Figure 119, the results for the natural frequency statistical observables are presented considering the two approaches discussed above: Fourier unfolded natural frequencies and analytical predictions corrected by degeneracy effects. For the Fourier unfolding process, a cut-off time of $t_c = 0.1194$ seconds was adopted.

As shown in Figure 119 (a), an excessive peak clearly occurs for the PDF bin associated with smaller spacings, demonstrating the establishment of degenerate natural frequencies. For other PDF bins, the numerical results agree satisfactorily with the scaled Poisson PDF prediction, showing a performance similar to that recently reported in the POT literature (100, 98, 99, 160).

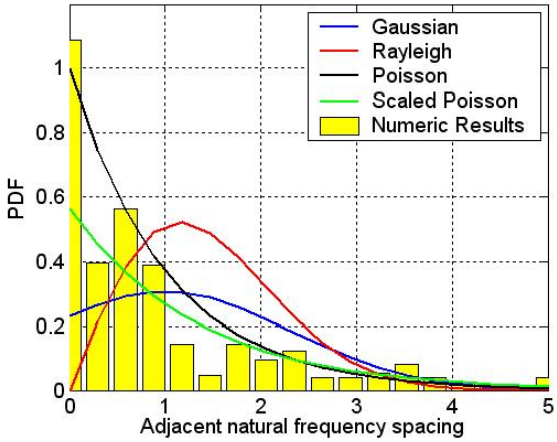

(a)

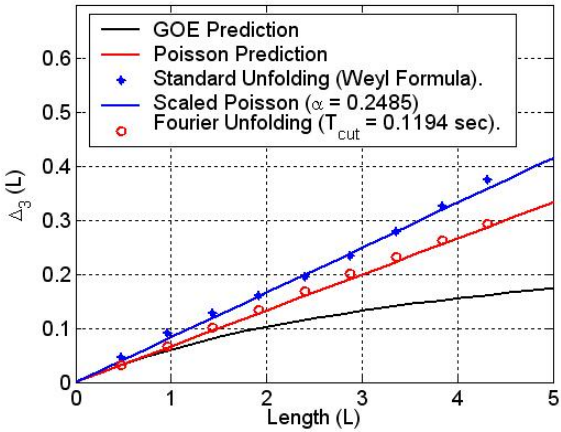

(b)

Figure 119: Natural frequency statistical observable results for the square plate (spectral averaging approach). Plot (a): PDF of adjacent natural frequency spacings. Plot (b): Δ_3 - statistics.

For the $\Delta_3(L)$ - statistics results, an excellent agreement between the numerical results and analytical predictions is observed for two approaches investigated herein, Figure 119 (b). Considering the scaled Poisson approach, the analytical predictions corrected by the mean degeneracy factor were shown to adequately represent the effects of the bouncing ball periodic orbits, which reduce the spectral rigidity characteristics of the natural frequency spectrum. In Figure 120, the individual and mean values of the degeneracy factors are presented and compared with the analytical value proposed in Equation (4.10).

The mean value and analytical prediction are very close, but the former is slightly larger than the latter. Additionally, the individual values have low dispersion characteristics around the mean and analytical prediction values. Indeed, the corrections provided by the degeneracy factor to the original prediction were efficient for the statistical observables associated with the long-range fluctuations.

Considering the numerical results based on the natural frequency spectrum obtained from the Fourier unfolding process, the value adopted for the cut-off time allowed a correct and complete removal of the bouncing ball

orbit contribution to the original staircase fluctuations. Hence, the resultant numerical results conform very well with the standard Poisson analytical prediction. In Figure 121, the effects of an inadequate choice of cut-off time for the Fourier unfolding process are illustrated for the square plate. The resultant fluctuations of the staircase function and corresponding Δ_3 - statistics results are presented for several cut-off times.

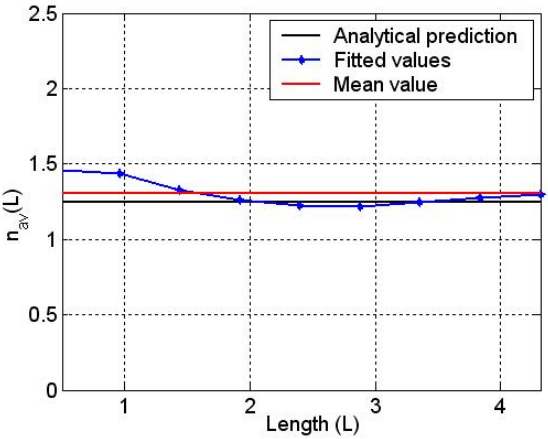

Figure 120: The natural frequency degeneracy factor (n_{av}) for the square plate: analytical prediction, individual and mean values.

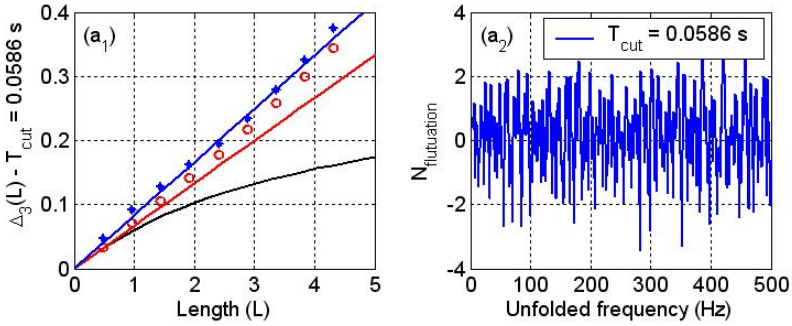

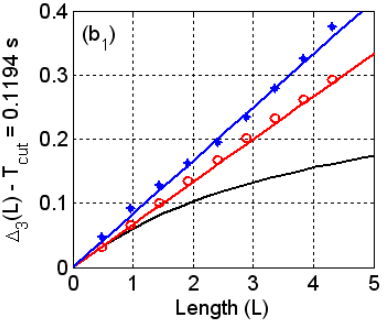
(b1)
Δ3(L) - Tcut = 0.1194 s
Length (L)

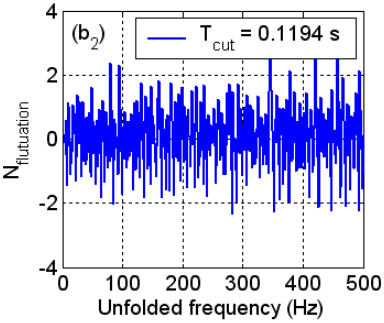
(b2)
Tcut = 0.1194 s
Nflutuation
Unfolded frequency (Hz)

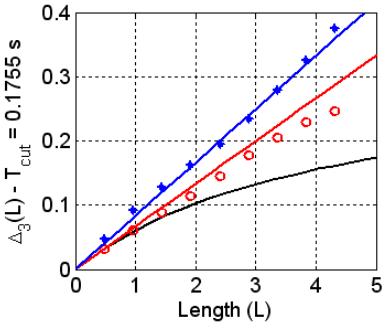
Δ3(L) - Tcut = 0.1755 s
Length (L)

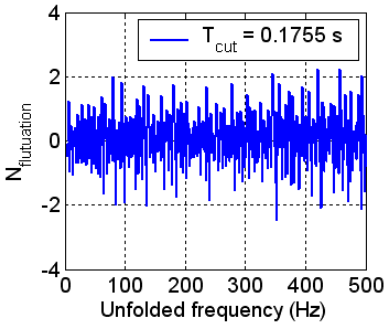
Tcut = 0.1755 s
Nflutuation
Unfolded frequency (Hz)

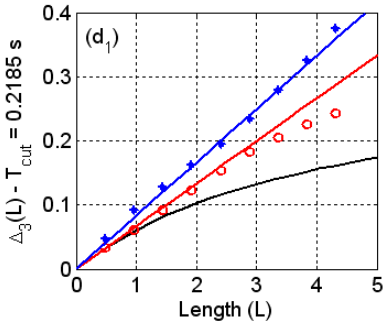
(d1)
Δ3(L) - Tcut = 0.2185 s
Length (L)

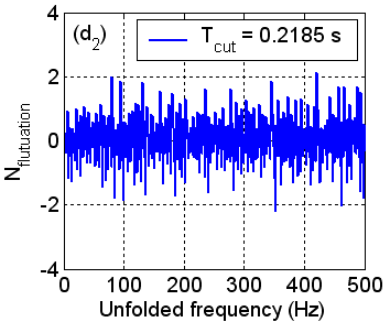
(d2)
Tcut = 0.2185 s
Nflutuation
Unfolded frequency (Hz)

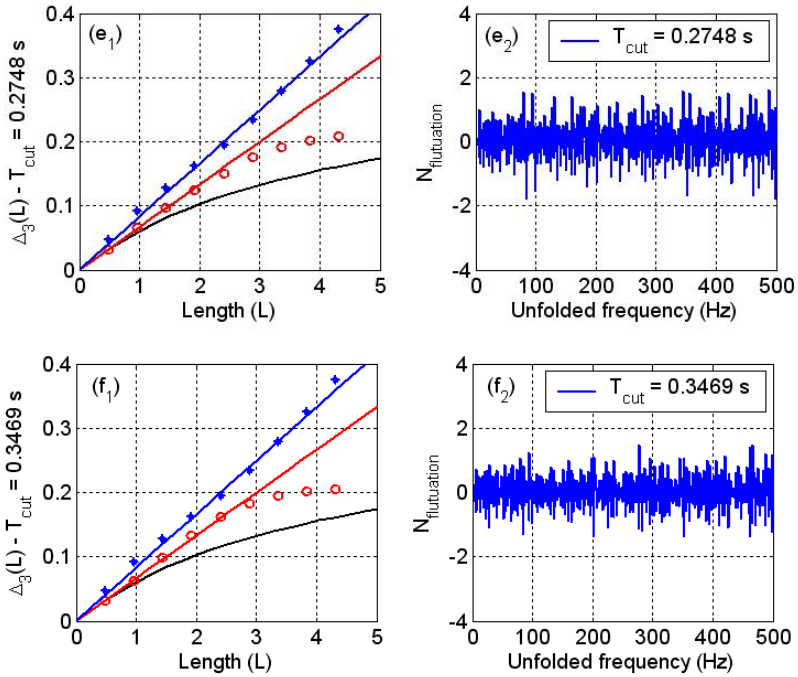

Figure 121: Analysis of the sensitivity of the Δ_3 - statistics results to the distinct magnitudes of the cut-off times used in the Fourier unfolding process (spectral averaging approach). The legends of Δ_3 - statistics results are that the same as those of Figure 119 (b).

As shown in Figure 121 (a), for small cut-off time values, the fluctuations have an oscillatory behavior with large amplitudes larger than the unitary natural frequency spacing, showing clearly that the bouncing ball orbit contributions were partially removed from the staircase fluctuations. The Δ_3 - statistics results present larger amplitudes than the analytical Poisson prediction which is directly associated with the low spectral rigidity. On the other hand, the large cut-off times can remove erroneously the *universal* characteristics of the resultant fluctuations, providing a saturation point of Δ_3 - statistics results for a given spectral length as observed in Figures 121 (c)-(f).

In Figure 122, the results for the natural frequency statistical observables are presented for the circular plate. The spacing PDF results show the occurrence of several natural frequency degeneracies, suggesting the establishment of the *Shnirelman peak* phenomenon, Figure 122 (a). Additionally, the scaled Poisson PDF prediction was also calculated through Equation (4.7). Based on the FEM results, a fraction of the degenerate spacings of 48.2 % was considered for the circle plate. As expected, a good agreement between the spacing PDF results and scaled Poisson prediction is observed beyond the second PDF bin.

As shown in Figures 122 (b) and (c), the results for the long-range fluctuation statistics are larger than the analytical predictions based on the Poisson model, showing that the natural frequencies have low spectral rigidity characteristics. In a manner similar to the square plate results, the Δ_3 - statistics results for the circular plate were also investigated using two different approaches, Figure 122 (c). The results obtained from the Fourier unfolded natural frequency spectrum with a cut-off time of 0.48 seconds show excellent agreement with the standard Poisson prediction. On the other hand, the results from the standard unfolded spectrum show small deviations in relation to the scaled Poisson prediction.

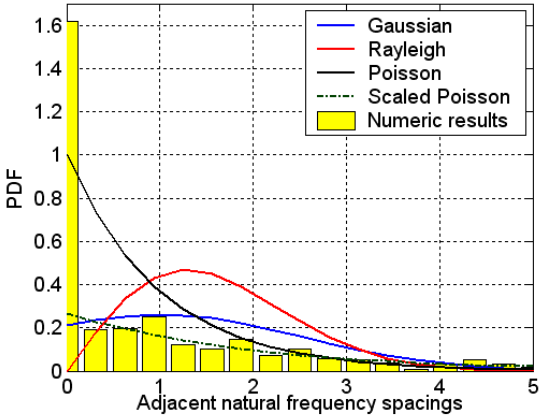

(a)

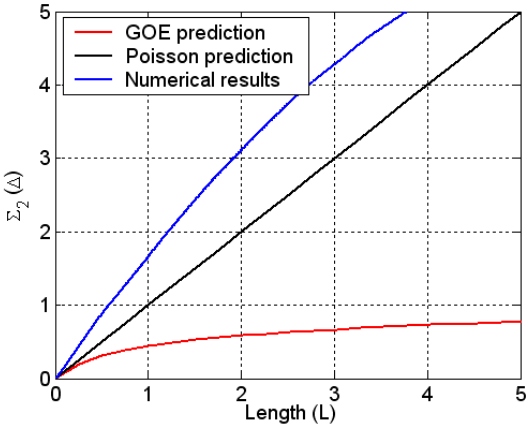

(b)

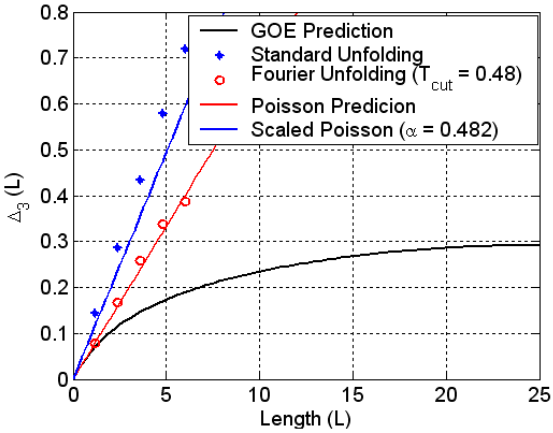

(c)

Figure 122: Natural frequency statistical observable results for the circular plate (spectral averaging approach). Plot (a): PDF of adjacent natural frequency spacings. Plot (b): number variance. Plot (c): Δ_3 - statistics.

Mixed Systems: Rectangular and Rectangular with one Arc Plates

In Figure 123, the results for the natural frequency statistical observables are presented for the rectangular plate. The spacing PDF results show a satisfactory agreement with the analytical prediction based on the Poisson model. However, the first PDF bin presents a probability lower than the corresponding value predicted by the Poisson model, Figure 123 (a). Indeed, this unexpected characteristic seems to suggest the incipient establishment of the *level repulsion* phenomenon in the natural frequencies. In Figure 123 (b), the natural frequency correlation coefficient results are presented and compared with the numerical results obtained from the perfect large Poisson and GOE matrices. The correlation coefficient results for the rectangular plate have, surprisingly, a negative value for $\Lambda \approx 1$, probably indicating the initial establishment of *veering* characteristics for the short-range fluctuations[2].

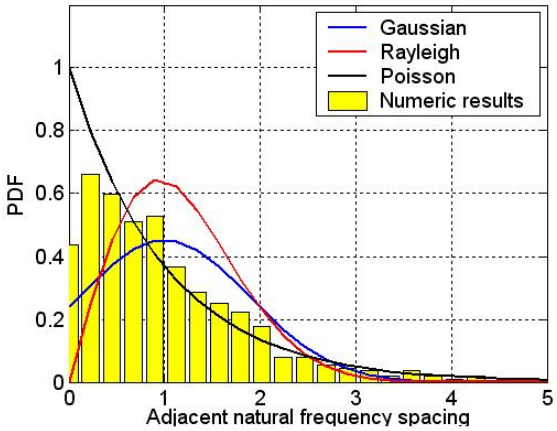

(a)

[2]According to Brown (1) the negative correlation coefficient result for $\Lambda = 1$ means also that a relatively large spacing is likely to be followed by a relatively small spacing.

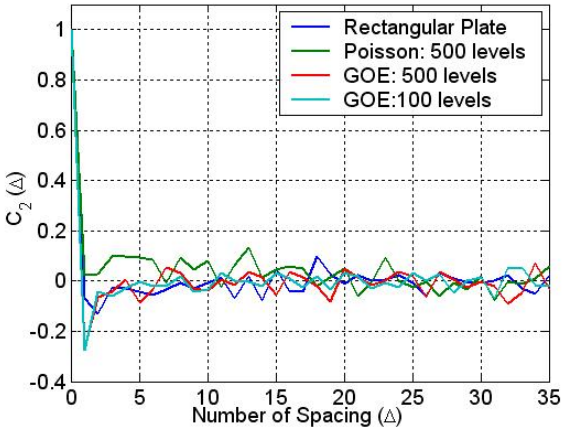
Rectangular Plate
Poisson: 500 levels
GOE: 500 levels
GOE:100 levels
$C_2(\Delta)$
Number of Spacing (Δ)

(b)

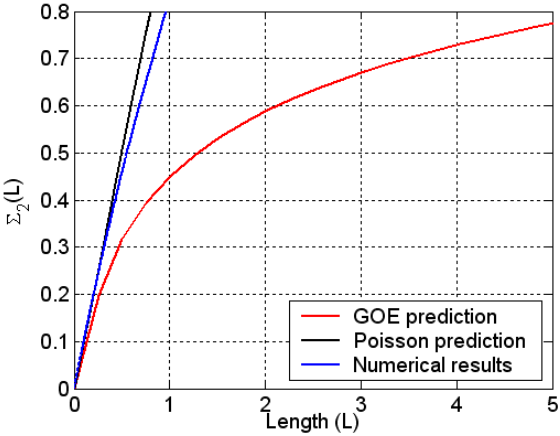
GOE prediction
Poisson prediction
Numerical results
$\Sigma_2(L)$
Length (L)

(c)

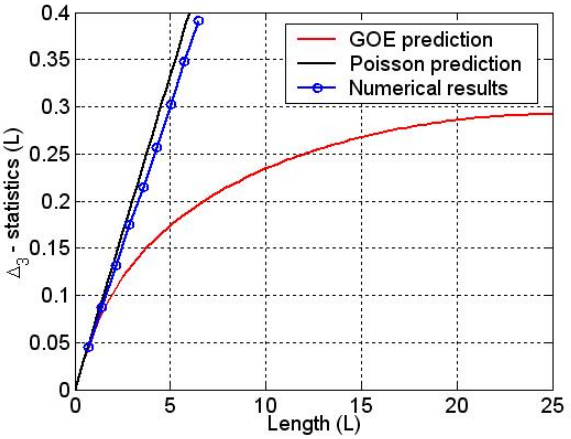

(d)

Figure 123: Natural frequency statistical observable results for rectangular plate (spectral averaging approach). Plot (a): PDF of adjacent natural frequency spacings. Plot (b): natural frequency correlation coefficient. Plot (c): number variance. Plot (d): Δ_3 - statistics.

For the long-range fluctuations, the number variance and Δ_3-statistics results are slightly lower than those predicted by the Poisson model, Figures 123 (c) and (d). In principle, the discrepancies observed can not be attributed to the establishment of periodic orbits for two main reasons. Firstly, these results clearly indicate higher spectral rigidity characteristics than those predicted by the Poisson model, which is the opposite characteristic to that expected, due to the effect of the establishment of the periodic orbits which reduces the spectral rigidity characteristics of the natural frequencies, (165, 95, 72). Another reason is associated with the fact that the geometrical ratio of the rectangular plate dimensions investigated herein is approximately the *gold ratio* (≈ 1.6180) which avoids spurious degeneracies, Bertelsen (90) and Schaadt (69).

In Figure 124, the results for the natural frequency statistical observables are presented for a rectangular plate with an arc at one corner. The results associated with the short-range fluctuations show good agreement with the GOE predictions in the small-spacing range. As shown in Figure 124 (a), the level repulsion characteristics lead to low PDF values for small adjacent

natural frequency spacings. Additionally, the correlation coefficient results conform satisfactorily with numerical results from the large GOE matrices in the small-spacing range, Figure 124 (b).

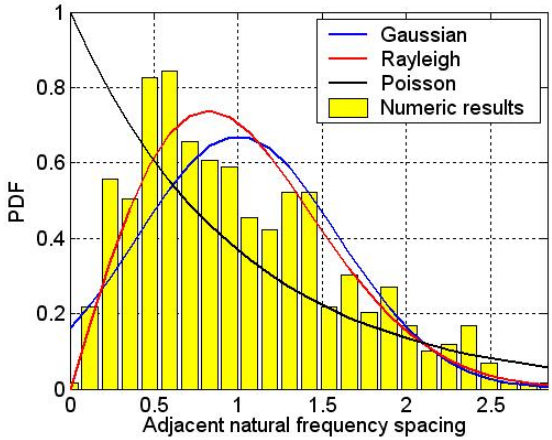

(a)

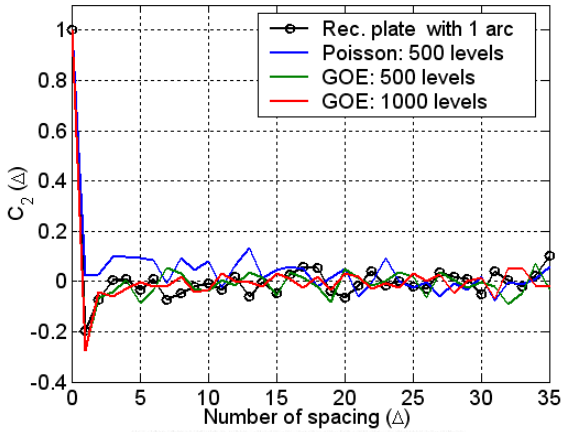

(b)

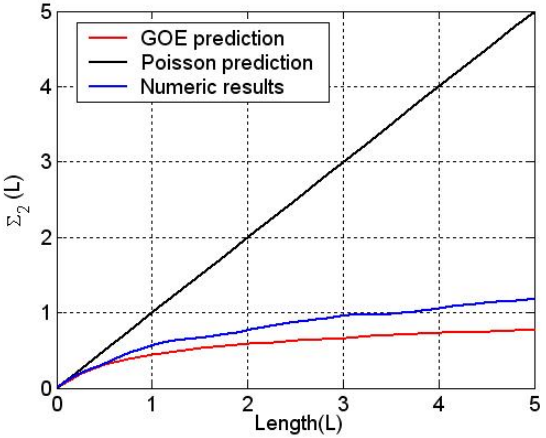

(c)

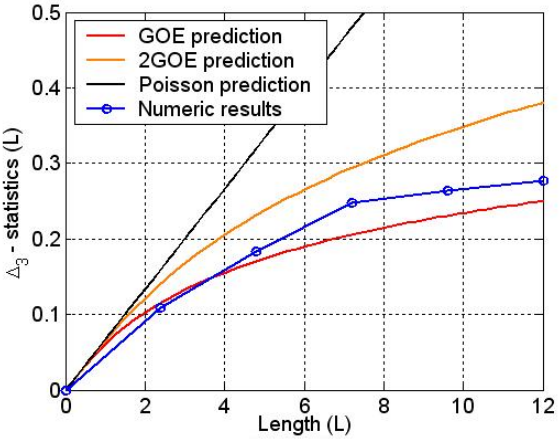

(d)

Figure 124: Natural frequency statistical observable results for the rectangular plate with an arc at one corner (spectral averaging approach). Plot (a): PDF of the adjacent natural frequency spacings. Plot (b): natural frequency correlation coefficient. Plot (c): number variance. Plot (d): Δ_3 - statistics.

As observed in Figures 124 (c) and (d), the results for the long-range fluctuation statistical observables show that the natural frequencies have an intermediate statistics between the 2 GOE and GOE model predictions. Although the statistics results associated with the small-spacing range present a partial establishment of the *universal* characteristics, the discrepancies observed in relation to the GOE model predictions in the large-spacing range yield, indirectly, trace information on the system geometry, for example, the level of symmetry.

The circular arc introduced at one corner of the perfect rectangular plate acts as a defocusing element which partially reduces the effects associated with the regular characteristics of system symmetries, leading to the establishment of some *deterministic* disorder in the modal parameter statistics, (72, 95, 113). Indeed, the natural frequency statistical observable results show clearly an incomplete establishment of the GOE statistics, partially evidencing the effects of the *level repulsion* and *spectral rigidity* phenomena. Additionally, it also believed that the spectral natural frequency correlations are associated with the existence of some stable periodic orbits, (72, 113).

Chaotic Systems: 1/4 Sinai Stadium and Polygon Plates

In Figure 125, the results for the natural frequency statistical observables are presented for 1/4 Sinai stadium plate. As expected, a good agreement with the GOE model prediction is readily observed, since the Sinai geometry is *classically* chaotic and shows the *universal* statistics described by the GOE model. Indeed, the breaking of system symmetries leads to a high dispersion of wave fronts over the spatial domain of the plate system.

The results for the short-range fluctuation statistical observables demonstrate a complete establishment of the *level repulsion* phenomenon, similarly to those associated with the classically chaotic systems. In Figure 125 (a), the PDF of adjacent natural frequency spacings shows a low probability for small and excessively large natural frequency spacings, conforming very well with the Rayleigh PDF. In a similar manner, a good agreement with the GOE statistics is also observed for natural frequency correlation coefficient results, Figure 125 (b).

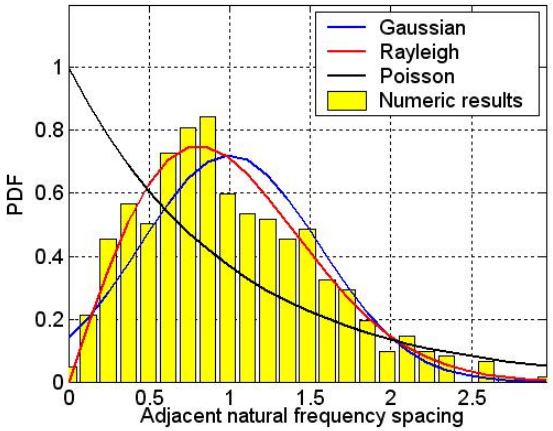
Gaussian
Rayleigh
Poisson
Numeric results
PDF
Adjacent natural frequency spacing
0
0.2
0.4
0.6
0.8
1
0.5
1.5
2
2.5

(a)

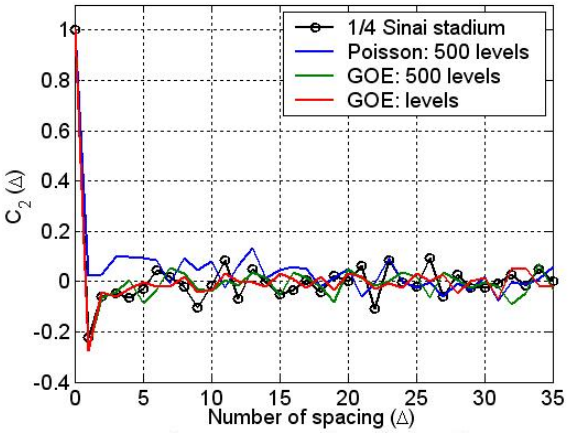
1/4 Sinai stadium
Poisson: 500 levels
GOE: 500 levels
GOE: levels
C2 (Δ)
Number of spacing (Δ)
-0.4
-0.2
0
0.2
0.4
0.6
0.8
1
5
10
15
20
25
30
35

(b)

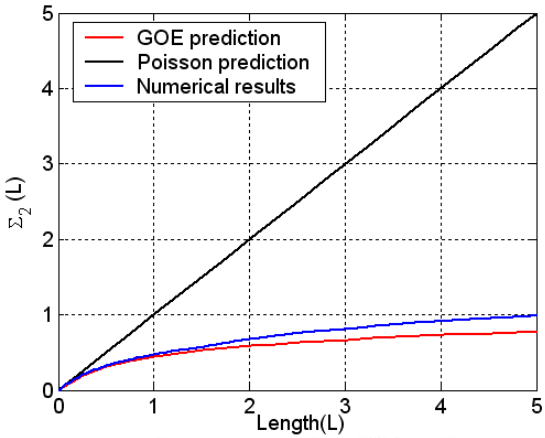

(c)

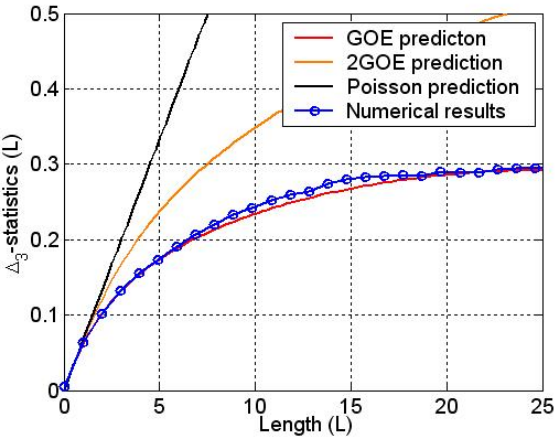

(d)

Figure 125: Natural frequency statistical observable results for the 1/4 Sinai stadium plate (spectral averaging approach). Plot (a): PDF of the adjacent natural frequency spacings. Plot (b): natural frequency correlation coefficient. Plot (c): number variance. Plot (d): Δ_3 - statistics.

As shown in Figures 125 (c) and (d), the establishment of the spectral rigidity characteristics is clearly observed for the long-range fluctuation statistical observable results. Indeed, a low probability for the establishment of small and large spacings is expected and most natural frequencies are uniformly distributed over the spectral domain, their spacing amplitudes being close to the spectral average value.

In Figure 126, the results for the natural frequency statistical observables are shown for the polygonal plate[3]. The natural frequency statistics show a surprising agreement with the GOE model predictions. Indeed, the non-parallel sizes of the polygonal plate prohibit the establishment of bouncing ball periodic orbits. The sloped sizes also act as defocusing elements and lead to a high and fast dispersion of waveguides over the spatial domain of the plate system, establishing a *deterministic chaos*.

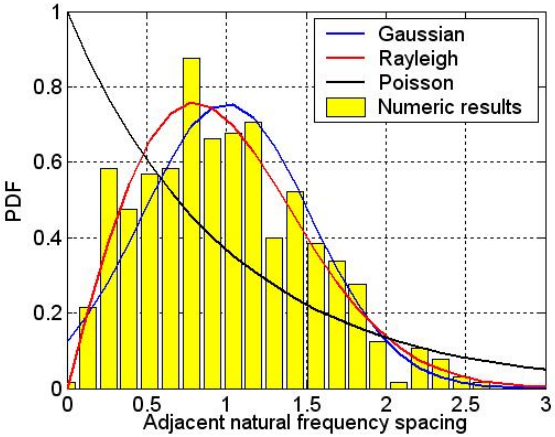

(a)

[3] In the current study, the aspect ratio of the sides of the polygonal plate was chosen in order to guarantee the establishment of a high level of spectral disorder in the modal parameter statistics, Cordioli (20) and Bertelsen (90).

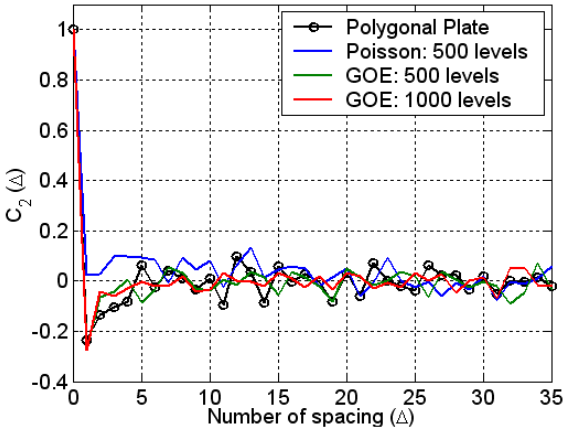
Polygonal Plate
Poisson: 500 levels
GOE: 500 levels
GOE: 1000 levels
C2 (Δ)
Number of spacing (Δ)
1
0.8
0.6
0.4
0.2
0
-0.2
-0.4
0
5
10
15
20
25
30
35

(b)

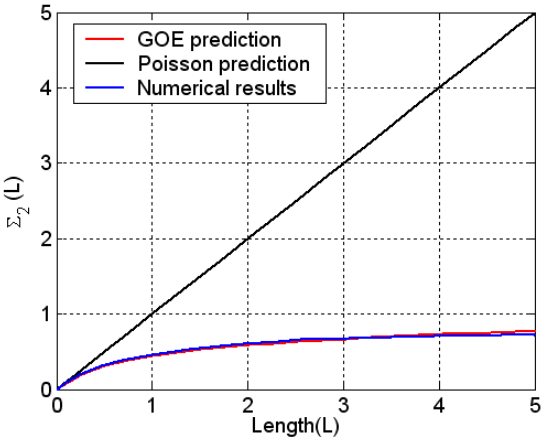
GOE prediction
Poisson prediction
Numerical results
Σ2 (L)
Length(L)
5
4
3
2
1
0
0
1
2
3
4
5

(c)

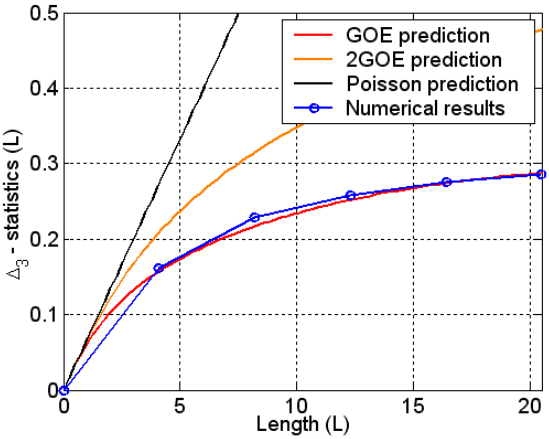

(d)

Figure 126: Natural frequency statistical observable results for polygonal plate (spectral averaging approach). Plot (a): PDF of the adjacent natural frequency spacings. Plot (b): natural frequency correlation coefficient. Plot (c): number variance. Plot (d): Δ_3 - statistics.

As discussed in the current physics literature (141, 72, 90, 69, 70), the geometrical characteristics of a given system are very significant for the determination of the spectral characteristics of the modal parameter statistics. Indeed, the natural frequency results for the polygonal plate suggest that the introduction of a certain level of irregularity in the system geometry could lead to the establishment of disordered statistics with spectral characteristics similar to those predicted by the GOE model.

Disordered System: Mass-Loaded Plate

In Figure 127, the results for the natural frequency statistical observables are presented for the mass-loaded rectangular plate. The spectral natural frequency statistics results associated with the short-range fluctuation characteristics conform well with the analytical predictions based on the GOE model. Indeed, the PDF of the adjacent natural frequency spacings shows clearly the establishment of level repulsion and spectral rigidity characteristics, that is, a low probability for small and excessively large natural frequency spa-

cings, Figure 127 (a). In a similar manner, a good agreement with the numerical results of large GOE matrices is also observed for the natural frequency correlation coefficient results, Figure 127 (b).

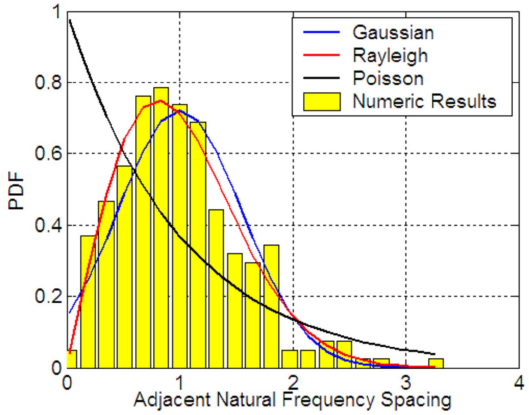

(a)

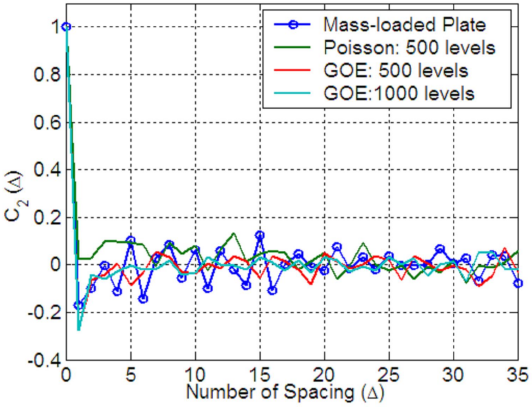

(b)

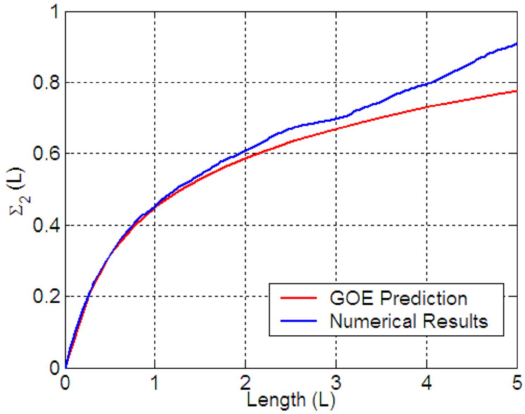

(c)

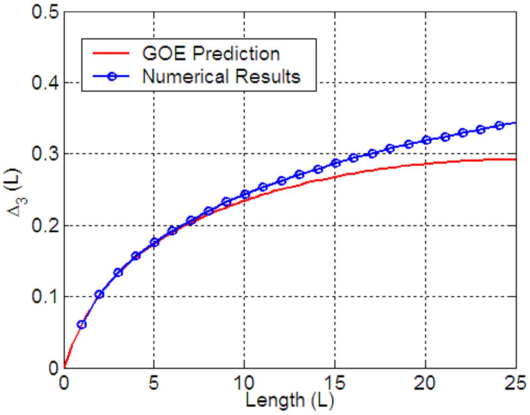

(d)

Figure 127: Natural frequency statistical observable results for the mass-loaded rectangular plate (spectral averaging approach). Plot (a): PDF of the adjacent natural frequency spacings. Plot (b): natural frequency correlation coefficient. Plot (c): number variance. Plot (d): Δ_3 - statistics results.

As expected the point masses led to the coupling of natural frequen-

cies and introduced *universal* characteristics in the high-frequency statistics similar to those expected for classically chaotic systems. Similar results in the quantum billiard field have been established for rectangular billiards perturbed by the point scatterers; Weaver *et al* (166, 167), Shigehara (168), Sridhar *et al.* (71, 73, 74).

As shown in Figures 127 (c) and (d), the results for the long-range fluctuation statistical observables show that spectral rigidity characteristics are strongly established for the mass-loaded plate. However, some small discrepancies occur in relation to the GOE prediction mainly for larger spectral distances, where the natural frequencies are separated from each other on the frequency axis by a large number of other natural frequencies. Indeed, the longer-range natural frequency statistics are slightly non-universal since the spectral correlations are influenced by the detailed nature of the system, Langley (23).

4.3.2 Spatial and Spectral Mode Shape Statistics

In this subsection the mode shape statistics are investigated considering the spatial and spectral mode shape averaging approaches. The results for the eigenvector statistical observables are compared with the analytical predictions based on sinusoidal functions and GOE eigenvectors. As in the case of the natural frequency statistics results, the spatial and spectral mode shape statistics results are also presented considering the following the major classes of statistics: integrable (or regular), mixed, chaotic and disordered.

Integrable Systems: Square and Circular Plates

In Figure 128, the spatial kurtosis and corresponding Lilliefors Test results are shown for the square plate. As shown in Figure 128 (a), most of the kurtosis values are surprisingly close to the Gaussian value, that is $K \sim 3$ and the spectral mean value of the spatial kurtosis is $K = 2.9$. Although it will not be shown here, a sharp and peaked kurtosis distribution centered at the spectral mean value occurs for spatial kurtosis values.

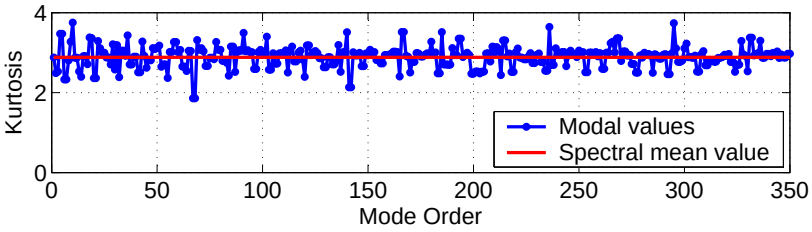

(a)

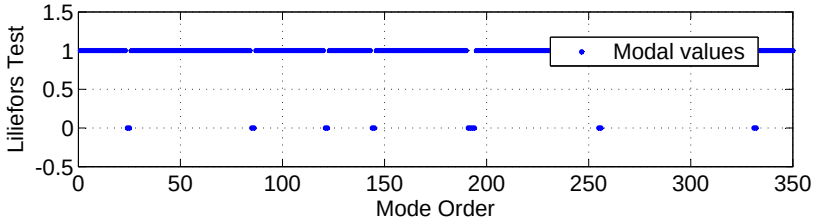

(b)

Figure 128: Spatial mode shape statistical observable results for square plate (spatial averaging approach). Plot (a): kurtosis results. Plot (b): Lilliefors Test results.

On the other hand, the spatial Lilliefors Test results showed that the hypothesis of a Gaussian distribution is approved only for some discrete mode orders, Figure 128 (b). Indeed, the free-free boundary condition leads to the establishment of non-sinusoidal mode shapes, where the nodal lines have slightly disordered spatial orientations, but a good agreement with chaotic mode shapes is not expected, A. Leissa (169).

In Figures 129 and 130, the spatial characteristics of the mode shape components over the system domain are presented for modes 145 and 255, respectively. As discussed above these mode shapes are expected, in principle, to have *near-Gaussian* characteristics. The spatial PDF of the mode shape components, spatial configurations and Porter-Thomas distribution results are shown in detail. The analytical predictions for the Gaussian and sinusoidal mode shapes are also plotted.

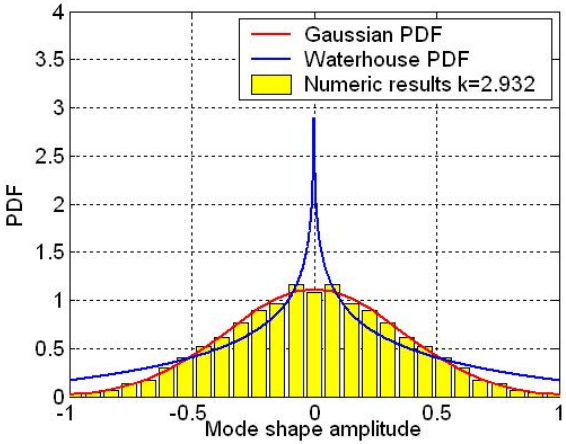
Gaussian PDF
Waterhouse PDF
Numeric results k=2.932
PDF
Mode shape amplitude
4
3.5
3
2.5
2
1.5
1
0.5
0
-1
-0.5
0
0.5
1

(a)

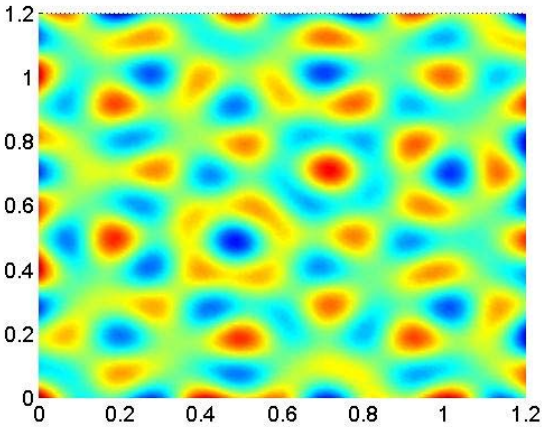
1.2
1
0.8
0.6
0.4
0.2
0
0
0.2
0.4
0.6
0.8
1
1.2

(b)

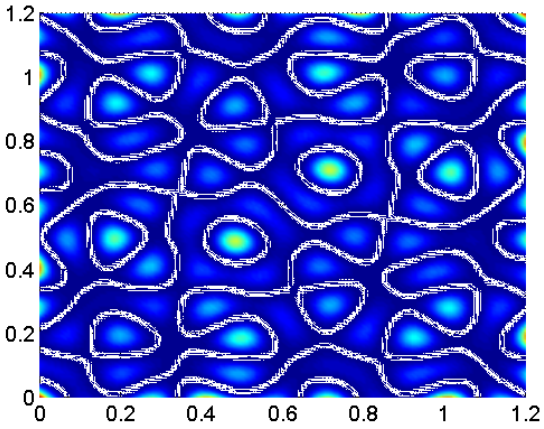

(c)

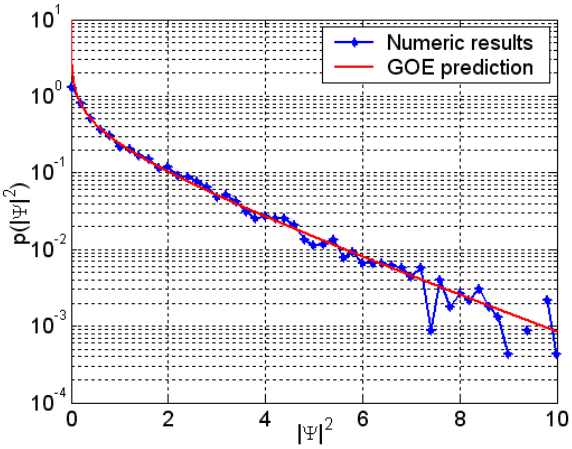

(d)

Figure 129: Mode shape statistical observable results for square plate: Mode 145 (spatial averaging approach). Plot (a): spatial PDF of mode shape components. Plot (b): spatial configuration. Plot (c): squared mode shape amplitudes. Plot (d): Porter-Thomas distribution.

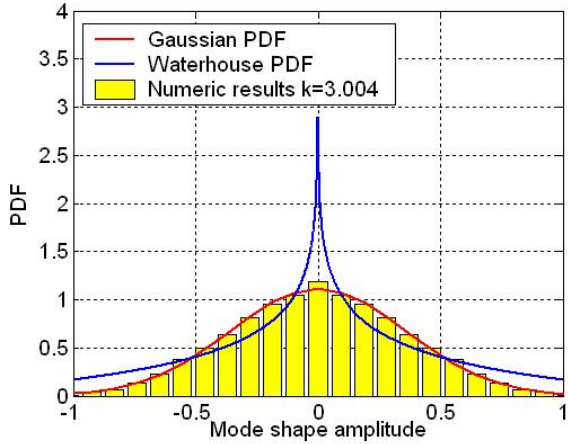
Gaussian PDF
Waterhouse PDF
Numeric results k=3.004
PDF
Mode shape amplitude
4
3.5
3
2.5
2
1.5
1
0.5
0
-1
-0.5
0
0.5
1

(a)

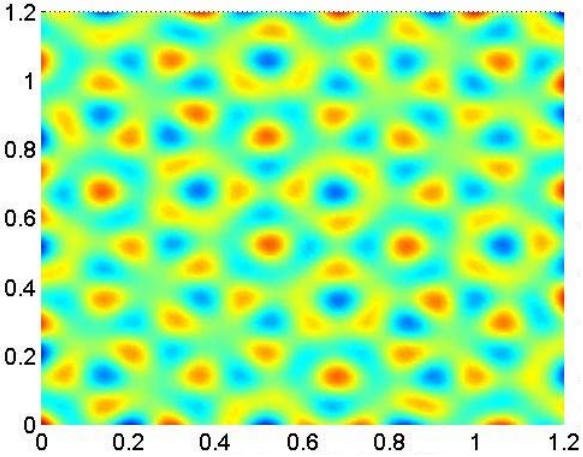
1.2
1
0.8
0.6
0.4
0.2
0
0
0.2
0.4
0.6
0.8
1
1.2

(b)

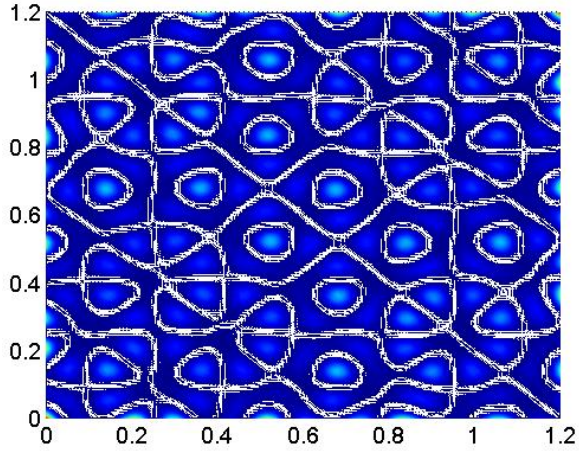

(c)

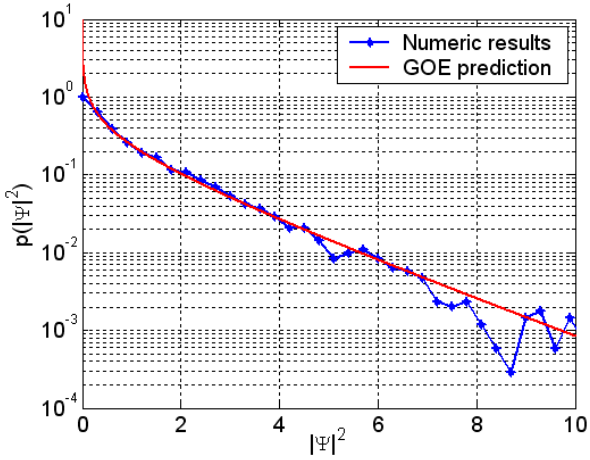

(d)

Figure 130: Mode shape statistical observable results for square plate: Mode 255 (spatial averaging approach). Plot (a): spatial PDF of mode shape components. Plot (c): spatial configuration. Plot (b): squared mode shape amplitudes. Plot (d): Porter-Thomas distribution.

As shown in Figures 129 and 130, both mode shapes are delocalized on the spatial domain of the plate system and present nodal lines with arbitrary directions similar to those of the perfect chaotic mode shapes, (73, 126). The spatial PDF of the mode shape components as well as the PT-distribution results show good agreement with the GOE model predictions. On the other hand, the symmetry characteristics of these mode shapes seem to be unbroken along one of the main diagonals. In other words, the symmetry level of the mode shape amplitudes is ensured in relation to the main diagonal direction. It is interesting to note that the results for the mode shape statistical observables seem not to be able to identify or quantify this characteristic of the regular mode shape statistics.

The spatial characteristics of the mode shape amplitudes for modes 145 and 255 are likely associated with the occurrence of the mode coupling phenomenon between degenerate flexural (vertical transverse) and extension (longitudinal) modes. Bertelsen (90) investigated experimentally this physical phenomenon in terms of natural frequency statistics using aluminum plates. A similar investigation was carried out by Schaadt (69, 70) in terms of wave function statistics.

From the Theory of Elasticity, it is known that the vibration modes of a plate can usually be classified into two main classes: flexural or extensional. Additionally, the extensional modes can be further divided or separated into two major groups: horizontal transverse or longitudinal modes. In Figure 131, the flexural (vertical transverse) and extensional (longitudinal and horizontal transverse) mode shapes are illustrated.

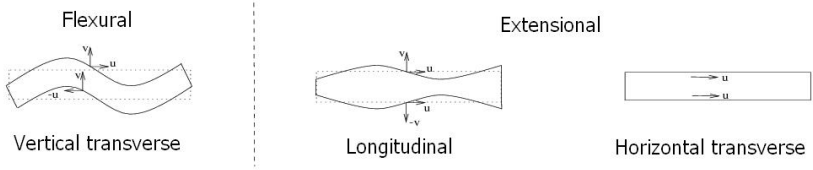

Figure 131: Representation of two classes of modes and their symmetry characteristics, Bertelsen (90, 66).

In Figure 132, the resultant characteristics of the mode shape amplitudes are illustrated for a superposition of two mode shapes with the same

natural frequencies, Schaadt (69). In order to provide a didactic illustration of the mode superposition phenomenon, the symmetry with respect to the y axis is initially considered. The same principle can also be extended to the case of a reflection with respect to the x axis.

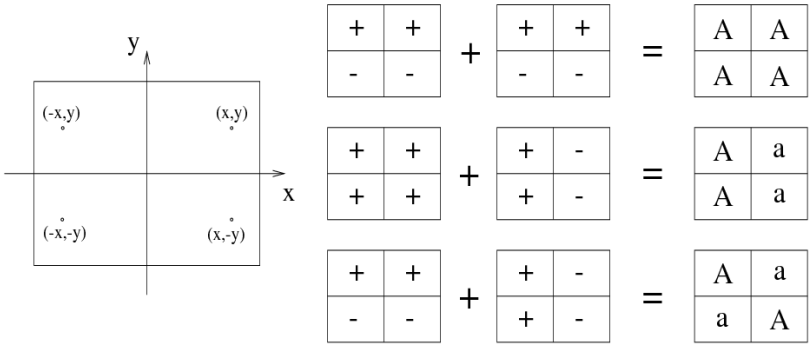

Figure 132: Schematic illustration of the superposition of modes, Schaadt (69).

As shown in Figure 132, any mode is either symmetric or anti-symmetric with the y axis. Hence, two results are expected for the modal superposition, either *destructive interference* which gives small amplitudes (a), provided by opposite signs, or *constructive interference* (A), provided by matching signs. Further information regarding the mode superposition phenomenon in plates is available in A. Leissa (169).

In this regard, it seems reasonable to assume that modes 145 and 255 are superposition of the flexural and longitudinal mode shapes with degenerate natural frequencies. Although the occurrence of an exact, or very near, degeneracy of two flexural modes is possible, this case is very rare, since the flexural modes do not couple with each other. Therefore, it is believed that the *chaotic* characteristics emerge from the contributions of the longitudinal modes. Indeed, Bertelsen and Schaadt's results (90, 66, 69, 70) demonstrated that the extensional modes, longitudinal and horizontal transverse, are strongly coupled due to the mode conversion phenomenon at the system boundaries, leading to *chaotic* characteristics independent of the system geometry.

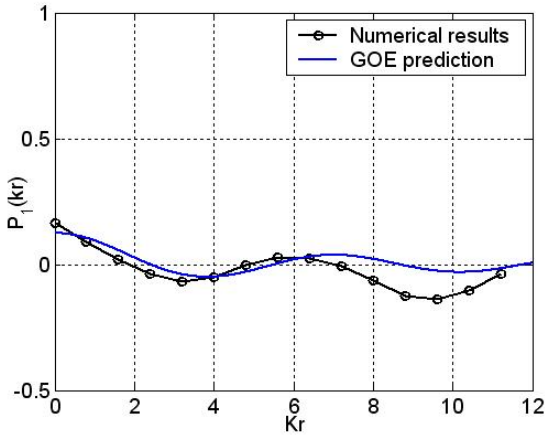

(a)

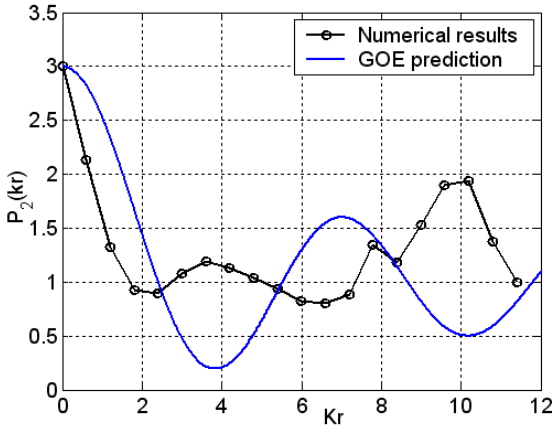

(b)

Figure 133: Spatial normalized mode shape correlation results for the square plate: Mode 255 (spatial averaging approach). Plot (a): linear correlation function (P_1). Plot (b): squared correlation function (P_2).

In Figure 133, the linear and squared spatial correlation functions of the normalized mode shape components are presented for mode 255.

These numerical results are compared with the GOE model predictions for bi-dimensional systems, Equations (2.40) and (2.44), respectively. Although the numerical results for mode 145 are not shown here, similar characteristics to those of mode 255 were observed.

As observed in Figure 133 (a), a good agreement between the numerical results and GOE model prediction is observed mainly for small values of $k_f r$. Indeed, two important conclusions can be drawn: (*i*) the value of k_f evaluated using the analytical formula based on the corresponding infinite plate system seems to represent a good estimate for finite flexural plates and, (*ii*) mode 255 can also be classified as a flexural mode. It is important to observe that some relevant discrepancies occur for large values of $k_f r$ and they seem to be associated with the regular characteristics of the degenerate flexural mode shape. For the spatial correlation function of the squared mode shape components, the discrepancies in relation to the GOE prediction are clearly observed and the contributions of the regular mode shape statistics seem to be more relevant mainly for large values of $k_f r$, Figure 133 (b). These results verify that mode 255 is not perfectly chaotic and presents some of the non-universal characteristics of the regular flexural mode shape associated with the modal superposition phenomenon. Further investigations are necessary to describe systematically the individual characteristics of the mode shape statistics associated with the degeneration phenomenon of the extensional and flexural mode shapes.

Considering the spectral mode shape averaging approach, the kurtosis and corresponding Lillierfors Test results were calculated for each mode shape component of the square plate. The spectral mode shape statistical observable results are presented in Figure 134.

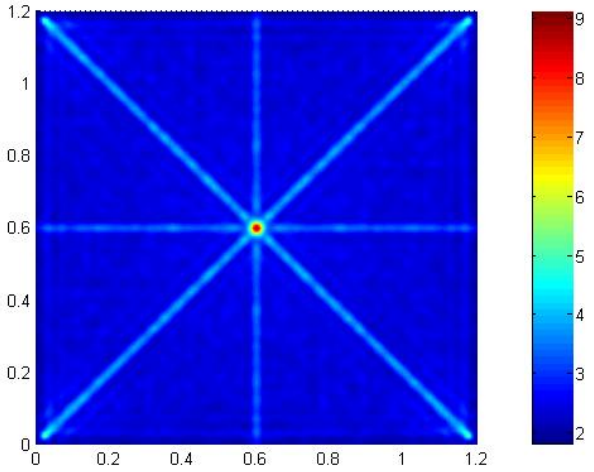

(a)

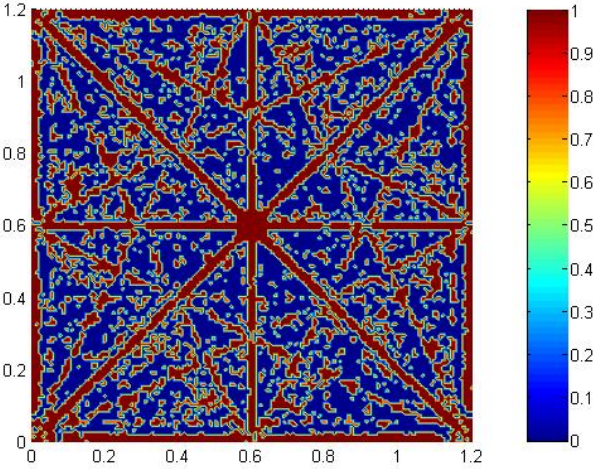

(b)

Figure 134: Spectral mode shape statistical observable results for the square plate (spectral averaging approach). Plot (a): kurtosis results. Plot (b): Lilliefors Test results.

As observed in Figure 134 (a), most of the spectral kurtosis results are close to $K \sim 2.5$ suggesting that a large number of mode shape components is not Gaussian distributed along the spectral domain. In addition, the largest values obtained for the spectral kurtosis occur for the mode shape components located on the main diagonals and on the middle lines parallel to plate sides. Indeed, the remarkably large spectral kurtosis values can be directly associated with the symmetry characteristics of the regular systems.

The corresponding spectral Lilliefors Test results allowed the accurate identification of the effects associated with the presence of the system symmetries as well as an indirect estimate of the spectral correlation strength for a given mode shape component. In Figure 134 (b), the mode shape components not approved by the Lilliefors Test results can be easily associated with the establishment of the periodic orbits. In a similar manner to the results for the spectral kurtosis, the bouncing ball and main diagonal periodic orbits were detected by the spectral Lilliefors Test results. However, surprisingly, the Lilliefors Test results allowed an accurate identification of the periodic orbits along the secondary diagonal and a perfect characterization of the symmetry effects on the spectral mode shape statistics.

In Figure 135, the spatial kurtosis and Lilliefors Test results are shown for the circular plate. Although, in principle, it is expected that the mode shapes of the circular plate are well-behaved, since the geometry of this system is perfectly symmetric, several discrete peaks in the spatial kurtosis results are observed along the mode order domain.

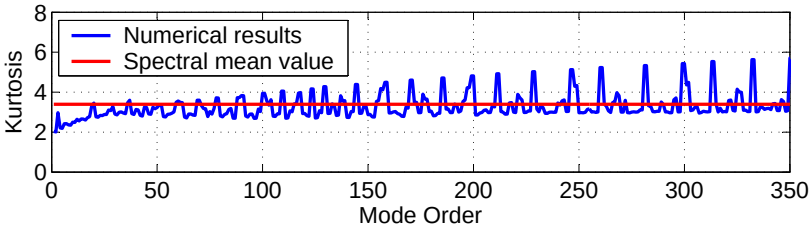

(a)

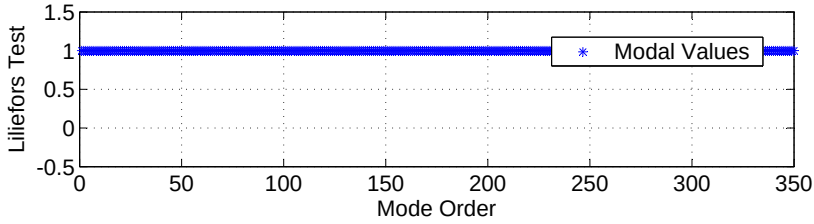

(b)

Figure 135: Spatial mode shape statistical observable results for the circular plate (spatial averaging approach). Plot (a): kurtosis values. Plot (b): Lilliefors Test results.

According to Figure 135 (a), the mode shapes seem to be classified into two major groups. The first group corresponds to mode shapes for which, apart from the first mode orders, the spatial kurtosis results are weakly localized with kurtosis values close to $K \sim 3.2$. On the other hand, the second group comprises the mode shapes for which the spatial kurtosis values are peaked, suggesting the establishment of characteristics similar to those expected for the mode shapes under the moderate localization regime. It is also interesting to note that the values of these peaked spatial kurtosis results increase asymptotically toward the high mode order range. Additionally, the spatial Lilliefors Test results show clearly that all mode shapes reject the Gaussian distribution hypothesis, although most of the spatial kurtosis values are close to the GOE value ($K^{GOE} = 3$), Figure 135 (b).

In order to obtain a better understanding of the physical phenomena associated with each one of these mode shape groups, one typical mode shape from each group was investigated using the complementary mode shape statistical observables. In Figures 136 and 137, the spatial representation of squared mode shape components, PDF of the mode shape components (normalized to have zero mean amplitude) and Porter Thomas-distribution results are presented for modes 142 and 229, respectively.

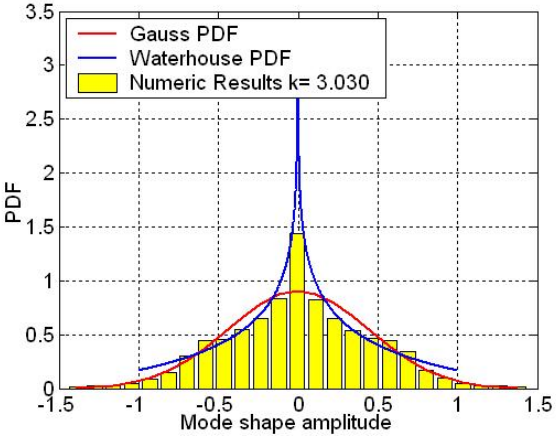
Gauss PDF
Waterhouse PDF
Numeric Results k= 3.030
PDF
Mode shape amplitude
3.5
3
2.5
2
1.5
1
0.5
0
-1.5
-1
-0.5
0
0.5
1
1.5

(a)

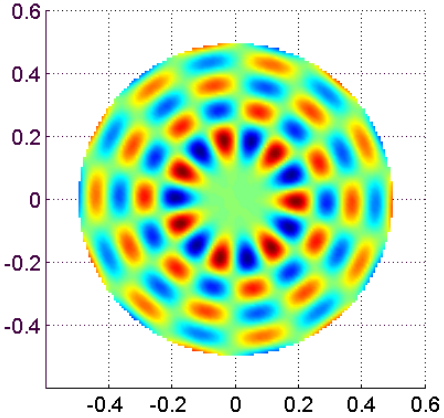
0.6
0.4
0.2
0
-0.2
-0.4
-0.4
-0.2
0
0.2
0.4
0.6

(b)

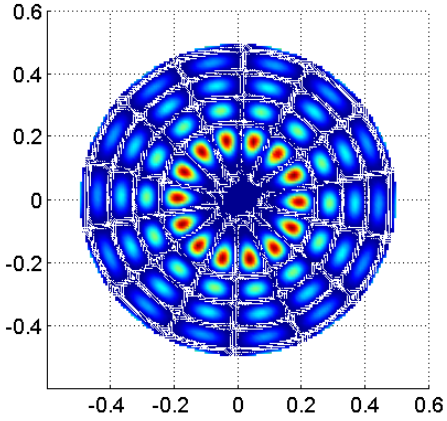

(c)

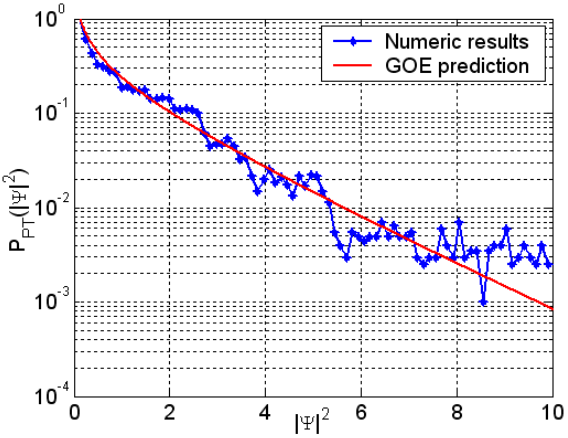

(d)

Figure 136: Spatial mode shape characteristics for the circular plate: Mode 142 (spatial averaging approach). Plot (a): spatial PDF of mode shape components. Plot (b): spatial configuration. Plot (c): squared mode shape amplitudes. Plot (d): Porter-Thomas distribution.

As shown in Figure 136, the nodal lines are well-defined along the ra-

dial direction and have a high degree of geometrical regularity. For mode 142, the amplitudes of the mode shape components located near the circle center are practically null while the adjacent ones are slightly larger than the others. These characteristics can also be observed in the spatial PDF results for the mode shape components, where a peak centered on null amplitude is clearly pronounced. On the other hand, the mode shapes with spatial characteristics similar to those of mode 229 have larger amplitudes in the region close to the circle edge, where the mode shape component amplitudes of other regions are practically null, Figure 137 (b).

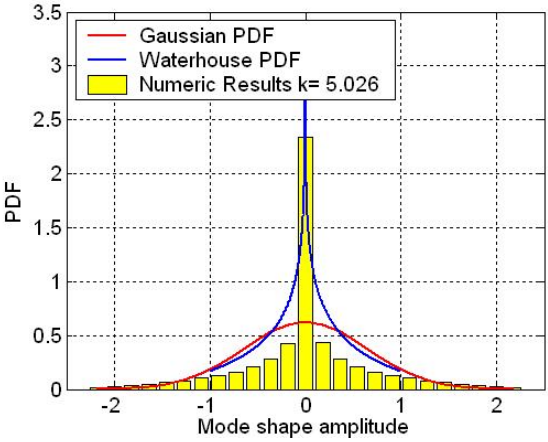

(a)

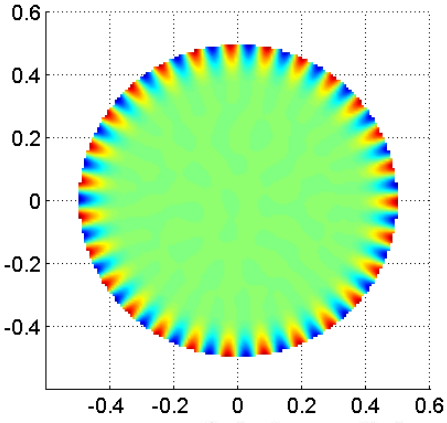

(b)

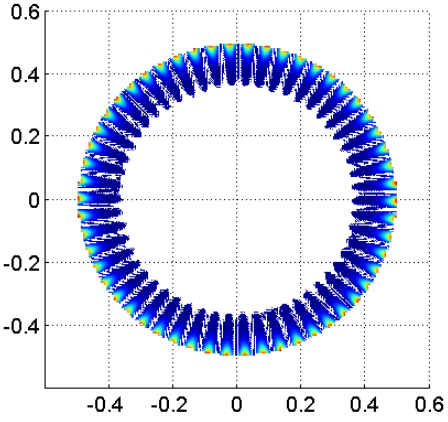

(c)

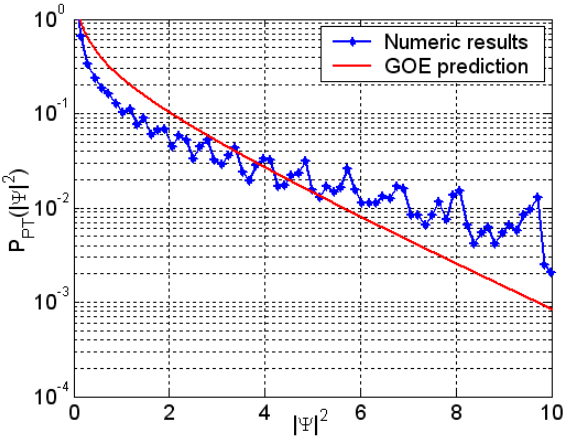

(d)

Figure 137: Spatial mode shape characteristics for the circular plate: Mode 229 (spatial averaging approach). Plot (a): spatial PDF of mode shape components. Plot (b): spatial configuration. Plot (c): squared mode shape amplitudes. Plot (d): Porter-Thomas distribution.

As shown in Figure 137 (a), a large peak centered on null mode shape component amplitude is clearly observed, suggesting, in principle, the establishment of spatial characteristics similar to those associated with the structural localization phenomenon. Similar conclusions were reached on considering the PT-distribution results, where the *non-universal* characteristics in relation to the Gaussian prediction were observed, Figure 137 (d).

Although the spatial mode shape characteristics described above are completely distinct to those expected for rectangular quantum billiards, it is important to note that the two groups of mode shapes investigated herein have also been observed in studies with circular billiards carried out by Arnd Bäcker (127), where these spatial characteristics were also associated with the regular statistics.

The spectral characteristics of the mode shapes for the circular plate are demonstrated in Figure 138. The spectral kurtosis values showed that almost-GOE characteristics are expected to be established in the ring region close to the edge, Figure 138 (a).

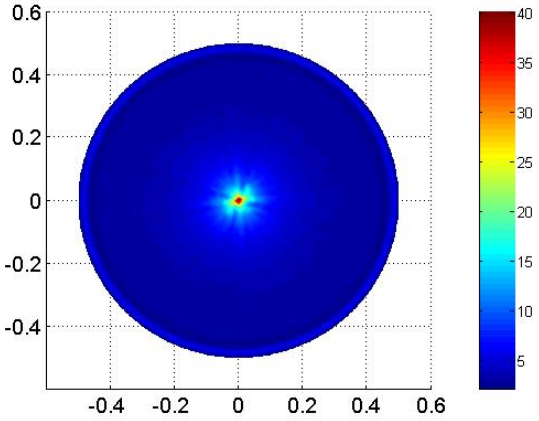

(a)

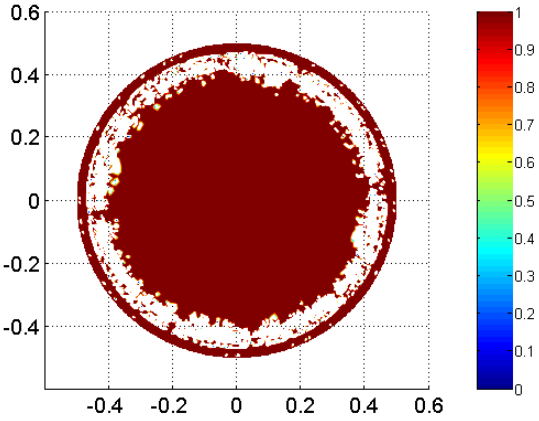

(b)

Figure 138: Spectral mode shape characteristics of the circular plate (spectral averaging approach). Plot (a): kurtosis values. Plot (b): Lilliefors Test results.

As shown in Figure 138 (b), the Lilliefors Test results confirm the establishment of a Gaussian distribution for the mode shape components located in the ring region close to the edge, suggesting that these mode shape

components are likely *uncorrelated* along the mode order domain.

Mixed Systems: Rectangular and Rectangular with One Arc Plates

Considering the mode shapes of the rectangular plate, the spatial kurtosis and corresponding Lilliefors Test results are shown in Figure 139.

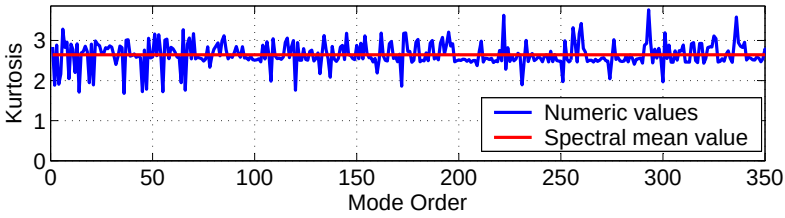

(a)

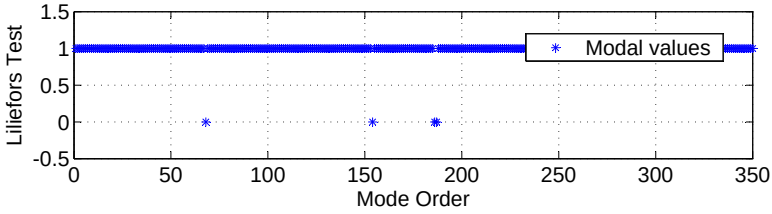

(b)

Figure 139: Spatial mode shape statistical observable results for the rectangular plate (spatial averaging approach). Plot (a): spatial kurtosis. Plot (b): Lilliefors Test.

As shown in Figure 139(a), most of the kurtosis values are slightly larger than the expected kurtosis value for 2D-sinusoidal mode shapes, that is, $K \sim 2.6 > 2.25 = K_{sin}^{2D}$. Additionally, some small and discrete peaks and anti-peaks are observed. Although not shown here, a sharp and peaked distribution centered around the spectral mean value ($\bar{K} = 2.64$) occurs for the spatial kurtosis values.

The spatial Lilliefors Test results suggest that the hypothesis of Gaussian distribution is approved only for some discrete mode orders, Figure

139(b). Leissa in (169) demonstrated that the free-free boundary condition leads to the establishment of non-sinusoidal mode shapes for rectangular plates, where the nodal lines are not perfectly parallel to the plate sides.

According to Figure 139, the mode shapes 68 and 186 are expected to be almost-Gaussian and to have good agreement with the GOE eigenvector statistics. In Figures 140 and 141, the spatial characteristics of the mode shape components are presented for modes 68 and 186, respectively. The spatial PDF of the mode shape components, spatial configurations and Porter-Thomas distribution results are plotted and compared with the analytical predictions for Gaussian and sinusoidal mode shape statistics.

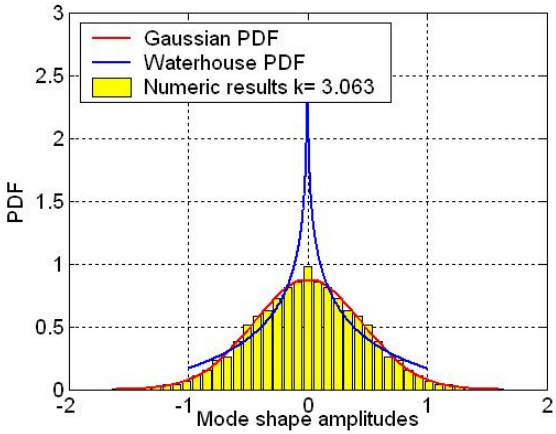

(a)

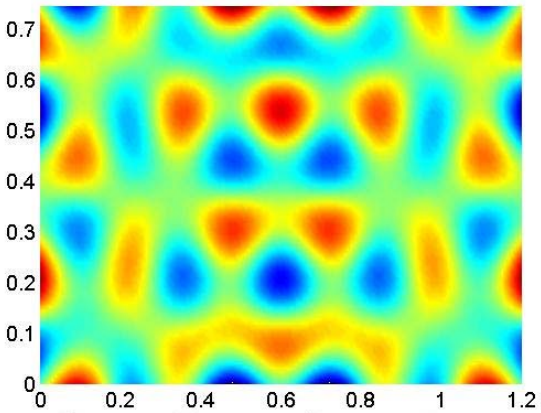
0.7
0.6
0.5
0.4
0.3
0.2
0.1
0
0
0.2
0.4
0.6
0.8
1
1.2

(b)

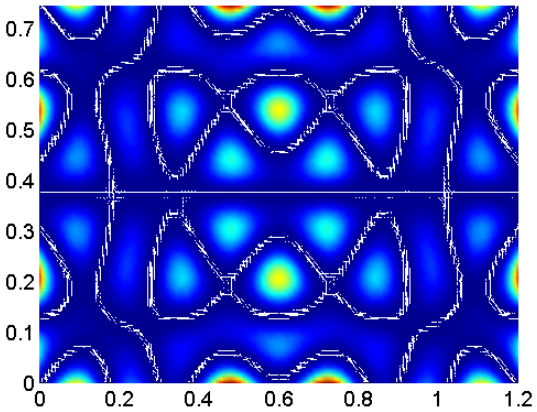
0.7
0.6
0.5
0.4
0.3
0.2
0.1
0
0
0.2
0.4
0.6
0.8
1
1.2

(c)

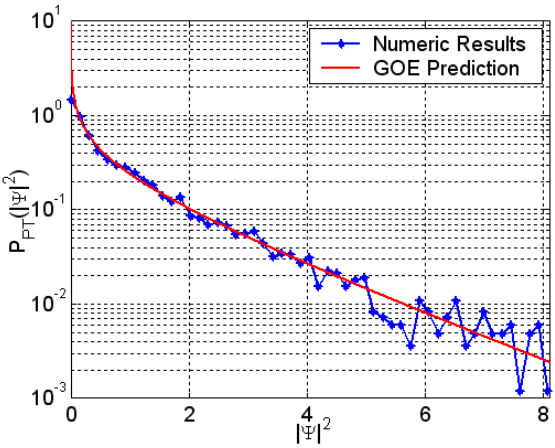

(d)

Figure 140: Spatial mode shape statistical observable results for the rectangular plate: Mode 68 (spatial averaging approach). Plot (a): spatial PDF of mode shape components. Plot (b): spatial configuration. Plot (c): squared mode shape component amplitudes. Plot (d): Porter-Thomas distribution.

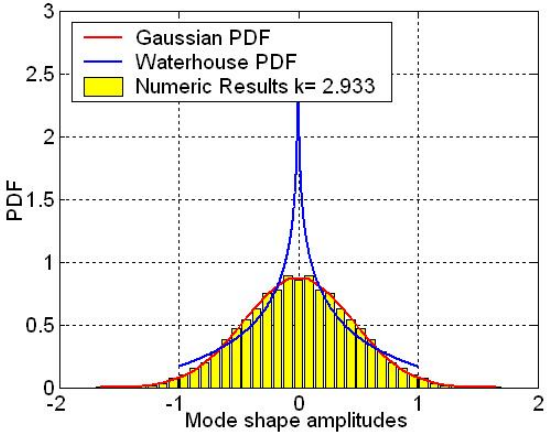
Gaussian PDF
Waterhouse PDF
Numeric Results k= 2.933
PDF
Mode shape amplitudes
3
2.5
2
1.5
1
0.5
0
-2
-1
0
1
2

(a)

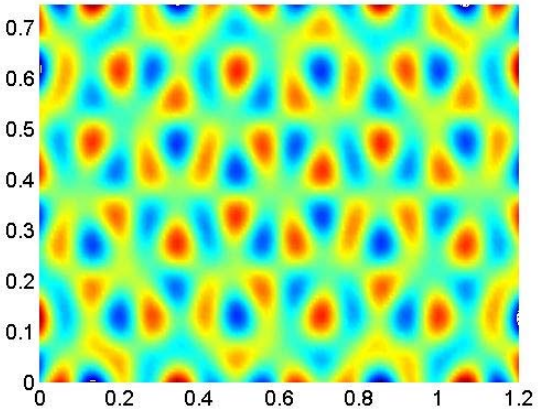
0.7
0.6
0.5
0.4
0.3
0.2
0.1
0
0
0.2
0.4
0.6
0.8
1
1.2

(b)

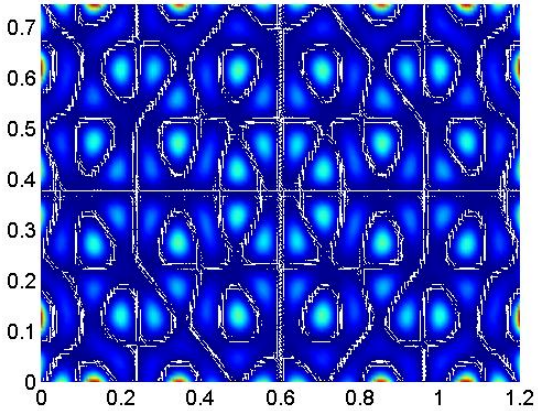

(c)

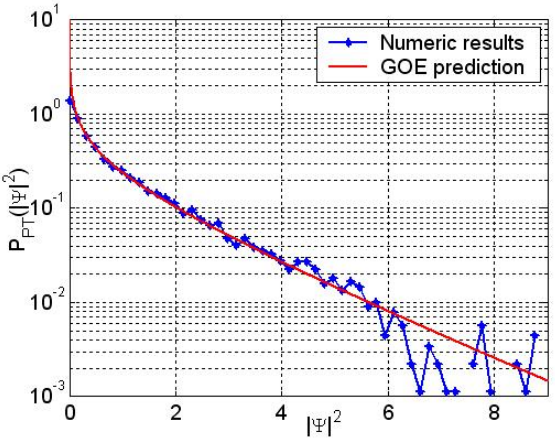

(d)

Figure 141: Spatial mode shape statistical observable results for the rectangular plate: Mode 186 (spatial averaging approach). Plot (a): spatial PDF of mode shape components. Plot (b): spatial configuration. Plot (c): squared mode shape component amplitudes. Plot (d): Porter-Thomas distribution.

As shown in Figures 140 and 141, both mode shapes are delocalized on the spatial system domain and present nodal lines with arbitrary directions. The PDF of mode shape components and PT-distribution results show a good agreement with GOE model predictions. On the other hand, the symmetry characteristics of these mode shapes are clearly unbroken along the horizontal axis. Indeed, substantial contributions of the effects associated with the geometrical regularity, such as the establishment of the *bouncing ball* periodic orbits, are expected for rectangular plates due to the parallel sides.

In a similar manner to the mode shapes of the square plate which have Gaussian characteristics, it is probable that the mode shapes 68 and 186 of the rectangular plate can be defined as modal superpositions of degenerate flexural (vertical transverse) and extension (longitudinal) modes, Schaadt (69) and A. Leissa (169). In principle, it is expected that the surprising Gaussian characteristics of modes 68 and 186 arise from the contributions of the chaotic characteristics associated with the extensional mode. Indeed, due to the mode conversion phenomenon at the system boundaries, the longitudinal and horizontal transverse extensional modes are strongly coupled and present chaotic characteristics, regardless of the symmetry characteristics of the system geometry, Bertelsen (90, 66) and Schaadt (69, 70).

In Figure 142, the linear and squared spatial correlation functions of the normalized mode shape components are presented for mode 186. These numerical results are compared with GOE model predictions for bidimensional systems, Equations (2.40) and (2.44), respectively.

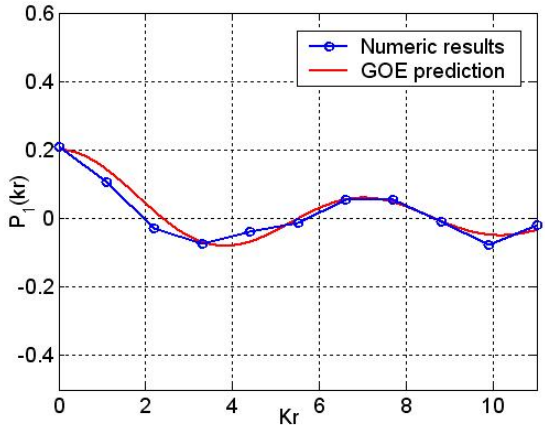

(a)

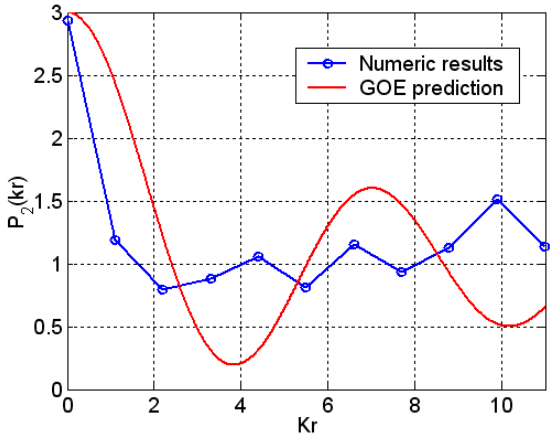

(b)

Figure 142: Spatial normalized mode shape correlation function results for the rectangular plate: Mode 186 (spatial averaging approach). Plot (a): linear correlation function (P_1). Plot (b): squared correlation function (P_2).

As observed in Figure 142 (a), the numerical results for small values of $k_f r$ conform well with the analytical prediction based on the GOE model.

This good agreement is likely associated with the relevant chaotic characteristics of the longitudinal mode.

For the squared spatial mode shape correlation function results, the existing discrepancies, in relation to prediction based on the GOE model, observed for large values of $k_f r$ seem to be directly associated with the relevant contributions of the regular characteristics of the flexural mode shapes, Figure 142 (b). Indeed, these results suggest that the mode shape 186 is not perfectly chaotic and presents *non-universal* characteristics certainly associated with the regular flexural mode shape.

In Figure 143, the spectral kurtosis and corresponding Lilliefors Test results are presented for each mode shape component of the rectangular plate.

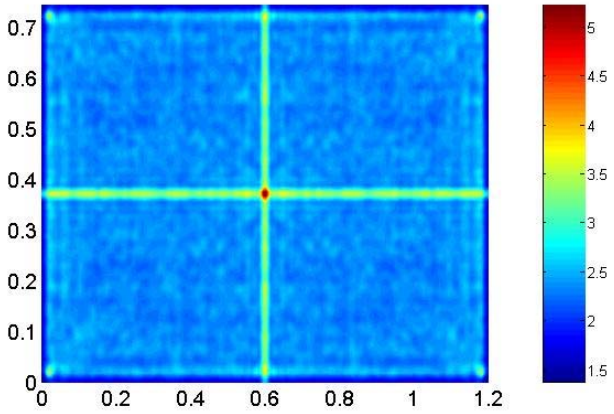

(a)

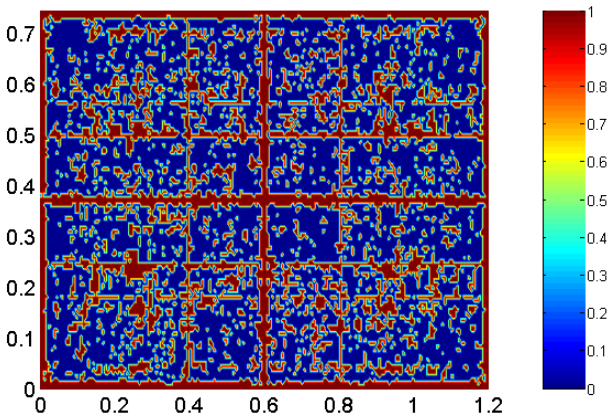

(b)

Figure 143: Spectral mode shape statistical observable results for the rectangular plate (spectral averaging approach). Plot (a): kurtosis results. Plot (b): Lilliefors Test results.

As observed in Figure 143(a), most of the mode shape components are not Gaussian distributed and have spectral kurtosis values close to $K \sim 2.4$. For the mode shape components located on the middle lines parallel to the plate sides large values occur for the spectral kurtosis, which can be associated with the establishment of the bouncing ball periodic orbits. The corresponding spectral Lilliefors Test results allow the effects associated with the presence of system symmetries to be clearly identified, Figure 143 (b). Differently from the spectral mode shape results for the square plate, the spectral kurtosis and Lilliefors Test results for the rectangular plate showed that the symmetry effects associated with the establishment of periodic orbits on the secondary diagonal are clearly reduced for the rectangular plate.

In Figure 144, the spatial kurtosis and Lilliefors Test results are shown for the rectangular plate with a circular arc at one corner. The spatial kurtosis values are slightly higher than those expected for perfect Gaussian mode shapes. Additionally, these results suggest that the mode shapes are homogeneously perturbed by the effect of the arc along the mode order domain investigated herein.

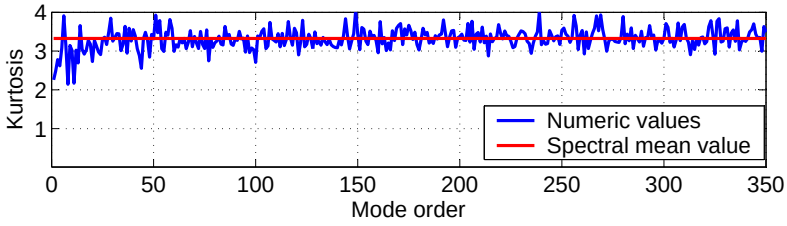

(a)

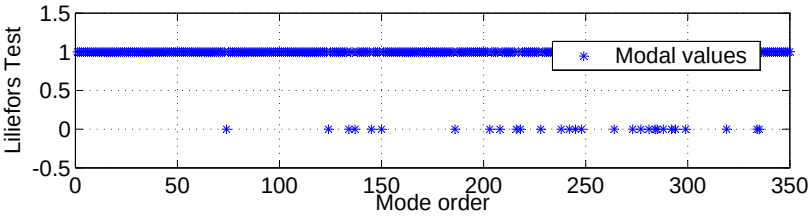

(b)

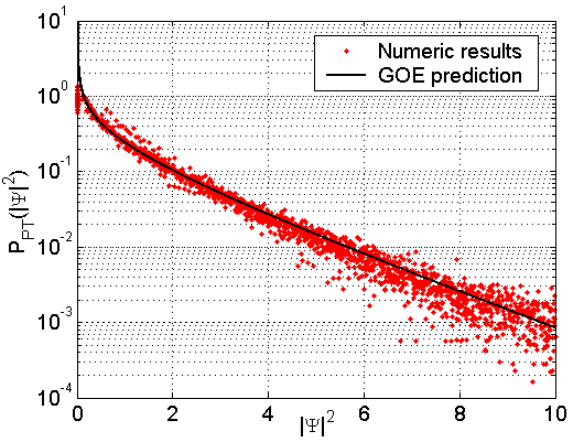

(c)

Figure 144: Spatial mode shape statistical observable results for the rectangular plate with an arc at one corner. Plot (a): kurtosis values (spatial averaging approach). Plot (b): Lilliefors Test results. Plot (c): PT-distribution results.

According to Figure 144 (b), the Lilliefors Test results show that, apart from the first mode orders, a Gaussian distribution for the mode shape components is expected for several mode shapes. Indeed, the focusing and defocusing effects associated with the presence of the arc lead to the establishment of a *deterministic chaos* for mid and high-frequency mode shapes. In Figure 144 (c), the PT-distribution results confirm the trend of the establishment of *universal* characteristics for the mode shapes, although small discrepancies are observed in the range associated with the large squared mode shape amplitudes.

In Figure 145, the spatial representation of the mode shape components and corresponding PT-distribution results are presented for some modes with *almost-Gaussian* characteristics.

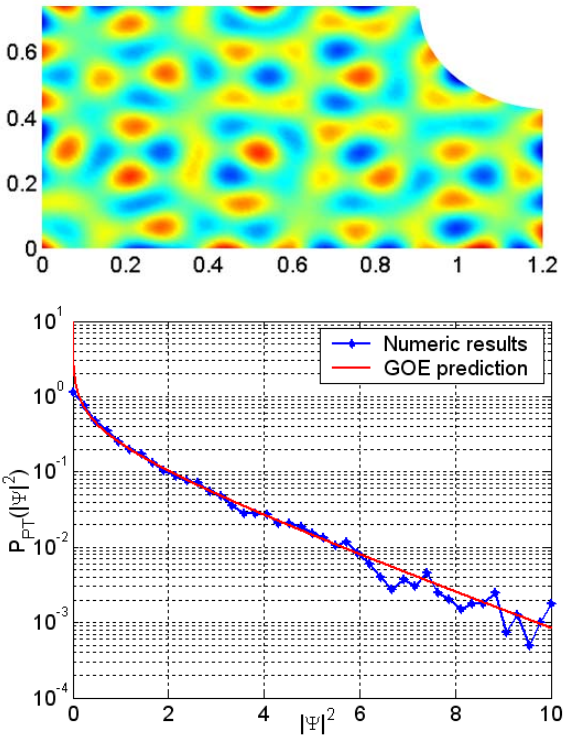

(a_2)

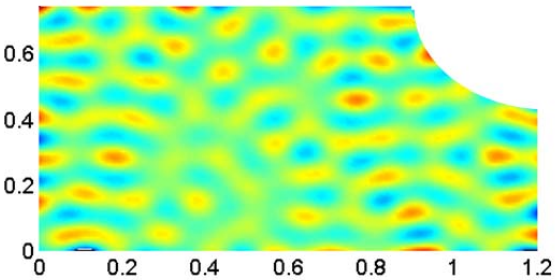

(b_1)

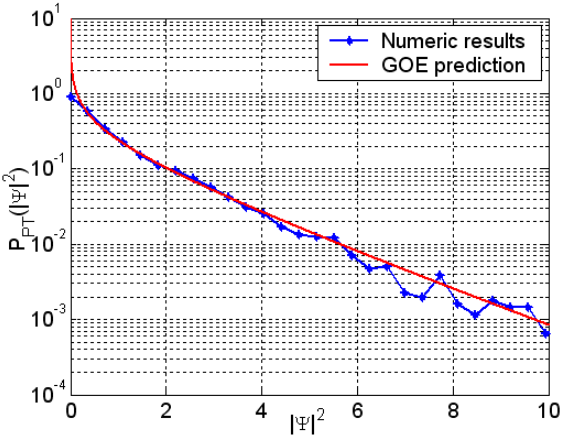

(b_2)

Figure 145: Spatial representation of the mode shape components and corresponding PT-distribution results for some almost-Gaussian mode shapes of the rectangular plate with an arc at one corner (spatial averaging approach). Plot (a): mode 137. Plot (b): mode 218.

For modes 137 and 218, the spatial layout of their nodal lines confirms the establishment of *chaotic* characteristics, evidencing the breaking of system symmetries by the arc effects. However, the low-frequency mode shapes are weakly influenced by the arc effects, since the typical wavelengths are larger than the circle radius. Additionally, bouncing ball periodic orbit effects are certainly expected due to the residual degree of system symmetry associ-

ated with the parallel sides of a perfect rectangular plate. In Figure 146, the statistical observable results of some low-frequency mode shapes are shown in detail.

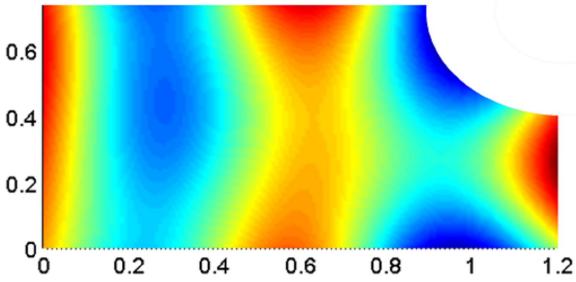

(a_1)

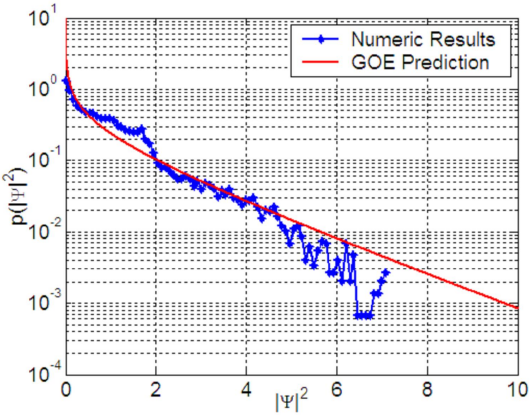

(a_2)

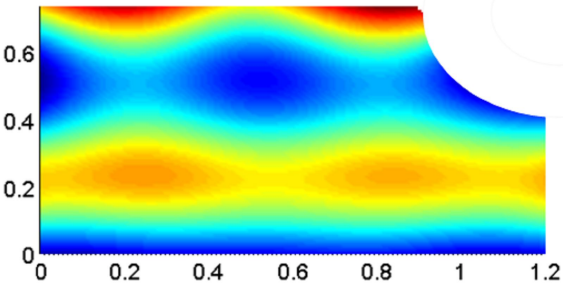
0.6
0.4
0.2
0
0
0.2
0.4
0.6
0.8
1
1.2

(b_1)

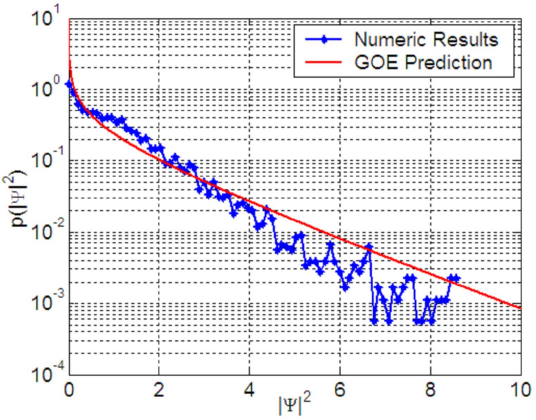
Numeric Results
GOE Prediction
10^{1}
10^{0}
10^{-1}
10^{-2}
10^{-3}
10^{-4}
$p(|\Psi|^2)$
0
2
4
6
8
10
$|\Psi|^2$

(b_2)

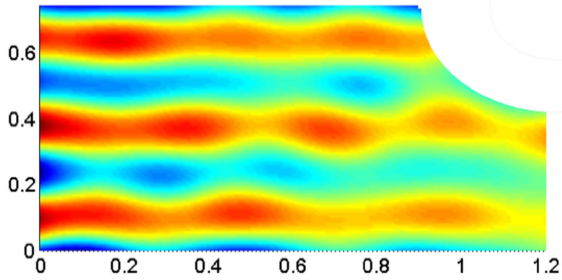

(c_1)

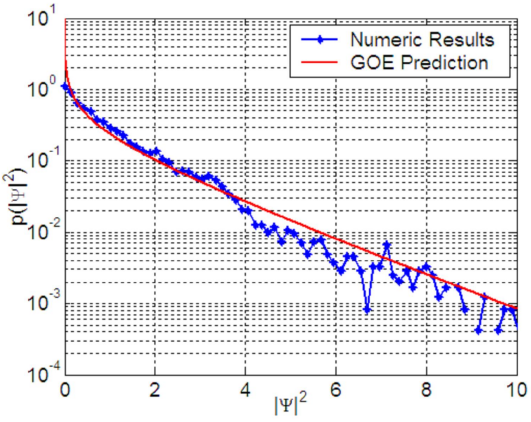

(c_2)

Figure 146: Spatial representation of the mode shape components and corresponding PT-distribution results for some low-frequency mode shapes of the rectangular plate with an arc at one corner (spatial averaging approach). Plot (a): mode 08. Plot (b): mode 11. Plot (c): mode 44.

As shown in Figure 146, the nodal lines are practically parallel to the plate sides, showing characteristics similar to those associated with the regular billiard systems with a perfect rectangular shape. The PT-distribution results in the tail region (*i.e.*, large normalized mode shape amplitudes) are

lower than the analytical prediction based on the GOE model, suggesting a relevant contribution of the bouncing ball periodic orbit effects to the mode shape statistics.

Chaotic Systems: 1/4 Sinai Stadium and Polygon Plates

In Figure 147, the spatial kurtosis and Lilliefors Test results are shown for the 1/4 Sinai stadium plate. The spatial kurtosis results suggest that most of the mode shapes are Gaussian, that is, $K \approx 3$. It is important to observe that the kurtosis values are not constant along the mode order domain and a narrow mode-to-mode fluctuation occurs around the GOE kurtosis value due to the effects associated with the finite characteristics of the system domain.

As shown in Figure 147 (b), the spatial Lilliefors Test results also suggest that a Gaussian distribution is expected for the mode shape components in the mid and high-mode order ranges. Indeed, the focusing and defocusing effects associated with the non-parallel and non-concentric circular sides lead to the establishment of chaotic statistics for mode shapes.

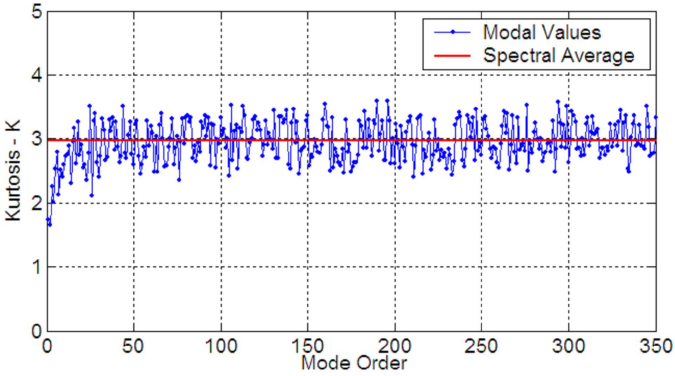

(a)

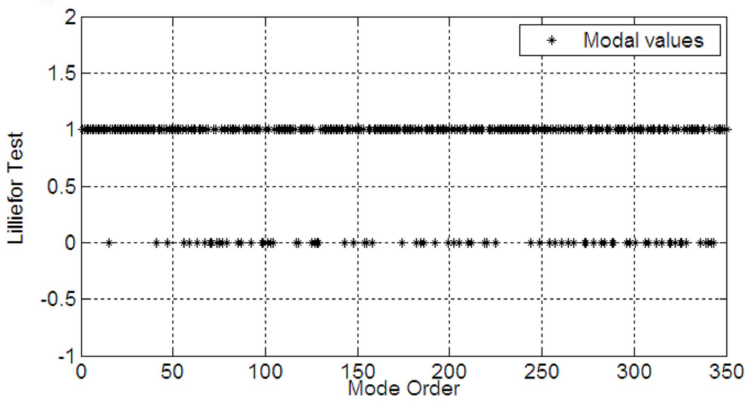

(b)

Figure 147: Spatial mode shape statistical observable results for 1/4 Sinai stadium plate (spatial averaging approach). Plot (a): kurtosis values. Plot (b): Lilliefors Test results.

In Figure 148, the spatial representation of the mode shape components and corresponding PT-distribution results are presented for some examples of the modes with *almost*-Gaussian characteristics.

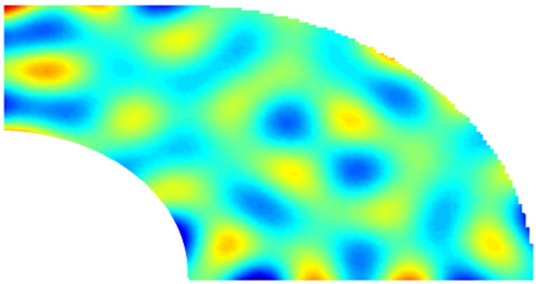

(a_1)

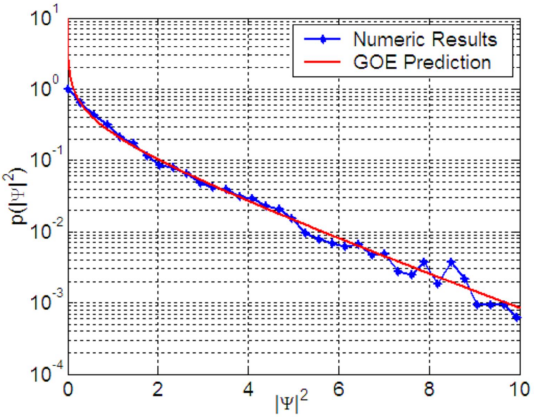
Numeric Results
GOE Prediction
p(|Ψ|²)
|Ψ|²
10¹
10⁰
10⁻¹
10⁻²
10⁻³
10⁻⁴
0
2
4
6
8
10

(a_2)

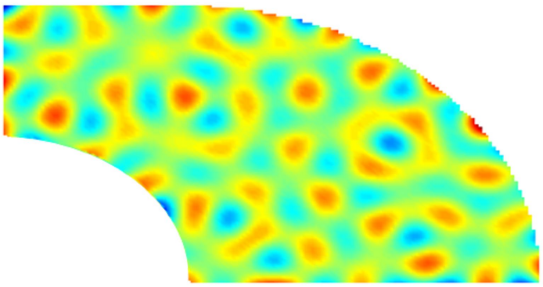

(b_1)

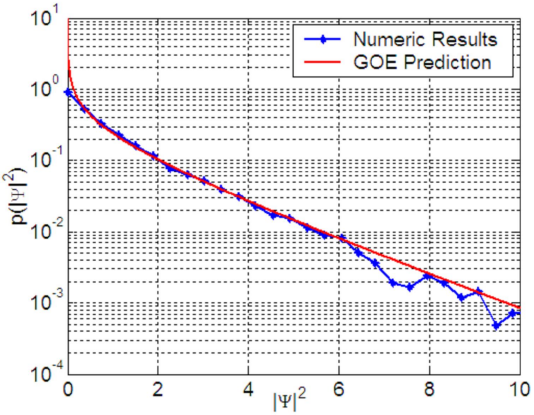
Numeric Results
GOE Prediction
p(|Ψ|²)
|Ψ|²
10^1
10^0
10^-1
10^-2
10^-3
10^-4
0
2
4
6
8
10

(b_2)

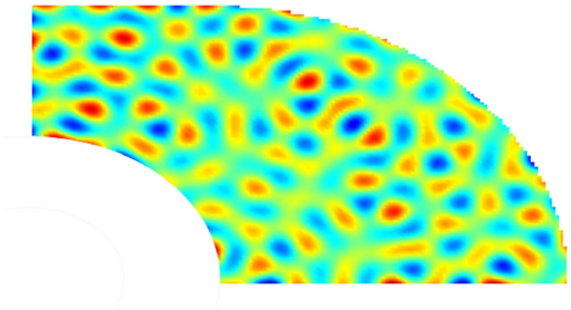

(c_1)

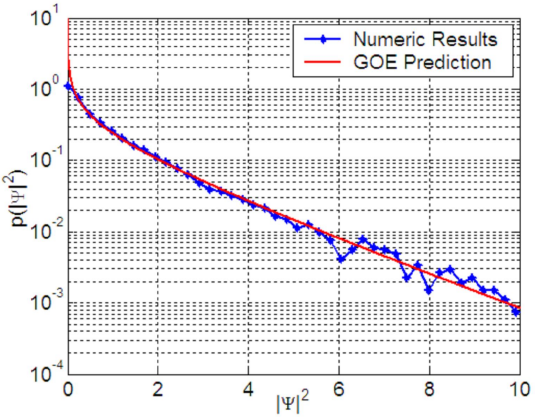

(c_2)

Figure 148: Spatial representation of the mode shape components and corresponding PT-distribution results for the 1/4 Sinai stadium plate (spatial averaging approach). Plot (a): mode 61. Plot (b): mode 186. Plot (c): mode 249.

As observed in Figure 148, the disordered spatial layout of the nodal lines and non-localized mode shape amplitudes strongly suggest the establishment of chaotic characteristics. The corresponding PT-results conform very well with the GOE prediction. Although it is not predicted by RMT, a small dispersion around the GOE prediction is observed over the range of large squared mode shape amplitudes. Indeed, these discrepancies are established due to incipient *non-universal* contributions associated with the effects of the finite nature of the system.

In Figure 149, the spectral mode shape statistics results are presented for the 1/4 Sinai stadium plate. As observed in Figure 149 (a), the most of spectral kurtosis values are also close to the expected Gaussian value, that is, $K \approx 3$.

The corresponding spectral Lilliefors Test results also suggest that most of the mode shape components have a Gaussian distribution, Figure 149 (b). Indeed, the spatial and spectral mode shape statistics results demonstrate that the *universal* characteristics are certainly established for several mode shapes of the 1/4 Sinai stadium plate.

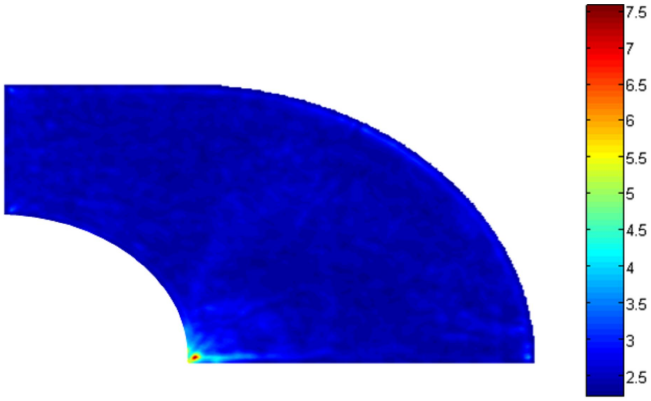

(a)

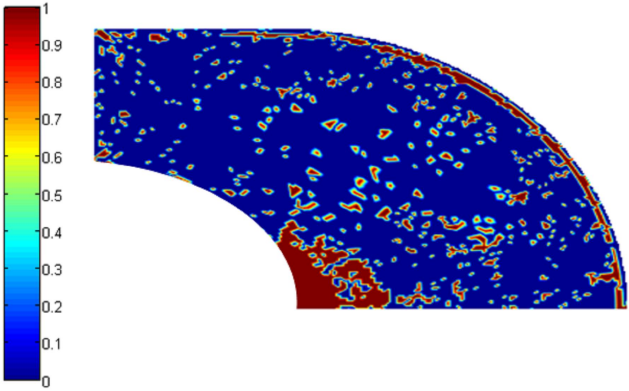

(b)

Figure 149: Spectral mode shape statistics results for the 1/4 Sinai stadium plate (spectral averaging approach). Plot (a): kurtosis results. Plot (b): Lilliefors Test results.

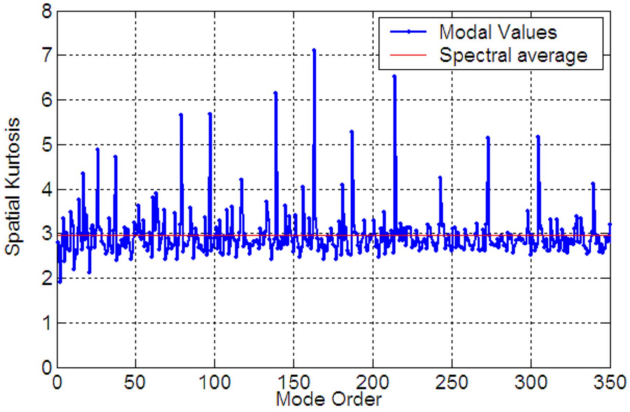

(a)

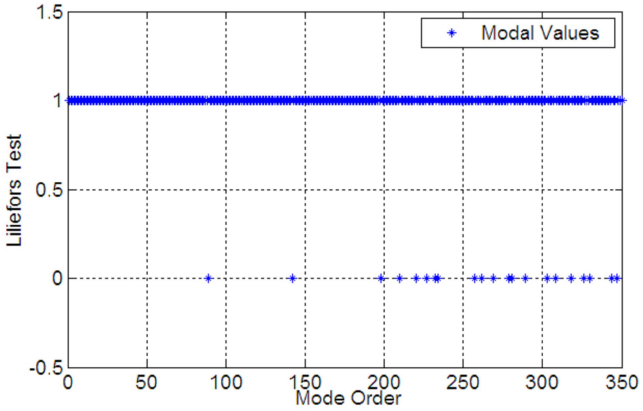

(b)

Figure 150: Spatial mode shape statistical observable results for the polygonal plate (spatial averaging approach). Plot (a): kurtosis values. Plot (b): Lilliefors Test results.

In Figure 150, the spatial kurtosis and Lilliefors Test results are shown for the polygonal plate. In a similar manner to the mode shape statistics results for the 1/4 Sinai stadium plate, the spatial kurtosis results also suggest that several mode shapes are *near*-Gaussian,Figure 150 (a). Indeed, the two

non-parallel sides of the polygonal plate seem to remove completely the effects of the system symmetry on the mode shape statistics. As is known, the effects associated with the finite nature of the system on the mode shapes are clearly expressed through a narrow mode-to-mode fluctuation around the GOE kurtosis value.

As shown in Figure 150 (b), the spatial Lilliefors Test results also showed that a Gaussian distribution occurs for several mode orders, suggesting the establishment of chaotic statistics for mid and high-frequency mode shapes.

In Figure 151, the spatial representation of the mode shape components and corresponding PT-distribution results are presented for some modes with almost-Gaussian characteristics.

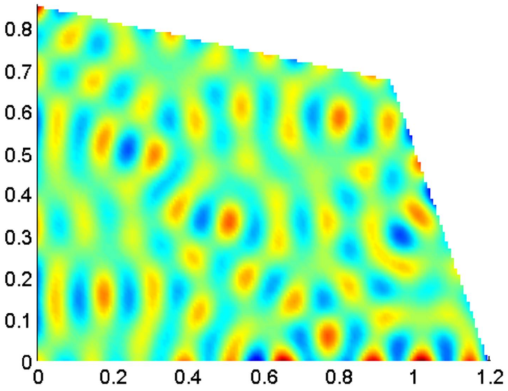

(a_1)

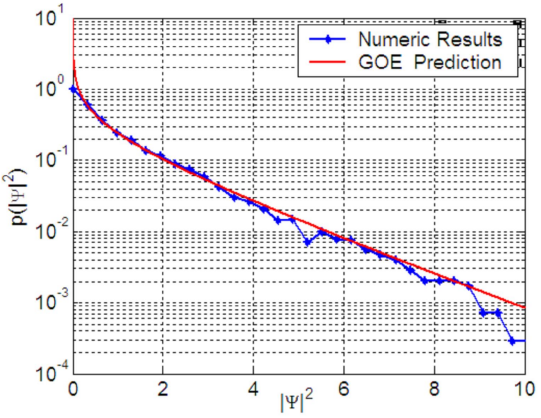
Numeric Results
GOE Prediction
p(|Ψ|²)
|Ψ|²
10^1
10^0
10^-1
10^-2
10^-3
10^-4
0
2
4
6
8
10

(a_2)

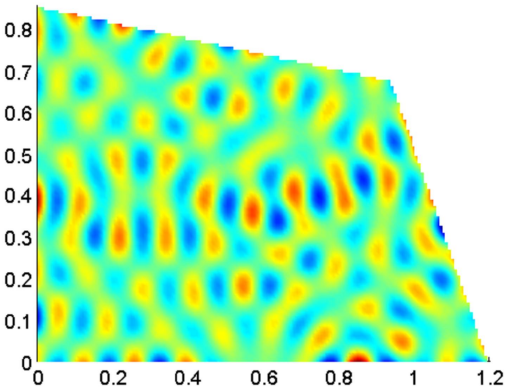
0.8
0.7
0.6
0.5
0.4
0.3
0.2
0.1
0
0
0.2
0.4
0.6
0.8
1
1.2

(b_1)

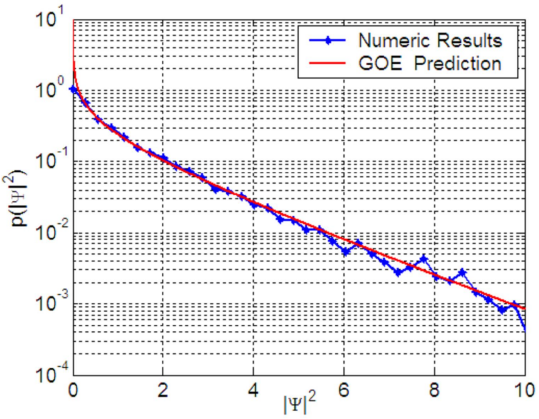

(b_2)

Figure 151: Spatial representation of the mode shape components and corresponding PT-distribution results for some mode shapes of the polygonal plate (spatial averaging approach). Plot (a): mode 198. Plot (b): mode 220.

As observed in Figure 151, the disordered spatial orientation of the nodal lines suggests a *deterministic* establishment of chaotic characteristics for the mode shapes of the polygonal plate. In Figure 152, the spectral mode shape statistics results for the polygonal plate are presented. The kurtosis and Lilliefors Test results seem to demonstrate that *universal* characteristics are established for several mode shape statistics.

Although the polygon plate does not present a classically chaotic geometry, similar results to those of the 1/4 Sinai stadium plate were surprisingly observed. Indeed, this good agreement with the GOE statistics demonstrates that the geometrical perturbation of the system symmetries through the breaking of the geometrical regularity leads to the establishment of substantial effects on the modal parameter statistics. As discussed in the RMT and POT literature, the disorder strength of these effects is associated with the magnitude of the ratio of the frequency wavelength to the typical size of the focusing or defocusing elements, (113, 65, 72).

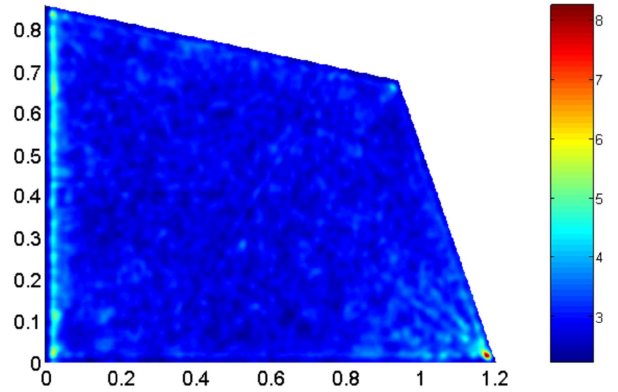

(a)

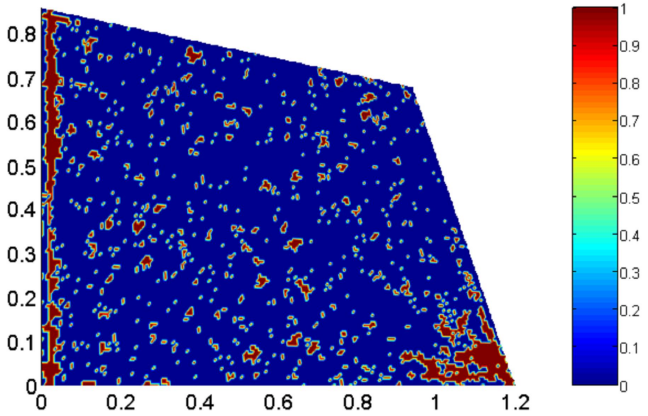

(b)

Figure 152: Spectral mode shape statistics results for the polygonal plate (spectral averaging approach). Plot (a): kurtosis results. Plot (b): Lilliefors Test results.

Disordered System: Point Mass-loaded Rectangular Plate

In Figure 153, the spatial kurtosis and Lilliefors Test results are shown for the mass-loaded rectangular plate. The spatial kurtosis results suggest that most of the mode shapes are near-Gaussian, where the probabilistic mode value is $K \sim 3.1$ and the spectral mean value is $\bar{K} = 3.26$. It is important to observe that the kurtosis values are not constant along the mode order domain and a mode-to-mode fluctuation occurs around the typically expected kurtosis value.

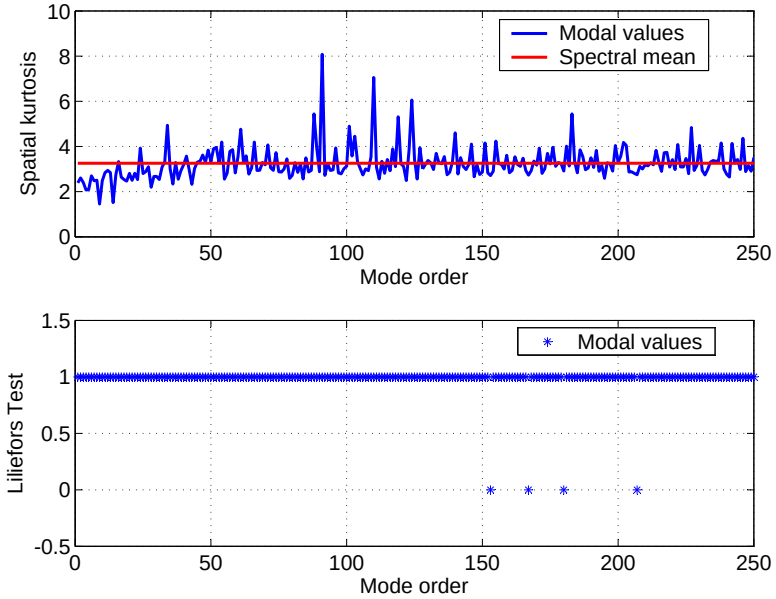

Figure 153: Spatial mode shape statistical observable results for the mass-loaded rectangular plate (spatial averaging approach). Plot (a): kurtosis values. Plot (b): Lilliefors Test results.

As observed in Figure 153 (a), a good agreement is observed between the numerical results and the GOE prediction beyond mode 50. For the low-order mode shapes, a gradual transition from almost-nominal to Gaussian

statistics is expected as the mode order increases. Additionally, some discrete peaks in the kurtosis curve suggest the establishment of an incipient structural localization.

The corresponding spatial Lilliefors Test results are shown in Figure 153 (b) and suggest that only a reduced number of mode shapes have components with Gaussian distribution, although the spatial kurtosis values of several modes are close to the value expected for Gaussian mode shapes. In Figures154 (a) and (b), histograms of the skewness coefficient and spatial kurtosis can be observed. These results show that for most of the mode shapes the components have an approximately symmetric distribution. Additionally, the spatial kurtosis results have an almost-Gaussian distribution with probabilistic mode value of close to $K^{GOE} \sim 3$.

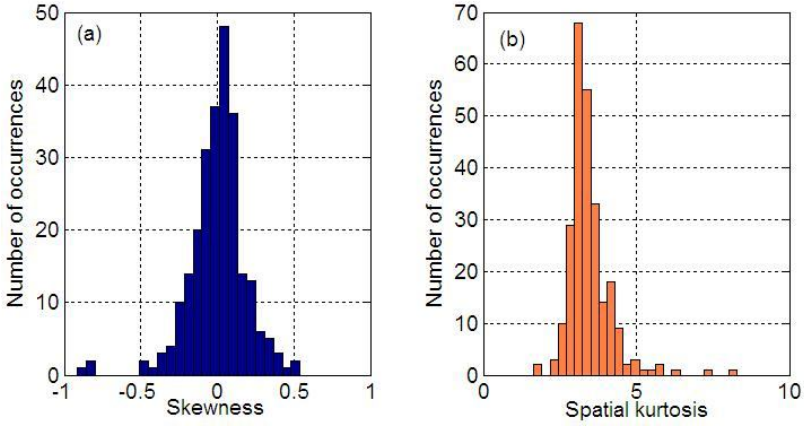

Figure 154: Histograms of the spatial skewness coefficients and kurtosis values for the mass-loaded rectangular plate.

Based on these spatial mode shape statistics results, three major classes of spatial mode shape statistics are clearly established: almost-nominal, almost-Gaussian and weakly localized. In Figure 155, the PDF of the mode shape components and the spatial representation of squared mode shape amplitudes are presented for a typical mode shape of these statistical mode shape classes.

In Figure 155 (a), the main spatial characteristics of the almost-Gaussian mode shape statistics are demonstrated for mode 207. The spatial distribution of the mode shape components of mode 207 is Gaussian, as expected for GOE eigenvectors. Additionally, the mode shape amplitudes are delocalized throughout the spatial domain of the plate system and the nodal lines have random orientations, characterizing a good agreement with the GOE model.

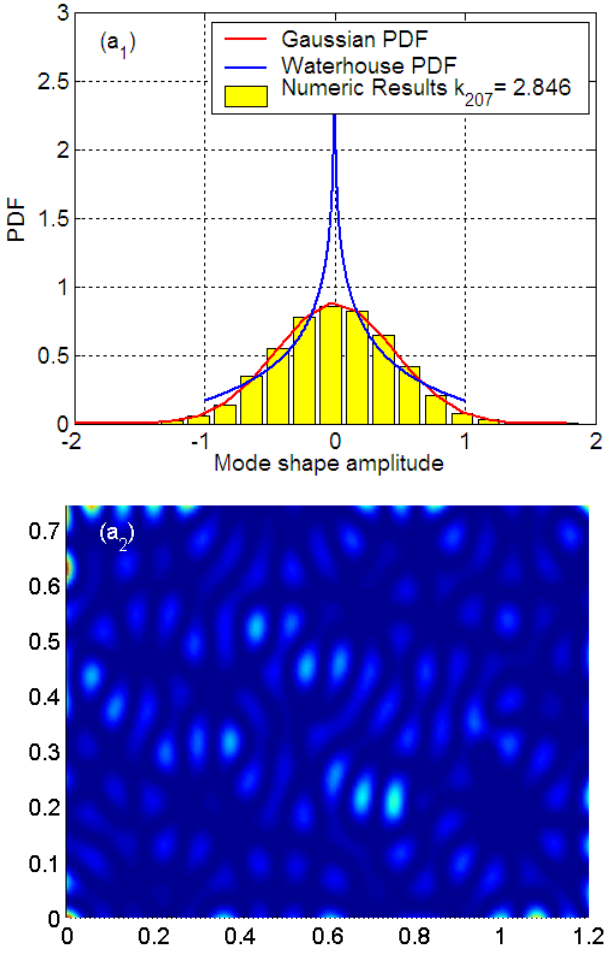

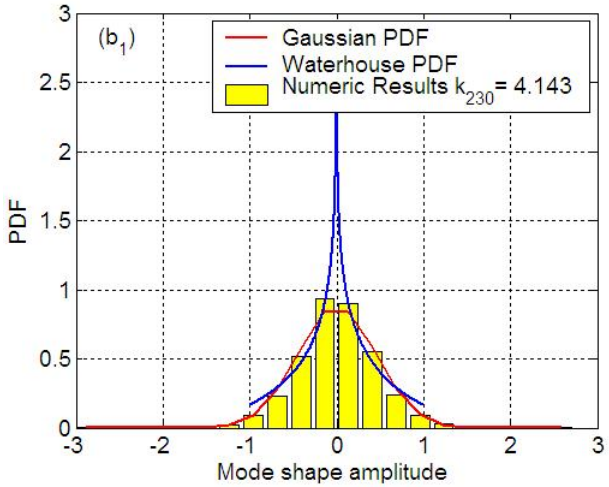
(b1)
Gaussian PDF
Waterhouse PDF
Numeric Results k230= 4.143
PDF
Mode shape amplitude
3
2.5
2
1.5
1
0.5
0
-3
-2
-1
0
1
2
3

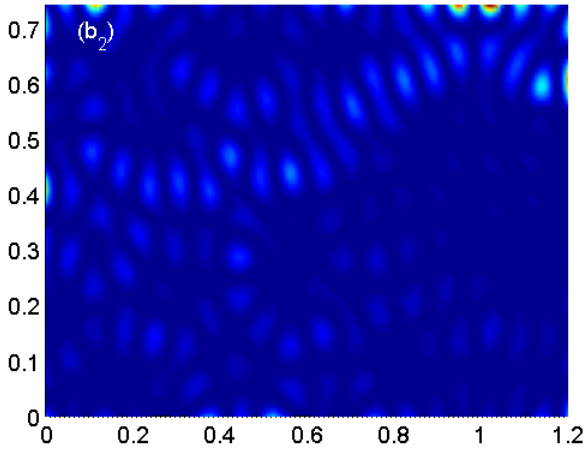
(b2)
0.7
0.6
0.5
0.4
0.3
0.2
0.1
0
0
0.2
0.4
0.6
0.8
1
1.2

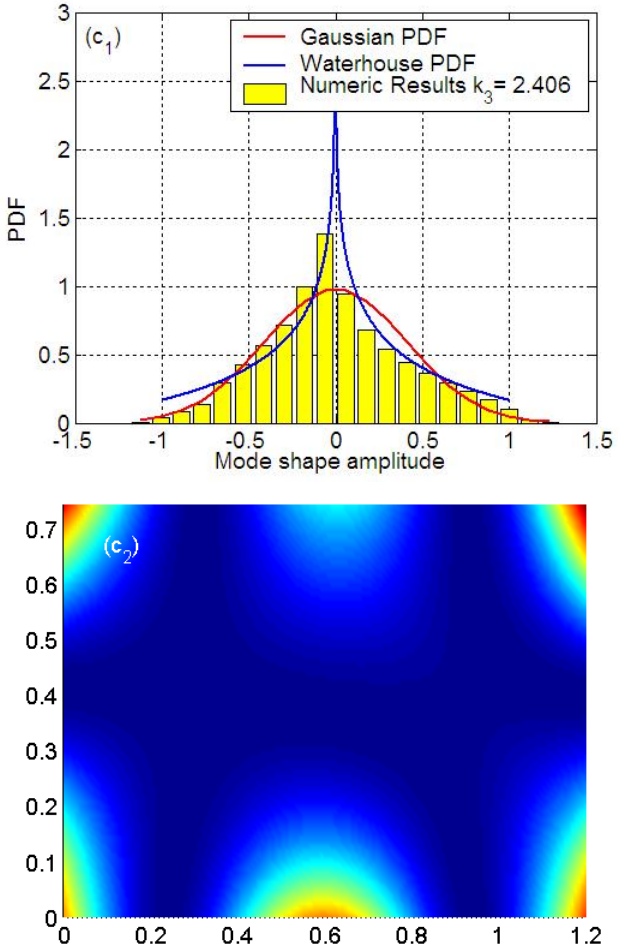

Figure 155: Spatial mode shape characteristics of the mass-loaded rectangular plate: PDF of the mode shape components and spatial representation of the squared mode shape amplitudes (spatial averaging approach). Plot (a): Mode 207 - almost-Gaussian. Plot (b): Mode 230 - weakly localized. Plot (c): Mode 003 - almost-nominal.

As observed in Figure 155 (b), the spatial characteristics of mode 230

show the establishment of the incipient or weak localization characteristics which are associated with the kurtosis values slightly higher than $k = 3$. The amplitudes of the mode shape components localized in the upper region of the plate are slightly larger than those localized in the bottom region. In Figure 155 (c), the main spatial characteristics of the almost-nominal mode shape statistics are demonstrated for mode 003. The spatial distribution of the mode shape components presents intermediate characteristics between the Waterhouse and Gaussian PDF predictions. The establishment of the nodal lines parallel to the plate sides shows that mode shape symmetries remained unbroken in relation to the plate sides. Indeed, for low-order mode shape the wavelengths are larger than the typical distances between two point masses and thus the effects of the scatter phenomenon are certainly minimized.

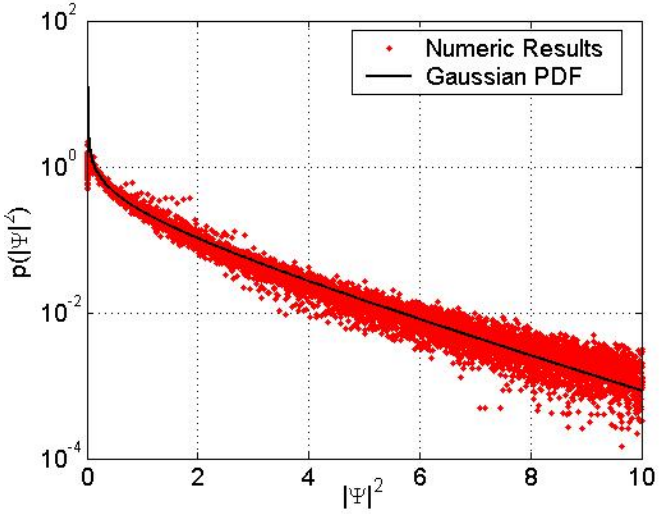

(a)

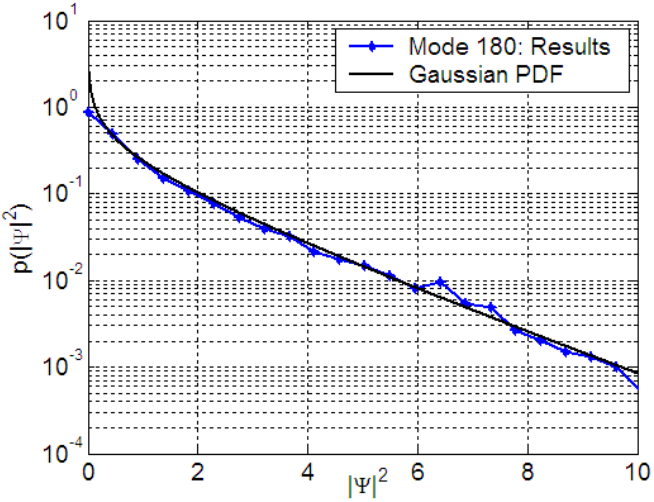
Mode 180: Results
Gaussian PDF
$p(|\Psi|^2)$
$|\Psi|^2$
10^{1}
10^{0}
10^{-1}
10^{-2}
10^{-3}
10^{-4}
0
2
4
6
8
10

(b)

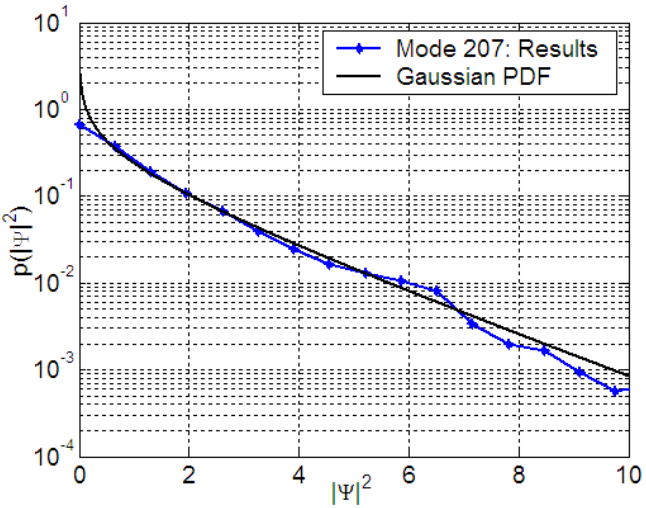
Mode 207: Results
Gaussian PDF
$p(|\Psi|^2)$
$|\Psi|^2$
10^{1}
10^{0}
10^{-1}
10^{-2}
10^{-3}
10^{-4}
0
2
4
6
8
10

(c)

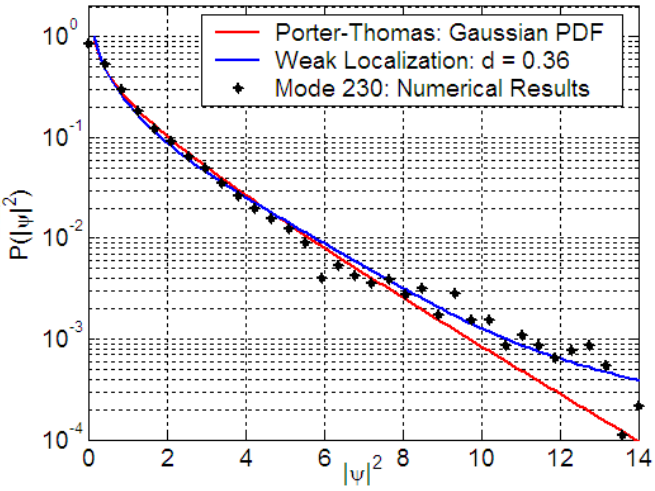

(d)

Figure 156: Porter-Thomas distribution results for the mass-loaded rectangular plate (spatial averaging approach). Plot (a): some typical mode orders. Plots (b) and (c): modes 180 and 207 (almost-Gaussian mode shape statistics), respectively. Plot (d): mode 230 (weak localization statistics) and non-linear sigma model expression (fitted with $d_L = 0.36$ - Equation 2.53).

As shown in Figure 156 (a), the Porter-Thomas distribution results are presented for most of the mode shapes. Small discrepancies in relation to the GOE model predictions are observed mainly in the range associated with the large normalized mode shape amplitudes (*i.e.*, the tail region of the distribution) which is strongly sensitive to details of the system nature. Two examples of almost-Gaussian mode shapes are shown in Figures 156 (b) and (c). A good agreement with the analytical prediction based on the GOE model is observed for the distribution of normalized mode shape components of modes 180 and 207, showing a perfect compatibility with the Lilliefors Test results shown in Figure 153 (b).

In Figure 156 (d), the PT-distribution results for mode 230 are presented and the incipient elevation of the distribution tail suggests the establishment of weak localization characteristics. In this regard the numerical results were fitted by the non-linear sigma model expression for a weak localization

regime, proposed by Equation (2.53). Good performance is observed when a disorder localization parameter equal to $d_L = 0.36$ is considered.

Considering the spatial correlation characteristics of the mode shape components of the mass-loaded rectangular plate, the linear and squared spatial correlation functions of the normalized mode shape components were evaluated for some modes with almost-Gaussian statistics characteristics. In Figure 157, the numerical results are compared with the GOE model predictions for bi-dimensional systems, Equations (2.40) and (2.44), respectively.

As shown in Figure 157 (a), a small dispersion is observed around the analytical GOE prediction when only the individual results are considered. In this regard, the mean value seems to be a robust and representative parameter to describe the spatial correlation statistics[4]. The agreement between the analytical GOE prediction and numerical results is certainly improved as the averaging process is considered in the evaluation of the spatial correlation functions of normalized mode shape components.

On other hand, the results for the squared correlation function of the normalized mode shape components seem to be more sensitive to small non-universal characteristics associated with the details of the system nature and thus some discrepancies in relation to the prediction based on the GOE model occur mainly for large values of $k_f r$, Figure 157 (b). It is important to note that these results seem to demonstrate that the application of the dispersion relation of infinite plate, Equation (4.2), is also sufficiently accurate for finite and almost-homogeneous plates, such as the mass-loaded plate system investigated here. To the best of the author's knowledge, this is the first application of non-linear sigma model expressions to describe the spatial correlation characteristics of the mode shape statistics of almost-chaotic engineering systems, since the mass-loaded plate system could be considered to be very similar to an equipment-loaded satellite panel, Brown *et al.* (1, 18).

The statistical characteristics of the mode shape components considering the spectral averaging approach are presented in Figure 158. The spectral kurtosis results are close to the Gaussian value, that is, $K \approx 3$, except for the small and isolated peaks observed, which are likely associated with the weak localization characteristics, Figure 158 (a). Although not shown here in detail, most of the spectral kurtosis values lie within the following range: $2.7 \lesssim K \lesssim 3.1$, where the spatial mean and typically expected, or probabilistic mode, values are 3.02 and 2.85, respectively.

[4]This hypothesis has been successfully adopted by several researchers in the Quantum Physics field, (71, 69, 74, 70).

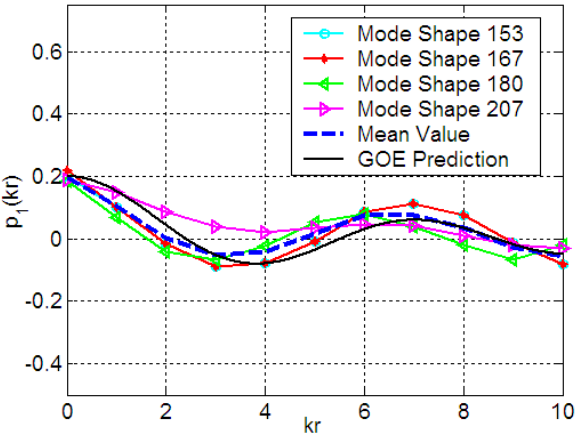

(a)

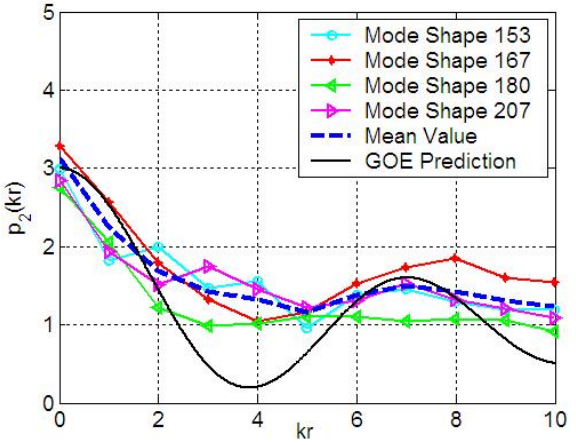

(b)

Figure 157: Spatial normalized mode shape correlation results for the mass-loaded rectangular plate: modes 153, 167,180, and 207 (spatial averaging approach). Plot (a): linear correlation function (P_1). Plot (b): squared function (P_2).

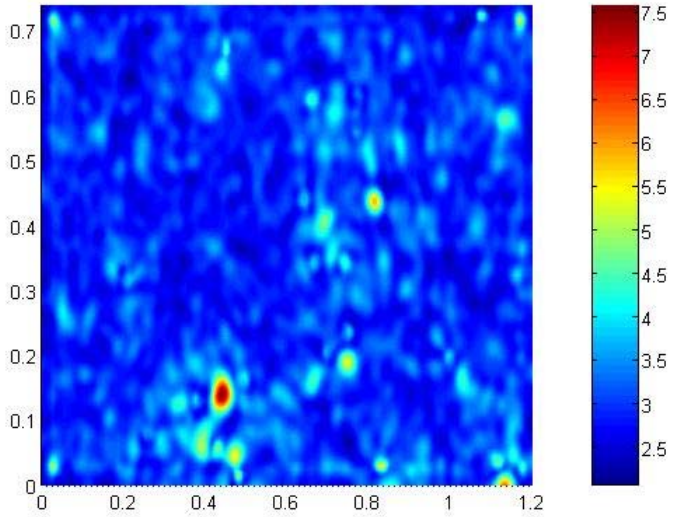

(a)

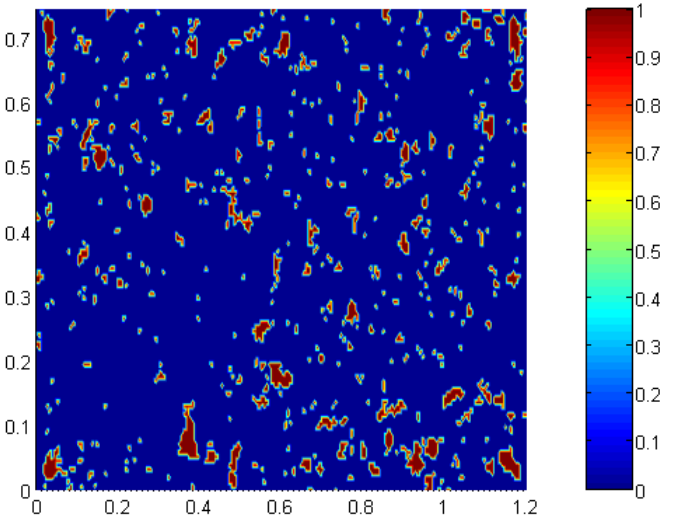

(b)

Figure 158: Spectral mode shape statistics results for the mass-loaded rectangular plate (spectral averaging approach). Plot (a): kurtosis results. Plot (b): Lilliefors Test results.

As shown in Figure 158 (b), most of the mode shape components were approved in the Lilliefors Test, suggesting the establishment of a Gaussian distribution. Indeed, similar characteristics are observed for perfect GOE eigenvectors, where the eigenvectors are almost statistically independent and their inter-modal correlations can be neglected when large matrix dimensions are considered, Brody *et al.* (56). On the other hand, most of the plate locations, for which the mode shape components were not approved by the Lilliefors Test, can be directly associated with the mode shape component locations where the kurtosis values are larger than the Gaussian kurtosis value, that is, $K > 3$. Thus, these particular mode shape components are expected to be influenced by the incipient structural localization effects, where their spatial distributions are slightly asymmetric and have long-tail characteristics.

4.3.3 Kinetic Energy Density Statistics

In this subsection the spectral statistics of the kinetic energy density results for the bare and mass-loaded rectangular plates are investigated considering two types of excitations: single-point and spatially-averaged. The spectral mean and relative variance of the kinetic energy density results are compared with SEA predictions based on GOE and Poisson models.

SEA Prediction

For an excited single subsystem, the SEA power balance showed that the power input (Π_{in}) to the structure is equal to the dissipated power (Π_{diss}). Indeed, the total energy of the flexural plates investigated here can be adequately expressed in terms of the real part of the input mobility results of an infinite plate system, $Y_\infty(\omega)$. This assumption is usually adopted in the analytical SEA field, Lyon and Dejong (29). A generic expression for the SEA predicted energy is given by:

$$E_{SEA} = \frac{Re\,(Y_\infty(\omega))}{2\omega\eta}. \tag{4.11}$$

Therefore, the kinetic energy density for a flexural plate is given by:

$$T_{SEA} = \frac{E_{SEA}}{2R_a} = \frac{Re\,(Y_\infty(\omega))}{4R_a\omega\eta}, \tag{4.12}$$

where R_a is the area of the plate.

The analytical mobility expression for an infinite plate subjected to a

single-point excitation is available in the literature, (29, 38, 5). According to Fahy and Walker (5), the analytical mobility expression for an infinite plate system is given by:

$$Y_{\infty}(\omega) = \frac{\pi n(\omega)}{2M}, \tag{4.13}$$

where M and $n(\omega)$ are the total mass and modal density of the flexural plate, respectively.

Lyon and Dejong (29) showed that the expression for the modal density of an isotropic plate is given by:

$$n(\omega) = \frac{R_a A\sqrt{3}}{2\pi h c_L^p}, \tag{4.14}$$

where c_L^p is the longitudinal wave speed in a plate and is given by:

$$c_L^p = \sqrt{\frac{E_{ym}}{\rho(1-\nu^2)}}. \tag{4.15}$$

Substituting the previous analytical mobility expression, Equation (4.13), into Equation (4.12), the kinetic energy density for a flexural plate is given by:

$$T_{SEA} = \frac{\pi n(\omega)}{8MR_a\omega\eta}. \tag{4.16}$$

Spectral Kinetic Energy Density Statistics: General Considerations

In the following, the spectral averaging approach was adopted to investigate the statistical characteristics of the kinetic energy density responses for the bare and mass-loaded rectangular plates. The first two statistical moments of the kinetic energy density responses were evaluated within the 1/3 octave frequency band limits.

Two types of loadings were considered: unitary single-point and spatially-averaged excitations. For the single-point case, the spatial location of the excitation point (X_0) was an arbitrary choice and was considered to be the same for the two plates investigated herein. The spatial coordinates of the excitation point are given by $X_0 = (0.923, 0.227)$ m.

Additionally, the damping loss factor (DLF) was considered *frequency-constant*, since the mechanical loss mechanisms for metal plates

are considered to be approximately spatially-distributed, (28). In this regard, three distinct DLF values were considered in order to provide distinct levels of modal superposition. The DLF values adopted are η = 0.010, 0.015 and 0.030. The free-free boundary condition was also adopted for both flexural plates investigated herein.

The kinetic energy density results for the bare and mass-loaded rectangular plates are initially evaluated for each DLF in terms of the narrow frequency band domain with intervals of 10 Hz. The excitation frequency range considered was from 0 to 1400 Hz. A sufficiently large number of modes was assumed in the superposition process to ensure the response convergence in the frequency range investigated.

Spectral Kinetic Energy Density Statistics: Spatially-Averaged Excitation

For the evaluation of the spatially-averaged kinetic energy density results, the single-point responses were evaluated for 100 distinct excitation points with arbitrary locations. In Figure 159 (a), the individual kinetic energy density responses and arithmetic mean values are presented for the bare rectangular plate along with the SEA analytical prediction for a damping loss factor magnitude of 1%, that is, $\eta = 0.010$. The corresponding 1/3 octave frequency band kinetic energy density results are presented in Figure 159 (b). An excellent agreement is observed between the SEA prediction and averaged numerical results, regardless of the frequency band domain considered.

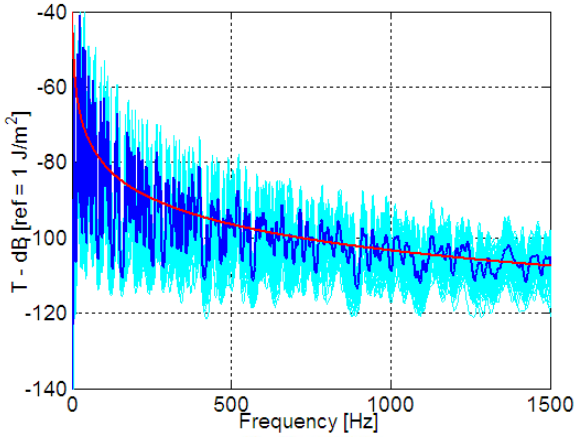
-40
-60
-80
-100
-120
-140
T - dB [ref = 1 J/m2]
0
500
1000
1500
Frequency [Hz]

(a)

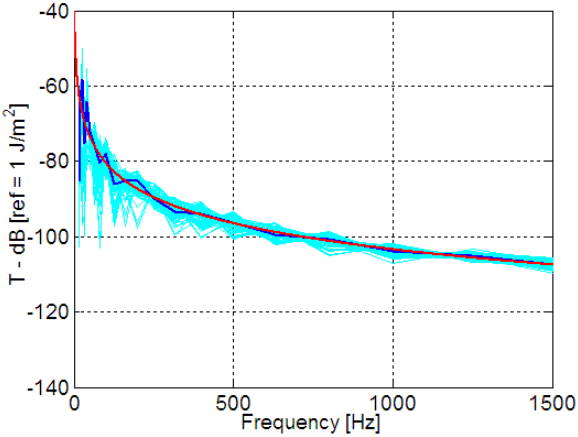
-40
-60
-80
-100
-120
-140
T - dB [ref = 1 J/m2]
0
500
1000
1500
Frequency [Hz]

(b)

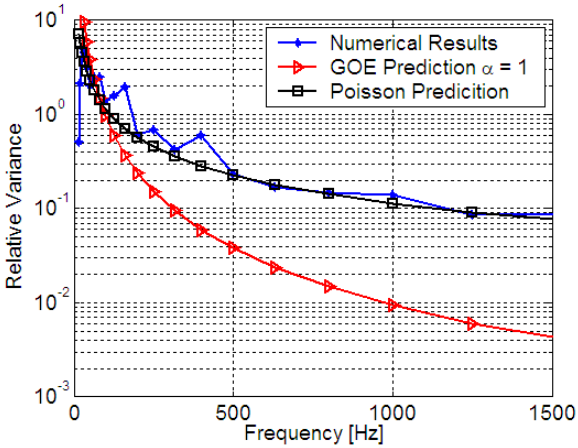

(c)

Figure 159: Spatially-averaged kinetic energy density results for the bare rectangular plates with $\eta = 0.010$. Plot (a): individual responses and spatially-averaged value - narrow frequency band domain (spatial averaging approach). Plot (b): individual responses and spatially-averaged value - 1/3 oct. frequency band domain (spatial averaging approach). Plot (c): spectral relative variance of spatially-averaged kinetic energy density response (spectral averaging approach).

The spectral relative variance of the spatially-averaged kinetic energy density response is presented in Figure 159 (c). As expected, the numerical results conform very well with the Poisson prediction mainly in the mid and high-frequency ranges. This agreement is supported by two factors: (*i*) the spatially-averaged excitation completely removes the contribution of the mode shape statistics to the kinetic energy responses and (*ii*) the spectral natural frequency statistics are approximately Poissonian.

In Figure 160, the relative variance results associated with the other two values for the DLF are plotted along with the analytical predictions based on the Poisson and GOE models.

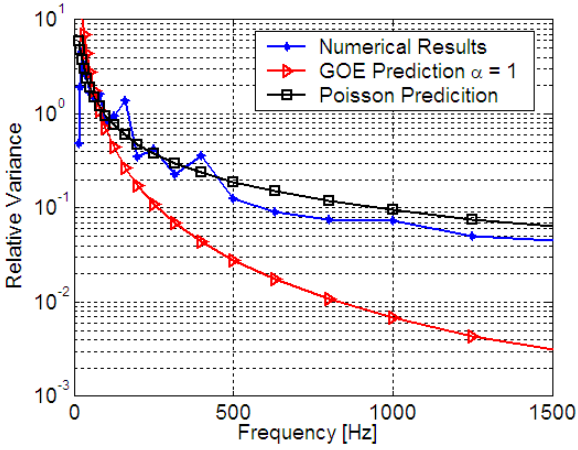

(a)

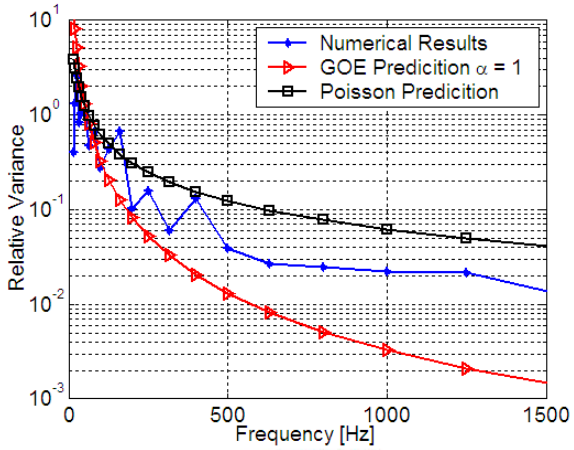

(b)

Figure 160: Relative variance of the spatially-averaged kinetic energy density results for the bare rectangular plate with $\eta = 0.015$ and 0.030, respectively (spectral averaging approach).

As shown in Figures 160 (a) and (b), the analytical prediction based

on the Poisson model overestimates both numerical results. Additionally, it is observed that the spectral relative variance results are gradually reduced as the damping loss factor increases. Indeed, as the damping mechanism effects become substantial a large number of modes contribute to the energy response, and thus the small discrepancies in the long-range fluctuations (*i.e.*, large spectral distances) between the statistics of the Poisson eigenvalues and the natural frequencies may become relevant in terms of the kinetic energy density responses.

As observed previously in Figure 123, the spectral natural frequency statistics of the bare rectangular plate are slightly more rigid than those described by the Poisson model. Therefore, the reduction in the spectral variability of the spatially-averaged kinetic energy density results could be associated with the establishment of the inter-modal correlations which reinforce the spectral rigidity characteristics of the natural frequencies along the frequency domain.

Similarly to the case of the bare rectangular plates, the evaluation of the spatially-averaged kinetic energy density response for the mass-loaded rectangular plate was based on the single-point responses for 100 distinct excitation points[5].The individual kinetic energy density responses and arithmetic mean value are presented along with the SEA analytical prediction for a damping loss factor of 1%, that is, $\eta = 0.010$, Figure 161 (a). The 1/3 octave frequency band kinetic energy density results are plotted in Figure 161 (b). As in the case of the bare rectangular plate, the averaged numerical results conform very well with the SEA prediction, regardless of the frequency domain considered.

[5]Although not shown here, convergence analysis of the first two statistical moments of the kinetic energy results was carried out in relation to the number of excitation points in order to guarantee the efficiency of the spatial averaging process.

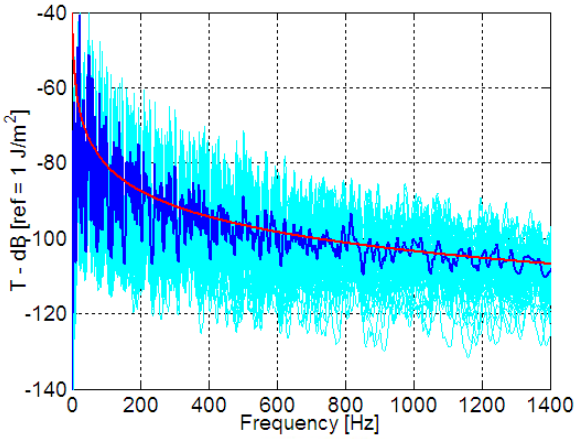
-40
-60
-80
-100
-120
-140
T - dB [ref = 1 J/m^2]
0
200
400
600
800
1000
1200
1400
Frequency [Hz]

(a)

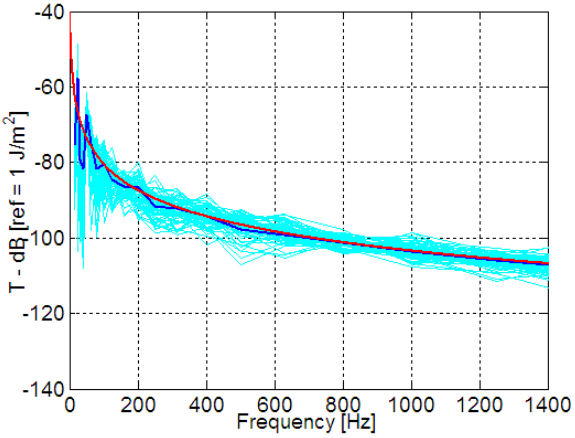
-40
-60
-80
-100
-120
-140
T - dB [ref = 1 J/m^2]
0
200
400
600
800
1000
1200
1400
Frequency [Hz]

(b)

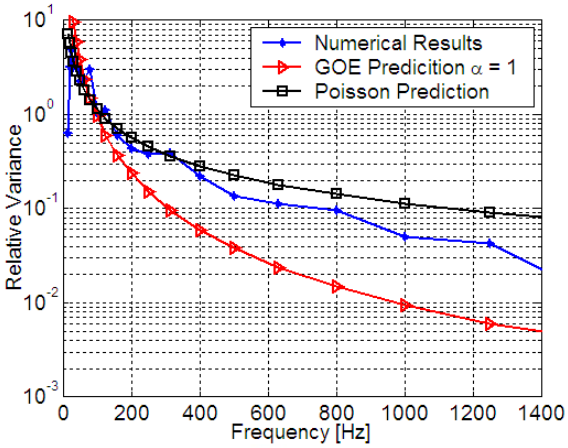

(c)

Figure 161: Spatially-averaged kinetic energy density results for the mass-loaded rectangular plates with $\eta = 0.010$. Plot (a): individual responses and spatially-averaged value - narrow frequency band domain (spatial averaging approach). Plot (b): individual responses and spatially-averaged value - 1/3 oct. frequency band domain (spatial averaging approach). Plot (c): spectral relative variance of the spatially-averaged kinetic energy density response (spectral averaging approach).

As observed in Figure 161 (c), the spectral relative variance of the spatially-averaged kinetic energy density response shows intermediate characteristics between the Poisson and GOE model predictions. As discussed in the SEA and Physics literature (167, 168, 16, 18), the introduction of the point masses to the bare rectangular plate probably leads to coupling of the natural frequencies, changing substantially their statistical characteristics along the spectral domain. Indeed, the spectral natural frequency statistical observable results for the mass-loaded rectangular plate also suggest the establishment of the *level repulsion* phenomenon and *spectral rigidity* characteristics for the natural frequencies, which reduces the relative variance of the spatially-averaged kinetic energy density response.

In Figure 162, the relative variance results for the mass-loaded rectangular plate associated with $\eta = 0.015$ and 0.030 are plotted along with the analytical predictions based on Poisson and GOE models.

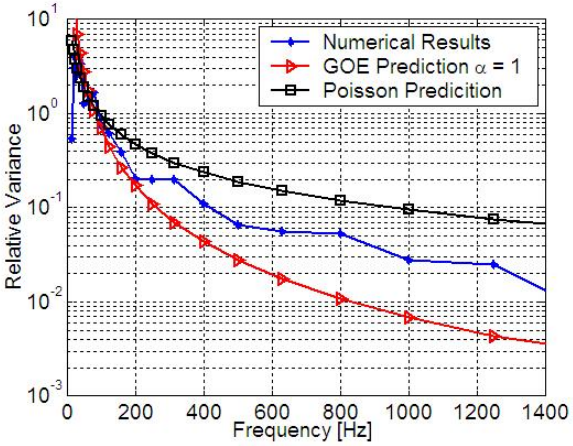

(a)

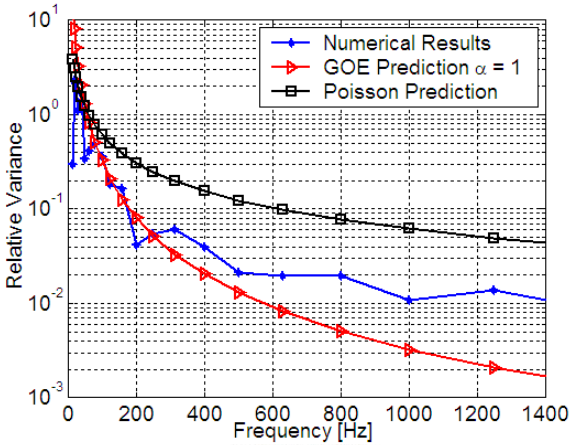

(b)

Figure 162: Relative variance of the spatially-averaged kinetic energy density responses for the mass-loaded rectangular plates with $\eta = 0.015$ and 0.030, respectively (spectral averaging approach).

As shown in Figures 162 (a) and (b), the spectral relative variance re-

sults have intermediate characteristics between the predictions based on the Poisson and GOE models. As observed previously in Figure 127, the spectral natural frequency statistics of the mass-loaded rectangular plate are slightly less rigid than those described by the GOE model, mainly for the long-range fluctuation statistics (*i.e.*, statistics of the large spectral distances). Therefore, the existing discrepancies between the numerical results and GOE predictions could be associated with the *non-universal* characteristics of the spectral natural frequency statistics which are reinforced as the damping loss factor increases.

Spectral Kinetic Energy Density Statistics: Single Point-Loading

In Figure 163, the spectral mean and relative kinetic energy density responses are shown for the bare and mass-loaded rectangular plates subjected to a unitary single-point loading at excitation point X_0. The kinetic energy density results expressed in the narrow and 1/3 oct. frequency band domains are presented along with the SEA analytical predictions based on the Poisson and GOE models.

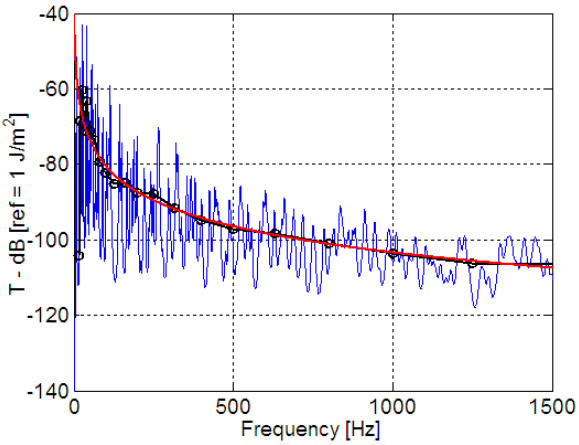

(a)

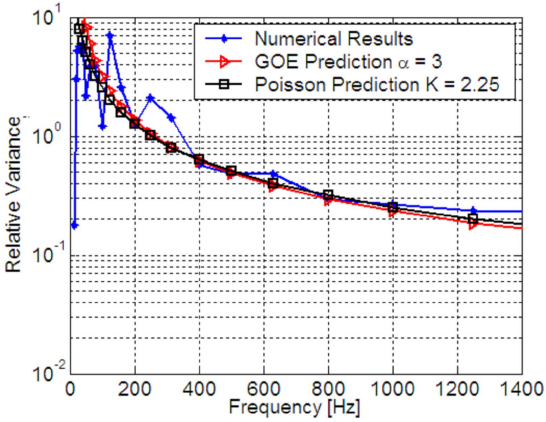
Numerical Results
GOE Prediction α = 3
Poisson Prediction K = 2.25
Relative Variance
Frequency [Hz]
10^1
10^0
10^-1
10^-2
0
200
400
600
800
1000
1200
1400

(b)

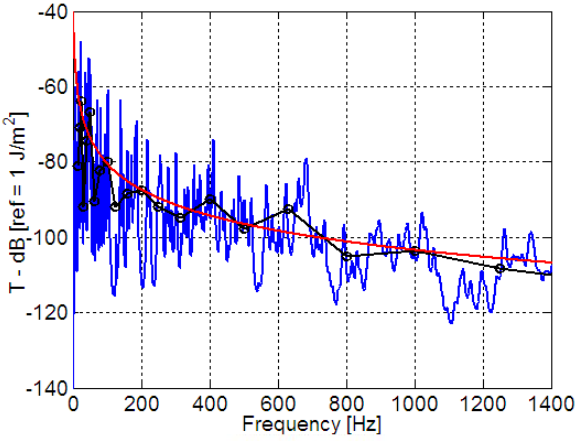
T - dB [ref = 1 J/m^2]
Frequency [Hz]
-40
-60
-80
-100
-120
-140
0
200
400
600
800
1000
1200
1400

(c)

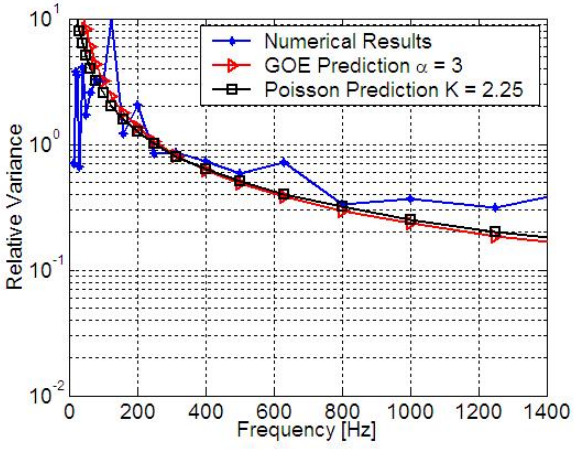

(d)

Figure 163: Spectral mean and relative variance values of the kinetic energy response for the bare and mass-loaded rectangular plates subjected to single-point loading with $\eta = 0.010$ (spectral averaging approach). Plot (a): kinetic energy density response of the bare rectangular plate - narrow and 1/3 oct. frequency domains. Plot (b): relative variance of the bare rectangular plate - 1/3 oct. frequency band domain. Plot (c): kinetic energy density response of the mass-loaded rectangular plate - narrow and 1/3 oct. frequency domains. Plot (d): relative variance of the mass-loaded rectangular plate - 1/3 oct. frequency band domain.

As observed in Figure 163 (a), the SEA predicted values describe very well the overall spectral tendency of the kinetic energy density results expressed in terms of the narrow frequency band domain. Additionally, the 1/3 oct. frequency band numerical results conform very well with the SEA predictions, mainly in the mid and high-frequency ranges. Figure 163 (c) shows that the corresponding narrow frequency band kinetic energy density response for the mass-loaded rectangular plate has large and well-defined peaks and anti-peaks in the mid and high-frequency ranges, suggesting that the current single-point energy results are probably affected strongly by the contribution from the weakly localized mode shapes. The small discrepancies observed between the 1/3 oct. frequency band numerical results and SEA predictions suggest that the reverberant characteristics are partially ensured

over the spatial domain for the energy field of the mass-loaded plate.

Figures 163 (b) e (d) show that the spectral relative variance of the single-point kinetic energy density responses for the bare and mass-loaded rectangular plates are slightly higher than the Poisson prediction, mainly in the mid and high-frequency ranges. This discrepancy can be explained by the following factors: (i) the large number of modes contributing, since the modal overlap factor is proportional to the excitation frequency, and; (ii) some high-order mode shapes have weak localization characteristics, see Figures 155 (b) and 156 (d). These relative variance results are typical examples which demonstrate that the mode shape contribution to the kinetic energy density response is more relevant than the corresponding natural frequency contribution for the case of single point-loading.

In Figure 164, the relative variance results associated with the other two DLF values are plotted for the bare and mass-loaded rectangular plates.

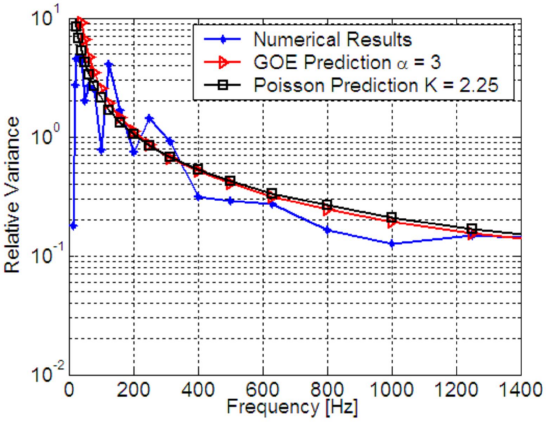

(a)

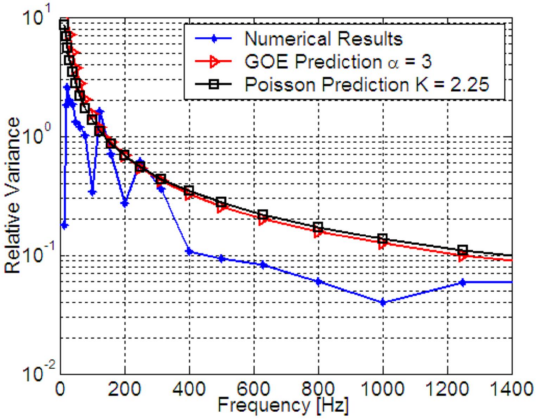
Numerical Results
GOE Prediction α = 3
Poisson Prediction K = 2.25
Relative Variance
Frequency [Hz]
10^1
10^0
10^-1
10^-2
0
200
400
600
800
1000
1200
1400

(b)

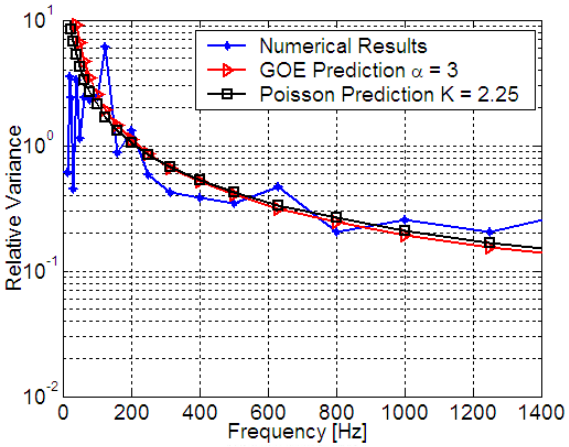
Numerical Results
GOE Prediction α = 3
Poisson Prediction K = 2.25
Relative Variance
Frequency [Hz]
10^1
10^0
10^-1
10^-2
0
200
400
600
800
1000
1200
1400

(c)

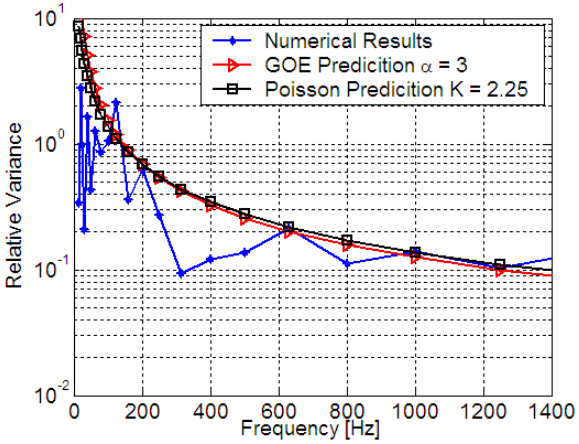

(d)

Figure 164: Relative variance of the single-point loading kinetic energy density responses for the bare and mass-loaded rectangular plates with $\eta = 0.015$ and 0.030 (spectral averaging approach). Plot (a): spectral relative variance of the single-point loading kinetic energy density response for a bare rectangular plate with $\eta = 0.015$. Plot (b): spectral relative variance of the single-point loading kinetic energy density response for a bare rectangular plate with $\eta = 0.030$. Plot (c): spectral relative variance of the single-point loading kinetic energy density result for a mass-loaded rectangular plate with $\eta = 0.015$. Plot (d): spectral relative variance of the single-point loading kinetic energy density response for a mass-loaded rectangular plate with $\eta = 0.030$.

The numerical results show a reduction in the spectral variance as the damping loss factor increases. It is interesting to note that the mass-loaded plate results are always higher than those of the bare rectangular plate, regardless of the DLF magnitude. As discussed previously, the differences are directly associated with mode shape contributions of the weakly localized mode shapes which are amplified as the frequency or DLF increases.

4.3.4 Discussion and Remarks

In this section the statistical characteristics of the modal parameters of plate systems with several geometries were investigated through the results for the statistical observables. The main effects of some particular physical phenomena, which can be established in real engineering systems and affect substantially the modal parameter statistics, were quantified using the results for the statistical observables. Their possible impacts on the performance of the SEA variance predictions based on the Poisson and GOE models were discussed in detail.

The statistical investigation of the natural frequencies of integrable systems, as such the square and circle plates, allowed the main effects of the degenerate natural frequencies on the statistical observable results to be assessed. As expected, the results for the natural frequency statistics showed that the spectral rigidity characteristics are substantially reduced with the occurrence of degenerate modes. In this study, two distinct approaches were considered to investigate the statistical characteristics of degenerate natural frequency spectra.

The first approach, employing the Fourier unfolding process, applied a low-pass filter to the staircase function fluctuations removing the non-universal contributions from the original staircase function. As observed in Figures 119 (b) and 122 (d), an excellent agreement was ensured between the numerical results from the Fourier unfolding process and the standard Poisson model prediction when a suitable cut-off time is adopted. The effects of an inadequate choice for the cut-off time on the long-range statistical observable results were demonstrated in Figure 121.

The second approach proposes the use of the *scaled* Poisson model predictions based on a degeneracy parameter. This corrective procedure is supported by the Shnirelman peak theory (99), where the degeneracy parameter is defined as the fraction of the number of degenerate natural frequencies in relation to the total number of natural frequencies. For the integrable plate systems investigated herein, the fraction of the degenerate natural frequencies was determined using the FEM model results. Thus, the scaled Poisson predictions were evaluated and conformed very well with the numerical results for short and long-range fluctuation statistics. Indeed, these two investigation approaches can be considered to have equivalent performance for the natural frequency statistical observable results of the regular systems with degenerate natural frequencies investigated herein.

For plate systems with rectangular-like shapes, the spatial mode shape

statistics showed strong evidence of the establishment of the modal superposition phenomenon for two degenerate mode shapes of distinct mode classes, where the resultant characteristics of the mode shape statistics are *almost*-Gaussian, Figures 129 - 130 and 140 - 141. As demonstrated for square and rectangular plates, the spatial representations of these mode shapes showed clearly delocalized amplitudes and nodal lines with arbitrary directions, although some geometrical symmetries remain unbroken. As reported in the literature (169, 69), these mode shapes are typical examples of the modal superposition of degenerate modes: flexural (vertical transverse) mode which has the characteristics of regular statistics and the extensional (longitudinal) mode which has the characteristics of chaotic statistics.

It is important note that only the results for the linear and squared spatial correlation functions of the normalized mode shape components were able to identify explicitly the regular statistics contributions from the flexural mode shape. Additionally, the spectral mode shape statistics results showed that these mode shapes are not perfectly Gaussian and that some regular or non-universal characteristics remain. As observed in Figures 134 and 143, the good performance of the spectral kurtosis and Lilliefors Test results suggests that these functions are efficient mode shape metrics to obtain an accurate identification of the establishment of the bouncing ball or stable periodic orbits on the spatial domain of the plate systems investigated herein.

The corresponding effects of the modal superposition of the flexural and extensional mode shapes on the natural frequency statistics were clearly visualized in the natural frequency statistical observable results of the rectangular plate, since the ratio of the sides of this system is close to the gold ratio, which avoids spurious degeneracies. The results for the natural frequency statistical observables show the establishment of incipient level repulsion characteristics in the short-range fluctuation range. For the long-range fluctuation statistics, a gradual increase in the spectral rigidity occurs as the spectral distance between the natural frequencies increases, leading to discrepancies in relation to the analytical prediction based on the Poisson model.

As discussed in Chapter 2, 2D-systems such as flexural plates are convenient systems to carry out systematic investigations on the effects of breaking symmetry on the modal parameter statistics. Considering all of the plate geometries investigated herein, the statistical observable results were able to describe the main effect on the spectral natural frequency statistics when the symmetry characteristics were altered or perturbed. Overall, a gradual statistical transition from regular to disordered statistics was established for the modal parameters.

Special importance is given to two particular systems investigated herein: the rectangular plate with an arc at one corner and the mass-loaded rectangular plate. These systems present statistical characteristics similar to those presented for real engineering systems, where the modal parameter statistics are strongly dependent on the excitation frequency. In the case of the rectangular plate with one arc, the statistical observable results show that the breaking of the system symmetries through the focusing and defocusing geometrical elements may provide the establishment of a high-frequency *deterministic chaos* in which the long-range fluctuation statistics of the modal parameters deviate slightly from the GOE model due to the *non-universal* effects originating from the pseudo-integrable nature of the system.

In the case of the mass-loaded rectangular plate, small perturbations in the mass or stiffness characteristics of a regular system lead to significant effects on the modal parameter statistics and the strength of these effects is dependent on the excitation frequency. The current spatial and spectral results for the mode shape statistics of the mass-loaded plate showed an overall agreement with the GOE model in the mid and high-frequency ranges. However, some discrete modes in the highest frequency range do not conform with the GOE model, showing incipient structural localization characteristics, as demonstrated by mode 230 in Figures 155 (b) and 156 (d). Additionally, these weak localization effects are expected for corresponding natural frequencies, leading to an incipient establishment of the *non-universal* characteristics in the long-range fluctuation range.

In last subsections, the analysis of the statistical characteristics of the kinetic energy responses for the bare and mass-loaded rectangular plates subjected to single-point and spatially-averaged excitations allowed the systematic investigation of the contribution of each modal parameter statistics to the kinetic energy density results as well as to its first two statistical moments when a spectral averaging process is adopted.

In the cases of plates subjected to the spatially-averaged excitation, the kinetic energy density results conformed very well to standard SEA predictions for the two classes of plates investigated herein, regardless of the frequency band domain considered. Indeed, this excellent agreement can be attributed to the following factors: (*i*) the spectral mean values are weakly affected by the natural frequency contributions, and (*ii*) the averaging process over the spatial domain of the system removes the non-reverberant mode shape contributions, such as those associated with the establishment of the structural localization phenomenon (*i.e.*, the spatial confinement of energy close to the excitation point).

The corresponding spectral relative variance results are strongly influenced by the statistical properties of the natural frequencies along the spectrum, showing distinct characteristics for the bare and mass-loaded rectangular plates. As observed in Figures 123 and 127, the spectral natural frequency statistics for the bare rectangular plate are almost-Poissonian while those for the mass-loaded rectangular plate conform with the GOE model. Therefore, satisfactory agreement between the spectral relative variance numerical results and the SEA analytical predictions based on the Poisson and GOE model was obtained for the bare and mass-loaded rectangular plates, respectively.

However, as the damping loss factor increases, inter-modal correlations are likely established between the natural frequencies along the frequency domain and the small discrepancies between the spectral natural frequency statistics and the well-defined statistics (Poisson and GOE models) may become relevant, directly affecting the level of agreement with the analytical predictions as observed in Figures 160 and 162. Indeed, the main characteristics of the damping mechanism effects are a substantial reduction in the oscillatory behavior of the energy response and a decrease in the spectral variability, mainly in the mid and high-frequency ranges where a large number of modes contribute to the energy response.

In the case of plates subjected to a single-point excitation, the kinetic energy density results are expected to be strongly influenced by the statistical mode shape properties at the excitation point.

As observed in Figures 163 and 164, the difference between the 1/3 octave frequency band energy responses for the bare and mass-loaded rectangular plates can be associated with distinct characteristics of the mode shape statistics. Indeed, the characteristics of the spatial mode shape statistics for the bare rectangular plate are well-behaved along the mode order domain while those of the mass-loaded rectangular plate have some high-order mode shapes with weak localization characteristics which introduce a peak or anti-peak in the energy response, see Figures 139 and 153, respectively. Additionally, it is interesting to note that the attachment of the point masses affects substantially the spectral mode shape statistics, breaking the symmetry effects and dissolve the bouncing ball periodic orbits.

In this regard, these notable differences in the modal parameter statistics support the very distinct spectral variance results observed for bare and mass-loaded rectangular plates mainly in the mid and high-frequency ranges.

4.4 Ensemble Averaging Approach

4.4.1 Random Rectangular Plates

In this study, a first ensemble composed of 500 random rectangular plates was investigated. The plate ensemble was artificially generated based on a *nominal* structure which is identical to the rectangular plate investigated previously in Section 4.3.

In the randomization process, the plate sides of each member, a and b, were considered to be independent Gaussian variables, Manohar and Keane (15) and Cordioli (20). For each ensemble member, the plate sides are calculated using the following equations:

$$a = a_0\,(1+\varepsilon_p U_g) \text{ and } b = b_0\,(1+\varepsilon_p U_g)\,, \tag{4.17}$$

where a_0 and b_0 are the sides of the nominal rectangular plate[6], U_g is a Gaussian random variable with zero mean and unit standard deviation, and ε_p is a parameter which describes the randomness level of the system. Additionally, geometrical regularity was assumed for each plate member such that the opposite sides were considered identical and parallel, ensuring a perfect rectangular shape for all ensemble members.

In order to guarantee that the strength of the level of the system randomness assumed for the plate sides has a significant effect on the modal parameter statistics, a value of $\varepsilon_p = 0.12$ was adopted for both plate sides. The free-free boundary condition was considered in the development of the FEM models. Thus, the natural frequencies and corresponding mode shapes were numerically evaluated for each plate member of the ensemble through the FEM modal analysis.

In the following sections, the best-known RMT statistical observables were evaluated for the first 250 modes, considering the ensemble averaging process approach for the natural frequencies and the ensemble, spatial and spectral averaging process approaches for the corresponding mode shapes[7].

[6] It is important to note that this randomization approach allows that the typically expected values for the plate sides across the ensemble are identical to those presented for a *nominal* rectangular plate, that is, $E[a] = a_0$ and $E[b] = b_0$.

[7] A similar statistical investigation with random rectangular plates was previously carried out by Cordioli (20). In his work the natural frequency statistics were assessed using ensemble averaging approach. The statistical analysis of the mode shape statistics at excitation point was only investigated considering the ensemble averaging approach, through the values obtained for the mode shape statistics factor (K). Additionally, the kinetic energy density results considered a type of excitation field, the single-point loading. In this section of current work, two types

These numerical results are compared to analytical predictions based on GOE and Poisson models. Additionally, the performance of the main SEA parameters applied traditionally to verify the establishment of GOE statistics for modal parameters was verified in relation to the conclusions drawn from the statistical observable results.

Natural Frequency Statistics

In Figure 165, the PDF of adjacent natural frequency spacings and Δ_3 - statistics results are shown for several mode orders (or natural frequency spacings).

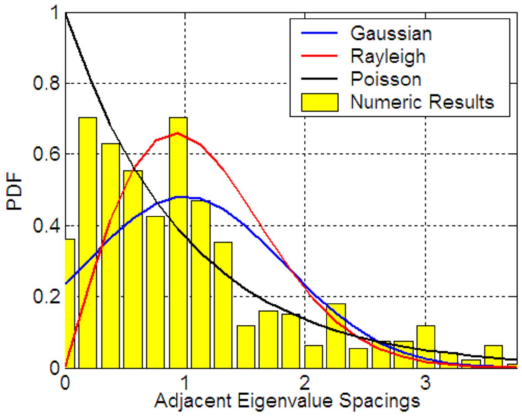

(a_1)

of excitation field are considered in the statistical analysis of the kinetic energy density results: single-point and spatially-averaged excitations. For the obtaining of the mode shape statistical observable results, the spatial and spectral averaging approaches are also considered, since their results contribute significantly for an improved and systematically understanding of the *non-universal* deviations observed in the literature results of SEA variance.

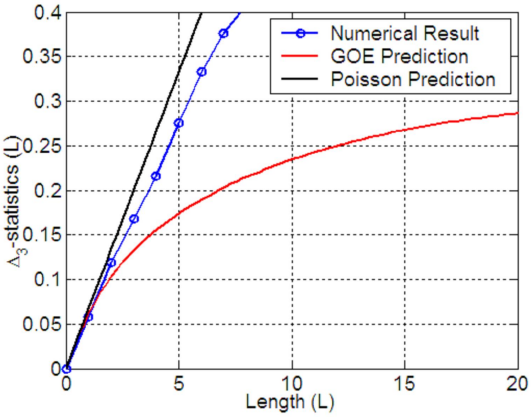
Numerical Result
GOE Prediction
Poisson Prediction
Δ3-statistics (L)
Length (L)
0.4
0.35
0.3
0.25
0.2
0.15
0.1
0.05
0
0
5
10
15
20

(a_2)

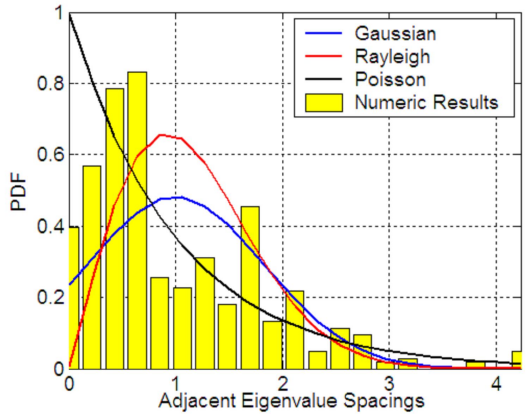
Gaussian
Rayleigh
Poisson
Numeric Results
PDF
Adjacent Eigenvalue Spacings
1
0.8
0.6
0.4
0.2
0
0
1
2
3
4

(b_1)

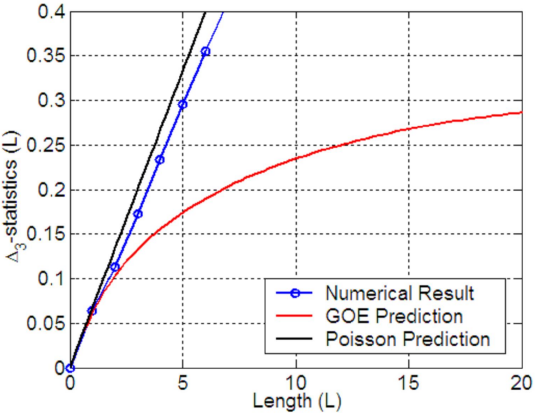
0.4
0.35
0.3
0.25
0.2
0.15
0.1
0.05
0
Δ_3-statistics (L)
0
5
10
15
20
Length (L)
Numerical Result
GOE Prediction
Poisson Prediction

(b_2)

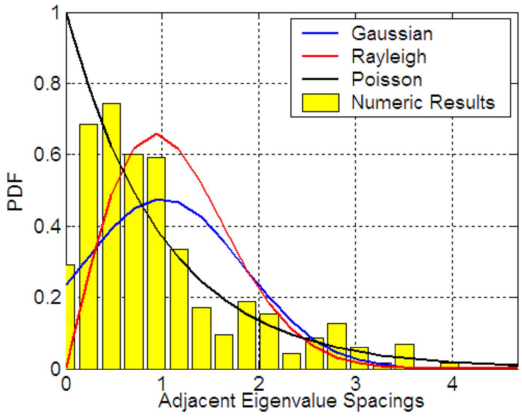
1
0.8
0.6
0.4
0.2
0
PDF
0
1
2
3
4
Adjacent Eigenvalue Spacings
Gaussian
Rayleigh
Poisson
Numeric Results

(c_1)

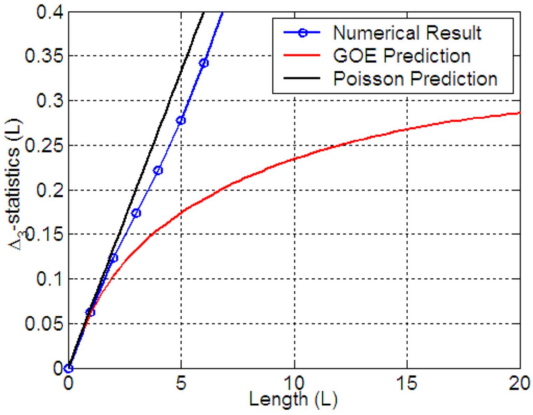
Numerical Result
GOE Prediction
Poisson Prediction
Δ_3-statistics (L)
Length (L)
0.4
0.35
0.3
0.25
0.2
0.15
0.1
0.05
0
0
5
10
15
20

(c_2)

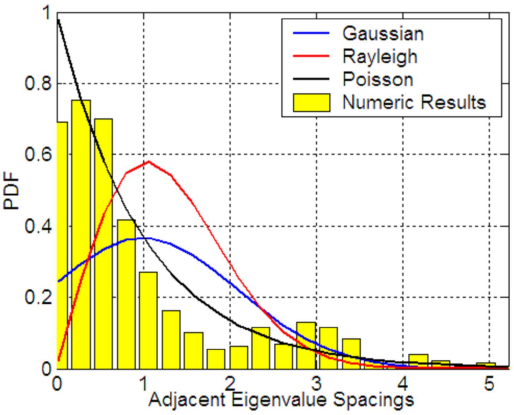
Gaussian
Rayleigh
Poisson
Numeric Results
PDF
Adjacent Eigenvalue Spacings
1
0.8
0.6
0.4
0.2
0
0
1
2
3
4
5

(d_1)

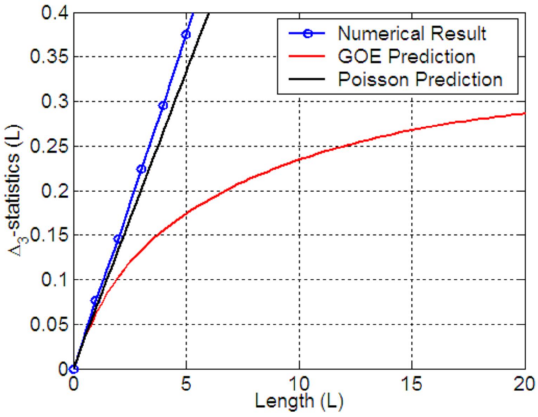

(d_2)

Figure 165: Natural frequency statistical observable results for the random rectangular plates (ensemble averaging approach). Plot (a): Mode 20. Plot (b): Mode 80. Plot (c): Mode 120. Plot (d): Mode 200.

As shown in Figure 165, the ensemble natural frequency statistical observable results showed a satisfactory agreement with the analytical predictions based on the Poisson model. Only small discrepancies are observed for the first bins of the PDF of the adjacent natural frequency spacings, suggesting an incipient establishment of *level repulsion* characteristics for the natural frequencies. On the other hand, the Δ_3 - statistics results suggest that the discrepancies observed between the analytical prediction based on the Poisson model and numerical results are amplified as the natural frequency spacing increases.

Based on the current results for the natural frequency statistical observables, the Poisson model is expected to perform well in representing the natural frequency statistics across the ensemble only for plates with very light damping levels. Indeed, for these plates, the number of resonant modes which contribute substantially to the kinetic energy density response is not high and the actual differences between the numerical results and analytical predictions based on the Poisson model are minimized for the natural frequency statistics.

In Figure 166, the spectral natural frequency statistical observable results of the *nominal* rectangular plate investigated in section 4.3.1 are compa-

red to the ensemble natural frequency statistical observable results.

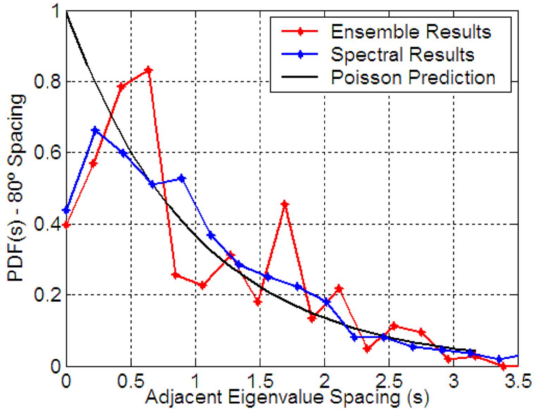

(a_1)

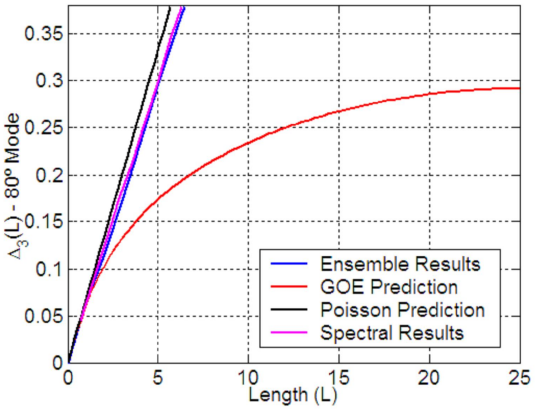

(a_2)

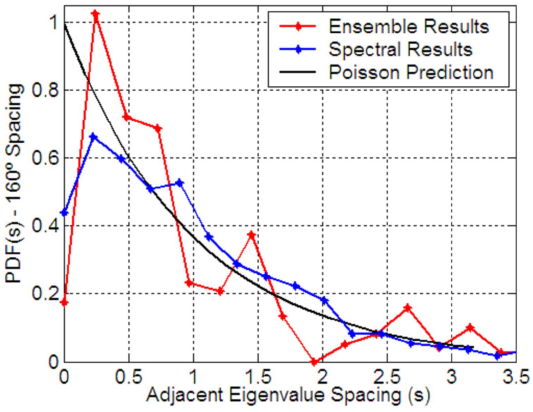
Ensemble Results
Spectral Results
Poisson Prediction
PDF(s) - 160º Spacing
Adjacent Eigenvalue Spacing (s)
0
0.2
0.4
0.6
0.8
1
0.5
1
1.5
2
2.5
3
3.5

(b_1)

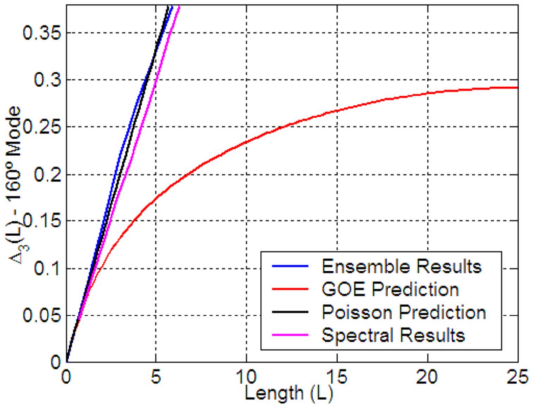
Ensemble Results
GOE Prediction
Poisson Prediction
Spectral Results
Δ3(L) - 160º Mode
Length (L)
0
0.05
0.1
0.15
0.2
0.25
0.3
0.35
5
10
15
20
25

(b_2)

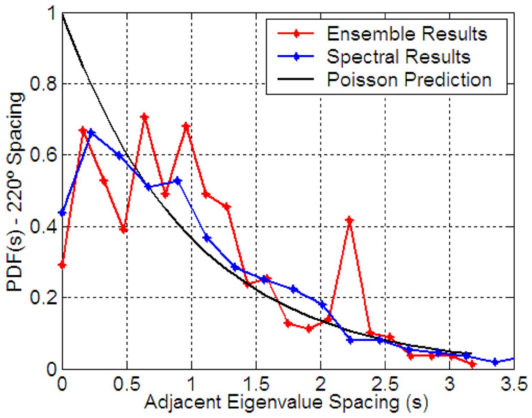

(c_1)

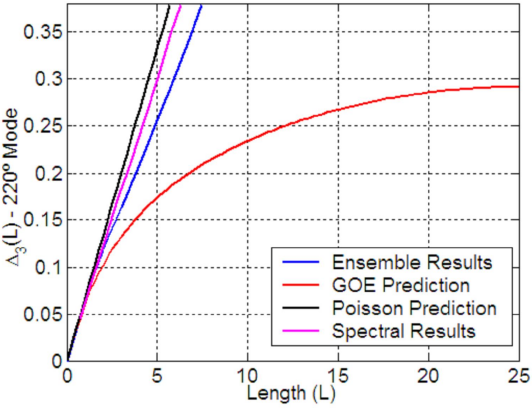

(c_2)

Figure 166: Natural frequency statistical observable results for nominal and random rectangular plates: spectral and ensemble averaging approaches.

As observed in Figure 166, a satisfactory equivalence is observed between the ensemble and spectral natural frequency statistics mainly in the

small spacing domain and thus the validity of the *spectral-ensemble* ergodicity is ensured *locally sense*[8] for natural frequencies. On the other hand, for large natural frequency spacings, the differences between the spectral and ensemble natural frequency statistics results become substantial and the spectral-ensemble ergodicity assumption is no longer valid for natural frequency statistics.

Natural Frequency SEA Parameter: Statistical Overlap Factor

The statistical overlap factor is a natural frequency SEA parameter which is traditionally used to quantify the level of randomness of an ensemble composed of random engineering structures, (18, 3, 4, 14). In the SEA context, the statistical overlap factor can be defined using: the *local mean spacing* between natural frequencies (15), or *global mean spacing* concept which represents the mean value for the spacings over ensemble and spectral domains, (18, 35, 4). In Figure 167, the statistical overlap factor results are shown for a random rectangular plate ensemble.

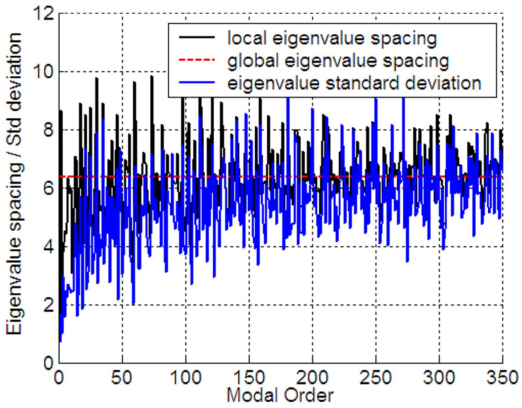

(a)

[8] According to Langley (23), *local sense* term means a group of neighboring natural frequencies with nearly constant mean spacing.

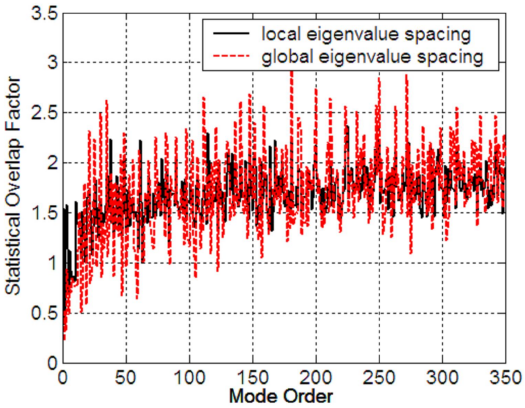

(b)

Figure 167: Statistical overlap factor results for an ensemble of the random rectangular plates (ensemble averaging approach). Plot (a): global natural frequency spacing, local natural frequency spacings, natural frequency standard deviations. Plot (b): Statistical overlap factor: based on global and local mean values of the natural frequency spacings.

As shown in Figure 167 (b), the statistical overlap factor results suggest approximately that, for mode orders greater than mode 20 (corresponding approximately the frequency of 100 Hz), the statistical overlap factor values are greater than unity. According to Langley *et al* (18, 4), the establishment of the GOE model for modal parameter statistics would be expected for modes where the statistical overlap factor values are greater than unity. Additionally, Figure 167 (a) shows that large standard deviations are also observed in the mid and high mode order ranges, leading to large statistical overlap factor values.

It is important to emphasize that the statistical overlap factor results lead to the opposite conclusions compared with the results obtained previously for the natural frequency statistical observable results. Indeed, the reliability of the statistical overlap factor performance in terms of verifying the applicability of the GOE model to the modal parameter statistics is not totally consolidated in the analytical SEA field and further systematic investigations are certainly needed, kessissoglou *et al* (80). Indeed, the statistical overlap

factor results are based on the ensemble natural frequency statistics only and any preliminary conclusion regarding to the establishment of GOE statistics for the modal parameters should be avoided, since the definition of the statistical overlap factor does not take into account the ensemble statistics for the corresponding mode shapes.

Mode Shape Statistics

In this section, a statistical analysis of the corresponding mode shapes is performed in order to provide a detailed understanding of the modal parameter statistics characteristics as well as of the conditions required for the establishment of *universal* statistics described by the GOE model.

In Figure 168, the spatial kurtosis and Lilliefors Test results for each member are presented in terms of the mode order domain. The arithmetic and geometric mean values are also presented along with the analytical predictions based on sinusoidal and GOE mode shapes.

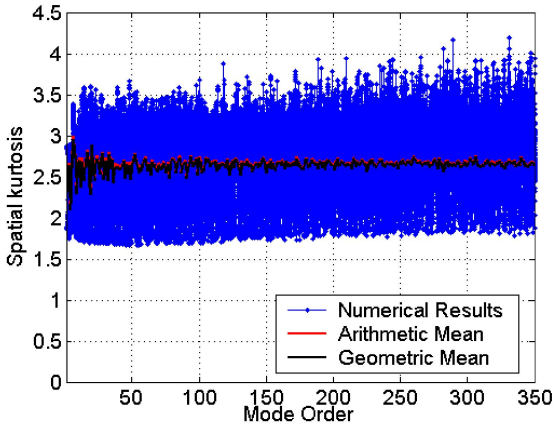

(a)

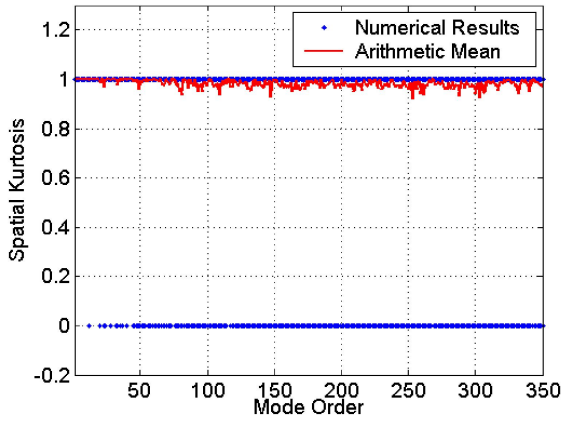

(b)

Figure 168: Spatial mode shape statistics results for the random rectangular plates (spatial averaging approach). Plot (a): spatial kurtosis results: individual members, arithmetic and geometric mean values and analytical predictions (sinusoidal and GOE). Plot (b): spatial Lilliefors Test results: individual member values and arithmetic mean values.

As observed in Figure 168 (a), a moderate level of dispersion is observed for the spatial kurtosis values throughout the mode order domain. The mean values obtained from the arithmetic and geometric averaging processes are very similar suggesting that the traditional arithmetic mean value is sufficiently accurate to represent the typically expected or probabilistic mode value. Indeed, the spatial kurtosis results show that most values are slightly larger than the 2D-sinusoidal kurtosis value, that is, $K \simeq 2.6 > 2.25 = K_{sin}^{2D}$, regardless of mode order value across the ensemble.

The corresponding Lilliefors Test results clearly show that most of the mode shapes are not Gaussian, although a small number of the mode shapes are accepted, Figure 168 (b). These modes with Gaussian characteristics may be associated with a particular group of mode shapes resulting from the modal superposition of two degenerate mode shapes: flexural (vertical transverse) and extension (longitudinal), where the flexural modes present regular statistics while the extensional modes have chaotic statistics, Schaadt (69, 70).

Another relevant characteristics of the mode shapes is the degree of

statistical independence at a fixed mode shape component, for example, that associated with a given excitation point. In the case of the GOE eigenvectors, their components are statistically independent and their distribution is expected to be Gaussian. In Figure 169, the spectral kurtosis and Lilliefors Test results at excitation point X_0[9] are presented for each plate member. As shown in Figure 169(a), the spectral kurtosis results are approximately constant across the ensemble and a small dispersion is also observed around the ensemble kurtosis mean value ($\overline{K} = 2.33$).

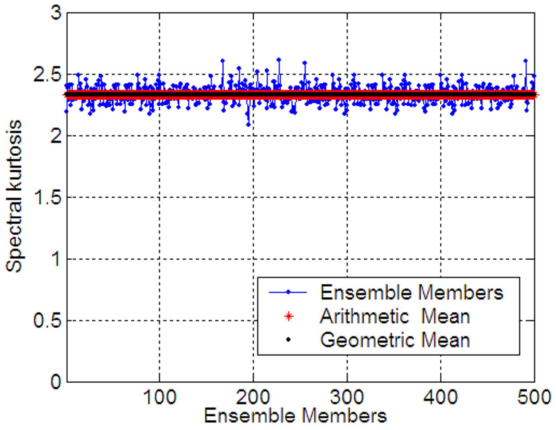

(a)

[9]The spatial coordinates of excitation point X_0 are identical to those adopted previously in the spectral analysis of the kinetic energy density results of the nominal rectangular plate described in subsection 4.3.3, that is, $X_0 = (0.923, 0.227)$ m.

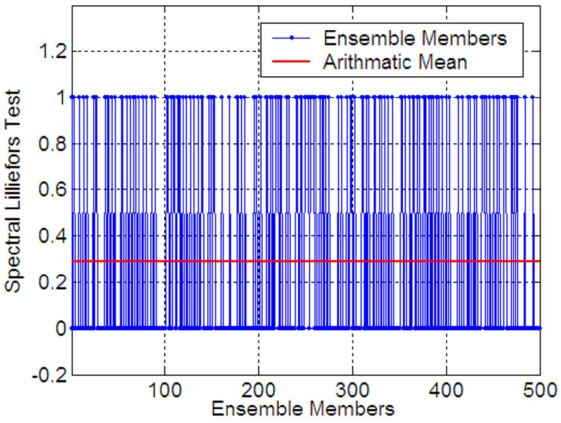

(b)

Figure 169: Spectral mode shape statistics results at excitation point X_0 for the random rectangular plates (spectral averaging approach). Plot (a): spectral kurtosis: individual members, arithmetic and geometric mean values and analytical predictions (sinusoidal and GOE models). Plot (b): spectral Lilliefors Test results: individual member and arithmetic mean values.

In Figure 169(b), the spectral Lilliefors Test results at excitation point X_0 are presented for random rectangular plate members. The arithmetic mean value suggests, surprisingly, that for approximately 70% of the plate members the mode shape components have a Gaussian distribution at excitation point X_0. However, the corresponding spectral kurtosis results are substantially lower than the GOE value ($K = 3$) and suggest that intermediate statistics between the sinusoidal and GOE models is established for these mode shapes, where the distribution of the mode shape amplitudes associated with the excitation point X_0 is slightly more spread out around the mean value than the corresponding Gaussian distribution, see Figure 169. Indeed, these results for the spectral mode shape statistics illustrate the difficulty involved in obtaining an exclusive eigenvector statistical observable which is able to verify, with sufficient accuracy, not considering the other eigenvector statistical observable results, the agreement with the GOE model.

As discussed in the previous chapter, the modal parameter statistics of a given random system is only correctly characterized when all available

results for the statistical observables are analyzed together and compared to each other, regardless of their individual performance in the characterization of the modal parameter statistics.

In Figure 170 the ensemble kurtosis values associated with the excitation point X_0 and their corresponding Lilliefors Test results are shown for the random rectangular plates. As observed in Figure 170 (a), the ensemble kurtosis values have a small dispersion around the spectral mean value ($\bar{K} = 2.36$). Although not shown here in detail, the distribution of the mode shape component associated with the excitation X_0 across the ensemble is almost symmetric and presents a well-defined peak. Thus, the spectral mean value is sufficiently representative to determine the typically expected value for the ensemble kurtosis along the mode order domain.

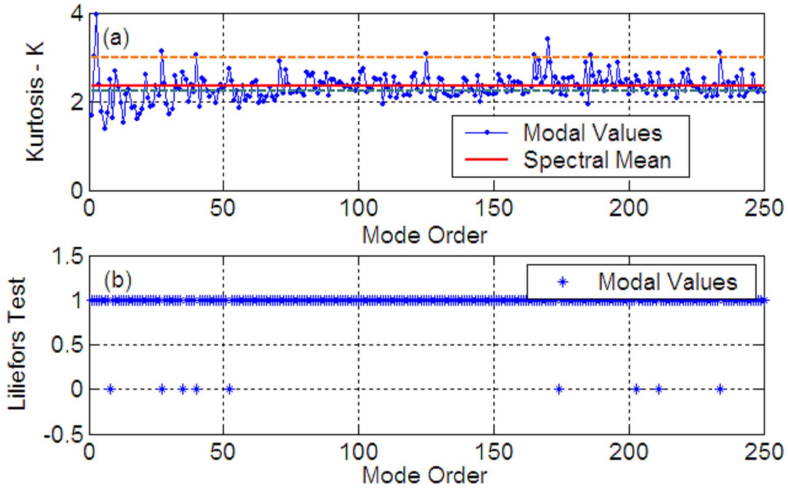

Figure 170: Ensemble mode shape statistics results at excitation point X_0 for the random rectangular plates (ensemble averaging approach). Plot (a): ensemble kurtosis, spectral arithmetic mean value and analytical predictions (sinusoidal and GOE models). Plot (b): ensemble Lilliefors Test results.

The corresponding ensemble Lilliefors Test results associated with the excitation point X_0 suggest that most of the mode shape amplitudes do not have a Gaussian distribution. Although some mode shapes are approved in the Lilliefors Test, the corresponding kurtosis results clearly show that these mode shapes have an incomplete establishment of *universal* statistics described by the GOE model.

It is interesting to note that the spectral and ensemble kurtosis curves have very similar characteristics along the respective domains. In Figure 171, the PDF values for the mode shape components associated with the excitation point X_0 are plotted considering the spectral and ensemble domains. For the evaluation of the spectral results at excitation point X_0, a typical plate member was considered, for which the spectral kurtosis value is the same as the typically expected value across the ensemble. For the evaluation of the ensemble results, three spacings along the mode order domain were considered.

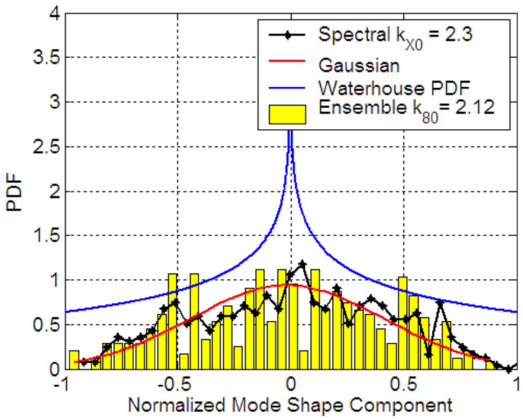

(a)

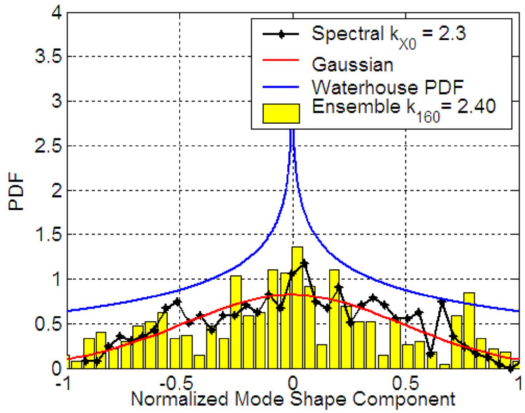

(b)

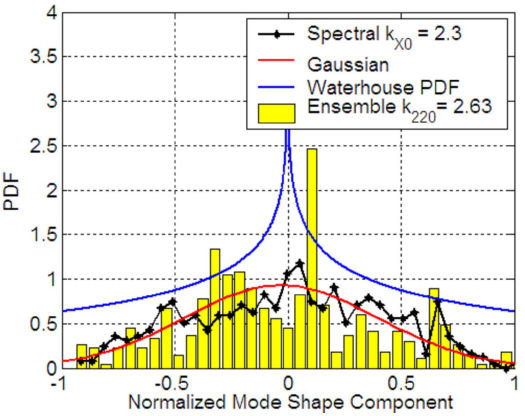

(c)

Figure 171: PDF values of the mode shape amplitudes associated with the excitation point X_0 for the random rectangular plates: spectral and ensemble averaging approaches.

As observed in Figure 171, the spectral and ensemble PDF results are similar, although some small discrepancies can be clearly observed. The ensemble PDF results are discontinuous and incipiently disordered while the spectral results are approximately continuous and well-behaved, showing a distribution close to the Gaussian pattern.

Considering the mode shape SEA parameters P and Q proposed originally by Cordioli (20), their evaluations consider a fixed number of components for the ith-mode shapes of members across the ensemble; see Equations (2.46) and (2.49), respectively. In the case of the random rectangular ensemble investigated herein, for all plate members a fixed mesh size was adopted for the development of the FEM model . As a direct consequence, the number of nodes (or mode shape components) for each plate member can not be fixed across the ensemble since the plate sides are independent Gaussian variables, and thus the evaluation of these mode shape SEA parameters becomes inappropriate.

Kinetic Energy Density Statistics: General Considerations

The ensemble averaging approach was then adopted to assess the statistical characteristics of the kinetic energy density results for the random rectangular plates.

In order to investigate the effects of distinct modal parameter statistics on the kinetic energy density statistics, two distinct excitation classes are considered. The first is a unitary longitudinal single point-loading which provides an energy response dependent on both modal parameter statistics. In this analysis, the location of the excitation point was considered to be the same for all plate members and identical to that adopted previously during the spectral analysis of the kinetic energy density statistics, that is, $X_0 = (0.923, 0.227)$ m.

The second excitation class considers a spatially-averaged excitation which provides energy results identical to those obtained for rain-on-the-roof excitation. It is important to emphasize that the contributions of the mode shape statistics are removed for this second excitation class and thus the kinetic energy density statistics are dependent only on the natural frequency statistics, Brown (1).

Based on a similar analysis reported in the current SEA literature (1, 3, 35, 18), the damping loss factor (DLF) was considered to be *frequency-constant* and three distinct values were considered to ensure distinct levels of modal superposition, that is, η = 0.010, 0.015 and 0.030. Additionally, the

free-free boundary condition was adopted for the random rectangular plates. Thus, the single-point and spatially-averaged kinetic energy density results were evaluated for the narrow frequency band domain with intervals of 10 Hz. The excitation frequency range considered was from 0 to 1400 Hz. It is also important to note that a sufficient number of modes was adopted in the superposition process so as to provide the correct response convergence in the frequency range investigated.

Kinetic Energy Density Statistics: Spatially-Averaged Excitation

In Figure 172, the mean and relative variance results are shown for the spatially-averaged excited rectangular plates with $\eta = 0.01$. The numerical results are compared with the SEA predictions based on the Poisson and GOE models.

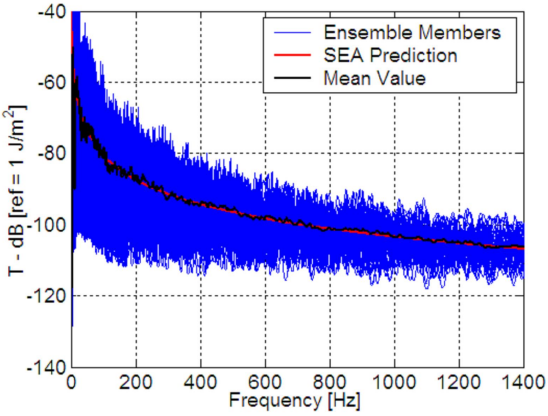

(a)

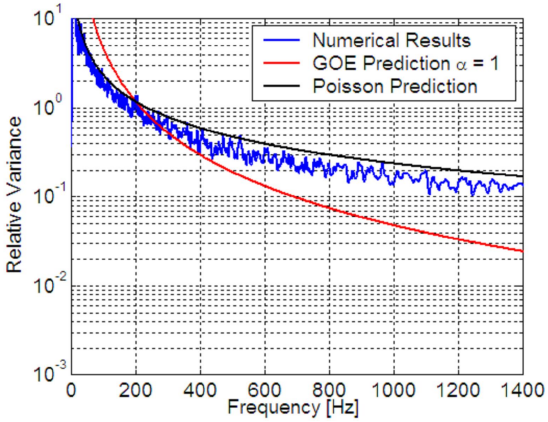

(b)

Figure 172: Mean and relative variance of the spatially-averaged kinetic energy density results for the random rectangular plates with $\eta = 0.01$ (ensemble averaging approach). Plot (a): mean values. Plot (b): relative variance values.

As observed in Figure 172 (a), an excellent agreement with the SEA prediction is observed for the frequency range considered. Indeed, the statistical characteristics of the mean value for the spatially-averaged kinetic energy density results are expected to be weakly dependent on the natural frequency statistical characteristics (*i.e.*, spacing distribution, spectral correlations, etc), (84, 154).

Considering the corresponding relative variance results, some discrepancies are clearly observed between the numerical results and the SEA prediction. As shown in Figure 172 (b), the analytical prediction based on the Poisson model slightly overpredicts the numerical results. Indeed, good agreement with the SEA prediction based on the Poisson model is strictly associated with the following factors: (i) the ensemble natural frequency statistics are almost-Poissonian; and (ii) the contributions of the mode shape statistics to the spatially-averaged kinetic energy density results are neglected, Brown (1). Therefore, the slight overprediction of the SEA formulation based on the Poisson model is easily explained by the small discrepancies observed in the Δ_3 - statistics results. Indeed, the statistical characteristics of the natural frequencies are slightly more rigid than those expected for perfect Poissonian

eigenvalues.

In Figures 173 and 174, the mean and relative variance results are shown for the spatially-averaged excited rectangular plates with $\eta = 0.015$ and $\eta = 0.030$, respectively. The numerical results are compared with SEA predictions based on Poisson and GOE models.

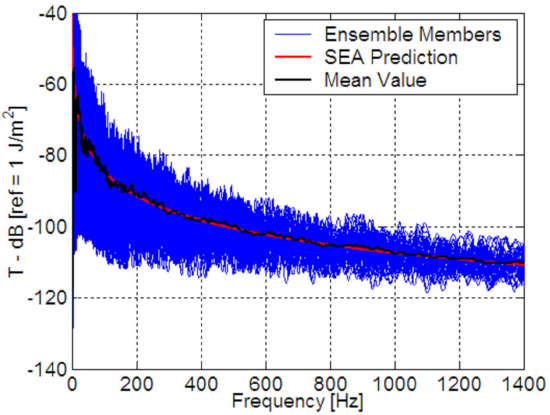

(a)

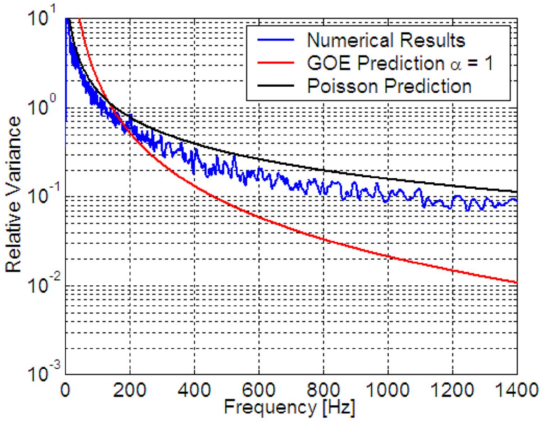

(b)

Figure 173: Mean and relative variance for the spatially-averaged kinetic energy density results of the random rectangular plates with $\eta = 0.015$ (ensemble averaging approach). Plot (a): mean values. Plot (b): relative variance values.

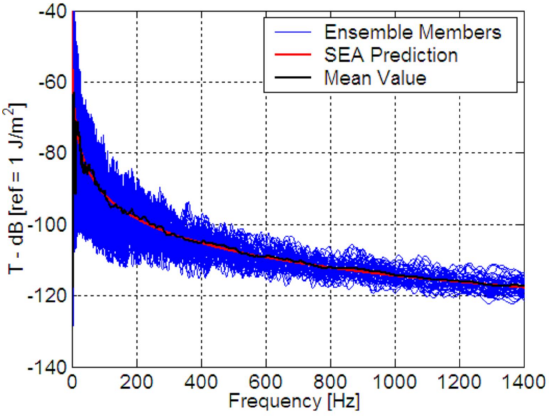

(a)

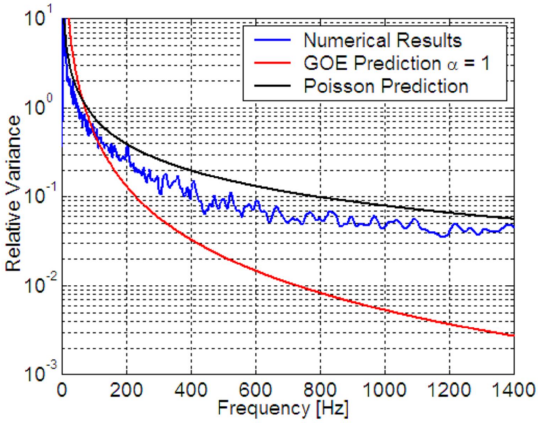

(b)

Figure 174: Mean and relative variance of the spatially-averaged kinetic energy density results for the random rectangular plates with $\eta = 0.030$ (ensemble averaging approach). Plot (a): mean values. Plot (b): relative variance values.

As observed in Figures 172 - 174, the variability of the kinetic energy results across the ensemble is gradually reduced as the damping loss factor increases. The increase in the DLF value leads to an increase in the modal superposition and thus the difference between the ensemble natural frequency and the Poisson model statistics becomes substantial and strong spectral correlations between the natural frequencies are established, which reduces the energy response variability over the spectral and ensemble domains.

Kinetic Energy Density Statistics: Single Point-Loading

In Figure 175, the mean and relative variance values of the single-point kinetic energy density results are shown for the rectangular plates with $\eta = 0.01$. The numerical results are compared with the SEA predictions based on the Poisson and GOE models.

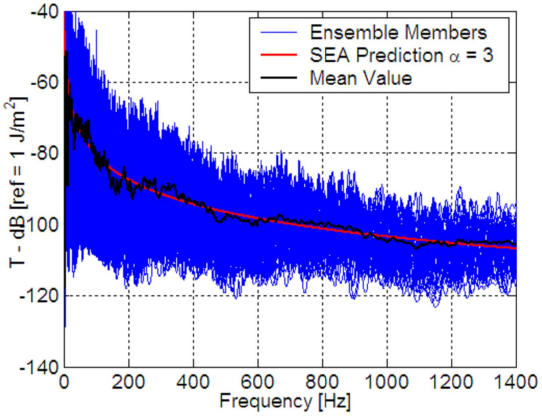

(a)

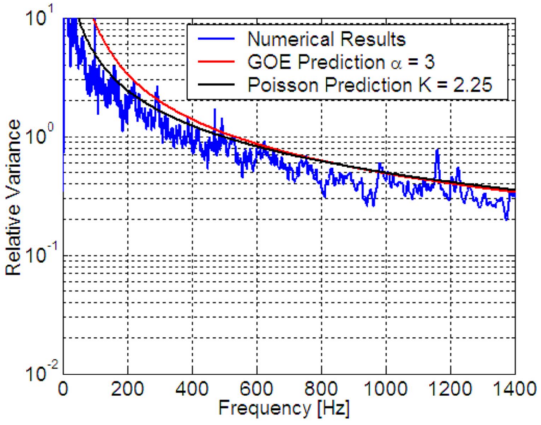

(b)

Figure 175: Mean and relative variance of the single-point kinetic energy density results for the random rectangular plates with $\eta = 0.01$ (ensemble averaging approach). Plot (a): mean value. Plot (b): relative variance values.

As observed in Figure 175 (a), an excellent agreement is observed between the SEA prediction and the mean values. The corresponding relative variance results also show, surprisingly, agreement with the SEA prediction

based on the Poisson model, Figures 175 (b). As demonstrated by the ensemble modal parameter statistics results, the incipient discrepancies were clearly identified in relation to the Poisson model for the natural frequencies and in relation to the sinusoidal statistics for the corresponding mode shapes. Indeed the natural frequencies are slightly more rigid than the Poisson eigenvalues and the corresponding mode shapes are not perfectly sinusoidal, since the free-free boundary condition was adopted. Thus, it would be expected that the numerical results do not conform very well with the analytical prediction based on the Poisson model, where the natural frequencies are perfectly uncorrelated and the mode shapes are assumed to be the product of sinusoidal functions. Therefore, the unexpected good agreement observed in Figure 175 (b) seems to be due to the fact that these possible non-Poisson effects of the modal parameter statistics could be sufficiently compensated in the modal superposition process, since the single-point kinetic energy density results are affected by the statistical contributions from the natural frequencies and mode shapes.

In Figures 176 and 177, the mean and relative variance values of the single-point kinetic energy density results are shown for the rectangular plates with $\eta = 0.015$ and $\eta = 0.030$, respectively. The numerical results are compared with the SEA predictions based on the Poisson and GOE models.

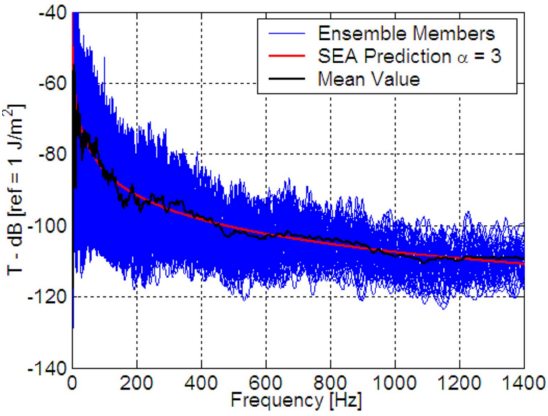

(a)

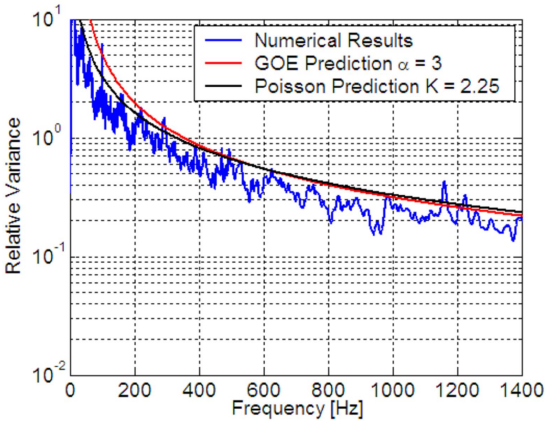

(b)

Figure 176: Mean and relative variance of the single-point kinetic energy density results for the random rectangular plates with $\eta = 0.015$ (ensemble averaging approach). Plot (a): mean values. Plot (b): relative variance values.

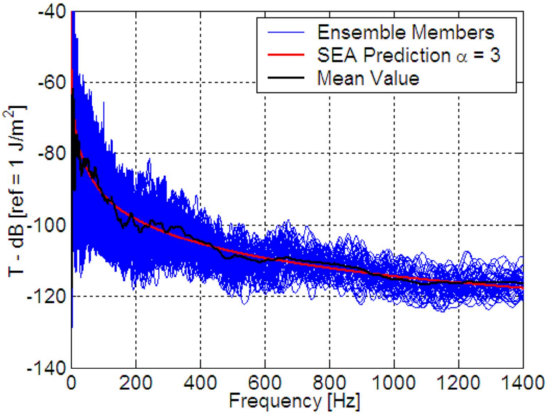

(a)

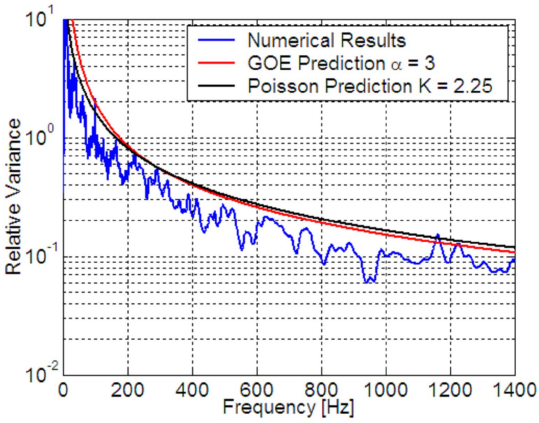

(b)

Figure 177: Mean and relative variance of the single-point kinetic energy density results for the random rectangular plates with $\eta = 0.030$ (ensemble averaging approach). Plot (a): mean values. Plot (b): relative variance values.

As observed in Figures 175-177, as the damping loss factor increases the variability of the single-point kinetic energy density results across the ensemble is gradually reduced and the level of agreement with the analytical Poisson prediction seems to become lower, mainly in the high-frequency range. It is important to note that, despite the strong spectral correlations which are introduced by the increase in the modal superposition, relevant contributions from the mode shape statistics associated with the excitation point X_0 can be expected for single-point kinetic energy density statistics since the mode shape statistics are very sensitive to the detailed nature of the system.

4.4.2 Random Mass-Loaded Plates

In this study, the statistical characteristics of a second ensemble composed of the 500 random mass-loaded rectangular plates are investigated across the ensemble. The structural irregularities of the mass distribution along the spatial domain of the system associated with the manufacturing uncertainties were represented by small point masses attached to the surface of each plate member.

For each mass-loaded rectangular plate member, 20 point masses

(each point mass with 1% of the total mass of the bare rectangular plate) are randomly distributed over the surface of the nominal rectangular plate. In this study, the ensemble size adopted guaranteed the convergence of the statistical results of the kinetic energy density statistics as well as of the modal parameter statistics across the ensemble.

As discussed on the previous chapters, the statistical investigation of modal parameters from the mass-loaded plate systems has been extensively carried out by several researchers, considering ensemble averaging approach Langley *et al.* (16, 3, 18, 4, 35, 17), Brown (1), Cordioli *et al.* (19) and Cordioli (20). However, in this section of current work, the spatial and spectral averaging approaches are also considered for the obtaining of the mode shape statistical observable results. Additionally, two types of excitation field are considered in the statistical analysis of the kinetic energy density results: single-point and spatially-averaged excitations. In this context, the comparison between the energy results and modal parameter statistical observables results evaluated under several averaging approach provide significant contributions for an improved and systematically understanding of the non-universal deviations observed in the literature results of SEA variance.

Natural Frequency Statistics

In Figure 178, the PDF values for adjacent natural frequency spacings and the Δ_3 - statistics results are shown for several mode orders. The statistical characteristics of the transition from Poisson to GOE statistics are demonstrated in Figures 178 (a) - (c). Additionally, the natural frequency results for mode 35 suggest that the establishment of *universal* statistics for the natural frequencies of the mass-loaded plate occurs initially for the short-range fluctuations (*i.e.*, small natural frequency distances), Figure 178(b).

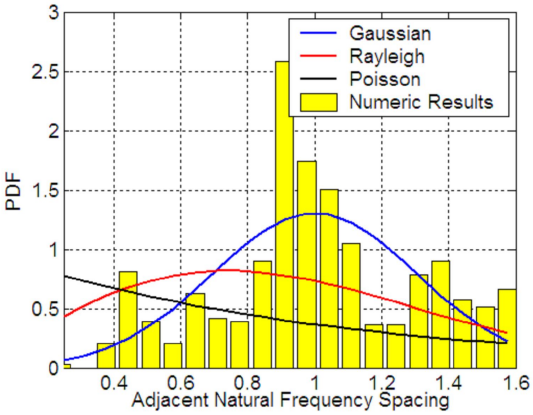
Gaussian
Rayleigh
Poisson
Numeric Results
PDF
Adjacent Natural Frequency Spacing
0
0.5
1
1.5
2
2.5
3
0.4
0.6
0.8
1
1.2
1.4
1.6

(a_1)

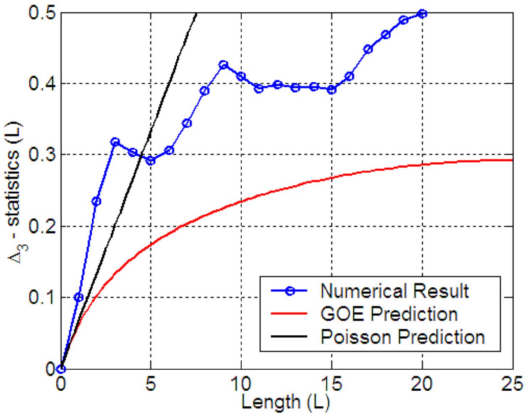
Numerical Result
GOE Prediction
Poisson Prediction
Δ3 - statistics (L)
Length (L)
0
0.1
0.2
0.3
0.4
0.5
0
5
10
15
20
25

(a_2)

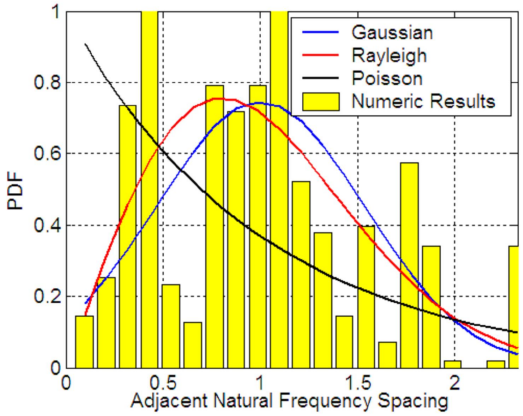
Gaussian
Rayleigh
Poisson
Numeric Results
PDF
Adjacent Natural Frequency Spacing
0
0.2
0.4
0.6
0.8
1
0.5
1.5
2

(b_1)

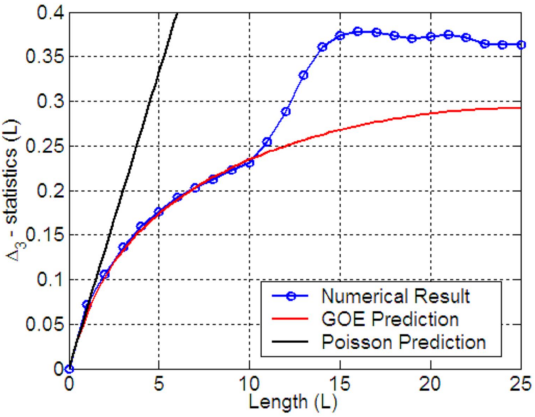
Numerical Result
GOE Prediction
Poisson Prediction
Length (L)
0
0.05
0.1
0.15
0.2
0.25
0.3
0.35
0.4
5
10
15
20
25

(b_2)

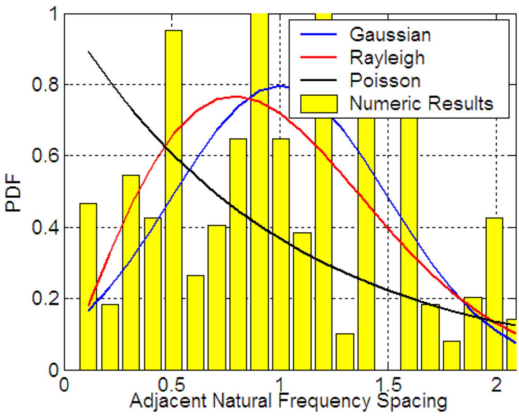
Gaussian
Rayleigh
Poisson
Numeric Results
PDF
Adjacent Natural Frequency Spacing
0
0.2
0.4
0.6
0.8
1
0.5
1.5
2

(c_1)

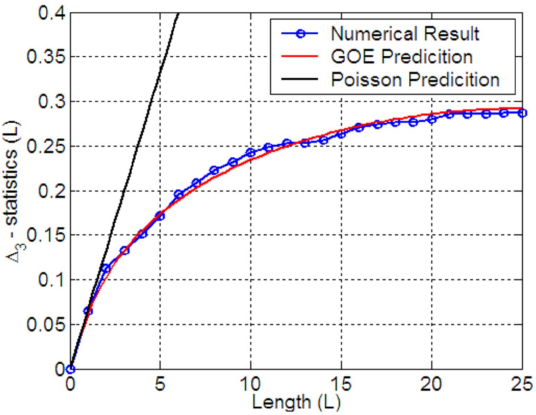
Numerical Result
GOE Predicition
Poisson Predicition
Δ3 - statistics (L)
Length (L)
0
0.05
0.1
0.15
0.2
0.25
0.3
0.35
0.4
5
10
15
20
25

(c_2)

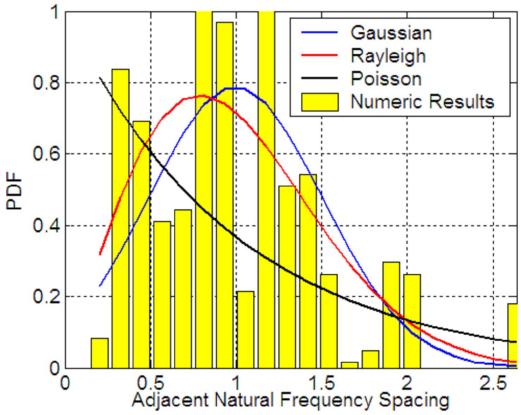
Gaussian
Rayleigh
Poisson
Numeric Results
PDF
Adjacent Natural Frequency Spacing
0
0.2
0.4
0.6
0.8
1
0.5
1
1.5
2
2.5

(d_1)

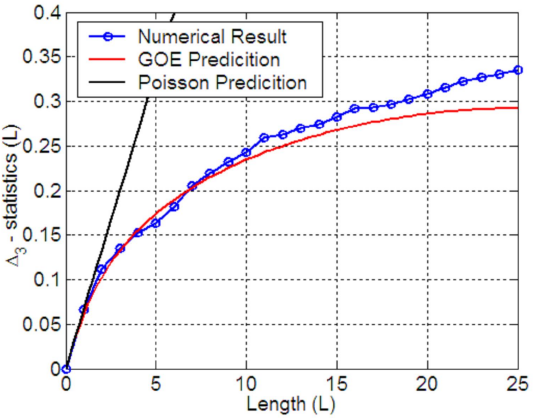
Numerical Result
GOE Predicition
Poisson Predicition
Δ3 - statistics (L)
Length (L)
0
0.05
0.1
0.15
0.2
0.25
0.3
0.35
0.4
5
10
15
20
25

(d_2)

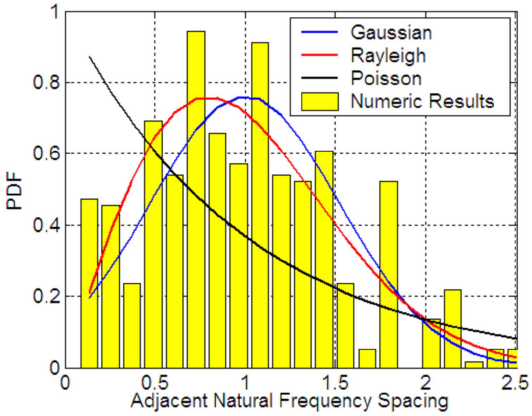
Gaussian
Rayleigh
Poisson
Numeric Results
PDF
Adjacent Natural Frequency Spacing
0
0.2
0.4
0.6
0.8
1
0.5
1.5
2
2.5

(e_1)

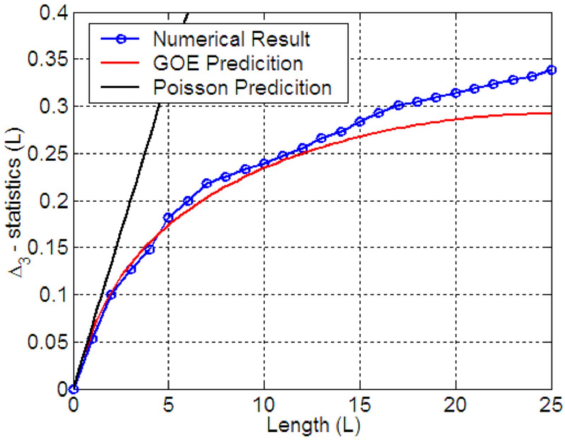
Numerical Result
GOE Predicition
Poisson Predicition
Δ3 - statistics (L)
Length (L)
0
0.05
0.1
0.15
0.2
0.25
0.3
0.35
0.4
5
10
15
20
25

(e_2)

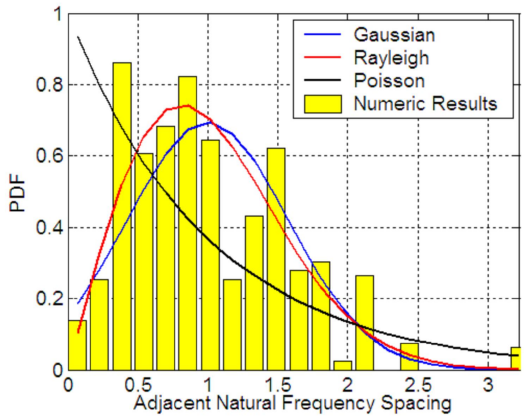

(f_1)

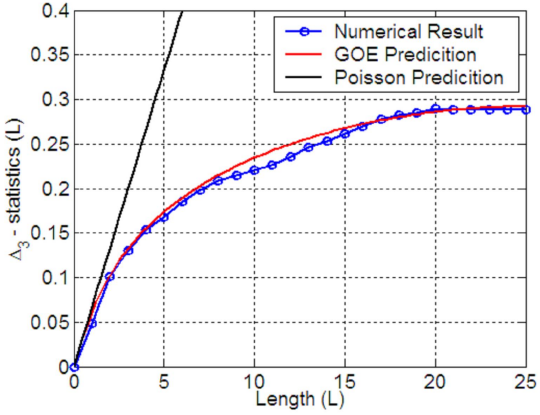

(f_2)

Figure 178: Natural frequency statistical observable results for the mass-loaded rectangular plates (ensemble averaging approach). Plot (a): Mode 30. Plot (b): Mode 35. Plot (c): Mode 50. Plot (d): Mode 175. Plot (e): Mode 230. Plot (f): Mode 250.

As observed in Figures 178 (d) - (f), the ensemble natural frequency statistical observable results show satisfactory agreement with the analytical predictions based on the GOE model. The establishment of level repulsion characteristics is clearly observed in the short-range fluctuation statistical observable results. However, the Δ_3 - statistics results showed small deviations in relation to GOE model prediction for large natural frequency distances.

Based on the current results for the natural frequency statistical observables, the application of the GOE model for the natural frequency statistics across the ensemble is considered to hold in the *local* sense only. In other words, *universal* statistics would only be established for a limited frequency range where the neighboring natural frequencies have a nearly frequency-constant spacing mean value, since for long-range variations in the mean spacing, non-universal characteristics associated with system-dependent effects are certainly established, Langley (23).

In Figure 179, the spectral natural frequency statistical observable results of the mass-loaded rectangular plate investigated in section 4.3.1 are compared to the ensemble natural frequency statistical observable results.

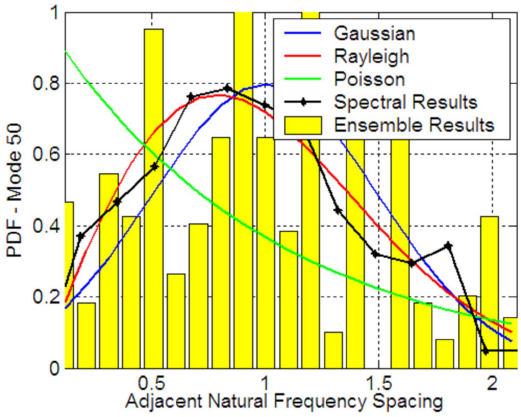

(a_1)

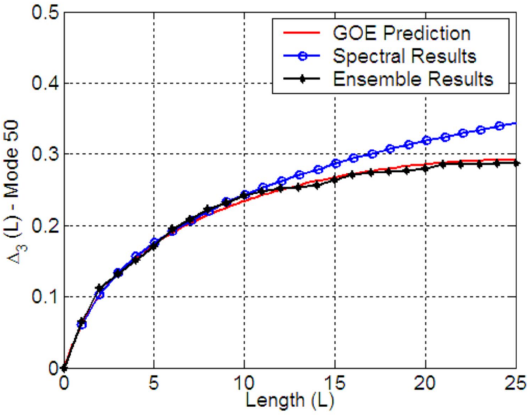
GOE Prediction
Spectral Results
Ensemble Results
Δ_3 (L) - Mode 50
Length (L)
0.5
0.4
0.3
0.2
0.1
0
0
5
10
15
20
25

(a_2)

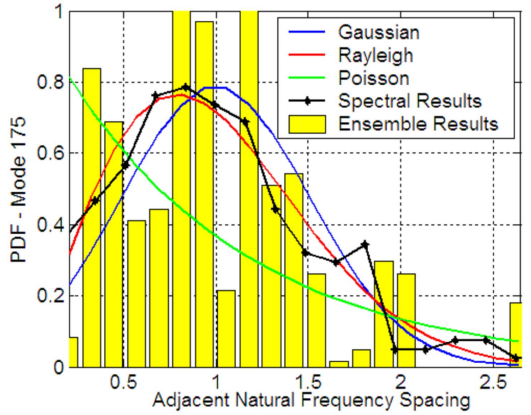
Gaussian
Rayleigh
Poisson
Spectral Results
Ensemble Results
PDF - Mode 175
Adjacent Natural Frequency Spacing
1
0.8
0.6
0.4
0.2
0
0.5
1
1.5
2
2.5

(b_1)

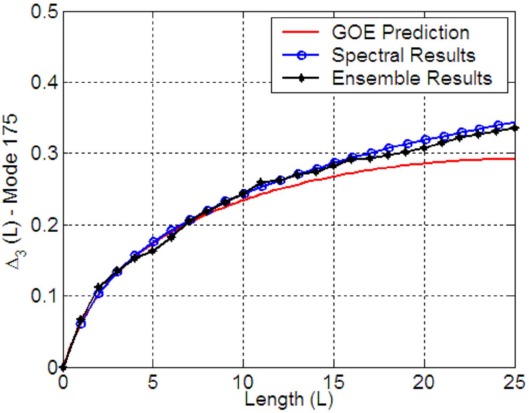
GOE Prediction
Spectral Results
Ensemble Results
Δ_3 (L) - Mode 175
Length (L)
0
0.1
0.2
0.3
0.4
0.5
0
5
10
15
20
25

(b_2)

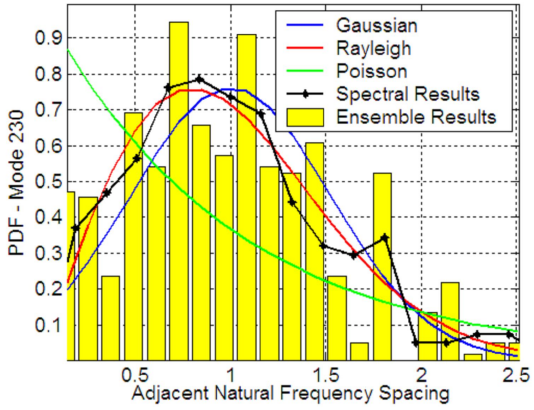
Gaussian
Rayleigh
Poisson
Spectral Results
Ensemble Results
PDF - Mode 230
Adjacent Natural Frequency Spacing
0.1
0.2
0.3
0.4
0.5
0.6
0.7
0.8
0.9
0.5
1
1.5
2
2.5

(c_1)

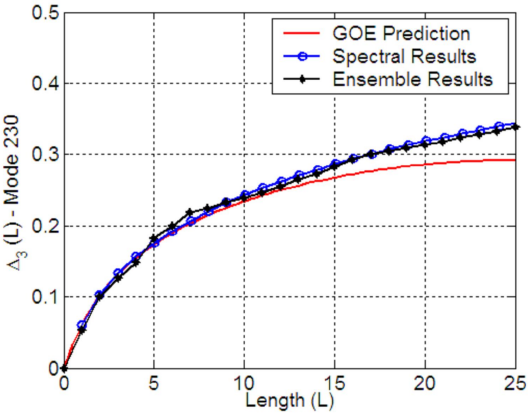

(c_2)

Figure 179: Natural frequency statistical observable results for mass-loaded rectangular plates: spectral and ensemble averaging approaches.

As can be seen in Figure 179, a satisfactory equivalence is observed between the ensemble and spectral statistics in the small spacing domain and thus, the validity of spectral-ensemble ergodicity is *locally* ensured for the mid and high natural frequencies of the mass-loaded rectangular plate.

On the other hand, the differences between the spectral and ensemble long-range fluctuation statistics become asymptotically relevant as the frequency increases, and thus the spectral-ensemble ergodicity assumption is no longer valid for natural frequency statistics.

Natural Frequency SEA Parameter: Statistical Overlap Factor

In Figure 180, the statistical overlap factor results are shown for the mass-loaded rectangular plate ensemble. The definitions based on the local and global mean spacings were considered for the evaluation of the statistical overlap factor results.

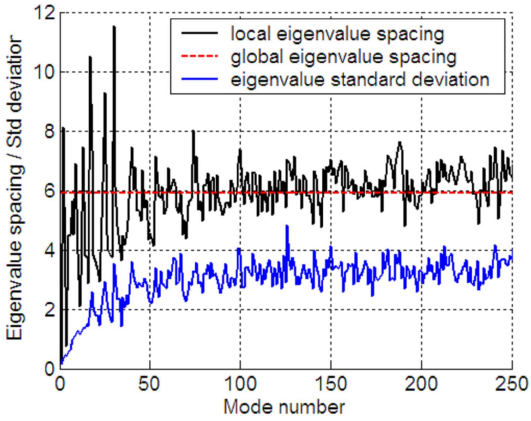

(a)

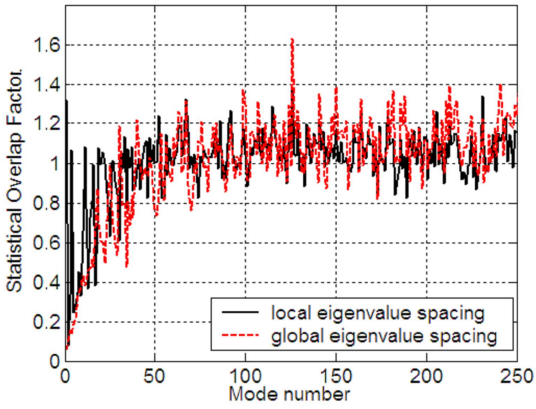

(b)

Figure 180: Statistical overlap factor results for an ensemble of the mass-loaded rectangular plates (ensemble averaging approach). Plot (a): global natural frequency spacing, local natural frequency spacings, natural frequency standard deviations. Plot (b): Statistical overlap factor: based on global and local mean values for the natural frequency spacings.

As observed in Figure 180 (a), the global mean spacing value seems to be sufficiently accurate to represent the typically expected value for the local mean spacings along the mode order domain. In Figure 180 (b), the statistical overlap factor results suggest that the establishment of the GOE model for the modal parameter statistics would be expected for mode orders greater than mode 50 (corresponding approximately to a frequency of 250 Hz), since the statistical overlap factor values are larger than unity.

It is important to emphasize that the conclusions of the statistical overlap factor analysis are in agreement with the results obtained previously for the natural frequency statistical observables. However, the reliability of the statistical overlap factor analysis in terms of verifying the applicability of the GOE model to modal parameter statistics is not totally consolidated. Indeed, some examples of the unsuccessful application of the statistical overlap factor analysis have been reported in the SEA literature and further investigations are certainly needed, Cordioli (20) and kessissoglou *et al* (80).

Mode Shape Statistics

In this section, a statistical analysis of the corresponding mode shapes is performed considering spatial, spectral and ensemble averaging approaches. In Figure 181, the spatial kurtosis and Lilliefors Test results for each mass-loaded plate member are presented in terms of the mode order domain. The arithmetic and geometric mean values are also presented along with the analytical predictions based on sinusoidal and GOE mode shapes.

As observed in Figure 181 (a), a moderate level of dispersion is observed for the spatial kurtosis values throughout the mode order domain. The mean values of the spatial kurtosis are slightly larger than GOE kurtosis value, suggesting an incipient establishment of the structural localization phenomenon. Additionally the small differences between the mean values obtained from the arithmetic and geometric averaging processes suggest that the traditional arithmetic mean value is sufficiently accurate to represent the typically expected or probabilistic mode value.

The corresponding Lilliefors Test results show clearly that most of the mode shapes are not Gaussian, although a small number of the mode shapes of some members are accepted in the high-frequency range, Figure 181 (b).

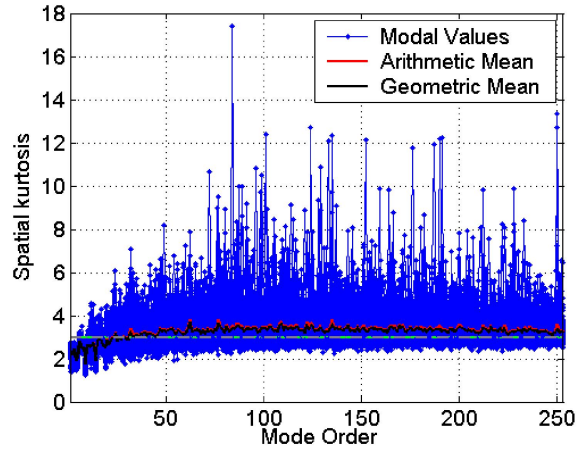

(a)

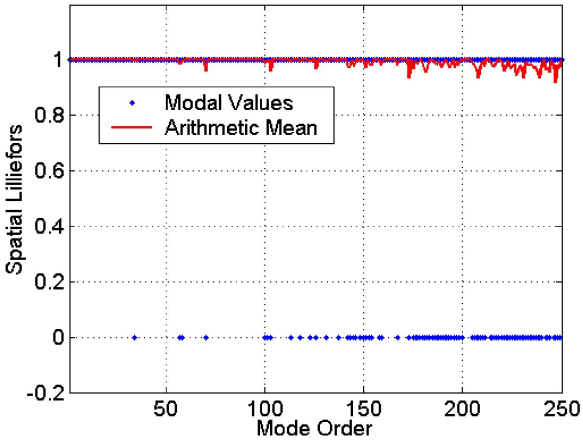

(b)

Figure 181: Spatial mode shape statistics results for the mass-loaded rectangular plates (spatial averaging approach). Plot (a): spatial kurtosis results: individual members, arithmetic and geometric mean values and analytical predictions (sinusoidal and GOE). Plot (b): spatial Lilliefors Test results: individual member values and arithmetic mean values.

In Figure 182, the spectral characteristics of mode shape component associated with the excitation point X_0 are presented for each mass-loaded plate member. The spectral kurtosis and Lilliefors Test results are plotted along with the GOE and sinusoidal model predictions.

As shown in Figure 182 (a), the spectral kurtosis results are approximately constant across the ensemble and a small dispersion is also observed around the ensemble kurtosis arithmetic mean value ($\bar{K} = 3.01$). Indeed, this good kurtosis agreement with the GOE values suggests that the mode shape components have a Gaussian distribution and are probably statistically independent at excitation point X_0.

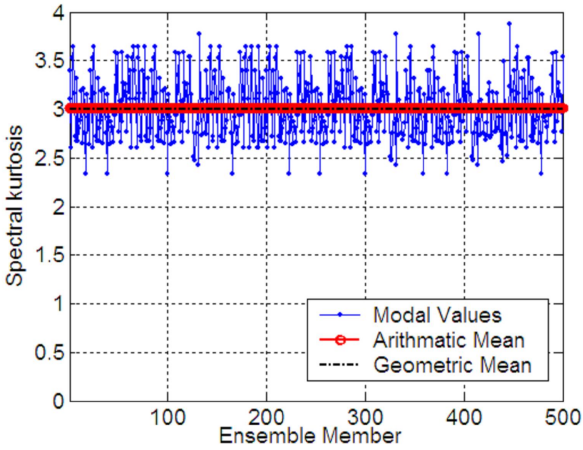

(a)

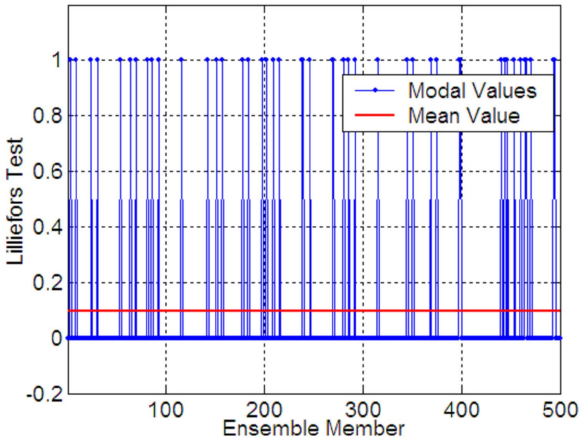

(b)

Figure 182: Spectral mode shape statistics results at excitation point X_0 for the mass-loaded rectangular plates (spectral averaging approach). Plot (a): spectral kurtosis: individual members, arithmetic and geometric mean values and analytical predictions (sinusoidal and GOE models). Plot (b): spectral Lilliefors Test results: individual member and arithmetic mean values

As shown in Figure 182 (b), the corresponding spectral Lilliefors Test results at excitation point X_0 are presented for mass-loaded rectangular plate members. The arithmetic mean value suggests that for approximately 90% of the mass-loaded plate members the mode shape components have a Gaussian distribution at excitation point X_0. These results suggest that the spectral mode shape statistics at excitation point X_0 are very close to those expected for perfect GOE eigenvectors, where the eigenvector components are statistically independent variables with Gaussian distribution characteristics, (56, 24).

In Figure 183 the ensemble kurtosis values associated with the excitation point X_0 and their corresponding Lilliefors Test results are shown for the mass-loaded rectangular plates. As observed in Figure 183 (a), the ensemble kurtosis values have a moderate dispersion around the spectral mean value ($\overline{K} = 2,73$). Although not shown here in detail, the distribution of the ensemble kurtosis results associated with the excitation point X_0 along the mode order domain is approximately symmetric, but the typically expected value is

lower than the spectral mean value, that is $K_{typ} = 2.60 \lesssim 2.73 = \overline{K}$.

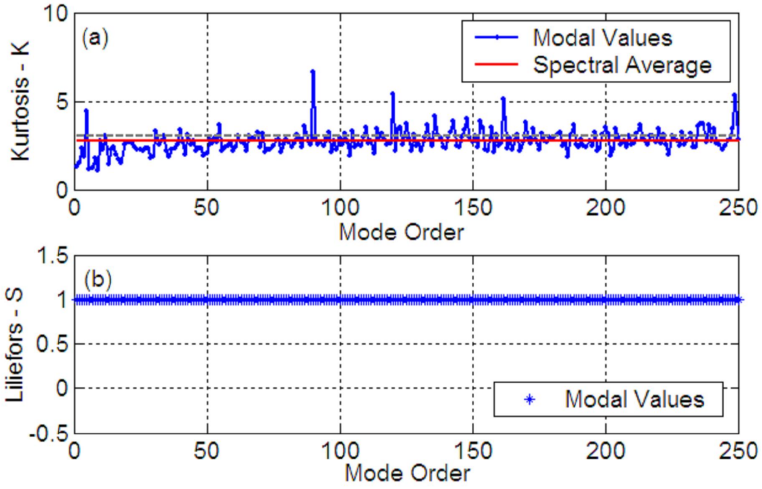

Figure 183: Ensemble mode shape statistics results at excitation point X_0 for the mass-loaded rectangular plates (ensemble averaging approach). Plot (a): ensemble kurtosis, spectral arithmetic mean value and analytical predictions (sinusoidal and GOE models). Plot (b): ensemble Lilliefors Test results.

The corresponding ensemble Lilliefors Test results associated with the excitation point X_0 suggest that most of the mode shape amplitudes do not have a Gaussian distribution. Although not shown here, the ensemble skewness coefficient results have dispersive characteristics along the mode order domain, showing that the distribution of the mode shape components associated with excitation point X_0 are strongly asymmetric for several mode orders.

In Figure 184, the PDF values for the mode shape components associated with the excitation point X_0 are plotted considering the spectral and ensemble domains. For the evaluation of the spectral results at excitation point X_0, a typical mass-loaded plate member was considered while for the evaluation of the ensemble results, three values along the mode order domain were considered.

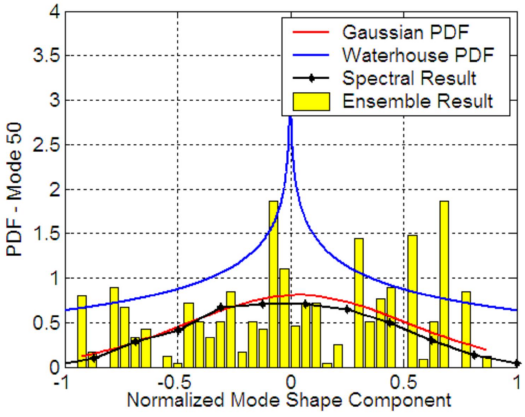
Gaussian PDF
Waterhouse PDF
Spectral Result
Ensemble Result
PDF - Mode 50
Normalized Mode Shape Component
4
3.5
3
2.5
2
1.5
1
0.5
0
-1
-0.5
0
0.5
1

(a)

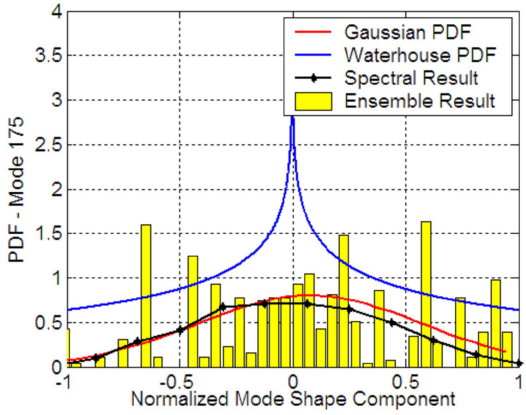
Gaussian PDF
Waterhouse PDF
Spectral Result
Ensemble Result
PDF - Mode 175
Normalized Mode Shape Component
4
3.5
3
2.5
2
1.5
1
0.5
0
-1
-0.5
0
0.5
1

(b)

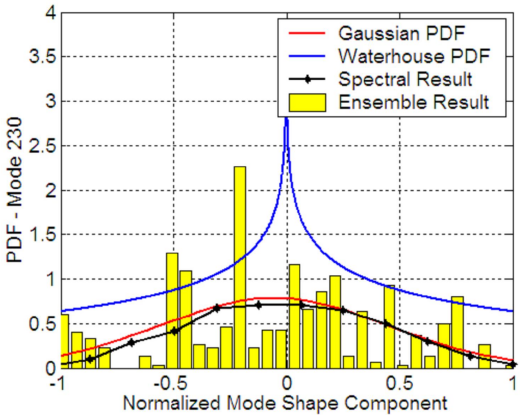

(c)

Figure 184: PDF values for the mode shape amplitudes associated with the excitation point X_0 for the mass-loaded rectangular plates: spectral and ensemble averaging approaches.

As observed in Figure 184, the spectral and ensemble PDF results are completely distinct. The ensemble PDF results are discontinuous while the spectral results are approximately continuous and have a well-behaved distribution. These notable differences between the characteristics of the spectral and ensemble mode shape statistics results clearly demonstrate the distinct levels of the establishment of chaotic statistics for the mode shapes.

Although the evaluations of the mode shape SEA parameters (P and Q) are ideally possible for the mode shapes of the random mass-loaded plates, computational limitations occurred during in their processing for the mathematical software used in the current work. Therefore, the calculation of these mode shape SEA parameters becomes prohibitive for this particular application. Additionally, it is important to emphasize that mode shapes consist on vectors with large dimensions since that a large number of the degrees of freedom are employed for the building of FEM model of each mass-loaded plate member of ensemble.

Kinetic Energy Density Statistics: Spatially-Averaged Excitation

In Figure 185, the mean and relative variance results are shown for the spatially-averaged excited mass-loaded plates with $\eta = 0.01$. The numerical results are compared with the SEA predictions based on the Poisson and GOE models.

As observed in Figure 185 (a), the mean value of the spatially-averaged kinetic energy density results conform very well with the SEA prediction. This excellent agreement can be attributed to the fact that the mean results are weakly dependent on the statistical characteristics of the natural frequencies, (84, 154).

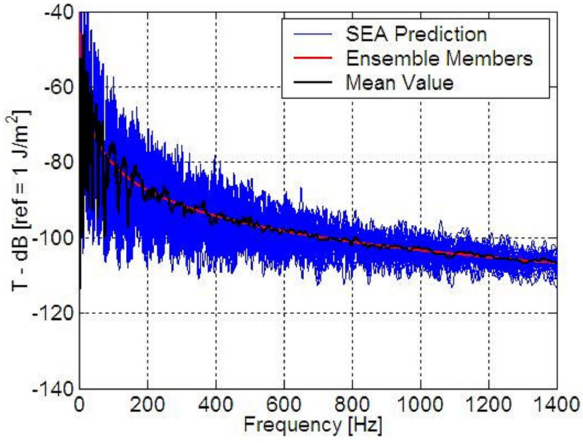

(a)

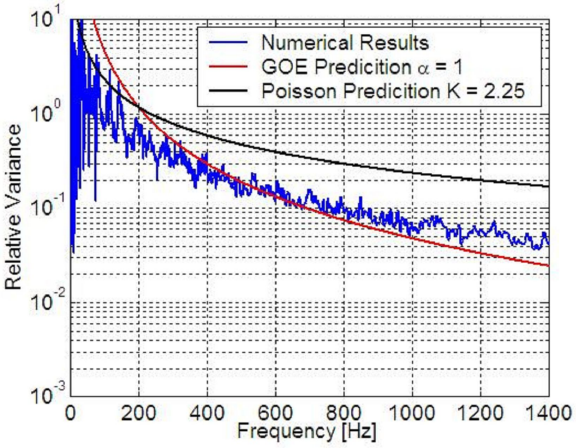

(b)

Figure 185: Mean and relative variance of the spatially-averaged kinetic energy density results for the mass-loaded rectangular plates with $\eta = 0.01$ (ensemble averaging approach). Plot (a): mean values. Plot (b): relative variance values.

The corresponding relative variance results conform well with the SEA prediction based on the GOE model, except for some small deviations observed in the high-frequency range. As shown in Figure 185 (b), the numerical results are slightly higher than the GOE model prediction and the deviations seem to be amplified as the excitation frequency increases. Indeed, a large number of modes contributes to the energy response in the high-frequency range, and thus the small discrepancies in the long-range fluctuation statistics become relevant to the statistical characteristics of the spatially-averaged kinetic energy density results. Therefore, the increase in the relative variance values in the high-frequency range is supported by the reduction in spectral rigidity characteristics of the natural frequencies which can be clearly observed in the results for the long-range fluctuation statistical observables in Figure 178.

In Figures 186 and 187, the mean and relative variance results are shown for the spatially-averaged excited mass-loaded plates with $\eta = 0.015$ and $\eta = 0.030$, respectively. The numerical results are compared with the SEA predictions based on the Poisson and GOE models.

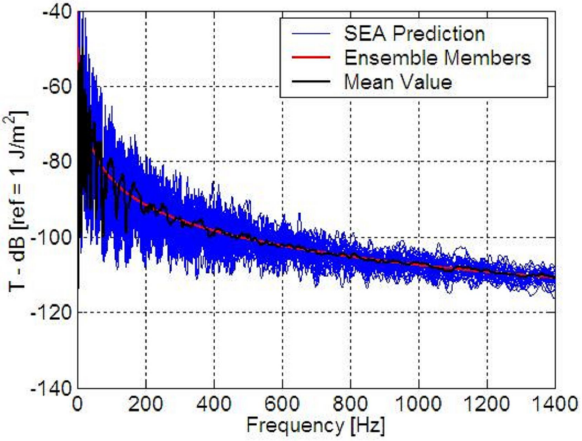

(a)

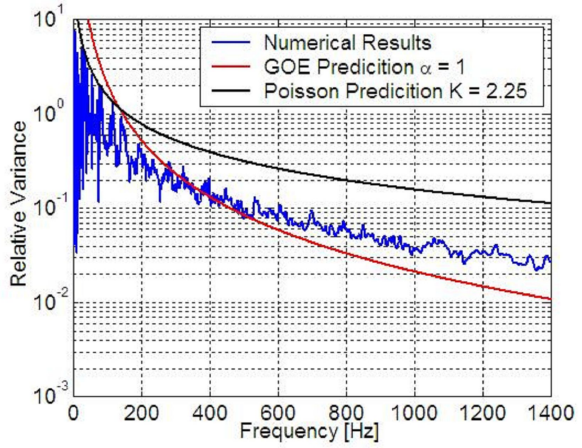

(b)

Figure 186: Mean and relative variance for the spatially-averaged kinetic energy density results for the mass-loaded rectangular plates with $\eta = 0.015$ (ensemble averaging approach). Plot (a): mean values. Plot (b): relative variance values.

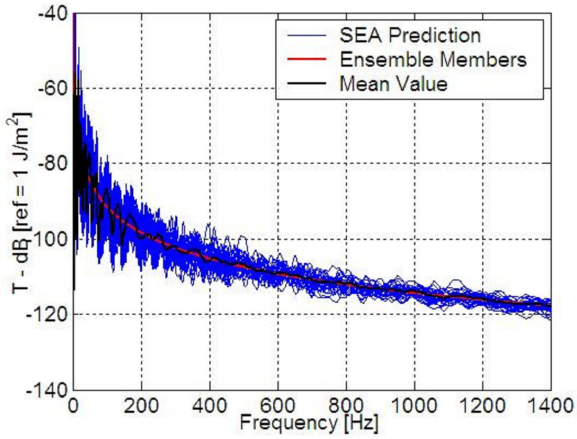

(a)

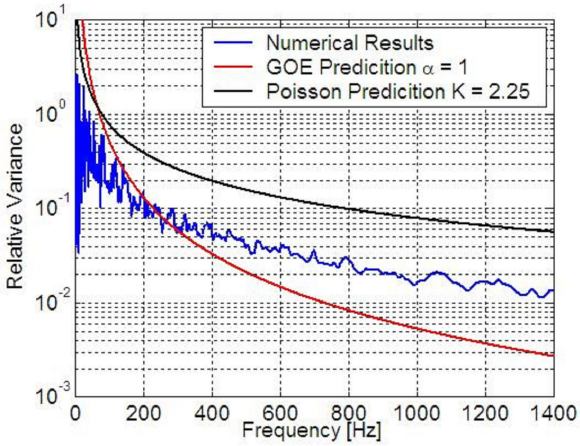

(b)

Figure 187: Mean and relative variance of the spatially-averaged kinetic energy density results for the mass-loaded rectangular plates with $\eta = 0.030$ (ensemble averaging approach). Plot (a): mean values. Plot (b): relative variance values.

As shown in Figures 185 - 187, the variability of the kinetic energy

results across the ensemble is gradually reduced as the damping loss factor increases. Additionally, the reduction in the level of agreement with the GOE model prediction suggests that the small long-range differences between the ensemble natural frequency and GOE model statistics are substantial in the high-frequency range due to the establishment of a high modal superposition condition.

Kinetic Energy Density Statistics: Single-Point Excitation

In Figure 188, the mean and relative variance values for the single-point kinetic energy density results are shown for the mass-loaded plates with $\eta = 0.01$. The numerical results are compared with the SEA predictions based on the Poisson and GOE models.

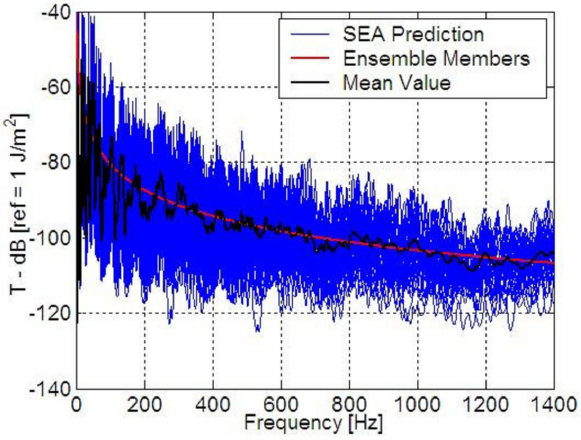

(a)

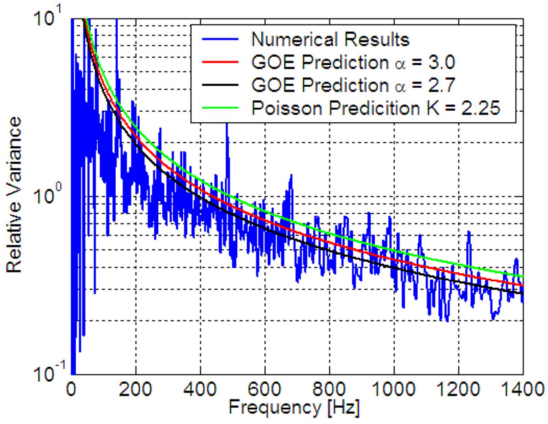

(b)

Figure 188: Mean and relative variance of the single-point kinetic energy density results for the mass-loaded rectangular plates with $\eta = 0.01$ (ensemble averaging approach). Plot (a): mean value. Plot (b): relative variance values.

As can be seen in Figure 188 (a), an excellent agreement is observed between the standard SEA formulation and the arithmetic mean values of the kinetic energy density results. Figure 188 (b) shows that the analytical prediction based on the GOE model overestimates the numerical results throughout the frequency domain investigated. Indeed, the discrepancies observed between the numerical results and the GOE prediction for the variance can be attributed to non-universal characteristics present in the mode shape statistics.

As discussed in the previous subsections, the mode shape statistics of the mass-loaded plates have significant deviations in relation to the statistics expected for perfect GOE eigenvectors. The main non-universal characteristics were identified in the results for the eigenvector statistical observables evaluated through the spatial and ensemble averaging processes.

In Figure 181, the ensemble mode shape statistics do not conform perfectly with the GOE model characteristics. The spectral mean of the ensemble kurtosis results is lower than the GOE kurtosis value and the corresponding Lilliefors Test results clearly reject the hypothesis that the mode shape components associated with excitation point X_0 have a Gaussian distribution across the ensemble. Additionally the spatial mode shape statistics suggest

an incipient establishment of the structural localization phenomenon in the mode shapes, which leads to large values for spatial kurtosis results.

On the other hand, the current variance results show, surprisingly, that an excellent agreement was obtained when a value of 2.7 was adopted for the mode shape statistics factor. This good performance of the GOE prediction with K modified may be attributed to the following factors: (*i*) the short-range fluctuation statistics of the natural frequencies conform well with the GOE model; and (*ii*) the corresponding mode shapes present some initial level of universal characteristics along the spectral domain.

As observed in Figure 182, the spectral characteristics of the fixed mode shape component associated with the excitation point X_0 are very similar to those expected for perfect GOE eigenvectors. The ensemble mean value for the spectral kurtosis results is approximately equal to 3 and only a small dispersion across the ensemble is observed. Additionally, the spectral Lilliefors Test results show that for approximately 90% of the mass-loaded plate members the mode shape components have a Gaussian distribution at excitation point X_0, suggesting that the spectral mode shape statistics at excitation point X_0 are very similar to those expected for perfect GOE eigenvectors, where the eigenvector components can be considered to be statistically independent variables with Gaussian distribution characteristics.

In Figures 189 and 190, the mean and relative variance values for the single-point kinetic energy density results are shown for the mass-loaded plates with $\eta = 0.015$ and $\eta = 0.030$, respectively. The numerical results are compared with the SEA predictions based on the Poisson and GOE models.

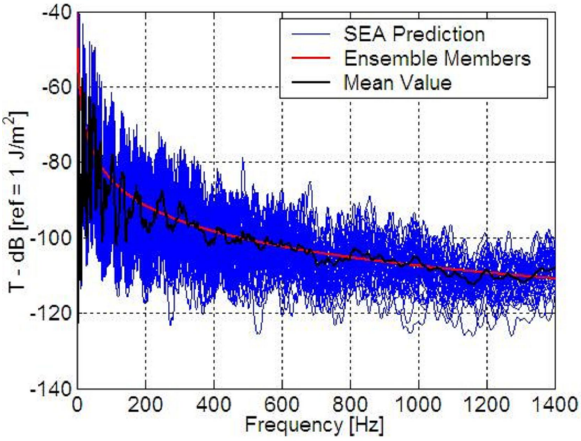

(a)

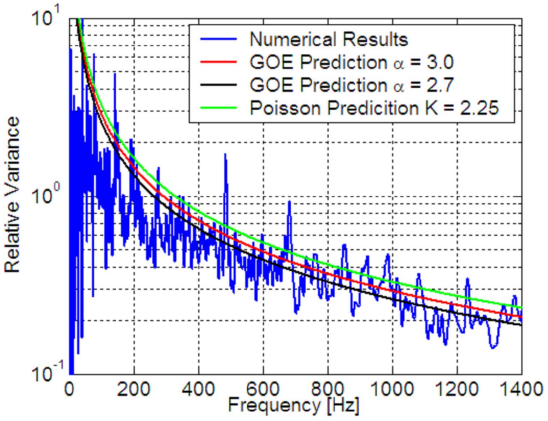

(b)

Figure 189: Mean and relative variance of the single-point kinetic energy density results for the rectangular mass-loaded plates with $\eta = 0.015$ (ensemble averaging approach). Plot (a): mean values. Plot (b): relative variance values.

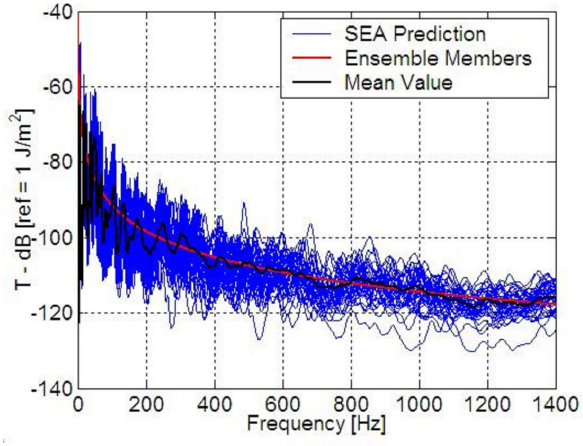

(a)

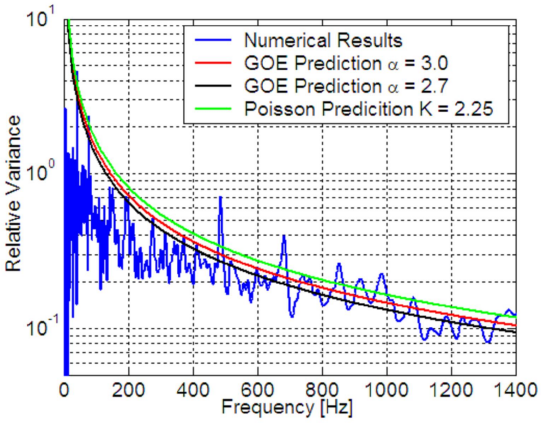

(b)

Figure 190: Mean and relative variance of the single-point kinetic energy density results for the mass-loaded rectangular plates with $\eta = 0.030$ (ensemble averaging approach). Plot (a): mean values. Plot (b): relative variance values.

The variance results shown in Figures 188-190 demonstrate that the variability of the single-point kinetic energy density results across the ensemble is gradually reduced as the damping loss factor increases. In principle, the level of agreement with the GOE model predictions with $K = 3$ or $K = 2.7$ seems to remain unaltered for the DLF values investigated herein. In general, the relative variance results become smoother as the damping effect increases.

4.4.3 Discussion and Remarks

In this second part of the statistical investigation of flexural plates, a complete statistical analysis of the modal parameters of two nominally identical ensembles of rectangular plates with distinct randomness natures was performed considering the ensemble averaging approach for the natural frequencies and the spatial, spectral and ensemble averaging approaches for the corresponding mode shapes.

The first ensemble investigated herein was composed of random rectangular plates the sides of which have a Gaussian distribution. The results for the eigenvalue statistical observables showed that the ensemble natural frequency statistics conform well with the analytical predictions based on the Poisson model and the small discrepancies suggested an incipient establishment of the level repulsion phenomenon which becomes more pronounced as the natural frequency spacing increases. Additionally, the comparisons with the previous natural frequency statistical observable results obtained using the spectral averaging approach demonstrated that the validity of the spectral-ensemble ergodicity only holds locally for the natural frequencies of random rectangular plates. On the other hand, the statistical overlap factor analysis led to the opposite conclusions to those obtained for the statistical observables results, which suggest a satisfactory agreement with the Poisson model throughout the frequency range investigated. Indeed, the statistical overlap factor results indicated erroneously that the universal establishment of GOE statistics for the natural frequencies would be expected for mode orders greater than mode 20 (that is, approximately a frequency of 100 Hz).

Overall, the results for the mode shape statistical observables showed the establishment of an intermediate statistics between sinusoidal and Gaussian statistics, that is, an incomplete establishment of the GOE model, regardless of the mode shape averaging approach adopted. The spatial mode shape statistics results suggested the establishment of a transitory state between the sinusoidal and Gaussian statistics, where the typically expected value for the spatial kurtosis is $K \simeq 2.6$ and most of the Lilliefors Test results rejected the

hypothesis of a Gaussian distribution for the mode shape components.

The spectral kurtosis values also suggested that the mode shape components associated with excitation point X_0 have a non-Gaussian distribution. However, the corresponding Lilliefors Test results suggested that for approximately 70% of plate members the mode shape components have a Gaussian distribution at excitation point X_0. Additionally, the ensemble mode shape statistics results confirmed the previous conclusions obtained from the spatial and spectral mode shape statistics analysis, where the establishment of an intermediate state between sinusoidal and Gaussian mode shape statistics is clearly observed.

The mean values for the spatially-averaged kinetic energy density results across the ensemble conformed very well with the standard SEA prediction, independently of the damping loss factor adopted. For the corresponding relative variance, the analytical prediction based on the Poisson model slightly overpredicted the numerical results since the ensemble natural frequency statistics are slightly more rigid than those expected for perfect Poissonian eigenvalues. As the damping loss factor was increased, the existing differences between the ensemble natural frequency statistics and Poisson model were amplified and introduced spectral or inter-modal correlations between the natural frequencies which reduce the energy response variability over the spectral and ensemble domains and also degrade the performance of the SEA variance prediction based on the Poisson model.

The point-loading kinetic energy density results allowed the assessment of the statistical contribution of each modal parameter to the first two statistical moments of the energy response across the ensemble. As expected, an excellent agreement was observed between the standard SEA prediction and the mean values for the numerical results. Additionally, the corresponding relative variance results conformed surprisingly well with the Poisson prediction. Indeed, this good agreement seems to be supported by the fact that the small deviations observed, in relation to the Poisson model for natural frequencies and in relation to the sinusoidal functions for the mode shapes, could be successfully compensated in the modal superposition process, since the point-loading kinetic energy density results are simultaneously affected by the statistical contributions from the natural frequencies and corresponding mode shapes.

However, as the damping loss factor increased, the level of agreement with the Poisson prediction became substantially lower. Indeed, despite the strong inter-modal correlations associated with the high modal superposition condition, relevant contributions from the mode shape statistics at the exci-

tation point can also be expected since the mode shape statistics are very sensitive to non-universal effects associated with the detailed nature of the system.

The second ensemble investigated herein is composed of mass-loaded rectangular plates. The ensemble natural frequency statistical observable results showed a transitory process from Poisson to GOE model statistics for the low-frequency range. On the other hand, a satisfactory agreement with the GOE model prediction was observed in the mid- and high-frequency ranges, particularly beyond mode 50 (corresponding approximately to a frequency of 250 Hz). Indeed, the establishment of the *level repulsion* characteristics in the short-range fluctuation statistics was clearly observed, although there were some small long-range deviations in the large natural frequency distances. Additionally, the universal establishment of GOE statistics for the natural frequencies was suggested by the statistical overlap factor results for mode orders greater than mode 50.

Considering the results for the corresponding mode shape statistical observables, they showed an incomplete establishment of the GOE model. The spatial mode shape statistics suggested an incipient establishment of the *structural localization* phenomenon, since the spatial kurtosis values are larger than the GOE kurtosis value and the Lilliefors Test confirmed that the mode shape components have a non-Gaussian distribution over the spatial domain of the plate system. In principle, these non-universal characteristics can be explained by the energy confinement phenomenon between the adjacent point-masses.

The spectral mode shape statistics results showed a satisfactory agreement with the GOE model since for most of ensemble members the spectral kurtosis values are close to $K = 3$, suggesting that the mode shape components associated with the excitation point X_0 have a Gaussian distribution along the spectral domain. Additionally, the corresponding Lilliefors Test results suggested that for approximately 90% of plate members the mode shape components have a Gaussian distribution at excitation point X_0, showing results similar to those expected for perfect GOE eigenvectors where their components are statistically independent variables with Gaussian distribution characteristics.

On the other hand, the ensemble mode shape statistics results also showed an incomplete establishment of the GOE model, since the spectral mean value for the ensemble kurtosis results associated with the excitation point X_0 is $K = 2.7 < K_{GOE} = 3$ and the corresponding Lilliefors Test results rejected the hypothesis of a Gaussian distribution for the mode shape com-

ponents. Therefore, it is interesting to note that the spectral and ensemble mode shape statistics results at excitation point X_0 have completely distinct characteristics along the respective domains.

As observed previously in Figures 185 - 187, the ensemble mean values for the spatially-averaged kinetic energy density results conformed very well with the standard SEA prediction, independently of the damping loss factor adopted. For the corresponding relative variance results, there was good agreement with the SEA prediction based on the GOE model, except for small discrepancies in the high-frequency range, which are associated with the reduction in the spectral rigidity characteristics of the natural frequencies. These discrepancies observed in the long-range fluctuations are expected to be amplified as the damping loss factor increases and thus the level of agreement with the GOE model prediction is substantially reduced in the mid and high-frequency ranges.

For the point-loading kinetic energy density results, an excellent agreement was observed between the standard SEA prediction and the mean values of the numerical results. The numerical relative variance results were clearly overpredicted by the analytical results based on the GOE model and $K = 3$ throughout the frequency domain investigated herein. Based on the results obtained for the mode shape statistical observables, these discrepancies are strongly associated with the incomplete establishment of the GOE model for mode shapes, which is demonstrated by the *non-universal* characteristics.

On the other hand, surprisingly, an excellent agreement with the GOE prediction was observed when the value of 2.7 was adopted for the mode shape statistics factor. Despite the natural frequency statistics are almost-GOE, this good performance of the GOE prediction with $K = 2.7$ can be attributed to the fact that an initial degree of universality is observed for the spectral statistical characteristics of the mode shape components associated with the excitation X_0.

Additionally, the spectral Lilliefors Test and kurtosis results for the mass-loaded rectangular plates demonstrated indirectly that the mode shape characteristics are very close to those expected for the perfect GOE eigenvector components, where the mode shape components associated with the forcing position would be considered *uncorrelated Gaussian* variables. In this regard, the occurrence of reduced agreement between the GOE prediction with $K = 3$ and current relative variance results suggested that the existence of inter-modal correlations between the mode shapes at the excitation point may not play an important role in the overprediction of the SEA variance prediction based on the complete GOE model. It is important to note that this new

finding can lead to conclusions which are the opposite to those of Langley and Brown who speculate that the correlation between the same component of different mode shapes at excitation point could be mainly responsible for the discrepancies in relation to the GOE model prediction, (18, 1). However, further systematic investigations are required to ascertain whether this unexpected conclusion can be extended to real engineering systems with different natures and dimensionality.

4.5 Summary and Final Discussion

The numerical analysis carried out with random flexural plates in this chapter allowed the systematic investigation of the modal parameter statistics. The main effects of the physical phenomena expected in real engineering 2D-systems were identified and measured through the statistical observable results.

Initially, the effects of the breaking of the geometrical regularity of plate systems on the modal parameter statistics were adequately characterized since the plate geometries investigated herein provided a gradual statistical transition from the *regular* to *disordered* statistics, where a *deterministic chaotic* statistics described by the GOE model was observed in the mid and high-frequency ranges when focusing and defocusing elements are introduced at the system boundaries (*i.e.*, circular arc elements, nonparallel or irregular sides, and non-concentric arc elements).

For plate systems with rectangular-like shapes, the main effects of the establishment of stable periodical orbits were promptly identified in the natural frequency statistics, which lead to a reduction in the spectral rigidity characteristics of the natural frequency statistics. As demonstrated for rectangular plates, these *non-universal* contributions can be accurately taken into account in the natural frequency statistical observable results through the use of the *Fourier unfolding process*. In this regard, the direct consequences of an incorrect choice for the cut-off time were highlighted and demonstrated through numerical results for the long-range statistical observables. For the corresponding mode shapes, the main effect of stable periodic orbits is the establishment of regular nodal lines, mainly for the case of the *bouncing ball* periodic orbits which lead to the occurrence of nodal lines within the parallel sides of the system. Additionally, the effects of the occurrence of perfect or quasi-degenerate modes on the natural frequencies statistics were investigated using the short and long-range fluctuation statistical observables. The analytical *scaled Poisson* predictions based on the Shnirelman Peak theory

showed good agreement with the numerical results.

The investigation of the square and perfect rectangular plates also demonstrated the existence of discrete mode shapes with almost-Gaussian characteristics, which are provided by the modal superposition phenomenon of two degenerate modes of different wave classes: the flexural (or vertical transverse) mode which has *regular* statistics characteristics and the extensional (or longitudinal) mode which has *chaotic* statistics characteristics. Indeed, these mode shape results for degenerate modes may explain the level repulsion characteristics observed in the natural frequency statistics.

Overall, the modal parameter results for the statistical observables allowed an accurate verification of the level of agreement with the GOE model (or Poisson model) as well as the classification and measurement of the deviations. Additionally, the expected performance of the SEA variance prediction based on the complete GOE model (or Poisson model) was estimated for the cases where the modal parameter statistics do not comply perfectly with GOE model (or Poisson model). It is important to emphasize that the statistical overlap factor analysis was inefficient in terms of verifying the application of the GOE model to the modal parameter statistics, mainly in the case of the ensemble of random rectangular plates. Indeed, the excellent performance of the statistical observable results in terms of characterizing the statistics of each modal parameter confirmed, definitively, that the statistical overlap factor analysis is not appropriate to verify the agreement with GOE model.

The statistical results obtained for the two plate ensembles investigated herein demonstrated that the nominally identical ensembles may have very distinct modal parameter and energy response statistics across the ensemble. As observed, the statistical analysis of the kinetic energy results suggested that the characteristics of the modal parameter statistics seem to have little influence on the mean values across the ensemble for the plate systems investigated herein.

The corresponding relative variance value for the spatially-averaged kinetic energy results was shown to be highly sensitive to the natural frequency statistics since the mode shape contributions were completely removed due to the averaging process over the spatial domain of the plate systems. Therefore, based on the ensemble natural frequency statistical observable results, good agreement with the different models was observed for each plate ensemble. For random rectangular plates, the numerical variance results conformed very well with the analytical prediction based on the Poisson model prediction while for the mass-loaded rectangular plates good agreement with

the GOE model prediction was locally observed across the ensemble. Additionally, small effects of long-range fluctuation deviations in relation to the Poisson model (or GOE model) were clearly observed in the high-frequency range and for the high superposition modal condition, where several modes contribute to the energy response and the establishment of non-universal inter-modal correlations possibly occurs between the natural frequencies.

Based on the modal parameter statistical observable results, the long-range fluctuation deviations observed for the natural frequency statistics of random rectangular plates can be explained by the modal superposition phenomenon of degenerate flexural and extensional modes which slightly increases the spectral rigidity characteristics of the natural frequencies along the frequency range. On the other hand, the long-range fluctuation deviations observed for the mass-loaded rectangular plates are probably associated with the incipient establishment of structural localization for the corresponding mode shapes.

The relative variance values of the point-loading kinetic energy density results demonstrated the substantial contributions of the mode shapes to the kinetic energy statistics across the ensemble. For the random rectangular plates, the numerical variance results conformed surprisingly well with the Poisson model prediction, although the natural frequency statistics do not agree perfectly with the Poisson model and the mode shape statistics deviate slightly from the sinusoidal eigenvector statistics. Indeed, this good agreement seems to be associated with the fact that the modal parameter deviations in relation to the Poisson model are successfully compensated in the modal superposition process. For mass-loaded plates, the GOE prediction with $K = 3$ overestimated the numerical variance results, suggesting the incomplete establishment of the GOE model for mode shape statistics, since good agreement with GOE prediction was observed for the natural frequency statistical observable results as well as for the relative variance of the spatially-averaged kinetic energy results. However, when the value of $K = 2.7$ was adopted for the mode shape statistics factor, an excellent agreement between the numerical values and GOE prediction was observed, since the natural frequency statistics are *almost-GOE* and the some *universal* characteristics are observed for the spectral mode shape statistics.

Important conclusions on the modal parameter statistics can be drawn when the current plate results are compared with the rod results investigated in the previous chapter. The different dimensionality of the mass-loaded system allowed the systematic investigation of the main aspects associated with the structural localization phenomenon, which is expected to affect substan-

tially the statistical moments of the high-frequency energy responses in real engineering systems.

For the same level of mass randomness (20%), different levels of the establishment of the structural localization phenomenon were observed for the modal parameters of the random mass-loaded systems investigated herein. The rod system, due to its one-dimensional characteristics, was shown to be a natural candidate for the establishment of the structural localization phenomenon in the high-frequency range. Indeed, the modal parameter statistical observable and localization factor results showed a simultaneously different regime for the structural localization along the frequency range investigated herein. On the other hand, the presence of point masses established a small degree of disorder in the mass-loaded rectangular plates, and thus only incipient localization effects on the natural frequencies and mode shapes were observed.

For both mass-loaded systems, good agreement was observed between the numerical mean value and standard SEA prediction for the spatially-averaged kinetic energy density results since the highly disordered mode shape contributions are completely removed by the spatial averaging of the excitation points.

However, for single point-excited structures, the structural localization effect becomes substantial as the excitation frequency increases. Due to the contributions of disordered mode shapes, the system dynamic characteristics do not conform well with the basic assumptions of the SEA theory, reducing strongly the performance of the SEA formulations, regardless of the statistical model adopted.

Considering the universal establishment of the GOE model for the modal parameters, distinct convergence characteristics were observed for the mass-loaded rod and plate ensembles with the same level of mass randomness (20% of total mass). For rod systems, the universal establishment of GOE model occurs simultaneously for the natural frequency and mode shape statistics over a small and limited frequency interval located in the mid-frequency range. On the other hand, for the mass-loaded rectangular plates, satisfactory establishment of the GOE model was only observed for the natural frequency statistics in the mid and high-frequency ranges. The corresponding mode shape statistics presented substantial *non-universal* characteristics since that the mode shape statistical observable results showed notable discrepancies in relation to the GOE model for the spatial and ensemble averaging approaches. It is interesting to note that the convergence characteristics of the modal parameter statistics for mass-loaded plate ensemble are very similar to those

proposed initially by Figure 12, which have been extensively reported in the SEA variance literature.

In this study, the statistical results for the Gaussian spatially-correlated rod ensemble showed an unexpected dynamical behavior which, to the best of the author's knowledge, has not previously been reported in the SEA variance literature. The individual results for the natural frequency and mode shape statistical observables showed that the universal establishment of GOE statistics may occur in separated frequency regions for each modal parameter. Additionally, the initial hypothesis, which states that the conditions necessary for the universal establishment of the GOE model for natural frequency statistics are less stringent than those for their corresponding mode shapes, that is, the mode shape statistics require a larger disorder in the system parameters than the corresponding natural frequency statistics for the universal establishment of the GOE model, was completely discarded considering the statistical results for the Gaussian spatially-correlated rods, where the mode shape universal limit occurs before the natural frequency limit along the frequency range.

Based on all of the numerical results obtained in this study, the convergence characteristics of the universal establishment of the GOE model for each modal parameter statistics seem to be a highly non-universal phenomenon, since the random systems investigated herein showed completely distinct characteristics, suggesting a strong dependence on the detailed nature of the system and the dimensionality.

Other important issue investigated in this study was the incomplete establishment of GOE statistics for the mode shapes and the possible impacts on the performance of the SEA variance prediction based on the complete GOE model. As discussed in the SEA variance literature, the inter-modal correlations at the excitation point are attributed as the main factor for the reduced performance of the SEA variance prediction based on the GOE model.

In the current model, the numerical point-loading variance results showed that good agreement with the GOE model prediction can be obtained, at least for a completely different level of agreement with the GOE statistics along the spectral domain, provided that the mode shape statistics at the excitation point across the ensemble ensure satisfactory establishment of the GOE model. Indeed, the random Gaussian spatially-correlated rod and mass-loaded plate results for the mode shape and point-loading energy statistics seem to suggest that the contributions of the spectral and spatial mode shape statistics are less expressive in comparison to that associated with the ensemble mode shape statistics at the excitation point, in terms of obtaining

good performance of the GOE model prediction.

For cases of random systems with the incomplete establishment of the GOE model for natural frequencies or mode shapes, good performance of the GOE prediction for point-loading with K modified is expected only for cases of random systems for which the modal parameter statistics do not deviate substantially from the GOE model characteristics. Indeed, the attribution of K value must be based on the engineering analysis, so that the possible effects of the *nonuniversal* phenomena associated with the detailed nature of the system and dimensionality are taken into account. For Gaussian spatially-correlated rods, the value which gave the best fit was $K = 4.5$, suggesting the incipient establishment of the structural localization phenomenon while for the mass-loaded rectangular plates the value of $K = 2.7$ is associated with the establishment of intermediate mode shape statistics between sinusoidal and perfect Gaussian mode shapes. It is important to emphasize that the numerical examples shown in this study are limited to the cases of simple one- and two-dimensional non-deterministic systems and further investigations are needed in order to extend the current conclusions and findings to cases of tri-dimensional random systems such as non-deterministic acoustical rooms.

5 CONCLUSIONS AND FURTHER WORK

In this last chapter, the initial research aims of the current work are reviewed. The main conclusions drawn in the previous chapters are restated and their possible implications in relation to results recently reported in the SEA literature are discussed. Based on these contributions and their possible extension to real engineering systems, some suggestions for further research are outlined.

5.1 Conclusions

The primary aim of this work was to obtain a better understanding of the statistical characteristics of the modal parameters of uncertain or non-deterministic structures in the mid to high-frequency ranges. In particular, considerable interest was focused on the complete description of the statistical characteristics of each modal parameter during the statistical transitory process of the *universal* establishment of GOE statistics.

In the introductory chapter, a literature review was carried out on the main effects of the system parameter uncertainties on the dynamic response statistics. In the low-frequency range, the uncertainty effects are almost negligible and traditional deterministic models, such as FEM, are sufficiently accurate to predict the dynamic response of the system. In the mid to high-frequency ranges, a wavelength reduction is expected and the uncertainty effects become increasingly substantial as the excitation frequency increases, leading to a large energy response variability. However, some SEA variance studies with artificially generated random systems have strongly suggested that the modal parameters as well as energy response statistics tends to have a universal behavior and thus the high-frequency energy response statistics becomes practically independent of the nature of the uncertainty of the physical parameters. Indeed, these results recently presented in the SEA literature also suggest the existence of a good agreement between the statistics of the GOE model and the high-frequency modal parameter statistics for real random engineering systems. Thus, the prediction problem of the maximum response variability becomes more appropriate from the analytical point of view. Langley and Brown (18, 3) took advantage of this fact and derived analytical expressions to predict the relative variance of kinetic energy density results for a generic excitation based on the GOE model for modal parameter statistics. Although satisfactory prediction results were observed for cases of random systems subjected to spatially-averaged excitations, a reduced per-

formance of the single point-loading relative variance was clearly observed at least for artificially generated random systems which are usually considered to be sufficiently random to ensure the complete establishment of GOE statistics for the modal parameters. As discussed previously, SEA results reported in the literature suggest that the deviations can probably be attributed to the incomplete establishment of GOE statistics for the mode shapes and thus non-universal system-dependent characteristics would be expected at least for the high-frequency mode shape statistics of real random engineering systems. Based on the results reported in the literature, it can be suggested, in principle, that the amount of randomness necessary to establish GOE statistics for mode shapes would probably be higher than the corresponding amount for natural frequencies and thus for real random engineering systems it would be expected that the universal establishment of GOE statistics is fulfilled more easily for natural frequencies than for the corresponding mode shapes. In this regard, several problematic issues were identified and the importance of a better understanding of the statistics characteristics during the process of the establishment of *universal* statistics for each modal parameter as well as the relevance of the development of metric functions to verify accurately the agreement with the GOE model were highlighted.

A review of the concepts of the Random Matrix Theory RMT applied to the prediction of the energy response statistics of random dynamical systems was performed. The main characteristics of well-defined statistical models, such as the Poisson and GOE models, were presented and discussed in terms of their application to the natural frequency statistics of real engineering systems. Special attention was given to the description of the statistical characteristics of a particular ensemble composed of large random symmetric matrices called the Gaussian Orthogonal Ensemble (GOE), since their eigenvalue statistics are expected to be very similar to the natural frequency statistics of sufficiently random vibroacoustic systems. The metric functions, denominated herein as statistical observables, were introduced to verify the level of agreement of the natural frequency statistics with GOE and Poisson models. Additionally, the results for the statistical observables demonstrated the occurrence of the main physical phenomena, such as level repulsion and spectral rigidity, of the natural frequency spectrum of real engineering systems. The possible effects of the finite wavelengths on the eigenvalue statistical results for the long-range fluctuations were investigated through a numerical methodology based on the Monte Carlo method. The numerical results showed that the finite wavelength effects can be significant for GOE random matrices and thus large fluctuations in the results for the natural fre-

quency statistical observables across the ensemble may be expected for random matrices of small dimensions.

As in the case of the natural frequencies, the main statistical aspects associated with the corresponding mode shapes of the dynamical systems were also reviewed in detail. The spatial, spectral and ensemble averaging approaches to the mode shape statistics were introduced and their relevance in the statistical analysis was highlighted. Results reported in the literature for the eigenvector statistical observables were used to describe the main statistical characteristics of the mode shapes of chaotic, regular and localized systems. The performance of the results for the statistical observables was discussed considering two main aspects: (i) verification of the level of agreement between the mode shape statistics of real engineering systems and the GOE eigenvector statistics, and (ii) direct characterization of the non-universal effects through the results for the mode shape statistical observables. Additionally, the main statistical issues associated with the establishment of the structural localization phenomenon were discussed and the analytical expressions of the non-linear sigma model from the Theory of Supersymmetry were introduced for weak and strong localization regimes.

Considering the SEA variance context, the derivations of the narrow and broad frequency band analytical predictions for the energy density variance were briefly reviewed for a single random dynamic system. The main aspects and limitations associated with the application of the Poisson and GOE models to the statistics of the natural frequencies of real engineering systems were presented. Based on recent results for the SEA variance reported in the literature, a detailed discussion was carried out regarding the main possible non-universal physical phenomena of the mode shape statistics which may contribute to the reduced performance of the point-loading SEA relative variance predictions.

In chapter 3 the modal parameter statistics of random longitudinal rods were systematically investigated using several averaging approaches. The most representative statistical observables for each modal parameter were selected and their results described adequately the main physical phenomena which are expected to be established in the modal parameters of real engineering systems. For the natural frequency statistics, the spectral rigidity and level repulsion characteristics were promptly identified, while for the mode shape statistics the main aspects associated with the establishment of structural localization were assessed along the excitation frequency range.

Based on the results for the statistical observables, the deviations from the universal statistics described by the GOE model were accurately identified

for each modal parameter. Therefore, the main impacts on the mean and relative variance of the kinetic energy density results as well as a possible reduction in the performance of the SEA variance prediction based on the complete GOE model (or Poisson model) were discussed in detail for the random rod ensembles investigated herein.

Regarding the convergence characteristics of the modal parameter statistics for the universal establishment of GOE model statistics, it is important to note that the current rod results for the natural frequency and mode shape statistical observables do not suggest the existence of a well-established priority order, or convergence sequence, between the modal parameters for the establishment of the universal statistics described by the GOE model, demonstrating that the hypothesis initially proposed in Figure 12 may be limited to a particular group of engineering systems. Indeed, the spatially-correlated Gaussian rod results showed that the establishment of GOE statistics may occur in separate frequency regions for each modal parameter. Additionally, the current results for the modal parameter statistics of random rods also suggested that the convergence speed and form characteristics of the statistical transition of each modal parameter required to conform to GOE statistics are non-universal characteristics which are strongly dependent on the nature of the randomness and system dimensionality.

The current relative variance results for random rods also suggested that for random vibroacoustic systems for which the establishment of universal statistics is incomplete or clearly separated over the frequency domain for each of the modal parameters, the performance of the SEA variance prediction based on the complete GOE model is strongly dependent on the nature and spatial characteristics of the excitation field.

In chapter 4 the statistical investigation of several geometries of flexural plates provided a better understanding of the effects of the breaking of the system symmetries on the modal parameter statistics. The presence of focusing and defocusing elements were shown to be a highly relevant factor for the establishment of a deterministic chaos on the modal parameter statistics in the mid to high-frequency ranges. Furthermore, special attention was focused on the identification and statistical description of the main physical phenomena associated with the random two-dimensional systems, for example: establishment of the stable periodic orbits, the occurrence of degenerate natural modes and structural localization aspects.

An important aspect investigated in this study was the possible effects of the inter-modal correlations at the excitation point on the performance of the SEA variance predicton based on the GOE model. The point-loading

variance results from the random rod ensembles showed that a good agreement with GOE prediction is equally obtained for two excitation points with completely distinct spectral mode shape statistics over the frequency range in which the ensemble mode shape component statistics are almost-Gaussian.

For the case of the mass-loaded plate ensemble, the spectral mode shape statistics associated with the excitation point location was found to be almost-Gaussian, but the best performance of the SEA variance prediction based on the GOE model was only obtained when a value of 2.7 was adopted for the mode shape statistics factor. Indeed, this good agreement can be explained by the current results for the mode shape statistical observables which suggest the incomplete establishment of Gaussian characteristics across the ensemble for the mode shape components associated with the excitation point. Thus, these results for the random rods and mass-loaded plates seem to reject the initial speculation that the inter-modal correlations at the force position are the main reason for the reduction in the performance of the SEA variance prediction based on the GOE model.

Finally, the findings in this study clarified some important issues regarding the modal parameter statistics and the *universal* establishment of GOE statistics. On the other hand, much work still needs to be carried out to extend these contributions to built-up complex real engineering systems in order to derive an efficient methodology with low computation cost characteristics for the prediction of high statistical moments of the energy responses.

5.2 Suggestions for Further Work

The numerical investigation of the modal parameter statistics described in this study revealed further research directions regarding the main aspects of the incomplete establishment of universal statistics in real engineering systems. In the author's opinion, the directions outlined below are examples of work areas which may warrant further research work:

- Modal parameter statistics of real engineering systems: Although the statistical observables can be applied to any generic vibroacoustic system, the investigation of the modal parameter statistics carried out in this study were limited to simple one- and bi-dimensional structures artificially randomized. Indeed, these randomized rod and plate system models are very simplified compared to "realistic" systems and were also investigated over a limited frequency range. In this regard, it would be of great interest to extend the current analysis of

the statistical modal parameters to more realistic systems with several shapes, boundary conditions and dimensionality. In real engineering structures, the uncertainties associated with manufacturing and assembly processes are expected to be much more complex than those investigated here. Typical examples might be non-homogeneities and discontinuities of the material, spot welds, holes for bolts or rivets and non-parallel edges. It is known that these structural irregularities will lead to the scattering phenomenon of the waveguide modes, which will probably result in the establishment of *universal* or disordered modal parameter statistics, depending on the dimensionality and symmetry characteristics of the system. Indeed, systematic investigations with more realistic systems from the naval, automotive and aeronautics fields are certainly necessary to characterize the typically expected modal parameter statistics in the high-frequency range.

- Accurate definition of the confidence limits: The currently available mean and variance analytical predictions of the kinetic energy density results are not sufficient to determine the maximum and minimum confidence intervals for an ensemble of structures. To undertake this task, a derivation of the statistical characteristics of the energy PDF for a generic system subjected to different types of excitation would be necessary. Considering the point process theory, a possible analytical approach is the use of high-order cumulants of the energy density. Some initial analysis to evaluate the high-order culmulants of modal parameters has been carried out for Poisson statistics and GOE statistics, (55, 35). For the well-defined statistics of modal parameters, results reported in the literature indicate that lognormal and Gaussian PDFs are expected for single point and spatially-averaged excitations, respectively. In this regard, it would be of interest to extend the analytical and numerical (or experimental) investigations on the form of PDF energy density to several types of excitation as well as to generic modal parameter statistics.

- Point-to-point transfer response statistics: Besides the evaluation of the spatially-averaged energy response variance results across the ensemble, the variance of the energy response at a given point remote from the excitation point is of interest to many engineering applications. The pioneering studies in this area were carried out in the room acoustics field, and they considered the natural frequency statistics described by the Poisson model. It is known that the establishment of the Poisson

model is unlikely in real engineering systems since the small random imperfections originating from manufacturing and assembly processes can greatly affect the modal parameter statistics, mainly in the high-frequency range. Considering that the energy response across the ensemble can be treated as a random point process, and the modal parameter statistics comply completely with the GOE model, Langley and Cotoni (35), based on the high-order culmulant values of the modal parameters, proposed analytical point-to-point relative variance predictions for response points located in the drive and far field positions. According to the modal parameter statistics results obtained in this study, it seems that the GOE statistics may not be completely established for modal parameters in some excitation frequency regions. Thus, further investigations are necessary to assess the main effects of different levels of agreement with the GOE model on the performance of the application of the point-to-point variance predictions in real engineering systems. Additionally, a systematic analysis needs to be carried out to determine the mean and variance values of the real and imaginary parts of the point-to-point transfer functions as well as to assess the statistical distributions of their amplitudes and phases.

- Damping effects on energy response statistics: Some basic studies using membranes with complex geometry have investigated the effects of distinct levels of the damping mechanism on the modal parameter statistics and the results indicated that the damped natural frequency spectra have spectral correlations which are consistent with GOE statistics, provided that the damping level is moderate (170, 106). However, for highly damped systems, the damping effects on the modal parameter statistics are substantial and thus their natural frequencies become strongly correlated in the spectral domain, and they may not conform with GOE statistics. Therefore, it would be of great interest to investigate the effects of different types and levels of damping mechanisms on the modal parameter statistics. Although it was not investigated here, the existence of variable modal damping factors is certainly expected for real engineering systems. In the elastodynamical literature, a good agreement with the chi-squared distribution has been observed for sufficient lightly damped systems. As discussed in the SEA variance literature, the possible mode-to-mode fluctuation of the modal damping loss factors may lead to important effects on the energy variance results. The results of some initial studies have been reported in the literature by Weaver *et al* (50, 75),

but the complete formulation of the two-level cluster function was not considered. The derivation of the complete variance prediction for the variable modal damping factor is a complex and interesting analytical task. Thus, there are good physical as well as mathematical reasons to carry out a systematic study of the effect of damping mechanisms on the *universal* establishment of GOE statistics for each of the modal parameters as well as an assessment of the expected contributions of the variable modal damping factors to the energy response statistics of real engineering systems.

- Semi-classical acoustics and non-linear sigma models: In this study, several conceptual results from the semi-classical acoustics area were considered in the statistical analysis of the modal parameters. In particular, the statistical investigation of the random rods and plates showed that the non-universal mode shape deviations due to the establishment of the structural localization phenomenon were accurately described in the weak and strong localization regimes by the non-linear sigma model expressions taken from the supersymmetry theory. Thus, one idea for future study would be to introduce non-universal deviations into the SEA variance theory through of use of non-linear sigma model expressions. However, this procedure is a complex analytical task and would probably provide an additional parameter associated with the level of disorder of systems and the localization phenomenon, moving away from the conceptual aim of SEA method which is to avoid the need for detailed information on the system geometry or the statistics of its parameters. Finally, further studies are required to explore the possible benefits of the semi-classical acoustics results on the theory of SEA variance.

REFERENCES

1 BROWN, A. W. M. *The Ensemble Statistics of the Response of Structural Components with Uncertain Properties*. Tese (Doutorado) — University of Cambridge, 2003.

2 ZIENKIEWICZ, O. C. *The Finite Element Method*. [S.l.]: McGraw-Hill, 1977.

3 LANGLEY, R. S.; BROWN, A. W. M. The ensemble statistics of the band-averaged energy of a random system. *Journal of Sound and Vibration*, v. 275, n. 3, p. 847–857, 2004.

4 LANGLEY, R. S.; SHORTER, P. J.; COTONI, V. Predicting the response statistics of uncertain structures using extended versions of sea. *Proceedings of Internoise 2005*, v. 1, p. 1 – 19, 2005.

5 FAHY, F. *Advanced Applications in Acoustics, Noise and Vibration*. [S.l.]: Taylor & Francis, 2004.

6 MACE, B.; WORDEN, K.; MANSON, G. Uncertainty in structural dynamics. *Journal of Sound and Vibration*, v. 288, p. 423–429, 2005.

7 FAHY, F. *Foundation of Engineering Acoustics*. [S.l.]: Academic Press, 2001.

8 KOMPELLA, M. S.; BERNHARD, R. J. Measurements of the statistical variation of structural-acoustics characteristics of automotive vehicles. *Proceedings of the SAE noise and Vibration Conference*, v. 1, p. 65–81, 1993.

9 KOMPELLA, M. S.; BERNHARD, R. J. Variation of structural-acoustic characteristics of automotive vehicles. *Noise Control Engineering*, v. 44, n. 2, p. 93–99, 1996.

10 GOMES, C. H. *Statistical Analysis of Mode Shapes from an Ensemble of Random Structures*. Doctorate Qualification, Federal University of Santa Catarina, 2006 (In Portuguese).

11 DAVIES, H. G.; WAHAB, M. A. Ensemble averages of power flow in randomly excited coupled beams. *Journal of Sound and Vibration*, v. 77, p. 311 – 321, 1981.

12 DAVIES, H. G.; KHANDOKER, S. I. Random point excitation of random beams. *Journal of Sound and Vibration*, v. 84, n. 4, p. 557 – 562, 1982.

13 FAHY, F. J.; MOHAMED, A. D. A study of uncertainty in applications of sea to coupled beam and plate systems, part 1: Computational experiments. *Journal of Sound and Vibration*, v. 158, n. 1, p. 45 – 67, 1992.

14 KEANE, A. J.; MANOHAR, C. S. Energy flow variability in a pair of coupled stochastic rods. *Journal of Sound and Vibration*, v. 168, n. 2, p. 253 – 284, 1993.

15 MANOHAR, C. S.; KEANE, A. J. Statistics of energy flows in spring-coupled one-dimensional subsystems. *Philosophical Transactions: Physical Sciences and Engineering*, v. 346, n. 1681, p. 525–542, March 1994.

16 LANGLEY, R. S.; COTONI, V. Response variance prediction in the statistical energy analysis of built-up systems. *Journal of the Acoustical Society of America*, v. 115, n. 2, p. 706–718, 2004.

17 COTONI, V.; LANGLEY, R. S.; KIDNER, M. R. F. Numerical and experimental validation of variance prediction in the statistical energy analysis of built-up systems. *Journal of Sound and Vibration*, v. 288, p. 701 – 728, 2005.

18 LANGLEY, R. S.; BROWN, A. W. M. The ensemble statistics of the energy of a random system subject to harmonic excitation. *Journal of Sound and Vibration*, v. 275, n. 3, p. 823 – 846, 2004.

19 CORDIOLI, J. A.; GERGES, S. N. Y.; KLUG, F. K. Energy statistics of different sea ensemble. *Proceedings of Inter-noise 2004*, v. 1, p. 1 – 11, 2004.

20 CORDIOLI, J. A. *Limits of the Applicability of Random Matrix Theory to the Dynamics of Structures with Uncertainties*. Tese (Doutorado) — Federal University of Santa Catarina, 2006.

21 JOHNSON, D. F. *Probabilistic and Possibilistic Models of Uncertainty for the Static and Dynamic Analysis of Structures*. Tese (Doutorado) — Department of Engineering, University of Cambridge, 2001.

22 MEIROVITCH, L. *Computational Methods in Structural Dynamics*. [S.l.]: Slithof and Noordhoff, 1980. 439 p.

23 LANGLEY, R. S. Natural frequency statistics and universality. *Proceeding of The 12th International Congress on Sound and Vibration*, v. 1, p. 1 – 10, 2005.

24 MEHTA, M. L. *Random Matrices Revised and Enlarged*. [S.l.]: Academic Press, 1991. 562 p.

25 HINKE, L. et al. A random field model for a laminate windshield. *Proceedings of Recent Advances in Structural Dynamics*, University of Southampton, 17 - 19 July, 1, p. 1–10, 2006.

26 ELISHAKOFF, I. Essay on uncertainties on elastic and viscoelastic structures: from a.m. freudenthal's criticisms to modern convex modelling. *Computer and Structures*, v. 56, n. 6, p. 871–895, 1995.

27 ANONYMOUS. *AutoSEA2 Variance 2004: Users Guide, Theory & QA*. July ESI Group Inc, 2004.

28 GOMES, C. H. *Characterization of the sound isolation of metal panels using Statistical Energy Analysis (SEA).* Dissertação (Mestrado) — Federal University of Santa Catarina, 2005 (In Portuguese).

29 LYON, R. H.; DEJONG, R. G. *Theory and Application of Statistical Energy Analysis*. [S.l.]: Butterworth-Heinemann, Boston - EUA, 1995.

30 FAHY, F. Statistical energy analysis: a critical overview. *Philosophical Transactions: Physical Sciences and Engineering*, v. 346, p. 431 – 447, 1994.

31 SOIZE, C. A nonparametric model of random uncertainties for reduced matrix models in structural dynamics. *Probabilistic Engineering Mechanics*, v. 15, n. 3, p. 277 – 294, 2000.

32 FAHY, F. *Statistical Energy Analysis: A guide for potential users. SEANET: Available in: <http://www.seanet.be/>*. 2006.

33 WOODHOUSE, J. An introduction to statistical energy analysis of structural vibration. *Applied Acoustics*, v. 14, p. 455 – 469, 1981.

34 GERGES, S. N. Y. *Ruido, Fundamentos e Controle*. [S.l.]: Editora NR, 2000.

35 LANGLEY, R. S.; COTONI, V. The ensemble statistics of the vibrational energy density of a random system subjected to single point harmonic excitation. *Journal of the Acoustical Society of America*, v. 118, p. 3064 – 3076, 2005.

36 FAHY, F. J.; RUIVO, H. M. Determination of statistical energy analysis loss factors by means of an input power modulation technique. *Journal of Sound and Vibration*, v. 203, n. 5, p. 763 – 779, 1997.

37 LANGHE, K. D. *High Frequency Vibrations: Contribution to Experimental and Computational SEA Parameter Identification Techniques*. Tese (Doutorado) — Katholieke Universiteit Leuven, Belgium, 1996.

38 CREMER, L.; HECKEL, M.; UNGAR, E. *Structure-Borne Sound*. [S.l.]: Berlin: Spriger-Verlag, 1988.

39 CLARKSON, B. L. The derivation of modal densities from point impedance. *Journal of Sound and Vibration*, v. 77, n. 4, p. 583 – 584, 1981.

40 CLARKSON, B. L. Experimental determination of modal density. *Random Vibration*, v. 1, p. 59 – 85, 1986.

41 BROWN, K. T.; NORTON, M. P. Some comments on the experimental determination of modal densities and loss factors for statistical energy analysis applications. *Journal of Sound and Vibration*, v. 102, n. 4, p. 588 – 594, 1985.

42 RANKY, M. F.; CLARKSON, B. L. Frequency average loss factors of plates and shells. *Journal of Sound and Vibration*, v. 89, n. 3, p. 309 – 323, 1983.

43 RODRIGUES, A. H. B. *Vibroacoustical characteristics of cylindrical shells*. Dissertação (Mestrado) — Federal University of Santa Catarina, 2002 (In Portuguese).

44 LANGLEY, R. S.; HERON, K. H. Elastic wave transmission through plate beam junctions. *Journal of Sound and Vibration*, v. 143, n. 2, p. 241 – 253, 1990.

45 CRAIK, R. J. M.; SMITH, R. S. Sound transmission through double leaf lightweight partitions part 2: structure-borne sound. *Applied Acoustic*, v. 61, p. 247 – 269, 2000.

46 BOSMANS, I.; VERMEIR, G. Diffuse transmission of structure-borne sound at periodic junctions of semi-infinite plates. *Journal of the Acoustical Society of America*, v. 101, n. 6, p. 3443 – 3456., 1997.

47 MEEDS, P.; VERMIER, G. Structure-borne sound transmission at elastically connected plates. *Journal of Sound and Vibration*, v. 166, n. 1, p. 55 – 76, 1993.

48 LYON, R. H. Statistical analysis of power injection and response in structures and rooms. *Journal of the Acoustical Society of America*, v. 45, n. 3, p. 545 – 565, 1969.

49 WEAVER, R. L. On the ensemble variance of reverberation room transmission functions, the effect of spectral rigidity. *Journal of Sound and Vibration*, v. 130, n. 3, p. 487 – 491, 1989.

50 LOBKIS, O. I.; WEAVER, R. L.; ROZHKOV, I. Power variances and decay curvature in a reverberant system. *Journal of Sound and Vibration*, v. 237, n. 2, p. 281 – 302, 2000.

51 LANGLEY, R. S. A non-poisson model for the vibration analysis of uncertain dynamic systems. *Royal Society of London A*, v. 455, p. 3325 – 3349, 1999.

52 SCHROEDER, M. R. Frequency- correlation functions of frequency responses in rooms. *Journal of the Acoustical Society of America*, v. 34, n. 12, p. 1819 – 1823, 1962.

53 DAVY, J. L. The relative variance of the transmission function of a reverberation room. *Journal of Sound and Vibration*, v. 77, n. 4, p. 455 – 479, 1981.

54 DAVY, J. L. Improvements to formulae for the ensemble relative variance of random noise in a reverberation room. *Journal of Sound and Vibration*, v. 115, n. 3, p. 145 – 161, 1987.

55 RICE, S. O.; WAX, N. *Mathematical Analysis of Random Noise*. Noise and Stochastic Processes, 1951.

56 BRODY, T. A. et al. Random-matrix physics: spectrum and strength fluctuations. *Reviews of Modern Physics*, v. 53, p. 385 – 479, 1981.

57 GUHR, T.; GROELING, A. M.; WEIDENMULLER, H. A. Random matrix theories in quantum physics: Common concepts. *Physics Reports*, v. 299, n. 4, p. 189 – 425, 1998.

58 ALMEIDA, A. M. O. *Sistemas Hamiltonianos - Caos e Quantização*. [S.l.]: Editora da Unicamp, 1995. 312 p.

59 SHORTER, P. J.; COTONI, V.; LANGLEY, R. S. Numerical and experimental validation of the hybrid fe-sea method. *Proceeding of Internoise 2005*, v. 1, p. 1 – 12, 2005.

60 LANGLEY, R. S.; SHORTER, P. J.; COTONI, V. A hybrid fe-sea method for the analysis of complex vibro-acoustic systems. *Proceedings of Noven 2005*, v. 1, p. 1 – 10, 2005.

61 WIGNER, E. P. Characteristic vectors of bordered matrices with infinite dimensions. *Annals of Mathematics*, v. 62, n. 3, p. 548 – 564, 1955.

62 WIGNER, E. P. On the distribution of the roots of certain symmetric matrices. *Annals of Mathematics*, v. 67, n. 2, p. 325 – 327, 1958.

63 GUHR, T. *Random Matrix in Physiscs*. Lunds Universitet, Sweden. Available in: <http://www.matfys.lth.se/staff/Thomas.Guhr/encrmt.pdf>, accessed on 22 may 2007.

64 WEAVER, R. L. Spectral statistics in elastodynamics. *Journal of the Acoustical Society of America*, v. 85, n. 3, p. 1005 – 1013, 1989.

65 ELLEGAARD, C. et al. Symmetry breaking and spectral statistics of acoustic resonances in quartz blocks. *Physical Review Letters*, v. 77, n. 24, p. 4918 – 4921, 1996.

66 BERTELSEN, P.; ELLEGAARD, C.; HUGUES, E. Distribution of eigenfrequencies for vibrating plates. *European Physical Journal B*, v. 15, p. 87 – 96, 2000.

67 BOHIGAS, O.; GIANNONI, M. J.; SCHIMIT, C. Characterization of chaotic quantum spectra and universality of level fluctuation laws. *Physical Review Letters*, v. 52, n. 1, p. 1 – 4, 1984.

68 ANDERSEN, A. *Topics in Random Matrix Theory*. Dissertação (Mestrado) — University of Compenhagen, Niels Bohr Institute, 1999.

69 SCHAADT, K. *The Quantum Chaology of Acoustic Resonators*. Dissertação (Mestrado) — University of Copenhagen, 1997.

70 SCHAADT, K. *Experiments on Acoustics Chaology and Statistical Elastodynamics*. Tese (Doutorado) — Niels Bohr Institute, 2001.

71 KUDROLLI, A.; KIDAMBI, V.; SRIDHAR, S. Experimental studies of chaos and localization in quantum wave functions. *Physical Review Letters*, v. 75, n. 5, p. 822 – 825, July 1995.

72 KUDROLLI, A.; SRIDHAR, S. Experiments on quantum chaos using microwave cavities: results for the pseudo-integrable l-billiard. *Pramana: Journal of Physics*, v. 48, n. 2, p. 459 – 467, 1997.

73 PRADHAN, P.; SRIDHAR, S. Correlations due to localization in quantum eigenfunctions of disordered microwave cavities. *Physical Review Letters*, v. 85, n. 11, p. 2360 – 2363, 2000.

74 PRADHAN, P.; SRIDHAR, S. From chaos to disorder: Statistics of the eigenfunctions of microwave cavities. *Pramana - Journal of Physics*, v. 58, n. 2, p. 333 – 341, 2002.

75 BURKHARDT, J.; WEAVER, R. L. The effect of decay rate variability on statistical response predictions in acoustic systems. *Journal of Sound and Vibration*, v. 196, n. 2, p. 147 – 164, 1996.

76 LANGLEY, R. S.; CORDIOLI, J. A. Personal Communication, March, 2006.

77 MIRLIN, A. D.; FYODOROV, Y. V. The statistics of eigenvector components of random band matrices: analytical results. *Journal of Physics A: Mathematical and Theoretical*, v. 26, p. L551–L558, 1993.

78 CASATI, G.; IZRAILEV, F.; MOLINARI, L. Scaling properties of the eigenvalue spacing distribution for band random matrices. *Journal of Physics A: Mathematical and General*, v. 24, p. 4755 – 4762, 1991.

79 CASATI, G.; IZRAILEV, F.; MOLINARI, L. Scaling properties of band random matrices. *Physical Review Letters*, v. 64, p. 1851 – 1854, 1990.

80 KESSISSOGLOU, N. J.; LANGLEY, R. S. Application of the statistical overlap factor to predict goe statistics. *Proceedings of Noven 2005*, v. 1, p. 1 – 8, 2005.

81 ZYCZKOWSKI, K. Indicators of quantum chaos based on eigenvector statistics. *Jounal of Physics A*, v. 23, p. 4427 – 4438, 1990.

82 LIN, Y. K. *Probabilistic Theory of Structural Dynamics*. [S.l.]: McGraw-Hill, 1967.

83 GOMES, C. H.; MACE, B. R. *Statistical Analysis of Mode Shapes from an Ensemble of Uncertain Engineering Structures*. Sandwich Doctorate Research Proposal, Institute of Sound and Vibration Research, University of Southampton, 2007.

84 GOMES, C. H. *Statistical Analysis of Mode Shapes from an Ensemble of Random Systems*. Doctorate Sandwich Report, Federal University of Santa Catarina, 2008 (In Portuguese).

85 GOMES, C. H.; GERGES, S. N. Y.; JORDAN, R. Measurements and sea modelling of the sound transmission of the ribbed-stiffened panels. *Proceedings of the 13th International Congress of Sound and Vibration*, v. 1, p. 1 – 8, 2006.

86 CORDIOLI, J. A. et al. Vibro-acoustic modelling of aircrafts using statistical energy analysis. *SAE Technical Paper 2004-01-3337*, v. 1, p. 1–12, 2004.

87 CALÇADA, M. *Métodos de predição de transmissão sonora através de placa revestida*. Tese (Doutorado) — Federal University of Santa Catarina, 2006.

88 GOMES, C. H.; CALÇADA, M.; GERGES, S. N. Y. Sea parameters to predict sound transmission through trimmed and ribbed-stiffened panels. *Proceedings of the Inter-noise*, v. 1, p. 1 – 10, 2006.

89 MEIROVITCH, L. *Fundamentals of Vibration*. New York, USA: McGraw-Hill, 2001.

90 BERTELSEN, P. *Quantum chaos and vibration of elastic plates*. Dissertação (Mestrado) — University of Copenhagen, 1997.

91 SANTOS, I. F. *Dinâmica de Sistemas Mecânicos*. [S.l.]: Makron Books, 2000.

92 STOCKMANN, H. J.; STEIN, J. Quantum chaos in billiards studies by microwave absorption. *Physical Review Letters*, v. 64, n. 19, p. 2215 – 2218, 1990.

93 GOMES, C. H.; GERGES, S. N. Y. *Analysis of Spectral Statistics of Dynamic Parameters from Chaotic System*. Proceeding of VI SEPEX: Week of Teaching, Research and Extension Activities – UFSC, Florianopolis – SC, Brazil, 2007 (In Portuguese).

94 FUJISAKA, Y.; TOHYAMA, M. Eigenfrequency spacing analysis and eigenmode breakdown for semi-stadium-type 2-d fields. *Journal of Sound and Vibration*, v. 267, p. 867 – 878, 2003.

95 DELANDE, D.; SORNETTE, D.; WEAVER, R. L. A reanalysis of experimental high-frequency spectra using periodic orbit theory. *Journal of the Acoustical Society of America*, v. 96, n. 3, p. 1873 – 1880, 1994.

96 GRAF, H. D. Distribution of eigenmodes in a superconducting stadium billiard with chaotic dynamics. *Physical Review Letters*, v. 69, n. 9, p. 1296 – 1299, 1992.

97 WRIGTH, M. C. M.; HAM, C. J. Periodic orbit theory in acoustics: spectral fluctuations in circular and annular waveguides. *Journal of Acoustical Society of America*, v. 121, n. 4, p. 1865 – 1872, 2007.

98 BISWAS, D.; AZAM, M.; LAWANDE, S. V. Spectral rigidity for degenerate integrable systems. *Physical Review A*, v. 43, p. 5694 – 5697, 1990.

99 CHIRIKOV, B. V.; SHEPELYANSKY, D. L. Shnirelman peak in level spacing statistics. *Physical Review Letters*, v. 74, p. 518 – 521, 1995.

100 FRAHM, K. M.; SHEPELYANSKY, D. L. Quantum localization in rough billiards. *Physical Review Letters*, v. 78, p. 1440 – 1443, 1997.

101 GOMES, C. H.; GERGES, S. N. Y. *Study of Statistical Observables in Spectral Analysis of Random Dynamic Systems*. Proceeding of VI SEPEX: Week of Teaching, Research and Extension Activities – UFSC, Florianopolis – SC, Brazil, 2007 (In Portuguese).

102 SONG, T. T. *Modelos Probabilisticos em Engenharias e Ciências*. [S.l.]: LTC, 1986.

103 MONTGOMERY, D. C.; RUNGER, G. C. *Applied Statistics and Probability for Engineers*. [S.l.]: John Wiley & Sons, 2003. 706 p.

104 STOCKMANN, H. J. *Quantum Chaos: An Introduction*. [S.l.]: Cambridge University Press, 1999.

105 KUDROLLI, A.; SRIDHAR, S. Experiments on quantum chaos using microwave cavities. *Proceedings of the 2nd Conference on Experimental Chaos*, v. 1, p. 184 – 189, 1993.

106 BURKHARDT, J.; WEAVER, R. L. Spectral statistics in damped systems. part 2. spectral density fluctuations. *Journal of the Acoustical Society of America*, v. 100, p. 327 – 334, 1996.

107 PLEROU, V.; GOPIKRISHNAN, P.; ROSENOW, B. A random matrix theory approach to financial cross-correlations. *Physica A*, v. 287, p. 374 – 382, 2000.

108 PANDEY, A. Statistical properties of many-particle spectra: ergodic behaviour in random matrix ensemble. *Annals of Physics*, v. 119, p. 170 – 191, 1979.

109 ELLEGAARD, C. et al. Spectral statistics of acoustic resonances in aluminum blocks. *Physical Review Letters*, v. 75, n. 8, p. 1546 – 1549, 1995.

110 SCHAADT, K.; KUDROLLI, A. Experimental investigation of universal parametric correlators using a vibrating plate. *Physical Review E*, v. 60, n. 4, p. R3479 – R3482, 1999.

111 KUHL, U.; STOCKMANN, H. J.; WEAVER, R. Classical wave experiments on chaotic scattering. *Journal of Physics A: Mathematical and General*, v. 38, n. 38, p. 10433 – 10463, 2005.

112 LI, B.; ROBNIK, M. Sensitivity of the eigenfunctions and the level curvature distribution in quantum billiards. *Journal of Physics A: Mathematical and General*, v. 29, p. 4387 – 4405, 1996.

113 BOHIGAS, O. et al. Comment on spectral statistics in elastodynamics. *Journal of the Acoustical Society of America*, v. 89, p. 1456 – 1458, 1991.

114 BOHIGAS, O.; HAQ, R. U.; PANDEY, A. Fluctuations properties of nuclear energy levels: Do theory and experiment agree? *Physical Review Letters*, v. 48, n. 16, p. 1086 – 1989, 1982.

115 HAM, C. *Periodic Orbit Analysis of The Helmholtz Equation in Two-Dimensional Enclosures*. Tese (Doutorado) — University of Southampton, Institute of Sound and Vibration Research, 2008.

116 HAAKE, F. *Quantum Signatures of Chaos*. [S.l.]: Springer, 2006. 479 p.

117 WRIGHT, M. C. M.; HOWLS, C. J. *Semiclassical acoustics: what can quantum physics teach us about plate vibration?* Institute of Sound and Vibration Research, University of Southampton, 2008.

118 EWINS, D. J. *Modal Testing: Theory and Practice*. [S.l.]: John Wiley & Sons Inc., 1984.

119 SRIDHAR, S. Experimental observation of scarred eigenfunctions of chaotic microwave cavities. *Physical Review Letters*, v. 67, n. 7, p. 785 – 788, 1991.

120 SRIDHAR, S. Quantum chaos, localization and tunnelling : microwave experiments on model geometries. *Philosophical Magazine B - Physics of Condensed Matter: Statistical Mechanics, Electronic, Optical and Magnetic Properties*, v. 80, n. 12, p. 2129 – 2141, 2000.

121 LU, W. et al. Microwave study of quantum n-disk scattering. *Physical Review E*, v. 61, n. 4, p. 3652 – 3663, 2000.

122 HELLER, E. J.; SRIDHAR, S. Physical and numerical experiments on the wave mechanics of classically chaotic systems. *Physical Review A*, v. 46, n. 4, p. R1728 – R1730, 1992.

123 PRADHAN, P.; SRIDHAR, S. *From chaos to disorder: Statistics of the eigenfunctions of microwave cavities*. Technical Report, Department of Physics, University of Northeastern, 2002.

124 BOGOMOLNY, E.; HUGUES, E. Semiclassical theory of flexural vibrations of plates. *Physical Review E*, v. 57, p. 5404 – 5424, 1998.

125 KUDROLLI, A.; SRIDHAR, S. Comment on gaussian orthogonal ensemble statistics in a microwave stadium billiard with chaotic dynamics: Porter-thomas distribution and algebraic decay of time correlations. *Physical Review Letters*, v. 76, n. 16, p. 3036, 1996.

126 MCDONALD, S. W.; KAUFMAN, A. N. Spectrum and eigenfunctions for a hamiltonian with stochastic trajectories. *Physical Review Letters*, v. 42, n. 18, p. 1189 – 1191, 1979.

127 BACKER, A. Quantum chaos in billiards. *Computing in Science and Engineering*, v. 9, n. 3, p. 60–64, 2007.

128 IZRAILEV, F. M. Chaotic structure of eigenfunctions in systems with maximal quantum chaos. *Physics Letters A*, v. 125, n. 5, p. 250 – 252, 1987.

129 CONOVER, W. J. *Practical Nonparametric Statistics*. [S.l.]: John Wiley & Sons, 1980.

130 WATERHOUSE, R. Sampling statistics for an acoustic mode. *Journal of the Acoustical Society of America*, v. 47, n. 4, p. 961 – 967, 1970.

131 MARTINEZ, W. L.; MARTINEZ, A. R. *Computational Statistics Handbook with Matlab*. [S.l.]: Chapman & Hall - CRC, 2002.

132 WILSON, H. B.; TURCOTTE, L. H.; HALPERN, D. *Advanced Mathematics and Mechanics Applications Using Matlab*. [S.l.]: Chapman & Hall - CRC, 2003. 665 p.

133 ANONYMOUS. *Statistics Toolbox For Use with Matlab: Computation, Visualization, and Programming*. [S.l.]: The Mathworks, Inc., User's Guide Version 4, 2002.

134 PRIGODIN, V. N. Spatial structure of chaotic wave functions. *Physical Review Letters*, v. 74, p. 1566 –1569, 1995.

135 PRIGODIN, V. N. et al. Mesoscopic dynamical echo in quantum dot. *Physical Review Letters*, v. 72, p. 546 – 549, 1994.

136 EFETOV, K. B. Supersymmetry and theory of disordered metals. *Advances in Physics*, v. 32, n. 1, p. 53 – 127, 1983.

137 SOUTO, G. *Decomposition in Singular Values*. Monograph in Mathematics. Federal University of Santa Catarina, 2000. (in Portuguese).

138 EFETOV, K. B. *Supersymmetry in disorder and chaos*. [S.l.]: Cambridge University Press, 1996. 453 p.

139 HODGES, C. H. Confinement of vibration by structural irregularity. *Journal of Sound and Vibration*, v. 82, n. 3, p. 411 – 424, 1982.

140 HODGE, C. H.; WOODHOUSE, J. Confinement of vibration by one-dimensional disorder 1: Theory of ensemble averaging. *Journal of Sound and Vibration*, v. 130, n. 2, p. 237 – 251, 1989.

141 HELLER, E. J. Bound-state eigenfunctions of classically chaotic hamiltonian systems:scars of periodic orbits. 1984. *Physical Review Letters*, v. 53, n. 16, p. 1515 –1518, 1984.

142 ANDERSON, P. W. Absence of diffusion in certain random lattices. *Physical Review*, American Physical Society, v. 109, n. 5, p. 1492–1505, 1958.

143 MIRLIN, A. D. *Statistics of energy levels and eigenfunctions in disordered systems*. Technical Report, Institut fur Theorie der kondensierten Materie, Universitat Karlsruhe, 1999.

144 FYODOROV, Y. V.; MIRLIN, A. D. Analytical derivation of the scaling law for the inverse participation ratio in quasi-one-dimensional disordered systems. *Physical Review Letters*, American Physical Society, v. 69, n. 7, p. 1093 – 1096, 1992.

145 PRIGODIN, V. N.; ALSHULER, B. L. Long-range spatial correlations of eigenfunctions in quantum disordered systems. *Physisical Review Letter*, American Physical Society, v. 80, n. 9, p. 1944– 1947, 1998.

146 ULLAH, N.; PORTER, C. E. Invariance hypothesis and hamiltonian matrix elements correlations. *Physics Letters*, v. 6, n. 3, p. 301 – 302, 1963.

147 WEISSTEIN, E. W. *Double Factorial*. Wolfram Research Inc., 2007. Disponível em: <http://mathworld.wolfram.com/DoubleFactorial-.html>.

148 PIERRE, C. Weak and strong vibration localization in disordered structures: a statistical investigation. *Journal of Sound and Vibration*, v. 139, n. 1, p. 111–132, 1990.

149 BENDIKSEN, O. O. Localization phenomena in structural dynamics. *Chaos, Solitons and Fractals*, v. 11, p. 1621 – 1660, 2000.

150 HODGES, C. H.; WOODHOUSE, J. Vibration isolation from irregularity in a nearly periodic structure: Theory and measurements. *The Journal of the Acoustical Society of America*, v. 74, n. 3, p. 894 – 905, 1983.

151 HODGES, C. H.; WOODHOUSE, J. Theories of noise and vibration transmission in complex structures. *Report of Progress in Physics*, v. 49, p. 107 – 170, 1986.

152 MEAD, D. J.; RICHARDS, E. J. *Noise and Acoustic Fatigue in Aeronautics*. [S.l.]: John Wiley and Sound LTD, 1968.

153 GOMES, C. H.; GERGES, S. N. Y. *Statistical Analysis of Mode Shapes from an Ensemble of Random Systems*. Doctorate Sandwich Proposal, Federal University of Santa Catarina, 2007 (In Portuguese).

154 GOMES, C. H.; MACE, B. R.; FERGUSON, N. S. *Statistical Analysis of Longitudinal Rods with Uncertain Parameters*. Technical Report on Sandwich Doctorate Activities, Institute of Sound and Vibration Research, University of Southampton, 2010.

155 TIMOSHENKO, S.; YOUNG, D. H. *Vibration Problems in Engineering*. [S.l.]: Van Nostrand Company, 1955.

156 ANONYMOUS. *Ansys Structural - Analysis Guide, Release 9.0*. [S.l.], ANSYS INC., 1994.

157 KOHNKE, P. *Ansys Theory - Release 5.7*. [S.l.], Ansys Inc.,2001.

158 THOMSON, W. T. *Theory of Vibration with Applications*. [S.l.]: Chapman and Hall, 1993.

159 HODGES, C. H.; WOODHOUSE, J. Confinament of vibration by one-dimensional disorder 2: Numerical experiment on different ensemble averages. *Journal of Sound and Vibration*, v. 130, n. 2, p. 253 – 268, 1989.

160 BRODIER, O.; NEICU, T.; KUDROLLI, A. Eigenvalues and eigenfunctions of a clover plate. *The European Physical Journal B*, v. 23, p. 365 – 372, 2001.

161 LANGLEY, R. S.; BREMNER, P. G. A hybrid method for the vibration analysis of complex structural-acoustic systems. *Journal of the Acoustical Society of America*, v. 105, n. 3, p. 1657 – 1671, 1999.

162 VANMAERCKE, E. *Random Fields: Analysis and Synthesis*. [S.l.]: MIT Press, Cambridge, MA, 1983.

163 SARKAR, A.; GHANEM, R. Mid-frequency structural dynamics with parameter uncertainty. *Computer Methods in Applied Mechanics and Engineering*, v. 191, p. 5499 – 5513, 2002.

164 GRAFF, K. F. *Wave Motion in Elastic Solids*. [S.l.]: Dover Publications, 1991.

165 KUDROLLI, A. et al. Signatures of chaos in quantum billiards: Microwave experiments. *Physical Review E*, American Physical Society, v. 49, n. 1, p. R11 – R14, 1994.

166 WEAVER, R. L.; SORNETTE, D. Range of spectral correlations in pseudointegrable systems: Gaussian-orthogonal-ensemble statistics in a rectangular membrane with a point scatterer. *Physysical Review E*, v. 52, n. 4, p. 3341 – 3350, 1995.

167 LEGRAND, O.; MORTESSAGNE, F.; WEAVER, R. L. Semiclassical analysis of spectral correlations in regular billiards with point scatterers. *Physical Review E*, v. 55, n. 6, p. 7741 – 7744, 1997.

168 SHIGEHARA, T. Conditions for the appearance of wave chaos in quantum singular systems with a pointlike scatterer. *Physical Review E*, v. 50, n. 6, p. 4357 – 4370, 1994.

169 LEISSA, A. W. *Vibration of Plates*. NASA, Technical Report, NASA SP – 160, 1969.

170 BURKHARDT, J.; WEAVER, R. L. Spectral statistics in damping systems. part 1. modal decay rate statistics. *Journal of Acoustical Society of America*, v. 100, n. 1, p. 320 – 326, 1996.

171 EFRON, B.; TIBSHIRANI, R. J. *An Introduction to the Bootstrap*. [S.l.]: Chapman & Hall, 1993.

APPENDIX A – STATISTICAL PROPERTIES OF SUPERIMPOSED SPECTRA

A.1 Two Independent GOE Eigenvalue Sequences

The analytical predictions for the eigenvalue statistical observables of a spectrum composed of two independent GOE eigenvalue sequences were proposed by Weaver (64) and they are given by:

$$P_{2GOE}(x) = \frac{1}{2}\left\{E\left(\frac{1}{2}x\right)P_{GOE}\left(\frac{1}{2}x\right) + \left[1 - F\left(\frac{1}{2}x\right)\right]^2\right\}, \tag{A.1}$$

$$\Sigma^2_{2GOE}(L) = 2\Sigma^2_{GOE}\left(\frac{L}{2}\right), \tag{A.2}$$

$$\Delta_3^{2GOE}(L) = 2\Delta_3^{GOE}\left(\frac{L}{2}\right), \tag{A.3}$$

where:

$$F(y) = \int_0^y P_{GOE}(z)\,dz, \tag{A.4}$$

$$E(y) = \int_y^\infty [1 - F(z)]\,dz. \tag{A.5}$$

A.2 Several Independent GOE Eigenvalue Sequences

For a composite spectrum which is composed of the superposition of several Gaussian ensembles with different relative densities, the analytical prediction of statistical observables were proposed by Mehta (24). The spacing PDF of a superposition of N spectra with individual spacing PDFs P_i and relative densities $g_i = \rho_i/\rho$ (where $\rho = \sum_{i=1}^N \rho_i$ is the total density), is given

by:

$$P(s) = E(s)\left[\sum_{i=1}^{N} g_i \frac{P(g_i s)}{E_i(g_i s)} + \left(\sum_{i=1}^{N} g_i \frac{1 - F_i(g_i s)}{E_i(g_i s)}\right)^2 - \sum_{i=1}^{N}\left(g_i \frac{1 - F_i(g_i s)}{E_i(g_i s)}\right)^2\right], \tag{A.6}$$

where the auxiliary functions are given by:

$$F_i(g_i s) = \int_0^{g_i s} P_i(t)\, dt, \tag{A.7}$$

$$E_i(g_i s) = \int_{g_i s}^{\infty} [1 - F_i(t)]\, dt, \tag{A.8}$$

$$E(s) = \prod_{i=1}^{N} Ei(g_i s). \tag{A.9}$$

For the analysis of long-range fluctuations, the analytical prediction of Δ_3 - statistics for independent superimposed GOE spectra is given by:

$$\Delta_3(L) = \sum \Delta_{3,i}(g_i L), \tag{A.10}$$

where g_i and $\Delta_{3,i}$ are the relative density and the Δ_3 - statistics associated with ith GOE spectrum, respectively.

In Figures 191 and 192, the PDFs and Δ_3 - statistics curves are shown for the 1 GOE, 2 GOE, 4 GOE and Poisson spectra, Gomes and Gerges (101).

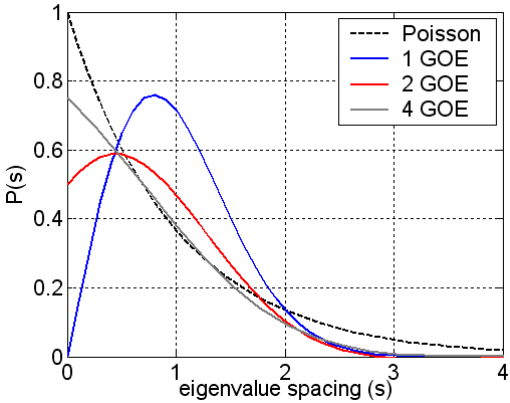

Figure 191: The spacing PDF predictions for the superimposed GOE and Poisson distributions, Gomes and Gerges (101).

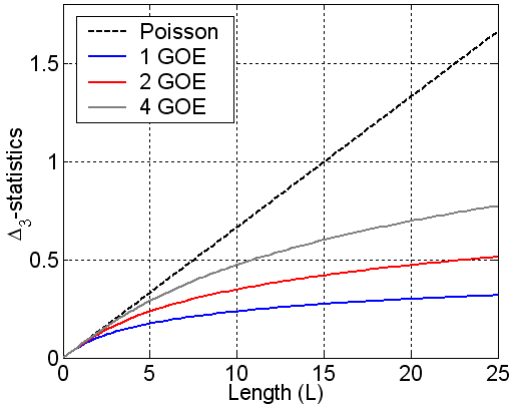

Figure 192: Δ_3 - statistics: superimposed GOE and Poisson predictions, Gomes and Gerges (101).

A.3 Two GOE Eigenvalue Sequences with Distinct Densities

In order to visualize the effects of the different relative densities, the spacing PDF and Δ_3 - statistics results of the 2 GOE spectra were plotted for several relative densities in Figure 193, Gomes and Gerges (101).

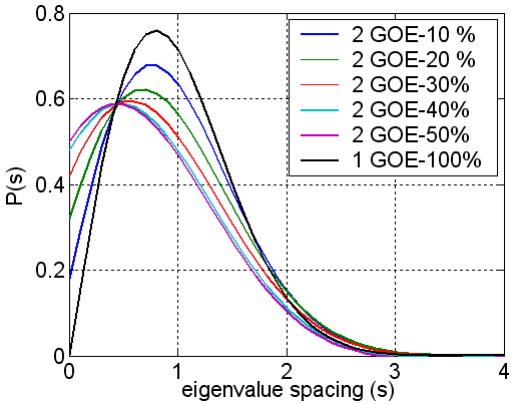

Figure 193: The spacing PDFs of several 2 GOE spectra with distinct relative densities, Gomes and Gerges (101).

As discusssed by Bertelsen (90), for $s = 0$, $P(0)$ is only dependent on the relative densities, $P(0) = 1 - \sum_{i=1}^{N} g_i^2$. Indeed, for relative densities close to $g_i = 0.5$, the results suggest that $P(0)$ is not very sensitive to small variations in g_i, Figure 193. Thus, 2 GOE behavior is expected when two independent classes coexist, even if they do not have exactly the same level density, Bertelsen (90). However, the results in Figure 193 also suggest significant deviations for relative densities outside the range of 30 to 70% in comparison to 2 GOE (with 50% relative densities).

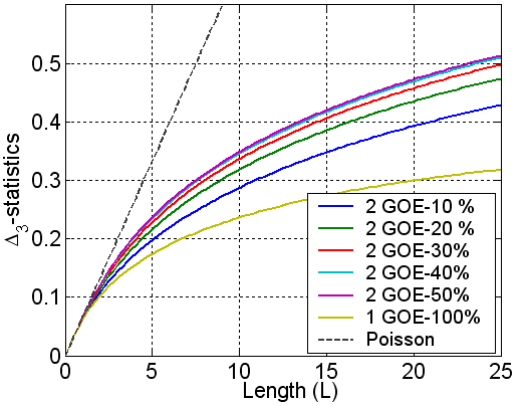

Figure 194: The Δ_3 - statistics results for several 2 GOE spectra with distinct relative densities, Gomes and Gerges (101).

As shown in Figure 194, the similar effects of the distinct relative densities are also observed for the evaluation of Δ_3 - statistics results. Therefore, for similar relative densities, the statistical behavior is almost the same obtained for 2 GOE with equal relative densities, Bertelsen (90).

The PDFs and Δ_3 - statistics results shown in Figures 193 and 194 were evaluated using Equations (A.6) and (A.10), respectively. The individual evaluations for each spectrum were made using the analytical definitions for all cases. Additional details regarding the superposition of independent spectra are beyond the scope of this initial analysis and will not be discussed here; further information is available in: Mehta (24), Brody *et al* (56), and Bertelsen (90).

APPENDIX B – NUMERICAL INVESTIGATION OF THE FINITE DIMENSION EFFECTS ON THE EIGENVALUE STATISTICS

The effects of the finite wavelengths are traditionally quantified using statistical tools such as the *Bootstrap* technique (171, 90, 69) or *Monte Carlo* method (114). In the present study, the Monte Carlo method was adopted to assess numerically the finite wavelength effects on the eigenvalue statistical observable results and to evaluate the expected range of fluctuations in the Δ_3 - statistics results[1], Gomes and Gerges (101).

Considering an ensemble composed of 100 GOE matrices with $dim(300\,\mathrm{x}\,300)$, the spectral mean value of $\Delta_3(L, Z_0)$-*statistics* results and the corresponding spectral variances[2], $Var\,\langle\Delta_3(L, Z_0)\rangle_s$, were evaluated for each GOE matrix member of the ensemble, Figures 195 (a) and (b), respectively. Additionally, the ensemble mean values were also determined for both parameters.

As shown in Figure 195 (a), a large ensemble variability (or dispersion across ensemble members) is expected as the spectral eigenvalue distance increases. For $\Delta_3(L)$ -*statistics* results, the ensemble mean value agrees very well with the GOE prediction. Additionally, the 95% confidence limits were calculated from the numerical results and showed good performance in quantifying the expected range of fluctuations across the ensemble.

Considering the corresponding spectral variance values from each GOE member, $Var\,\langle\Delta_3(L, Z_0)\rangle_{Z_0}$, a similar dispersive behavior across the ensemble is also observed as the spectral eigenvalue distance increases. In this case, the mean of the spectral variance values across the ensemble presents a approximately logarithmic pattern and does not conform very well to the asymptotic analytical prediction proposed by Bohigas *et al* (114), that is $Var^{GOE}\,\langle\Delta_3(L, Z_0)\rangle_{Z_0} \equiv 0.012$. As shown in Figure 195 (b), a good agreement with the numerical results is only expected for extremely large spectral eigenvalue distances, since the analytical prediction of the spectral variance is constant for all spectral eigenvalue distances.

[1] In this Appendix, the finite wavelength effects were investigated using the Δ_3-statistics, since the application of this statistical observable is one of the most popular long-range fluctuation metrics and also presents faster convergence characteristics, Cordioli (20), Bertelsen (90) and Gomes (101).

[2] For each GOE matrix, the spectral variability of the $\Delta_3(L, Z_0)$ -*statistics* results was evaluated over eigenvalue domain, considering all available starting points Z_0.

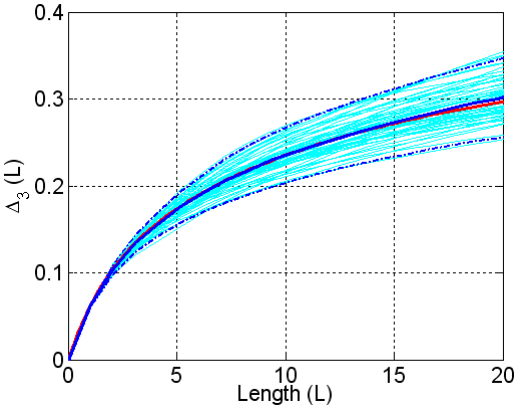

(a)

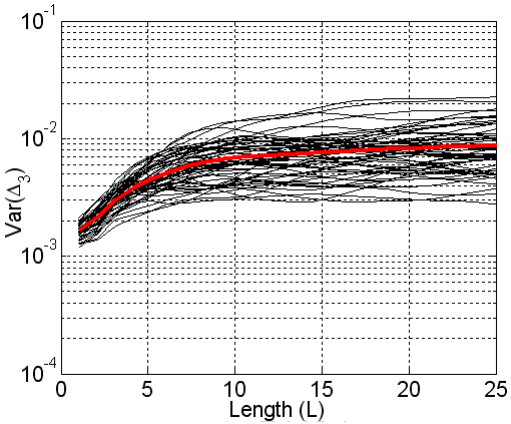

(b)

Figure 195: Δ_3-statistics results for the 100 GOE matrices with *dim* (300 x 300). Plot (a): individual spectral mean values and ensemble mean value. Plot (b): individual spectral variance values and ensemble mean value of spectral variances. Additionally, the analytical GOE predictions are also plotted, Gomes and Gerges (101).

In Figure 196 (a), the corresponding variance value of Δ_3 - statistics results evaluated across the ensemble is also presented. It can be noted that the ensemble mean value for the spectral variance is expected to be much larger than the ensemble variance value of Δ_3 -statistics results across the ensemble. In order to guarantee that the adopted size of the ensemble is large enough to provide representative numerical results, the statistical convergence of the spectral variance results was carefully evaluated in terms of the ensemble size for several spectral eigenvalue distances. The numerical results from the convergence analysis of the spectral variance values are presented for several eigenvalue spectral distances in Figure 196 (b). The numerical results are only shifted to better visualize the convergence characteristics associated with each spectral eigenvalue distance. The vertical amplitude scale remains unaltered.

As observed in Figure 196 (b), the size of the ensemble is adequate to obtain representative statistical results for the mean value of the spectral variance across the ensemble. Overall, a fast convergence along ensemble is expected for small spectral distances.

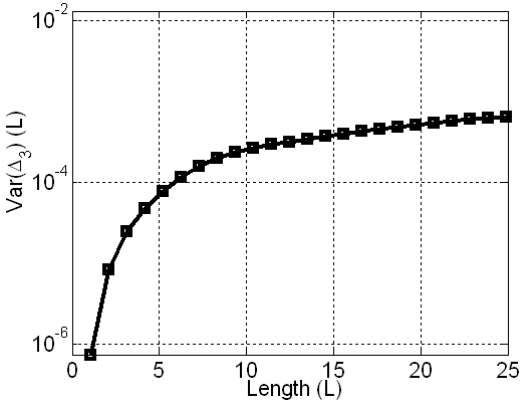

(a)

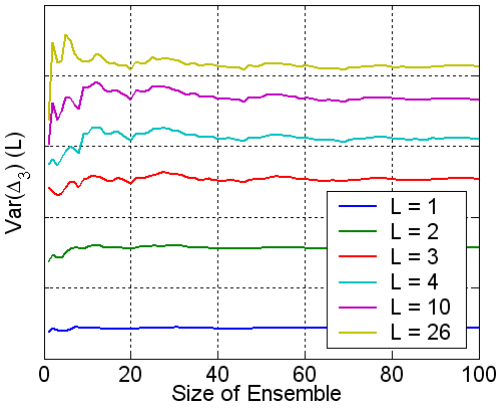

(b)

Figure 196: Plot (a): Ensemble variance value of Δ_3 - statistics results. Plot (b): statistical convergence analysis of the mean value of spectral variance results across the ensemble, Gomes and Gerges (101).

In order to verify the performance of the numerical methodology described above in evaluating the expected ensemble mean value for the spectral variance of the Δ_3 - statistics results, $E\left[Var\langle\Delta_3(L,Z_0)\rangle_{Z_0}\right]$, the ensemble mean value for the numerical spectral variance results is compared with that for the experimental results available in the RMT literature. The experimental results were obtained in a laboratory study on complex nuclei systems carried out by Bohigas *et al* (114). The nuclear data ensemble comprises 1407 resonance energies corresponding to 30 sequence of 27 different nuclei systems. In Figure 197, the Δ_3 - statistics and their spectral variance results for the nuclear data ensemble are compared with the numerical results for the Monte Carlo numerical method described above, as well as with asymptotic analytical predictions. The expected range of fluctuations in the Δ_3 - statistics across the ensemble is presented in terms of one standard deviation.

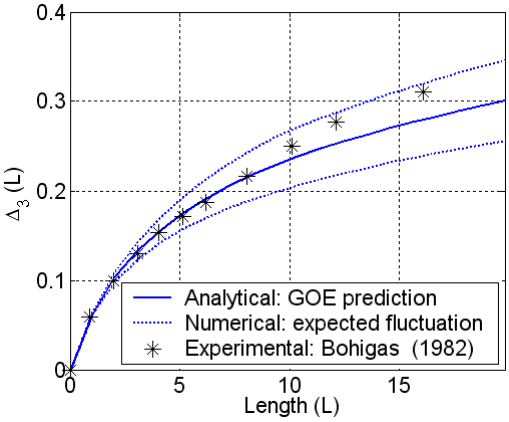

(a)

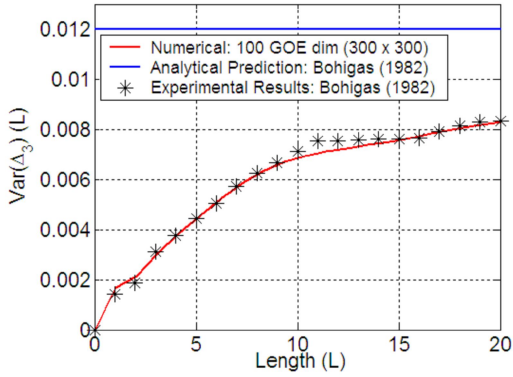

(b)

Figure 197: Results from the numerical methodology to estimate the ensemble mean values of Δ_3 - statistics results and corresponding spectral variance values. The experimental data from nuclei systems are also plotted, Bohigas *et al* (114). Plot (a): ensemble mean values of Δ_3- statistics results. Plot (b): ensemble mean value of the spectral variances of Δ_3 - statistics results, Gomes and Gerges (101).

As shown in Figures 197 (a) and (b), a good performance in obtaining the estimates from the numerical results is observed for ensemble mean values of Δ_3 -statistics results and their corresponding spectral variance values, respectively. Indeed, the ensemble mean value of spectral variance values from the numerical method, which takes into account the finite wavelength effects, presents an excellent agreement with that from the experimental values, clearly showing that this is an appropriate alternative methodology to estimate the ensemble mean value of spectral variance values and to replace asymptotic analytical predictions for large spectral eigenvalue distances.

Based on the excellent performance of the numerical methodology in describing the ensemble mean values of the Δ_3 - statistics results and their spectral variances, it is reasonable to consider that this methodology is appropriate to accurately estimate the expected variability of the Δ_3 - statistics results across the ensemble, that is, the expected fluctuation ranges of the Δ_3 - statistics due to finite wavelength effects.

In this regard, the expected fluctuation ranges of the Δ_3 - statistics across the ensemble were evaluated for several dimensions of random matrices with GOE statistics. Additionally, the convergence analysis of the first two statistical moments of the Δ_3 - statistics results across the ensemble was carried out to provide statistically representative results. In Figure 198, the numerical results for the ensemble variance of the Δ_3 - statistics are presented for three ensembles of GOE random matrices with the following dimensions: 100, 150 and 300 elements, respectively.

As observed in Figure 198, the finite wavelength effects are significant for GOE random matrices and thus large fluctuations in the Δ_3 - statistics results across the ensemble are expected for random matrices with small dimensions. Therefore, the numerical ensemble variance results presented in Figure 198 may eventually be employed together with respective RMT analytical predictions in this current work to express the expected fluctuation range across the ensemble due to finite wavelength effects.

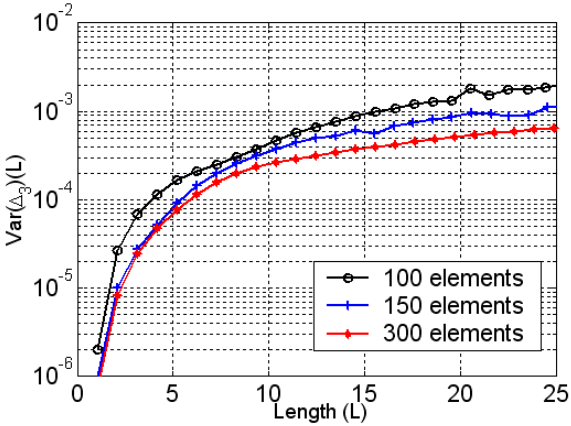

Figure 198: Numerical variance results of Δ_3 - statistics values from the ensembles of GOE random matrices with different dimensions, Gomes and Gerges (101).

APPENDIX C – NUMERICAL INVESTIGATION OF THE FINITE DIMENSION EFFECTS ON THE MODE SHAPE STATISTICS

In this Appendix the analytical estimates of the kurtosis values based on the prediction proposed by Equation (2.63) are compared to the numerical kurtosis results for perfect GOE matrices with several finite dimensions, Figure 199.

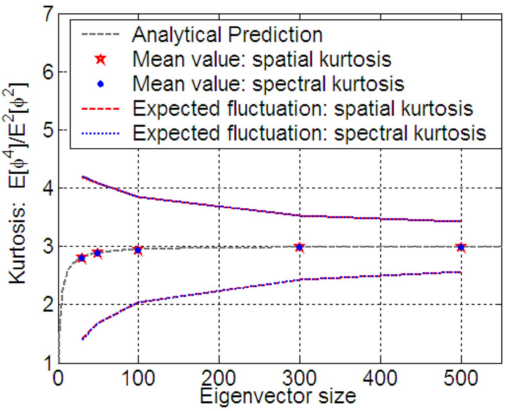

Figure 199: Numerical investigation of the finite dimension effects on the spatial and spectral kurtosis metrics: the expected ensemble kurtosis mean values and respective variance values from the finite GOE matrices with the following dimensions: 30, 50, 100, 300 and 500 elements are compared with available analytical predictions, using Equation (2.63).

As shown in Figure 199, finite GOE matrices with the following dimensions: 30 x 30, 50 x 50, 100 x 100, 300 x 300 and 500 x 500 elements were considered in current investigation. In order to guarantee the statistical convergence of the numerical kurtosis results, the matrix ensembles were composed of 2000 members. For each random GOE matrix, the individual spatial (and spectral) kurtosis values associated with each mode order value (or each mode shape component) were initially evaluated. Additionally, the

spatial and spectral kurtosis mean and variance values associated with each ensemble member were then calculated. Finally, the mean values of spatial and spectral kurtosis results across the ensemble were calculated for each one of the ensembles of the matrices with finite dimensions.

A good agreement was observed between the analytical prediction based on Equation (2.63) and the ensemble mean values of the numerical kurtosis results evaluated for spatial and spectral mode shape averaging approaches. Additionally, it can be observed that the ensemble mean and variance kurtosis results are almost identical for the spatial and spectral mode shape averaging approaches for all matrix dimensions investigated.

Based on the above numerical results, it appears that the finite dimension effects on the results for the eigenvector statistical observables associated with the spatial and ensemble mode shape approaches are expected to be almost negligible for the random structures investigated in this study. Indeed, the results for the statistical observables associated with the spatial eigenvector averaging approach are commonly evaluated using a large number of mode shape components from a typical FEM model of an engineering system which usually has several degrees of freedom. Similarly, the results for the mode shape statistical observables associated with the ensemble averaging approach are evaluated using a large number of ensemble members since the size of the ensemble should be large enough to guarantee the statistical convergence of the statistical moments of the energy results.

However, the results for the statistical observables associated with the spectral eigenvector averaging approach are clearly more susceptible to finite dimension effects since a limited number of the mode orders (or modes) is traditionally available from the typical engineering models and experimental measurements. Thus, it is recommended that the maximum number of available modes should be used during the evaluation of the results for the spectral statistical observables in order to minimize possible finite dimension effects.